

265

Topics in Current Chemistry

Editorial Board:

**V. Balzani · A. de Meijere · K. N. Houk · H. Kessler · J.-M. Lehn
S. V. Ley · S. L. Schreiber · J. Thiem · B. M. Trost · F. Vögtle
H. Yamamoto**

Topics in Current Chemistry

Recently Published and Forthcoming Volumes

Supramolecular Chirality

Volume Editors: Crego-Calama, M.,
Reinhoudt, D. N.
Vol. 265, 2006

Radicals in Synthesis II

Complex Molecules
Volume Editor: Gansäuer, A.
Vol. 264, 2006

Radicals in Synthesis I

Methods and Mechanisms
Volume Editor: Gansäuer, A.
Vol. 263, 2006

Molecular Machines

Volume Editor: Kelly, T. R.
Vol. 262, 2006

Immobilisation of DNA on Chips II

Volume Editor: Wittmann, C.
Vol. 261, 2005

Immobilisation of DNA on Chips I

Volume Editor: Wittmann, C.
Vol. 260, 2005

Prebiotic Chemistry

From Simple Amphiphiles to Protocell Models
Volume Editor: Walde, P.
Vol. 259, 2005

Supramolecular Dye Chemistry

Volume Editor: Würthner, F.
Vol. 258, 2005

Molecular Wires

From Design to Properties
Volume Editor: De Cola, L.
Vol. 257, 2005

Low Molecular Mass Gelators

Design, Self-Assembly, Function
Volume Editor: Fages, F.
Vol. 256, 2005

Anion Sensing

Volume Editor: Stibor, I.
Vol. 255, 2005

Organic Solid State Reactions

Volume Editor: Toda, F.
Vol. 254, 2005

DNA Binders and Related Subjects

Volume Editors: Waring, M. J., Chaires, J. B.
Vol. 253, 2005

Contrast Agents III

Volume Editor: Krause, W.
Vol. 252, 2005

Chalcogenocarboxylic Acid Derivatives

Volume Editor: Kato, S.
Vol. 251, 2005

New Aspects in Phosphorus Chemistry V

Volume Editor: Majoral, J.-P.
Vol. 250, 2005

Templates in Chemistry II

Volume Editors: Schalley, C. A., Vögtle, F., Dötz, K. H.
Vol. 249, 2005

Templates in Chemistry I

Volume Editors: Schalley, C. A., Vögtle, F., Dötz, K. H.
Vol. 248, 2004

Collagen

Volume Editors: Brinckmann, J., Notbohm, H., Müller, P. K.
Vol. 247, 2005

Supramolecular Chirality

Volume Editors:

Mercedes Crego-Calama · David N. Reinhoudt

With contributions by

D. B. Amabilino · V. V. Borovkov · K.-H. Ernst · Y. Inoue

D. A. Leigh · K. Maeda · E. M. Pérez · K. N. Raymond · J. Rebek Jr.

A. Scarso · G. Seeber · B. E. F. Tiedemann · J. Veciana · E. Yashima

The series *Topics in Current Chemistry* presents critical reviews of the present and future trends in modern chemical research. The scope of coverage includes all areas of chemical science including the interfaces with related disciplines such as biology, medicine and materials science. The goal of each thematic volume is to give the nonspecialist reader, whether at the university or in industry, a comprehensive overview of an area where new insights are emerging that are of interest to a larger scientific audience.

As a rule, contributions are specially commissioned. The editors and publishers will, however, always be pleased to receive suggestions and supplementary information. Papers are accepted for *Topics in Current Chemistry* in English.

In references *Topics in Current Chemistry* is abbreviated *Top Curr Chem* and is cited as a journal.

Visit the TCC content at springerlink.com

ISSN 0340-1022

ISBN-10 3-540-32151-9 Springer Berlin Heidelberg New York

ISBN-13 978-3-540-32151-4 Springer Berlin Heidelberg New York

DOI 10.1007/11406174

This work is subject to copyright. All rights are reserved, whether the whole or part of the material is concerned, specifically the rights of translation, reprinting, reuse of illustrations, recitation, broadcasting, reproduction on microfilm or in any other way, and storage in data banks. Duplication of this publication or parts thereof is permitted only under the provisions of the German Copyright Law of September 9, 1965, in its current version, and permission for use must always be obtained from Springer. Violations are liable for prosecution under the German Copyright Law.

Springer is a part of Springer Science+Business Media

springer.com

© Springer-Verlag Berlin Heidelberg 2006

Printed in Germany

The use of registered names, trademarks, etc. in this publication does not imply, even in the absence of a specific statement, that such names are exempt from the relevant protective laws and regulations and therefore free for general use.

Cover design: *Design & Production* GmbH, Heidelberg

Typesetting and Production: LE-TeX Jelonek, Schmidt & Vöckler GbR, Leipzig

Printed on acid-free paper 02/3100 YL – 5 4 3 2 1 0

Volume Editors

Dr. Mercedes Crego-Calama

MESA⁺ Inst. for Nanotechnology
Lab. Supramolecular Chemistry
and Technology
University of Twente
P.O. Box 217
7500 AE Enschede
The Netherlands
m.cregocalama@utwente.nl

Prof. Dr. David N. Reinhoudt

MESA⁺ Inst. for Nanotechnology
Lab. Supramolecular Chemistry
and Technology
University of Twente
P.O. Box 217
7500 AE Enschede
The Netherlands
d.n.reinhoudt@utwente.nl

Editorial Board

Prof. Vincenzo Balzani

Dipartimento di Chimica „G. Ciamician“
University of Bologna
via Selmi 2
40126 Bologna, Italy
vincenzo.balzani@unibo.it

Prof. Jean-Marie Lehn

ISIS
8, allée Gaspard Monge
BP 70028
67083 Strasbourg Cedex, France
lehn@isis.u-strasbg.fr

Prof. Dr. Armin de Meijere

Institut für Organische Chemie
der Georg-August-Universität
Tammanstr. 2
37077 Göttingen, Germany
ameijer1@uni-goettingen.de

Prof. Steven V. Ley

University Chemical Laboratory
Lensfield Road
Cambridge CB2 1EW
Great Britain
Svl1000@cus.cam.ac.uk

Prof. Dr. Kendall N. Houk

University of California
Department of Chemistry and
Biochemistry
405 Hilgard Avenue
Los Angeles, CA 90024-1589
USA
houk@chem.ucla.edu

Prof. Stuart L. Schreiber

Chemical Laboratories
Harvard University
12 Oxford Street
Cambridge, MA 02138-2902
USA
sls@slsiris.harvard.edu

Prof. Dr. Horst Kessler

Institut für Organische Chemie
TU München
Lichtenbergstraße 4
86747 Garching, Germany
kessler@ch.tum.de

Prof. Dr. Joachim Thiem

Institut für Organische Chemie
Universität Hamburg
Martin-Luther-King-Platz 6
20146 Hamburg, Germany
thiem@chemie.uni-hamburg.de

Prof. Barry M. Trost

Department of Chemistry
Stanford University
Stanford, CA 94305-5080
USA
bmtrost@leland.stanford.edu

Prof. Dr. Hisashi Yamamoto

Department of Chemistry
The University of Chicago
5735 South Ellis Avenue
Chicago, IL 60637
USA
yamamoto@uchicago.edu

Prof. Dr. F. Vögtle

Kekulé-Institut für Organische Chemie
und Biochemie
der Universität Bonn
Gerhard-Domagk-Str. 1
53121 Bonn, Germany
voegtle@uni-bonn.de

Topics in Current Chemistry **Also Available Electronically**

For all customers who have a standing order to Topics in Current Chemistry, we offer the electronic version via SpringerLink free of charge. Please contact your librarian who can receive a password or free access to the full articles by registering at:

springerlink.com

If you do not have a subscription, you can still view the tables of contents of the volumes and the abstract of each article by going to the SpringerLink Homepage, clicking on "Browse by Online Libraries", then "Chemical Sciences", and finally choose Topics in Current Chemistry.

You will find information about the

- Editorial Board
- Aims and Scope
- Instructions for Authors
- Sample Contribution

at springer.com using the search function.

Preface

One of the most important landmarks in the phenomenon of chirality was the first successful separation of a pair of enantiomers achieved by Louis Pasteur in 1848. Since then, huge progress has been made in the resolution of racemic mixtures and in the preparation by covalent synthesis of chiral molecules. The latter is still a major topic of interest especially because of its implication in the development of new drugs and catalysts. The advent of supramolecular chemistry 30 years ago with tools such as molecular recognition and molecular self-assembly has expanded the toolbox of chirality tremendously. However, the noncovalent synthesis of chiral self-assembled aggregates is not an easy task due to the highly dynamic character of noncovalent interactions. Recently, the field of supramolecular chirality (i.e. the nonsymmetric arrangement of molecules in a noncovalent assembly), has started to master control over many aspects of chirality. In the literature of the past 5–10 years beautiful examples of noncovalent systems have been described in which the process of self-assembly is fully controlled, resulting in the stereoselective synthesis of diastereomeric and enantiomeric assemblies. Intriguing concepts such as self-resolution, chiral memory and chiral amplification have emerged with very promising consequences. For applications, especially in the field of nanofabrication, the initial study and control of the supramolecular chirality in solution has been extended to the chirality of two-dimensional structures. There are now very interesting and novel examples dealing with the concept of two-dimensional chirality (chirality on surfaces). New paradigms such as the amplification of chirality in two-dimensional lattices have already been observed. It is obvious that control of supramolecular chirality of increasingly complex synthetic assemblies in solution and on surfaces will be of crucial importance to their application in the field of molecular recognition, asymmetric chemical synthesis, chiral separation, catalysis, material sciences, and especially nanotechnology and nanosciences.

This volume of *Topics in Current Chemistry* on supramolecular chirality aims to acquaint the researcher with the principles and applications of noncovalent chiral assemblies or aggregates. The first chapter illustrates the reader the state of the art on the construction of synthetic chiral supramolecular assemblies held together by means of weak intermolecular noncovalent forces in solution except metal–ligand coordination. The next chapter deals with dynamic heli-

cal polymers which respond to the chirality of optically active small molecules via noncovalent interactions. This chapter also includes recent representative examples of helical aggregates based on small molecules. A comprehensive review of the supramolecular chirogenesis in various porphyrinoid-containing systems is the topic of the third chapter, while the preparation and analysis of a variety of chiral architectures based on metal–ligand coordinative interactions are described in the fourth chapter. The following chapter discusses the relationship between mechanical motion and chirality at the (supra)molecular level. Next, in the sixth chapter, chirality induction due to confinement of molecules at surfaces and chiral recognition in two dimensions is discussed. Chiral amplification and homochirality are also presented in this chapter. The book concludes with a chapter concentrating on applications, focusing on supramolecular materials with a function—be it electronic, magnetic, optical, etc.—where the role of chirality is evident.

Hopefully, this volume will be useful to readers not currently working with chiral supramolecular structures as well as informative to those who are more familiar with the subject. This book written by recognized experts in their respective fields and not only provides an excellent and comprehensive overview of the supramolecular chirality, but also shows that there are many new aspects to be discovered, understood, and controlled.

Several supramolecular chiral systems were discovered as a result of “lucky breaks,” but one should not forget that even 100 years ago chemists thought Pasteur was lucky. On this topic Pasteur once said: “Chance favors the prepared mind.”

Enschede, March 2006

Mercedes Crego-Calama, David N. Reinhoudt

Contents

Chiral Spaces in Supramolecular Assemblies	
A. Scarso · J. Rebek, Jr.	1
Dynamic Helical Structures: Detection and Amplification of Chirality	
K. Maeda · E. Yashima	47
Supramolecular Chirogenesis in Host–Guest Systems Containing Porphyrinoids	
V. V. Borovkov · Y. Inoue	89
Supramolecular Chirality in Coordination Chemistry	
G. Seeber · B. E. F. Tiedemann · K. N. Raymond	147
Dynamic Chirality: Molecular Shuttles and Motors	
D. A. Leigh · E. M. Pérez	185
Supramolecular Surface Chirality	
K.-H. Ernst	209
Supramolecular Chiral Functional Materials	
D. B. Amabilino · J. Veciana	253
Author Index Volumes 251–265	303
Subject Index	311

Contents of Volume 258

Supramolecular Dye Chemistry

Volume Editor: Frank Würthner

ISBN: 3-540-27758-7

Chlorins Programmed for Self-Assembly

T. S. Balaban · H. Tamiaki · A. R. Holzwarth

Metallosupramolecular Dye Assemblies

C.-C. You · R. Dobrawa · C. R. Saha-Möller · F. Würthner

Hydrogen-Bonded Assemblies of Dyes and Extended π -Conjugated Systems

A. Ajayaghosh · S. J. George · A. P. H. J. Schenning

Dye-Based Organogels: Stimuli-Responsive Soft Materials Based on One-Dimensional Self-Assembling Aromatic Dyes

T. Ishi-i · S. Shinkai

Intercalation of Organic Dye Molecules into Double-Stranded DNA – General Principles and Recent Developments

H. Ihmels · D. Otto

Two-Dimensional Dye Assemblies on Surfaces Studied by Scanning Tunneling Microscopy

S. De Feyter · F. De Schryver

Self-Assembled Monolayers of Chromophores on Gold Surfaces

V. Kriegisch · C. Lambert

Chiral Spaces in Supramolecular Assemblies

Alessandro Scarso¹ (✉) · Julius Jr. Rebek²

¹Università Cà Foscari di Venezia, Calle Larga Santa Marta 2137, 30123 Venice, Italy
 alesca@unive.it

²The Skaggs Institute for Chemical Biology and The Department of Chemistry,
 The Scripps Research Institute, MB-26, 10550 North Torrey Pines Road,
 La Jolla, CA 92037, USA

1	Introduction: Chiral Spaces in Supramolecular Assemblies	3
1.1	Kinds and Strength of Weak Intermolecular Forces.	
	Multivalency and Cooperativity Concepts	4
1.2	Lifetime of Supramolecular Assemblies	6
1.3	Examples in Nature	7
1.4	Supramolecular Chirality in Artificial Systems	8
2	Chiral Assemblies Comprising Enantiopure Building Blocks	10
2.1	Achiral <i>tris</i> -Melamine with Chiral Cyanurate Assembly	10
2.2	Double Rosettes	11
2.2.1	Diastereoselective Non-Covalent Synthesis of Chiral Dimelamines— Barbituric Acid Assemblies	11
2.2.2	Chiral Amplification in Dimelamines-Cyanurate Assemblies	14
2.3	Capsules	16
2.3.1	Calix[4]arene Urea Dimeric Capsules	16
2.3.2	Peptido Calix[4]arene Capsules	19
2.3.3	Ion Pairing Dimeric Capsules	20
2.3.4	Tetrameric Capsule	21
2.3.5	Cylindrical Dimeric Capsule	23
2.4	G-Quadruplex Assemblies	25
2.5	Other Dimeric Assemblies	25
3	Chiral Assemblies Comprising Achiral Building Blocks	28
3.1	Racemic Capsules	29
3.1.1	Calix[4]arene Capsules	29
3.1.2	Tennis Ball Capsule	30
3.1.3	Softball Capsule	31
4	Enantioselective Synthesis via the Chiral Memory Effect	35
4.1	Enantiopure Double Rosettes	35
4.2	Chiral Enantioenriched Softball	37
5	Asymmetric Spaces within an Achiral Cylindrical Host	38
5.1	Single Encapsulation	39
5.2	Double Coencapsulation	40
5.3	Triple Coencapsulation	43

6	Conclusions	44
7	Outlook	44
	References	44

Abstract The present review is aimed at illustrating to the reader the state of the art on the construction of artificial chiral supramolecular assemblies held together by means of weak intermolecular non-covalent forces in solution except metal-ligand coordination. Chiral supramolecules are self-assembled finite aggregates characterized by the presence of chiral residues or by asymmetric arrangement of components. These assemblies have proven to be powerful tools to explore chirality and its effects in host-guest interactions and represents important steps toward a superior control in asymmetric non-covalent synthesis, which is still a peculiar prerogative of natural systems. The introduction serves as a quick overview of weak (non-covalent) interactions refreshing concepts like cooperativity and multivalency that are crucial to molecular assembly, as well as providing selected examples of supramolecular chiral systems found in nature. Four main strategies have been so far employed for the preparation of chiral supramolecular assemblies: these are discussed on the bases of the nature of the monomeric components employed. Intrinsically chiral scaffolds have been used both in the enantiopure or racemic mixture form to assemble into chiral aggregates. A second approach instead makes use of achiral building blocks to give racemic chiral supramolecules, and a step further consists of the enrichment of these species in one enantiomeric form exploiting the chiral memory effect. The last approach is based on encapsulation of chiral guests, which allows reciprocal sensing of chiral species confined in close proximity within an achiral host.

Keywords Supramolecular chemistry · Chirality · Non-covalent synthesis · Hydrogen bond · Weak interactions

Abbreviations

Alk	alkyl chain
Ar	aryl
BAR	barbiturate
Cbz	benzyloxycarbonyl
CD	circular dichroism
CYA	cyanurate
d.e.	diastereoisomeric excess
e.e.	enantiomeric excess
EXSY	exchange spectroscopy
¹ H-NMR	proton nuclear magnetic resonance
2D-NMR	bidimensional nuclear magnetic resonance
I	ionic strength
NOE	nuclear Overhauser Effect
PC	packing coefficient
Pr	propyl chain

1

Introduction: Chiral Spaces in Supramolecular Assemblies

The world where we live, and in particular living systems, appear to be symmetric in shape from a macroscopic point of view, but are indeed chiral if observed from a molecular point of view [1]. All the biopolymers in the living systems are made of chiral building blocks, (e.g. amino acids, nucleic acids, sugars, lipids, etc.) from primary up to quaternary structure and their functions are specifically related to their reciprocal supramolecular interactions. Even though it is not clear what the advantages of this are (whether a chiral world is more efficient than an achiral one in conserving and developing life), most of the reactions in living systems occur in a stereospecific manner, therefore preferring a particular pathway rather than the opposite one which leads to the mirror image species. The importance of chirality in chemistry is clear: with a myriad of examples provided by Mother Nature as references, some of the most challenging targets for chemists are the creation of artificial systems that resemble natural ones in terms of catalytic efficiency and stereoselectivity. From these challenges arises for scientists the great interest in the study of chirality, in particular in natural supramolecular assemblies.

Origins of chirality are still extensively debated, but since chemistry and other disciplines have gained insight into the molecular structure of living systems, they have highlighted the pivotal role played by chiral supramolecular structures in life. In biochemistry supramolecular chirality arises from the aggregation of intrinsically chiral biopolymers and this feature represents a superior tool, which allows that, in principle, a better stereocontrol of catalyzed reactions is possible to be achieved. Self-assembly has emerged as an important tool for the bottom-up approach to nanofabrication of a plethora of thermodynamically controlled supramolecular functional devices due also to particular features like reversibility and self correction. Parallel to this, the construction of (finite) chiral supramolecular aggregates is still in its infancy even though important steps have been made to master weak interactions and to develop more and more sophisticated scaffolds that bear specific functional groups.

Rather than aiming at compiling an exhaustive list of examples, this work has the purpose to rationalize the strategies employed for the creation of chiral artificial supramolecules and to sort the many artificial systems thus far reported in the literature into four main subcategories, addressing topics like supramolecular chirality both starting from chiral and achiral building blocks, chiral memory effect encapsulation, giving a broad overview of structures. Only chiral supramolecular finite assemblies held together by means of weak interactions (except metal-ligand coordination which is reviewed elsewhere in this volume) have been covered.

1.1

Kinds and Strength of Weak Intermolecular Forces.

Multivalency and Cooperativity Concepts

Within a molecule, covalent bonds have energies in the range 170–450 KJ/mol, while interactions between molecules are typically much weaker [2]: in general the enthalpy for intermolecular attractive forces spans from 8–80 KJ/mol for a hydrogen bond, to ~ 8 KJ/mol for ionic interactions, and as low as 0.4–2 KJ/mol for van der Waals or dispersive and CH – π interactions. These kinds of non-covalent forces have been thoroughly reviewed elsewhere [3–7], and in the present work we intend to remind the reader of a few characteristics of only hydrogen bonds and ionic interactions because these are the classes of intermolecular forces that are responsible for the chiral supramolecular assemblies known in the literature. Weaker attractive interactions like dispersive forces and CH – π interactions have not been used so far for the construction of artificial chiral supramolecular structures probably due to their low energy of binding which therefore requires the presence of many concomitant interactions (high level of multivalency) and do not ensure a high level of control over the geometry of the assemblies.

Hydrogen bonding prevails among other weak interactions in terms of diffusion in nature, importance and energy of binding: it is needless to state the pivotal role played by such a kind of attractive force in protein and many other natural macromolecule folding and how essential it is for their biological activity. Moreover, water with its unique properties as a solvent and as a biological reaction medium, represents the most striking example of the pervasive importance of the hydrogen bond because life on earth, in the forms that we know, is a direct consequence of water's hydrogen bond ability. Even the hydrophobic effect, which could be considered to be another form of weak interaction, is an indirect consequence of water's structure which squeezes out hydrophobic solutes from the network of hydrogen bonds and forces them to aggregate [7]. Multivalent hydrogen bonds, when present in close reciprocal distance, have an enthalpy of binding which is not a multiple of a single interaction, rather they are characterized by extra attractive and repulsive interactions as observed when comparing the three complexes A, B and C in Fig. 1. The same number of hydrogen bonds gives rise to binding constants that differ overall for three orders of magnitude [8, 9], attesting to these presumptions. This large binding affinity difference has been elucidated in terms of secondary interactions that are present between one donor group and those present in the other acceptor counterpart.

Ion pair interactions are also present in natural supramolecular systems (e.g. DNA-peptides, polyamine-nucleic acids and among proteins or enzymes). Such kinds of attractive forces are strongly dependent on the ionic strength (I) of the solution: if extrapolated to $I = 0$ the average value for the free energy of association for one cation–anion pair is about 8 KJ/mol, and

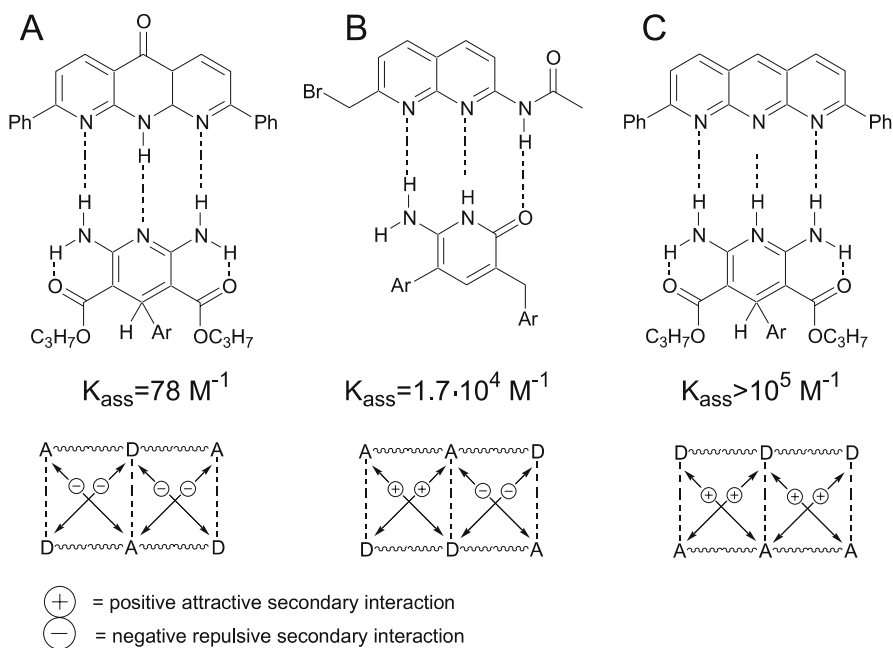


Fig. 1 Examples of positive and negative secondary hydrogen bond interactions on the binding affinity between triple donor D and acceptor A hydrogen bond partners

the value decreases down to 4 KJ/mol for $I = 0.02$. As observed in many synthetic systems, a certain level of tolerance is permitted for complexation between molecules bearing two or more charges, in other words pre-orientation and rigidity of the scaffold is not as important as in hydrogen bonded assemblies [4].

In nature weak interactions between two counterparts are rarely monotopic, more frequently multiple complementary interactions take place at the same time to strengthen the interaction between the counterparts [10, 11]. To ensure multivalent interactions, the proper functional group requires the adequate relative orientation which is ensured by the design of the system and by the architecture of the scaffold. The thermodynamic character of multivalent interactions is particularly interesting because this phenomenon is pervasive in nature, e.g. adenine–thymine is a divalent interaction and cytosine–guanine is trivalent. By means of careful design of counterparts it has been demonstrated that increasing the rigidity of the partners results in an increase of binding mainly because of less flexibility and a lower number of possible conformers, thus a smaller entropy loss. Cooperativity is often invoked in supramolecular systems when binding constants between n -valent species are higher the n monovalent binding constants. It has to be stressed that cooperativity is strictly peculiar for consecutive monovalent interactions

with a multivalent platform, and not directly applicable to two multivalent molecules: in other words cooperativity can be only assessed if the compared equilibrium constants have the same dimensions [12]. The presence of a few concomitant interactions can have a remarkable effect both on the thermodynamic and kinetic formation of a supramolecular complex: for example association and dissociation of many hydrogen bonds at a time give rise to higher activation energies and slower kinetics for dissociation of the species, which is a fundamental aspect in choosing which kind of spectroscopic methodology has to be used to follow the process.

1.2

Lifetime of Supramolecular Assemblies

All the processes that take place in solution have to deal with solvation and de-solvation phenomena; basically the solvent plays a crucial role both on a thermodynamic and kinetic point of view. When two molecules come together in solution and no special attractive interactions are present among them, the lifetime of this encounter complex is on the order of $< 10^{-9}$ sec. At the opposite extreme, for topological linked molecules like catenanes or rotaxanes that are not covalently bound together but simply interlocked, the lifetime is on the order of breaking a covalent bond, namely 10^{10} sec. Supramolecular complexes have a lifetime that is strictly related to the kind, strength and overall number of weak interactions. Assemblies like capsules with trapped guests have intermediate activation barriers and lifetimes for their association and dissociation in the order of 10^3 to 10^{-3} sec (Fig. 2) [13]. Often they can release the guest without complete disassembly of the multi-meric structure, but simply by means of gating through one of the walls of

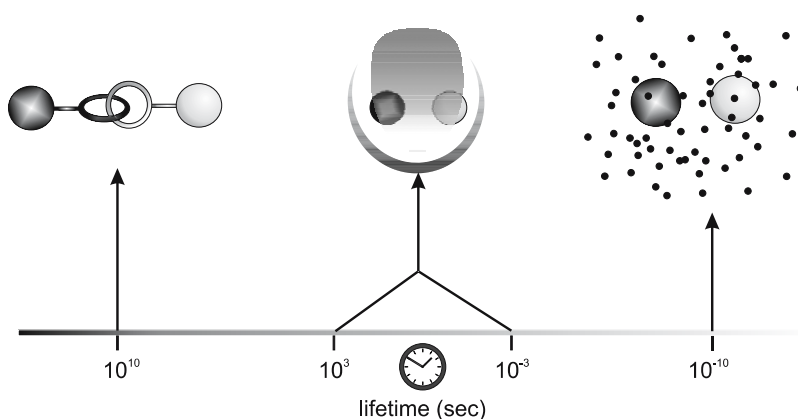


Fig. 2 Timescales for different intermolecular interactions: mechanically interlocked molecules, encapsulated species and solvated encounters

the monomers, thus limiting the enthalpic cost and favoring a chiral memory effect.

Monitoring of these phenomena requires tools able to “take snapshots” of the system at a rate faster than that of the process under investigation, thus allowing us to detect signals for each species present in solution. If this is not the case, the pictures taken are the average, during the time required for observation, of the system, with signals in between the species that exchanged during the shot. NMR spectroscopy is the most adequate/prevalent technique because the change between fast and slow exchange regime, compared to the chemical shift timescale, falls in the range from 0.1 ms up to a few seconds with the opportunity to tune temperature to regulate the exchange process rate. IR and UV-Visible spectroscopy are instead in the range of picoseconds, in which case the systems observed almost always reside in the slow exchange regime [14].

1.3

Examples in Nature

In nature, as well as in artificial systems, the most widely used tool for the construction of supramolecules is hydrogen bonding. The supremacy of this kind of weak interaction is related to the strength of such a kind of attractive force, as well as the extremely large choice of functional groups able to give hydrogen bonding that are easily implemented into more complex architectures. Bearing in mind that most of the natural building blocks are chiral and enantiopure, we will first consider the effect of this chirality on supramolecules based on biopolymers. As a leading example, the double helix of DNA represents a supramolecular assembly that exhibits a chiral quaternary structure. The complementarity between the nucleobases adenine–thymine and cytosine–guanine allow dimerization of the helices in an anti-parallel fashion leading to the well known double helix structure. With natural D-nucleotides, among the two mirror image helices which are diastereomeric, DNA-A assumes only a right-handed double helix as an indication of a very high level of supramolecular diastereoselection. The left-handed helix is not observed as a consequence of the chiral information implemented in the ribose ring of nucleotides: this transfer of chiral information from the building blocks to the tertiary structure adopted is a common phenomenon and is observed in other DNA structures. DNA-B also assumes only a right-handed conformation of the double helix, while DNA-Z, which is characterized by alternation of purine and pyrimidine nucleobases, exists as a double left-handed helix (Fig. 3) [15]. Proteins exhibit chiral tertiary structure too, like the one observed in the triple helix of collagen, where the L relative configuration of the amino acids forces the supramolecule to adopt a right-handed triple helical structure once again with complete diastereoselection on the supramolecular level of organization (Fig. 3). Natural organic chiral pigments display supra-

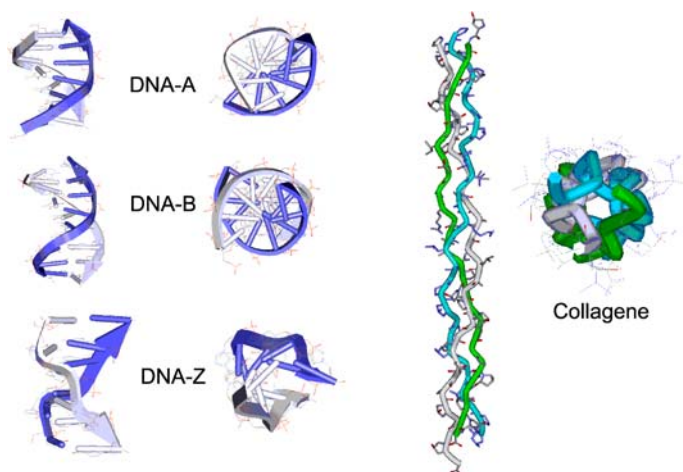


Fig. 3 Different handedness and supramolecular chirality of DNA (A, B and Z forms) arising from the same D-nucleotides, and the triple right-handed helix of polypeptide natural collagen made of natural L-aminoacids

molecular chirality as well, like complexes between six anthocyanines and six flavone units where both kinds of monomers assemble around a Mg^{2+} cation into a supramolecular right-handed propeller-like structure that is composed of three blades and exhibits chirality. Natural flavone components containing D-sugars form an intensely blue colored stacked complex only with anthocyanines with the same relative configuration on the sugar moiety. In fact, with L-sugars the proper supramolecular chiral assembly is not possible due to steric hindrance and only a weak color is observed for the system [16].

1.4

Supramolecular Chirality in Artificial Systems

Supramolecular chirality arises when finite molecular non-covalent assemblies are present in a non-symmetrical arrangement and it is distinguished from “chiral molecular recognition” which regards one to one host-guest chiral interaction, recently reviewed [17, 18], and will not be covered here. Typical properties of supramolecular aggregates are reversibility, self-correction and self-recognition, which are all fundamental tools for the creation of chiral aggregates. Figure 4 depicts the four different approaches to the construction of chiral supramolecular aggregates. All the chiral supramolecular aggregates reported so far in the literature can be classified into four different strategies [19].

The first approach (Fig. 4A) called “diastereoselective non-covalent synthesis” regards the self-assembly of chiral units which bear stereogenic centers or which are intrinsically chiral (for instance because of atropoisom-

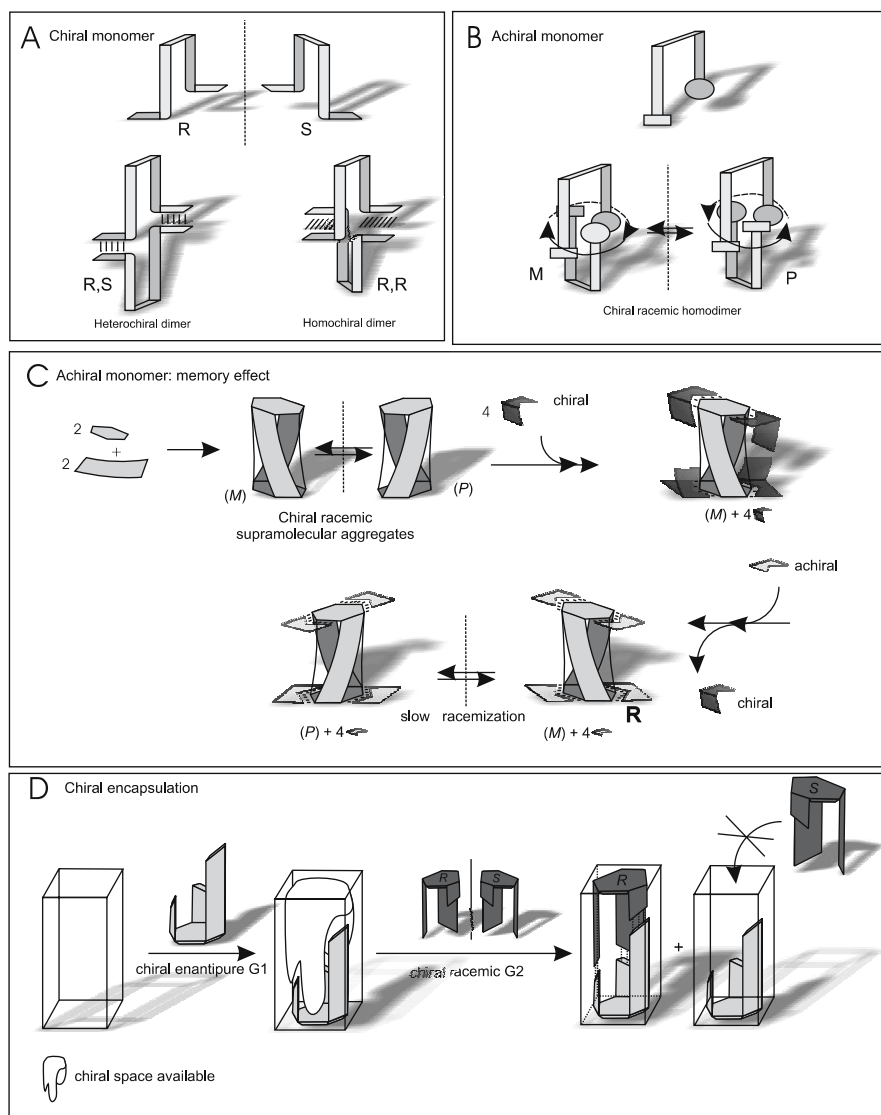


Fig. 4 Schematic representations of the possible pathways for the construction of chiral supramolecular aggregates. **A** Chiral supramolecular aggregates from chiral components. **B** Chiral racemic supramolecular aggregates from achiral components. **C** Chiral enantioenriched supramolecular aggregates from achiral components exploiting the chiral memory effect. **D** Chiral encapsulation: achiral capsule binds an enantiopure primary guest forming a chiral space in the cavity, which is filled preferentially by one of the two enantiomers of a secondary guest

merism). When chiral components associate by means of hydrogen bonding or other weak intermolecular forces, the overall three-dimensional structure can be characterized by a higher degree of asymmetry, for example helical shape, thus leading to diastereomeric structures. The second approach is based on the aggregation of achiral building blocks where only racemic enantiomeric assemblies are possible (Fig. 4B). To induce an imbalance into such kinds of enantiomeric supramolecules, the chiral memory effect can be exploited. This procedure takes advantage of the opportunity to create a chiral supramolecular enantioenriched structure starting from chiral building blocks in a highly diastereoisomeric excess, and, in virtue of the slow kinetic of association and dissociation of the assembly, chiral templating components can be replaced by achiral ones without modifying the supramolecular level of chirality (Fig. 4C). The structure thus obtained is chiral and with a certain degree of enantiopurity even though it is made of achiral components. It has to be noticed that this species is not under thermodynamic control and it racemizes slowly by means of dissociation and reassembly of the components.

Entrapment of guests within self-assembled capsules provides a fourth method for the construction of chiral supramolecular aggregates. In fact, confinement of guests into cavities with a proper shape and size limits their available space and allows the control over their reciprocal positioning. This reflects directly into their mutual electronic and steric interaction and, as a consequence, in their stereorecognition (Fig. 4D).

2

Chiral Assemblies Comprising Enantiopure Building Blocks

This section presents different kinds of chiral supramolecular aggregates based on various scaffolds endowed with stereogenic centers. This is the easiest approach to chiral supramolecular systems—present also in Nature—because of the high level of steric control that it permits.

2.1

Achiral *tris*-Melamine with Chiral Cyanurate Assembly

One of the earliest examples of chiral melamine–cyanurate was reported by Whitesides and collaborators, who studied the hydrogen-bonded aggregate between three molecules of chiral cyanurate and a complementary achiral *tris*-melamine unit based on a 1,3,5 trisubstituted benzene with a melamine unit appended at each arm (Fig. 5) [20]. The *tris*-melamine unit is not chiral itself, but in the complex with cyanurate forms a tightly bonded hydrogen bond platform with C_3 symmetry which is chiral at a supramolecular level due to the clockwise (*P*) and counterclockwise (*M*) conformation of the pendants (Fig. 5).

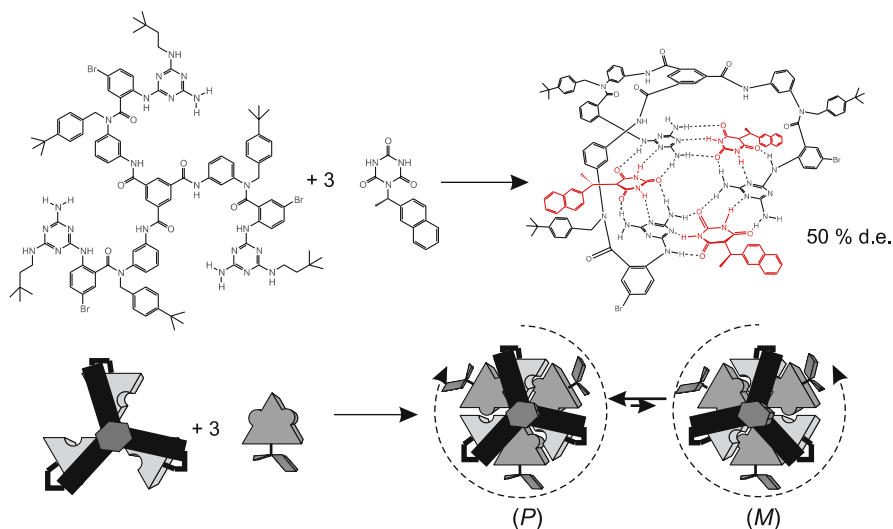


Fig. 5 Tetrameric diastereoisomeric complexes based on the assembling of achiral trisdimelamine unit with chiral isocyanuric acid

The ^1H -NMR spectrum showed two distinct diastereomeric complexes with C_3 symmetry each one characterized by two singlets for the NH resonances, in a 3 : 1 ratio (50% d.e.), that is a difference of 1.3 KJ/mol in free energy. C_1 symmetric diastereoisomers were also observed, but as minor complexes ($\sim 10\%$) and correct assignment remains uncertain. Both C_3/C_1 ratio and diastereomeric ratio were affected by the solvent employed with exchange rate for cyanurate that was larger in chloroform than in benzene or carbon tetrachloride, and by the temperature with expected increasing diastereomeric ratio at lower temperature. The activation energy barrier for the interconversion between these couples of diastereoisomers is high and requires the dissociation of one or more cyanurate units, which means breaking at least six hydrogen bonds. This is a slow process compared to the chemical shift timescale.

2.2

Double Rosettes

2.2.1

Diastereoselective Non-Covalent Synthesis of Chiral Dimelamines—Barbituric Acid Assemblies

The multimeric assembly reported in Fig. 6 forms spontaneously when three calix[4]arene dimelamine units and six barbiturates or cyanurate are mixed in a 1 : 2 ratio in apolar solvents. These assemblies, made of nine achiral com-

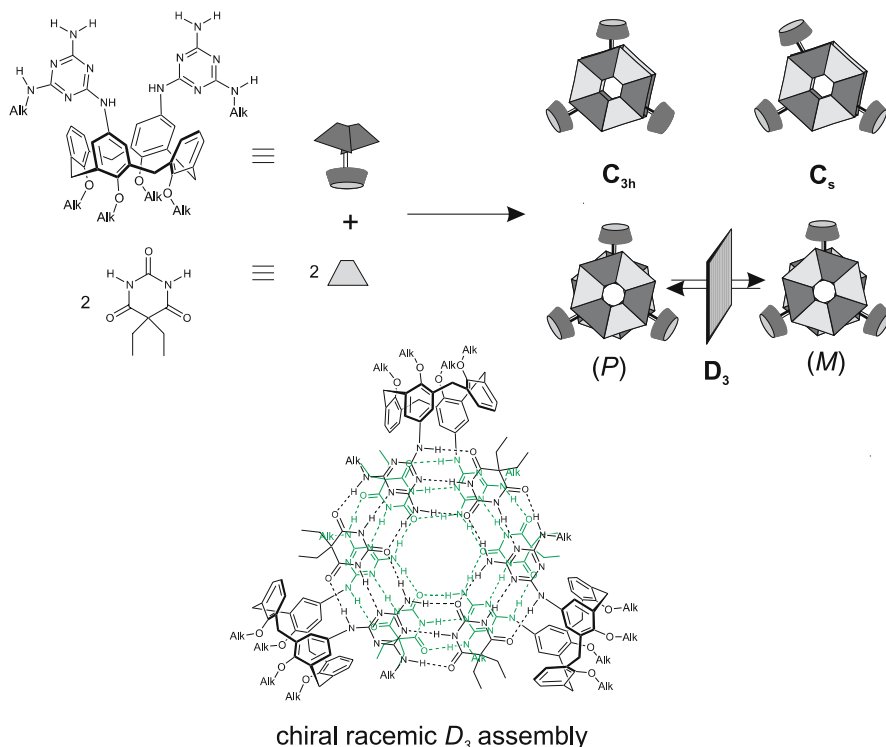


Fig. 6 Schematic representation of double rosette assemblies with three constitutional isomers with different symmetry. The D_3 symmetric assembly is chiral and exists as a racemic mixture

ponents, are held together by 36 hydrogen bonds and can adopt up to three diastereoisomeric forms with D_3 , C_{3h} and C_s symmetry due to the reciprocal staggering or aligning of the dimethylamine units. Only the D_3 species exists as a pair of enantiomers (P) and (M) as a function of the orientation of each calix[4]arene dimethylamine unit. The relative distribution between the isomers is related to the substituents on both the calix[4]arene and barbiturate or cyanurate, with a marked preference for D_3 symmetry if more hindered units are employed [21].

The chirality of the assembly was clear upon addition to the system of ten equivalents of enantiopure Pirkle's reagent that caused the splitting of the bridging methylene of the calix[4]arene into equally populated signals due to diastereomeric complexation of the reagent with the M and P enantiomeric assemblies. The interaction between the chiral shift reagent and the hydrogen bonded assemblies was too weak to induce an energy difference between the diastereomeric complexes and proved the existence of slowly interconverting chiral assemblies in solution [22].

With a chiral calix[4]arene bearing stereogenic centers in the dimelamine moieties (Fig. 7A), the complexation with achiral diethyl-barbiturate showed only two NH signals which implies the presence of only one of the two diastereomeric complexes with D_3 symmetry: (*M*) or (*P*) [23]. This turned out in an induced diastereomeric excess $\geq 98\%$ corresponding to a ΔH° (298 K) of 13.4 KJ/mol with different several chiral residues thus indicating that a high level of stereocontrol is implicit in such kinds of supramolecular well-defined aggregates: six homochiral stereogenic centers are present in each aggregate strongly inducing a very high control of supramolecular chirality. (*S*) stereogenic centers in the melamine moieties induce (*P*) chirality in the major diastereomeric assembly as demonstrated by spatial coupling observed with 2D-NMR experiments.

Chiral calix[4]arene dimelamines are weakly CD active, while on the contrary chiral double rosettes show strong absorptions with $|\Delta\epsilon_{\max}|$

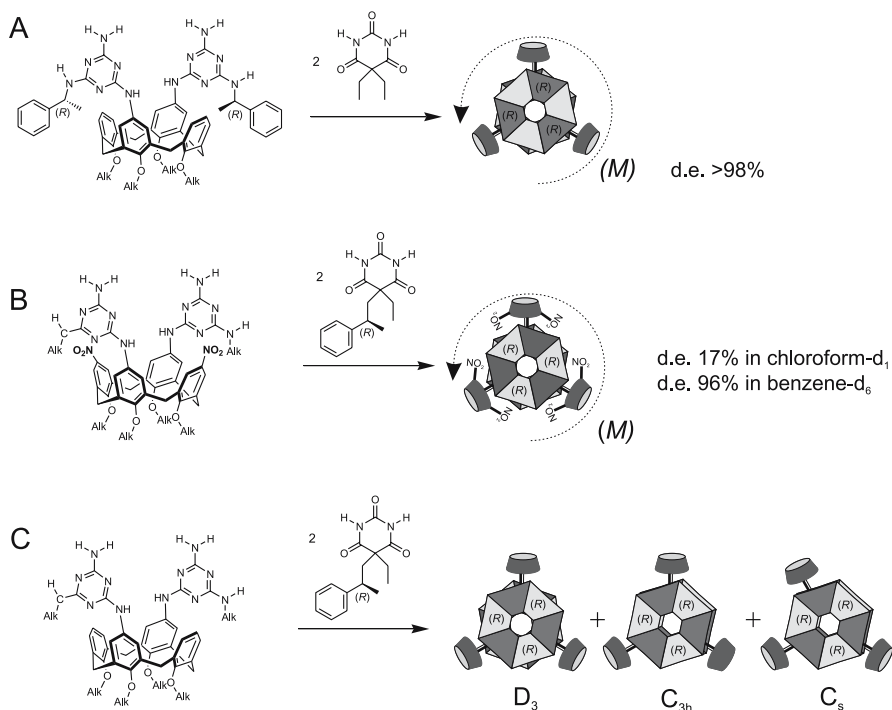


Fig. 7 Schematic representation of highly diastereoselective non-covalent synthesis: **A** (*R,R*) chiral dimelamine and achiral barbiturate components lead only to the (*M*) double rosettes with very high d.e. **B** Achiral hindered dimelamine and chiral barbiturate leads to highly solvent dependent asymmetric induction, while; **C** achiral alkyl dimelamine and chiral barbiturate components lead instead to all the isomeric double rosettes with different symmetry

$\sim 100 \text{ L}/(\text{mol} \cdot \text{cm})$ due to exciton coupling between the chromophores present in the core of the assembly. Titration of the (*R,R*)-(*M*) double-rosette with the enantiomer (*S,S*)-(*P*) showed a linear decrease of the CD activity that can be explained only assuming no interchange between (*R*) and (*S*) calix[4]arenes which means no heteromeric assemblies comprising (*R*) and (*S*) dimelamine components are present in the same assembly and complete chiral self-recognition of these units is achieved. Analogously an equimolar amount of (*R,R*) and (*S,S*) dimelamine in the presence of achiral barbiturate did not show the presence of any heterochiral complexes. Further evidence of the high degree of stereocontrol implemented in this kind of self-assembled structure was observed also employing the (*R,S*) dimelamine component with one *R* and one *S* stereogenic center on the same calix[4]arene unit. Only polymeric species and not finite aggregates were observed, underlining once again the pivotal role played by stereogenic centers in controlling supramolecular chirality in double-rosettes.

Chiral barbiturates can be employed as well for the construction of chiral double rosettes (Fig. 7B,C). Compared to chiral dimelamines, the higher average distance of the stereogenic center of the barbiturate (C_β) from the hydrogen-bonded network allows a good level of stereocontrol only if employing more sterically demanding nitro-substituted achiral calix[4]arene dimelamines. This time the asymmetric induction is strongly solvent dependent, with values as low as 17% in the more polar chloroform- d_1 and as high as 96% in benzene- d_6 or toluene- d_8 where hydrogen bond strength is likely to be higher with concomitant lower flexibility of the assembly and more pronounced steric effects (Fig. 7B). With calix[4]arenes lacking the NO_2 substituents, all the isomeric D_3 , C_{3h} and C_s complexes are present (Fig. 7C) in similar amounts and no clear interpretation of the spectra is possible. The smaller asymmetric inducing effect of chiral barbiturates compared to chiral dimelamines correlates with the higher distance in the former system between the chiral centers and the hydrogen-bonded network [22].

2.2.2

Chiral Amplification in Dimelamines-Cyanurate Assemblies

Similar chiral supramolecular assemblies are also observed from achiral calix[4]arene dimelamine derivatives with chiral cyanurates thus leading to D_3 symmetry species [21]. Analogously to chiral dimelamines, predominantly one of the two possible diastereomeric double-rosette assemblies was observed in most cases and it is noteworthy that the same (*R*) chiral moiety when mounted in the dimelamine is located on the left-hand side of the calix[4]arene and induces (*M*) chirality, while when implemented in the cyanurate is placed on the right-hand side and therefore promotes *P* chirality (Fig. 8).

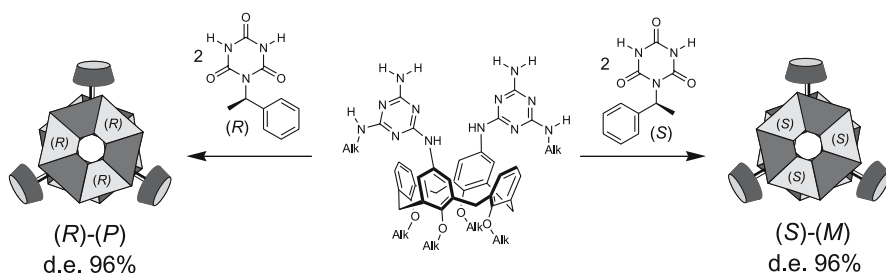


Fig. 8 Schematic representation of highly diastereoselective non-covalent synthesis: achiral dimelamine calix[4]arene with enantiopure chiral cyanurate components lead to chiral double rosettes with d.e. as high as 96%; (R)-cyanurate induces complete (P) chirality, while (S) favors only (M) chirality

Chiral amplification is the phenomenon observed when a chiral unit present in a small initial enantiomeric bias, induces a much higher stereo preference (high d.e. or e.e.) when introduced into a bigger aggregate. Double rosette assemblies are typical examples of such a relationship. From a theoretical point of view, mixing different amounts of an enantiopure complex comprising a chiral dimelamine unit with a second racemic one bearing a different achiral dimelamine residue should lead to a linear dependence of the CD intensities as a function of the molar ratio of the two complexes. On the contrary, experimental data showed a positive deviation from linearity as a direct consequence of the so-called “sergeants and soldiers principle”, which indicates that within the assembly the achiral units tend to follow the helicity of the chiral units, thus leading to higher d.e. than expected [24]. Moreover, when chiral dimelamine was present, the exchange of chiral components and (M) – (P) interconversion took place via identical pathways, while when chiral cyanurates were employed, exchange of chiral components was faster than (M) – (P) interconversion. This leads to a much stronger chiral amplification in the latter case, even though the overall number of stereocenters is the same in both cases.

Diastereoisomeric non-covalent synthesis was accomplished also on dimelamine–cyanurate double rosettes using an external chiral inductor of asymmetry. Employing a dimelamine unit with appended pyridine units, it was possible to prepare racemic rosettes and to amplify preferentially one of the enantiomers by complexation (ion pair formation) with chiral enantiopure monocarboxylic acids, with d.e. up to 50%. In particular the selectivity observed is strongly dependent on the structure of the acids, with interesting results with aromatic species, and on the number of equivalents employed [25]. It is worth noting that titration of the racemic rosette with (R)-2-phenylbutyric acid showed a sigmoidal profile for the CD signal, which was attributed to cooperativity in the binding process.

2.3

Capsules

A simpler approach to the construction of chiral supramolecules is based on concave-shaped molecules endowed with H-bond donor and acceptor residues capable of self-assembling into closed structures. The cavity thus formed can be created usually by two, but sometimes up to six units, and properties like size, shape and polarity of the capsule have reached a high level of sophistication due to the development of proper scaffold structures and hydrogen-bonding motifs. The encapsulation process can be easily studied because NMR resonances of the trapped guests are shifted upfield by the aromatic ring currents of the host, often kinetically stable and in slow exchange on the NMR chemical shift timescale, revealing two distinct species for the encapsulated and free guest. A common rule for succeeding in encapsulation is to choose the proper geometry, electronic properties and volume of the guest in agreement also with the general observation made for several liquids that feature packing coefficients in the range 45–55% [26].

2.3.1

Calix[4]arene Urea Dimeric Capsules

Calix[4]arene provides a suitable semi-rigid concave scaffold for the construction of dimeric capsules. Both the upper and lower rim can be decorated with a wide variety of functional groups, in particular the urea moiety is known to provide a good combination of hydrogen bond donor and acceptor character implemented in the same functional group and this sequence of atoms have been extensively employed in the constructions of calix[4]arene dimeric molecular capsules (Fig. 9). Characteristic of these dimers is the presence of a cyclic seam of hydrogen bonds that seal the capsule and provides an internal molecular cavity that easily accommodates molecules as big as benzene.

Chiral (due to the presence of stereogenic centers in the R groups) or achiral homodimeric capsules show clockwise or counterclockwise orientation of the hydrogen bond seam but the two different arrangements defines exactly the same molecule (Fig. 9B). On the contrary, the combination of two different urea calix[4]arene results in the formation of the corresponding homo- and heterodimers, with a remarkable shift of the equilibrium towards the latter species. For instance, if an aryl urea is mixed with an equimolar amount of sulfonyl urea calix[4]arene, in virtue of the higher hydrogen bond donor character of the latter and the attractive interactions between aromatics in the side chains, only the heterodimer capsules are observed. This time the capsule assumes a C_4 symmetry with the presence of distinct northern and southern hemispheres. In this capsule the head-to-tail hydrogen bond network defines two enantiomeric structures, more precisely; cyclo-enantiomers, which racemize via inversion of hydrogen bond orientation (Fig. 9C) [27]. The kinetic stability of these assem-

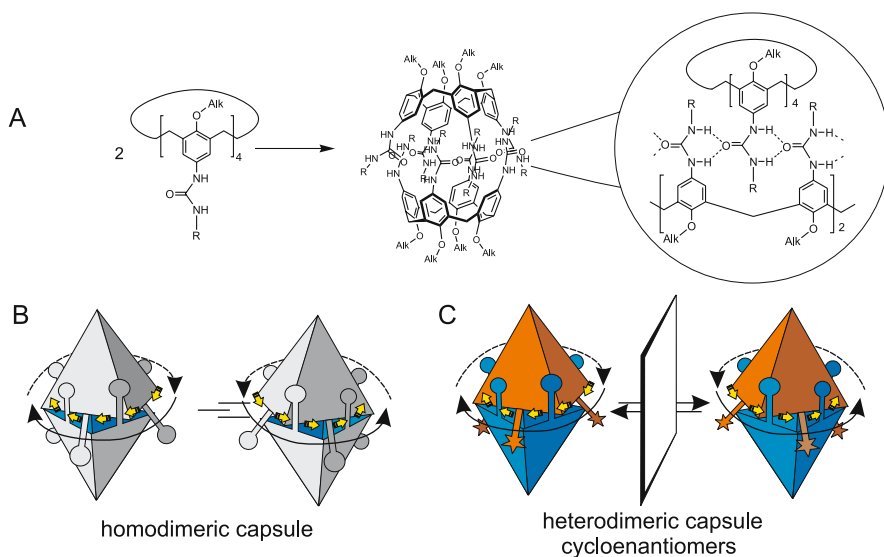


Fig. 9 **A** Calix[4]arene tetraurea dimeric capsules with a particular head-to-tail hydrogen bond network. **B** Achiral tetraurea units form achiral homodimeric capsules, while **C** two different achiral units forms chiral heterodimeric capsules

blies is a function of the guest's size and PC, and increases drastically increasing the steric hindrance around the urea groups [28, 29].

The easiest approach to the construction of chiral tetraurea calix[4]arene capsules is based on the covalent attachment of chiral residues (Fig. 10). The reaction of tetraamino calix[4]arene with isocyanates of aminoacid methyl esters or enantiopure α -methylbenzylamine provided easy access to chiral urea calix[4]arene, which has been thoroughly investigated by Rebek and collaborators in the formation of homo- and heterochiral capsular dimers [48]. Optically active tetraurea species **3–10** were singularly investigated in common non-polar solvents, but only the β -branched L-isoleucine **7** and L-valine **8** provided sharp spectra in agreement with a C_4 symmetric homodimeric capsule, with two distinct sets of signals, one for each half of the capsule. Unfortunately, no evidence of selective binding of chiral guests was observed. It is noteworthy that L-leucine calix[4]urea **9** with an amide functionality compared to **6** did not show homo- or heterodimerization because of the presence of extra hydrogen bonding species which tend to be intramolecular rather than intermolecular. If the amide bond links a second aminoacid with the opposite relative configuration like in **10**, homodimerization is again observed, because amide NH groups provide extra binding between lateral chains as an indication of the fine tuning of geometry and functional groups that is required for the construction of such kinds of chiral capsules [30].

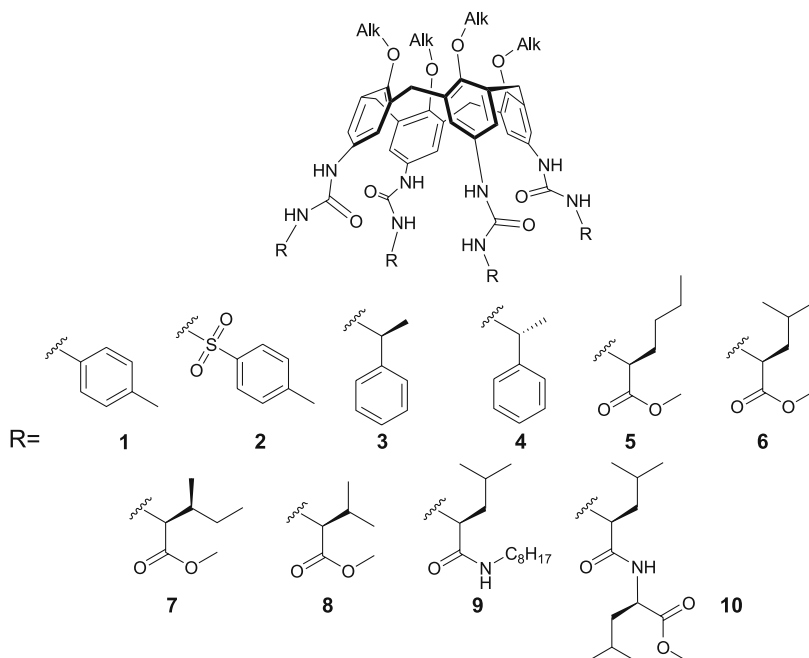


Fig. 10 Chiral Calix[4]arene tetraurea unit bearing stereogenic centers on the urea residues

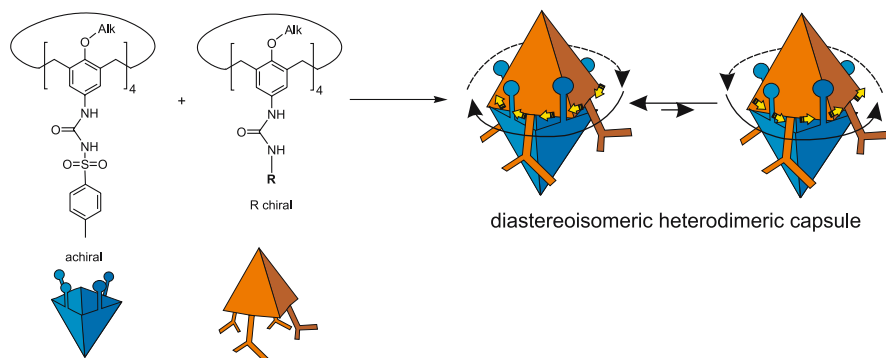


Fig. 11 Heterodimeric diastereoisomeric capsules arising from dimerization of achiral sulfonyl tetraurea and chiral tetraurea calix[4]arenes

Equimolar amounts of achiral urea **1** and the optically active calix[4]urea **5** give rise to the formation of a heterodimeric capsule with only one cyclic arrangement of the urea hydrogen bonds (Fig. 11), and in the presence of a chiral racemic substrate like norcamphor two diastereoisomeric complexes were present in a 1.3 to 1 ratio.

2.3.2

Peptido Calix[4]arene Capsules

Because of their efficiency in natural systems in giving supramolecular aggregates, aminoacids have been implemented extensively in calix[4]arene scaffolds. Di- and tetrasubstitution with aminoacid derivatives have been investigated observing different behaviors depending on the orientation of the chiral residues attached to the calix[4]arene scaffold. Derivatives compris-

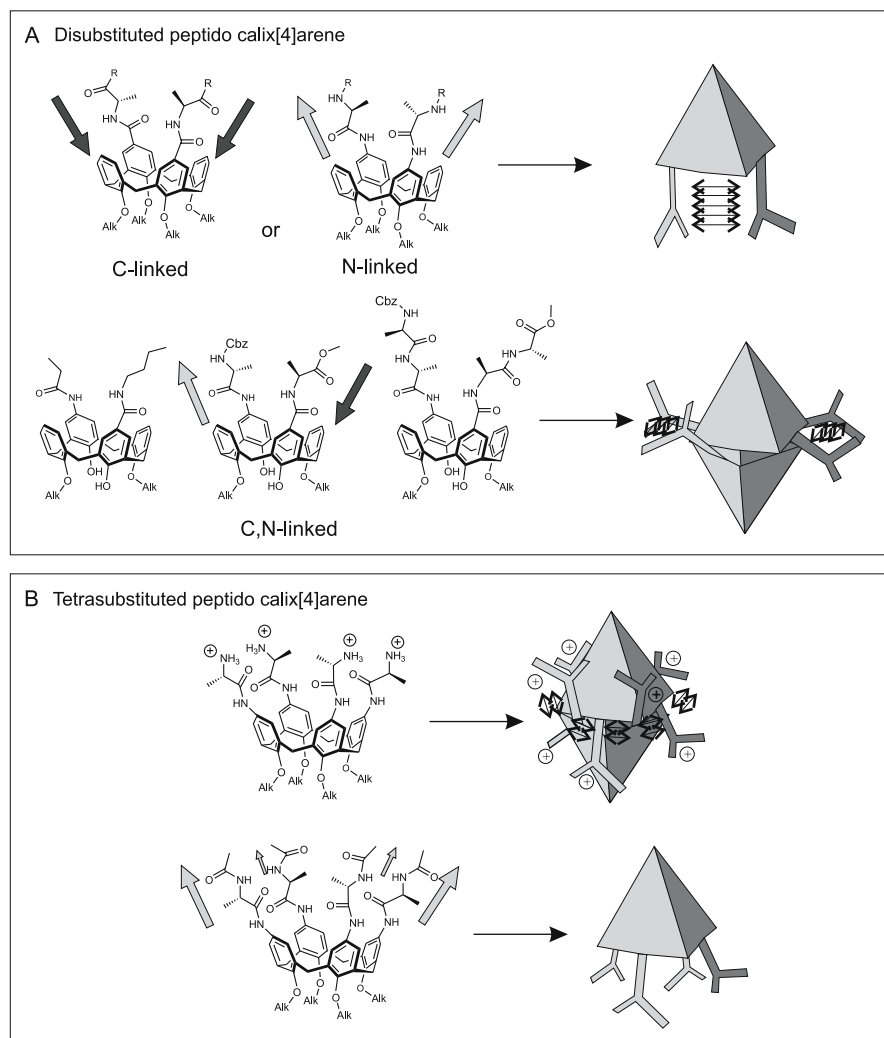


Fig. 12 Tendency to self-assembly formation of homodimeric chiral assemblies for disubstituted and tetrasubstituted peptido calix[4]arenes

ing two *C*-linked or *N*-linked aminoacids or peptides bound parallel on two facing aromatic rings of a calix[4]arene showed no dimeric capsule formation mainly because of the preference for the formation of intramolecular hydrogen bonds rather than intermolecular interaction (Fig. 12) [31]. On the contrary, if the aminoacids are connected one via the carboxylic group and one via the amino group (*N,C*-linked) on the calix[4]arene scaffold, dimerization occurs as observed by strongly concentration-dependent ^1H -NMR spectra [32]. The opposite directionality of the peptides is therefore crucial because it favors the dimerization of the *N,C*-linked peptido-calix[4]arene as depicted in Fig. 12 forming an antiparallel β -sheet hydrogen bond network that seals the capsule. Dimerization constants in apolar solvents depends on the number of hydrogen bonds and are of the order of $70\text{--}700\text{ M}^{-1}$; the assembly resides in the fast exchange compared to the NMR timescale. Unfortunately, no guest encapsulations except for the solvent have been investigated with this kind of chiral enantiopure molecular capsule, but they seem to be highly promising due to the easy substitution with different aminoacids, and the possible further elongation of the β -sheet motif that would increase the strength of the dimer.

Functionalization with L-alanine residues on each aromatic ring in the *N*-linked form with free amino groups provided a system which assembled in $\text{CD}_3\text{OD}/\text{D}_2\text{O}$ with association constants as high as $3 \cdot 10^4\text{ M}^{-1}$ [33]. The high association constant was ascribed to strong hydrogen bonds between charged $-\text{NH}_3^+$ residues and carbonyl as acceptors. The chiral enantiopure capsule showed affinity towards positively charged guests such as arginine or lysine, but the stoichiometry of the resulting structure turned out to be 1 : 1 between guest and calix[4]arene, ruling out capsule binding of the guest. Once again, little variations on the chemical structure, like acetylation of the free amino groups, changed the behavior and dimerization was not observed [31] (Fig. 12B).

2.3.3

Ion Pairing Dimeric Capsules

Ionic interactions between positively and negatively charged residues have been less thoroughly investigated compared to hydrogen bonds, and have rarely been implemented into supramolecular assemblies. In fact, due to solubility concerns, the construction of supramolecular aggregates held together by ionic couples is a more challenging task because often charge pairing could cause a net decrease of solubility of the aggregate resulting in precipitation. Reinhoudt and collaborators succeeded in adorning calix[4]arene scaffolds with *N*-coupled L-alanine carboxylate anionic groups or amidinium cationic moieties on the wider rim, thus providing two hemispherical units that in buffered water solution dimerized by means of four electrostatic ion-pair interactions (Fig. 13).

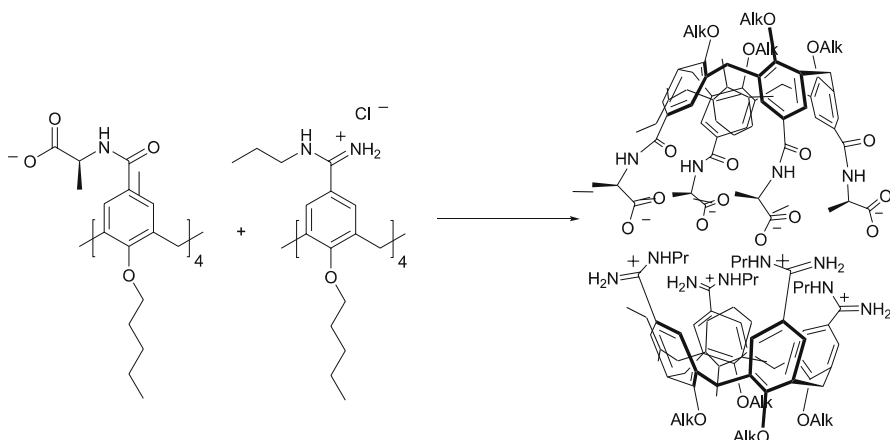


Fig. 13 Chiral heterodimeric capsule held together by means of ionic interactions

Dimerization was proved via NMR analysis that showed an upfield shift for the protons of the propyl amidinium chains compared to the simple tetracationic scaffold in solution, as an indication of dimer formation via inclusion of the alkyl chain inside the cavity [34]. The assembly was fast on the NMR chemical shift timescale, indicating a rather low activation energy barrier for capsule dissociation and reassembly. A wider range of possible guests was investigated [35], discovering some neutral ones characterized by high binding affinity. The presence of the L-alanine residues imparts chirality to the capsular assembly but thus far examples of enantioselective binding have not been observed, even though the ionic interactions that held together the capsule provide an association constant as high as 10^5 M^{-1} in pure water.

2.3.4

Tetrameric Capsule

A molecular capsule can be composed of more than two units; also a sphere can be obtained assembling together a generic number n of slices. Rebek and collaborators, in their extensive exploration of the properties and features of self-assembled capsules [36], developed a L-shaped molecule characterized by the presence at one end of the glycoluril hydrogen bond system, and at the other end, separated by an aromatic ring, a sulfamide moiety (Fig. 14).

This unit, decorated with an extra hydroxyl group in the aromatic spacer, is chiral and single enantiomer isolation was possible by means of chiral chromatography. In the presence of suitable guests, four enantiopure monomers self-assemble into a head-to-tail arrangement with eight hydrogen bonds between alternating glycoluril and sulfamide residues yielding a chiral tetrameric capsule with D_2 symmetry and an internal volume of

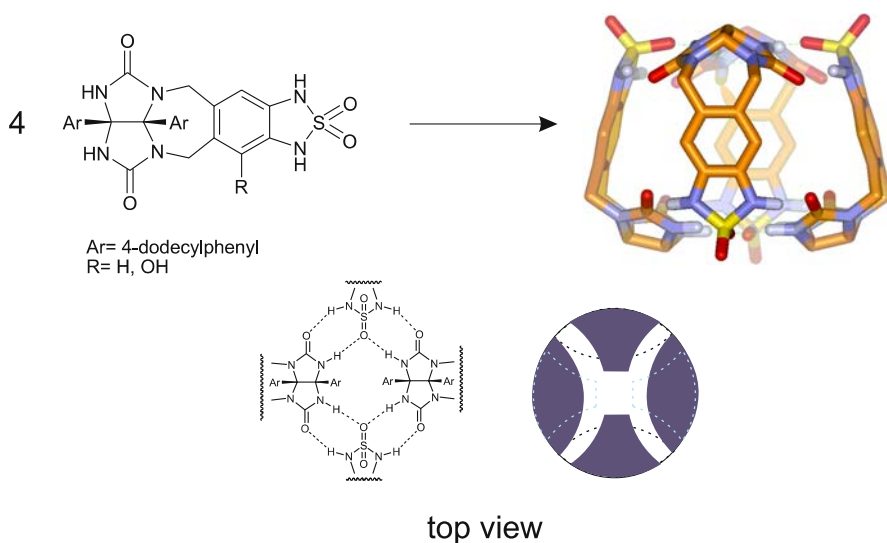


Fig. 14 Tetrameric capsule made of L-shaped components held together by 16 hydrogen bonds. Aryl and OH groups have been removed for clarity

Table 1 Diastereoselective excess in the binding of chiral racemic ketone guests by chiral enantiopure tetrameric capsule

Racemic guest	d.e. %	Volume (\AA^3)	Racemic guest	d.e. %	Volume (\AA^3)
	60	113		0	104
	13	98		23	111
	23	120		9	126

about 170 \AA^3 [37]. The presence of the phenol groups not only desymmetrizes the cavity, but also strengthens the assembly providing an additional hydrogen bond for the adjacent glycoluril carbonyls. This chiral capsule, analogously to the achiral counterpart, showed a remarkable preference for binding ketones. A variety of chiral ketones were investigated as guests for

this capsule in *m*- and *p*-xylene- d_{10} and in Table 1 a few examples are reported. Racemic (\pm)-3-methyl-cyclopentanone showed doubling of the NH resonances of the host due to the formation of the diastereoisomeric complexes in a 1.3 to 1 ratio. Analogously (\pm)-3-methyl-cyclohexanone was encapsulated in the cavity but with a 4 : 1 diastereoselective ratio, which was the result of a bigger size and a better fitting with the cavity. On the contrary a constitutional isomer of the latter guest like (\pm)-norcamphor is not discriminated at all. The presence of an extra carbonyl group in [2.2.1]-bicycloheptane-2,5-dione enhanced selectivity towards the enantiomers, with a 23% d.e. due to a more tight dual binding by hydrogen bonds with the polar extremities of the cavity, allowing a better sensing of the chirality of the capsule that is confined in the equatorial belt. From these data, no direct relationship was observed between guest size and enantio-discrimination, rather the positioning of the functional groups in the cavity was fundamental: this is evident considering the molecules examined which are sparsely functionalized. These results attest to the importance of close contact between the chiral counterparts, even if the assembly is composed of several chiral subunits.

2.3.5

Cylindrical Dimeric Capsule

Chirality is a pervasive property of an object, which means that in theory, a single remote asymmetric center in a macromolecule is enough to make the entire molecule chiral and, in principle, even the more distant residue could sense the asymmetry induced by the stereogenic center. On the contrary, experiences matured by synthetic chemists in the construction of molecular species for enantioselective recognition speak for the necessity of placing the asymmetric units in close contact to allow chiral sensing and discrimination. The latter, in fact, arises from attractive forces and steric interactions that require close contact between the counterparts. On the contrary, magnetic asymmetry is not a direct consequence of weak interactions, but is more a property of the space which surrounds a chiral object.

The cylindrical capsule depicted in Fig. 15 can be prepared with achiral or chiral pendants that reside external to the cavity. It resembles a tennis ball can and its elongated inner space allows up to three guests and impedes them slipping past each other. Therefore, an encapsulated guest is confined in a precise portion of the cavity for an average time that is a function of the strength of the assembly and that can allow ^1H -NMR observation of the phenomena involved due to the slow in-out exchange of guests from the capsule.

Coencapsulation of enantiomerically pure (*R*)-styrene oxide with a co-guest such as isopropyl chloride in the achiral capsule **11·11** showed doubling of the methyl resonances of the methyl groups of the halogenated guest,

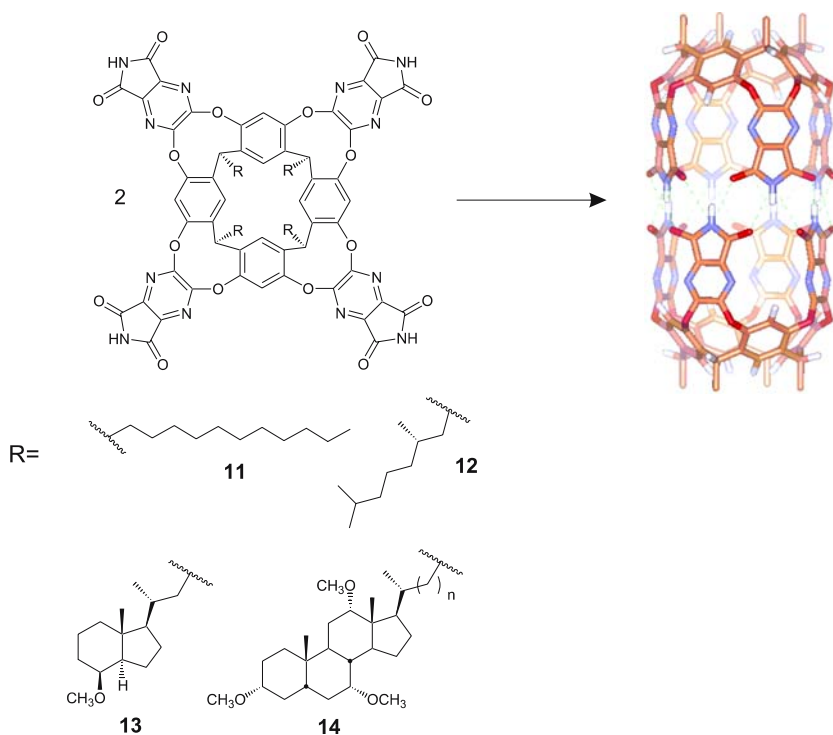


Fig. 15 Homodimeric cylindrical capsule held together by means of a seam of 16 hydrogen bonds. R groups have been removed for clarity

which are no longer magnetically equivalent [38]. Much more unexpected was the analogous observation made using the chiral capsules like 12·12, 13·13 and 14·14, where the chirality is placed outside the capsule. In this case, a single guest bearing an isopropyl ester moiety showed at the ^1H -NMR two doublets for the methyl groups, even though these are physically shielded by the capsule from the chiral steroidal pendants placed outside the cavity [39]. Moreover, the magnetic asymmetry experienced by the isopropyl group was related to the length of the spacer between the CH of the resorcin[4]arene scaffold and the steroidal parts, with a decreasing splitting in the resonances with an increase in length of the spacer.

Different asymmetric residues with a different number of stereocenters attached with the same spacer to the resorcin[4]arene part showed an important influence on the encapsulated guest, even though the overall number of stereocenters changes drastically from 88 for 14·14 to only 8 for 12·12. These complementary experiments are undoubtedly proof of principle that magnetic desymmetrization of closed space can be performed by placing a chiral object outside the immediate environment.

2.4

G-Quadruplex Assemblies

The hydrogen bond complementarity between purine and pyrimidine nucleobases is an example of the high level of recognition typical of most of the natural functional units. Nucleosides containing guanosine are known to arrange in tetramers via hydrogen bond self-assembly and to bind alkaline cations to provide G-quartets that stack to give G_8-M^+ sandwiches or higher-ordered G-quadruplets [40]. It is remarkable that in this kind of aggregate, enantiomeric self-recognition is present and it is dependent on the nature of the templating cation (Fig. 16A). In fact, racemic (D,L)-5'-silyl-2',3'-O-isopropylidene guanosine (G1) in the presence of Ba^{2+} picrate ($r = 1.42 \text{ \AA}$) formed only homochiral aggregates in organic chlorinated solvent. Eight guanosine with the same relative configuration created two G-quartets with a Ba^{2+} in between, while on switching to the monovalent K^+ ($r = 1.51 \text{ \AA}$) only heterochiral aggregates were observed, where diastereoisomeric quartets were present in the form of layers with interposed potassium cations (Fig. 16B) [41]. The structure self-assembled through hydrogen bonding while the cations triggered the stereoselective recognition. A pivotal role was played also by the picrate anion that provided hydrogen bond contacts between two $(G1)_8Ba^{2+}$ into a hexadecameric homochiral structure.

NMR experiments on freshly mixed $[(L)-G1]_{16}M_m^{n+}$ and $[(D)-G1]_{16}M_m^{n+}$ showed re-equilibration of the monomers for K^+ with new emerging NH resonances, while for Ba^{2+} no appearance of new signals was observed, as a clear indication of self-enantio-recognition. The latter divalent cation provides stronger cation-dipole interactions and strengthens hydrogen bonds, while the bridging picrate favors enantio-recognition between two G_8-Ba^{2+} octamers. With the isomeric nucleobases isoguanosine, a racemic mixture of D,L forms gave rise to the formation of homochiral pentamers that stack forming a *meso* decamer in the presence of Cs^+ cations. Once again, hydrogen bond complementarity assembles the structure and the metal ion directs the enantio-recognition [42].

2.5

Other Dimeric Assemblies

By means of proper tailoring of the shape and chirality of the monomer it is possible to prepare instructed chiral molecules capable of enantiomeric self-sorting. Two prerequisites are necessary: the proper functional groups must be chosen to act as recognition elements and the latter have to be mounted on an adequate molecular scaffold to promote formation of the desired assembly. One clear example is illustrated in Fig. 17A: achiral racemic clip molecules formed kinetically and thermodynamically stable homodimers in $CDCl_3$ with complete diastereoselectivity [43].

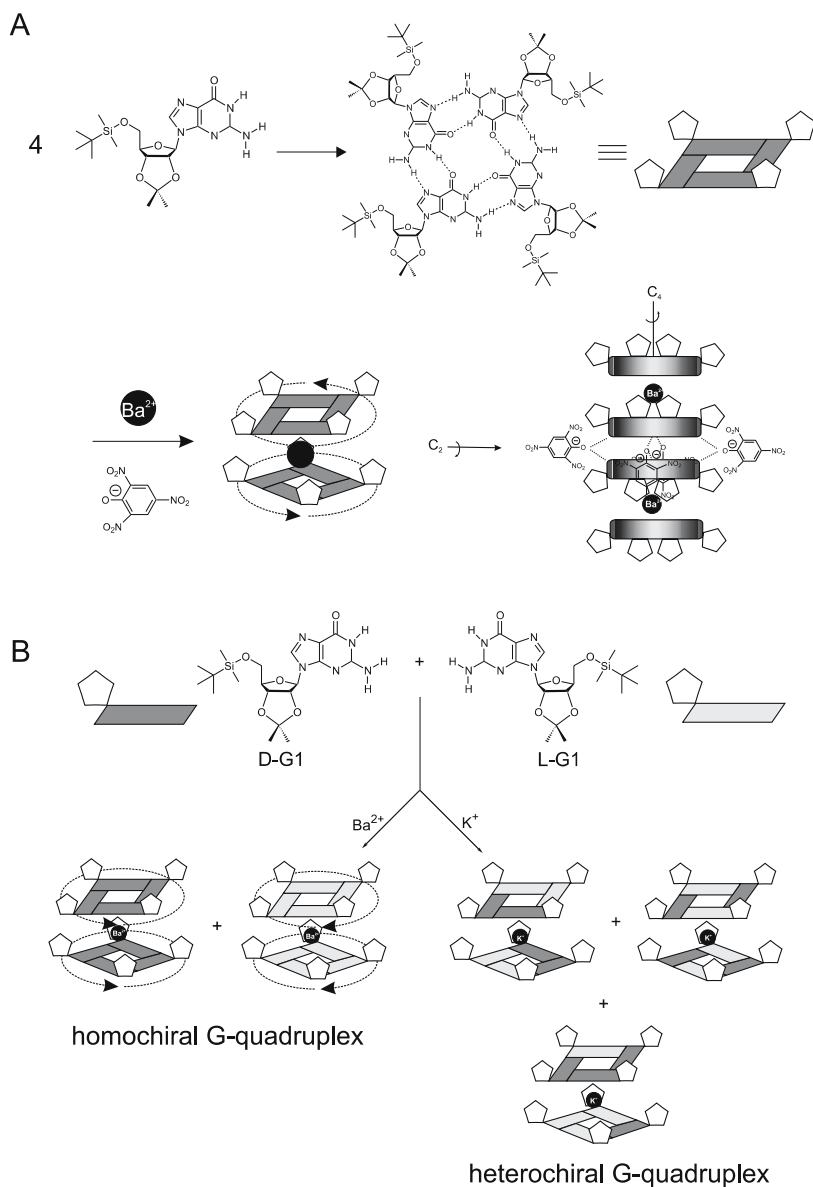


Fig. 16 **A** Self assembling of G-quadruplex chiral aggregates and their stacking by interposition of cations. **B** Stereospecific binding of Ba^{2+} cations to give homochiral G-quadruplex, while K^+ leads to heterochiral aggregates

In particular racemic **16** forms only heterochiral aggregates because this combination benefits from two hydrogen bonds from the amide groups and $\pi - \pi$ stacking, while in the homochiral complex one hydrogen bond is missing.

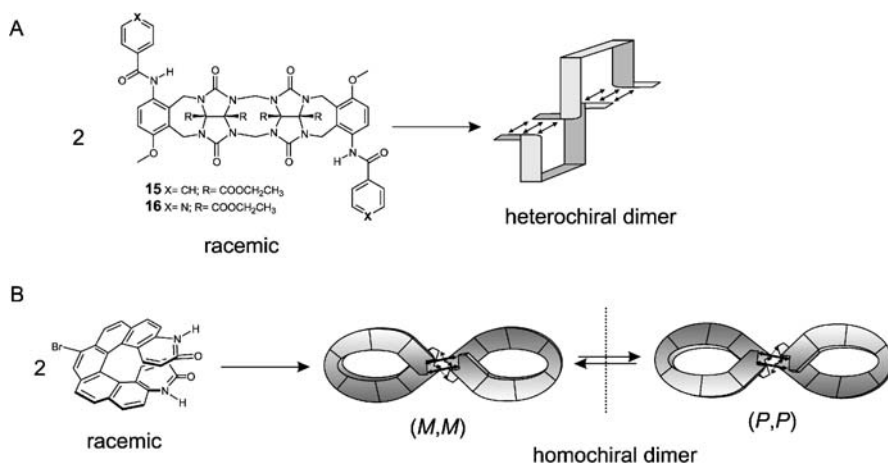


Fig. 17 Examples of intrinsically chiral molecules that associate into dimeric structures: **A** clip racemic molecule provides only heterochiral dimers, while **B** helicene-based molecules give only homochiral dimers

As observed for the molecular clips reported above, the chiral scaffold is pivotal in promoting homo- or heterochiral self-discrimination. Amide hydrogen bonds were implemented on helicene chiral scaffolds as well, but in this case dimerization of the monomers was characterized by homochiral enantioselective self-recognition, that is self-association between molecules with the same helicity (Fig. 17B) [44]. These species dimerized in solution with association constants of 207 M^{-1} by means of four non-covalent bonding interactions and, in combination with the peculiar helical shape of the monomers, forms only homochiral dimers.

Guanidinium cations are easily prepared functional groups characterized by both hydrogen bonding and an ionic interaction ability. Such kinds of derivatives have been implemented onto semirigid scaffolds like those reported in Fig. 18. The first is an elegant example of a chiral dimeric complex that was investigated by the group of de Mendoza. They prepared enantiopure bis-guanidinium and tetra-guanidinium cationic molecules bearing asymmetric centers in the bicyclic rings endowed with a CH_2SCH_2 spacer. These molecules have the peculiar property of folding in pairs around sulfate counter-anions into helical—well defined in length—structures resembling the double helix of DNA (Fig. 18A) [45].

(S,S) relative configuration on the guanidinium moieties induced complete (*M*) helicity in the complex as confirmed by 2D-NMR, because of the strong salt-bridged and $\text{N}-\text{H}\cdots\text{O}$ hydrogen bond pairs, which are responsible for the chiral supramolecular structure. Significantly weak CD traces for complexes comprising chloride as the anion were observed, as well as a lack of intermolecular NOE contacts as an indication of the importance

A



B

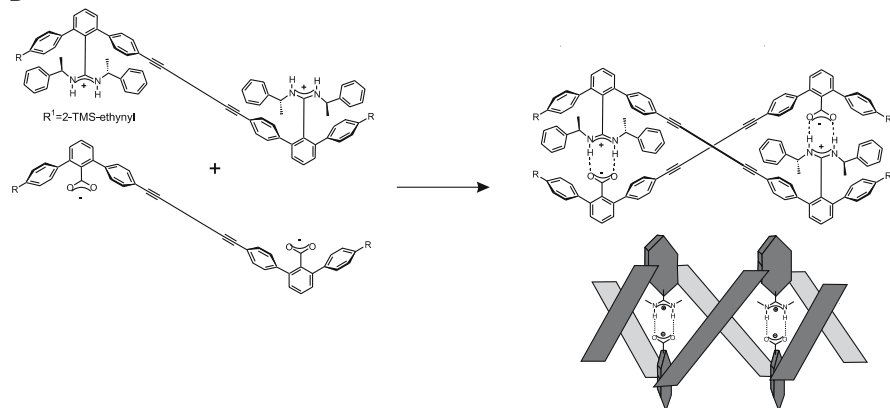


Fig. 18 Supramolecular chiral aggregates based on bis-guanidinium functional groups: **A** chiral tetra-guanidinium units self-assemble around sulfate anions into a left-handed double helical structure; **B** chiral bis-guanidinium unit associates with a complementary bis-anionic counterpart leading to a left-handed double helix

of H-bonds provided by the sulfate anion, which are not present with the chloride anion.

A second more recent example is depicted in Fig. 18B where a bis-guanidinium molecule bears chiral functional groups attached to the nitrogen atom of the amidinium residues. This species is coupled with a complementary dicarboxylic anionic counterpart with all the benzene rings twisted clockwise into a right-handed double helical structure that resembles the DNA double helix [46]. The chiral supramolecular structure was observed both in the solid state and in chloroform- d_1 solution as confirmed by NMR investigation and by the presence of a strong Cotton effect on the CD signals for the diacetylenic linkages.

3

Chiral Assemblies Comprising Achiral Building Blocks

This section collects examples based on the employment of achiral self-assembling components which aggregates to produce chiral supramolecular structures [47]. This strategy is much less costly in terms of time required for

the synthesis and purification of the enantiopure components, but allows the obtainment of only racemic chiral aggregates.

3.1

Racemic Capsules

3.1.1

Calix[4]arene Capsules

As mentioned before [27], equimolar amounts of the achiral calix[4]urea **1** and **2** (Fig. 10) provided only one set of signals as a clear cut indication of complete formation of the heterodimeric capsule that is chiral and racemic due to the clockwise or counterclockwise arrangement of the hydrogen bond network. Encapsulation of chiral enantiopure guests was investigated in these chiral racemic assemblies. Bicyclic (1*R*)-(-)-myrtenal clearly showed two sets of signals for the encapsulated guest due to the chirality imparted by the seam of hydrogen bonds that seals the capsule, while a racemic guest like norcamphor provided two sets of signals in a 1.3 to 1 ratio as an indication of a little stereorecognition in binding [27, 48].

The geometry of achiral dimeric calix[4]arene endowed with urea functionalities offers further possibilities to obtain homodimeric chiral capsules. In fact, simply employing two different substituents A and B on the urea or on the ether part of the calix[4]arene aromatic rings and considering all the possible combinations depicted in Fig. 19, it was possible to obtain up

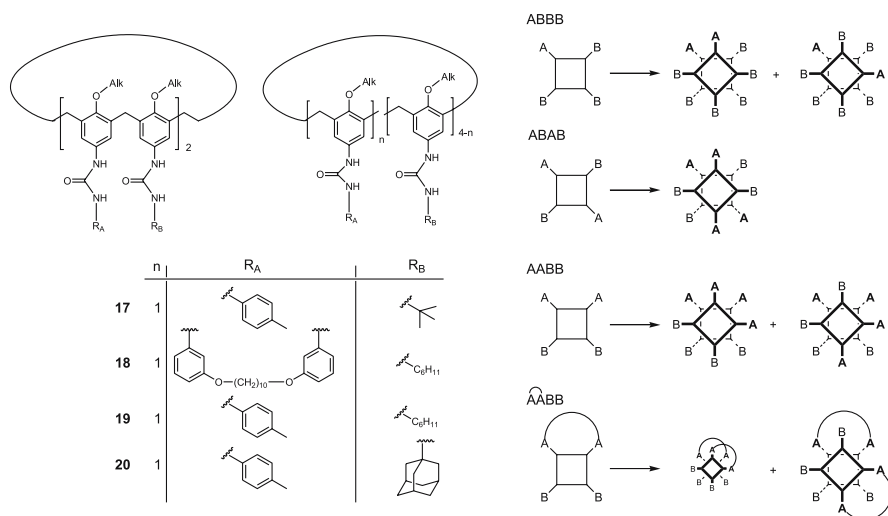


Fig. 19 Achiral calix[4]arenes with different substituents on the urea residues lead to diastereoisomeric chiral dimeric capsules

to five different chiral capsules, in some cases with a certain degree of diastereoselection [49]. For all these systems, the capsule is chiral and inversion of the directionality of the hydrogen bond seam does not create additional stereoisomers but simply maintains unchanged the structure.

For the AB₃B monomer, two diastereoisomeric chiral capsules were possible, with a diastereoisomeric ratio that varies from 6 : 1 in cyclohexane-*d*₁₂ to 1 : 1 in chloroform-*d*, with a strong solvent effect: the latter was also the guest and therefore influenced the stability of the capsules both from the inside and outside of the capsule. The ABAB monomer gave rise to only one chiral racemic capsule, while for AAB₂B two regioisomeric structures were possible, with a relative amount from 1 : 1 to 2 : 1 increasing the steric difference between A and B from *n*-hexyl to adamantyl residues. Moreover, the equilibrium between the regioisomeric forms could be shifted entirely on one side if two adjacent A and two B groups are covalently connected.

All these capsules are in principle stable enough for optical resolution by means of chromatographic methods, even though this has not been accomplished yet. In these systems, the weak asymmetry imparted on the cavity is not sufficient to allow chiral discrimination of chiral enantiopure guests.

3.1.2

Tennis Ball Capsule

Another remarkable example of chiral assemblies made of achiral components is provided by concave-shaped molecules which self-assemble into supramolecular capsules. These species are usually quite rigid, based on aromatic and cyclic structures and are specifically decorated on the extremities with complementary hydrogen bond donors and acceptors. For a capsule made of two identical achiral components, if the concave monomer has different extremities, the capsule obtained by homodimerization is chiral. The smaller chiral supramolecular capsule is derived from the so-called tennis ball [50] (Fig. 20). The monomeric unit based on the durene scaffold comprises two different glycoluril units at the extremities that provides eight hydrogen bonds to seal the capsule and form a cavity of approximately 60 Å³ that can accommodate gaseous guests like methane and ethane. Upon dimerization of the monomer four well-separated N–H signals were observed in the downfield region of the ¹H-NMR spectrum due to the chirality of the assembly, even though it is composed of achiral monomers. Racemization takes place by dissociation and re-assembly of the dimer and the activation energy for this process has been calculated to be ~ 73 KJ/mol at 295 K from EXSY experiments. Because of the small space inside the capsule, no encapsulation of chiral guests could be investigated.

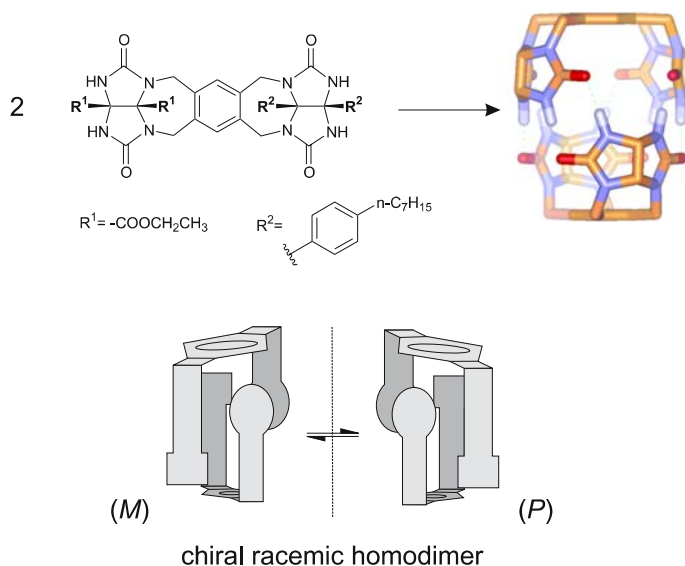


Fig. 20 Chiral homodimeric tennis ball capsule from an achiral component bearing two different glycoluril residues. The R^1 and R^2 groups have been removed for clarity

3.1.3

Softball Capsule

More insight into this class of systems came from the extensive investigation of the so-called chiral “softball” molecular capsules based on a rigid polycyclic scaffold with two different glycoluril moieties at the extremities. When two such achiral subunits associate, the chiral capsule obtained, maintains a C_2 symmetry axis but no longer has the planes of symmetry featured by the monomer (Fig. 21) [51]. Monomers assemble because of the proper filling of the inner cavity, and if the encapsulated guests were achiral no splitting was observed at the NMR for the NH signals of the capsule. If the trapped guest is chiral, like for (*R*)-(+)-camphor, two diastereoisomers are present and showed separate signals of the guest in the two diastereoisomeric complexes. No diastereoselectivity was observed because of the symmetry of the cavity.

This serves as proof of concept to underline how asymmetry can be easily sensed at a magnetic level more easily than at a binding level. To provide selectivity in the binding due to stereorecognition, closer interactions and tighter binding are pivotal requisites. Moreover, the asymmetry of the surfaces has to extend into the cavity, rather than be limited to the exterior. A step forward is presented by the evolution of the chiral softball in Fig. 22. In this case the monomer maintains the same glycoluril functional group at

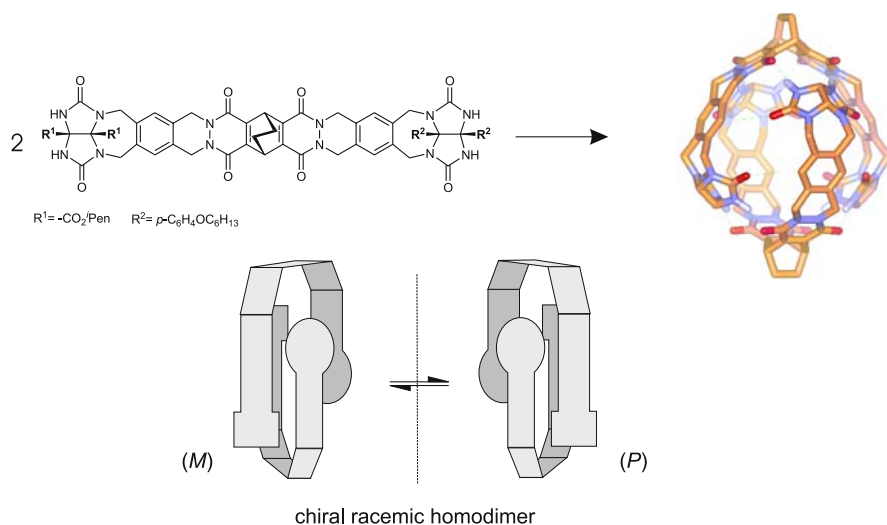


Fig. 21 Chiral homodimeric softball capsule from an achiral component bearing two different glycoluril residues. The R^1 and R^2 groups have been removed for clarity

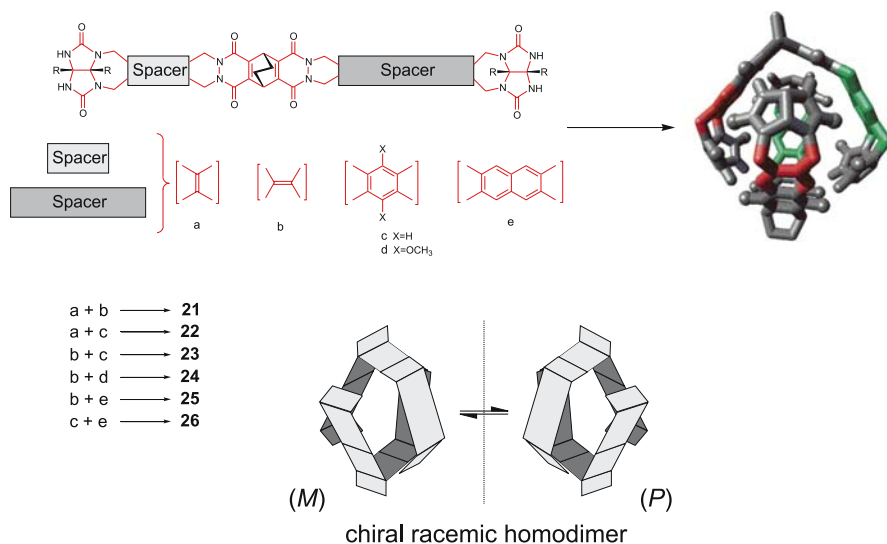


Fig. 22 Second generation of chiral dissymmetric softball capsules with the same glycoluril residues at the two extremities of the monomer but with different spacers. The R groups have been removed for clarity

the extremities but is characterized by different lengths of the two spacer residues. The monomer is still achiral due to the presence of a plane of symmetry, but leads to a chiral dimeric capsule characterized by a dissymmetric inner space [52].

Differently from the previous chiral softball, in this case the dissymmetric inner surface of the cavity easily sensed chiral guests, providing different diastereoisomeric complexes in different amounts. Each diastereoisomer is characterized by four different NH resonances because of the complete loss of symmetry of the complex. The system described was extensively investigated pursuing the synthesis of a total of six different glycoluril monomers (21–26) with various spacers in terms of size and electronic properties on the two sides of the bicyclic six-membered unit, and the relative homodimeric capsules were studied with a total of 20 chiral enantiopure guests (Fig. 23 and Table 2) [53].

The cavity volume varies from 190 to 390 Å³ and the average size of the guest is in the range 160–225 Å³ for camphor derivatives and 145–175 Å³ for pinane derivatives. Therefore, the proper matching of host and guest was crucial to obtain complexes characterized by the proper fitting and packing

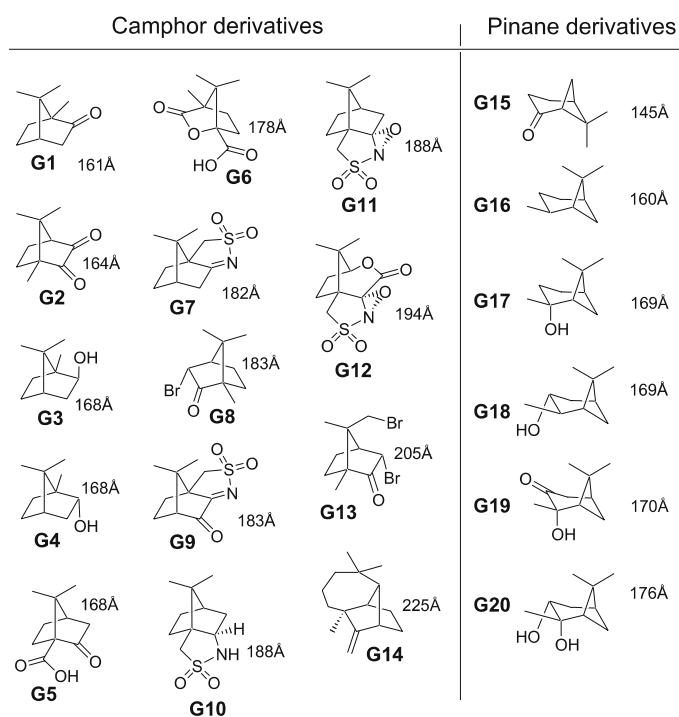


Fig. 23 Chiral enantiopure guests studied in the encapsulation in the chiral racemic softball and their relative molecular volume

Table 2 Diastereoisomeric excesses for chiral racemic softballs as a function of different chiral enantiopure guests

Guest	PC	d.e. %	Guest	PC	d.e. %
G@22·22					
G1	0.70	17	G16	0.69	16
G2	0.71	12	G17	0.73	20
G3	0.73	8	G18	0.73	10
G4	0.73	8	G19	0.74	29
G5	0.73	0	G20	0.76	35
G15	0.63	0			
G@23·23					
G1	0.67	12	G19	0.71	19
G2	0.68	6	G20	0.73	32
G15	0.60	0			
G@25·25					
G1	0.54	—	G12	0.65	44
G7	0.61	34	G14	0.75	—
G8	0.61	—	G15	0.48	—
G9	0.61	56	G19	0.57	—
G10	0.63	0	G20	0.59	—
G11	0.63	60			
G@26·26					
G6	0.46	—	G11	0.49	0
G7	0.47	6	G12	0.50	—
G8	0.47	—	G13	0.53	—
G9	0.47	—	G14	0.58	36
G10	0.49	44	G20	0.45	—

coefficient to allow reciprocal sensing and diastereoselectivity, as observed comparing hosts **23·23** with the smaller **22·22**, which provided higher selectivities for pinane guests (Table 2). Considering the most selective combination of host and guest emerged the clear indication that the presence of functional groups capable of hydrogen bonding to the host is important for affinity as well as selectivity, as observed comparing the alcohol (+)-pinanediol (d.e. 32%) with the ketone (+)-nopinone (d.e. 0%).

This effect is added to the steric interactions imparted by the asymmetric shape of the cavities, and to more weak interactions like CH/ π . Nevertheless, in a few cases d.e. was above 50% and never more than 60% probably because the average distance between the capsule and the chiral content is not optimized, bearing in mind also that even in the presence of a good fit and high PC, still about half of the cavity's volume is not filled and this space surrounds the guests and is also interposed between them.

4

Enantioselective Synthesis via the Chiral Memory Effect

This phenomenon consists of the preparation of a highly diastereoselective assembly using a chiral enantiopure unit, then the latter is exchanged with achiral counterparts that are characterized by a higher binding affinity. The result of these operations is an enantioenriched complex comprising only achiral units that is not thermodynamically stable, but if the kinetics of racemization is slow enough, it can persist long enough to ensure full characterization, even though it inexorably undergoes slow racemization by dissociation and reassembly until reaching the racemic mixture.

4.1

Enantiopure Double Rosettes

For hydrogen-bonded supramolecular chiral complexes, the interconversion between the enantiomers often takes place via dissociation and reassembly of one or more units, with an activation energy for racemization that is at least as high as the energy required to break the hydrogen bonds. Few supramolecular structures are so tightly connected to allow a half-life time of several hours for this process; one of these is the hydrogen-bonded double rosette. With this class of supramolecules it is possible to exploit the “chiral memory effect”. Reinhoudt and collaborators succeeded in this task preparing initially

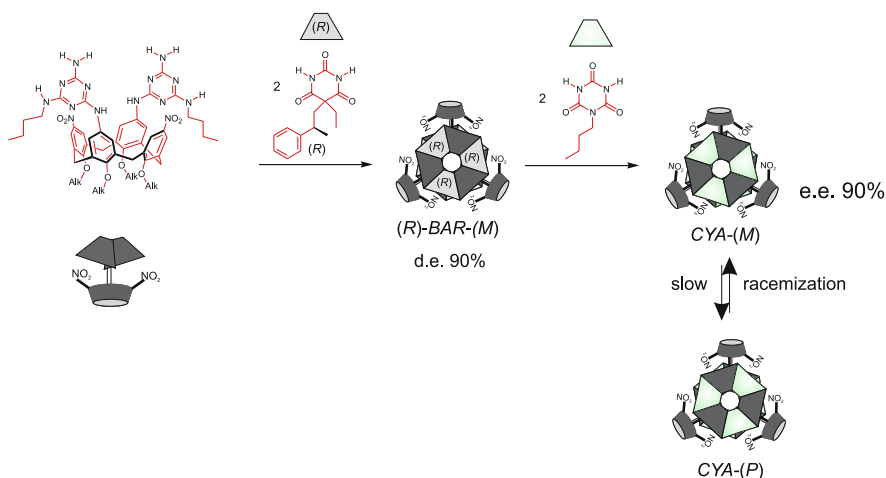


Fig. 24 Enantioselective non covalent synthesis of double rosettes exploiting the chiral memory effect. Exchange of chiral barbiturate with the achiral cyanurate occurs faster than racemization by dissociation of the supramolecular structure and allows temporary preservation of the asymmetry instructed in the first diastereoselective step

a double rosette from achiral calix[4]arene dimelamine and chiral (*R*)-BAR obtaining predominantly the (*M*) isomer in 98% d.e. (Fig. 24). Subsequently, in the presence of a slight excess of achiral cyanurate, which is characterized by a stronger hydrogen bond attitude than barbiturate due to the more acidic NH protons, the original chiral assembly released the (*R*)-BAR without complete dissociation of the structure, yielding a chiral double rosette made of achiral components with 90% e.e.

The chiral enantiopure double rosette therefore preserved the (*M*) chirality as a memory of the native form of the assembly, despite the fact that it no longer contains any chiral components [54, 55]. This complex is CD active with intensity of about $\Delta\epsilon \approx 90 \text{ L}/(\text{mol} \cdot \text{s})$, comparable to other chiral double-rosettes and much higher than the chiral barbiturate released ($< 5 \text{ L}/(\text{mol} \cdot \text{s})$). The kinetic analysis of the racemization reaction at different temperatures gave an activation energy of 106 KJ/mol with a half-life time of 4.5 days at room temperature, confirming the requirement of a high energy barrier to take advantage of such kinds of memory effect.

Exploiting the same concept, Reinhoudt and Shinkai were able to obtain another example of enantioenriched chiral double-rosette made of achiral components. In this case achiral calix[4]arene bearing dimelamine moieties with pyridine functionalities were assembled with achiral cyanurate leading to racemic chiral double rosettes. The latter are perfect counterparts for chiral D-dibenzoyl tartaric acid via two-point hydrogen-bonding interactions thus

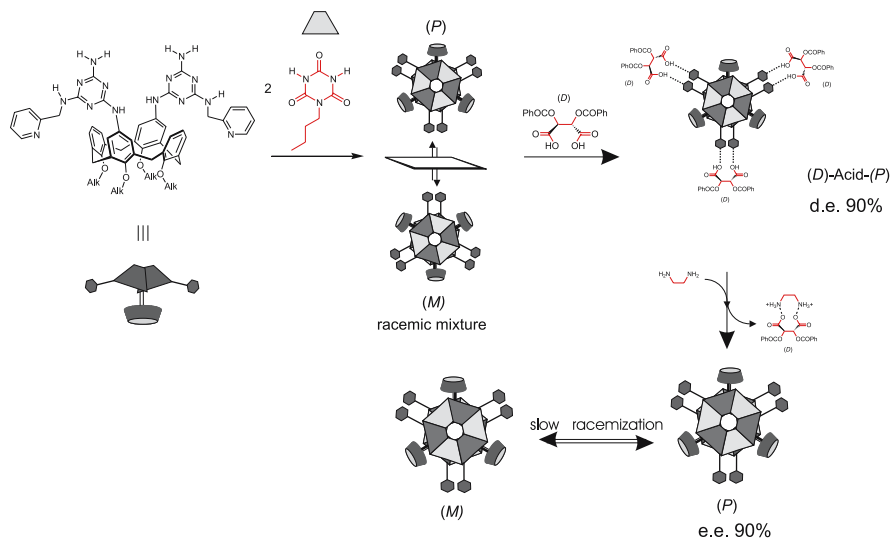


Fig. 25 Enantioselective non covalent synthesis of double rosettes exploiting the chiral memory effect. Pyridyl residues on the dimelamine units bind chiral dicarboxylic acids leading mainly to one diastereoisomer. Once the chiral templating carboxylic acid is removed by precipitation, the enantioenriched double rosette persists for several hours

giving with the pyridyl functionalities predominantly the (*P*) diastereomeric supramolecular complex with 90% d.e. (Fig. 25) [56].

The imbalance between the two diastereoisomers is prolonged when the chiral D-tartrate is removed by precipitation with ethylenediamine thus leading to an enantioenriched chiral double-rosette made of achiral components with 90% e.e. The memory effect in this case is even stronger than in the former example with activation energy towards racemization as high as 119 KJ/mol and a half-life time of one week at room temperature.

4.2

Chiral Enantioenriched Softball

In chiral supramolecular capsules made of achiral building blocks, guest sensing of chirality is a phenomenon that is directly connected to the lifetime of the capsule. If the latter is very high and in-out exchange of the guest is faster and allowed without complete dissociation of the closed structure, which causes racemization, it is possible to observe a chiral memory effect. In particular, it is possible to template the capsule with a chiral enantiopure guest thus favoring one of the two enantiomeric capsular structures, then the guest can be replaced with another one without racemization of the structure. Removal of the chiral template leaves a chiral non-racemic host capsule that slowly re-equilibrates to the thermodynamically most favorable enantiomer. With this purpose Rebek and collaborators endowed the chiral softball with extra phenolic groups to provide four extra hydrogen bonds and to increase the lifetime of the chiral capsule thus obtained (Fig. 26) [57].

In *p*-xylene- d_{10} the monomer assembled only in the presence of a suitable guest like (+)-pinanediol leading to two diastereoisomeric complexes in 2 : 1 ratio the inclusion phenomenon was rather slow to reach equilibrium, requiring several hours to reach completeness (half-life time 19 h). Providing the diastereoisomeric system with an excess of the opposite enantiomer (–)-pinanediol, the relative ratio between the two diastereoisomers was then altered from the equilibrium composition: the replacement of the (+)-enantiomer with the (–)-enantiomer occurs via opening of flaps of the pyridazinyl ring, characterized by a low energy barrier for inversion. In fact, the capsule imprinted with (+)-pinanediol and subsequently exchanged with an achiral guest and again with the enantiomer (–)-pinanediol showed the same d.e. 50% d.e. in favor of the less stable diastereoisomeric complex, which proved that the chiral memory is maintained even in the presence of the wrong enantiomeric guest. Then the system, in few days, slowly equilibrated to a 2 : 1 diastereoisomeric ratio in favor of the (–)-enantiomer complex.

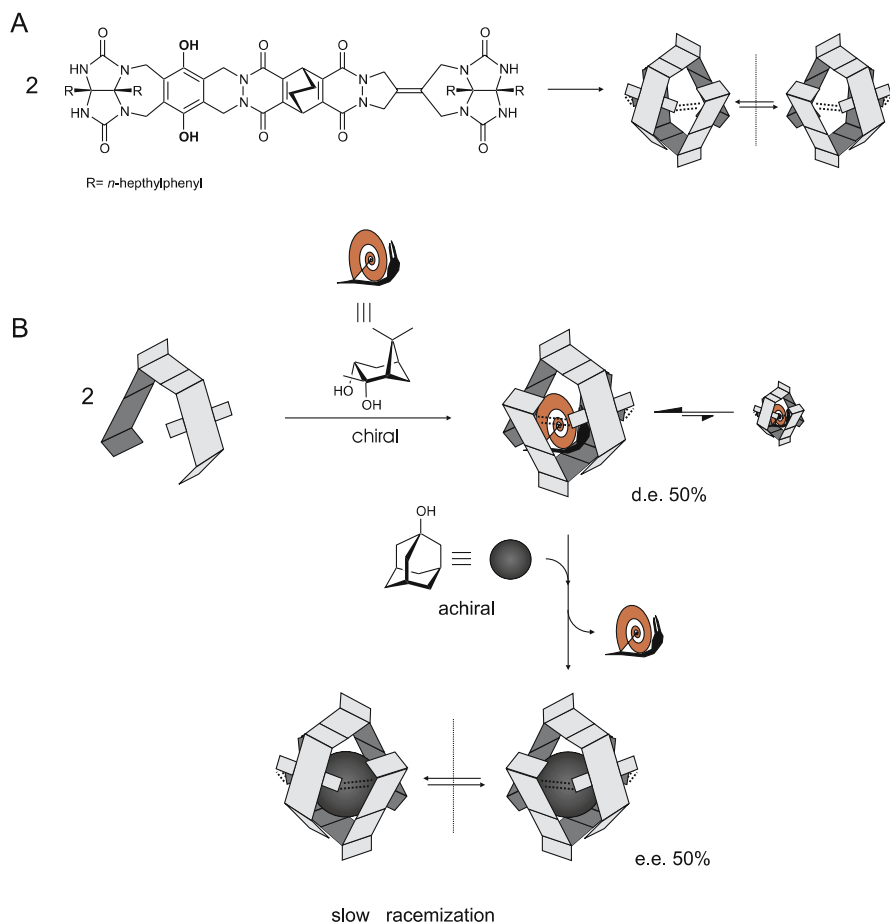


Fig. 26 **A** Chiral memory effect applied to the construction of a chiral softball homodimeric capsule made of achiral units. **B** Racemic softball binds a chiral guest leading preferentially to one diastereoisomer. Fast exchange, compared to capsule's racemization rate, with a better achiral guest allows preparation of enantioenriched capsule

5

Asymmetric Spaces within an Achiral Cylindrical Host

Coencapsulation is a process that limits the space provided to trapped guests and obliges them to sense reciprocally simply because they cannot avoid each other. Chirality is a feature related to the spatial distribution of objects, therefore any symmetric closed space becomes chiral if a chiral object is placed in it (Fig. 27A). This simple concept is then applied to spherical and cylindrical capsules: in both cases the correct orientation of two chiral guests is necessary to allow interactions between the asymmetric centers of the two partners. In

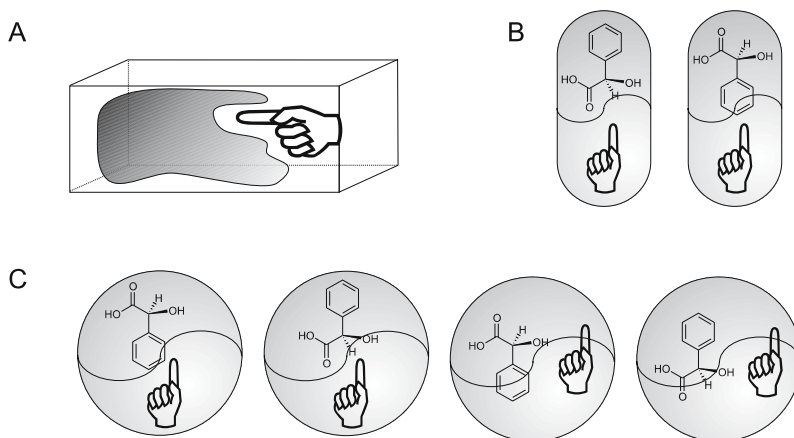


Fig. 27 **A** A chiral object like a hand in an achiral environment leaves a chiral space available. **B** Spherical supramolecular capsules are much less suitable compared to **C** cylindrical ones for enantiorecognition because of the greater number of possible reciprocal orientations of two co-guests encapsulated

a cylindrical space the number of possible reciprocal orientations of the two guests is lower compared to a spherical space because of the constrictions imposed by the geometry of the cavity (Fig. 27B and C). In addition, the polarity of the cavity can favor certain spatial arrangements among all the possible ones. This is the case for the cylindrical achiral capsule depicted in Fig. 15, which is composed of two resorcin[4]arene scaffolds with four pyrazine walls adorned with four imide groups that provide a seam of 16 hydrogen bonds that seal the capsule. All of the following encapsulation studies refer to the use of such kinds of capsule. The elongated shape hampers free tumbling for many guests and allows a better control over their reciprocal position.

5.1

Single Encapsulation

A guest that is achiral in its elongated antiparallel most stable conformation can become chiral if it assumes staggered conformations. Encapsulation in the achiral cylindrical capsule of a single achiral guest can force the latter to assume chiral conformations thus leading to chiral racemic complexes. This is the case observed in the complexation of extended hydrocarbon chains which are longer than the internal cavity of the capsule (Fig. 28). Encapsulation occurred but the hydrocarbon had to assume a helical chiral conformation as demonstrated by the presence of consistent NOE contacts along the hydrocarbon chain [58, 59]. The extra energetic cost due to the presence of several gauche interactions is overcome by a better fitting with the host and the pres-

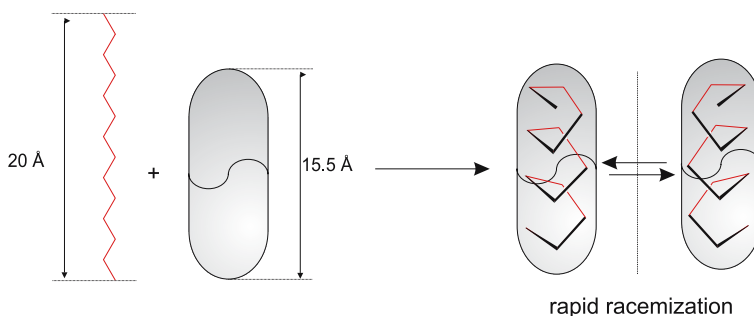


Fig. 28 Hydrocarbon encapsulation in the achiral cylindrical capsule occurs forcing the guest to assume a helical conformation in order to fit the available space

ence of many attractive CH – π interactions. The hydrocarbon helix is chiral and every proton of a methylene group is therefore diastereotopic; however, no geminal coupling was observed suggesting rapid helix–helix interconversion (racemization) on the chemical shift timescale. This phenomenon is likely to occur within the capsule by means of propagation of short-range uncoiling.

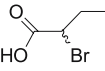
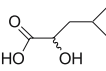
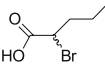
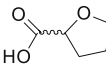
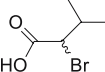
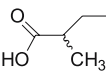
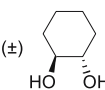
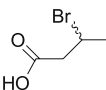
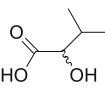
5.2

Double Coencapsulation

The easiest combination of two chiral guests in the cylindrical capsule comes by the double encapsulation of racemic species with adequate size, shape and polarity to be accommodated in pairs, giving two diastereoisomeric complexes, the homochiral couple (*R*) – (*R*)/(*S*) – (*S*) and the heterochiral (*R*) – (*S*) combination. (\pm)-*trans*-1,2-Cyclohexanediol has all the above requisites and showed a ~ 1.2 ratio between the two complexes in favor of the heterochiral combination [60]. This observation may be related to the preference in nature for centrosymmetric crystals or, alternatively stated, the higher melting points of racemates vs. enantiopure compounds where the resolution is driven by the less soluble pair [61, 62]. In the cylindrical capsule a single couple of chiral molecules is extrapolated from the bulk and the interactions between the two is governed by the shape of the cavity and their goodness of fit within the cavity.

The coencapsulation of chiral carboxylic acids was investigated in detail, seeking the weak forces that drive the coencapsulation to be homochiral or heterochiral depending on the nature of the chiral acid and on the relative orientation of the guests within the cylindrical capsule (Table 3) [63]. α -Halo or α -hydroxy acids are all suitable guests that are accommodated in pairs within the cavity, but only a few of them give rise to diastereoselective binding, all with energy differences < 6.3 KJ/mol. In particular, substitution in

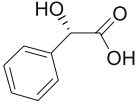
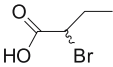
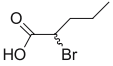
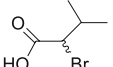
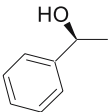
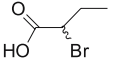
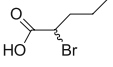
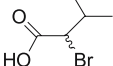
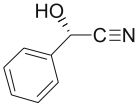
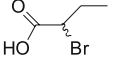
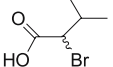
Table 3 Coencapsulation of racemic chiral guests within the achiral cylindrical capsule 11·11

Racemic guest	d.e. %	Preferred dimer	Racemic guest	d.e. %	Preferred dimer
	23	ND		9	homochiral
	13	ND		13	heterochiral
	20	homochiral		13	homochiral
	9	heterochiral		7	ND
	9	heterochiral			

the β position hinders the guests and this leads to a diastereoselective ratio of up to 1.6 : 1 in coencapsulation for bromo and hydroxy acids. In some cases the more stable combination is the heterochiral one like for (\pm)-3-methyl-2-hydroxy-butyric acid, while for (\pm)-3-methyl-2-bromo-butyric acid the homochiral couple is preferred. Computational Monte Carlo conformational search on these diastereoisomeric complexes revealed differences in energy between the complexes that are in agreement with the diastereoselective ratios determined by NMR. From the calculations, in general, a high packing coefficient favors hydrogen bonding between the carboxylic groups and the imide functional groups of the capsule, while a low packing coefficient allows linear carboxylic acid dimer formation. It is worth noting that in the latter orientation, the stereocenters in the α position on the chiral acids are some 7 Å apart, while if they interact by means of a hydrogen bond with the imide protons of the capsule, their stereocenters are on average closer to each other, and their reciprocal sensing gives rise to energy differences between the diastereoisomeric complexes.

Concomitant encapsulation also allows the reciprocal interaction between two different chiral guests. In the achiral cylindrical capsule 11·11, encapsulation of (*R*)-styrene oxide with racemic (\pm)-2-butyl chloride or the alcohols (\pm)-2-butanol or (\pm)-2-pentanol showed two coencapsulation diastereoisomeric complexes comprising the enantiopure oxide and one enantiomer of the secondary guest. Unfortunately, these combinations did not provide any

Table 4 Coencapsulation of two different chiral guests within the achiral cylindrical capsule 11·11

Enantiopure guest	Racemic guest	d.e. %
		9
		0
		9
		13
		17
		20
		5
		0

diastereoselectivity, even though the stereogenic centers of both guests face each other near the capsule's center. Better results were observed with the stronger hydrogen bond donor (*S*)-mandelic, which is easily coencapsulated with (\pm)-2-butanol giving rise to two diastereoisomeric complexes this time in the ratio 1.1 at 303 K and 1.3 at 283 K in favor of the combination (*S*)-mandelic acid with (*R*)-2-butanol because of the presence of attractive inter-guest hydrogen bonds that are instructed and favored by the shape and size of the cavity of the molecular capsule [38]. Many other combinations of chiral guests were explored and those that showed selectivity were characterized by the presence of good hydrogen bond donor or acceptor groups, the best example with a diastereoselective ratio of 1.5 provided by the couple (*S*)-1-phenylethanol and (\pm)-3-methyl-2-bromo-butyric acid (Table 4).

As observed above, d.e. are low unless contact between the two chiral guests is provided for example by weak attractive interactions like hydrogen bonds [26].

5.3

Triple Coencapsulation

A further step in the survey on encapsulation of chiral molecules is the study of the combinations of three chiral species in the achiral cylindrical capsule [64]. For this purpose propylene sulfide represents a good choice because of the proper small size, the presence of a stereo center and is characterized by well-resolved NMR resonances which do not overlap with the capsule's spectrum. Encapsulated enantiopure (*R*)-propylene sulfide provided two sets of methyl resonances up-field shifted for the molecules placed at the ends of the capsule and for the one in the middle: this indicates that these species do not exchange their position on the NMR chemical shift timescale. Decreasing gradually the enantiomeric purity of the guest caused the appearance of other diastereoisomeric capsules that were assigned on the basis of the relative statistical abundance (Fig. 29). The pattern of signals observed is direct consequence of the enantiomeric distribution of the guest. Formation of diastereoisomeric capsules allows the determination of the enantiopurity of the guest without any employment of external chiral source because coencapsulation forces the molecules of the chiral guest to sense their reciprocal chirality.

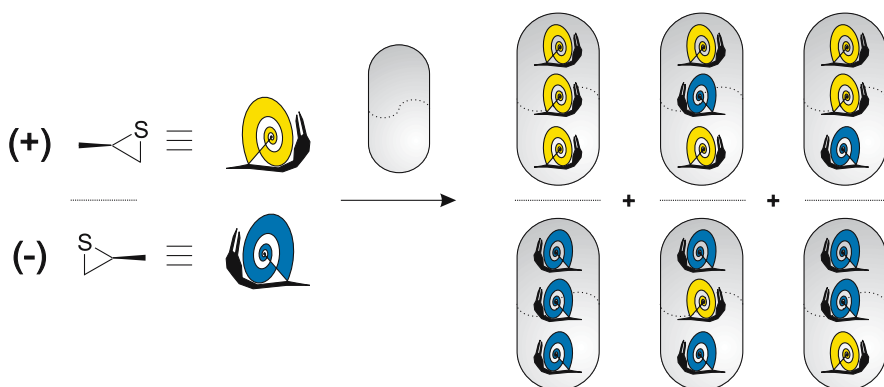


Fig. 29 Coencapsulation of three chiral molecules into an achiral cylindrical capsule leads to the formation of three racemic diastereoisomeric complexes. Their reciprocal ratio is a function of the enantiopurity of the guest

6

Conclusions

The strategies for the construction of chiral supramolecular aggregates have been reviewed with particular emphasis on their singular advantages as well as limits. In terms of stereocontrol, the use of intrinsically chiral components ensures better results, while the employment of achiral units opens the way to more synthetically accessible systems, and the chiral memory effect allows an elegant way to induce enantioselectivity in such kinds of assemblies. Encapsulation as an alternative approach that offers the advantage of being limited only by the size of the molecular chiral guests, and provides interesting results in asymmetric binding only if attractive forces are present between guests in agreement with what is observed in other systems.

7

Outlook

In parallel to the emerging interest for asymmetric organocatalysis seen in recent years, the potential development of supramolecular chirality for the construction of asymmetric self-assembling organocatalytic systems is evident. Moreover, the control over the entire space that surrounds a guest allows in theory fine construction of chiral nano-reactors with the ultimate goal of mimicking nature's efficiency and the selectivity observed in enzymes.

Acknowledgements The authors wish to thank Ms. E. Bosa for assistance in the preparation of figures and graphics, and Dr. M. Schramm for reviewing the manuscript.

References

1. Feringa BL, van Delden RA (1999) *Angew Chem Int Ed* 38:3418
2. Goshe AJ, Steele IM, Ceccarelli C, Rheingold AL, Bosnich B (2002) *Proc Natl Acad Sci USA* 99:4823
3. For hydrogen bond see Prins L, Reinhoudt DN, Timmerman P (2001) *Angew Chem Int Ed* 40:2383 and references therein
4. for ionic interactions see Hossain MA, Schneider H-J (1999) *Chemistry Eur J* 5:1284
5. for dispersive forces see Meyer EA, Castellano RK, Diederich F (2003) *Angew Chem Int Ed* 42:1210
6. for CH – π interactions see Nishio M (2005) *Tetrahedron* 61:6923
7. for hydrophobic effect see Blokzijl W, Engberts JBFN (1993) *Angew Chem Int Ed Engl* 32:1545
8. Jorgensen WL, Pranata J (1990) *J Am Chem Soc* 112:2008
9. Murray TJ, Zimmerman SC (1992) *J Am Chem Soc* 114:4010
10. Mulder A, Huskens J, Reinhoudt DN (2004) *Org Biomol Chem* 2:3409

11. Mammen M, Choi S-K, Whitesides GM (1998) *Angew Chem Int Ed Engl* 37:2754
12. Ercolani G (2003) *J Am Chem Soc* 125:16097
13. Palmer LC, Rebek J Jr (2004) *Org Biomol Chem* 2:3051
14. Atkins PW (1993) *Physical Chemistry*, 4th ed. Oxford University Press, Oxford
15. van Holde M (1990) *Biochemistry*. The Benjamin Cummings Publishing Company Inc, Redwood, CA
16. Kondo T, Oyama K-I, Yoshida K (2001) *Angew Chem Int Ed* 40:894
17. Chen H, Weiner WS, Hamilton AD (1997) *Curr Opin Chem Biol* 1:458
18. Fitzmaurice RJ, Kyne GM, Douheret D, Kilburn JD (2002) *J Chem Soc Perkin Trans* 1:841
19. Mateos-Timoneda MA, Crego-Calama M, Reinhoudt DN (2004) *Chem Soc Rev* 33:363
20. Simanek EE, Qiao S, Choi IS, Whitesides GM (1997) *J Org Chem* 62:2619
21. Prins LJ, Jolliffe KA, Hulst R, Timmerman P, Reinhoudt DN (2000) *J Am Chem Soc* 122:3617
22. Prins LJ, Hulst R, Timmerman P, Reinhoudt DN (2002) *Chem Eur J* 8:2288
23. Prins LJ, Huskens J, de Jong F, Timmerman P, Reinhoudt DN (1999) *Nature* 398:498
24. Prins LJ, Timmerman P, Reinhoudt DN (2001) *J Am Chem Soc* 123:10153
25. Ishi-I T, Crego-Calama M, Timmerman P, Reinhoudt DN (2002) *Angew Chem Int Ed* 41:1924
26. Mecozzi S, Rebek J Jr (1998) *Chem Eur J* 4:1016
27. Castellano RK, Kim BH, Rebek J Jr (1997) *J Am Chem Soc* 119:12671
28. Vysotsky MO, Böhmer V (2000) *Org Lett* 2:3571
29. Shivanyuk A, Spaniol TP, Rissanen K, Kolehmainen E, Böhmer V (2000) *Angew Chem Int Ed* 39:1264
30. Rincón AM, Prados P, de Mendoza J (2001) *J Am Chem Soc* 123:3493
31. Casnati A, Sansone F, Ungaro R (2003) *Acc Chem Res* 36:246
32. Sonson F, Baldini L, Casnati A, Chierici E, Faimani G, Ugozzoli F, Ungaro R (2004) *J Am Chem Soc* 126:6204
33. Brewster RE, Beckham Shuker S (2002) *J Am Chem Soc* 124:7902
34. Corbellini F, Di Costanzo L, Crego-Calama M, Geremia S, Reinhoudt DN (2003) *J Am Chem Soc* 125:9946
35. Corbellini F, Knegtel RMA, Grootenhuys PDJ, Crego-Calama M, Reinhoudt DN (2005) *Chemistry Eur J* 11:298
36. Rebek J Jr (2005) *Angew Chem Int Ed* 44:2068
37. Nuckolls C, Hof F, Martín T, Rebek J Jr (1999) *J Am Chem Soc* 121:10281
38. Scarso A, Shivanyuk A, Hayashida O, Rebek J Jr (2003) *J Am Chem Soc* 125:6239
39. Amaya T, Rebek J Jr (2004) *J Am Chem Soc* 126:6216
40. Davis JT (2004) *Angew Chem Int Ed* 43:668
41. Shi X, Fettinger JC, Davis JT (2001) *J Am Chem Soc* 123:6738
42. Shi XD, Fettinger JC, Cai MM, Davis JT (2000) *Angew Chem Int Ed* 39:3124
43. Wu A, Chakraborty A, Fettinger JC, Flowers II RA, Isaacs L (2002) *Angew Chem Int Ed* 41:4028
44. Murguly E, McDonald R, Branda NR (2000) *Org Lett* 2:3169
45. Sanchez-Quesada J, Seel C, Prados P, de Mendoza J (1996) *J Am Chem Soc* 118:277
46. Tanaka Y, Katagiri H, Furusho Y, Yashima E (2005) *Angew Chem Int Ed* 44:3867
47. Scarso A, Shivanyuk A, Hayashida O, Rebek J Jr (2004) *Chiral Spaces in Encapsulation Complexes*, chap. 22. In: Palyi G, Zucchi C, Caglioti L (eds) *Progress in Biological Chirality*. Elsevier, Oxford
48. Castellano RK, Nuckolls C, Rebek J Jr (1999) *J Am Chem Soc* 121:11156
49. Pop A, Vysotsky MO, Saadioui M, Böhmer V (2003) *Chem Commun* 1124
50. Szabo T, Hilmersson G, Rebek J Jr (1998) *J Am Chem Soc* 120:6193

51. Tokunaga Y, Rebek J Jr (1998) *J Am Chem Soc* 120:66
52. Rivera JM, Martín T, Rebek J Jr (1998) *Science* 279:1021
53. Rivera JM, Martín T, Rebek J Jr (2001) *J Am Chem Soc* 123:5213
54. Prins LJ, De Jong F, Timmerman P, Reinhoudt DN (2000) *Nature* 408:181
55. Prins LJ, Verhage JJ, de Jong F, Timmerman P, Reinhoudt DN (2002) *Chem Eur J* 8:2302
56. Ishi-I T, Crego-Calama M, Timmerman P, Reinhoudt DN, Shinkai S (2002) *J Am Chem Soc* 124:14631
57. Rivera JM, Craig SL, Martín T, Rebek J Jr (2000) *Angew Chem Int Ed* 39:2130
58. Scarso A, Trembleau L, Rebek J Jr (2003) *Angew Chem Int Ed* 42:5499
59. Scarso A, Trembleau L, Rebek J Jr (2004) *J Am Chem Soc* 126:13512
60. Heinz T, Rudkevich DM, Rebek J Jr (1999) *Angew Chem Int Ed* 38:1136
61. Pérez-García L, Amabilino DB (2002) *Chem Soc Rev* 31:342
62. Kimbara K, Saigo K (2003) *Top Stereochem* 12:207
63. Palmer LC, Zhao Y-L, Houk KN, Rebek J Jr (2005) *Chem Commun* 29:3667
64. Yamanaka M, Rebek J Jr (2004) *Chem Commun* 1691

Dynamic Helical Structures: Detection and Amplification of Chirality

Katsuhiro Maeda¹ · Eiji Yashima^{1,2} (✉)

¹Department of Molecular Design and Engineering, Graduate School of Engineering,
Nagoya University, Furo-cho, Chikusa-ku, 464-8603 Nagoya, Japan
yashima@apchem.nagoya-u.ac.jp

²Yashima Super-Structured Helix Project,
Exploratory Research for Advanced Technology (ERATO),
Japan Science and Technology Agency (JST), Creation Core Nagoya 101, 2266-22,
Anagahora, Shimoshidami, Moriyama-ku, 463-0003 Nagoya, Japan
yashima@apchem.nagoya-u.ac.jp

1	Introduction	48
2	Helical Aggregates	49
2.1	Helical Aggregates Based on Small Molecules	49
2.2	Chiral Amplification by Helical Aggregates	55
2.3	Chirality Sensing by Helical Aggregates	60
3	Helical Macromolecules and Oligomers	61
3.1	Poly(phenylacetylene)s	62
3.2	Other Helical Polymers and Oligomers	67
3.3	Chirality Sensing by Helix Inversion	71
3.4	Memory and Storage of Helical Chirality	74
3.5	Chirality Sensing in Gel and Solid	78
3.6	Sensing and Amplification of Chirality in Liquid Crystal	79
4	Supramolecular Assembly of Helical Polymers	80
5	Conclusion	83
	References	84

Abstract A unique feature of dynamic helical, chromophoric macromolecules that enables the detection of a small imbalance in chiral guest molecules through a noncovalent bonding interaction with high cooperativity is described. In sharp contrast to host–guest and supramolecular systems based on small synthetic receptor molecules, the chiral information of nonracemic guest molecules transfers with a significant amplification in a helical polymer as an excess of a single-handed helix, resulting in a highly efficient chirality-sensing system. Helical aggregates with controlled helicity based on small molecules and their chiral amplification and use in chirality sensing are also briefly described in this review.

Keywords Chiral amplification · Chirality sensing · Helical aggregates · Helical macromolecules · Helix

1

Introduction

Living organisms often show quite different biological activities toward a pair of enantiomers, particularly chiral drugs. Therefore, the detection and assignment of the chirality of molecules at molecular and supramolecular levels has become significantly important in recent years. To this end, a number of artificial receptor molecules, supramolecules and π -conjugated macromolecules have been developed. Among them, achiral or dynamically racemic, but chromophoric supramolecular and macromolecular helical systems are particularly interesting, because upon noncovalent binding to a nonracemic guest, the chirality is transferred to the receptors, resulting in the generation of one of the enantiomeric or diastereomeric twisted or helical conformers, thus producing a characteristic induced circular dichroism (ICD) in the absorption region of the receptors. Such systems will provide the basis to construct a novel chirality-sensing probe to determine the absolute configuration and enantiomeric excess (ee) of the guest molecules.

The macromolecular and supramolecular helicities are one of the most important and unique chiralities, as exemplified by biological macromolecules, such as proteins and nucleic acids and their helical assemblies, for example, the coiled-coils (helix-bundles) and super-helices of DNA plasmids. These elaborate helical structures appear to play an essential role for exercising their sophisticated functions in nature that involve recognition, replication and catalytic activity [1, 2]. Bioinspired by such discrete helical structures of biopolymers, chemists have been challenged to construct artificial helical macromolecules and supramolecules from small component molecules through self-assembly with controlled helicity that mimic the structures and functions of biological helices. To date, several synthetic helical polymers exhibiting an optical activity due to their one-handed helicity have been successfully prepared and the details have been thoroughly reviewed elsewhere [3–7]. This review will focus on dynamic helical polymers such as π -conjugated poly(phenylacetylene)s with functional pendant groups, which respond to the chirality of optically active small molecules via noncovalent bonding interactions [8–11]. The complexes exhibit a characteristic ICD in the main chain absorption region due to the induced macromolecular helicity with an excess helical sense, which reflects the chirality of the chiral guest molecules. Similar sensing of the chirality of molecules is possible with achiral or dynamically racemic chromophoric small molecules as a receptor [12–15]. However, they usually require stoichiometric complexation with the guest molecules. In sharp contrast, chirality is significantly amplified in dynamic helical polymers with a high cooperativity, that enables the highly sensitive detection of chiral guests.

On the other hand, in the field of supramolecular chemistry, a variety of helical supramolecular assemblies have been constructed using various types

of noncovalent bonding interactions, such as hydrogen bonding, $\pi - \pi$ stacking, ion-dipolar, electrostatic interactions, and their combinations [16–23]. In this review, recent representative examples of helical aggregates based on small molecules are also briefly described from the viewpoints of their formation and chirality amplification, and use for chirality sensing. A large number of helical architectures including single, double and triple helices have also been developed from small molecular components or oligomers based on directional, strong coordinate bonding with metal ions, which are known as “helicates” [24–27]. However, helicate chemistry studies are numerous and they are beyond the scope of this work. Chiral amphiphilic lipids [28–31], organogelators [32, 33], and dendron rodcoils [34] are also known to self-assemble into helical supramolecular structures with optical activity in water or organic solvents. These results have been reviewed [30–33] and are described in detail elsewhere within this volume.

2

Helical Aggregates

A large number of helical aggregates with a well-defined structure have been constructed from small molecules based on self-assembly and/or supramolecular assembly through noncovalent interactions, such as $\pi - \pi$ stacking, hydrogen bonding, ion-dipolar, and charge-transfer interactions. Advanced microscopy techniques including scanning force microscopy (SFM), atomic force microscopy (AFM) and transmission electron microscopy (TEM) combined with circular dichroism (CD) spectroscopy and scattering techniques such as small-angle neutron and X-ray scattering (SANS and SAXS) clearly reveal the structures of helical aggregates and their helix-senses.

2.1

Helical Aggregates Based on Small Molecules

The phthalocyanine derivative **1** bearing four benzo crown ether moieties with optically active tails self-assembles into long columns driven by $\pi - \pi$ stacking interactions in chloroform, resulting in the formation of fibers with a right-handed helix as evidenced by the appearance of an ICD. The fibers further assemble into superhelices with an opposite left-handed helix to that of each fiber, as demonstrated by TEM observations of the helical aggregates (Fig. 1) [35]. This process is a typical example of the hierarchical self-assembly of small components into a complex architecture with helical chirality. The helical structure of the aggregate can be turned off by the addition of potassium (K^+) ions without breaking their fiber structures. Metal phthalocyanines **2** fused to four chiral [7]helicenes also form helical columnar

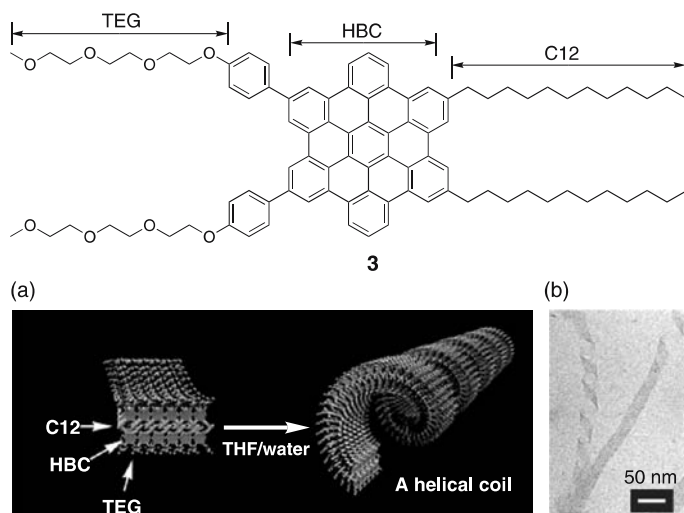


Fig. 2 **a** Schematic illustration of the formation of a helical supramolecular graphitic nanotube of **3**. **b** TEM image of self-assembled **3**. (Reprinted with permission from [37]. Copyright 2004 American Association for the Advancement of Science)

helical arrays of π -stacked coronenes covered with hydrophilic TEG chains, formed by loose rolling-up of a bilayer graphite tape composed of π -stacked HBC **3**. The helical coils are a mixture of right- and left-handed helices. However, optically active HBCs bearing nonracemic side groups produce an excess one-handed helix with significant chiral amplification, thus showing an intense ICD (see Sect. 2.2) [38].

Alkoxy-substituted triphenylenes form charge-transfer $\pi - \pi$ stacked complexes with electron-accepting aromatic compounds, producing cylindrical helical aggregates of alternating donors and acceptors. Schuster et al. demonstrated that an achiral triphenylene **4** forms charge-transfer complexes with an optically active electron acceptor **5** bearing a bulky (–)-menthyl group. The intercalation of **5** into the columnar aggregates induced a preferential helical twist into the columns, which was evidenced by the appearance of an ICD in the triphenylene chromophore region (Fig. 3) [39].

Helicenes have an intrinsic, rigid helical shape and can be separated into enantiomers. Katz et al. found that the nonracemic helicene **6** with quinone residues self-assembles into one-handed helical columns in apolar solvents, where the molecules are stacked along their helix axes as shown in Fig. 4 [40–42]. In this case, the π -donor–acceptor interactions appear to induce aggregations and stabilize the columnar stacks. Interestingly, unlike the non-racemic **6**, the corresponding racemic **6** produced no such aggregation.

Similar helical columnar aggregates have also been synthesized through the combination of $\pi - \pi$ interactions and hydrogen bonding and/or ion-

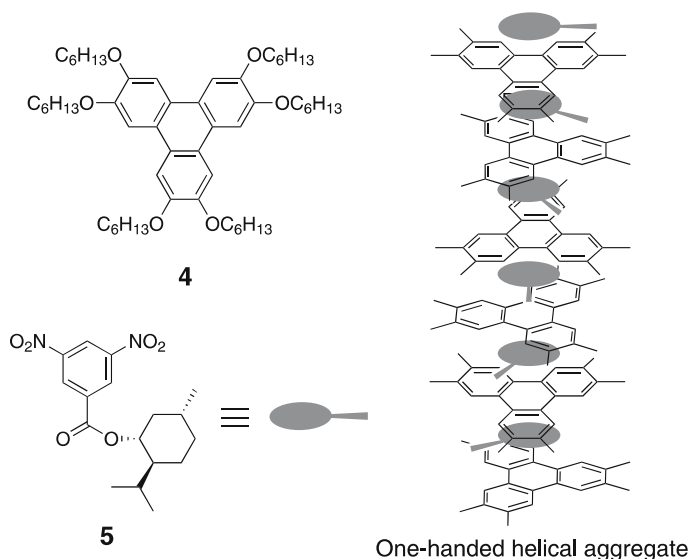


Fig. 3 Schematic illustration of one-handed helical aggregates of **4** doped with chiral **5**

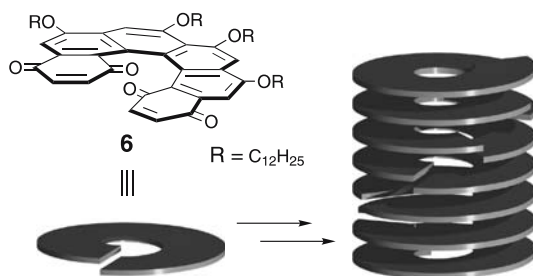


Fig. 4 Schematic illustration of aggregation of nonracemic helicene **6** into helical columns

dipolar interactions. Gottarelli and Spada et al. utilized a biologically important structural motif of the tetrameric cyclic arrangement of guanosine derivatives (G-quartet) and prepared helical columns with a controlled helix-sense (Fig. 5). The oligomeric deoxyguanosines **7**, the guanosine units of which form G-quartets through hydrogen bonding, subsequently stack into helicoidal columnar structures in water [43, 44]. The addition of K^+ ions that bind to the inner carbonyl groups of the G-quartets stabilize the columnar aggregates increasing columnar length. In concentrated aqueous solutions, **7** forms lyotropic cholesteric and hexagonal liquid crystalline phases. Unlike the polar **7**, the lipophilic deoxyguanosine derivatives **8** form an octamer in the presence of K^+ ions in apolar solvents, where the K^+ ion is sandwiched between two G-quartets. At a higher K^+ ion concentration, the G-quartets further assemble into longer helical columnar aggregates through

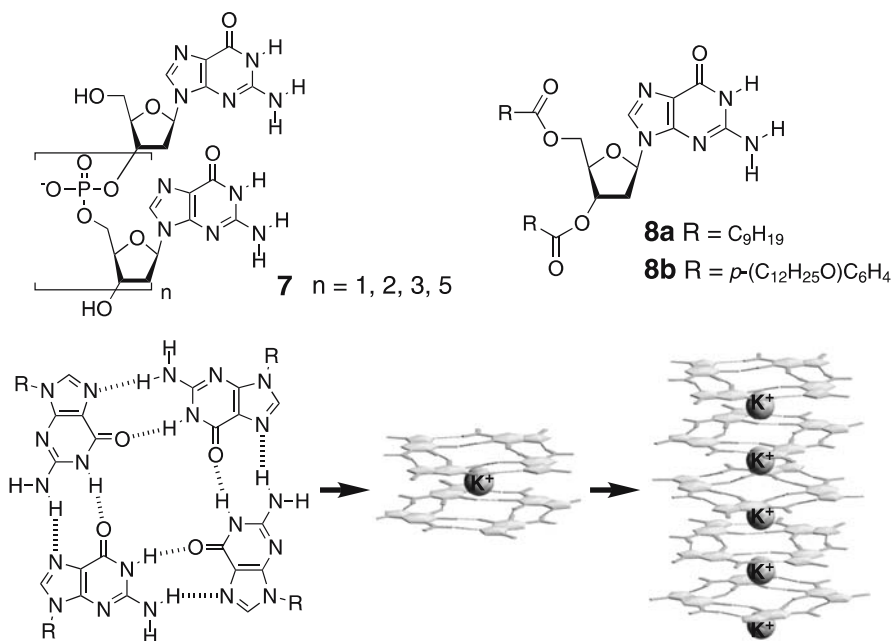


Fig. 5 Schematic illustration of the formation of the disk-shaped tetramers of deoxyguanosine **7** and **8** by intermolecular hydrogen bonding and the subsequent stacking of the disks into helical columns in the presence of potassium ions

ion-dipolar interactions (Fig. 5) [45]. Interestingly, the one-handed helical columnar aggregates of **8a** can discriminate enantiomers of the K^+ salts of amino acids and enantioselectively extract one of the enantiomers from an aqueous solution into an organic phase of **8a** [46]. Folic acid derivatives **9** bearing a pterin residue also form disk-shaped tetramers through intermolecular hydrogen bonding in water and organic solvents. In the presence of Na^+ ions, the tetramers stack to form helical columns through ion-dipolar interactions similar to the guanosine derivatives (Fig. 6) [47–49], while **9a** can self-assemble to form similar helical columns through a lipophilic interaction in apolar solvents without the aid of alkali metal ions [49].

Meijer and coworkers have reported a series of hierarchical self-assemblies of π -conjugated systems to develop nanowires for “supramolecular electronics”. A chiral π -conjugated oligo(*p*-phenylene vinylene) **10** possessing a ureido-*s*-triazine unit forms a dimer through complementary quadruple hydrogen bonding [50], which subsequently stacks into helical columns by $\pi - \pi$ interactions in apolar solvents (Fig. 7) [51–54]. A negative bisignated Cotton effect observed in the $\pi - \pi^*$ transition region suggests left-handed helical arrays of the dimers. Meijer et al. extended the concept in Fig. 8 to triple-hydrogen bonded 1 : 2 triad helical aggregates composed of achiral perylene bisimide **11** and chiral oligo(*p*-phenylene vinylene) **12**. The 12–11–12 triad

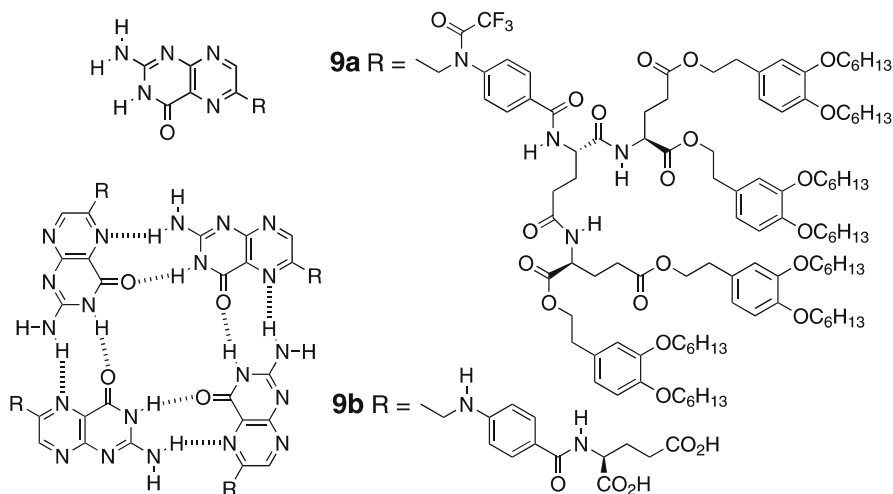


Fig. 6 Formation of the disk-shaped tetramers of folic acids **9** by intermolecular hydrogen bonding

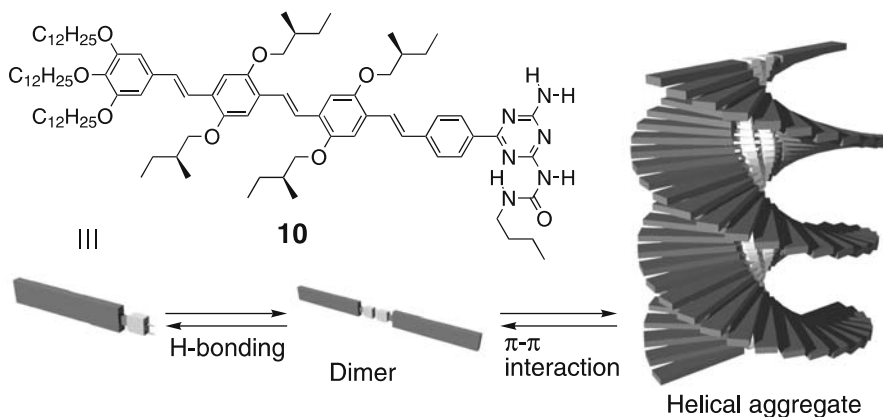


Fig. 7 Schematic representation of the formation of a helical columnar structure by hierarchical self-assembly of a chiral oligo(*p*-phenylene vinylene) **10** bearing ureido-*s*-triazine units in *n*-dodecane. (Reproduced with permission from [51]. Copyright 2005 American Chemical Society)

first self-assembles in a hierarchical fashion into rodlike aggregates with a left-handed helical structure by π – π interactions in methylcyclohexane (Fig. 8a) [55, 56], which further assemble into right-handed nanometer-scale supercoils, as visualized by AFM measurements (Fig. 8b). These π -conjugated helical aggregates are of particular interest for the development of electro-optical devices such as light emitting diodes (LEDs) and field effect transistors (FETs).

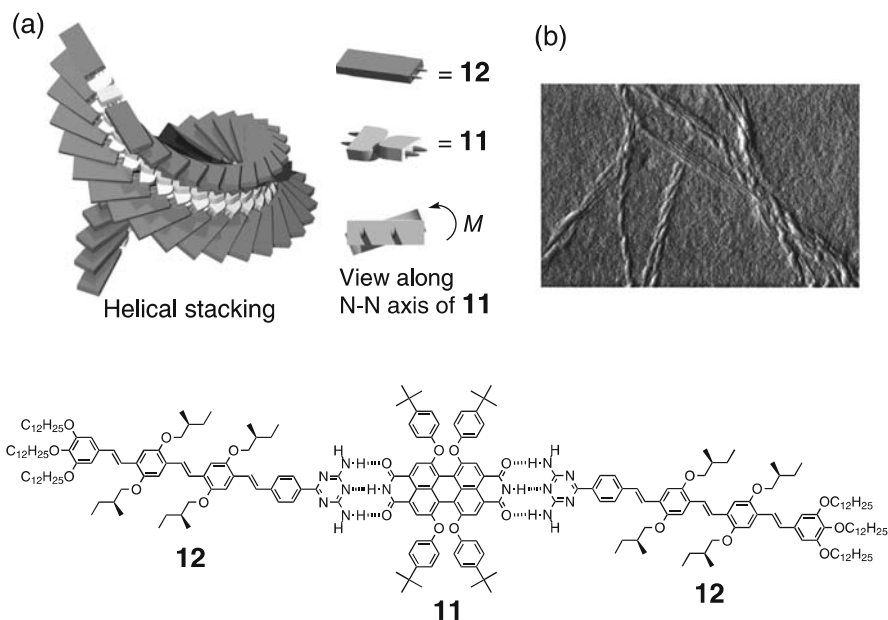


Fig. 8 **a** Schematic representation of the formation of triple-hydrogen-bonded 1 : 2 complex of a perylene bisimide **11** and a chiral oligo(*p*-phenylene vinylene) **12** and its helical stacking in apolar solvents. (Reproduced with permission from [55]. Copyright 2004 American Chemical Society.) **b** AFM image of right-handed supercoiled aggregates from **12**–**11**–**12** complex. (Reprinted with permission from [56]. Copyright 2002 American Chemical Society)

2.2

Chiral Amplification by Helical Aggregates

Chiral amplification is a unique process from which a small chiral bias is significantly enhanced through covalently and/or noncovalently bonded systems. This phenomenon is also interesting in connection with not only the origin of biomolecular homochirality in nature [57, 58], but also the development of ideal methods to produce optically active compounds [59, 60]. Green et al. discovered chiral amplification in polyisocyanates, typically stiff, rod-like polymers and combined experimental and theoretical work revealed the substantial nature of their dynamic macromolecular helicity [61]. Dynamic helical polyisocyanates are composed of right- and left-handed helical conformations separated by helical reversals, whose helix-sense readily inverts in solution due to the relatively small barrier energy for helical reversals in these polymers. Therefore, the copolymerization of achiral isocyanates with a small amount of optically active ones can produce optically active polyisocyanates with a prevailing one-handed helical conformation. This process is highly cooperative and was called the “sergeants and soldiers rule” by Green

et al. [61, 62]. They further demonstrated that the copolymers of isocyanates composed of a mixture of (*R*)- and (*S*)-enantiomers with a small ee also form an excess single-handed helical conformation [63]. The minority units obey the helical sense of the majority units in order to avoid introducing energetic helical reversals. Green et al. termed this phenomenon (positive nonlinear effect in asymmetric synthesis) the “majority rule”. Consequently, chiral information of a tiny amount of a pendant group covalently bonded to the polymer backbone is significantly amplified and transformed into the entire polymer chain through a significant cooperative manner, resulting in a higher optical activity than that expected from the monomer unit components.

This concept of the chiral amplification has been applied to supramolecular systems that involve self-assemblies composed of chiral–achiral and chiral–chiral (*R/S*) components, resulting in the formation of chiral supramolecules [20] including helical aggregates.

The bifunctional ureido-*s*-triazines (13, 14) and ureidopyrimidinones (17) connected by a spacer can dimerize through self-complementary quadruple

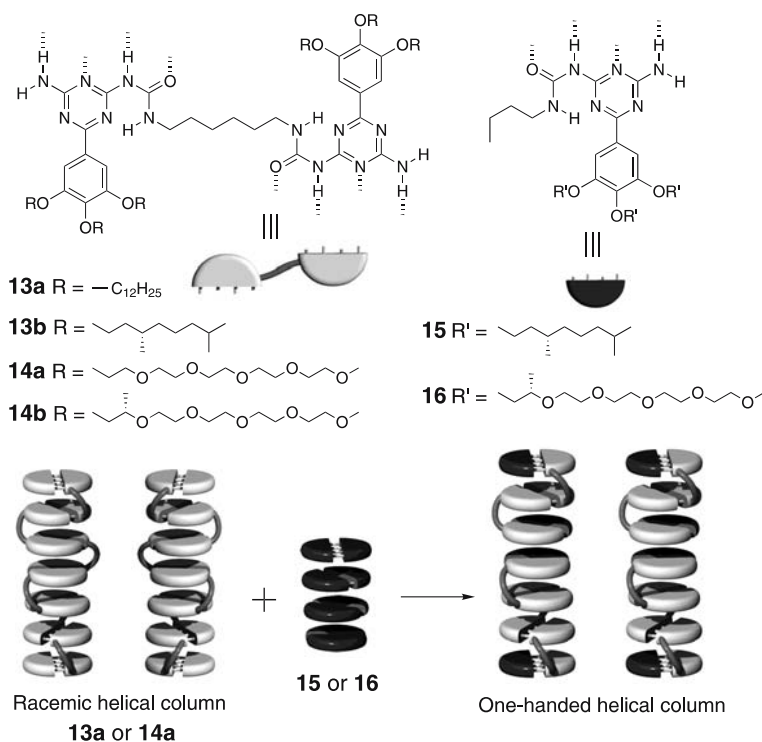


Fig. 9 Schematic illustration of supramolecular assembly of bifunctional 13 and 14 into helical columns and amplification of chirality in mixtures of achiral 13a and 14a and chiral 15 and 16, respectively

Percentage chiral monofunctional 16	$g^{\ddagger}_{\text{gas}} \times 10^5$ (TS, dotted line)	$g^{\ddagger}_{\text{gas}} \times 10^5$ (Reactants, dashed line)
0	0.0	0.0
10	-1.0	-3.5
15	-1.5	-3.8
20	-2.0	-9.5
30	-3.0	-11.0
60	-5.0	-12.5
75	-6.5	-11.5
85	-7.5	-11.0
100	-9.5	-10.0

17a R = $-\text{C}_{12}\text{H}_{25}$ **17b** R =

Meijer et al. also reported that C_3 -symmetrical disk-shaped molecules (**18–21**) form a helical columnar assembly through π – π stacking interactions together with hydrogen-bonding in water and polar solvents such as alcohols as well as in apolar solvents (Fig. 11) [67–71]. These systems also showed an extremely strong chiral amplification (sergeants and soldiers effect) (Fig. 12a). The addition of a small amount of chiral sergeant molecules into achiral soldier molecules produced a one-handed helical supramolecular assembly. Recently, Meijer et al. reported the first example of the majority rule effect for noncovalently bonded helical aggregate formation in the non-racemic **18** [38, 72]. As shown in Fig. 12b, the anisotropy factor g exhibits a positive nonlinear dependence on the ee of **18**.

Trialkyl-1,3,5-benzenetricarboxamides (**22–24**) also self-assemble to form helical columns through a 3-fold intermolecular hydrogen bonding in apolar solvents, and the sergeants and soldiers effect was observed in this system [73, 74]. A one-handed helical column of the major achiral **24** bearing a sorbyl moiety induced by a small amount (0.1 equiv.) of chiral **22**, followed by bridging each achiral **24** unit through the 1,4-polymerization of the sorbyl moiety produced a linear polymer with optical activity after removal of the

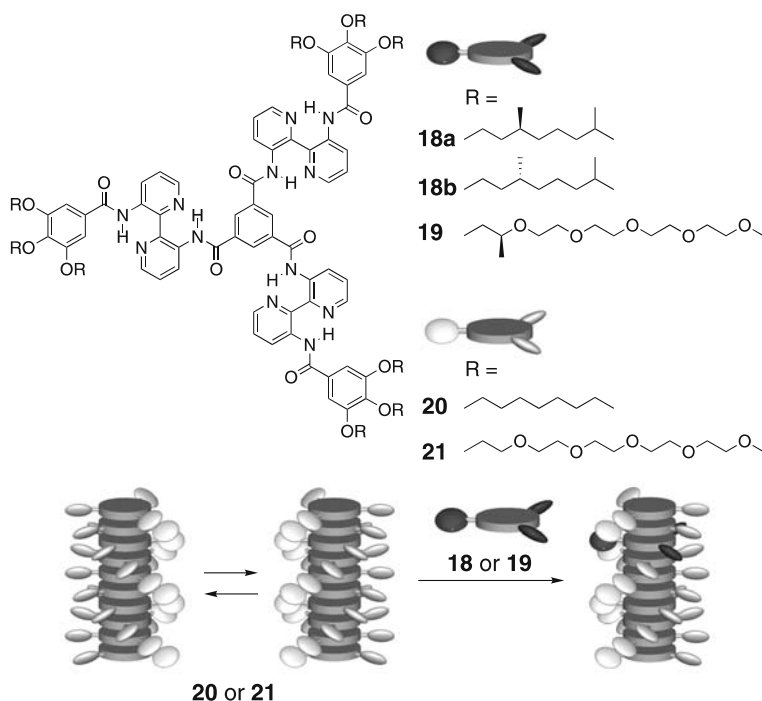


Fig. 11 Schematic illustration of helical supramolecular assembly of C_3 -symmetrical disk-shaped molecules **18–21**

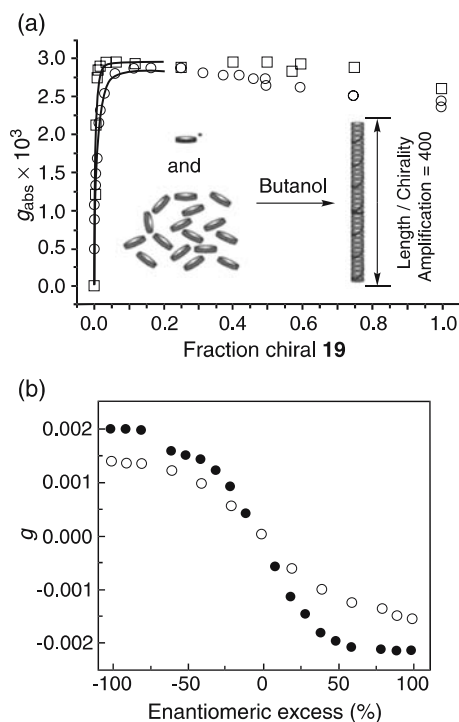
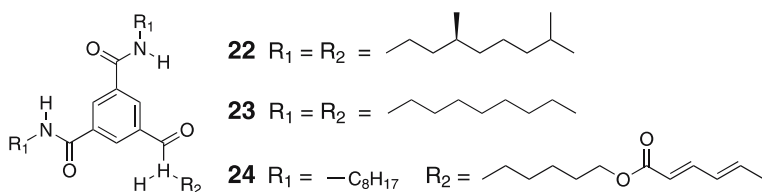
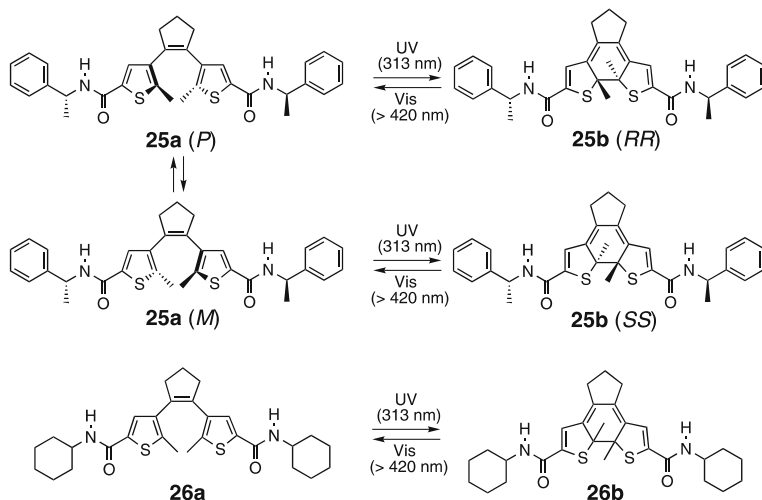


Fig. 12 **a** “Sergeants and soldiers” effect: plots of anisotropy factor g versus the mole fraction of chiral **19** for helical supramolecular assembly of chiral **19** and achiral **21** in *n*-butanol at 10^{-5} (O) and 10^{-4} M (□). (Reproduced with permission from [71]. Copyright 2001 Springer.) **b** “Majority rule” effect: plots of g versus the enantiomeric excess of **18a** and **18b** for helical supramolecular assembly of chiral **18a** and **18b** in *n*-octane at 20 (●) and 50 °C (○). (Reproduced with permission from [72]. Copyright 2005 American Chemical Society)

chiral template **22** in specific solvents where helical columnar formation takes place [75]. The chiral information seems to be encoded in the stereochemistry of the sorbyl main chain, leading to a kind of chiral memory effect.

The photochromic dithienylethene (**25a**) bearing amide groups exists in two interconvertible conformations with *P*- and *M*-helicity in solution. However, **25a** can take either the *P*- or *M*-helical conformation giving a supramolecular helical fibrous network when they aggregate in apolar solvents due to the multiple hydrogen bonding formation between the amide groups to form gels [76]. Subsequent photochemical ring-closure to **25b** in the gel state proceeds with the remarkably high diastereoselectivity (96% diastereomeric excess). Feringa et al. demonstrated that the sergeants and soldiers effect was observed for the coaggregation of achiral **26a** with a small amount of chiral **25a** [77]. Moreover, the supramolecular chirality information of **26a** co-operatively induced by coaggregation with chiral **25a** could be fixed as the

**Structure 3****Structure 4**

molecular chirality of the dithienylethene units in **26b** by the photochemical ring-closure with irradiation of UV light.

2.3

Chirality Sensing by Helical Aggregates

Fenniri et al. found that the heterocyclic molecule **27** possessing two hydrogen bonding arrays based on guanine and cytosine and a benzo-18-crown-6 ether residue spontaneously forms a disk-shaped hexamer (rosette) through intermolecular hydrogen bonding, and then the rosettes further self-assemble to form right- or left-handed nanotube structures (Fig. 13) [78, 79]. The addition of chiral amino acids, such as L-alanine, induced the formation of one-handed helical nanotubes, resulting in the appearance of a characteristic ICD. Other amino acids also gave the same Cotton effect sign if the configurations are the same. Moreover, the majority rule effect was observed in this system, which will contribute to detecting small enantiomeric imbalances in chiral amino acids. Therefore, this supramolecular system can be used as a probe for the chirality sensing of amino acids.

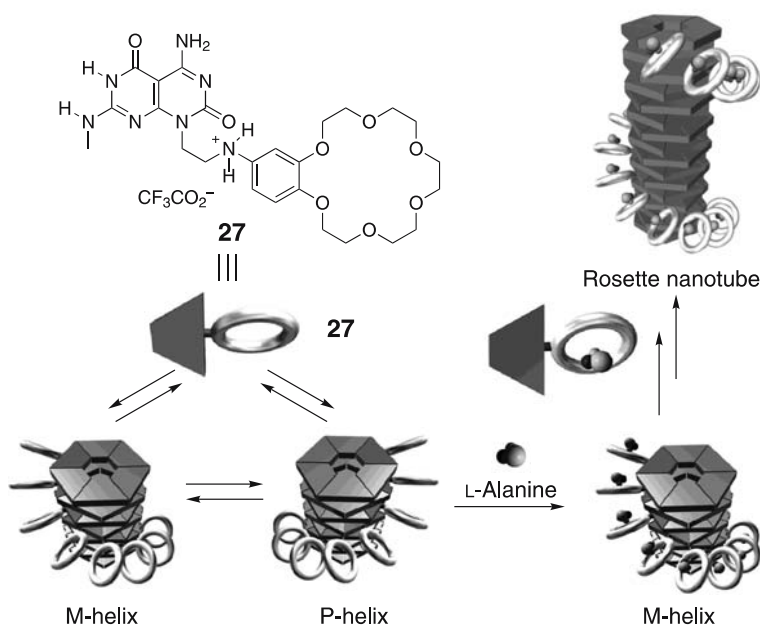


Fig. 13 Schematic illustration of supramolecular self-assembly of **27** forming a left-handed rosette nanotube with L-alanine

3

Helical Macromolecules and Oligomers

Artificial helical macromolecules and oligomers with a predominantly one-handed helix-sense have attracted great interest not only to mimic biological macromolecules such as DNA and proteins, but also for their possible applications in materials science including enantioselective adsorbents and catalysts. Optically active helical polymers can be prepared by either the polymerization of optically active monomers or the asymmetric polymerization of achiral or prochiral monomers with chiral initiators or catalysts [5]. In these synthetic methods, the helical structures of the polymers including a helix-sense and a helical pitch are determined by chiral substituents covalently bonded to the polymer backbone or kinetically during the polymerization. In 1995, we reported that the macromolecular helicity with an excess helical sense could be induced in an optically inactive, dynamic helical poly(phenylacetylene) bearing a functional group by optically active small molecules (Fig. 14) [8–11]. The polymer has a chromophoric dynamic helical backbone with a functional pendant group, so that upon complexation with specific chiral guests, the complexes exhibit a characteristic ICD in the UV-visible region of the polymer backbone. The Cotton effect signs corresponding to the helical sense can be used as a novel probe for the chirality

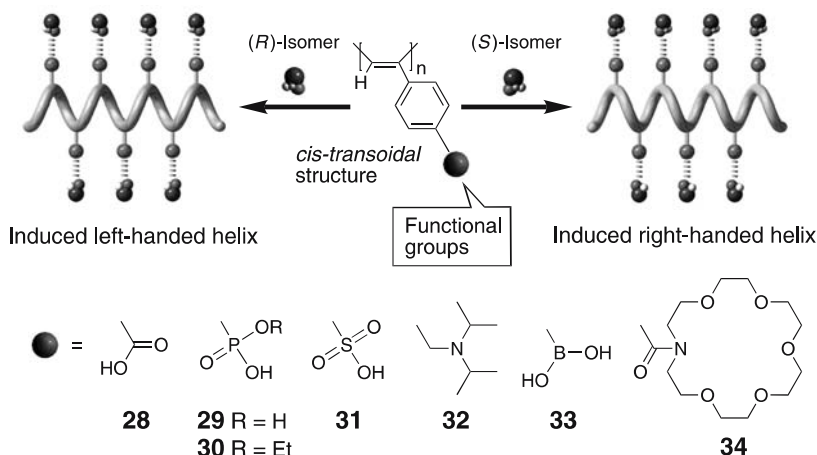


Fig. 14 Schematic illustration of helicity induction on poly(phenylacetylene)s upon complexation with chiral compounds

assignments of the guest molecules. In addition, this one-handed helicity induction concept involves a significant cooperative interaction with a considerable amplification of chirality, which enables the detection of a small chiral bias and can be used as a highly sensitive chirality sensor by utilizing the signals of the ICDs.

This section mainly describes our studies of the helicity induction on poly(phenylacetylene)s through noncovalent chiral interactions together with other interesting chiroptical properties of helical polymers and oligomers.

3.1

Poly(phenylacetylene)s

A *cis-transoidal* stereoregular poly(phenylacetylene) bearing a carboxy group **28** forms a complex with optically active amines through an acid–base interaction, and a one-handed helical conformation is instantaneously induced on the polymer (Fig. 14) [8, 9]. The predominantly one-handed helix formation can be monitored by the appearance of a characteristic ICD in the UV-visible region of the polymer backbone. The typical CD spectra of **28** in the presence of various optically active amines (**35**–**39**) in DMSO are depicted in Fig. 15. There is a good relation between the Cotton effect signs reflecting the helix-sense of **28** and the absolute configurations of the chiral amines; all primary amines gave the same Cotton effect signs when the configurations were the same. Therefore, the Cotton effect sign of **28** can be used as a probe for sensing the chirality of various primary chiral amines. Moreover, the magnitude of the ICD tends to increase with an increase in the bulkiness of the

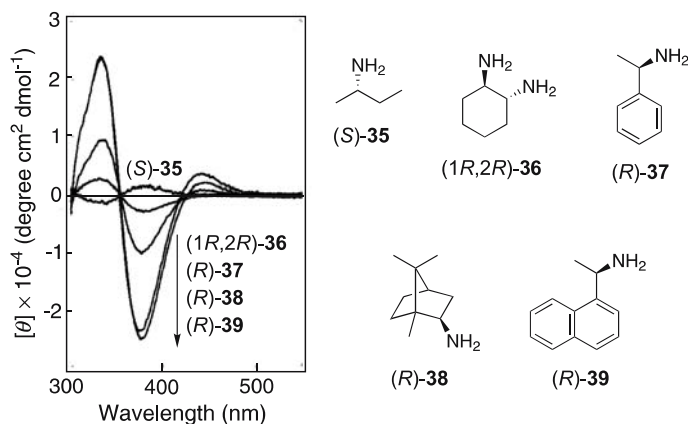


Fig. 15 CD spectra of **28** upon complexation with chiral amines in DMSO. (Reprinted with permission from [9]. Copyright 1997 American Chemical Society)

amines, $35 < 36 < 37 \ll 38 < 39$, suggesting that the bulky groups introduced at the para position of **28** contribute more efficiently for the polymer to take an excess helix-sense.

Taking advantage of this helicity induction concept, a variety of chirality-sensing poly(phenylacetylene)s responding to the chirality of target chiral molecules can be designed and synthesized by introducing a specific functional group as the pendant group. For example, poly(phenylacetylene)s bearing phosphonate (**29**, **30**) [80, 81], sulfonate (**31**), amino (**32**) [82–84], and boronate groups (**33**) [85, 86] as the pendant groups can respond to the chirality of chiral amines, ammoniums, acids, diols and sugars, respectively, and their complexes show a characteristic ICD due to the predominantly one-handed helix formation (Fig. 14).

The underlying principle for these phenomena is considered to be the fact that the poly(phenylacetylene)s are a dynamic helical polymer of which right- and left-handed helical conformations are interconvertibly separated by helical reversals like polyisocyanates as mentioned above. Therefore, the remarkable CD induction arises from a drastic change in the population of the right- and left-handed helices of the polymers.

Chiral amplification phenomena of sergeants and soldiers and majority rule effects, which are characteristic features for dynamic helical polymers [4, 58], are, therefore, observed for the noncovalent helix induction in the poly(phenylacetylene)s. For example, when **28** was mixed with 50% ee of 2-amino-1-propanol in DMSO, the complex showed an intense ICD like that of 100% ee. In the presence of a small amount of (*R*)-**39**, **28** showed a very weak ICD due to the lack of a single-handed helical conformation. However, the coaddition of the excess bulky, achiral 1-naphthylmethylamine **40** with

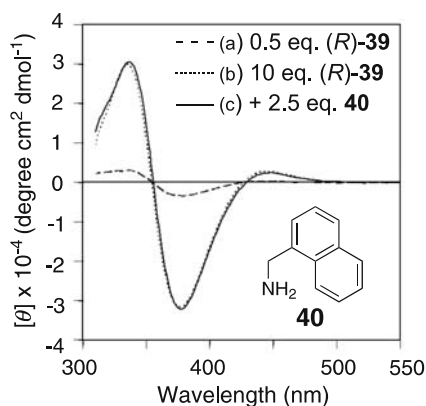


Fig. 16 CD spectra of **28**–(*R*)-**39** complexes in the absence ($[(R)\text{-}39]/[28] = 0.5$ (a) and 10 (b)) and presence of **40** ($[(R)\text{-}39]/[40]/[28] = 0.5/2.5/1$) in DMSO. (Reprinted with permission from [87]. Copyright 2004 Wiley)

a small amount of (*R*)-**39** caused a dramatic increase in the ICD magnitude being comparable to the full ICD by excess (*R*)-**39** (Fig. 16) [87]. This indicates that an almost one-handed helix can be induced on **28** upon complexation with a small amount of (*R*)-**39** assisted by the achiral **40**.

The introduction of bulky substituents, such as the aza-18-crown-6-ether, a typical host molecule in host–guest chemistry, as the functional pendant group of a poly(phenylacetylene) (**34**) was expected to improve the rigidity of the polymer backbone, so as to increase the helical segments separated by rarely occurring helix reversals. In fact, **34** can detect the chirality of chiral amino acids with an extremely high sensitivity [88–90]. An almost one-handed helix was induced in **34** in the presence of 0.1 equiv. *L*-alanine (*L*-Ala) in acetonitrile (Fig. 17a,b). In addition, **34** showed an apparent ICD even with 0.01 equiv. of *L*-Ala, indicating a strong chiral amplification with cooperative interaction in the pendant groups through noncovalent interactions. A very small chiral bias in the pendant crown units complexed with *L*-Ala is significantly amplified and induces the same helix on the major free crown ether units. Because of the high sensitivity of **34** to the chirality of amino acids, all the common 19 *L*-amino acids as well as some amino alcohols derived from the amino acids produced the same Cotton effect signs. This indicates that for detecting the amino acid chirality, **34** is indeed among the most sensitive and practically useful synthetic receptors.

Interestingly, even a 5% ee of alanine gave rise to the full ICD in **34** as induced by optically pure alanine (Fig. 17c), indicating a very strong majority rule (positive nonlinear) effect between the ee of amino acids and the observed ICD intensity [88]. This noticeable chiral amplification of **34** made it possible to detect an extremely small enantiomeric imbalance in the amino

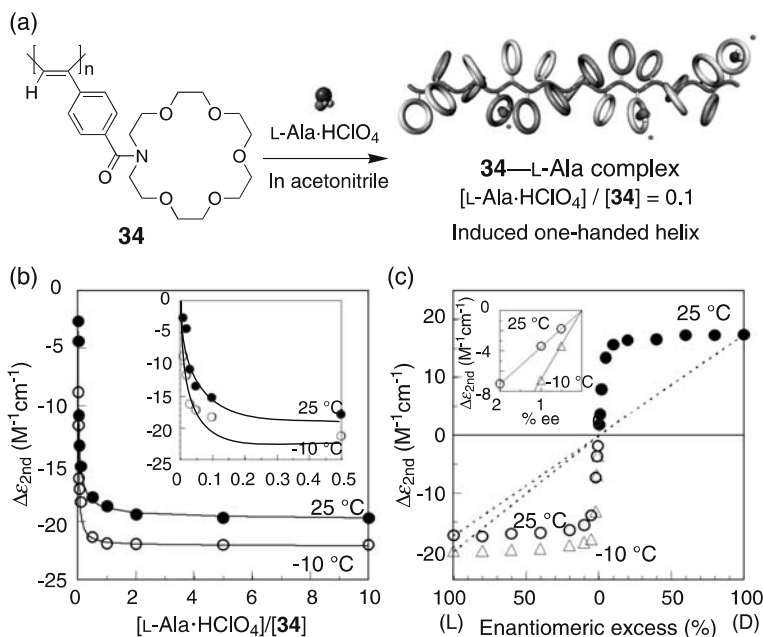


Fig. 17 Schematic illustration of helicity induction on **34** upon complexation with a small amount of L-Ala·HClO₄ (a). Titration curves of **34** with L-Ala·HClO₄ in acetonitrile at 25 and -10 °C (b). Changes in ICD intensity ($\Delta\epsilon_{2nd}$) of **34** versus the % ee of L-Ala·HClO₄ during the complexation with **34** in acetonitrile at 25 and -10 °C (c). (Reprinted with permission from [88]. Copyright 2003 American Chemical Society)

acids, for instance, alanine of less than 0.005% ee, showing an apparent ICD. This method will enable the detection of the chirality of the amino acids with a very small ee and determine their optical purities without derivatization (Fig. 17c). Because of the recent remarkable developments in nanotechnology, the right- and left-handed helically twisted **34** induced by L- and D-Ala, respectively, can be directly observed using AFM when the complexes were deposited on mica (Fig. 18) [91].

In order to mimic the specific interactions occurring in biological events, a number of synthetic receptor molecules have been prepared, but they usually show a chiral or chirality recognition in organic media, and the chiral recognition of charged biomolecules in water through polar interactions remains very difficult. This is because small electrolytes predominantly dissociate into free ions in water by hydration, so that attractive polar interactions such as hydrogen bonding and electrostatic interactions between the host and guest molecules may not be anticipated in water. On the other hand, biological macromolecules such as DNA and proteins are typical polyelectrolytes and have a sophisticated molecular recognition

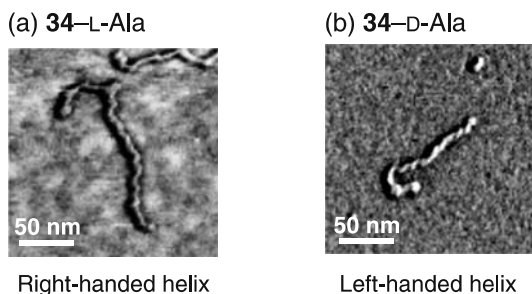


Fig. 18 Typical tapping-mode AFM images of **34** in the presence of L-Ala (a) and D-Ala (b) on mica. (Reprinted with permission from [91]. Copyright 2004 Wiley)

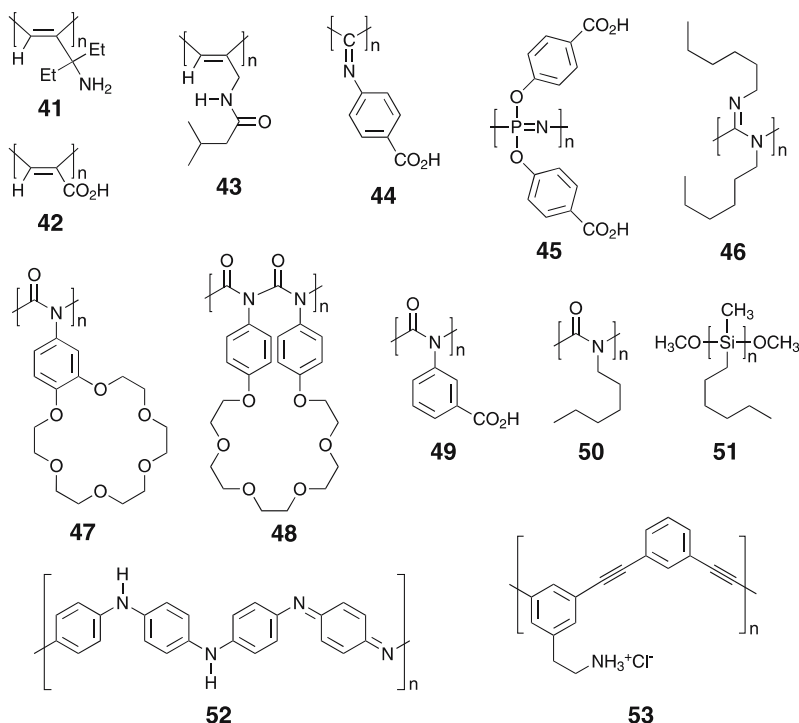
and catalytic activity in aqueous solution, since a portion of the counterions are bound to charged polyelectrolytes, which enables the interaction with small charged molecules even in water. This counter ion condensation effect is a characteristic feature of polyelectrolytes, and may provide an important clue for designing charged synthetic receptors for biomolecular recognition in water [92]. On the basis of these considerations, we attempted the one-handed helicity induction in chromophoric polyelectrolytes (**29**, **30**, and the sodium salt of **28**) (Fig. 14) and found that these polyelectrolytes can interact with a variety of charged and noncharged biomolecules including amino acids, aminosugars, carbohydrates, and peptides in water. The complexes formed supramolecular assemblies with controlled helicity through electrostatic and hydrogen bonding interactions in water and exhibited characteristic ICDs in the UV-visible regions [80, 93]. **29** and **30** bearing a phosphonate group as the pendant group, bioinspired by the interaction motifs of nucleic acids, exhibited the ICDs in the presence of L-amino acids without derivatization in water. Especially, **30** produced the same Cotton effect sign in response to all 19 of the common free L-amino acids, demonstrating that the polyelectrolyte is the first powerful chirality-sensing probe in water.

The hydrochloride of **32** (**32-HCl**) bearing an ammonium group is a positively charged polyelectrolyte, and can respond to the chirality of various acids including carboxylic, phosphoric, and sulfonic acids in water with an extremely high sensitivity, thus forming a single-handed helical conformation in the presence of a small amount of chiral acids ($[\text{chiral acid}]/[\text{32-HCl}] = 0.1$) even with a low ee in water [94]. The polyelectrolyte function of the **32-HCl** plays an important role in the high chiral amplification property of this polymer in water, because the neutral **32** is not sensitive to the chirality of chiral acids in organic solvents [83] and requires a large excess amount of chiral acids to exhibit the full ICD. This finding will contribute to the design and construction of more sensitive helical polyacetylenes for the detection of chirality of target molecules in water.

3.2

Other Helical Polymers and Oligomers

The one-handed helicity induction concept has also been applied to other optically inactive, chromophoric polymers or oligomers through noncovalent bonding interactions. Aliphatic polyacetylenes (**41**, **42**, **43**) [95–97], poly(phenyl isocyanide) (**44**) [98], poly(organophosphazene) (**45**) [99], polyguanidine (**46**) [100], polyisocyanates (**47–50**) [101–104], polysilane (**51**) [105], polyaniline (**52**) [106], and poly(*m*-phenylene ethynylene) (**53**) [107] are such examples, in which chiral ionic and hydrogen bonding interactions as well as acid-base interactions are used for the helicity induction. A similar, but weak chiral amplification was observed in **45** and **47**. Chiral solvation can also be used to induce a helical conformation with an excess helix-sense in dynamic helical polyisocyanate (**50**) and polysilanes (**51**, **54**) with no functional pendant groups, although its chiral bias seems to be very weak. The helicity induction was detected by the appearance of ICD in the UV-visible region of the polymer backbones. However, this method may not be applicable for general use as a chirality-sensing probe of chiral solvents due to the complexity of the interaction mechanism and practical nonfeasibility.



Structure 5

Fujuki et al. reported supramolecular helical aggregates of a dynamically racemic helical **54** in solution containing chiral alcohols such as **55** as the co-solvent, resulting in the appearance of an ICD through amplification of the chirality of alcohols (Fig. 19) [108]. The ICD sign reflects the position of the hydroxyl group and the absolute configuration of the alcohols. Therefore, this system has great potential to be of general use for the chirality sensing of chiral alcohols.

A similar helicity induction may be possible for dynamic helical peptides when a suitable functional group is attached to the end or pendant group. Inai et al. took advantage of the helicity induction concept combined with the dynamic helical feature of an optically inactive oligopeptide **56** with the *N*-terminal amino group [109, 110]. The peptide produced an ICD derived from the one-handed helical conformation of the entire peptide chain upon complexation with chiral carboxylic acids to the *N*-terminal amino group. This phenomenon was called the “noncovalent domino effect”. A similar, but covalent terminus-triggered one-handed helicity induction has been reported for polyisocyanates [111–113] and oligosilanes [114].

A zinc(II) meso-meso linked porphyrin oligomer **57** exists in a nonhelical conformation in solution, but may adopt a dynamic helical conformation upon complexation with an achiral urea **58** through complementary hydrogen bonding interactions [115]. In the presence of the chiral diamine (*S*)-**59**, the **57**–**58** complex forms a predominantly one-handed helical conformation, thus showing a characteristic ICD in the absorption region of the porphyrin chromophore. This system may be used to sense the chirality of chiral diamines.

The π -conjugated achiral oligo(*m*-phenylene ethynylene) **60** (Fig. 20) adopts a random conformation in solvophilic solvents such as chloroform,

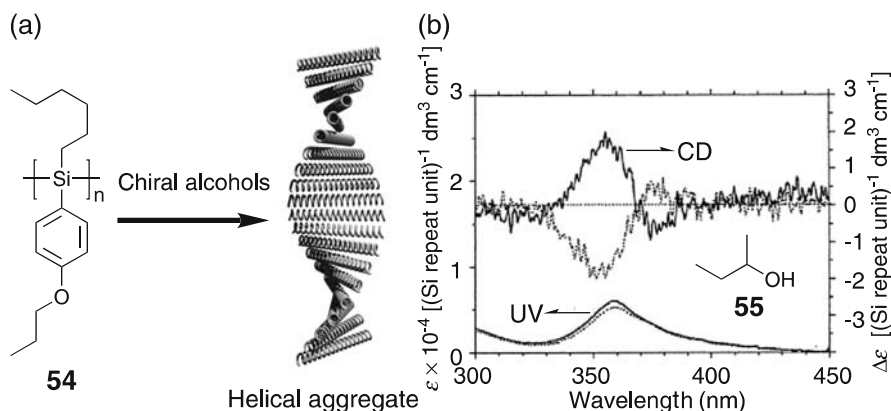
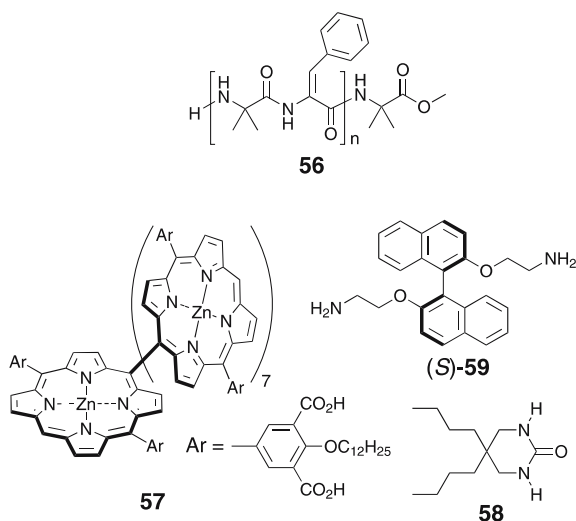


Fig. 19 **a** Schematic illustration of the formation of one-handed helical aggregates of polysilane **54** in the presence of chiral alcohols. **b** CD and UV spectra of **54** aggregates in the presence of chiral alcohol **55** in toluene-methanol mixtures at 20 °C. (Reprinted with permission from [108]. Copyright 2001 American Chemical Society)



Structure 6

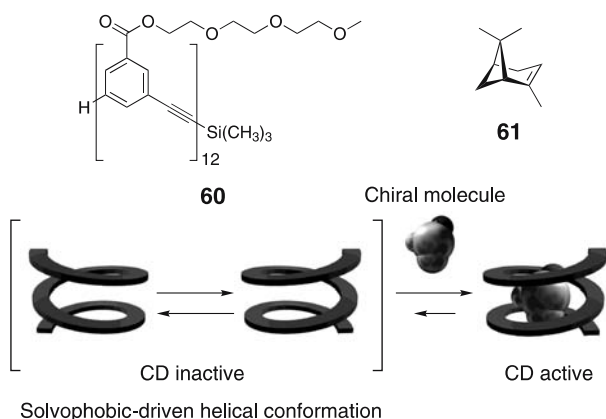
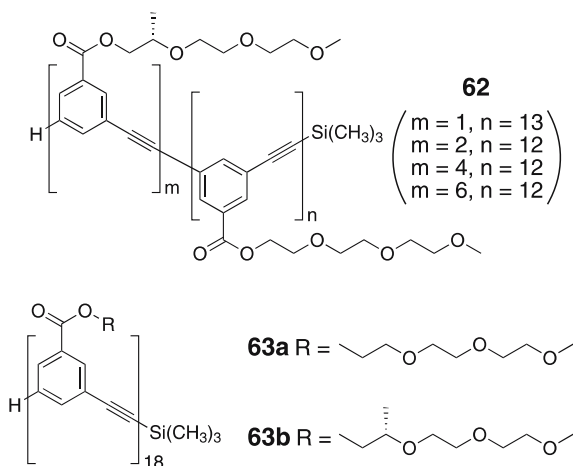


Fig. 20 Schematic illustration of a predominant one-handed helix induction in **60** by inclusion complex formation with a chiral guest molecule **61**

which solvophobically folds into right- and left-handed helical conformations in polar solvents such as acetonitrile and in aqueous solution. Oligomers like **60** possessing a strong tendency to adopt a specific folded conformation are called “foldamers” [16, 116]. The foldamer **60**, both helices of which are at equilibrium, has a specific tubular hydrophobic cavity. As a result, **60** forms a predominantly one-handed helical conformation by the diastereoselective complexation with chiral monoterpenes such as **61** in polar solvents and the complex exhibits a characteristic ICD (Fig. 20) [117]. The introduction of a small amount of chiral side chains into the foldamers (**62**) can also cooperatively bias the helical handedness of a solvophobically folded heli-

cal conformation, thus showing a positive nonlinear dependence of the ICD magnitude against the amount of the chiral side chains [118]. Mixtures of the chiral and achiral oligomers **63** form columnar aggregates of stacked helices in an aqueous acetonitrile solution, where the noncovalent intermolecular sergeants and soldiers effect takes place, resulting in the formation of a one-handed helical column composed of the major achiral **63a** units assisted by a small amount of chiral **63b** [119]. By introducing pyridyl groups, the resulting *m*-ethynylpyridine oligomer **64** folds into a one-handed helical conformation in the presence of saccharides such as **65** through intermolecular hydrogen bonding in apolar solvents, thus showing a similar ICD in the long-wavelength region (Fig. 21) [120].



Structure 7

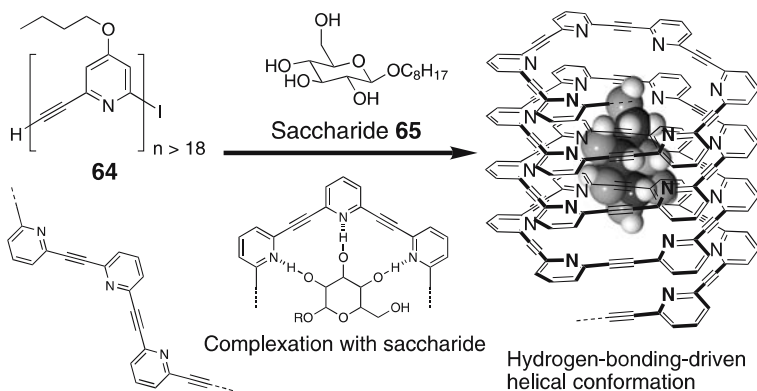


Fig. 21 Schematic illustration of a predominantly one-handed helix induction in **64** by hydrogen bonded complex formation with a chiral saccharide **65**

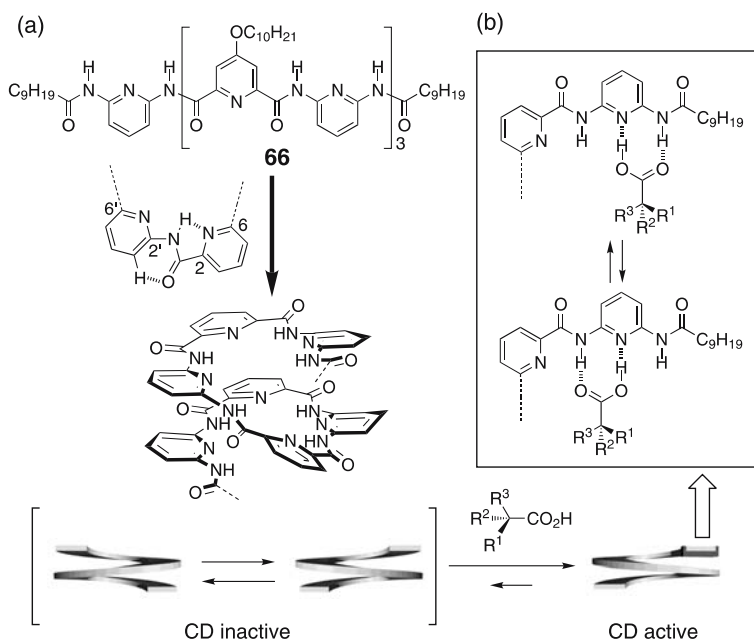


Fig. 22 **a** Schematic illustration of a predominantly one-handed helix induction in **66** upon complexation with chiral carboxylic acids. **b** Expected hydrogen-bonding modes

The pyridinedicarboxamide oligomer **66** folds into a helical conformation by intramolecular hydrogen bonding (Fig. 22) [121]. Although **66** exists in a mixture of right- and left-handed helices, the helical handedness of **66** can be biased through chiral hydrogen bonding interactions at the terminal acyl aminopyridine units of **66** in the presence of chiral carboxylic acids, and the complexes exhibit an ICD. Interestingly, the single helices of **66** can form a double helical molecular duplex depending on the concentration of **66** and temperature [122]. A similar one-handed helicity induction will be applicable for the duplex of **66**.

3.3

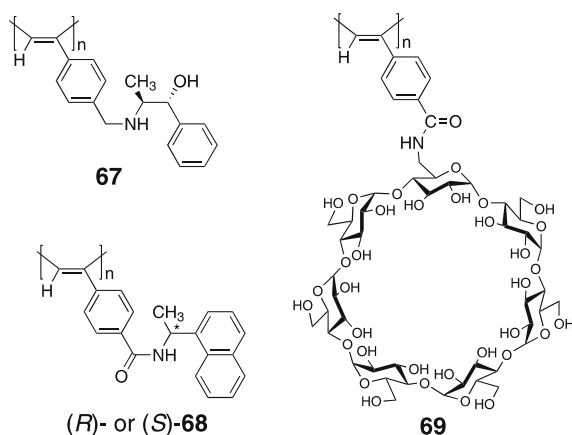
Chirality Sensing by Helix Inversion

Several biopolymers and synthetic optically active polymers are known to exhibit an inversion of helicity (helix–helix transition) between right- and left-handed helical conformations when changing the external conditions, such as solvent, temperature, or by light irradiation. However, switching of the macromolecular helicity by chiral stimuli is rare, and can be used to sense the chirality of specific chiral guests. The helicity of optically active helical poly(phenylacetylene)s **67–69** can be switched by external chiral and achiral stimuli [123–126]. The first example of such a helix inversion induced by

external chiral stimuli through diastereomeric, noncovalent acid-base interactions was reported for a poly(phenylacetylene) **67** bearing an optically active (1*R*, 2*S*)-norephedrin residue [124]. **67** is an optically active polymer and exhibited an ICD in the long-wavelength region due to a predominantly one-handed helical conformation in DMSO. However, the addition of (*R*)-mandelic acid ((*R*)-**70**) produced an inversion of the Cotton effect signs, suggesting that **67** undergoes a transition from one helix to another in the presence of (*R*)-**70** in DMSO (Fig. 23). On the other hand, the ICD of **67** hardly changed even in the presence of excess (*S*)-**70**. The underlying principle for this phenomenon may be based on the small difference in the free energy between the right- and left-handed helices of the polyacetylene, even though the polymer is optically active. Such a delicate balance between the helices may lead to such a helix inversion by responding to the chirality of the acids. In this particular system, the chirality can be determined by the change in the CD.

A similar chiral stimuli-responsive, macromolecular helicity inversion was also observed for (*R*)- or (*S*)-**68** bearing an optically active (1-(1-naphthyl)ethyl)carbamoyl group by interacting with optically active small molecules, such as (*R*)- and (*S*)-**39** (Fig. 15) [126]. The ICD of (*R*)-**68** or (*S*)-**68** in DMF changed to almost a mirror image in the presence of an excess of (*R*)- or (*S*)-**39**, respectively. Thus, optically active **39** can be used to regulate the helix-sense of **68**.

The introduction of an optically active host molecule such as β -cyclodextrin at the pendant group of a poly(phenylacetylene) (**69**) results in a particularly interesting chirality-sensing system. The optically active **69** exhibits a remarkable macromolecular helicity inversion accompanied by a visible color change induced by inclusion complexation with particular guest molecules into the cyclodextrin cavity as well as by solvent and temperature [125]. **69** showed a color change (from yellow to orange to red) with a negative first



Structure 8

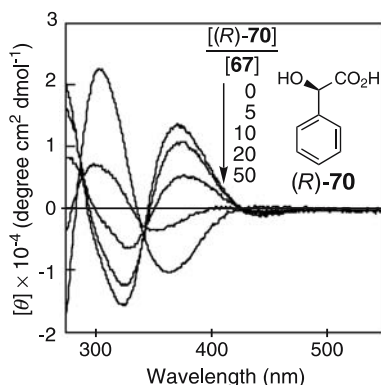


Fig. 23 CD spectral changes of **67** (1 mg mL^{-1}) with (*R*)-**70** in DMSO at room temperature. (Reproduced with permission from [124]. Copyright 1998 American Chemical Society)

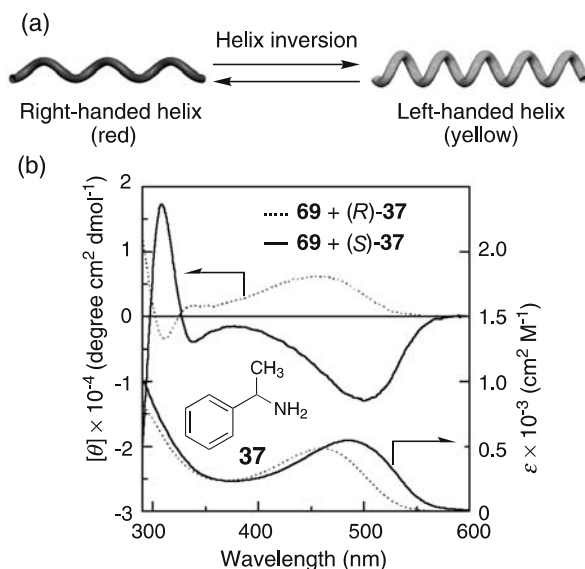


Fig. 24 **a** Schematic illustration of interconvertible right- (*red*) and left-handed (*yellow*) helices of **69**. **b** CD and absorption spectra of **69** (1 mg mL^{-1}) with (*S*)-**37** (solid lines) and (*R*)-**37** (dotted lines) in DMSO-alkaline water (pH 11.7) (3/7, v/v) at room temperature. (Reproduced with permission from [125]. Copyright 2001 American Chemical Society)

Cotton effect sign in the presence of (*S*)-**37** in DMSO/alkaline water (3/7, v/v), while the solution color remained yellow with a positive first Cotton effect sign in the presence of (*R*)-**37** (Fig. 24). The chirality of **37** might induce the macromolecular helicity inversion of **69**, which can be readily visible with the naked eye. The color change may be due to a change in the twist angle of

the conjugated double bonds. As a result, the helical pitch can be tunable. This system seems to be a conceptually new chirality-sensing method using a helical polymer as a color indicator.

3.4

Memory and Storage of Helical Chirality

The macromolecular helicity induced in poly(phenylacetylene)s **28–30** (Fig. 14) upon complexation with chiral amines is dynamic in nature, and therefore, the ICD due to the helical chirality immediately disappears when exposed to a stronger acid such as trifluoroacetic acid. However, during the intensive exploration of the helicity induction and chirality amplification mechanism of the poly(phenylacetylene)s, such an induced helical chirality of **28–30** by an optically active amine such as (*R*)-**39** has been found to be maintained, namely “memorized”, when the chiral amine is completely removed and replaced by various achiral amines, for example, **71** and **72** for **28** and diamines such as ethylenediamine for **29** and **30** in

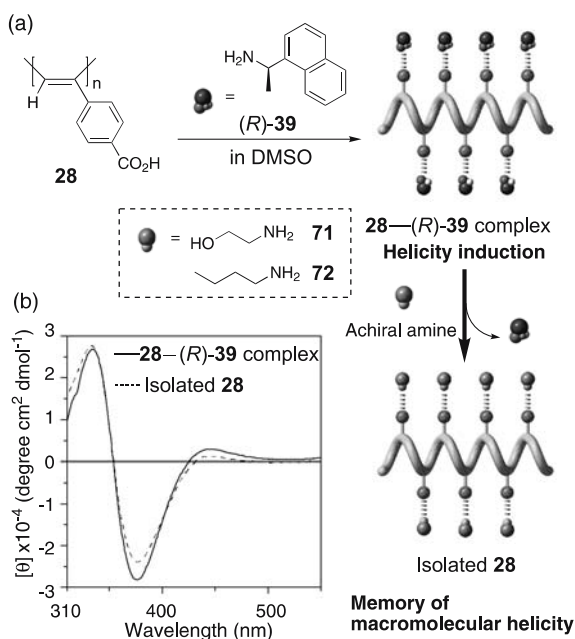


Fig. 25 **a** Schematic illustration of helicity induction in **28** upon complexation with (*R*)-**39** and memory of the induced macromolecular helicity after replacement by achiral amines (**71**, **72**). **b** CD spectra of the **28**-(*R*)-**39** complex (solid line) and the isolated **28** by SEC fractionation using a DMSO solution containing an achiral amine **71** as the eluent (dashed line) in DMSO. (Reproduced with permission from [128]. Copyright 2004 American Chemical Society)

DMSO (Fig. 25) [81, 127, 128]. The memory of the macromolecular helicity was not transient but lasted for an extremely long time (over two years). The memory efficiency was influenced by small structural changes in the achiral amines.

The one-handed helicity of **28** induced by a small amount of chiral (*R*)-**39** and subsequently amplified by an achiral amine **40** (Fig. 16) can also be memorized in the same way by the replacement of (*R*)-**39** and **40** with achiral amines [87]. The chiral amplification combined with the macromolecular helicity memory will offer a highly sensitive, chirality sensing method for chiral molecules even when their optical activities are too small to detect by conventional spectroscopic means.

The noncovalent helicity induction and chiral memory concept is versatile enough to produce and maintain either a right- or left-handed helix because the helix-sense is predetermined by the chirality of the enantiomeric amines used. Consequently, the opposite enantiomeric helicity induction and the memory requires the opposite enantiomeric amine, followed by replacement with achiral amines. However, both mirror-image enantiomeric helices can be produced with a high efficiency from a helical poly(phenylacetylene) induced by a single enantiomer (Fig. 26) [129]. This “dual memory” of enantiomeric

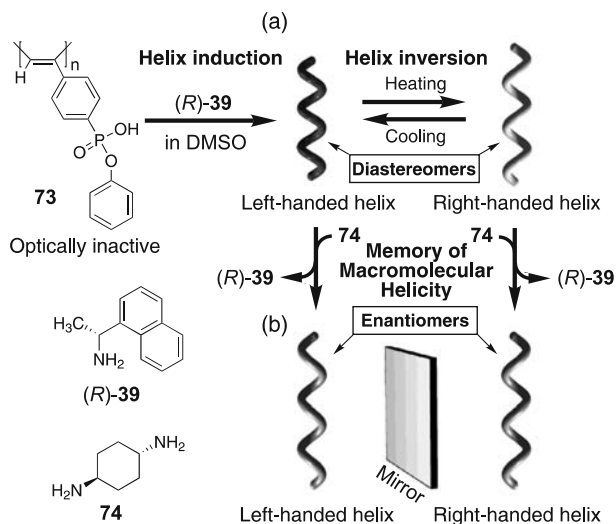


Fig. 26 Schematic illustration of an induced one-handed helicity in optically inactive **73**, helix inversion with temperature, and subsequent memory of the diastereomeric macromolecular helicity at different temperatures. The left-handed helical conformation of **73** induced by (*R*)-**39** at low temperature reversibly changes into the opposite right-handed helix at high temperature (a), and these diastereomeric helices of **73** are memorized at different temperatures by replacement of the (*R*)-**39** with achiral **74**, resulting in the formation of the enantiomeric mirror image helices of **73** (b). (Reproduced with permission from [129]. Copyright 2005 American Chemical Society)

helices is based on the inversion of the macromolecular helicity with temperature. A *cis-transoidal* poly(phenylacetylene) **73** forms a one-handed helix induced by (*R*)-**39** at 25 °C in DMSO, whose helix-sense inverts at 65 °C, as evidenced by the inversion of the Cotton effect signs. These diastereomeric right- and left-handed helices of **73** obtained at 25 and 65 °C can be further memorized by an achiral diamine such as **74** at those temperatures, thus showing the perfect mirror image Cotton effects and identical absorption spectra.

Macromolecular helicity memory is possible in organic solvents, but was difficult to realize in water, because the polymer retains the helicity memory only when complexed with achiral molecules such as achiral amines; therefore, the memory in water is lost. However, a new approach based on the fabrication of layer-by-layer (LbL) assembled multilayer thin films has made possible the macromolecular helicity memory in water (Fig. 27) [130]. A one-handed helicity in a negatively charged poly(phenylacetylene) **30** was first induced by a chiral amine such as (*S*)-**75** in water, thus showing a full ICD. Subsequently, the **30**-(*S*)-**75** complex was deposited on a substrate and then an achiral positively charged vinylpolymer such as the hydrochloride of poly(allylamine) (PAH) was LbL assembled. The chiral guest molecules used as a helix inducer were automatically removed during the LbL assembly process, resulting in optically active thin films with a macromolecular helicity memory. When a positively charged, induced helical **32**-HCl was used instead, the alternative deposition of an achiral vinylpolymer with opposite charges

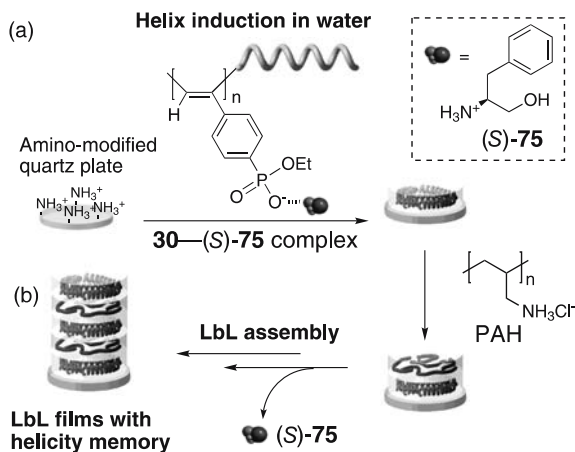


Fig. 27 Schematic illustration of the LbL self-assembly of a charged poly(phenylacetylene) with induced macromolecular helicity. **a** An excess of the one-handed helical sense is induced in **30** upon complexation with the optically active (*S*)-**75** in water. **b** An induced helical **30** can be LbL assembled with an achiral polyelectrolyte having opposite charges (PAH), resulting in multilayer thin films with an induced macromolecular helicity on a substrate

produced a similar thin film with the macromolecular helicity memory. These optically active multilayer thin films will be used as novel chiral materials for enantioseparation and catalysis after the deposition of specific metals.

The chiral memory effect has also been observed in other supramolecular systems [131–142] as well as in helical poly(phenylacetylene)s, but the use of achiral guests is indispensable for the maintenance of the memory effect. That is, in the absence of the achiral guest, the memory will be instantly lost. However, such a dynamic memory in **30** bearing a phosphonic acid mono ethyl ester as the pendant group can be “stored” after the pendant group is converted to its methyl ester with diazomethane, resulting in the generation of a phosphorus stereogenic center with optical activity (Fig. 28) [143]. The esterification enantioselectively proceeds through chirality transfer from the induced helical conformation or the helicity memory of the polyacetylene backbone. Although the enantioselectivity is low (4–11% ee), the pendant chirality is significantly amplified in the polymer backbone at low temperatures, resulting in a higher optical activity as an excess single-handed helix than that expected from the ee of the pendant groups; the helix-sense excess of the polymer is in the range of 15–62% ee at -95°C . This helicity storage concept may be applicable for the detection and sensing of chirality of a particular guest when the induced one of the enantiomeric twisted or helical conformers by the guest is too labile to measure the optical activity.

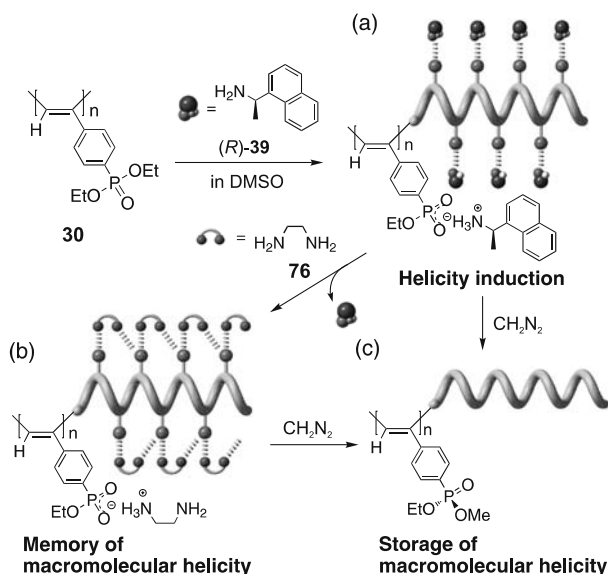


Fig. 28 Schematic illustration of a helicity induction in **30** upon complexation with *(R)*-**39** (a), memory of the induced macromolecular helicity after replacement by achiral **76** (b), and storage of the induced helicity or helicity memory by asymmetric esterification with diazomethane (c)

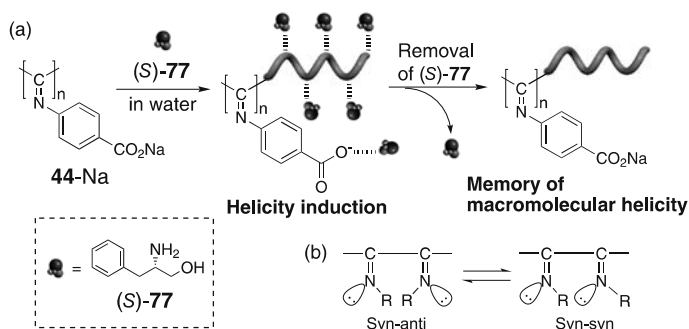


Fig. 29 **a** Schematic illustration of a helicity induction in **44-Na** upon complexation with (S)-77 and memory of the induced macromolecular helicity after complete removal of (S)-77. **b** *Syn-anti* configurational isomerization of the C = N double bond of polyisocyanide backbone

A similar, but unprecedented memory of macromolecular helicity induced in an achiral charged poly(phenyl isocyanide), the sodium salt of **44** (**44-Na**) in water, has recently been reported (Fig. 29) [144]. The polymer folds into a one-handed helix induced by interactions with optically active amines such as (S)-77 and this helicity is automatically memorized even after complete removal of the optically active amine in water. In sharp contrast to the conformational memory of poly(phenylacetylene)s, configurational isomerization around the C = N double bonds (*syn-anti* isomerization) may take place during the helix formation of **44-Na**; that is, an imino configurational mixture of *syn* and *anti* of the optically inactive **44** is transformed into one of a single configuration upon complexation with chiral amines, and this configurational homogeneity then forces a helical conformation on the polymer backbone, which is influenced by the chiral amines, to take an excess helical sense (Fig. 29b). The significant advantage of this helicity memory over that of helical poly(phenylacetylene)s is that there is no longer a need to have the achiral chaperoning amines to retain the helicity in the polymer, so that further modifications of the side groups with a variety of functional groups can be possible along with maintaining the macromolecular helicity memory.

3.5

Chirality Sensing in Gel and Solid

A predominantly one-handed helix can be induced in poly(phenylacetylene) gels (**78**, **79**) and solid films (**28**) bearing a carboxy pendant group as well as in solution. The gels **78** and **79** were synthesized either by the copolymerization of (4-carboxyphenyl)acetylene with a bis(phenylacetylene) as the cross-linker using a rhodium catalyst or by the cross-linking of **28** with a diamine, respectively. The gels significantly swelled and exhibited an ICD in the main chain

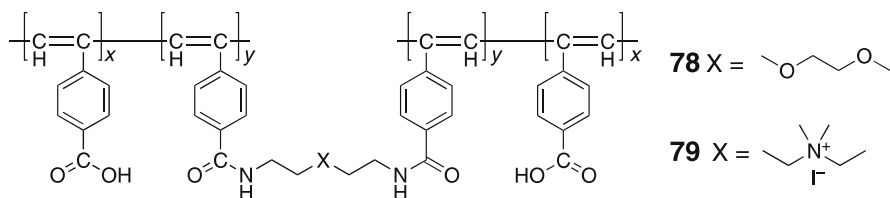
absorption region in the presence of optically active amines in DMSO and alkaline water [145], resulting in the first example of a chirality-responsive gel. The aza-18-crown-6 ether-bound poly(phenylacetylene) (**34**) also forms a predominantly one-handed helix upon complexation with optically active bis(amino acid)s such as L-homocystine perchlorate (L-HCys) in acetonitrile, resulting in an optically active gel, exhibiting an ICD [146]. The gelation of **34** is highly sensitive to the structure and chirality of the bisammoniums with a different distance between the separated charges, and achiral diamines with a similar structure to L-HCys gave rise to no gelation. In addition, the racemic L-HCys did not gel **34**, while HCys of more than 60% ee produced gelation with a full ICD as intense as that of the 100% ee of HCys. This is the first observation of a helical gel induced and assisted by noncovalent chiral interactions in an enantioselective fashion.

A cast film of **28** also responded to the chirality of liquid and solid chiral amines, and exhibited an ICD in the UV-visible region. The observed Cotton effect patterns were similar to those of **28** induced by the chiral amines in solution [147]. These methods are more convenient and practically feasible to sense the chirality of chiral amines than the solution method, and may be applicable to other dynamic helical polyacetylenes.

3.6

Sensing and Amplification of Chirality in Liquid Crystal

Doping nematic liquid crystal (LC) phases with nonracemic molecules can induce cholesteric or twisted nematic LC phases. This process is highly sensitive to a small bias of chirality and is a powerful tool for amplifying and detecting chirality [148, 149]. This implies that, if dynamic helical poly(phenylacetylene)s formed a cholesteric LC phase induced by a chiral dopant, their helix-sense excesses would be further amplified in the LC state over that in dilute solution because each helical polymer chain can interact with others, thus leading to a tightening of the cholesteric pitch [150]. In fact, water-soluble **32-HCl** (Fig. 30) has been found to form a lyotropic, nematic LC in concentrated water (> 8 wt %) and the LC phase changed into a cholesteric one by the addition of a tiny amount of optically active acids such as (S)-**80**. This first example of the liquid crystalline poly(phenylacetylene) is based on its main chain stiffness in water [151]. The macromolecular helicity induced in **32-HCl** by (S)-**80** in dilute solution was further amplified in the LC state (Fig. 30). The helical pitch reached an almost constant value at 0.01 to 0.1 equiv. of (S)-**80** in the LC state, while a higher excess (S)-**80** (0.1–0.3 equiv.) was required in dilute solution for the appearance of the full ICD. Because of its high sensitivity in the LC state, the **32-HCl** showed an apparent cholesteric LC phase of well-defined fingerprint patterns even in the presence of 0.0005 equiv. of (S)-**80**. Furthermore, **32-HCl** exhibited an extremely strong nonlinear effect (majority rule) for the ee of **80** in the LC phase (Fig. 31); the helical



Structure 9

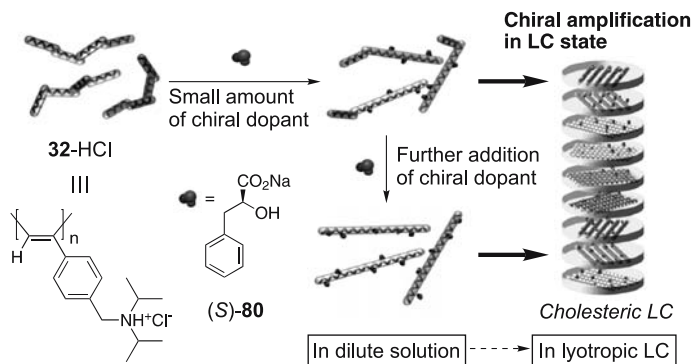


Fig. 30 Schematic illustration of chiral amplification in macromolecular helicity of 32-HCl in dilute solution and liquid crystalline (LC) state. (Reproduced with permission from [151]. Copyright 2004 American Chemical Society)

pitch decreased with the increasing ee and reached a constant value at about 10% ee, whereas in dilute solution, the ICD value became constant at over 60% ee. In the LC state, once an excess of one helical sense is induced in a 32-HCl chain with nonracemic dopants, the same helical sense can be induced in the dynamically racemic helical 32-HCl chains of the nearest neighbors through interchain interactions in the LC state, so that all the polymer chains are transformed into a one-handed helix, resulting in the cholesteric LC phase with amplification of the helical chirality (Fig. 30).

4

Supramolecular Assembly of Helical Polymers

Biological macromolecules such as DNA and proteins are typical polyelectrolytes, which further hierarchically self-assemble into complicated supramolecular structures such as coiled coil (helix bundle) superstructures, which are responsible for their sophisticated functions [152, 153]. Therefore, with implications for biological superstructures and functions, the design and synthesis of supramolecular helical assemblies with a controlled helicity have attracted great interest.

44-Na with a macromolecular helicity memory is an optically active polyelectrolyte with negative charges, which can serve as the template for further helicity induction in a different achiral polyelectrolyte with opposite charges in water (“helicity-replication”), resulting in biomimetic helix bundles and helical assemblies with controlled helicity in water (Fig. 32) [154]. As described above, **44-Na** forms a one-handed helix upon complexation with chiral amines in water and the induced macromolecular helicity can be memorized after complete removal of the chiral helix inducers. Although the polymer no longer has any chiral components and stereogenic centers, the macromolecular helicity memory of the polymer is efficiently transformed into an optically inactive, cationic polyelectrolyte **32-HCl** through electrostatic interaction, resulting in the appearance of an ICD in the **32-HCl** chromophore region due to an excess one-handed helicity induced in **32-HCl**. These he-

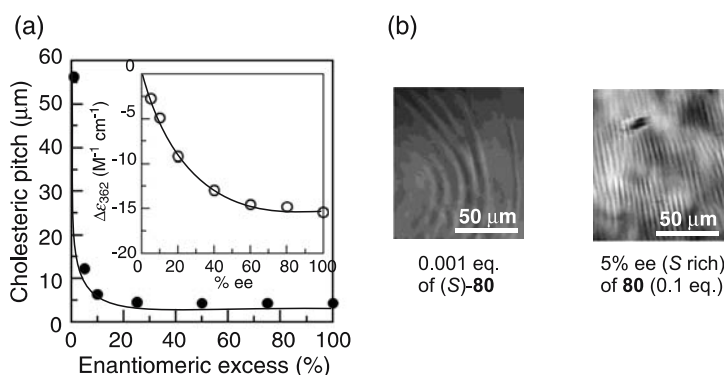


Fig. 31 **a** Changes in the cholesteric pitch and ICD intensity of **32-HCl** versus the enantiomeric excess (% ee) of **80** (S rich) in concentrated (20 wt %) and dilute (*inset*, 1 mg mL⁻¹) water solutions. **b** Polarized optical micrographs of cholesteric liquid crystalline phases of **32-HCl** (20 wt %) in the presence of 0.001 equivalent of (S)-**80** and 5% ee (S rich) of **80** (0.1 equivalent) in water. (Reprinted with permission from [151]. Copyright 2004 American Chemical Society)

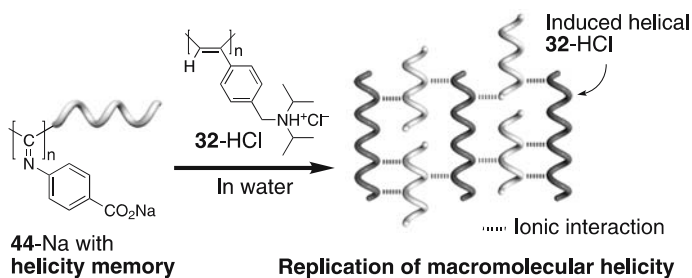


Fig. 32 Schematic illustration of the replication of the macromolecular helicity

lical polyelectrolytes are held together by the simple attraction of opposite charges, but their interpolymer complexations were more difficult to control compared to the complexation between a polymer and small molecules and highly influenced by external conditions such as the pH and salt concentration. This result further provided a new approach for the stepwise replication of the macromolecular helicity through layered helical assemblies with a controlled helix-sense (Fig. 27).

Inganäs et al. have taken advantage of chromophoric, luminescent, and water-soluble π -conjugated polythiophenes and developed sensory systems to detect biopolymers in water. A negatively charged, optically inactive polythiophene **81** and a positively charged, artificial peptide **82** with a random coil conformation self-assemble into a helix bundle in an aqueous solution (Fig. 33) [155]. Interestingly, a one-handed helical conformation and an α -helix are simultaneously induced in both polymers upon complexation through electrostatic interactions by mixing the two polymers in water. When optically active zwitterionic polythiophenes are used instead, their helical assembly properties as detected by CD and emission spectra can be used as a novel sensor for peptide helix bundles [156] and DNA hybridization [157].

Nolte et al. found that an amphiphilic block copolymer **83** composed of a hydrophobic tail of poly(styrene) and a hydrophilic head group of a charged, right-handed helical poly(isocyanide), which is referred to as a “superamphiphile”, self-assembles in a hierarchical fashion in water to form left-handed superhelices (Fig. 34) [158]. They suggest that this type of copolymer will serve as an experimental model for the theoretical study of the packing of helices due to their versatility and easy accessibility.

A noncovalent chiral amplification based on the sergeants and soldiers effect between chiral and achiral polymers in the film state has been developed by Fujiki et al., which results in the formation of helix bundles (Fig. 35) [159]. An optically active, helical polysilane **84** with an almost single-handed screw-sense was chemically bonded or spin-coated on the surface of a quartz plate, followed by further spin-coating of an optically inactive polysilane **85** to give

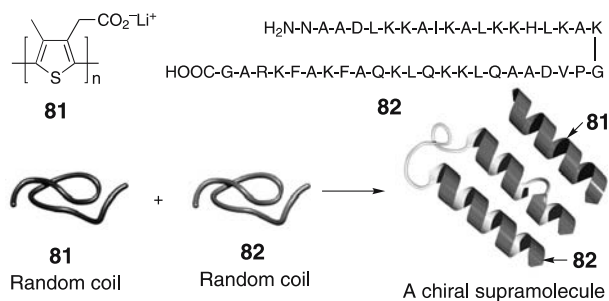


Fig. 33 Schematic illustration of self-assembly of a chiral supramolecule from nonchiral polythiophene polyanion **81** and random coil synthetic peptide **82**

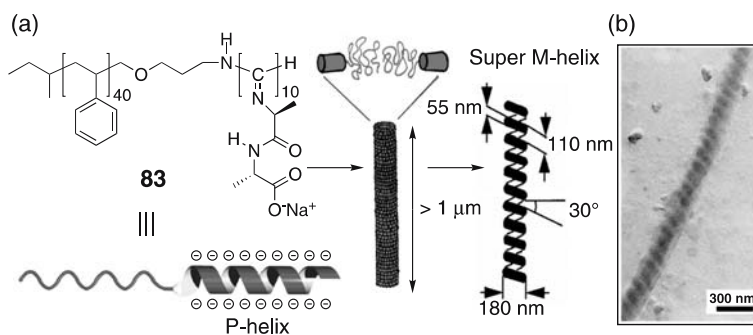


Fig. 34 **a** Schematic illustration of the formation of a superhelix by hierarchical self-assembly of a block-copolymer of isocyanide and styrene **83**. **b** TEM image of a left-handed superhelix from **83**. (Reprinted with permission from [158]. Copyright 1998 American Association for the Advancement of Science)

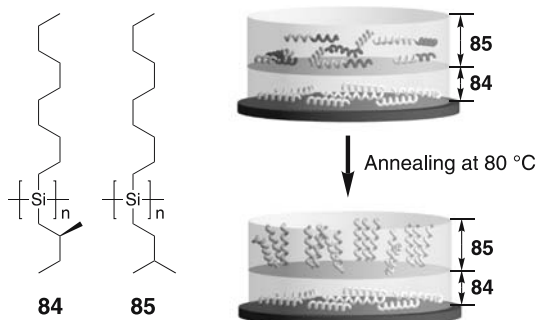


Fig. 35 Schematic illustration of thermally driven chiroptical transfer and amplification of helicity into dynamically racemic helical **85** from one-handed helical **84**

a binary polysilane film. The film showed a dramatic increase in the CD intensity by thermal annealing at 80 °C, while no significant change in the CD intensity was observed for the single layer film composed of only **84** immobilized on a quartz plate. These results indicate that an excess helical sense is induced in the optically inactive **85** as a result of chirality transfer either from the chiral side chain or one-handed helical backbone of **84** through a weak van der Waals interaction between these two different polymers. This effect is also called the “command surface” [160].

5

Conclusion

A large number of chromophoric, helical macromolecules and oligomers, and supramolecular helical assemblies have been constructed by utilizing vari-

ous types of noncovalent bonding interactions. Some have a dynamic feature and may form a dynamic one-handed helix or helical assembly responding to the chirality of guest molecules as evidenced by the examples presented in this review. Here, we have mainly concentrated our attention on the detection and amplification of chirality by dynamic macromolecular and supramolecular helical systems. Chiral amplification, that requires cooperativity, during the transfer of chiral information from nonracemic guests to the helical systems is essential for developing a highly efficient chirality-sensing probe. On the basis of this concept, the rational design of macromolecular and supramolecular receptors is possible by using chromophoric helical (macro)molecules or components for further helical assembly with a dynamic characteristic, combined with functional groups or a suitable cavity for the target chiral guest molecules. In addition, such receptors may be further applied for developing novel chiroptical devices and chiral materials as enantioselective catalysts and adsorbents.

References

1. Saenger W (1984) Principles of nucleic acid structure. Springer, Berlin Heidelberg New York
2. Schulz GE, Schirmer RH (1979) Principles of protein structure. Springer, Berlin Heidelberg New York
3. Okamoto Y, Nakano T (1994) Chem Rev 94:349
4. Green MM, Peterson NC, Sato T, Teramoto A, Cook R, Lifson S (1995) Science 268:1860
5. Nakano T, Okamoto Y (2001) Chem Rev 101:4013
6. Cornelissen JJLM, Rowan AE, Nolte RJM, Sommerdijk NAJM (2001) Chem Rev 101:4039
7. Fujiki M (2001) Macromol Rapid Commun 22:539
8. Yashima E, Matsushima T, Okamoto Y (1995) J Am Chem Soc 117:11596
9. Yashima E, Matsushima T, Okamoto Y (1997) J Am Chem Soc 119:6345
10. Yashima E (2002) Anal Sci 18:3
11. Yashima E, Maeda K, Nishimura T (2004) Chem Eur J 10:43
12. Berova N, Nakanishi K, Woody RW (2000) Circular dichroism: principles and applications, 2nd edn. Wiley, New York
13. Canary JW, Holmes AE, Liu J (2001) Enantiomer 6:181
14. Tsukube H, Shinoda S (2002) Chem Rev 102:2389
15. Allenmark S (2003) Chirality 15:409
16. Hill DJ, Mio MJ, Prince RB, Hughes TS, Moore JS (2001) Chem Rev 101:3893
17. Rowan AE, Nolte RJM (1998) Angew Chem Int Ed 37:63
18. Brunsveld L, Folmer BJB, Meijer EW, Sijbesma RP (2001) Chem Rev 101:4071
19. Schmuck C (2003) Angew Chem Int Ed 42:2448
20. Mateos-Timoneda MA, Crego-Calama M, Reinhoudt DN (2004) Chem Soc Rev 33:363
21. Hoebe FJM, Jonkheijm P, Meijer EW, Schenning APHJ (2005) Chem Rev 105:1491
22. Zhang J, Albelda T, Liu Y, Canary JW (2005) Chirality 17:404
23. Keizer HM, Sijbesma RP (2005) Chem Soc Rev 34:226

24. Constable EC (1992) *Tetrahedron* 48:10013
25. Lehn J-M (1995) *Supramolecular chemistry*. Wiley-VCH, Weinheim, Germany
26. Piguet C, Bernardinelli G, Hopfgartner G (1997) *Chem Rev* 97:2005
27. Albrecht M (2001) *Chem Rev* 101:3457
28. Tachibana T, Kambara H (1965) *J Am Chem Soc* 87:3015
29. Nakashima N, Asakuma S, Kunitake T (1985) *J Am Chem Soc* 107:509
30. Fuhrhop JH, Helfrich W (1993) *Chem Rev* 93:1565
31. Shimizu T, Masuda M, Minamikawa H (2005) *Chem Rev* 105:1401
32. Terech P, Weiss RG (1997) *Chem Rev* 97:3133
33. Van Bommel KJC, Friggeri A, Shinkai S (2003) *Angew Chem Int Ed* 42:980
34. Messmore BW, Sukerkar PA, Stupp SI (2005) *J Am Chem Soc* 127:7992
35. Engelkamp H, Middelbeek S, Nolte RJM (1999) *Science* 284:785
36. Fox JM, Katz TJ, Van Elshocht S, Verbiest T, Kauranen M, Persoons A, Thongpanchang T, Krauss T, Brus L (1999) *J Am Chem Soc* 121:3453
37. Hill JP, Jin W, Kosaka A, Fukushima T, Ichihara H, Shimomura T, Ito K, Hashizume T, Ishii N, Aida T (2004) *Science* 304:1481
38. Jin W, Fukushima T, Niki M, Kosaka A, Ishii N, Aida T (2005) *Proc Natl Acad Sci USA* 102:10801
39. Gallivan JP, Schuster GB (1995) *J Org Chem* 60:2423
40. Nuckolls C, Katz TJ, Castellanos L (1996) *J Am Chem Soc* 118:3767
41. Lovinger AJ, Nuckolls C, Katz TJ (1998) *J Am Chem Soc* 120:264
42. Nuckolls C, Katz TJ, Katz G, Collings PJ, Castellanos L (1999) *J Am Chem Soc* 121:79
43. Mariani P, Mazabard C, Garbesi A, Spada GP (1989) *J Am Chem Soc* 111:6369
44. Bonazzi S, Capobianco M, De Morais MM, Garbesi A, Gottarelli G, Mariani P, Ponzi Bossi MG, Spada GP, Tondelli L (1991) *J Am Chem Soc* 113:5809
45. Gottarelli G, Spada GP (2004) *Chem Rec* 4:39
46. Andrisano V, Gottarelli G, Masiero S, Heijne EH, Pieraccini S, Spada GP (1999) *Angew Chem Int Ed* 38:2386
47. Ciuchi F, Di Nicola G, Franz H, Gottarelli G, Mariani P, Ponzi Bossi MG, Spada GP (1994) *J Am Chem Soc* 116:7064
48. Gottarelli G, Mezzina E, Spada GP, Carsughi F, Di Nicola G, Mariani P, Sabatucci A, Bonazzi S (1996) *Helv Chim Acta* 79:220
49. Kamikawa Y, Nishii M, Kato T (2004) *Chem Eur J* 10:5942
50. Sijbesma RP, Meijer EW (2003) *Chem Commun* 5
51. Jeukens CRLPN, Jonkheijm P, Wijnen FJP, Gielen JC, Christianen PCM, Schenning APHJ, Meijer EW, Maan JC (2005) *J Am Chem Soc* 127:8280
52. Hoebe FJM, Herz LM, Daniel C, Jonkheijm P, Schenning APHJ, Silva C, Meskers SCJ, Beljonne D, Phillips RT, Friend RH, Meijer EW (2004) *Angew Chem Int Ed* 43:1976
53. Jonkheijm P, Hoebe FJM, Kleppinger R, van Herrikhuyzen J, Schenning APHJ, Meijer EW (2003) *J Am Chem Soc* 125:15941
54. Schenning APHJ, Jonkheijm P, Peeters E, Meijer EW (2001) *J Am Chem Soc* 123:409
55. Wurthner F, Chen ZJ, Hoebe FJM, Osswald P, You CC, Jonkheijm P, van Herrikhuyzen J, Schenning APHJ, van der Schoot PPAM, Meijer EW, Beckers EHA, Meskers SCJ, Janssen RAJ (2004) *J Am Chem Soc* 126:10611
56. Schenning APHJ, von Herrikhuyzen J, Jonkheijm P, Chen Z, Wurthner F, Meijer EW (2002) *J Am Chem Soc* 124:10252
57. Feringa BL, van Delden RA (1999) *Angew Chem Int Ed* 38:3419
58. Green MM, Park JW, Sato T, Teramoto A, Lifson S, Selinger RLB, Selinger JV (1999) *Angew Chem Int Ed* 38:3139

59. Soai K, Shibata T, Sato I (2000) *Acc Chem Res* 33:382
60. Noyori R (2002) *Angew Chem Int Ed* 41:2008
61. Green MM, Reidy MP, Johnson RJ, Darling G, O'leary DJ, Willson G (1989) *J Am Chem Soc* 111:6452
62. Jha SK, Cheon KS, Green MM, Selinger JV (1999) *J Am Chem Soc* 121:1665
63. Green MM, Garetz BA, Munoz B, Chang HP, Hoke S, Cooks RG (1995) *J Am Chem Soc* 117:4181
64. Hirschberg JHKK, Brunsveld L, Ramzi A, Vekemans JAJM, Sijbesma RP, Meijer EW (2000) *Nature* 407:167
65. Hirschberg JHKK, Koevoets RA, Sijbesma RP, Meijer EW (2003) *Chem Eur J* 9:4222
66. Brunsveld L, Vekemans JAJM, Hirschberg JHKK, Sijbesma RP, Meijer EW (2002) *Proc Natl Acad Sci USA* 99:4977
67. Palmans ARA, Vekemans JAJM, Havinga EE, Meijer EW (1997) *Angew Chem Int Ed Engl* 36:2648
68. Brunsveld L, Lohmeijer BGG, Vekemans JAJM, Meijer EW (2000) *Chem Commun* 2305
69. Brunsveld L, Zhang H, Glasbeek M, Vekemans JAJM, Meijer EW (2000) *J Am Chem Soc* 122:6175
70. van Gorp JJ, Vekemans JAJM, Meijer EW (2002) *J Am Chem Soc* 124:14759
71. Brunsveld L, Lohmeijer BGG, Vekemans JAJM, Meijer EW (2001) *J Inclusion Phenom* 41:61
72. van Gestel J, Palmans ARA, Titulaer B, Vekemans JAJM, Meijer EW (2005) *J Am Chem Soc* 127:5490
73. Brunsveld L, Schenning APHJ, Broeren MAC, Janssen HM, Vekemans JAJM, Meijer EW (2000) *Chem Lett* 292
74. Lightfoot MP, Mair FS, Pritchard RG, Warren JE (1999) *Chem Commun* 1945
75. Wilson AJ, Masuda M, Sijbesma RP, Meijer EW (2005) *Angew Chem Int Ed* 44:2275
76. de Jong JJD, Lucas LN, Kellogg RM, van Esch JH, Feringa BL (2004) *Science* 304:278
77. de Jong JJD, Tiemersma-Wegman TD, van Esch JH, Feringa BL (2005) *J Am Chem Soc* 127:13804
78. Fenniri H, Deng BL, Ribbe AE (2002) *J Am Chem Soc* 124:11064
79. Fenniri H, Deng BL, Ribbe AE, Hallenga K, Jacob J, Thiagarajan P (2002) *Proc Natl Acad Sci USA* 99:6487
80. Onouchi H, Maeda K, Yashima E (2001) *J Am Chem Soc* 123:7441
81. Onouchi H, Kashiwagi D, Hayashi K, Maeda K, Yashima E (2004) *Macromolecules* 37:5495
82. Yashima E, Maeda Y, Okamoto Y (1996) *Chem Lett* 955
83. Yashima E, Maeda Y, Matsushima T, Okamoto Y (1997) *Chirality* 9:593
84. Maeda K, Okada S, Yashima E, Okamoto Y (2001) *J Polym Sci, Part A: Polym Chem* 39:3180
85. Yashima E, Nimura T, Matsushima T, Okamoto Y (1996) *J Am Chem Soc* 118:9800
86. Kawamura H, Maeda K, Okamoto Y, Yashima E (2001) *Chem Lett* 58
87. Morino K, Watase N, Maeda K, Yashima E (2004) *Chem Eur J* 10:4703
88. Nonokawa R, Yashima E (2003) *J Am Chem Soc* 125:1278
89. Nonokawa R, Obo M, Yashima E (2003) *Macromolecules* 36:6599
90. Nonokawa R, Yashima E (2003) *J Polym Sci, Part A: Polym Chem* 41:1004
91. Sakurai S, Kuroyanagi K, Nonokawa R, Yashima E (2004) *J Polym Sci, Part A: Polym Chem* 42:5838
92. Manning GS (1979) *Acc Chem Res* 12:443
93. Saito MA, Maeda K, Onouchi H, Yashima E (2000) *Macromolecules* 33:4616

94. Nagai K, Maeda K, Takeyama Y, Sakajiri K, Yashima E (2005) *Macromolecules* 38:5444
95. Yashima E, Goto H, Okamoto Y (1998) *Polym J* 30:69
96. Maeda K, Goto H, Yashima E (2001) *Macromolecules* 34:1160
97. Tabei J, Nomura R, Sanda F, Masuda T (2003) *Macromolecules* 36:8603
98. Ishikawa M, Maeda K, Yashima E (2002) *J Am Chem Soc* 124:7448
99. Yashima E, Maeda K, Yamanaka T (2000) *J Am Chem Soc* 122:7813
100. Schlitzer DS, Novak BM (1998) *J Am Chem Soc* 120:2196
101. Maeda K, Yamamoto N, Okamoto Y (1998) *Macromolecules* 31:5924
102. Sakai R, Satoh T, Kakuchi R, Kaga H, Kakuchi T (2003) *Macromolecules* 36:3709
103. Sakai R, Satoh T, Kakuchi R, Kaga H, Kakuchi T (2004) *Macromolecules* 37:3996
104. Green MM, Khatri C, Peterson NC (1993) *J Am Chem Soc* 115:4941
105. Dellaportas P, Jones RG, Holder SJ (2002) *Macromol Rapid Commun* 23:99
106. Majidi MR, Kane-Maguire LAP, Wallace GG (1995) *Polymer* 36:3597
107. Arnt L, Tew GN (2004) *Macromolecules* 37:1283
108. Nakashima H, Koe JR, Torimitsu K, Fujiki M (2001) *J Am Chem Soc* 123:4847
109. Inai Y, Tagawa K, Takasu A, Hirabayashi T, Oshikawa T, Yamashita M (2000) *J Am Chem Soc* 122:11731
110. Inai Y, Ousaka N, Okabe T (2003) *J Am Chem Soc* 125:8151
111. Okamoto Y, Matsuda M, Nakano T, Yashima E (1993) *Polym J* 25:391
112. Okamoto Y, Matsuda M, Nakano T, Yashima E (1994) *J Polym Sci, Part A: Polym Chem* 32:309
113. Maeda K, Matsuda M, Nakano T, Okamoto Y (1995) *Polym J* 27:141
114. Obata K, Kabuto C, Kira M (1997) *J Am Chem Soc* 119:11345
115. Ikeda C, Yoon ZS, Park M, Inoue H, Kim D, Osuka A (2005) *J Am Chem Soc* 127:534
116. Gellman SH (1998) *Acc Chem Res* 31:173
117. Prince RB, Barnes SA, Moore JS (2000) *J Am Chem Soc* 122:2758
118. Prince RB, Moore JS, Brunsveld L, Meijer EW (2001) *Chem Eur J* 7:4150
119. Brunsveld L, Meijer EW, Prince RB, Moore JS (2001) *J Am Chem Soc* 123:7978
120. Inouye M, Waki M, Abe H (2004) *J Am Chem Soc* 126:2022
121. Maurizot V, Dolain C, Huc I (2005) *Eur J Org Chem* 1293
122. Berl V, Huc I, Khoury RG, Krische MJ, Lehn JM (2000) *Nature* 407:720
123. Maeda K, Morino K, Yashima E (2003) *Macromol Symp* 201:135
124. Yashima E, Maeda Y, Okamoto Y (1998) *J Am Chem Soc* 120:8895
125. Yashima E, Maeda K, Sato O (2001) *J Am Chem Soc* 123:8159
126. Morino K, Maeda K, Yashima E (2003) *Macromolecules* 36:1480
127. Yashima E, Maeda K, Okamoto Y (1999) *Nature* 399:449
128. Maeda K, Morino K, Okamoto Y, Sato T, Yashima E (2004) *J Am Chem Soc* 126:4329
129. Miyagawa T, Furuko A, Maeda K, Katagiri H, Furusho Y, Yashima E (2005) *J Am Chem Soc* 127:5018
130. Maeda K, Matsushita Y, Ezaka M, Yashima E (2005) *Chem Commun* 4152
131. Furusho Y, Kimura T, Mizuno Y, Aida T (1997) *J Am Chem Soc* 119:5267
132. Bellacchio E, Lauceri R, Gurrieri S, Scolaro LM, Romeo A, Purrello R (1998) *J Am Chem Soc* 120:12353
133. Sugasaki A, Ikeda M, Takeuchi M, Robertson A, Shinkai S (1999) *J Chem Soc, Perkin Trans 1* 3259
134. Rivera JM, Craig SL, Martin T, Rebek J Jr (2000) *Angew Chem Int Ed* 39:2130
135. Prins LJ, De Jong F, Timmerman P, Reinhoudt DN (2000) *Nature* 408:181
136. Kubo Y, Ohno T, Yamanaka J, Tokita S, Iida T, Ishimaru Y (2001) *J Am Chem Soc* 123:12700

137. Ishi-i T, Crego-Calama M, Timmerman P, Reinhoudt DN, Shinkai S (2002) *J Am Chem Soc* 124:14631
138. Prins LJ, Verhage JJ, de Jong F, Timmerman P, Reinhoudt DN (2002) *Chem Eur J* 8:2302
139. Purrello R (2003) *Nat Mater* 2:216
140. Ziegler M, Davis AV, Johnson DW, Raymond KN (2003) *Angew Chem Int Ed* 42:665
141. Lauceri R, Raudino A, Scolaro LM, Micali N, Purrello R (2002) *J Am Chem Soc* 124:894
142. Lauceri R, Purrello R (2005) *Supramol Chem* 17:61
143. Onouchi H, Miyagawa T, Furuko A, Maeda K, Yashima E (2005) *J Am Chem Soc* 127:2960
144. Ishikawa M, Maeda K, Mitsutsuji Y, Yashima E (2004) *J Am Chem Soc* 126:732
145. Goto H, Zhang HQ, Yashima E (2003) *J Am Chem Soc* 125:2516
146. Morino K, Oobo M, Yashima E (2005) *Macromolecules* 38:3461
147. Maeda K, Hatanaka K, Yashima E (2004) *Mendeleev Commun* 231
148. Proni G, Spada GP (2001) *Enantiomer* 6:171
149. Huck NPM, Jager WF, deLange B, Feringa BL (1996) *Science* 273:1686
150. Green MM, Zanella S, Gu H, Sato T, Gottarelli G, Jha SK, Spada GP, Schoevaars AM, Feringa B, Teramoto A (1998) *J Am Chem Soc* 120:9810
151. Maeda K, Takeyama Y, Sakajiri K, Yashima E (2004) *J Am Chem Soc* 126:16284
152. Lupas A (1996) *Trends Biochem Sci* 21:375
153. Burkhard P, Stetefeld J, Strelkov SV (2001) *Trends Cell Biol* 11:82
154. Maeda K, Ishikawa M, Yashima E (2004) *J Am Chem Soc* 126:15161
155. Nilsson KPR, Rydberg J, Baltzer L, Inganäs O (2004) *Proc Natl Acad Sci USA* 101:11197
156. Nilsson KPR, Rydberg J, Baltzer L, Inganäs O (2003) *Proc Natl Acad Sci USA* 100:10170
157. Nilsson KPR, Inganäs O (2003) *Nat Mater* 2:419
158. Cornelissen JJLM, Fischer M, Sommerdijk NAJM, Nolte RJM (1998) *Science* 280:1427
159. Saxena A, Guo GQ, Fujiki M, Yang YG, Ohira A, Okoshi K, Naito M (2004) *Macromolecules* 37:3081
160. Ichimura K (2000) *Chem Rev* 100:1847

Supramolecular Chirogenesis in Host–Guest Systems Containing Porphyrinoids

Victor V. Borovkov (✉) · Yoshihisa Inoue (✉)

Entropy Control Project, ICORP, Japan Science and Technology Agency,
 Kamishinden 4-6-3, Toyonaka-shi, 560-0085 Osaka, Japan
victrb@inoue.jst.go.jp, inoue@chem.eng.osaka-u.ac.jp

1	Introduction	90
1.1	Supramolecular Chirogenesis: Definition, Significance, and Occurrence in Natural Systems	90
1.2	Overview of Latest Reviews	91
2	Supramolecular Systems on the Basis of Monomeric Porphyrinoids	93
2.1	Achiral/Racemic Porphyrinoids	93
2.2	Chiral Porphyrinoids	97
3	Chiral Dimeric/Oligomeric Porphyrinoids Constructed from Achiral Monomers Fixed by Noncovalent Bridges	99
4	Supramolecular Systems on the Basis of Dimeric/Oligomeric Porphyrinoids	105
4.1	Achiral/Racemic Porphyrinoids	105
4.2	Chiral Porphyrinoids	117
4.2.1	Interactions with Achiral Counterparts	118
4.2.2	Interactions with Chiral Counterparts	121
5	Supramolecular Systems on the Basis of Aggregated Porphyrinoids	126
5.1	Monomeric Achiral/Racemic Porphyrinoids	126
5.1.1	Spontaneous Resolution and Stirring Induced Chirality	126
5.1.2	Interactions with Chiral Counterparts	129
5.2	Monomeric Chiral Porphyrinoids	131
5.3	Dimeric/Oligomeric Porphyrinoids	139
6	Concluding Remarks and Future Perspectives	141
	References	142

Abstract Supramolecular chirogenesis is a smart combination of supramolecular chemistry and molecular chirality resulting in effective functioning of living organisms and important implications in modern sciences, technologies and medicines. Recently, amongst the vast number of molecules employed in studying this phenomenon, porphyrinoids have repeatedly been shown to be one of the most suited and versatile chromophores owing to their spectral and physicochemical properties, easy handling and versatile modification, great biological importance, and wide applicability. This is the first comprehensive review of the supramolecular chirogenesis in various porphyrinoid-containing systems, covering the progress made in this field during the last 10 years. In

particular, a variety of chirogenic assemblies based on monomeric, dimeric/oligomeric and self-assembled/aggregated porphyrinoids (both achiral and chiral) upon interaction with chiral/achiral counterparts or external chiral field are described, and the role of various external and internal controlling factors are discussed. The results and subsequent concepts arising from these studies are of consequence and general applicability to various fields of science and technology.

Keywords Supramolecular chemistry · Chirality · Porphyrinoids · Host–guest · Aggregation

Abbreviations

TPP	5,10,15,20-tetraphenylporphyrin
TMP	5,10,15,20-tetra(4- <i>N</i> -methylpyridyl)porphyrin
CE	Cotton effect
CD	circular dichroism
BNP	1,1'-binaphthyl
AA	amino acid
DACH	<i>trans</i> -1,2-diaminocyclohexane
A	CD amplitude

1

Introduction

1.1

Supramolecular Chirogenesis:

Definition, Significance, and Occurrence in Natural Systems

In recent years the considerable progress in the field of supramolecular chemistry and its combination with new insights into molecular chirality has given rise to a new interdisciplinary area of chemistry—supramolecular chirogenesis. The rapid growth in this area derives from its direct relevance to many natural processes and artificial systems, as well as its importance in understanding fundamental chemical principles and vital biological functions, and its applicability to various chiroptical devices, modern molecular technologies, and medicine. This area includes the processes of immediate asymmetry transfer from a chiral guest to an achiral host (or vice versa) via noncovalent interactions, chirality induction in achiral supramolecular complexes affected by the external chiral field and environment, optical activity modulation in supramolecular systems by various controlling factors, chirality amplification of whole assemblies upon association of the individual elements with a low degree of asymmetry, and spontaneous resolution of racemic supramolecular systems.

Supramolecular chirogenesis is widely observed and plays a vital role in a large number of natural systems such as the DNA double helix, the sec-

ondary α -helical structure of proteins, heme proteins, photosynthetic apparatus, etc. [1–4]. In particular, tetrapyrrolic structures are one of the key elements of many important biomolecular assemblies. Hence, this prompted various research groups to investigate various chirality aspects of porphyrinoid-containing natural systems for better understanding of the functional mechanisms and various influencing factors [5–12]. Indeed, the extraordinary intricacy of biological objects gave impetus to the research of a large number of model supramolecules on the basis of tetrapyrrolic pigments. These kinds of macrocycles turned out to be well-suited for studying the processes involved in supramolecular chirality owing to their unique spectral and physicochemical properties, easy handling and versatile modification, thus resulting in numerous examples of various structures and different applications that will be discussed in subsequent sections.

So far, several reviews have been published, some of which refer to supramolecular chirogenic porphyrinoid-containing systems to a greater or lesser extent. Therefore, before moving to specific examples of this area, we shall give an overview of some of these articles.

1.2

Overview of Latest Reviews

The review articles dealing with some aspects of supramolecular chirogenesis can be conventionally divided into four major categories: devoted to various supramolecular systems including chiral and porphyrinoid-containing assemblies; summarizing different molecular and chiral receptors on the basis of porphyrinoids; dealing primarily with circular dichroism (CD) phenomena, enantiomeric excess (ee), and other chirality issues and presenting porphyrinoid structures as examples; and focusing on an alternative subject, while referring to chirogenic phenomena in porphyrins.

The first type includes several recent reviews written by Lawrence, van Nostrum, Hupp, Miyake, MacGillivray and their colleagues, which described various supramolecular and self-assembled systems [13–17]. Amongst the systems described there were several porphyrinoid-based natural and artificial chiral assemblies, such as hemoglobin, porphyrins inside lipid bilayers, porphyrin–cyclodextrin conjugates, porphyrinoid-containing liquid crystals, porphyrin–chiral ligand complexes. Our recent article that summarized some advances in the supramolecular chirogenesis phenomenon in bis-porphyrinoids also fits into this category [18].

To the second class belong a number of articles describing different synthetic receptors possessing molecular and chiral recognition abilities. Ogoshi et al. in several comprehensive reviews summarized the results of using synthetic monomeric and dimeric porphyrins for molecular recognition purposes with few specific examples of chiral porphyrins applicable for chiral recognition and achiral porphyrins interacting with various chiral counter-

parts [19–22]. More specialized articles devoted to porphyrins with different structural features and their application to asymmetric catalysis, chiral recognition, memory systems, CD studies, etc., by Marchon and Ramasseul [23] and by Berova et al. [24] were also recently published. Shinkai et al. thoroughly analyzed a variety of synthetic receptors including those that were porphyrin-based with a particular emphasis placed on saccharide sensing [25–28]. Also a chapter devoted to porphyrin-containing saccharide receptors was included in a broad review on synthetic receptors by Hartley, James, and Ward [29]. Tsukube et al. examined in close detail another type of molecular and chiral sensor—different lanthanide complexes including many porphyrinoid structures [30–32], while Simonneaux and Maux analyzed the application of optically active ruthenium porphyrins for chiral recognition and asymmetric catalysis [33]. Additionally, a few examples of porphyrin-based metalloreceptors for anion binding including chiral recognition were presented by Bondy and Loeb [34].

The third type of review primarily focused on the different aspects of chirality and contained some porphyrin-based supramolecular chirogenic systems as examples. For example, Finn, Wenzel, and Wilcox discussed various methods and reagents for the determination of *ee* and absolute configuration using different spectroscopic approaches [35, 36]; whilst Allenmark, Pasternack, Kobayashi, Formaggio et al. addressed the induced and electronic CD upon the intra- and intermolecular interactions considering several porphyrinoid chromophores [37–40].

The last category was concerned with miscellaneous subjects, while citing some chirogenic porphyrin-based systems. Representative reviews include chiral lanthanide complexes by Aspinall [41], coordination chemistry of tin porphyrins by Arnold and Blok [42], photoprocesses of copper complexes that bind to DNA by McMillin and McNett [43], nonplanar porphyrins and their significance in proteins by Shelnutt et al. [44], cytochrome P450 biomimetic systems by Feiters, Rowan, and Nolte [45] and phthalocyanines by Kobayashi [46, 47].

Thus, this brief overview clearly demonstrates the importance, large diversity, and wide applicability of supramolecular chirogenesis in various fields of chemistry. Although there were numerous reviews devoted to different subjects, which discussed the chirogenic phenomenon in a greater or lesser extent, to-date there has not been a review comprehensively describing the chirogenic behavior of porphyrinoids in supramolecular systems. To fill this gap, we have summarized the most representative developments in this area over the last 10 years to illustrate the major principles, mechanisms, driving forces, and various controlling factors of this phenomenon. The presented examples are classified into several categories according to the complexity of the supramolecular systems: on the basis of monomeric, dimeric/oligomeric and aggregated porphyrinoids, and as intrinsically achiral and chirally modified ones. However, the complex supramolecular systems on the basis of such

structurally sophisticated natural and bio-related compounds, such as proteins, polypeptides, cyclodextrins, DNA/RNA, etc., which are able to form three-dimensional chiral spatial conformations, are out of the scope of this review.

2

Supramolecular Systems on the Basis of Monomeric Porphyrinoids

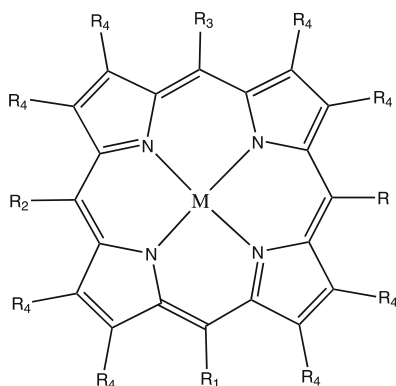
As the simplest, and thus most easily understandable and widely applicable structural type, supramolecular chirogenic systems based on monomeric achiral and racemic porphyrinoids will be discussed first.

2.1

Achiral/Racemic Porphyrinoids

Chirogenic processes in this type of supramolecular system can be achieved only upon interaction with an external chiral field, such as a single optically active guest or host molecule, artificial self-organized chiral assembly, various natural biopolymers and superstructures. The occurrence of asymmetry transfer to achiral or racemic porphyrinoids usually results in a corresponding chirogenic response, which can be detected by various spectroscopic techniques. In general, the supramolecular systems in this section can be classified according to the type of porphyrin co-binder, functionality, and chiroptical response.

Despite apparent simplicity of the monomeric porphyrin-based systems, they may possess some intriguing properties. For example, Aida's group prepared a series of saddle-shaped fully substituted porphyrins 1–3 [48, 49]. Their nonplanarity derived from the steric repulsion among the neighboring substituents resulting in two enantiomeric forms, which rapidly interconverted to yield a racemic mixture. This equilibrium was shifted to one particular conformation (higher than 98%) upon interaction with various enantiopure acids via hydrogen bonding of two carboxylates to the pyrrole nitrogens of the porphyrin ring from opposite sides to give a 1 : 2 complex. The supramolecular complexes exhibited a noticeable induced CD signal in the region of the Soret band, the sign of which was correlated with the relative steric bulk at the asymmetric center allowing the absolute configuration determination excepting some bulkiness borderline cases. Although the authors have not discussed the electronic origin of the observed optical activity, the induced chirality was found to show remarkable chirality memory properties upon replacement of the chiral acid with an achiral one. Other examples included a group of various saccharide sensors. Shinkai et al. designed a selective porphyrin sensor exclusively for D-lactulose on the basis of distance matching between the binding sites of this sugar and two boronic acid groups

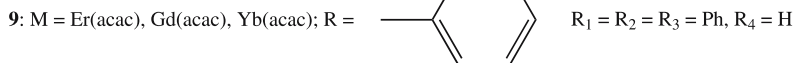
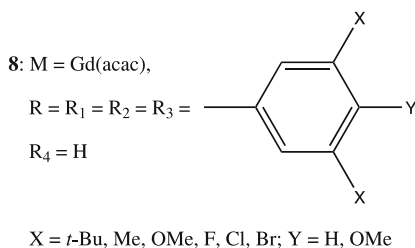
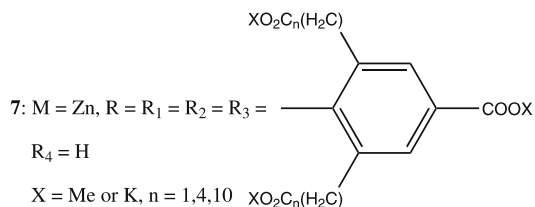


1: $M = 2H$, $R = Ph(OMe)_2-o,o$, $R_1 = R_2 = R_3 = Ph$, $R_4 = Me$

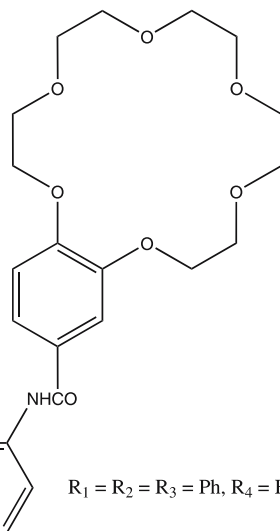
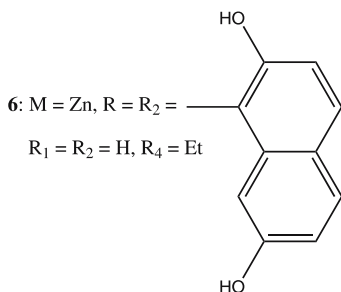
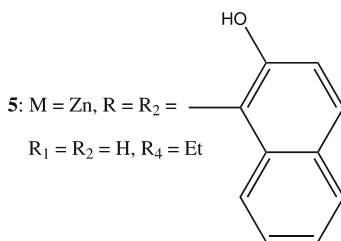
2: $M = 2H$, $R = R_2 = Ph(OMe)_2-o,o$, $R_1 = R_3 = Ph$, $R_4 = Me$

3: $M = 2H$, $R = R_1 = R_2 = Ph(OMe)_2-o,o$, $R_3 = Ph$, $R_4 = Me$

4: $M = 2H$, $R = R_2 = PhB(OH)_2-o$, $R_1 = R_3 = Ph$, $R_4 = H$



10: $M = 2H$, $R = R_1 = R_2 = R_3 = PhSO_3H-p$, $R_4 = H$

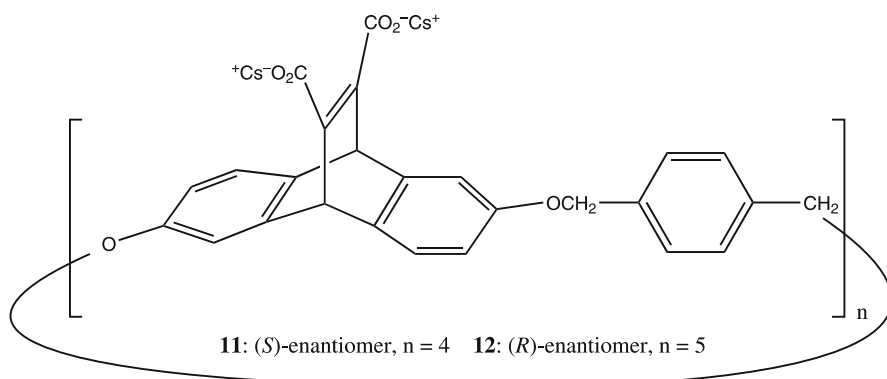


in *cis-4* that yielded a 1 : 1 complex with a monosignate CD response in the Soret band region [50].

Another type of supramolecular system is based on amino acids (AAs) as chiral guests. Hence, Mizutani, Ogoshi and their coworkers using the *trans*-isomers of **5** and **6** developed a receptor for AAs with particular selectivity found for Asp-OMe (the binding constant was found to be as large

as $6.98 \times 10^4 \text{ M}^{-1}$) because of the conformational matching for a three-point fixation mode ensured by the coordination and two hydrogen-bonding interactions [51]. All the systems studied exhibited a small-to-moderate negative couplet in the Soret region induced, as suggested, via the porphyrin-carbonyl coupling mechanism, although other factors could also contribute. To expand the applicability of the AA receptors, a series of porphyrins **7** were proposed for a dual use, in nonpolar organic solvents as the ester derivatives, and in aqueous media as the hydrolyzed derivatives [52]. Interestingly, it was found that two driving forces competitively contribute to the binding: the electrostatic interactions upon coordination of the amino group to the Zn central ion in organic solvents (enthalpic forces) and the host–guest dispersion interactions (an enthalpic force) along with the desolvation-driven binding (an entropic force) which were dominant in water. To sense the chirality of unprotected zwitterionic AAs, Tamiaki et al. applied a biphasic organic solvent–water system using **8** for extraction of AAs from the aqueous phase [53]. The resulting 1 : 1 complexes gave two well-resolved CD couplets of opposite sign, which were matched to the split Soret band and Q transitions in UV-vis spectra. The CD amplitude (*A*) value was strongly dependent upon the solvent used and the Ph ring substituents, with the highest sensitivity found for aromatic solvents and $X = t\text{-Bu}$, and the sign of the induced CD followed the chirality of AAs, though with several reported exceptions. Although the chiroptical properties and observed dependencies were not rationalized, the authors suggested the use of this method for determination of the absolute configuration of unprotected α -AAs. The sensitivity of this method was further improved by using a synergistic binding approach upon incorporation of the crown ether moiety to yield **9** [54]. Apparent co-coordinations of the CO_2^- group of AA to the lanthanide center and the NH_3^+ group to the crown ether along with appropriate metal choice considerably enhanced the extraction abilities and *A* values. Another approach for sensing unprotected AAs was demonstrated by Harmon et al. by using solid-state optical detection [55]. This method was based on the hypsochromic shifts in UV-vis spectra of **10** immobilized as a monolayer onto a cellulose film caused by interaction with AAs. The degree of spectral change was dependent upon the structure of the AA, making it possible to quantify different AA in solutions, although the operating mechanism was not reported.

Besides the host functions, porphyrin structures may serve as the achiral guests for certain chiral hosts possessing specific binding sites. For example, Dougherty et al. reported several interesting effects upon complexation of simple 5,10,15,20-tetra(4-*N*-methylpyridyl)porphyrin (TMP) and **10** with anionic cyclophane hosts **11**, **12** [56]. Thus, while the interaction of cationic TMP with smaller **11** induced a noticeable asymmetric negative couplet ($A = -166.6 \text{ M}^{-1}\text{cm}^{-1}$), enlarging the cavity in **12** resulted in stoichiometry controlled CD changes. Particularly, the induced chirality, expressed also as a negative couplet regardless of the host's opposite absolute configuration,



was inverted upon increasing the TMP concentration, apparently due to the complex stoichiometry switching from 1 : 1 to 1 : 2. Another surprising result was a generation of the monosignate CD signal upon binding of **10** with **11** and **12** despite the expected electrostatic repulsions between the negatively charged guest and hosts. The rationale of these phenomena was not presented making it difficult to understand the corresponding origins and driving forces, although these supramolecular systems obviously deserve further investigation as interesting and rare examples of stoichiometry-controlled chirogenic processes.

As the last supramolecular chirogenic system presented in this section, a three-component assembly consisting of an achiral monomeric porphyrin and two chiral units, which exhibited selective optical differentiation properties is worthwhile of discussion [57]. As shown above, while achiral lanthanide porphyrin **8** served as an effective chiral sensor in biphasic conditions, replacement of the acac external ligand with enantiopure 3-acetylcamphors resulted in the corresponding chiral complexes, which in turn could be applied for chirality recognition. Indeed, this was nicely demonstrated by the complexation with two antipodal AA dipeptides, the CD response of which gave opposite bisignate couplets of different intensities depending upon the corresponding diastereomeric composition. However, the sensitivity of this system was not high enough to detect antipodal alanines.

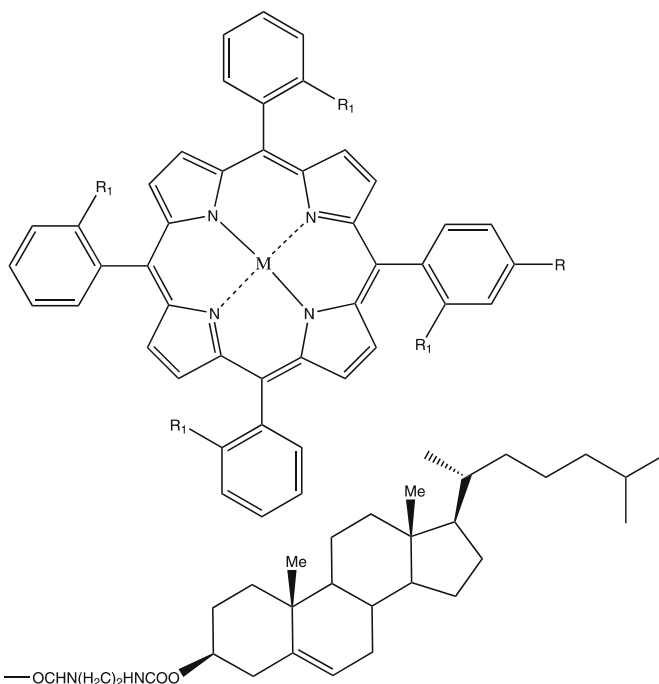
The representative examples of chirogenic assemblies on the basis of achiral monomeric porphyrinoids exposed to a chiral influence clearly show their great importance and wide applicability in various fields. The major chiroptical properties of these relatively simple supramolecular systems include transferring the chiral information and controlling the induced asymmetry by different factors. However, another type of chirogenic process—modulation of inherent chirality is going to be illustrated for chiral porphyrins in the next sections.

2.2

Chiral Porphyrinoids

In contrast to achiral/racemic porphyrinoids, the chirogenic properties of chiral porphyrinoids have been scantily investigated despite their prime importance for chiral recognition, asymmetric catalysis, medical purposes, and various biomimetic studies.

Shinkai et al. reported an interesting example of the association between chiral **13** and [60]fullerene forming the corresponding 2 : 1 complex, which enhanced the gelation ability of **13** [58]. In the gel phase, this complex yielded a strong negative exciton couplet in the region of the Soret band indicating an anticlockwise orientation of the corresponding interaction transitions, although a more detailed rationalization of the chiroptical properties seems



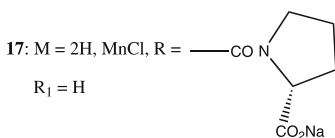
13: $M = \text{Zn}$, $R = \text{---OCHN}(\text{H}_2\text{C}_2\text{H}_4\text{NCOO})$

$R_1 = \text{H}$

14: $M = \text{Zn}$, $R = \text{H}$, $R_1 = \text{NHCOCH}(\text{NHBoc})\text{Me}$

15: $M = \text{Zn}$, $R = \text{H}$, $R_1 = \text{NHCOCH}(\text{NHBoc})\text{Pro}$

16: $M = \text{Zn}$, $R = \text{H}$, $R_1 = \text{NHCOCH}(\text{NHBz})\text{Gln}$



to be an arduous task due to the uncertainty of the molecular organization within the gel.

In another example one of the most effective recognitions of AA esters with an enantioselectivity as high as 21.54 (for PheOMe) was reported by Zhu et al. upon applying the AA substituted 14–16 [59]. It was shown that the enantioselectivity was exponentially dependent upon the temperature, and that the diastereomeric complexes exhibited different CD responses. Specifically, the CD spectrum of 14 in the presence of weakly bound L-AlaOMe was essentially similar to that of uncomplexed 14 yielding a single negative CE in the region of the Soret band, whilst strongly bound D-AlaOMe produced a positive couplet, apparently due to the excitonic interactions between the porphyrin and AA's carbonyl transitions, although this chiroptical effect was not explained.

The use of organized media for studying various aspects of chiral supramolecular systems was effectively exploited by Monti et al. [60,61]. Thus, the selective interactions between proline-substituted 5,10,15,20-tetraphenylporphyrin (TPP) 17 and chiral micelles made of sodium *N*-dodecanoyl-L-prolinate were analyzed. The inclusion complexes yielded different chiroptical responses for the free base and Mn complex of 17, a negative and positive bisignate CD signal, respectively, caused by exciton coupling between the chirally arranged chromophores, although porphyrin aggregation was ruled out by the authors. In contrast, upon using achiral micelles constructed from sodium dodecyl sulfate, the formation of chiral porphyrin aggregates leading to CD couplets of opposite sign was suggested. Although these astonishing transformations have yet to be rationalized, the usefulness of this chiral supramolecular assembly for stereoselective epoxidation was demonstrated by applying the corresponding Mn complex with (*R*)-limonene as a test substrate. The reaction carried out with this system proceeded with the highest regioselectivity (> 95%) and de (up to 42%) in comparison to the other catalytic systems, in which one of the components was replaced with the corresponding achiral analog.

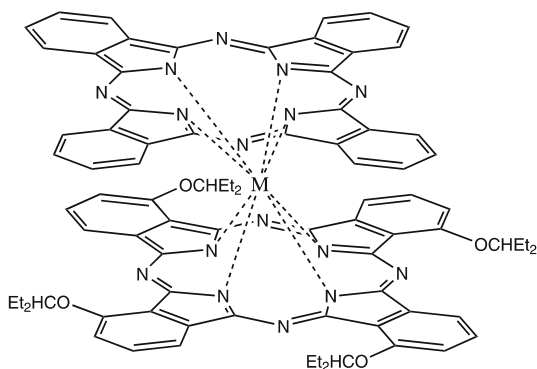
The aforementioned representative examples of chirogenic supramolecular systems based on monomeric porphyrinoids clearly demonstrate their vital importance and wide applicability in various fields, while many aspects of the operating mechanisms and especially chiroptical properties have yet to be comprehensively investigated and well understood. However, in many cases just a monomeric porphyrin cannot function properly without the synergetic assistance of another porphyrin unit (or several porphyrins) that give rise to chirogenic supramolecular assemblies built upon the dimeric/oligomeric porphyrinoids, which will be discussed in subsequent sections.

3

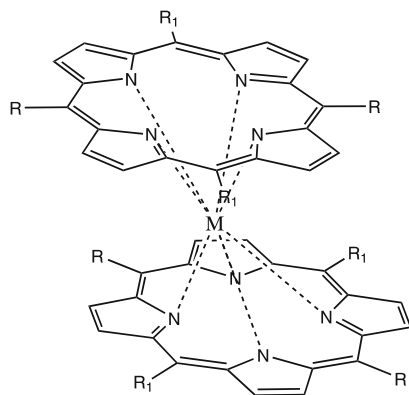
**Chiral Dimeric/Oligomeric Porphyrinoids
Constructed from Achiral Monomers Fixed by Noncovalent Bridges**

Chirogenic supramolecular systems based on dimeric/oligomeric porphyrinoids can also be classified according to their complexity and structural features. First, the assemblies consisting of two or more monomeric porphyrins fixed in an asymmetrical fashion by chiral bridges via supramolecular binding will be examined.

The most facile approach in designing such systems lies in the center-to-center fixation of two porphyrin macrocycles through a multivalent metal ion or bidentate spacer. Using this methodology Jiang, Ng and coworkers synthesized racemic mixtures of the metal-bound chiral double-decker bis-phthalocyanines **18** [62]. While optical resolution was not achieved, these compounds crystallized as racemates in a monoclinic system with two pairs of enantiomeric **18** per unit cell. In contrast, Aida's group succeeded in the separation of the corresponding antipodes of some double-decker bis-porphyrins **19–22**, which was confirmed by the corresponding mirror-image CD spectra [63, 64]. The CD spectral profiles consisted of several bisignate CEs apparently arisen from the excitonic interactions of two pairs of the porphyrin electronic transitions arranged in a chiral fashion, although the band assignment has not been done. The chiroptical properties were strongly affected by the nature of the central metal and its oxidation state. For example, reduction of the Ce complex of **22** considerably enhanced the porphyrin rotation around the central metal ion leading to easier racemization, while the oxidized forms of the Zr complex of **19** in contrast decelerated the complex racemization by 21 and 99 times for monocationic and dicationic forms, respectively. These redox effects, as assumed, were a result of weakening the π -electronic interporphyrin interactions upon enlargement of the reduced Ce ion and enhancing the bonding character of the π -electronic interactions upon decreasing of the number of electrons in the antibonding orbital of the oxidized forms. Another approach for the fixation of two porphyrinoids via chiral linkers to obtain **23** and **24** was used by Durfee, Kobayashi, Ceulemans and coworkers [65, 66]. In particular, two subphthalocyanine units connected by an (*R*)-1,1'-binaphthyl (BNP) bridge in **23** produced intense CD signal in the region of low energy Q transitions, the complex shape of which was rationalized in terms of the excitonic interactions by analyzing band deconvolution results. In the case of **24** a pair of phthalocyanine chromophores were brought together in chiral arrangement by the hematoxylin bridge. The chiroptical response consisted of an intense negative-to-positive bisignate and several weak CD signals in the Q- and Soret band regions arising from the excitonic interaction between two phthalocyanines. The induced optical activity was unambiguously confirmed by ab initio geometry optimization combined with a Kuhn–Kirkwood coupled-oscillator mechanism, which add-



18: M = Sm, Eu, Gd



19: M = Ce, Zr, R = Tol, R₁ = H

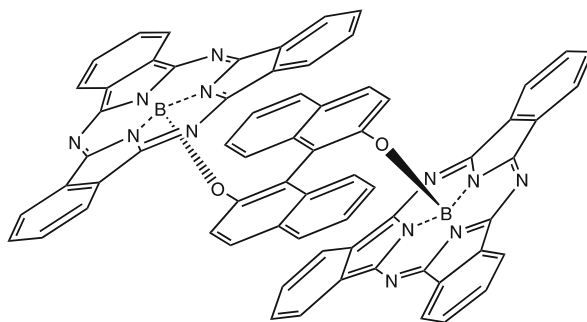
20: M = Ce, Zr, R = PhPr-*i*-4, R₁ = H

21: M = Ce, Zr, R = Ph(OMe)_{2-3,5}, R₁ = Tol

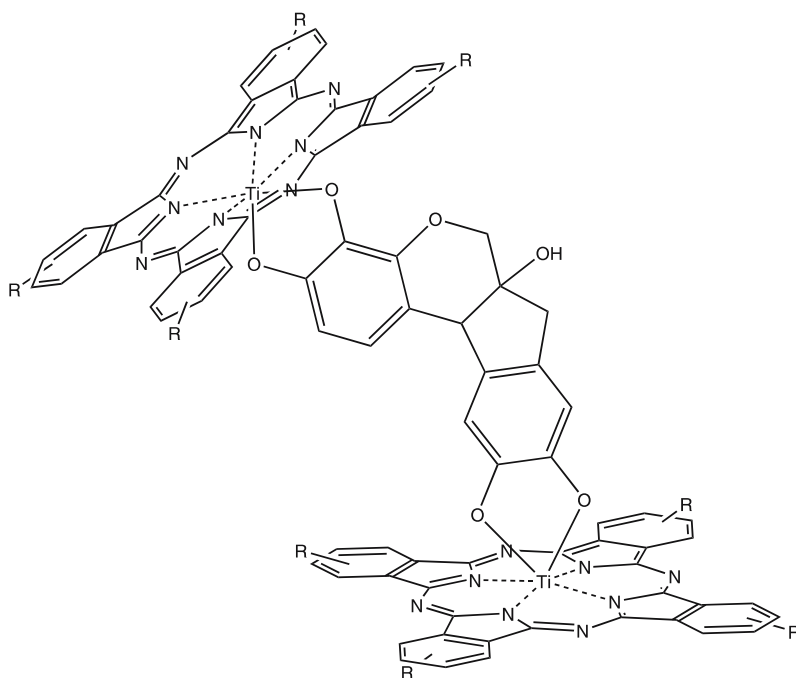
22: M = Ce, Zr, R = Ph(OMe)_{2-3,5}, R₁ = PhF₅

itionally allowed determination of the absolute configuration of hematoxylin as the (6a*S*,11*bR*)-form. Although this method provides a powerful tool for assigning stereochemistry, the practical application is rather limited due to its overall complexity.

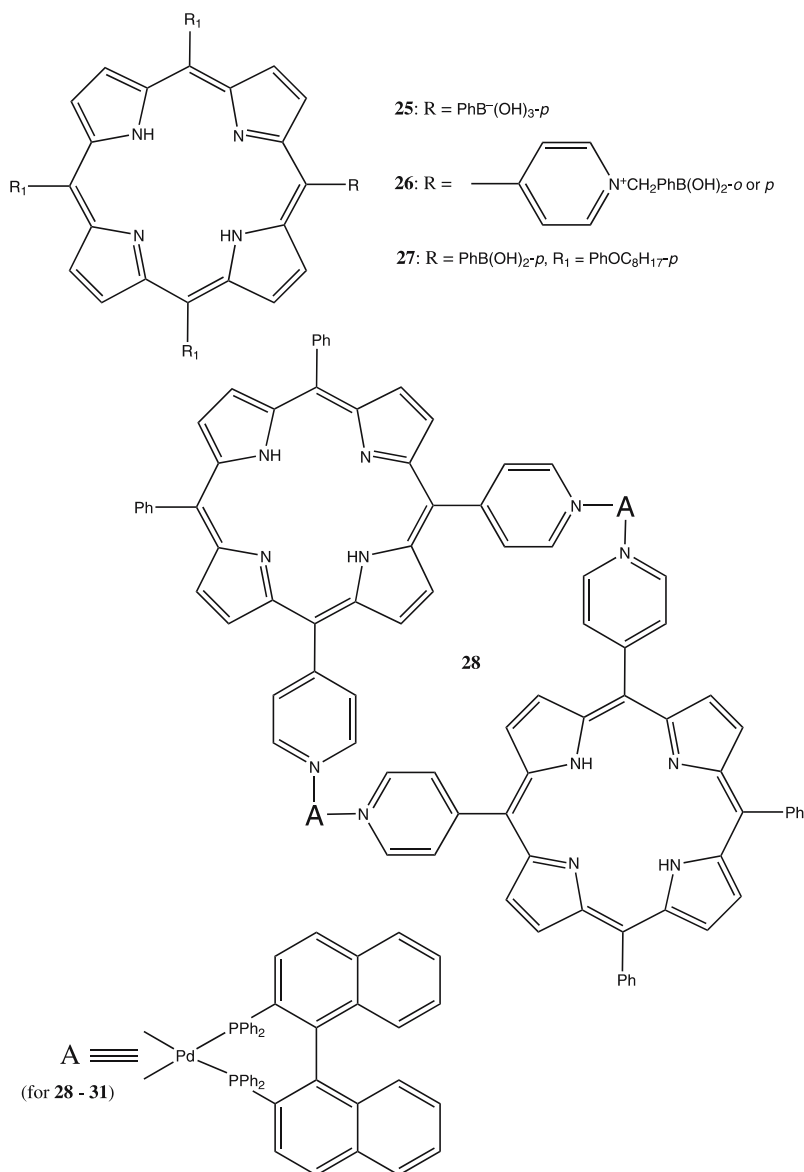
Shinkai's group applied another method for the chiral spatial fixation of two porphyrins via peripheral substitution at the corresponding *meso*-position with boronic acid residue [67, 68]. Thus, anionic **25** and cationic **26** formed an optically active 1 : 1 complex only in the presence of glucose and xylose in aqueous solution as a result of the boronic acid binding to the sac-



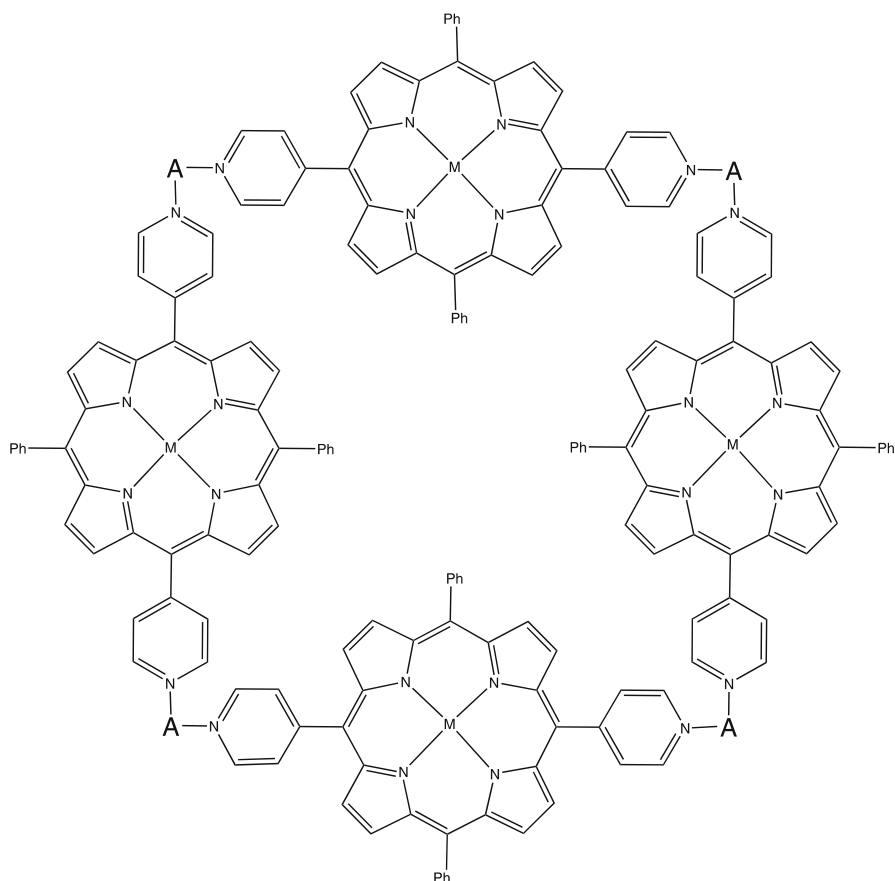
23

24: R = H or *t*-Bu

charide diols. However, 27 was found to be more versatile in interacting with different saccharides to form the bis-porphyrin chiral complexes upon binding of two molecules of 27 with one molecule of sugar in CH_2Cl_2 . The induced bisignate exciton-coupling CD in the Soret region was strongly dependent upon the saccharide and porphyrin structures, while not always following the sugar's absolute configuration. Further exploiting the *meso*-substituent

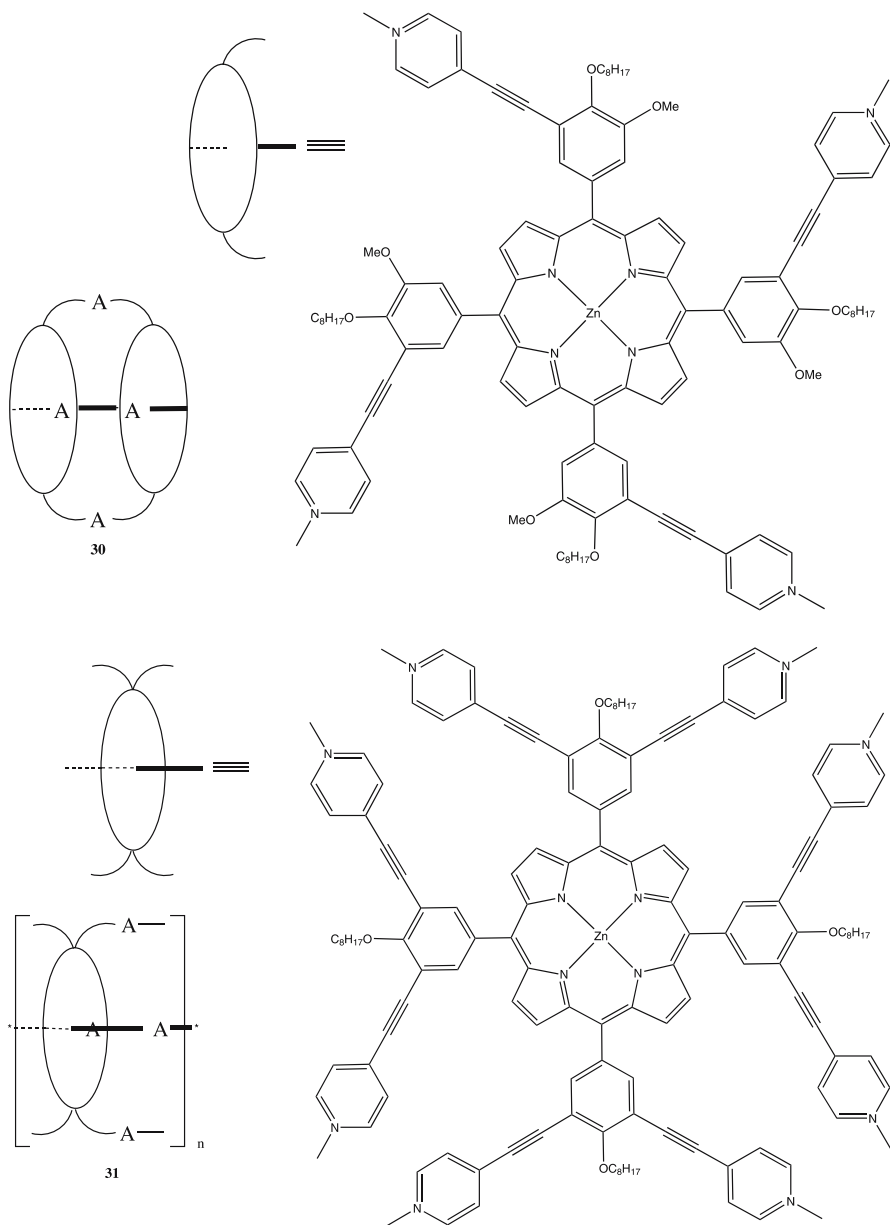


strategy, Stang and coworkers obtained chiral dimeric and tetrameric porphyrins **28** and **29**, respectively, by self-assembly via the enantiopure BNP bridge [69]. The chiroptical properties were distinguished for these systems exhibiting a strong bisignate Soret CD signal ($A = 1800 \text{ M}^{-1} \text{ cm}^{-1}$) in the case of the free bases of **29** apparently due to the multiporphyrin exciton coupling, a moderate monosignate CE ($300 \text{ M}^{-1} \text{ cm}^{-1}$) in the case of **28**, and no



29: M = 2H, Zn

CD of the Zn complexes of **29**. This remarkable behavior was suggested to be governed by the difference in the chromophore's symmetry and spatial geometry, although the detailed rationale is yet to be elaborated. A very similar self-assembly procedure and the same BNP bridge were used by Shinkai et al. to construct a different capsule-type geometry of the chiral di- and polymeric **30** and **31** [70]. The asymmetry of BNP forced the face-to-face orientated porphyrins to adopt a twisted conformation resulting in the unidirectional (clockwise or anticlockwise) coupling of the porphyrin electronic transitions. For example, in the case of the (*R*)-enantiomer, porphyrins formed the left-handed helical twisting structure, as confirmed by computational methods, yielding a negative exciton couplet in CD spectra of the Soret region, the intensity of which was markedly increased by oligoporphyrin interactions in **31**.



The conformational stability and structural rigidity of these systems makes it difficult to comprehensively investigate the various controlling factors that influencing the chirogenic processes. For this purpose, achiral or racemic bis- or oligoporphyrins connected by a sufficiently flexible covalent bridge, which are able to finely sense the chirality of the interacting counter-

part and facilely respond to various external and internal stimuli are of most promise. These supramolecular systems will be discussed in the subsequent sections.

4

Supramolecular Systems on the Basis of Dimeric/Oligomeric Porphyrinoids

Supramolecular systems on the basis of dimeric and oligomeric porphyrinoids are varied depending upon the chirality of the supramolecular counterparts, type of the covalent linkage, and number of the porphyrin subunits. Firstly, we shall examine examples of the assemblies consisting of achiral and racemic bis-porphyrinoid hosts and chiral guests.

4.1

Achiral/Racemic Porphyrinoids

This kind of chirogenic system primarily serves for sensing the asymmetry of the interacting chiral guest. Although there are different mechanisms of the chirality information transfer, generally this process can be schematically depicted in Fig. 1. An achiral bis-porphyrinoid should possess at least two interaction sites and a flexible enough covalent bridge in order to adopt a stereospecific three-dimensional conformation induced by a chiral guest, hence generating chirality in the whole supramolecular assembly.

The importance of these two factors can be easily understood by the following examples. Shinkai and coworkers widely employed a double-decker architecture of the center-to-center bound bis-porphyrins **32–39** designed on the basis of μ -oxo dimers and Ce complexes to sense the chirality of

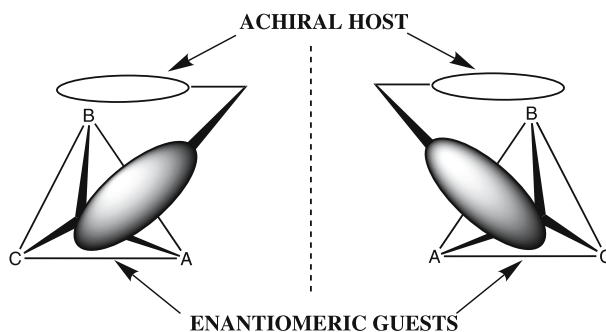
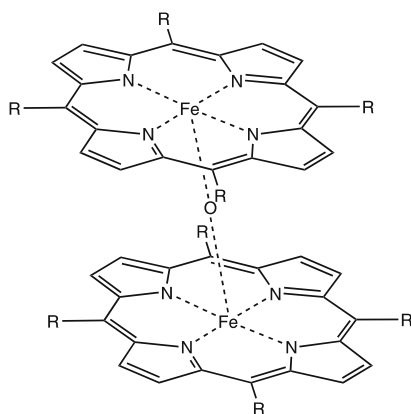
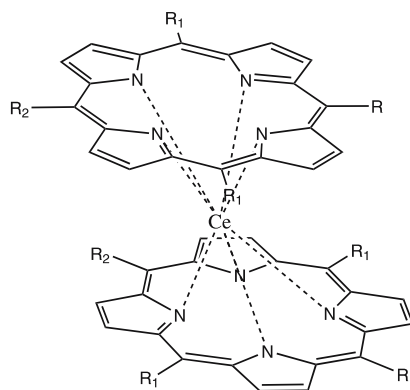


Fig. 1 Schematic representation of chirality sensing of enantiomeric guests by achiral bis-porphyrinoids



32: $R = \text{PhB(OH)}_2\text{-}m$ **33:** $R = \text{PhB(OH)}_2\text{-}p$



34: $R = R_1 = R_2 = p\text{-pyridyl}$ **35:** $R = R_2 = p\text{-pyridyl}, R_1 = \text{Ph}$

36: $R = R_2 = p\text{-pyridyl}, R_1 = \text{Ph(OMe)}_2\text{-}m,m$

37: $R = R_2 = p\text{-(N-CH}_2\text{PhB(OH)}_2\text{-}p\text{)pyridyl}, R_1 = \text{PhOMe-}p$

38: $R = p\text{-(N-CH}_2\text{PhB(OH)}_2\text{-}p\text{)pyridyl}, R_1 = R_2 = \text{PhOMe-}p$

39: $R = R_2 = p\text{-(N-Me)pyridyl}, R_1 = \text{PhOMe-}p$

various chiral guests [71–76]. The association mechanism was unambiguously established and included the interaction of a bidentate guest with two binding groups of the neighboring porphyrins, forcing these porphyrins to rotate around the central axis and subsequently to twist the macrocycles in the right- or left-handed direction, depending on the guest's stereochemistry

(Fig. 2). This asymmetry transfer resulted in noticeable optical activity in the region of the porphyrin absorption caused by interporphyrin exciton coupling. Although the electronic origin of the induced CD has not been fully rationalized, these systems were successfully applied for sensing the chirality of saccharides (for 32, 33, 37, 38), dicarboxylic acids (for 34, 35, 36), dianions (for 39) and memorizing chirality (for 36). The generated chiral memory was remarkably preserved for 3 days at 0 °C and even for 1 year at – 37 °C. The host–guest binding occurred in a highly cooperative manner exhibiting a positive allosteric effect, and the CD response was strongly affected by the guest's structure [71, 72], solvent [76], and pH [75]. Interestingly, in the case of maltooligosaccharide guests, a chirality switching effect controlled by the number of saccharide units was reported for 37.

The entropically unfavorable face-to-face architecture of bis-porphyrins could also be preserved by two oppositely located covalent bridges as in the case of cryptand-containing 40, 41 prepared by Schmidtchen et al. [77]. These hosts were also able to bind various saccharides presumably via an encapsulation mode, while only a very weak CD induction in the Soret region was reported, as a result of the inability of the bis-porphyrins to follow the guest's stereochemistry apparently caused by structural peculiarity of this particular linkage. The Aida's group applied more flexible covalent bridges of different structure and length to obtain a face-to-face arrangement in 42–44 [78, 79]. The bis-porphyrins 42, 43 with longer linkage showed high specificity toward bis-pyridyl substituted chiral guests of appropriate length to form stable 1 : 1 inclusion complexes with association constants of up to $2.3 \times 10^6 \text{ M}^{-1}$ (Fig. 3). It was found that the helicity of the guest played a key role in transferring

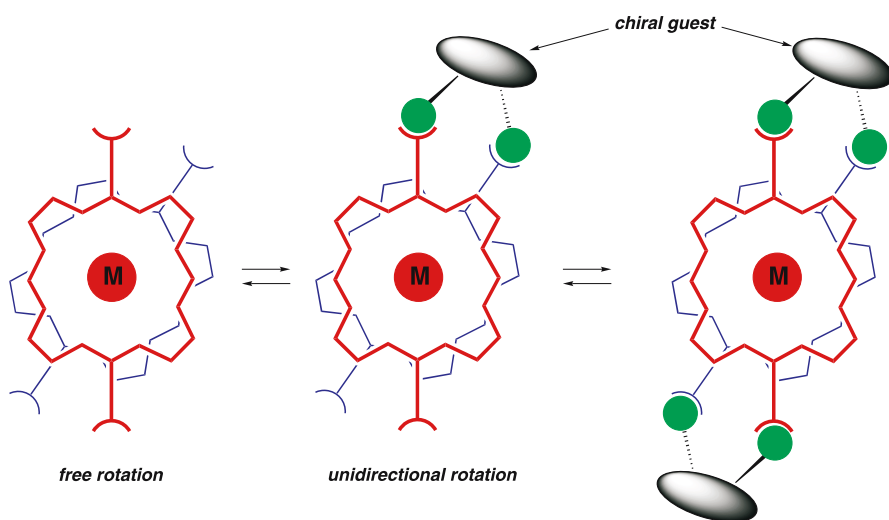
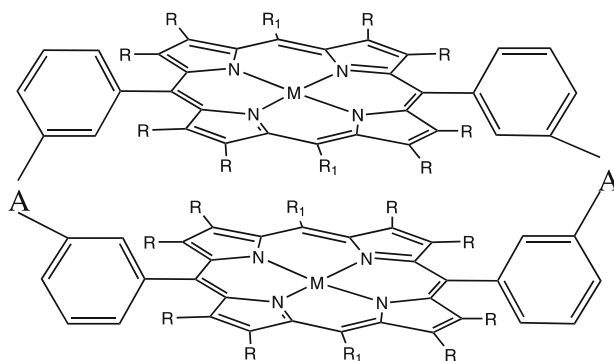
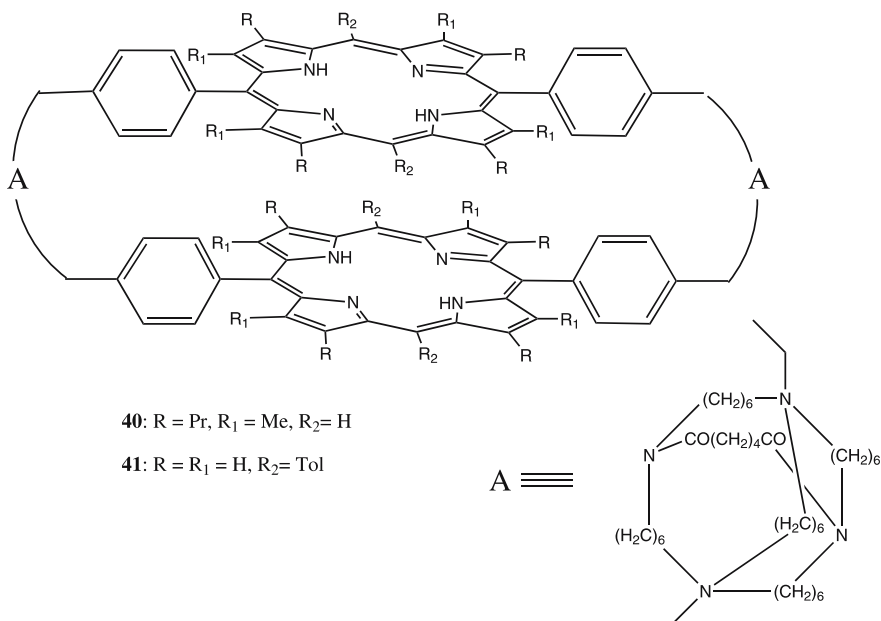


Fig. 2 Schematic representation of chirality transfer from enantiomeric guests to 32–39



42: $M = \text{Zn}$, $R = \text{H}$, $R_1 = \text{Mes}$, $A = -\text{CO}(\text{NHCMe}_2\text{CO})_9\text{NH}^-$

43: $M = \text{Zn}$, $R = \text{H}$, $R_1 = \text{Mes}$,

$A = -\text{CO}(\text{NHCMe}_2\text{CO})_3\text{NHC}(\text{CHPh})\text{CONHCH}_2\text{CONH}(\text{CHPh})\text{CO}(\text{NHCMe}_2\text{CO})_3\text{NH}^-$

44: $M = 2\text{H}$, $R = \text{Me}$, $R_1 = \text{Ph}(\text{OMe})_2$ -*o,o*-, $A = -\text{OCH}_2\text{PhCH}_2\text{O}^-$

the chiral information and inducing a strong exciton coupling in the Soret region. bis-Porphyrin **44** with a shorter bridge was used for complexation with the smaller mandelic acid, exhibiting significant amplification (more than 7 times) of the CD activity ($A = 260 \text{ M}^{-1}\text{cm}^{-1}$) in comparison to the corresponding monomer, owing, as assumed, to the translation of the nonplanar chirality of the porphyrin ring into the helical chirality of the entire assembly. A step-

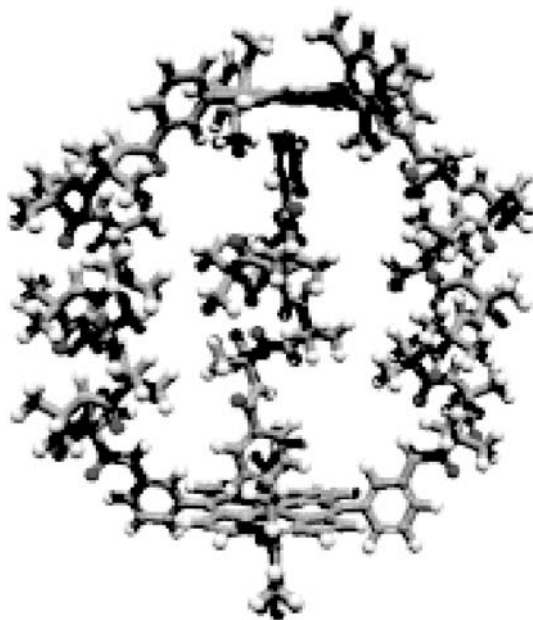
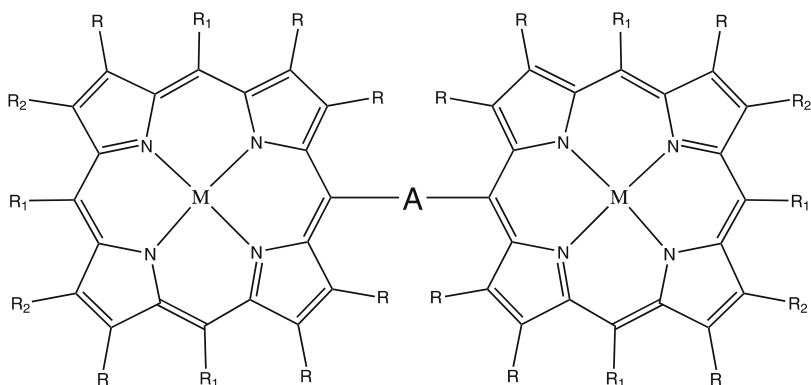


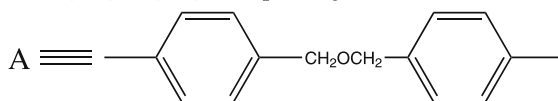
Fig. 3 Molecular model of inclusion complex of **42** with a chiral guest (reprinted in part with permission from Guo et al. [78]. Copyright (2004) American Chemical Society)

wise increasing of the guest concentration resulted in complicated changes of CD signals apparently reflecting the multistep equilibrium of the binding process. Although the observed chiral responses have not been clearly rationalized as yet, these chiroptical systems are of certain interest as potential chirality sensors for reading the stereochemistry of interacting guests.

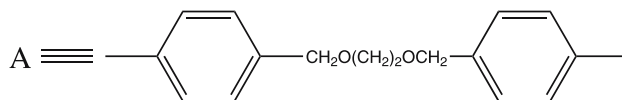
Another structural type of bis-porphyrin is based on connecting the two chromophoric units by a single covalent bridge. While the spatial arrangement becomes less predictable in this case due to decreasing the overall system's rigidity, some additional factors, such as bidentate guest complexation or shortening the linkage, can bring two porphyrin units close to each other and fix the bis-porphyrin in a face-to-face or linear conformation, respectively. Hence, Tsukube et al. prepared a series of lanthanide bis-porphyrins **45**, **46** connected by ether bridges of different length as potential hosts for binding cystine polyions [80]. These receptors exhibited a remarkable size selectivity for sensing chiral guests. For example, the Yb complex of **45** with a short bridge efficiently extracted cystine from an aqueous solution into the organic phase, while cystathionine, homocystine, and methionine were only modestly extracted. In contrast **46** favored longer homocystine. The complexation proceeded through the formation of 1 : 1 complexes of presumably a tweezer type resulting in a complex CD response in the Soret region, which was markedly enhanced in comparison to that of the corresponding



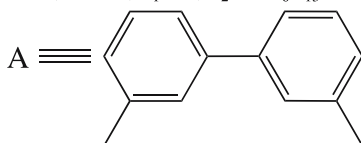
45: $M = \text{Yb}(\text{acac}), \text{Gd}(\text{acac}), R = R_2 = \text{H}, R_1 = \text{Ph}$



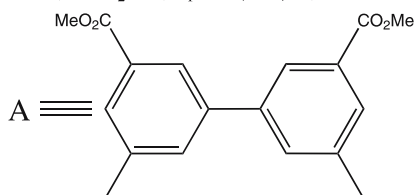
46: $M = \text{Yb}(\text{acac}), \text{Gd}(\text{acac}), R = R_2 = \text{H}, R_1 = \text{Ph}$



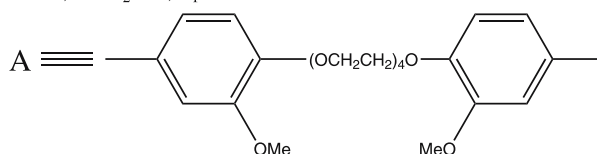
47: $M = \text{Zn}, R = \text{Me}, R_1 = \text{H}, R_2 = n\text{-C}_6\text{H}_{13}$



48: $M = \text{Zn}, R = R_2 = \text{H}, R_1 = \text{Ph}(t\text{-Bu})\text{-}m,m$

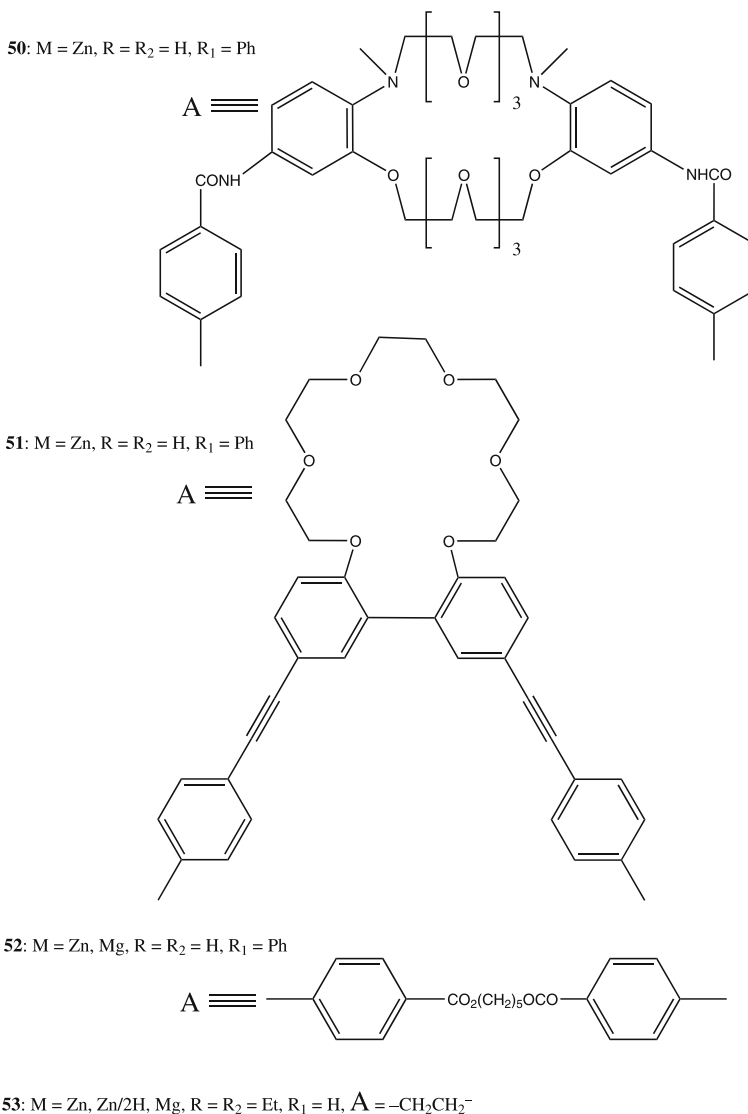


49: $M = \text{Zn}, R = R_2 = \text{H}, R_1 = \text{Ph}$



monomer but the origin of which has yet to be understood. Even more drastic length selectivity in binding chiral diamines was reported by Hayashi and coworkers for the rigidly linked **47**, **48** [81]. The host–guest size matching was an important requirement for effective complexation with the association constant determined as high as $2.4 \times 10^6 \text{ M}^{-1}$ for the best pair. The induced CD was strongly affected by the bulkiness and the number of stereogenic centers, porphyrin peripheral substituents, and temperature. For example,

the greatest A value ($1340 \text{ M}^{-1}\text{cm}^{-1}$) was a further 1.5-fold increased upon lowering the temperature to -45°C . However, for potential application of these supramolecular systems as chiral sensors, a comprehensive rationale of the observed effects would be needed. A crown ether type of linkage gave additional stimuli for controlling the bis-porphyrin conformation via specific complexation with alkali metal ions that was exploited by the groups of Monti and Kubo [82–84]. This effect was nicely demonstrated by an almost 2-fold increase of the binding constant (from $2.6 \times 10^5 \text{ M}^{-1}$ to $4.5 \times 10^5 \text{ M}^{-1}$)



upon addition of Na ions to the **49**/*trans*-1,2-diaminocyclohexane (DACH) tweezer system as a result of the bis-porphyrin preorganization. The corresponding chiroptical properties have also been tuned by the addition of Na⁺ markedly enhancing the A value of the induced CD couplet. A very similar effect of the binding and CD amplification was found for **50** upon interaction with *N*-alkyl-substituted DACH [83]. However, a larger crown ether cavity required a bigger K ion in this case. In addition, **50** could read out the chirality of potassium salts of carboxylates such as camphorates and mandelates inducing the corresponding exciton couplet CD through the solid/liquid two-phase extraction. Furthermore, the induced chirality in the tweezer conformation of **51** was effectively preserved upon replacement of a chiral diamine with an achiral one in the presence of Ba ions, with the CD intensity showing only a little decrease after one day [84]. Although the discussed tweezer systems produced rather high optical activity due to the chiral spatial arrangements of two porphyrin chromophores, no efforts have been undertaken to provide a detailed explanation of the electronic and structural factors involved.

One of the first attempts to resolve this issue in the case of bis-porphyrin systems was undertaken by Nakanishi and coworkers using the more flexible **52**, which was able to adopt a tweezer conformation upon complexation with bidentate ligands (Fig. 4) [85–95]. The chirogenesis mechanism was found to be based upon the stereospecific differentiation of the substituents' relative bulkiness at the asymmetric carbon by forcing the bis-porphyrin to adopt in general the least sterically hindered conformation, although it was also reported that other factors such as hydrogen bonding, presence of heteroatoms, solvent, etc., might affect the overall geometry of assembly. This resulted in formation of the directional orientation of two porphyrins in **52**, thus inducing an exciton couplet CD, the sign of which was suggested to be used as a tool for the absolute configuration determination of various bidentate guests. In the cases when the relative bulkiness could not be directly determined, molecular mechanics calculations were applied for the conformational analysis to explain the observed inconsistency between the predicted and obtained chirality. Although it is well known that a metalloporphyrin chromophore consists of two degenerate (or nearly degenerate owing to the asymmetry imposed by the *meso*-substitution) transitions along the *meso* 5–15 and 10–20 axes, only the excitonic coupling of the pair of 5–15 oscillators was chosen for the rationalization of induced optical activity in **52**, without further in-depth analysis. However, contribution of the 10–20 oscillators via homo- and heterocoupling may play an important role as well, especially in some certain conformations. Some dependencies of induced CD upon solvent, guest's structure, and temperature were also reported, although not comprehensively studied.

In order to comprehensively investigate various chiroptical aspects of the bis-porphyrin-based supramolecular systems and unambiguously rationalize

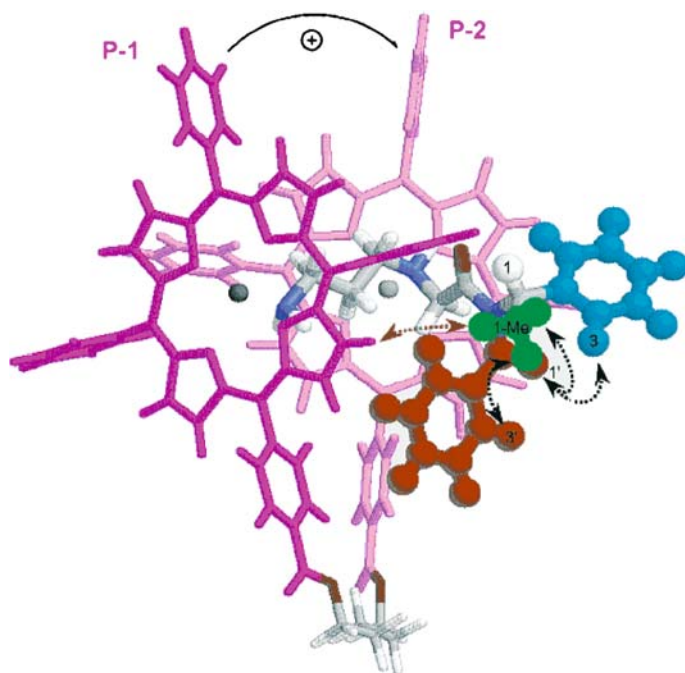


Fig. 4 Molecular model of complex of **52** with a chiral guest (reprinted in part with permission from Huang et al. [91]. Copyright (2002) American Chemical Society)

the chirality induction mechanism, our group used a simple ethane-bridged host **53** [18, 96–109]. In sharp contrast to the above-discussed bis-porphyrin systems, this host was able to sense chirality of not only bidentate but also monodentate guests owing to the linkage's semi-flexibility/semi-rigidity provided by the relatively short but flexible enough C_2 chain via formation of the stable extended 1 : 2 host–guest complexes in a cooperative manner with the Gibbs free energy ranged from -6.7 to -8.4 kcal mol $^{-1}$ for primary amines as determined by analyzing the corresponding UV-vis/CD spectral changes [96–105]. The specific chirogenic mechanism in **53** by monodentate guests included competitive repulsive interactions between the two most bulky substituents at the ligand's stereogenic center and the ethyl groups of the neighboring porphyrin ring (Fig. 5). The bulkiest group forced the neighboring macrocycle to move outwards, thus generating a unidirectional twist, which resulted in a moderate-to-strong exciton couplet CD signal in the Soret region. The chirality sign correlated with the induced helicity allowing straightforward determination of the absolute configuration of monodentate guests. A fully rationalized host–guest interaction mechanism allowed the detailed investigation of various external and internal factors influencing the chirality induction processes. For example, it was shown that the

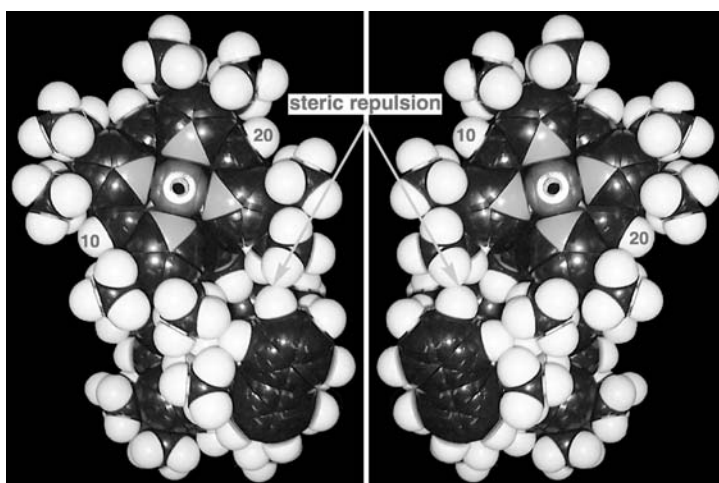


Fig. 5 The mechanism of chirality induction in **53** upon interaction with chiral guests (reprinted in part with permission from Borovkov et al. [18]. Copyright (2004) American Chemical Society)

A value was linearly dependent upon the size of the largest substituent at the stereogenic center for homologous ligands, thus allowing prediction of the induced chirality [96, 97, 99]. Also, a decisive role of solvent as an active part of the overall supramolecular system was clearly understood through judicious analysis of the selective solute–solvent interactions in the borderline cases where the difference between the competitive chiral interactions were small and the substituent’s relative bulkiness could be modulated upon formation of a specific solvation shell [104, 105]. Temperature was found to be another important factor controlling the chirogenic processes considerably increasing the *A* values upon lowering the temperature via enhancing the binding affinity, thus allowing the chirality induction by alcohols possessing a well-known low affinity for Zn porphyrins [100–102]. However, the alcohol binding, and thus the chirogenic ability was considerably increased by the replacement of the Zn central ion with a Mg ion [103]. Interaction of **53** with bidentate guests resulted in the formation of extremely stable 1 : 1 tweezer complexes with the binding constants estimated as high as $> 10^7 \text{ M}^{-1}$. However, further increasing the bidentate guest concentration could shift the supramolecular equilibria toward the extended 1 : 2 complex, hence allowing investigation of the corresponding stoichiometry effect [106–109]. In the case of enantiomeric 1,2-diphenylethylenediamine a remarkable phenomenon of chirality switching controlled exclusively by the stoichiometry of the supramolecular system as a result of the opposite spatial orientation of the 1 : 1 and 1 : 2 complexes was discovered. More importantly, a full and unambiguous rationalization of the induced optical activity in the bisporphyrin-based supramolecular system was achieved for the first time by

using chiral DACH. Particularly, on the basis of the obtained crystallographic structure of the **53**/(*R,R*)-DACH tweezer complex (Fig. 6) and the Kuhn–Kirkwood coupled-oscillator mechanism, the CD signal was assigned to be a combination of the two $B_{||} - B_{||}$ and $B_{\perp} - B_{\perp}$ homocouplings, both of which were orientated in an anticlockwise manner, thus resulting in an intense negative CD couplet ($A = -590 \text{ M}^{-1} \text{ cm}^{-1}$), while the contribution of the corresponding $B_{||} - B_{\perp}$ heterocouplings was found to be negligible [109]. Thus, high sensitivity, full rationalization, and wide applicability for various types of guests showed that **53** could serve as a powerful tool for studying various aspects of supramolecular chirogenesis and additionally for use as a versatile chirality sensor.

Another single bridged bis-porphyrin host **54** was proposed by Shinkai et al. for selective binding of oligosaccharides in a cooperative manner by virtues of the enhanced rigidity of the system [75, 110]. Particularly, the fixed porphyrin–porphyrin distance was well matched to the maltotetraose size producing a stable 1 : 2 complex, which resulted in a complex chiroptical response in the Soret region consisting of three nonequivalent and asymmetrical CEs, presumably due to the overlapping of two or more exciton couplets. A further increase of the porphyrin multiplicity in the corresponding meso-meso linked oligomers **55** led to considerable amplification of the induced chirality as observed by Kim, Osuka and coworkers [111]. These oligomers formed a helical structure by clipping the *meso*-aryl substituents with hydrogen bonding between carboxyl groups and a cyclic urea guest. The direction of the helix was then controlled by complexation with a chiral diamine derivative of BNP resulting in an induced CD of similar shape. However, the CD intensity as judged by the corresponding anisotropy factor was enhanced by three times upon increasing the number of porphyrin units

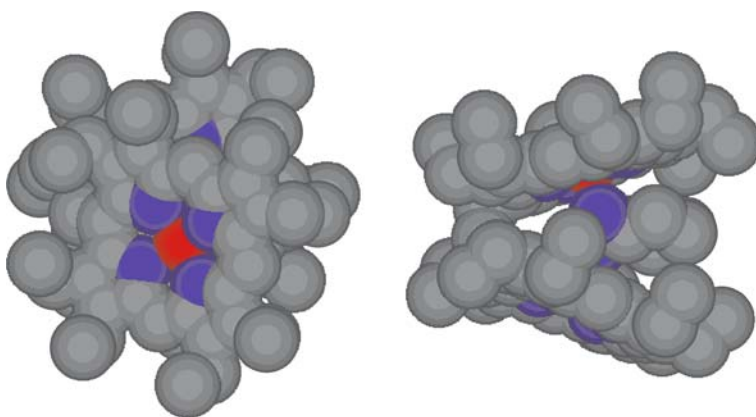
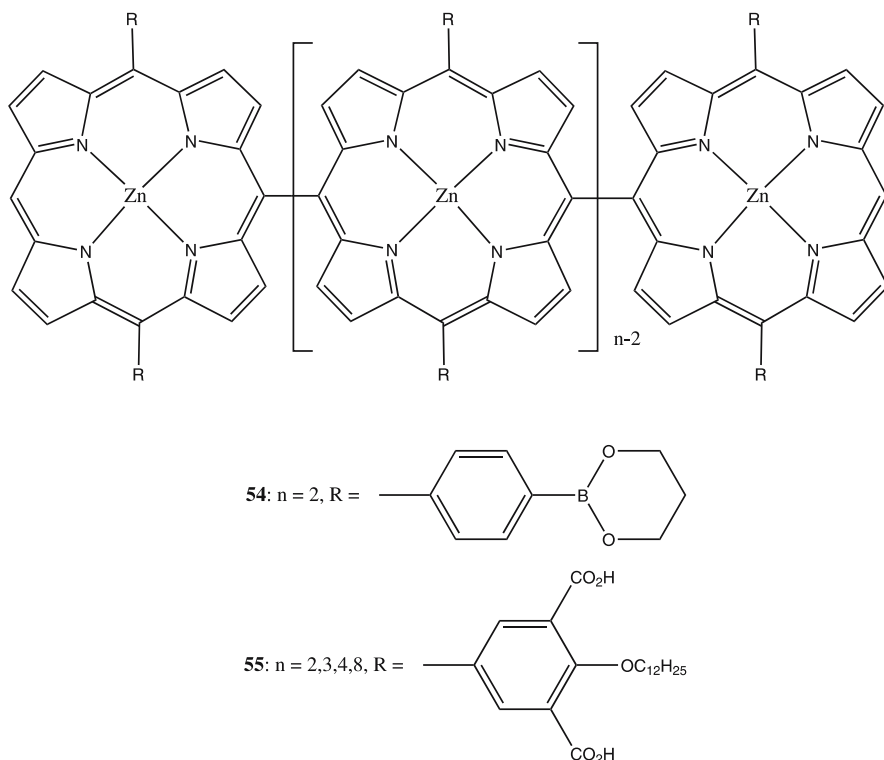


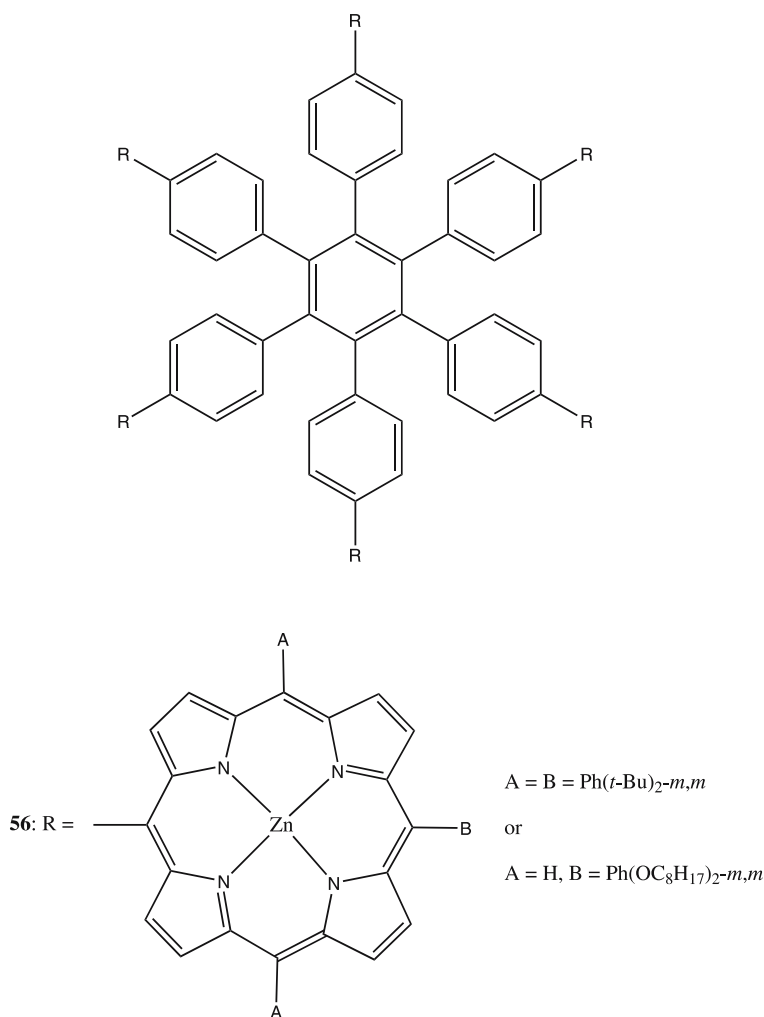
Fig. 6 The crystallographic structure of the **53**/(*R,R*)-DACH tweezer complex (*top and side views*)



from $n = 2$ to $n = 8$. Although the chiroptical properties were not rationalized, an interesting effect of chirality memory was reported for **55** ($n = 8$). Upon addition of the antipode to the helical array formed by the opposite enantiomer the sign of induced chirality, while reduced, could not be completely switched.

A different type of two-dimensional multiporphyrin arrangement was explored by the groups of Kim, Osuka, Jiang, and Aida to test its corresponding chirogenic properties [112, 113]. It was found that the hexamer **56** induced a strong bisignate CD signal in the Soret region in the presence of enantiopure (1-naphthyl)ethylamines exclusively, while other chiral amines led to only weak CEs indicating that the host-guest size matching was an essential requirement for effective chirogenesis in these systems. Even more drastic chiral selectivity was found for a series of dendric porphyrins **57–60** upon binding with a bidentate chiral guest. Particularly, the induced CD was strongly dependent upon the porphyrin multiplicity with the highest A value ($2693 \text{ M}^{-1} \text{ cm}^{-1}$) observed for **58**. However, these intriguing chiroptical effects have yet to be comprehensively investigated.

In order to fulfill the function of chiral discrimination and enantioselective catalysis as well as some others, the corresponding dimeric and oligomeric

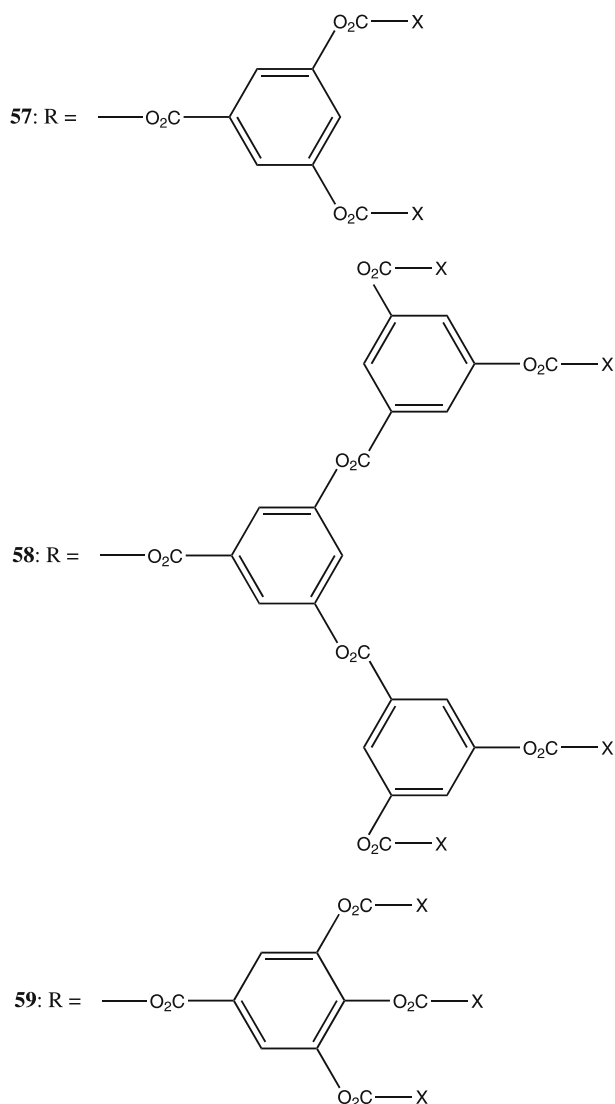


chiral porphyrinoids were used. Therefore, in the following section we shall show some recent representative examples of supramolecular systems based on this category of porphyrinoids.

4.2

Chiral Porphyrinoids

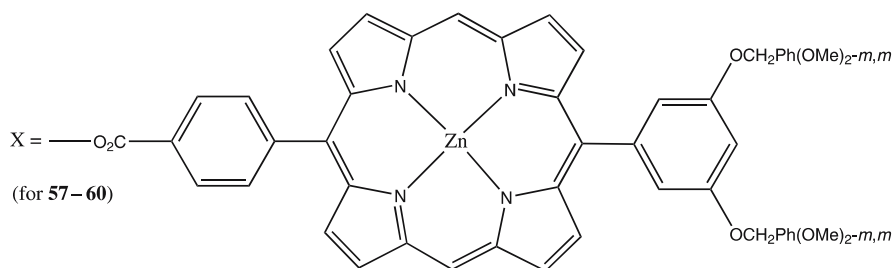
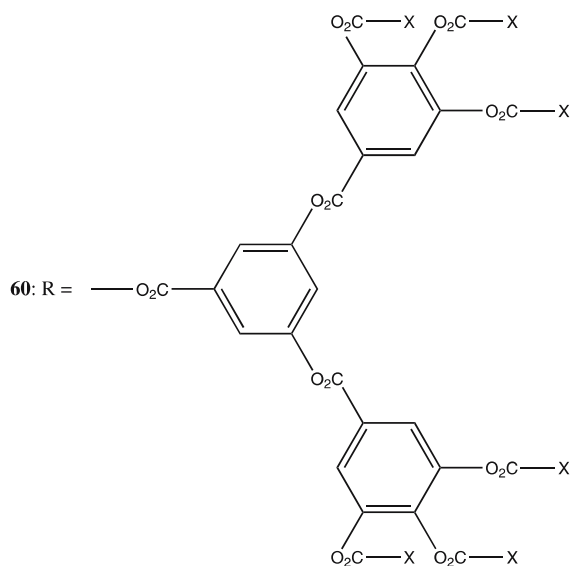
This type of porphyrin host can also interact with achiral guests and with chiral guests to generate corresponding supramolecular systems, and interaction with the achiral supramolecular counterparts will be discussed first.



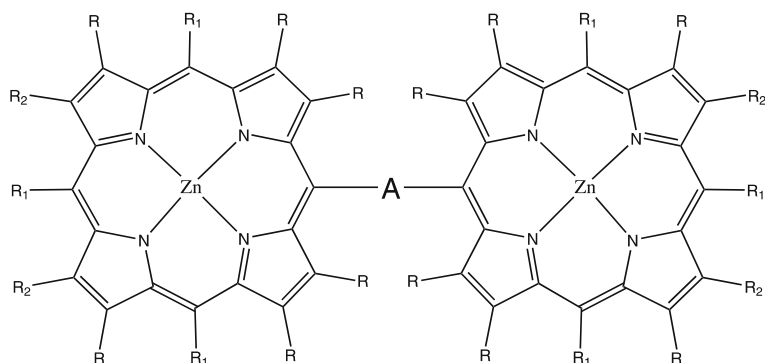
4.2.1

Interactions with Achiral Counterparts

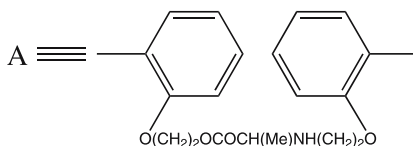
Because of the limited utility of this type of supramolecular system, there were only a few examples found in the literature. Particularly, Ji et al. linked two TPPs via a covalent bridge containing AA residues to obtain the conformationally flexible **61–63** [114, 115]. Upon interaction with achiral monodentate amines, the induced CD was dramatically diminished apparently due to breaking the attractive intramolecular interactions between two por-



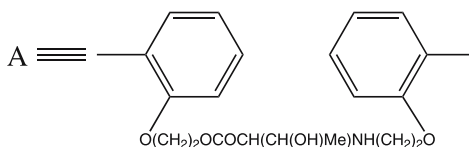
phyrin macrocycles. However, bidentate ligands behaved differently. For example, the short ethylenediamine resulted in CD sign inversion at a 1 : 1 molar ratio, while further addition led to decreasing the CD intensity. In the case of the longer 1,10-diaminodecane, the behavior was found to be the same as for monodentate ligands. Although the detailed mechanism of this chirality switching was not investigated, the authors interpreted this observation in terms of formation of chiral linear porphyrin arrays. However, the 1 : 1 tweezer structure would be more reasonable as in the case of above- and below-described supramolecular systems on the basis of achiral and chiral bis-porphyrins. A thorough analysis of the distance dependent host–guest complexation was undertaken by Ema, Utaka and coworkers using the



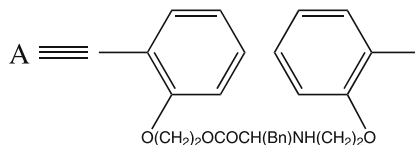
61: $R = R_2 = H$, $R_1 = Ph$



62: $R = R_2 = H$, $R_1 = Ph$

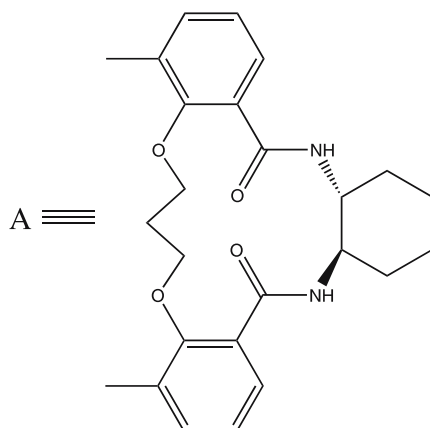


63: $R = R_2 = H$, $R_1 = Ph$

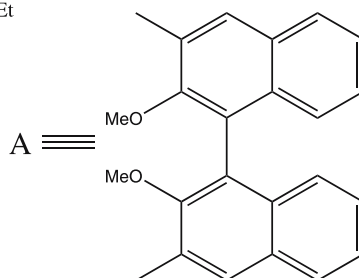


more rigidly bound **64** [116]. While the binding constants were found to be $> 10^7 \text{ M}^{-1}$ in all cases, this host exhibited a remarkable CD selectivity for the binding of a series of diamines $\text{NH}_2(\text{CH}_2)_n\text{NH}_2$ ($n = 2 - 7$) upon forming the corresponding 1 : 1 tweezers by tuning the chiroptical response. Particularly, the greatest amplification of negative CD couplet was found for $n = 6$, presumably caused by a good distance matching between the two Zn ions of **64** and the two amino groups of the diamine. Similar results were obtained by Hayashi, Ogoshi and coworkers upon using the BNP strapped rigid **65**, which gave the greatest exciton couplet ($A = +1788 \text{ M}^{-1} \text{ cm}^{-1}$) upon interaction with the longer diamine ($n = 8$), apparently due to the enlarged chiral cavity [117]. Although the observed effects opened an interesting opportunity for the chirality amplification of supramolecular systems, none of the reported distance dependences have been comprehensively rationalized.

64: $R = R_2 = H$, $R_1 = Ph$



65: $R = Me$, $R_1 = H$, $R_2 = Et$

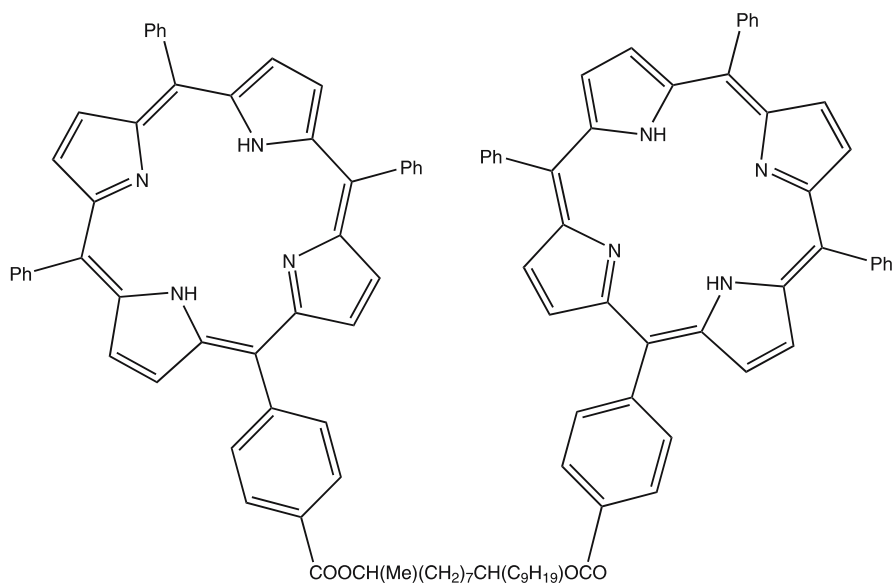


4.2.2

Interactions with Chiral Counterparts

Chirogenic supramolecular systems consisting of both optically active counterparts gained wider acceptance in different fields owing to some specific properties. For example, flexible and chiral bis-porphyrin **66** was used by Molinski et al. for determination of the absolute configuration of camonoxide A upon incorporation into liposomes prepared from 1,2-distearoyl-*sn*-glycero-3-phosphocholine and subsequent application of the exciton coupling CD method [118]. While the liposome environment played a rather ordering role to fix the spatial orientation of two porphyrins in **66**, empirical analysis of the chiroptical response from four possible stereoisomeric complexes and its comparison with the reference bis-porphyrin of known stereochemistry led to assignment of the C10 configuration as *R*.

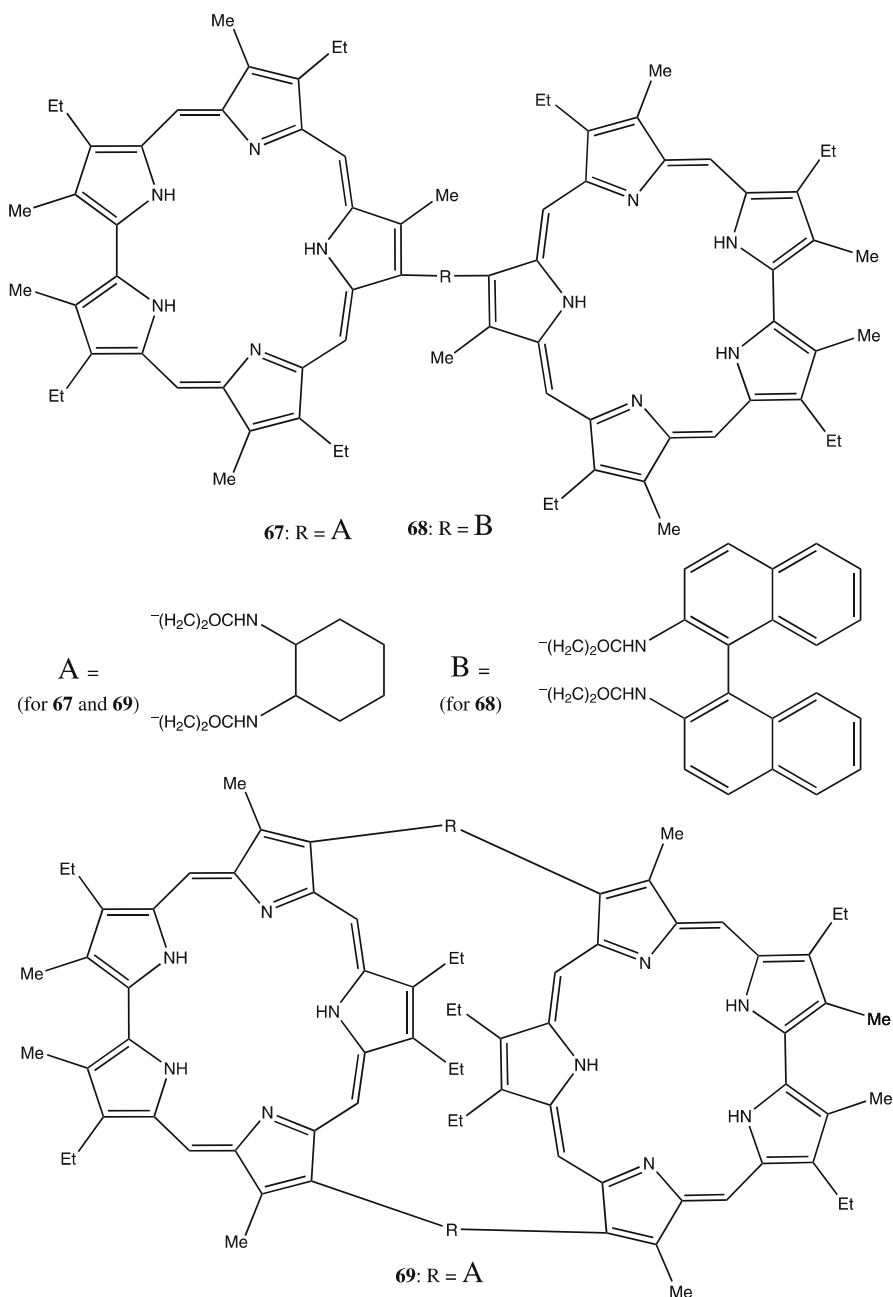
However, chiral recognition was the most common field of application of various chiral bis-porphyrinoids. Hence, Sessler's group prepared a series of bis-sapphyrins **67–69** for the chiral recognition of dicarboxylate anions via a combination of Coulombic attractions and hydrogen bonding [119]. While



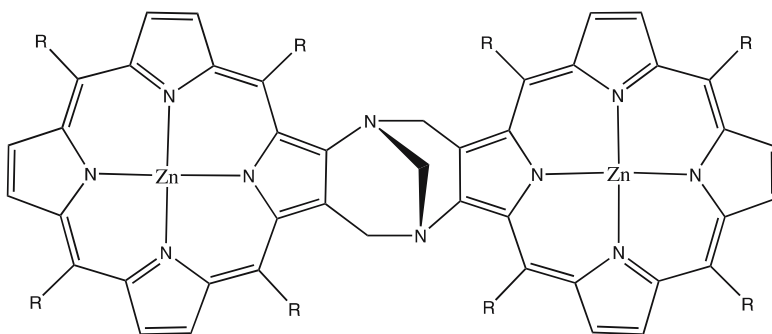
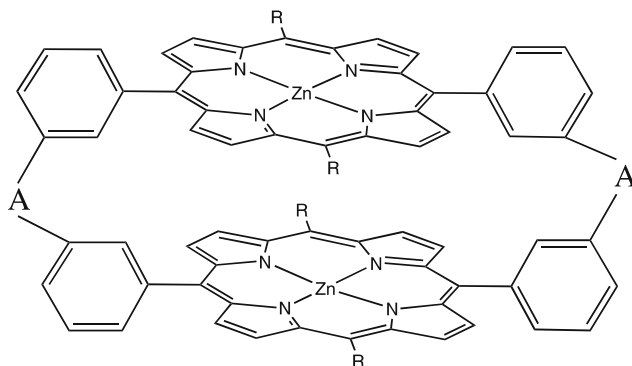
66

flexible **67** and **68** were found to form strong complexes with *N*-Cbz-Asp and *N*-Cbz-Glu with the association constants in the range of 10^4 – 10^5 M⁻¹, and displayed a preference for Glu over Asp, with **68** showing a modest level of enantiomeric selectivity, cyclic and more rigid **69** exhibited low affinity for these guests but showed significant chiral discrimination. Apparently, this arose from a good size and shape match between the host and guest as a result of the fixation of two porphyrinoids by two covalent bridges, however, the detailed recognition mechanism has yet to be understood. Crossley et al. were able to obtain 80–86% and 48% ee for the binding of histidine and lysine esters, respectively, by using the spatially fixed **70** owing to the ditopic interaction of the two nitrogen sites on the guest with the two zinc centers leading to the corresponding tweezer structure [120]. Similarly, Hayashi and coworkers also applied the rigidly BNP linked **65** for the chiral recognition of AA derivatives [81]. This host exhibited a particularly high (11–12 fold) ee for the lysine derivatives due to tweezer formation. The host–guest complex optimization revealed that the selectivity mechanism was based on steric repulsion occurring between the two methoxy groups of **65** and the amide group of the AA derivative in the unfavorable diastereomeric complex.

Oike, Aida and coworkers after chiral insertion of the leucine residue into the covalent bridge of achiral **43** obtained the corresponding chiral **71**, which was used for optical resolution of a series of artificial oligopeptides of different lengths containing the two terminal pyridines for ensuring the ditopic binding and a leucine group in the middle as a chiral source [121]. The ee



value was determined to be as high as 80%, with significant enhancement of the CD signal in the Soret region upon formation of the favorable tweezer complex. While the detailed mechanism of the chirality amplification was

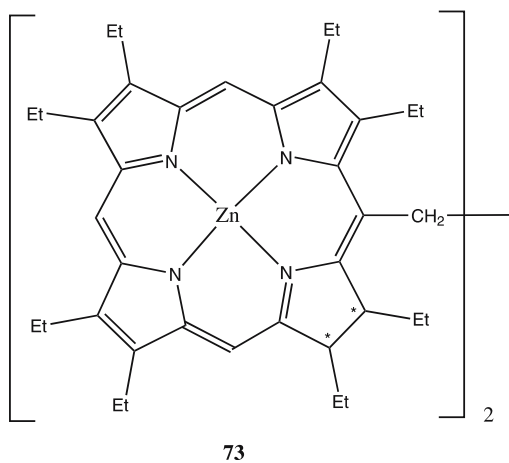
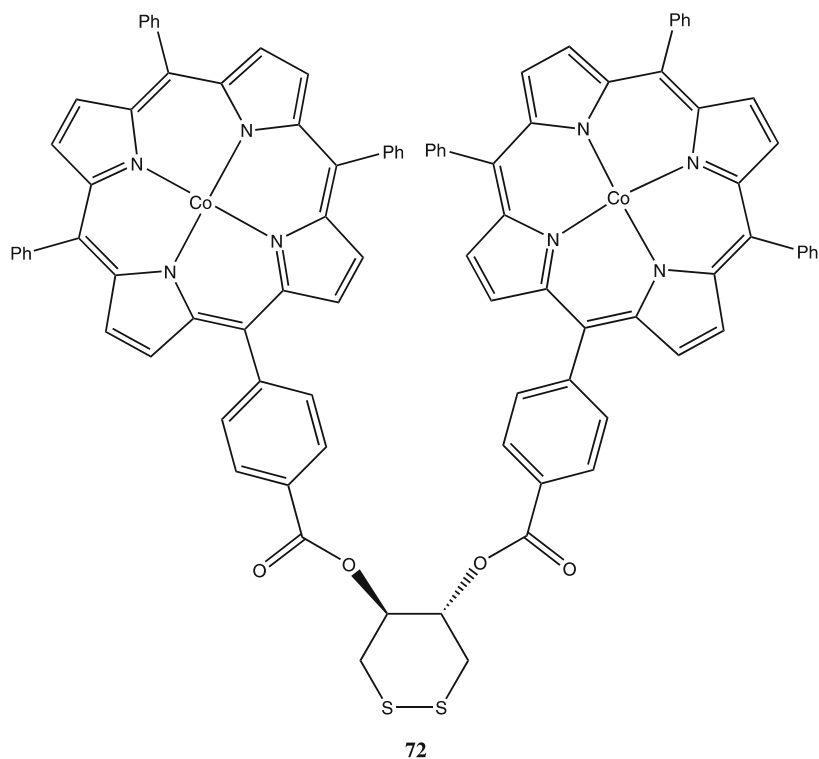
70: R = Ph(*t*-Bu)-*m,m*

71: R = Mes,



not presented, a comparative study revealed that the observed effect was apparently due to the directional stabilization of the twisted geometry of the host by the guest's helicity. An opposite tendency of chirality quenching upon host-guest interaction was reported by Paolesse et al. [122]. In particular, the negative monosignate CD signal of **72** was noticeably diminished and hypsochromically shifted in the presence of limonene with a different degree of the chirality modulation for the two enantiomers. Although neither chiroptical behavior nor recognition mechanism were rationalized, **72** was successfully applied to the enantiodiscrimination of this particular guest in the solid state upon deposition onto the gold electrodes of quartz crystal microbalances and exposure to the guest containing gas phase as the first step for developing nanogravimetric sensors.

Our group discovered a similar property of the CD signal reduction in the case of chiral bis-chlorin **73** upon interaction with chiral ligands due to the



induced conformational changes, while the chiroptical response was found to be noticeably different for the corresponding antipodal ligands [123]. This makes it possible to apply **73** for the purposes of chiral recognition utilizing a new principle of enantioselectivity on the basis of only a two-point host–

guest interaction model combined with the coupling electronic transitions of chromophoric host, the chiral orientation of which was controlled by the guest stereochemistry.

Despite the excessive complexity from the synthetic viewpoint, the above-discussed supramolecular systems are of obvious interest for various application fields, especially for chiral recognition purposes. However, the specific host–guest matching, which is one of the key elements for enantioselective processes, requires fine design of the chiral host that in turn imposes limitations on the scope of the host's applicability.

In contrast, the last type of chirogenic supramolecular systems consisting of aggregated porphyrinoids to be considered in the next section brings wider structural variability at a sacrifice in the geometrical certainty.

5

Supramolecular Systems on the Basis of Aggregated Porphyrinoids

The supramolecular assemblies involving aggregated porphyrinoids similarly to other types of previously discussed systems could be reasonably divided into different categories: on the basis of achiral, chiral monomeric, and dimeric porphyrinoids. Again, the simplest monomeric achiral porphyrinoids will be presented first.

5.1

Monomeric Achiral/Racemic Porphyrinoids

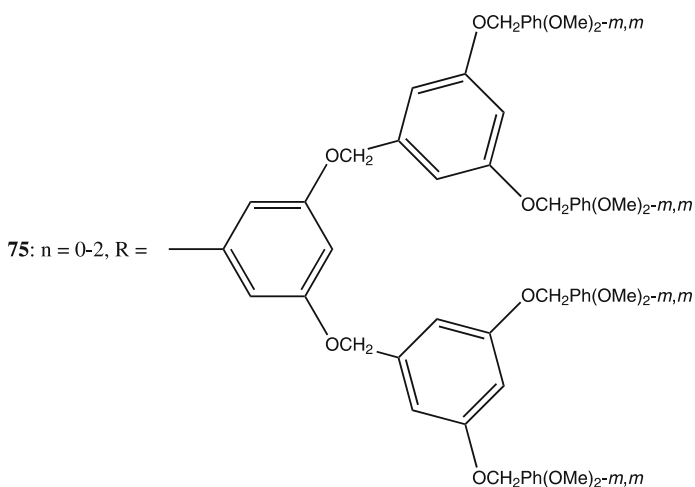
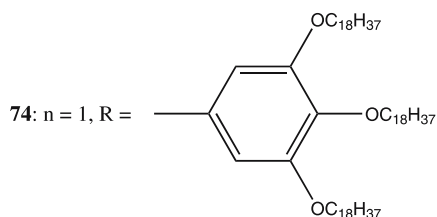
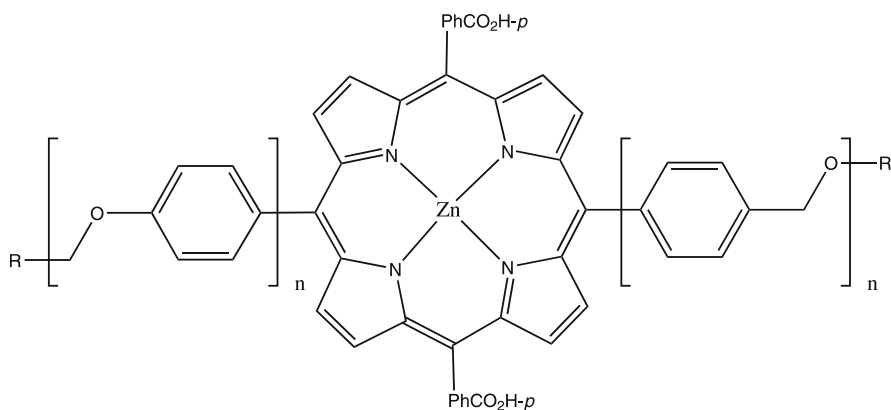
Although the aggregation process is responsible for greater supramolecular and chiroptical uncertainty and uncontrollability, the repeated intermolecular interactions make it possible to considerably amplify any small (and even almost negligible) chiral deformations within assembly leading to a significant chiroptical response. This results in two recently observed remarkable chirality phenomena that are spontaneous optical resolution and stirring induced chirality in porphyrin aggregates, which can be hardly seen in other types of supramolecular systems.

5.1.1

Spontaneous Resolution and Stirring Induced Chirality

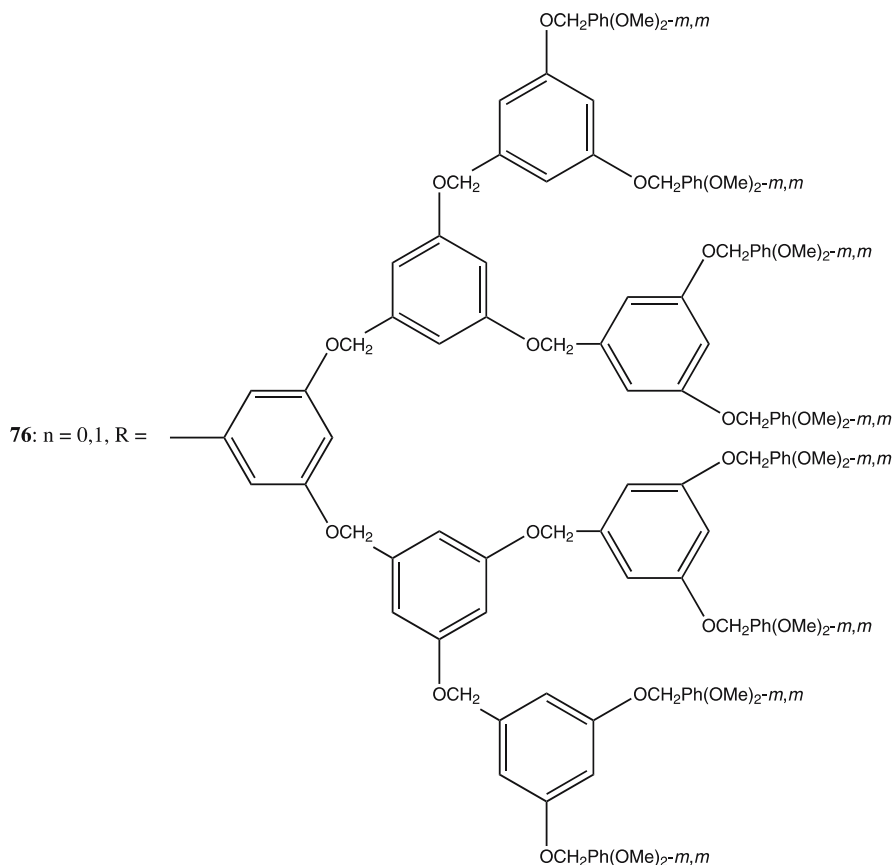
For example, Wakayama and coworkers discovered the formation of two oppositely orientated domains of 5,10,15,20-tetrakis(3,5-di-*tert*-butylphenyl)-porphine deposited onto a Cu surface using low-temperature scanning tunneling microscopy [124]. It was demonstrated that the twin domains were produced by a pair of chiral conformations induced by a combination of symmetrical tilting and twisting rotation of the phenyl rings with respect to

the porphyrin macrocycle upon surface adsorption. The tilting and twisting angles were estimated as 46 and 49°, respectively. In another development, Langmuir–Schaefer films made of achiral **10** and different amphiphiles exhibited significant optical activity in the Soret and Q band regions as a result of interporphyrin excitonic coupling occurring in spontaneously optically re-



solved J-aggregates as reported by Liu et al. [125]. The intensity of induced CD signal was dependent upon the nature of amphiphiles with the greatest observed for cetyltrimethylammonium bromide, while the chirality sign could not be controlled and appeared with equal probability. However, the chiroptical and resolution mechanisms have yet to be rationalized.

Ribó and coworkers reported an intriguing phenomenon of chirality control in the J-aggregates of **10** and related meso-sulfonatophenyl-substituted porphyrins by vortex motion during the aggregation process caused by the intermolecular association between the positively charged porphyrin ring and the negatively charged sulfonato groups [126–129]. While without stirring equal amounts of left- and right-handed aggregates were formed, upon stirring the porphyrins were arranged with a unidirectional helical orientation with about 85% probability, having the helicity dependent upon the vortex (i.e. stirring) direction. Clockwise and anticlockwise stirring generated right- and left-handed chirality, respectively, that corresponded to a strong positive and negative CD couplet in the porphyrin absorption re-



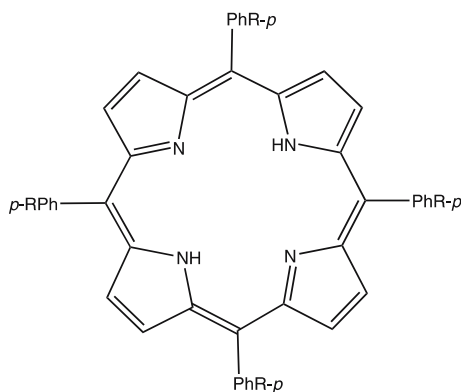
gion as a result of the interchromophoric exciton coupling. While the detailed mechanisms of the chirality induction and amplification remained unclear, it was suggested that the chiral vortex acted at the mesoscale level upon the kinetically controlled growth of the supramolecular assembly and spontaneous symmetry-breaking processes in the diffusion-limited generation of the high-molecular-weight homo-associates. This assumption was further supported by the direct visualization of 3D homochiral helices using atomic force microscopy. A similar approach was undertaken by Aida et al. to induce chirality in the hydrogen-bonded J-aggregates of dendritic **74–76** by spin-coating [130]. The chirality sign was also governed by the spin direction with clockwise and anticlockwise rotation generating a positive and negative exciton couplet, respectively, while the CD intensity was strongly affected by the structure of the dendritic periphery with the largest A value detected for **75** ($n = 1$). While the origin and driving forces of this phenomenon have yet to be rationalized, the generation of these 2D supramolecular sheets, which adopt a twisted geometry relative to one another upon rotational force, was proposed.

Besides the relatively weak asymmetry fields discussed above, chirogenic processes in various aggregated and self-assembled systems on the basis of achiral porphyrinoids can be driven by more conventional (and more powerful) chiroptical influences upon interacting with a supramolecular counterpart possessing optical activity.

5.1.2

Interactions with Chiral Counterparts

The well-known ability of porphyrins to aggregate in the solid state was utilized by Shinkai's, Liu's and our groups to generate supramolecular chirality using different interaction modes [131–133]. For example, **77** formed a one-dimensional face-to-face assembly in an organogel phase via combining the $\pi - \pi$ interporphyrin stacking and hydrogen-bonding interactions among urea moieties, which turned into an optically active aggregate in the presence of (*R*)- or (*S*)-*N*-(1-phenylethyl)-*N'*-dodecyl urea, thus resulting in an exciton-coupling CD signal in the Soret region [131]. A different type of the solid state structure was used to induce chirality in the aggregates of **10** [132]. Upon deposition of **10** onto a multilayer film consisting of enantiomeric tryptophan hexa- or octadecyl ester, the formed porphyrin J-aggregate adopted the chiral structure of the Trp surface resulting in bisignate and monosignate CD signals in the Soret and Q band regions, respectively, the sign of which was governed by the Trp absolute configuration. The third type of solid state supramolecular system was obtained on the basis of simple zinc octaethylporphyrin incorporated into a glassy KBr matrix in the presence of enantiopure 1-cyclohexylethylamine [133]. An interesting feature of the observed chirogenic process was a time-dependent gradual development of highly stable



77: R = $-\text{NHCONH}(\text{CH}_2)_{11}\text{Me}$

and optically active J-aggregates with the rate constant of $0.026\text{--}0.030\text{ h}^{-1}$ and helicity controlled by the amine's absolute configuration. While in general the chirality induction was a result of interporphyrin excitonic interaction within the chirally orientated assembly, elaboration of the precise chirality transfer mechanism in the solid state appeared to be an arduous task due to a great variability of possible conformations and aggregation modes as well as a rather limited number of available investigation methods. In connection with this, solution phase studies always open more opportunities for elucidation of the chirogenic processes in various aggregates.

Thus, Purrello et al. reported a self-assembly effect of oppositely charged **10** and CuTMP in the presence of enantiopure aromatic AAs yielding optically active aggregates that exhibited an exciton couplet type of CD signal in the Soret region [134]. A remarkable long lasting chirality memory effect expressed in terms of retaining the CD signal was observed upon removing the AA template. The initiation role of AA clusters (ca. 10^{-13} M for Phe) for the formation of similar concentrations of chiral porphyrin assemblies followed by the self-propagation process was established as a driving force for the chirogenic mechanism in this system. Further insight into the self-assembly of **10** onto polylysine was gained by Purrello, Periasamy and co-workers [135, 136]. This system also exhibited efficient chirality transfer from the optically active matrix to the porphyrin J-aggregates. This process was controlled by pH and rationalized in terms of the monomer-aggregate equilibrium, which shifted towards the aggregation state at low pHs due to the protonation of polylysine. Additionally, it was reported that metallation could strongly affect the aggregation behavior, and consequently the chiroptical properties: the corresponding Zn complex presumably favored the face-to-face arrangement yielding a complicated multicomponent CD signal, while the hexacoordinate Sn complex exhibited strong resistance towards aggregation. Another attractive development for this matrix was, as in the case of

monomeric AA, a combination of cationic and anionic porphyrins [137–140]. Particularly, **10** and various metal complexes of TMP formed stable chiral aggregates on poly(glutamic acid) resulting in a strong chiroptical response in the Soret region ($A = 2500 \text{ M}^{-1} \text{ cm}^{-1}$ for the Zn complex). Using CuTMP promoted further stability of this heteroporphyrin assembly allowing the chiral information to be memorized even when the chiral matrix was disrupted by raising pH. The chiral memory was retained for several days decreasing only by 30% in about 4 weeks owing to the kinetic inertness of the aggregates.

The last example to be cited in this section is an intermediate type of aggregated system consisting of racemic porphyrins. Thus, Bischoff et al. reported spontaneous optical resolution of a racemic mixture of diacetyl derivative of hematoporphyrin IX upon aggregation via $\pi - \pi$ and hydrogen-bonding interactions [141]. While the CD sign was always unpredictable, unexpectedly, increasing the temperature above 25°C at low salt concentration ($< 40 \text{ mM}$) produced drastic chiroptical changes resulting in a strong bisignate signal with an always positive first CE. The mechanism of such directional transformation is difficult to perceive in the absence of an external chiral field. However, the interaction with a chiral template such as DNA yielded a negative CD signal in the Soret region as a result of the porphyrin–DNA interactions.

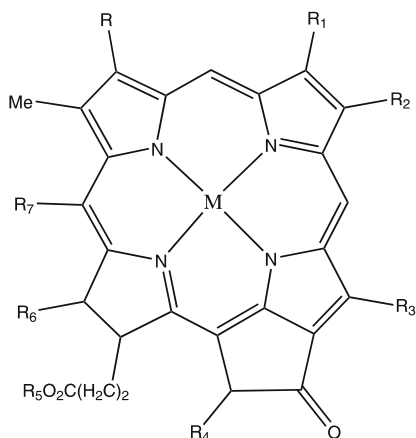
After examining the aggregates consisting of achiral/racemic porphyrins, it is reasonable to discuss the self-assembled systems based on chiral porphyrinoid.

5.2

Monomeric Chiral Porphyrinoids

This class of supramolecular systems is directly related to many biomimetic systems, including photosynthetic models and new materials, which have attracted much attention of the scientific community for years.

The largest part of research works in this field have been devoted to investigation of the aggregation behavior and self-assembly of different naturally occurring and artificial chlorin derivatives to mimic the photosynthetic special pairs and light-harvesting antennae. In general, this type of aggregation is driven by three binding forces: coordination to the central metal, H-bonding, and $\pi - \pi$ interactions, the individual contribution of which is varied depending upon a particular pigment structure, and characterized by considerable bathochromic shifts of the Q bands in comparison to the corresponding monomeric form. For example, Holzwarth, Oba, Watanabe et al. reported aggregation of chlorophylls and bacteriochlorophylls extracted from natural sources [142–144]. Using bacteriochlorophyll **78**, they observed autocatalyzed chlorosomal-like self-assembling, with an induction period followed by an exponential build-up, leading to a sigmoidal growth of the aggregate [142]. These chiral associates were characterized by a particular low



78: M = Mg, R = R₂ = R₃ = Et, R₁ = R₇ = Me, R₄ = R₆ = H, R₅ = phytlyl

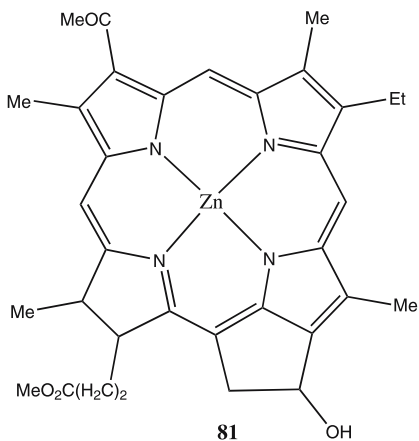
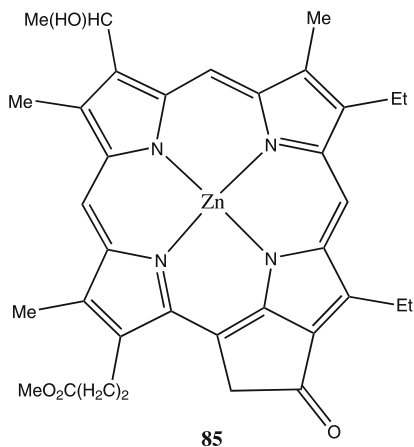
79: M = Mg, R = CH(OH)Me, R₁ = CHO, R₂ = Et or Pr or *i*-Bu, R₃ = Et, R₄ = H, R₅ = phytlyl, R₆ = R₇ = Me

80: M = Zn, R = CH(OH)Me or CH₂OH or CHCH₂, R₁ = Me or CH₂OH, R₂ = Et or Pr or *i*-Bu, R₃ = Me or Et, R₄ = H, R₅ = Me or stearyl or phytlyl, R₆ = Me, R₇ = H or Me

82: M = Zn, R = CH₂OH or (CH₂)₂OH or (CH₂)₃OH or CHCHCH₂OH or CHNOH, R₁ = R₃ = R₅ = R₆ = Me, R₂ = Et, R₄ = R₇ = H

83: M = Zn, R = CH₂OH, R₁ = R₃ = R₆ = Me, R₂ = Et, R₄ = R₇ = H, R₅ = CH₂Ph(OC₁₂H₂₅)₂-*m,m*

84: M = Cd, R = CH(OH)Me, R₁ = R₃ = R₆ = Me, R₂ = Et, R₄ = R₇ = H, R₅ = Me or stearyl



energy absorption at 739 nm yielding a strong negative CD excitonic couplet. The chiroptical properties of the aggregates were found to be largely affected by the epimeric compositions of chlorophyll *a/a'* (distinguished by the ab-

solute configuration at the 13² position) [143]. Surprisingly, the CD signal of the epimeric mixture comprising of a negative couplet (CEs at 765 nm and 742 nm) could not be reproduced by a linear combination of the CD spectra of the pure epimers, both of which were high-energy shifted negative couplets at 754/715 nm and 706/694 nm. This was an indication of different supramolecular architectures of the aggregates, but with the same orientation of coupling electronic transitions, however, the structural details have yet to be understood. Further insight into the diastereoselective control was obtained by studying a series of bacteriochlorophylls **79** distinguished by the stereochemistry of the hydroxy ethyl group at the 3 position [144]. It was found that the *S* absolute configuration promoted the formation of chlorosome-like structures as judged by the appearance of absorption at about 717 nm. Besides, **79** ($R_2 = i\text{-Bu}$) showed a clear solvent dependence of the chiroptical response even resulting in a chirality switching effect from negative in hexane to positive in a water–lecitin mixture.

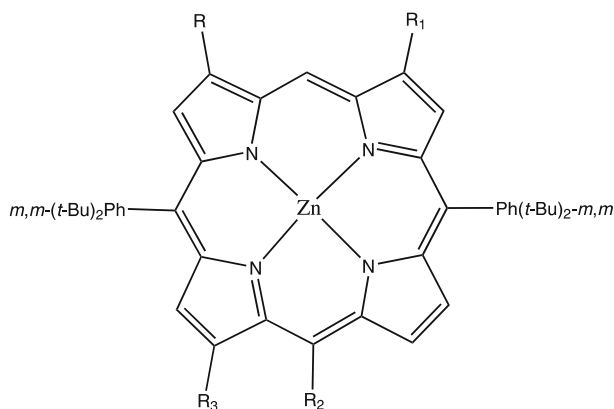
Among the synthetic analogs of natural pigments, Zn complexes of chlorins were the most frequently used for self-assembly owing to their well-determined pentacoordinate ability. This approach was undertaken by Tamaki, Knapp, Potenza, Schugar, Würthner et al. [145–149]. As in the case of natural chlorophylls, Zn complexes of **80** exhibited a tendency to form J-aggregates in the water–lecitin solution, the structures and subsequent chiroptical properties of which were dependent upon the substituent's stereochemistry at the 3 position and other peripheral substituents [145]. Again the epimeric mixture resulted in new spectral profiles, which were not reproducible by a spectral combination of the individual components. More pronounced and better understood diastereomeric control over aggregation was obtained by changing stereochemistry at the 13' position of **81** [146]. The self-assembly pathways were found to be different for the two epimers yielding an energetically stable face-to-face dimer for the (*R*)-diastereomer and large oligomers for the (*S*)-diastereomer with a significant difference in the stabilization energy. Also, the CD signal of (*R*)-diastereomer, consisting of a negative couplet in the Q_y region, was consistent with the anticlockwise coupling of the corresponding electronic transitions in the optimized dimeric structure. Another structural modification of the substituent at the 3 position allowed investigation of the distance dependence on the self-assembly [147]. Particularly, it was found that increasing the distance between the hydroxyl group and the chlorin moiety in **82** diminished the aggregation abilities as was found by smaller red-shifts of the Q_y band absorption and reduction of the negative CD couplet arising from an increase of the conformational flexibility. In contrast, enhancement of the substituent's rigidity by introduction of the double bond resulted in structurally ordered large aggregates yielding precipitates. Further replacement with the oxime group yielded a dimeric structure in solution with a special pair like pyrrole-over-pyrrole overlap and a positive Q_y exciton couplet in the CD spectrum, which correlated with the

obtained crystallographic structure [148]. Changing the ester group as in the case of **83** was another stimuli to control the self-organization process [149]. It was shown that **83** formed well-defined rod aggregates, spin-coating samples of which were visualized by atomic force microscopy. The chiroptical response consisted of an intense negative Q_y exciton couplet, which was reversibly controlled by the temperature resulting in its considerable reduction upon increasing the temperature. Additional information regarding the influence of the ester group on the aggregation behavior was obtained by Matysik, de Groot and coworkers upon using Cd complexes **84** [150]. While the truncated tail of the methyl ester yielded a microcrystalline solid with a head-to-tail orientation of the chlorin layers, the long stearyl tail gave more disordered aggregates having both *syn* and *anti* layers, as suggested by NMR, which resemble the chlorosomal antennae.

Besides chlorins, chiral porphyrins were also successfully used for photosynthetic mimicking. For example, Fajer et al. revealed supramolecular organization of the bacteriochlorophyll *d* analog **85** on the basis of crystallographic analysis [151]. The formed aggregates were comprised of hydrogen-bonded dimers with the assistance of $\pi - \pi$ interactions, surprisingly without the expected Zn – O coordination, with the interporphyrin distance being 3.33 Å. These dimers were subsequently connected to each other via the $\pi - \pi$ interactions with a separation of 3.54 Å between successive dimer units. A series of chiral porphyrins **86–88** were applied by Balaban and coworkers to obtain the corresponding self-aggregates, which were characterized by an intense CD exciton couplet and a monosignate signal in the Soret and Q band regions, respectively. The chirality sign was found to be governed by the absolute configuration of the stereogenic carbon, while the CD induction was dependent upon the solvent [152, 153].

Aside from photosynthetic models, the aggregation and self-assembly properties of various chiral porphyrinoids were investigated. For example, a porphyrin–cyclodextrin conjugate **89** was reported by Carofiglio, Fornasier and coworkers to have unusual pH-controlled chiroptical properties upon self-assembling [154]. In particular, a negative CD exciton couplet in the Soret region induced in alkaline conditions as a result of intermolecular interactions was switched into a positive bisignate CD signal of a complex profile in acidic media arising from the split absorption bands. Although some aggregation modes (inclusion complexes, face-to-face, and J-type arrangement) were proposed, none of them gave a clear rationale for the observed chirality switching phenomenon.

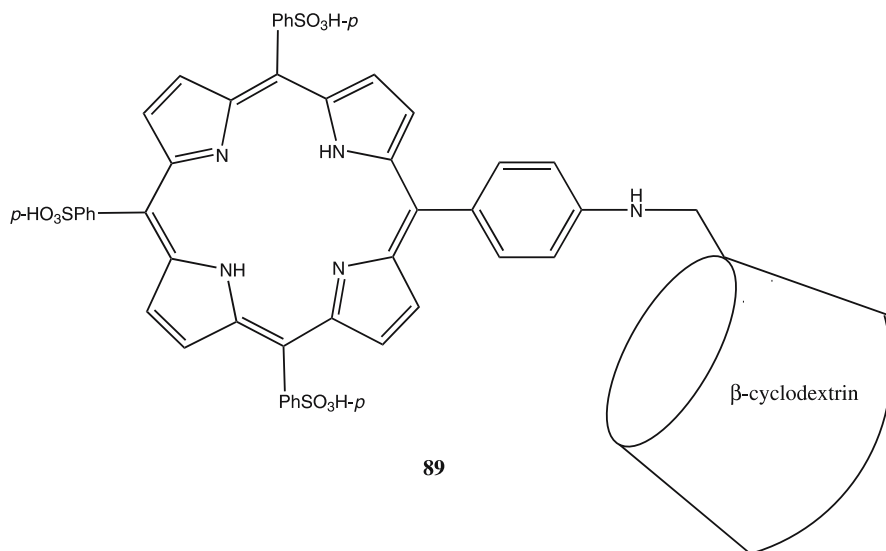
A different type of chiral porphyrin bearing the guanidine moieties **90** exhibited a strong aggregation ability caused by the Coulombic and H-bonding attraction forces of the guanidine residues combined with $\pi - \pi$ interporphyrin stacking as reported by Kral, Schmidtchen et al. [155]. These self-assemblies produced a CD exciton couplet in the Soret region, the intensity and surprisingly even sign of which were controlled by the nature of the



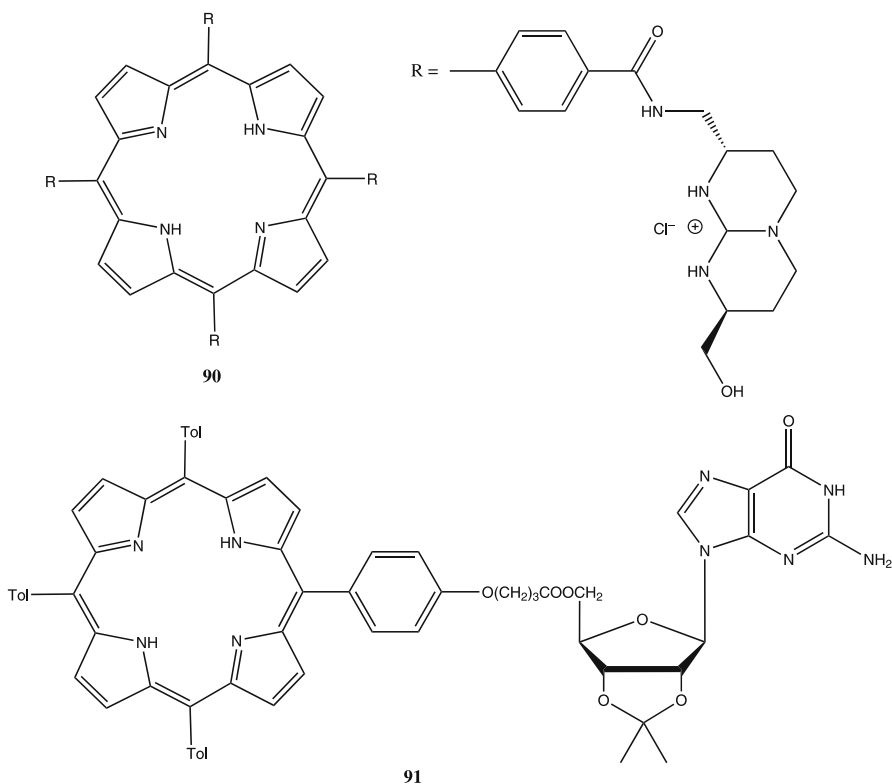
86: R = CH(OH)Me, R₁ = R₂ = H, R₃ = COMe

87: R = R₂ = H, R₁ = CH(OH)Me, R₃ = COMe

88: R = CH(OH)Me, R₁ = R₃ = H, R₂ = CHO

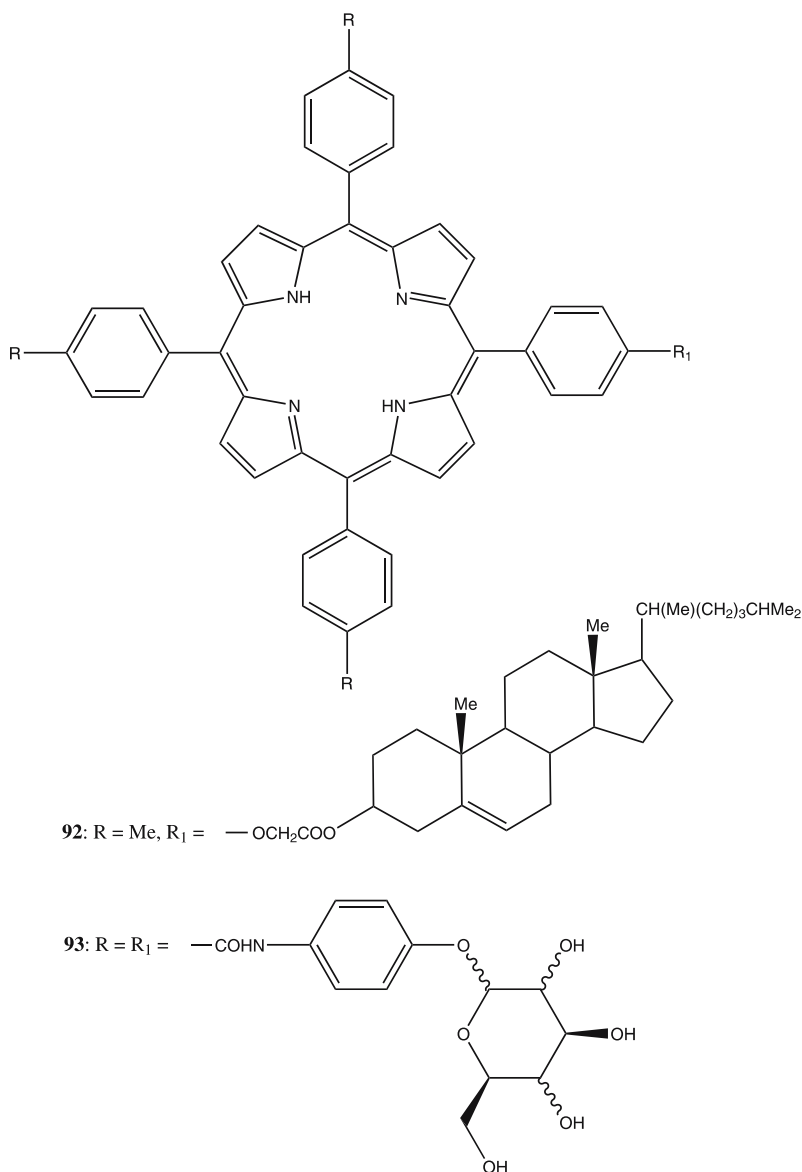


counteranion, which apparently affected the supramolecular structure of the aggregates, while particular relationships between the anion structure and chiroptical response have not been established. A more directional approach to obtaining self-assemblies of predictable structure was exploited by Masiero et al. by using a porphyrin–guanosine conjugate **91** [156]. This conjugate formed an octameric supramolecular complex consisting of two G-quartets in

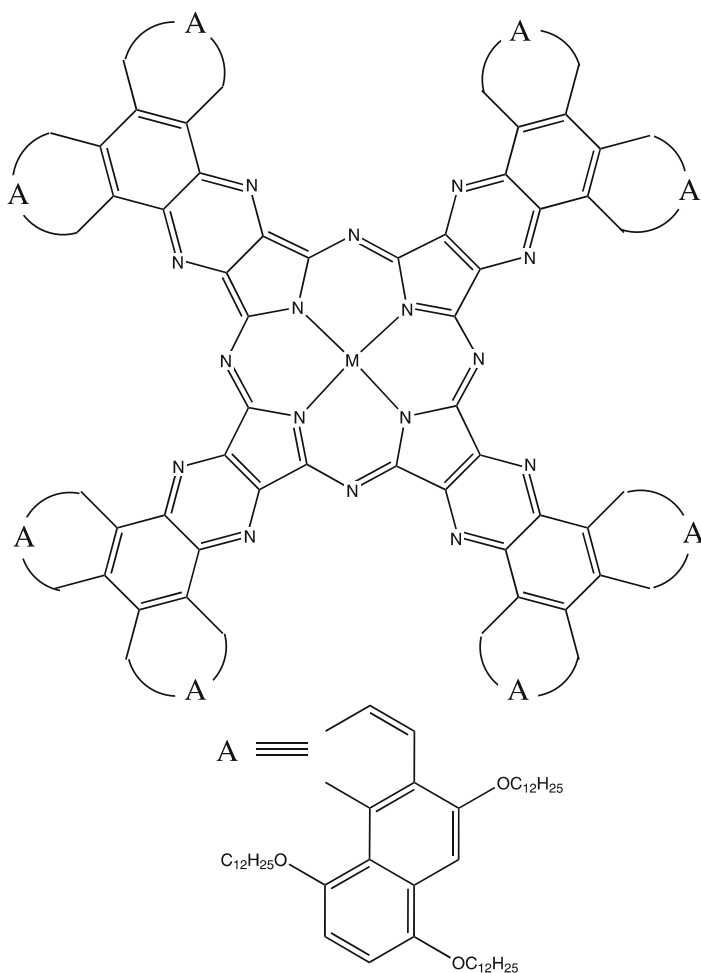


the presence of potassium picrate inducing a positive CD exciton couplet in the Soret region, a relatively low intensity of which was likely to be as a result of the conformational freedom of the porphyrin chromophores owing to the flexible linkage.

Besides the above-mentioned applications, new chiral materials were prepared by Shinkai, Katz and coworkers utilizing the aggregation properties of optically active porphyrinoids [157–160]. Thus, cholesterol-containing porphyrins **92** exhibited gelation properties, which were strongly dependent upon the stereochemistry at the C-3 position of the cholesterol moiety with the (*S*)-configuration being exclusively able to form a gel phase [157]. The chiroptical response was also changed from a monosignate negative CE to a complex red-shifted CD signal that consisted of several CE of opposite signs, probably due to porphyrin stacking according to the J-aggregation mode. More intelligent control of the gel structure was achieved via the synergetic effect of $\pi - \pi$ interporphyrin interactions and hydrogen bonding between the saccharide moieties in **93** [158, 159]. It was demonstrated that these porphyrins formed a one-dimensional aggregate, the helical orientation of which was governed by the chirality of the appended sugar residue. For example, the aggregates made of α - and β -D-galactopyranoside moieties yielded nega-



tive and positive CD couplets in the Soret region indicating a right- and left-handed helical orientation, respectively, which were further visualized by scanning electron microscopy. Moreover, these organic helices were successfully transcribed into inorganic helical silica fibers. A similar type of interchromophore stacking was obtained by using optically active phthalocyanines **94** resulting in a CD exciton couplet in the Q band region [160]. The observed spectral profile was essentially preserved in a casting film,



94: M = Cu, Ni

while the obtained Langmuir–Blodgett films exhibited large second-order nonlinear optical responses owing to the chirality of these supramolecular systems.

While self-assembled and aggregated chirogenic systems are mainly based on monomeric porphyrinoids, a further increase of the pigment multiplicity, despite raising the overall complexity of supramolecular structures, may lead to novel functional properties and new applications. Therefore, in the last section we shall show a few examples of self-assembled and aggregated systems constructed from dimeric and oligomeric porphyrins.

5.3

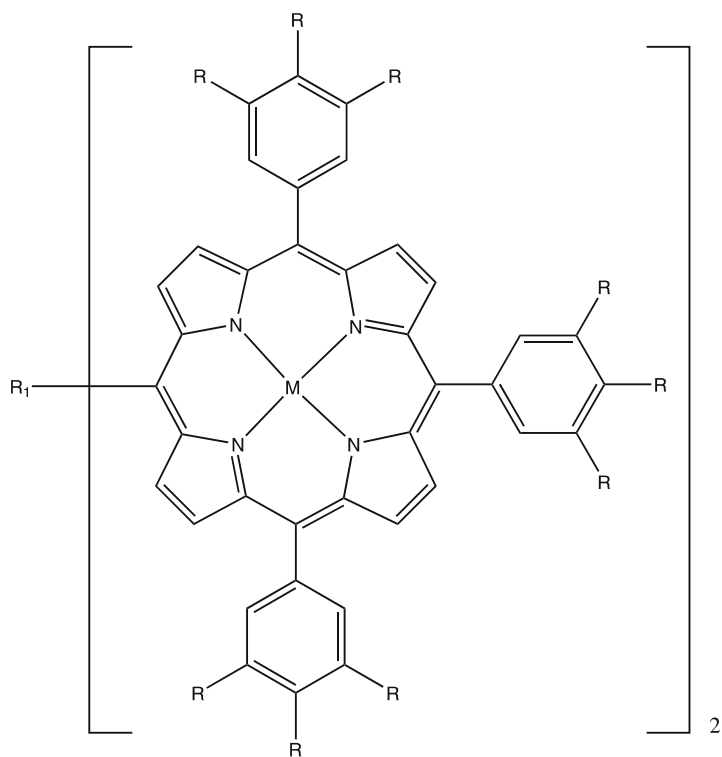
Dimeric/Oligomeric Porphyrinoids

Since this class of supramolecular assemblies is represented by a small number of examples due to the enhanced structural intricacy and synthetic complexity, we shall present both chiral and achiral dimeric/oligomeric porphyrinoid-based systems in one section.

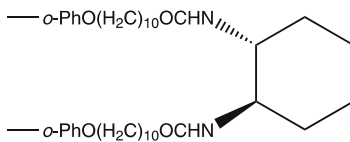
Hence, our group, while studying a phase transition effect on supramolecular chirogenesis, has found that **53** ($M = \text{Zn}$) formed chiral aggregates in a solid KBr matrix in the presence of enantiopure monoamines [161]. These structures were characterized by a bathochromic shift in comparison to the solution phase CD signal of complex shape due to simultaneous contribution of the inter- and intramolecular exciton couplings and considerable enhancement of the anisotropy factors by a factor of 1.6–9.1 due to the asymmetry amplification effect in the aggregates. Surprisingly, the chirality sign was also switched reflecting opposite orientation of the inter- and intramolecular helicity, although the detailed mechanism of the supramolecular chirality induction in the solid state has yet to be understood.

Kimura, Shirai and coworkers used two chiral dimeric porphyrins **95** and **96** to investigate their self-assembling behavior [162, 163]. While incorporation into fibers made of the alkylamide derivatives of (*R,R*)-DACH, **95** formed stable well-resolved fibrous assemblies as visualized by transmission electron microscopy, the fluorescence of which was not quenched by external electron acceptors [162]. However, the induced CD was not detected indicating an inability of **95** to form chirally orientated aggregates under the applied conditions. In contrast, **96** was able to produce optically active intermolecular self-assemblies with an enhanced chiroptical response through the μ -oxo bridging in an alkali solution, while intramolecular μ -oxo dimer formation was excluded on the basis of steric reasons [163].

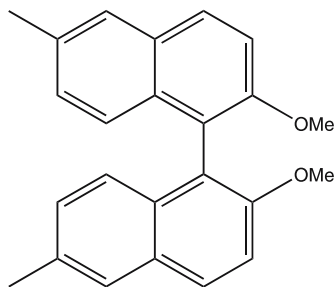
Osuka's and Kim's groups reported more controllable self-assembly of dimeric porphyrins **97** into chiral porphyrin boxes of well-defined structure that were comprised of four dimeric molecules by using the pentacoordinate ability of Zn porphyrins [164]. The obtained self-assemblies exhibited a complex CD signal in the Soret region, the intensity of which was considerably enhanced (more than 10 times) in comparison to the CD signal of **97** due to multiple exciton coupling interactions. While the precise band assignment has not been done, an exciton coupling model was proposed upon empirical consideration of the fixed geometry of these supramolecular systems. In addition, the well-defined spatial arrangement ensured the effective exciton energy migration described by the Förster-type incoherent energy hopping model depending upon the size of porphyrin boxes.

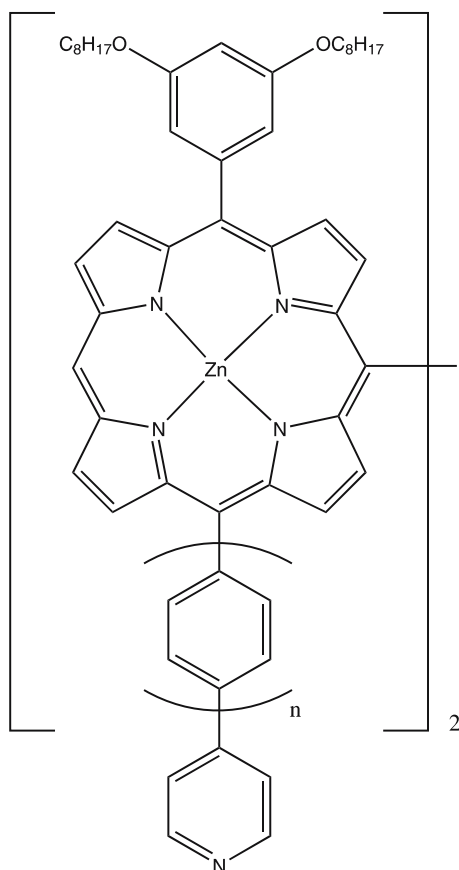


95: $M = \text{Zn}$, $R = \text{H}$, $R_1 =$



96: $M = \text{FeCl}$, $R = \text{OMe}$, $R_1 =$





97: $n = 0, 1, 2$

6

Concluding Remarks and Future Perspectives

In conclusion, this review demonstrated recent progress on supramolecular chirogenesis in different porphyrinoid-based assemblies. In particular, the wide structural diversity of these systems was emphasized in light of high demand from various fields of science, technology and medicine. However, despite a great number of presented examples, and the apparent importance of the obtained asymmetries, the detailed origin of the chiroptical properties of many of them have been only perfunctorily examined. Furthermore, there are only a few examples of comprehensive and unambiguous rationalization of optical activity in these assemblies. Also, although supramolecular chemistry offers a unique tool for fine-tuning the chiroptical properties via various controlling factors, this opportunity has been scarcely exploited. These are

serious setbacks for designing optimal systems for fulfilling a particularly desired function, since the optical activity outcome is often directly related to various chiroptical applications. Therefore, further efforts in this field should be concentrated on closing this gap, which should have an immediate positive impact in such important applications as asymmetric synthesis and catalysis, photodynamic therapy and magnetic resonance imaging, structural and stereochemical assignment, chemical and chiroptical sensors and biomimetic studies. Furthermore, recent advances in this field exhibited considerable promise for newly emerged molecular technologies such as chiral nanotechnology, intelligent molecular devices and chiroptical memory.

Acknowledgements We thank Dr. G. A. Hembury for assistance in the preparation of this manuscript.

References

1. Voet D, Voet JG (1995) *Biochemistry*, 2nd edn. Wiley, New York
2. Steed JW, Atwood JL (2000) *Supramolecular chemistry*. Wiley, Chichester
3. Kyte J (1995) *Structure in protein chemistry*. Garland Publishing, Inc., New York
4. Rodger A, Nördén B (1997) *Circular dichroism and linear dichroism*. Oxford University Press, Oxford
5. Hsu M-C, Woody RW (1971) *J Am Chem Soc* 93:3515
6. Blauer G, Sreerama N, Woody RW (1993) *Biochem* 32:6674
7. Björling SC, Goldbeck RA, Paquette SJ, Milder SJ, Kliger DS (1996) *Biochem* 35:8619
8. Boffi A, Wittenberg JB, Chiancone E (1997) *FEBS Lett* 411:335
9. Santucci R, Ascoli F (1997) *J Inorg Biochem* 211
10. Linnanto J, Korppi-Tommola JFI, Helenius VM (1999) *J Phys Chem B* 103:8739
11. Georgakopoulou S, Frese RN, Johnson E, Koolhaas C, Cogdell RJ, van Grondelle R, van der Zwan G (2002) *Biophys J* 82:2184
12. Iida K, Ohya N, Kashiwada A, Mimuro M, Nango M (2000) *Bull Chem Soc Jpn* 73:221
13. Lawrence DS, Jiang T, Levett M (1995) *Chem Rev* 95:2229
14. van Nostrum CF, Nolte RJM (1996) *Chem Commun* 2385
15. Dinolfo PH, Hupp JT (2001) *Chem Mater* 13:3113
16. Miyake H, Tsukube H (2005) *Supramol Chem* 17:53
17. Hamilton TD, MacGillivray LR (2004) *Cryst Growth Des* 4:419
18. Borovkov VV, Hembury GA, Inoue Y (2004) *Acc Chem Res* 37:449
19. Ogoshi H, Mizutani T (1996) *J Synth Org Chem Jpn* 54:906
20. Ogoshi H, Mizutani T (1998) *Acc Chem Res* 31:81
21. Ogoshi H, Mizutani T (1999) *Curr Opin Chem Biol* 3:736
22. Ogoshi H, Mizutani T, Hayashi T, Kuroda Y (2000) In: Kadish KM, Smith KM, Guillard R (eds) *The porphyrin handbook*, vol 6. Academic Press, New York, p 279
23. Marchon J-C, Ramasseul R (2003) In: Kadish KM, Smith KM, Guillard R (eds) *The porphyrin handbook*, vol 11. Academic Press, New York, p 75
24. Huang X, Nakanishi K, Berova N (2000) *Chirality* 12:237
25. James TD, Sandanayake KRAS, Shinkai S (1996) *Angew Chem Int Ed Engl* 35:1911
26. Robertson A, Shinkai S (2000) *Coord Chem Rev* 205:157
27. Shinkai S, Ikeda M, Sugasaki A, Takeuchi M (2001) *Acc Chem Res* 34:494

28. Shinkai S, Takeuchi M (2004) *Biosens Bioelectron* 20:1250
29. Hartley JH, James TD, Ward CJ (2000) *J Chem Soc, Perkin Trans* 1:3155
30. Tsukube H, Shinoda S (2000) *Enantiomer* 5:13
31. Tsukube H, Shinoda S, Tamiaki H (2002) *Coord Chem Rev* 226:227
32. Tsukube H, Shinoda S (2002) *Chem Rev* 102:2389
33. Simonneaux G, Maux PL (2002) *Coord Chem Rev* 228:43
34. Bondy CR, Loeb SJ (2003) *Coord Chem Rev* 240:77
35. Finn MG (2002) *Chirality* 14:534
36. Wenzel TJ, Wilcox JD (2003) *Chirality* 15:256
37. Allenmark S (2003) *Chirality* 15:409
38. Pasternack RF (2003) *Chirality* 15:329
39. Kobayashi N (2001) *Coord Chem Rev* 219–221:99
40. Formaggio F, Peggion C, Crisma M, Kaptein B, Broxterman QB, Mazaleyrat J-P, Wakselman M, Toniolo C (2004) *Chirality* 16:388
41. Aspinall HC (2002) *Chem Rev* 102:1807
42. Arnold DP, Blok J (2004) *Coord Chem Rev* 248:299
43. McMillin DR, McNett KM (1998) *Chem Rev* 98:1201
44. Shelnutt JA, Song X-Z, Ma J-G, Jia S-L, Jentzen W, Medforth CJ (1998) *Chem Soc Rev* 27:31
45. Feiters MC, Rowan AE, Nolte RJM (2000) *Chem Soc Rev* 29:375
46. Kobayashi N (2002) *Bull Chem Soc Jpn* 75:1
47. Kobayashi N (2003) In: Kadish KM, Smith KM, Guillard R (eds) *The porphyrin handbook*, vol 15. Academic Press, New York, p 161
48. Furusho Y, Kimura T, Mizuno Y, Aida T (1997) *J Am Chem Soc* 119:5267
49. Mizuno Y, Aida T, Yamaguchi K (2000) *J Am Chem Soc* 122:5278
50. Kijima H, Takeuchi M, Shinkai S (1998) *Chem Lett* 781
51. Mizutani T, Murakami T, Kurahashi T, Ogoshi H (1996) *J Org Chem* 61:539
52. Mizutani T, Wada K, Kitagawa S (2000) *J Org Chem* 65:6097
53. Tamiaki H, Matsumoto N, Unno S, Shinoda S, Tsukube H (2000) *Inorg Chim Acta* 300–302:243
54. Tsukube H, Wada M, Shinoda S, Tamiaki H (1999) *Chem Commun* 1007
55. Awawdeh MA, Legako JA, Harmon HJ (2003) *Sens Actuator B* 91:227
56. Forman JE, Barrans RE Jr, Dougherty DA (1995) *J Am Chem Soc* 117:9213
57. Tamiaki H, Unno S, Takeuchi E, Tameshige N, Shinoda S, Tsukube H (2003) *Tetrahedron* 59:10477
58. Ishi-i T, Jung JH, Shinkai S (2000) *J Mater Chem* 10:2238
59. Wang CZ, Zhu ZA, Li Y, Chen YT, Wen X, Miao FM, Chan WL, Chan ASC (2001) *New J Chem* 25:801
60. Monti D, Cantonetti V, Venanzi M, Ceccacci F, Bombelli C, Mancini G (2004) *Chem Commun* 972
61. Cantonetti V, Monti D, Venanzi M, Bombelli C, Ceccacci F, Mancini G (2004) *Tetrahedron: Asym* 15:1969
62. Bian Y, Wang R, Jiang J, Lee C-H, Wang J, Ng DKP (2003) *Chem Commun* 1194
63. Tashiro K, Konishi K, Aida T (1997) *Angew Chem Int Ed Engl* 36:856
64. Tashiro K, Konishi K, Aida T (2000) *J Am Chem Soc* 122:7921
65. Fukuda T, Olmstead MM, Durfee WS, Kobayashi N (2003) *Chem Commun* 1256
66. Muranaka A, Okuda M, Kobayashi N, Somers K, Ceulemans A (2004) *J Am Chem Soc* 126:4596
67. Arimori S, Takeuchi M, Shinkai S (1996) *Chem Lett* 77
68. Takeuchi M, Chin Y, Imada T, Shinkai S (1996) *Chem Commun* 1867

69. Fan J, Whiteford JA, Olenyuk B, Levin MD, Stang PJ, Fleischer EB (1999) *J Am Chem Soc* 121:2741
70. Ayabe M, Yamashita K, Sada S, Ikeda A, Sakamoto S, Yamaguchi K (2003) *J Org Chem* 68:1059
71. Takeuchi M, Imada T, Shinkai S (1998) *Bull Chem Soc Jpn* 71:1117
72. Takeuchi M, Imada T, Shinkai S (1998) *Angew Chem Int Ed Engl* 37:2096
73. Sugasaki A, Ikeda M, Takeuchi M, Robertson A, Shinkai S (1999) *J Chem Soc, Perkin Trans 1*:3259
74. Sugasaki A, Ikeda M, Takeuchi M, Shinkai S (2000) *Angew Chem Int Ed* 39:3839
75. Sugasaki A, Sugiyasu K, Ikeda M, Takeuchi M, Shinkai S (2001) *J Am Chem Soc* 123:10239
76. Yamamoto M, Sugasaki A, Ikeda M, Takeuchi M, Frimat K, James TD, Shinkai S (2001) *Chem Lett* 520
77. Kral V, Rusin O, Schmidtchen FP (2001) *Org Lett* 3:873
78. Guo Y-M, Oike H, Aida T (2004) *J Am Chem Soc* 126:716
79. Mizuno Y, Aida T (2003) *Chem Commun* 20
80. Tsukube H, Tameshige N, Shinoda S, Unno S, Tamiaki H (2002) *Chem Commun* 2574
81. Hayashi T, Aya T, Nonoguchi M, Mizutani T, Hisaeda Y, Kitagawa S, Ogoshi H (2002) *Tetrahedron* 58:2803
82. Monti D, Monica LL, Scipioni A, Mancini G (2001) *New J Chem* 25:780
83. Kubo Y, Ishii Y, Yoshizawa T, Tokita S (2004) *Chem Commun* 1394
84. Kubo Y, Ohno T, Yamanaka J-i, Tokita S, Iida T, Ishimaru Y (2001) *J Am Chem Soc* 123:12700
85. Huang X, Rickman BH, Borhan B, Berova N, Nakanishi K (1998) *J Am Chem Soc* 120:6185
86. Huang X, Borhan B, Rickman BH, Nakanishi K, Berova N (2000) *Chem Eur J* 6:216
87. Kurtan T, Nesnas N, Li Y-Q, Huang X, Nakanishi K, Berova N (2001) *J Am Chem Soc* 123:5962
88. Kurtan T, Nesnas N, Koehn FE, Li Y-Q, Nakanishi K, Berova N (2001) *J Am Chem Soc* 123:5974
89. Yang Q, Olmsted C, Borhan B (2002) *Org Lett* 4:3423
90. Proni G, Pescitelli G, Huang X, Quraishi NQ, Nakanishi K, Berova N (2002) *Chem Commun* 1590
91. Huang X, Fujioka N, Pescitelli G, Koehn FE, Williamson RT, Nakanishi K, Berova N (2002) *J Am Chem Soc* 124:10320
92. Proni G, Pescitelli G, Huang X, Nakanishi K, Berova N (2003) *J Am Chem Soc* 125:12914
93. Ishii H, Chen Y, Miller RA, Karady S, Nakanishi K, Berova N (2005) *Chirality* 17:305
94. Solladié-Cavallo A, Marsol C, Pescitelli G, Bari LD, Salvadori P, Huang X, Fujioka N, Berova N, Cao X, Freedman TB, Nafie (2002) *Eur J Org Chem* 1788
95. Ishii H, Krane S, Itagaki Y, Berova N, Nakanishi K, Weldon PJ (2004) *J Nat Prod* 67:1426
96. Borovkov VV, Lintuluoto JM, Inoue Y (2000) *Org Lett* 2:1565
97. Borovkov VV, Lintuluoto JM, Inoue Y (2001) *J Am Chem Soc* 123:2979
98. Borovkov VV, Lintuluoto JM, Inoue Y (2000) *J Phys Chem A* 104:9213
99. Borovkov VV, Yamamoto N, Lintuluoto JM, Tanaka T, Inoue Y (2001) *Chirality* 13:329
100. Borovkov VV, Lintuluoto JM, Sugeta H, Fujiki M, Arakawa R, Inoue Y (2002) *J Am Chem Soc* 124:2993
101. Borovkov VV, Lintuluoto JM, Fujiki M, Inoue Y (2000) *J Am Chem Soc* 122:4403

102. Borovkov VV, Hembury GA, Inoue Y (2003) *J Porphyrins Phthalocyanines* 7:337
103. Lintuluoto JM, Borovkov VV, Inoue Y (2002) *J Am Chem Soc* 124:13676
104. Borovkov VV, Hembury GA, Yamamoto N, Inoue Y (2003) *J Phys Chem A* 107:8677
105. Borovkov VV, Hembury GA, Inoue Y (2003) *Angew Chem Int Ed* 42:5310
106. Borovkov VV, Lintuluoto JM, Inoue Y (2002) *Org Lett* 4:169
107. Borovkov VV, Lintuluoto JM, Sugiura M, Inoue Y, Kuroda R (2002) *J Am Chem Soc* 124:11282
108. Borovkov VV, Lintuluoto JM, Hembury GA, Sugiura M, Arakawa R, Inoue Y (2003) *J Org Chem* 68:7176
109. Borovkov VV, Fujii I, Muranaka A, Hembury GA, Tanaka T, Ceulemans A, Kobayashi N, Inoue Y (2004) *Angew Chem Int Ed* 43:5481
110. Ikeda M, Shinkai S, Osuka A (2000) *Chem Commun* 1047
111. Ikeda C, Yoon ZS, Park M, Inoue H, Kim D, Osuka A (2005) *J Am Chem Soc* 127:534
112. Takase M, Ismael R, Murakami R, Ikeda M, Kim D, Shinmori H, Furuta H, Osuka A (2002) *Tetrahedron Lett* 43:5157
113. Li W-S, Jiang D-L, Suna Y, Aida T (2005) *J Am Chem Soc* 127:7700
114. Liu H-y, Huang J-w, Tian X, Jiao X-d, Luo G-t, Ji L-n (1997) *Chem Commun* 1575
115. Liu H-y, Huang J-w, Tian X, Jiao X-d, Luo G-t, Ji L-n (1998) *Inorg Chim Acta* 272:295
116. Ema T, Misawa S, Nemugaki S, Sakai T, Utaka M (1997) *Chem Lett* 487
117. Hayashi T, Nonoguchi M, Aya T, Ogoshi H (1997) *Tetrahedron Lett* 38:1603
118. MacMillan JB, Linington RG, Andersen RJ, Molinski TF (2004) *Angew Chem Int Ed* 43:5946
119. Sessler JL, Andrievsky A, Kral V, Lynch V (1997) *J Am Chem Soc* 119:9385
120. Crossley MJ, Mackay LG, Try AC (1995) *J Chem Soc, Chem Commun* 1925
121. Gou Y-M, Oike H, Saeki N, Aida T (2004) *Angew Chem Int Ed* 43:4915
122. Paolesse R, Monti D, Monica LL, Venanzi M, Froio A, Nardis S, Natale CD, Martinelli E, D'Amico A (2002) *Chem Eur J* 8:2476
123. Borovkov VV, Hembury GA, Inoue Y (2005) *J Org Chem* 70:8743
124. Sekiguchi T, Wakayama Y, Yokoyama S, Kamikado T, Mashiko S (2004) *Thin Solid Films* 464–465:393
125. Zhang L, Lu Q, Liu M (2003) *J Phys Chem B* 107:2565
126. Rubires R, Crusats J, El-Hachemi Z, Jaramillo T, López M, Valls E, Farrera J-A, Ribó JM (1999) *New J Chem* 189
127. Ribó JM, Crusats J, Sagués F, Claret J, Rubires R (2001) *Science* 292:2063
128. Rubires R, Farrera J-A, Ribó JM (2001) *Chem Eur J* 7:436
129. Crusats J, Claret J, Diez-Pérez I, El-Hachemi Z, Garcia-Ortega H, Rubires R, Sagués F, Ribó JM (2003) *Chem Commun* 1588
130. Yamaguchi T, Kimura T, Matsuda H, Aida T (2004) *Angew Chem Int Ed* 43:6350
131. Tamaru S-i, Uchino S-y, Takeuchi M, Ikeda M, Hatano T, Shinkai S (2002) *Tetrahedron Lett* 43:3751
132. Zhang L, Yuan J, Liu M (2003) *J Phys Chem B* 107:12768
133. Borovkov VV, Harada T, Hembury GA, Inoue Y, Kuroda R (2003) *Angew Chem Int Ed* 42:1746
134. Lauceri R, Napoli MD, Mammana A, Nardis S, Romeo A, Purrello R (2004) *Synthetic Metals* 147:49
135. Purrello R, Bellacchio E, Gurrieri S, Lauceri R, Raudino A, Scolaro LM, Santoro AM (1998) *J Phys Chem B* 102:8852
136. Koti ASR, Periasamy N (2003) *Chem Mater* 15:369
137. Purrello R, Scolaro LM, Bellacchio E, Gurrieri S, Romeo A (1998) *Inorg Chem* 37:3647

138. Bellacchio E, Lauceri R, Gurrieri S, Scolaro LM, Romeo A, Purrello R (1998) *J Am Chem Soc* 120:12353
139. Purrello R, Raudino A, Scolaro LM, Loisi A, Bellacchio E, Lauceri R (2000) *J Phys Chem B* 104:10900
140. Lauceri R, Purrello R (2005) *Supramol Chem* 17:61
141. Bischoff G, Bischoff R, Hoffmann S (2001) *J Porphyrins Phthalocyanines* 5:691
142. Balaban TS, Leitich J, Holzwarth AR, Schaffner K (2000) *J Phys Chem B* 104:1362
143. Furukawa H, Oba T, Tamiaki H, Watanabe T (1999) *J Phys Chem B* 103:7398
144. Steensgaard DB, Wackerbarth H, Hildebrandt P, Holzwarth AR (2000) *J Phys Chem B* 104:10379
145. Miyatake T, Oba T, Tamiaki H (2001) *Chembiochem* 2:335
146. Yagai S, Miyatake T, Tamiaki H (2002) *J Org Chem* 67:49
147. Yagai S, Tamiaki H (2001) *J Chem Soc, Perkin Trans* 1:3135
148. Knapp S, Huang B, Emge TJ, Sheng S, Krogh-Jespersen K, Potenza JA, Schugar HJ (1999) *J Am Chem Soc* 121:7977
149. Huber V, Katterle M, Lysetska M, Würthner F (2005) *Angew Chem Int Ed* 44:3147
150. de Boer I, Matysik J, Erkelens K, Sasaki S-i, Miyatake T, Yagai S, Tamiaki H, Holzwarth AR, de Groot HJM (2004) *J Phys Chem B* 108:16556
151. Barkigia KM, Melamed D, Sweet RM, Smith KM, Fajer J (1997) *Spectrochim Acta A* 53:463
152. Balaban TS, Bhise AD, Fischer M, Linke-Schaetzel M, Roussel C, Vanthuyne N (2003) *Angew Chem Int Ed* 42:2140
153. Balaban TS, Linke-Schaetzel M, Bhise AD, Vanthuyne N, Roussel C (2004) *Eur J Org Chem* 3919
154. Carofiglio T, Fornasier R, Lucchini V, Simonato L, Tonellato U (2000) *J Org Chem* 65:9013
155. Kral V, Schmidtchen FP, Lang K, Berger M (2002) *Org Lett* 4:51
156. Masiero S, Gottarelli G, Pieraccini S (2000) *Chem Commun* 1995
157. Tian HJ, Inoue K, Yoza K, Ishi-i T, Shinkai S (1998) *Chem Lett* 871
158. Tamaru S-I, Nakamura M, Takeuchi M, Shinkai S (2001) *Org Lett* 3:3631
159. Kawano S-i, Tamaru S-i, Fujita N, Shinkai S (2004) *Chem Eur J* 10:343
160. Fox JM, Katz TJ, Elshocht SV, Verbiest T, Kauranen M, Persoons A, Thongpanchang T, Krauss T, Brus L (1999) *J Am Chem Soc* 121:3453
161. Borovkov VV, Harada T, Inoue Y, Kuroda R (2002) *Angew Chem Int Ed* 41:1378
162. Kimura M, Kitamura T, Muto T, Hanabusa K, Shirai H, Kobayashi N (2000) *Chem Lett* 1088
163. Kimura M, Kitamura T, Sano M, Muto T, Hanabusa K, Shirai H, Kobayashi N (2000) *New J Chem* 24:113
164. Hwang I-W, Kamada T, Ahn TK, Ko DM, Nakamura T, Tsuda A, Osuka A, Kim D (2004) *J Am Chem Soc* 126:1618

Supramolecular Chirality in Coordination Chemistry

Georg Seeber · Bryan E. F. Tiedemann · Kenneth N. Raymond (✉)

Department of Chemistry, University of California, Berkeley, CA 94720-1460, USA
 raymond@socrates.berkeley.edu

1	Introduction	148
1.1	Generation of Chirality	152
1.2	Overview of Coordination Assemblies	153
1.3	Racemization of Coordination Assemblies	155
2	Chiral Supramolecular Architectures	159
2.1	Helicates	159
2.1.1	Single-Stranded Helicates	159
2.1.2	Double-Stranded Helicates	160
2.1.3	Triple-Stranded Helicates	160
2.1.4	Quadruple-Stranded Helicates	161
2.1.5	Circular Helicates	162
2.2	Trigonal (Anti)prism	162
2.3	Tetrahedra	166
2.3.1	M ₄ L ₆ Stoichiometry	166
2.3.2	M ₄ L ₄ Stoichiometry	171
2.3.3	M ₆ L ₄ Stoichiometry	172
2.4	Trigonal Bipyramid	173
2.5	Octahedra	175
2.6	Cuboctahedra	175
3	Conclusions and Outlook	176
	References	178

Abstract Supramolecular chirality is generated from assemblies based on supramolecular interactions such as hydrogen bonding, van der Waals and metal-ligand coordinative interactions. In this chapter, we discuss chiral supramolecular architectures that are based on metal-ligand coordination. Emphasis is given to ensembles that are formed exclusively from achiral building units and thus rely on metal coordination geometries or asymmetric ligand arrangements in order to generate chirality via supramolecular (coordinative) interactions. Particular interest is given to assemblies that exhibit chiral cavities with potential for guest encapsulation for recognition, storage, and utilization as nano-reaction vessels. Examples of chiral architectures are presented that resemble molecular symmetries of helicates, trigonal (anti)prisms, tetrahedra, trigonal bipyramids, octahedra and cuboctahedra.

Keywords Chirality · Coordination compounds · Guest inclusion · Host-guest interactions · Supramolecular chemistry

1 Introduction

Chirality is widespread in nature and is expressed ubiquitously in the most abundant forms of matter. As an example, the basic structure of quartz minerals consists of covalently linked silicon-oxygen tetrahedra, which are corner-connected and twisted in a helical fashion around three- and six-fold screw axes, rendering individual quartz crystals chiral (Fig. 1) [1]. Although crystalline quartz aggregation exemplifies a form of static chirality only found in the solid state, it is most noteworthy that it is generated exclusively from the spatial arrangements of achiral building units. Contrary to static chirality, assemblies based on dynamic equilibria—mediated by non-covalent, supramolecular interactions allow the formation of thermodynamically stable ensembles exhibiting *supramolecular chirality*. With a plethora of chiral compounds based on supramolecular interactions, a series of questions arise: How can chirality principally be generated from achiral building units? What enables the formation of chiral architectures based on dynamic equilibria of individual building units? How can the formation of specific assemblies be controlled?

In order to answer some of these outstanding questions, this chapter presents and analyzes a variety of chiral architectures based on metal-ligand coordinative interactions. Although there are a number of ways in which chirality can be introduced into coordination assemblies [2], we will concentrate on ensembles formed from achiral components, where chirality arises from metal coordination geometries or asymmetric ligand arrangements. Particular focus lies with assemblies that show host-guest encapsulation potential and maintain their chirality in solution.

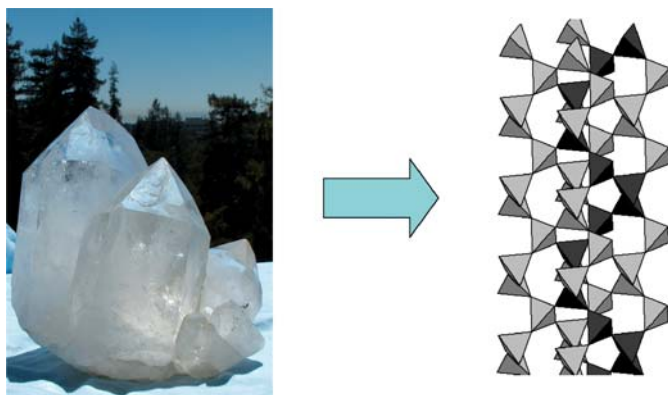


Fig. 1 Quartz minerals consisting of covalently linked silicon-oxygen tetrahedra that are corner-connected and twisted in a helical fashion around three- and six-fold screw axes, rendering individual quartz crystals chiral

Biology is chiral. The design and synthesis of self-assembled and chiral supramolecular architectures is inspired by the stunning variety of non-covalently linked ensembles that are found in nature. The assembly of such macromolecular structures is a fundamental biological process, and the well-ordered assembly pathways that typically form one polymeric arrangement have been characterized most thoroughly in viral systems. As one example, human rhinovirus 14, a member of the major rhinovirus receptor class, possesses a protein capsid that is composed of 60 protomers arranged in an icosahedrally symmetric array [4–6]. Many viruses exhibit such high symmetry, which is illustrated by comparison of an example virus [7] to a man-made wooden ball-and-stick puzzle (Fig. 2). Both assemblies exhibit the highest molecular chiral symmetry, icosahedral *I*-symmetry with 6 C_5 -, 10 C_3 - and 15 C_2 -symmetry axes. It is important to note that the formation of the complex wooden, and chiral, icosahedron is achieved entirely from achiral ball and stick building units.

The existence of chirality in nature is of particular importance in numerous recognition processes, often illustrated by examples detectable by non-spectroscopic methods such as the different orange and lemon odors of *R*-(+)- and *S*-(-)-limonene, respectively (Fig. 3) [8]. As such, chiral discrimination is also of considerable consequence in the medical sciences, as often one enantiomer is pharmaceutically active whereas the other may show adverse side effects. A historic example is the anti-emetic activity of one of the enantiomers of thalidomide, while the other can cause fetal damage [9, 10]. These considerations highlight the importance of chiral discrimination in the production of biologically active materials, whereas on the other hand, the design of routes to asymmetric synthesis presents an active challenge to synthetic chemists worldwide.

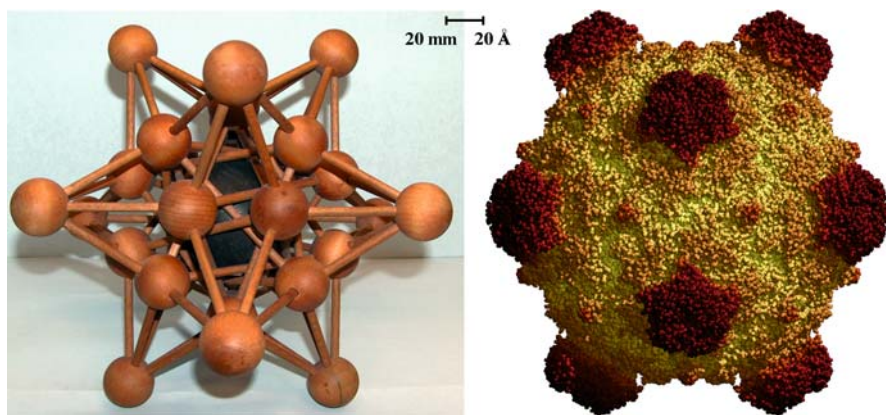


Fig. 2 Comparison of an icosahedral wooden model and enterobacteria phage PhiX174. Reprinted with permission from [3]

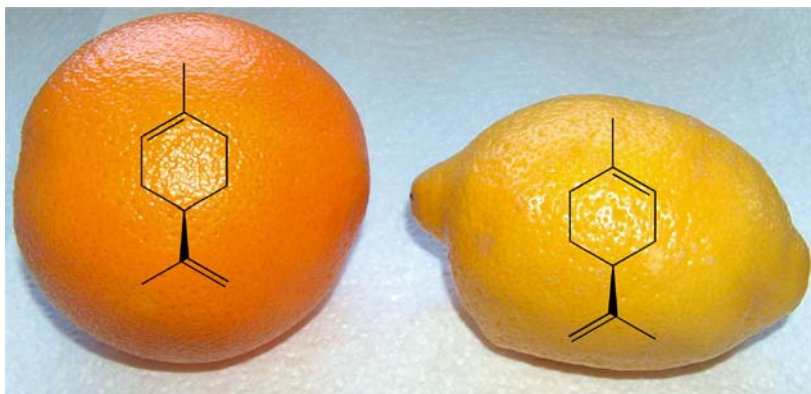


Fig. 3 Orange and lemon odor in mirror image molecules: *R*-(+)- and *S*-(-)-limonene, respectively

In this respect, one fascinating aspect of the highly symmetric architectures present in nature is the fact that they are constructed via the self-assembly of just a small number of identical subunits. Most importantly, they form enclosed environments that are vital to the functioning of many biological processes, e.g., in the protection of genetic material in the wide range of viral species or in the storage of iron in apoferritin [11]. The simplicity of self-assembling building blocks into highly symmetric containers or protective shells inspires the vision of chemists in creating molecular systems that can act as vessels for a variety of purposes [12, 13]. Such functions include storage and recognition of ions [14–19] or molecules [20–22], as well as utilization of such encapsulated spaces as nano-reaction vessels in chemical transformations and catalysis [23–29].

Synthesis of supramolecular assemblies can be achieved utilizing an assortment of non-covalent interactions such as van der Waals, hydrogen bonding, and metal-ligand coordinative interactions. The latter are advantageous as they typically possess the strong directionality and higher stability that are crucial in the geometric control of the overall architecture. But whereas the individual interactions involved in cluster formation are relatively well understood, less is known about the mechanics that favor the construction of specific architectures with defined stoichiometries and high symmetry, rather than a mixture of random polymorphs. Synthetic coordination clusters of various sizes, stoichiometries, and symmetries have been the subject of a number of review articles [30–32], and it appears that careful consideration of the geometric requirements of a particular cluster symmetry and stoichiometry can lead to the controlled formation of “designer” assemblies [31, 33]. Once such a model has been established, it is then possible to create a library of assemblies by the combination of different subunits of available ligands and metals.

Of the wealth of supramolecular architectures reported, many structures have attracted particular attention due to interesting topological, dynamic and electronic properties [34–36], as they represent promising models for the production of molecular switches, motors and machines [37–41]. Significant examples of these include the design and synthesis of rotaxanes [42, 43], catenanes [44–48] and knots [49, 50], as well as various polyhedra such as boxes [51–53], tetrahedra [14, 54, 55], octahedra, cubes, dodeca- and icosahedra [13, 56–59]. Unlike the great variety of common organic host compounds such as crown ethers, acyclic podands, macropolycyclic cryptands, calixarenes, cyclodextrins and spherands [60–62] that display a rich host-guest chemistry, fewer examples of cavity containing, metal-ligand based ensembles have been utilized for molecular guest encapsulation [15, 19, 29, 45, 63]. However, there are a variety of metal-ligand based host systems that encapsulate small ions such as Li^+ , Na^+ , K^+ , Cl^- and NH_4^+ [14–19].

Uncertainty can arise concerning the formation of supramolecular compounds that encapsulate guest molecules. Such architectures are often synthesized in the presence of suitable guests, leaving ambiguity as to whether the structure was pre-formed for guest encapsulation or, alternatively, whether the presence of the guest facilitated the formation of the host by acting as a template. A variety of examples have been reported where assemblies form without the influence of guest molecules [12, 14, 47, 54, 55, 64–70]. However, guest molecules have also been found to play an important role in the synthesis of many metal-ligand architectures [15, 71] either by driving cluster formation via host-guest interactions [14, 45, 72–74] or by establishing guest-mediated equilibria between multiple clusters [75, 76]. Rather than interpreting the role of these templates as adhering to the classical “lock and key” [77] concept found in molecular recognition processes in nature [77, 78], Busch and coworkers have defined the template effect as either a kinetic or a thermodynamic phenomenon, where “*the chemical template organizes an assembly of atoms [...] in order to achieve a particular linking of atoms.*” [79]. In addition, Busch states that the role of the template should not be thought of in terms of the molecular lock-and-key interaction, which resembles a construct in which the key is a constituent part of the assembly. A true template should be removable and leave behind the desired product, as in the case of many macrocycles, macrobicycles and catenanes etc. [80–82]. The definition of template as “*a pattern, mold, or the like, usually consisting of a thin plate of wood or metal, serving as a gauge or guide in mechanical work*” [83] implies that this is a repeatable (e.g., catalytic) process as opposed to a stoichiometric reaction. Hence, one can differentiate between a *thermodynamic* (template becomes integral part of the architecture) versus *kinetic* (template is removable after formation of the desired product) templated host-guest interaction in metal-ligand cluster formation [79].

1.1

Generation of Chirality

The term chirality describes objects (molecules) that exist as pairs of enantiomers, which are non-superimposable mirror images of each other. Various alternative definitions exist, e.g., the necessary and sufficient condition of the lack of improper rotational axes S_n (where $S_1 = \sigma$ (mirror plane) and $S_2 = i$ (inversion center)). Different elements of chirality can be identified in molecules; (i) *chirality center* or *chirotopic stereogenic center* as suggested by IUPAC [84]—created around a single point in space, e.g., tetrahedrally substituted atoms with four different substituents, (ii) *chirality axis*—created with respect to a molecular axis, as for example found in a tetra-substituted allene with four different substituents, and (iii) *chirality plane*—with respect to a plane within a molecule, for example as found in (*E*)-cyclo-octene. These three elements of chirality in three-dimensional space, which have themselves the dimensions 0, 1 and 2, are described in the classical publications by Cahn, Ingold and Prelog [85, 86] that led to the definition of the *R*- and *S*-descriptors of chirality according to the *CIP*-system. Furthermore, structures comprising *chirality axes* and *chirality planes* can alternatively be viewed as *helical*. As this type of chirality is the most predominant in coordination chemistry, it is important to systematically analyze the origin of chirality within different parts of the molecule. This subject has been extensively covered [87] and is therefore just briefly summarized here. Chirality can principally be introduced into metal-ligand assemblies (Fig. 4) by (i) coordination of differ-

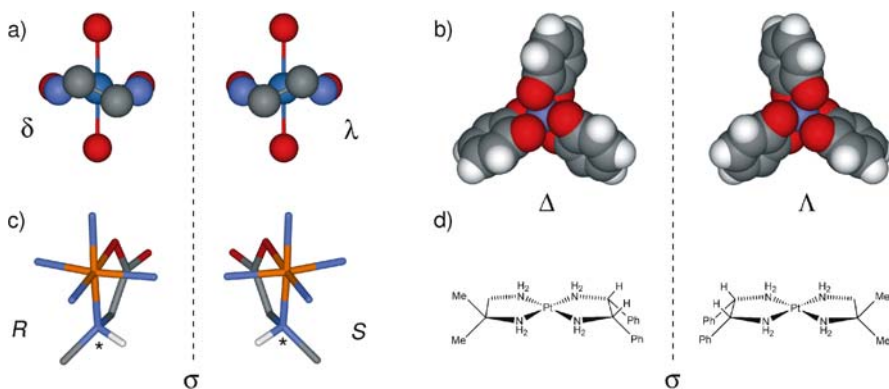


Fig. 4 Generation of chirality upon metal ligand coordination from **a** orientation of individual chelating ligands (δ/λ) ($[\text{Ni}(\text{en})(\text{OH}_2)_4]^{2+}$); **b** *tris*-bidentate octahedral coordination (Δ/Λ) ($[\text{Fe}(\text{cat}^{2-})_3]^{3-}$ [88]); **c** coordination of chiral ligands (*R/S*) ($[\text{Co}(\text{NH}_3)_4(\text{sarcosinato})]^{2+}$); **d** loss of improper symmetry axes of individual ligands upon coordination ($[\text{Pt}(\text{iso-butylenediamine})(\text{meso-stilbenediamine})]^{2+}$ [89]; en = 1,2-ethylenediamine; cat²⁻ = 1,2-catecholate dianion

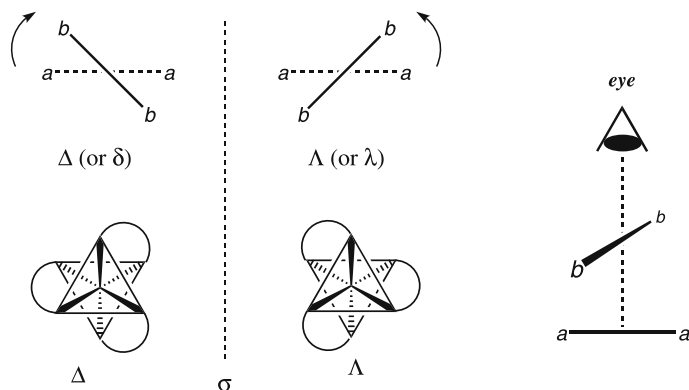


Fig. 5 Definition of skew-line chirality descriptors with rotational right- (δ/Δ) and left- (λ/Λ) handed orientations

ent types of monodentate ligands, (ii) chiral conformations within individual chelating rings (δ/λ , Fig. 4a), (iii) formation of helical structures utilizing chelating ligands (Δ/Λ , Fig. 4b) [88], iv) coordination of chiral ligands (*R/S*, Fig. 4c), v) coordination of one or more ligands that lose improper symmetry axes upon coordination (Fig. 4d) [89].

The chiral identity of a molecule is included in the nomenclature of inorganic compounds, and today's comprehensive system is based upon suggestions made in 1990 in IUPAC's *Recommendations on Nomenclature of Inorganic Chemistry* [84], and ACS's *Inorganic Chemical Nomenclature* [90]. The basis for the usage of stereochemical descriptors was laid by Brown [91, 92], from which three types of chiral descriptor conventions were developed: (i) *Steering-wheel-convention* [93], (ii) *Skew-lines convention* [94] and (iii) *Oriented-skew-lines convention* [95].

The IUPAC recommended nomenclature of chirality is the skew-lines convention in cases where the CIP system does not apply. It can be formulated for any complex where two non-intersecting skew lines uniquely define a helical system. Examples of two skew lines that generate chirality are the projection of two planar chelating rings about a metal center or any non-planar chelating ring (Fig. 5). The descriptors for right and left handed helical chirality are Δ/Λ for chirality involving the whole molecule and δ/λ for chirality caused by molecular fragments (such as conformations of chelating rings), respectively.

1.2

Overview of Coordination Assemblies

Molecular systems formed from metal-ligand coordinative interactions are generally kinetically more labile and thus, dynamically more flexible than covalently bound systems. This is important since supramolecular architectures

are formed under thermodynamic control, allowing self-correction to enable the formation of the thermodynamically most stable product. Additionally, metal-ligand interactions are highly directional due to preferred coordination environments of the chosen metal ions. In combination with suitable ligand geometries, this directionality allows a certain predictability of the architecture formed. A common feature of such design approaches is the use of rigid and poly-functional organic ligands as geometrically pre-determined building blocks. Rigidity is an important factor to ensure the formation of the desired architecture that represents the most favored structure as a function of the geometrical restraints. Elegant examples of the rational design approach can be seen in the architectures based both on chelating ligands used by Lehn [96, 97], Raymond [30, 31] and Saalfrank [14, 98] that show increased pre-organization and high formation constants [99] and on monodentate ligands [32, 100–103] exemplified by the work of Stang [33, 64] and Fujita [104].

These two rational design approaches are based on either control of the bonding vector direction between the building units (*symmetry interaction model*) or on control of the overall symmetry by the molecular components (*molecular library model*) (Fig. 6) [30, 33].

The *symmetry interaction* model takes advantage of multibranching chelating ligands, which show increased pre-organization and stronger binding energies as a result of the chelate effect [99]. Geometric relationships between the ligand and metal ion form the conceptual basis to understand the formation of a given supramolecular architecture. The predominant coordination geometry for *tris*-bidentate coordination is the pseudo-octahedral coordination geometry with idealized D_3 symmetry. This arrangement results in inherently chiral structures, where the helical Δ or Λ chirality is induced by the trigo-

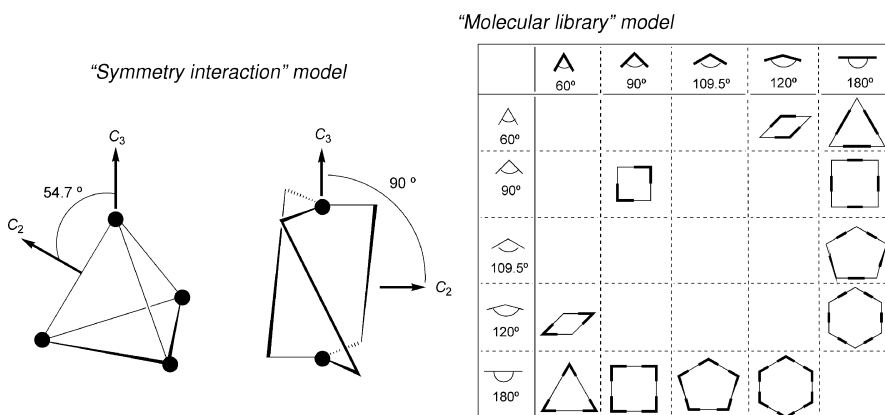


Fig. 6 Illustration of two rational design approaches to construct coordinative supramolecular architectures. The *symmetry interaction* model is based on controlling the bonding vector direction between individual building units, whereas the *molecular library* model relies on control of the overall symmetry by the molecular components

nal twist of the three chelating ligands around the metal center. For example, a tetrahedron with T symmetry contains four C_3 and six C_2 axes. The structure may be formed from the combination of four C_3 -symmetric *tris*-bidentate chelated octahedral metal centers spanned by six C_2 -symmetric *bis*-bidentate ligands (M_4L_6 tetrahedron). This approach places the metal ions at the vertices of the tetrahedron and the ligands on the edges. However, not every combination of C_2 -symmetric *bis*-bidentate ligands and octahedrally coordinated metal centers will generate a tetrahedron. The structure of the ligand is critical in achieving the correct orientation of symmetry elements in the target assembly, e.g., 54.7° between the C_2 and C_3 axes for a tetrahedron and 90° for a triple helicate (Fig. 6) [33]. The importance of geometric design criteria in order to assemble the desired architectures over entropically favored lower stoichiometry compounds has been discussed in depth previously [68, 105, 106]. Advantages of this design approach lie with the utilization of pseudo-octahedrally coordinated metal ions, which upon *tris*-bidentate coordination generate helical chirality from achiral building blocks.

Contrary to this, the *molecular library* model takes advantage of multi-branched monodentate ligands as first applied by Verkade [102]. It describes metal and ligand components as angular and linear pieces to be combined in the formation of two-dimensional polygons and three-dimensional polyhedra. A matrix of combinations of these simplified elements provides a formula for the synthesis of an array of self-assembled architectures (Fig. 6). For example, a molecular square can be assembled in several different ways, such as combining four linear with four 90° angular building blocks or by combining four 90° angular subunits. Similarly, three-dimensional polyhedra can be constructed where a minimum of one building unit has to be a tritopic subunit [33]. Although an elegant approach to high symmetry coordination assemblies, the *molecular library* approach lacks the generality of creating chiral architectures from achiral components upon coordination. Although chirality can be induced by introducing chiral ligands, this approach is not the subject of this overview and is discussed elsewhere [107–113]. Throughout this chapter we will concentrate on assemblies that generate chirality from achiral components upon coordination, regardless if the resulting racemic mixtures were separated into its enantiomers. Independent of the chosen synthetic approach, an important factor in utilizing chiral architectures as nano-reaction vessels is their enantioselectivity in solution. Hence, inertness to racemization or diastereomeric isomerization is an important factor and the potential pathways to isomerization of coordination compounds need to be evaluated.

1.3

Racemization of Coordination Assemblies

Although racemization represents an energetically spontaneous process, activation barriers need to be overcome along the reaction coordinate that can

lead to one or more transition intermediates. In an achiral environment, the racemization enthalpy (ΔH) is zero, whereas the entropy ($\Delta S = R \ln 2$) equals a purely statistical distribution of both enantiomers leading to a free Gibbs energy ($\Delta G = 1.72 \text{ kJ mol}^{-1}$ standard conditions $T = 298 \text{ K}$) in favor of the racemate. The height of the energy barrier, and thus the timescale on which racemization occurs, determines if the separation of enantiomers is principally possible.

Trivial racemization mechanisms represent dissociation of the metal-ligand coordinative bonds. The magnitude of the energy barrier is thereby dependent on the type of ligands (e.g., denticity) and kinetic inertness of the metal ions. Utilizing multi-dentate ligands in combination with kinetically inert metal ions can dramatically increase the energy barrier for dissociation and completely prevent this pathway from occurring. However, alternative racemization pathways with lower energy barriers represent *intra*-molecular racemization mechanisms. Two such non-dissociative reaction mechanisms are available for pseudo-octahedral, D_3 symmetric complexes that represent the most utilized coordination geometry in generating chirality upon metal-ligand coordination [114]: (i) the *Bailar twist* with a trigonal D_{3h} transition state and (ii) the *Ray-Dùtt twist* with a rhombic C_{2v} transition state (Fig. 7).

Both mechanisms proceed via trigonal prismatic transition states. In the Bailar twist, all three chelating rings remain equivalent throughout the racemization, whereas in the case of the Ray-Dùtt twist, the ligands are grouped into non-equivalent pairs of one and two ligands, respectively. The

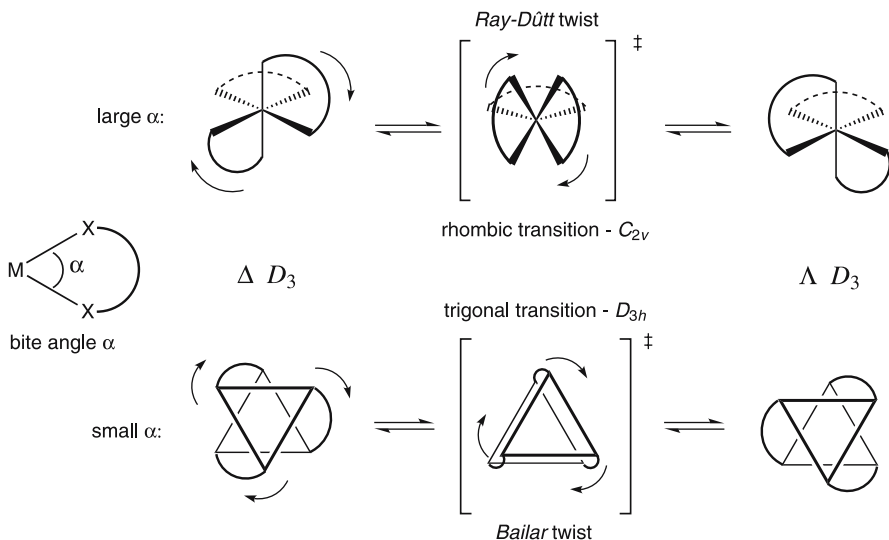


Fig. 7 Definition of the chelating bite angle α . Large angles α facilitate Ray-Dùtt twists with rhombic (C_{2v}) transition states, whereas small angles α favor Bailar-twists with trigonal (D_{3h}) transition states

differentiation between the two racemization pathways is not trivial but theoretical studies indicate a dependence on the chelating bite angle α (Fig. 7). Small bite angles will favor the Bailar twist, whereas large angles favor Ray-Dûtt twists [114, 115].

In the case of poly-metallic assemblies that are linked via organic bridging ligands, racemization is strongly dependent on the conformational rigidity of the organic linker, as rigid linkages lead to an increase in the activation barriers for intra-molecular racemization pathways. This increase in activation energy can be expressed as *mechanical coupling* between multiple metal centers [116], which has been investigated in triple-stranded dinuclear helicates [117, 118], where distinctions were identifiable between different racemization pathways involving individual racemization of metal centers and simultaneous racemization of multiple metal centers. In the case of flexible organic linkers that allow conformational freedom upon coordination, each metal vertex racemizes at rates comparable to those of mononuclear complexes, indicating little or no communication between different metals.

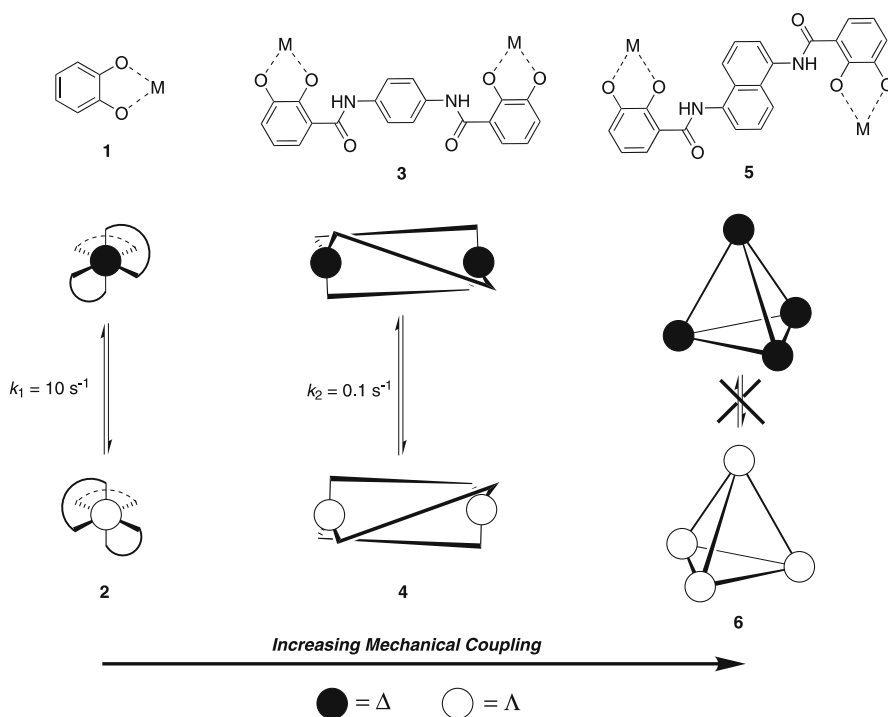


Fig. 8 Series of chelating ligands **1**, **3** and **5**, forming the three complexes **2** (mononuclear), **4** (dinuclear) and **6** (tetranuclear), respectively, illustrating the concept of *mechanical coupling* by slowing racemization rates of individual metal centers from 10 s^{-1} (**2**) [118] to 0.1 s^{-1} (**4**) [117] and no observed racemization (**6**) [119]

Contrary to this, mechanical coupling is observed if the ligand exhibits structural rigidity. This is illustrated in the coordinative series of mononuclear *tris*-catecholate **2**, helical dinuclear *tris*-catecholate **4** and the tetranuclear *tris*-catecholate assembly **6** (Fig. 8).

Utilization of the conformationally rigid bridging ligand **3** results in a 100-fold decrease in racemization rate (0.1 s^{-1}) [117] of the dinuclear helicate **4** compared to the mononuclear complex **2** (10 s^{-1}) built from the simple catecholate ligand **1** [118]. More dramatically, coupling of four metal centers via six rigid bridging ligands **5**, entirely prevents the assembly **6** from racemization [119] (Fig. 8). As a direct result of the rigidity of the ligands (strong mechanical coupling), the metals communicate their Δ/Λ chirality to each vertex and the architectures formed are found to exhibit identical chirality at all metal vertices (homoconfigurational or *homochiral* ensembles) [31, 106, 120]. In such cases, it has been shown that calculated energies for the formation of *heterochiral* assemblies are higher than those for their *homochiral* counterparts, being a direct measurement for the magnitude of mechanical coupling. This magnitude difference of mechanical coupling is further illustrated for tetrahedral coordination assemblies (Fig. 9) where racemization of individual metal centers (a) [121], synchronous racemization of four metal centers (b) [122] or no racemization (c) [119] can be observed.

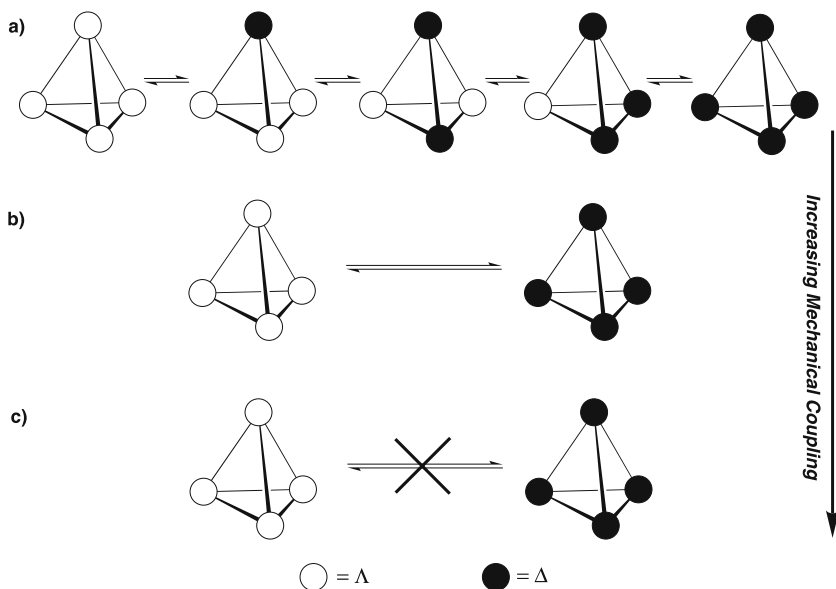


Fig. 9 Schematic representation of racemization processes in tetrahedral complexes depending on increasing mechanical coupling between the metal vertices: **a** individual racemization of each metal vertex; **b** Synchronous racemization of four metal vertices; **c** no racemization

2

Chiral Supramolecular Architectures

Supramolecular architectures formed upon metal-ligand coordination from achiral building units without the use of chiral auxiliaries are usually obtained as racemic mixtures. Resolution of enantiostable racemic ensembles is principally possible but not always synthetically achieved. We therefore also include compounds that are reported only as racemic mixtures in the literature. Albeit helicates principally do not fall into our categorization of guest encapsulating systems, we include a brief categorization of helical systems as they represent the first examples of inherently chiral, supramolecular architectures formed via metal-ligand coordinative interactions.

2.1

Helicates

Although the term “helicate” was introduced into coordination chemistry by Lehn and coworkers in 1987 [123], the first example of a coordination helix, ferric rhodotorulate—a di-iron(III) triple-stranded helicate, was proposed a decade earlier by Raymond and coworkers [124]. Since then, the concept of helicates extends the idea of classical coordination complexes towards more complex “supermolecules” in which two or more metal ions lie on a helical axis [123, 125–127]. Thus, helicates are discrete supramolecular structures formed by one or more covalent organic strands entwined and coordinated to a series of metal-ions defining the helical axes. Helical arrangements implicitly result in chirality, producing right- ($\Delta = Plus = P$) or left-handed ($\Lambda = Minus = M$) helicity around the principal axis [127–130]. Variations in helical arrangements can be described (i) by the number of coordinated strands, corresponding to single-, double- and triple-stranded helicates and (ii) by the symmetry of the coordinating strands¹. From the myriad of reported helical structures, only a few examples are represented in this chapter and more examples can be found in recent reviews [131, 132].

2.1.1

Single-Stranded Helicates

The quinquepyridine ligand **7** forms a dinuclear, single-stranded helicate with ruthenium(II) ions (**8**) [133]. The crystal structure shows two different six-coordinate metallic sites, with one ruthenium(II) coordinated to a terpyridine subunit of **7** and the second ruthenium(II) bound to the remaining bipyridine subunit (Fig. 10). The helical twist of the strand (74.9°) results

¹ Identical strands correspond to homotopic arrangements, whereas non-symmetrical strands represent heterotopic helicates, which can form isomers by different orientations of the coordinating binding units (Head to Head or Head to Tail)

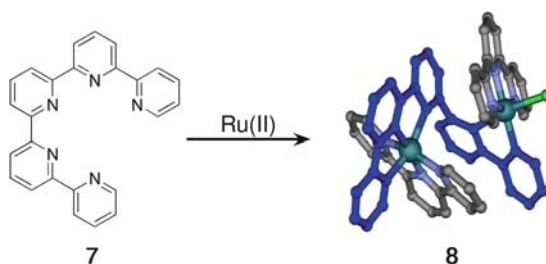


Fig. 10 Representation of the single-stranded helicate **8** formed from quinquepyridine ligand **7** and ruthenium(II) ions [133]. Ligand **7** is shown in *blue* to illustrate the helical twist

from the torsion between the two connected pyridine rings of each subunit. The remaining vacant coordination sites around the ruthenium(II) ions are occupied by a chloro and two tridentate terpyridine ligands.

2.1.2

Double-Stranded Helicates

The double-stranded helicate **10**, reported by Constable and coworkers [134, 135], was characterized both in the solid state and in solution. In this D_2 symmetric structure, two *tris*-bidentate sexipyridine ligands **9** wrap around two octahedral cadmium(II) ions forming the dinuclear double-stranded helicate **10** (Fig. 11).

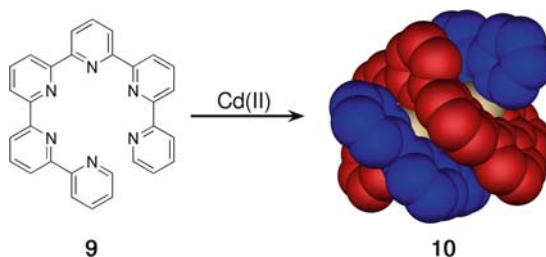


Fig. 11 Representation of the double-stranded helicate **10** formed from sexipyridine ligand **9** and cadmium(II) ions [134]. The two sexipyridines are shown in *blue* and *red* to illustrate the helical twist

2.1.3

Triple-Stranded Helicates

The spontaneous, highly selective process of helicate formation has been reported to exhibit self-recognition [120, 136]. Amongst a variety of examples, Raymond and coworkers have reported that gallium(III) and iron(III) coordination by the *bis*-bidentate catecholate ligands **3**, **11** and **12** facilitate

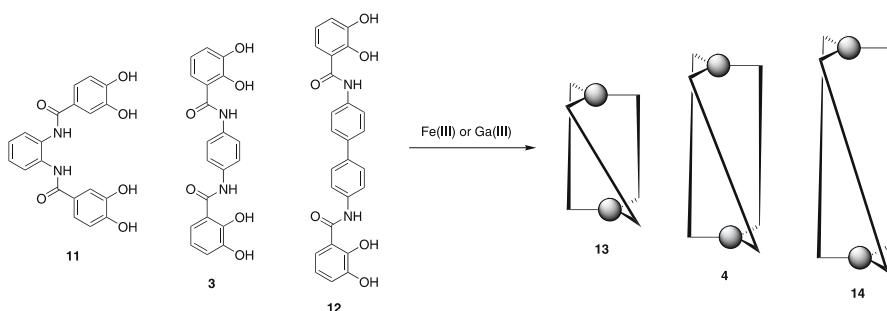


Fig. 12 Self-recognition and formation of triple-stranded helicates **13**, **4**, and **14** from *bis*-catechol ligands **11**, **3**, and **12** and iron(III) or gallium(III) ions, respectively [120]

exclusive formation of the complementary *homo*-triple helicates **4**, **13** and **14** in high yield without traces of oligomeric or mixed species (Fig. 12) [120]. This is remarkable in as much as principally 27 *homo*- and *hetero* ligand combinations are possible. The high degree of conformational rigidity of each donor subunit in **3**, **11** and **12**, combined with different spacer lengths between the catecholate binding sites provide a possible explanation for the self-recognition and formation of exclusively *homo*-triple helicates.

2.1.4

Quadruple-Stranded Helicates

A rare example of higher stranded helicates is found in the decanuclear quadruple-helicate **16**. Lehn and coworkers reported the dynamic equilibrium

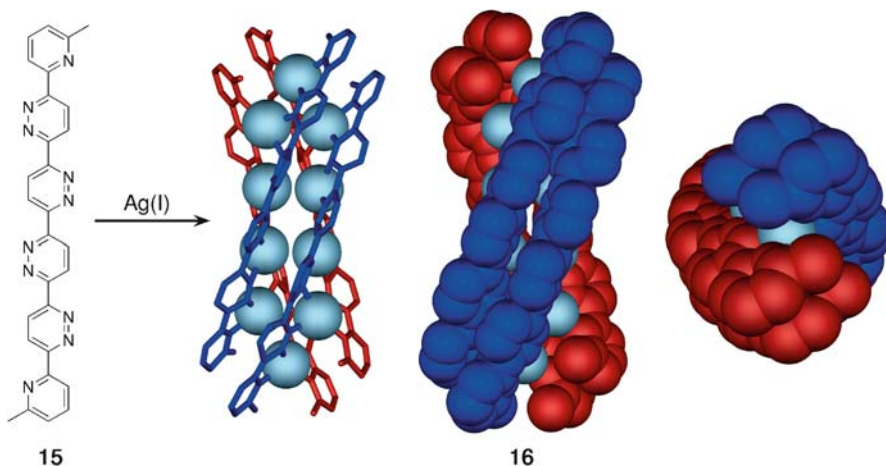


Fig. 13 Three representations of the decanuclear, quadruple-stranded helicate **16** formed from the polydentate ligand **15** and silver(I) ions [137]. The two sets of ligands **15** are shown in *red* and *blue* to illustrate the helical twist

between silver(I) helicate **16** and an $[4 \times 5]$ -icosanuclear silver(I) grid [137]. In the quadruple-helicate **16**, eight silver(I) ions are arranged into two parallel and nearly linear rows of four silver(I) ions, with the top and bottom capped by the two remaining silver(I) ions (Fig. 13). Each row of four silver(I) ions is coordinated by two strands of ligands **15** that additionally interconnect both silver(I) rows by alternating coordination to the top and bottom silver(I) caps. The quadruple strand can be seen as two subsets from two pairs of ligands that are wrapped around the helical axis.

2.1.5

Circular Helicates

Circular helicates exhibit a particular aesthetic appeal as they comprise closed tori of chiral architectures. Hannon and coworkers [138] have reported the self-assembly of the “chiral ball” $([\text{Cu}_3\text{17}_3])_4^{12+}$ (**19**) assembled from four homochiral, circular helicates $[\text{Cu}_3\text{17}_3]^{3+}$ (**18**) that are held together via CH- π interactions (Fig. 14). Each copper(I) ion is tetrahedrally coordinated by two imine-ligands **17**, resulting in the solution-stable trimeric helicate **18**. The resulting chiral tetramer **19** is quite remarkable as it is self-assembled from a one-pot reaction of 48 simple and achiral building units.

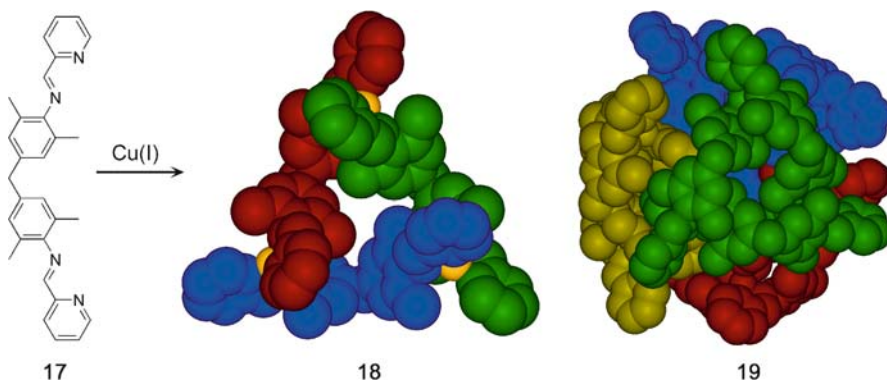


Fig. 14 Formation of the “chiral ball” $([\text{Cu}_3\text{17}_3])_4^{12+}$ (**19**) assembled via CH- π interactions from four circular helicates $[\text{Cu}_3\text{17}_3]^{3+}$ (**18**), where each copper(I) ion is tetrahedrally coordinated by two imine-ligands **17** [138]

2.2

Trigonal (Anti)prism

Trigonal prismatic assemblies can be formed from only five building blocks; two angular tritopic subunits such as tripyridine ligand **20** and three angular connectors such as the square planar palladium(II) complex **21**. Formation of these cage-like molecules were reported by Fujita and coworkers upon guest

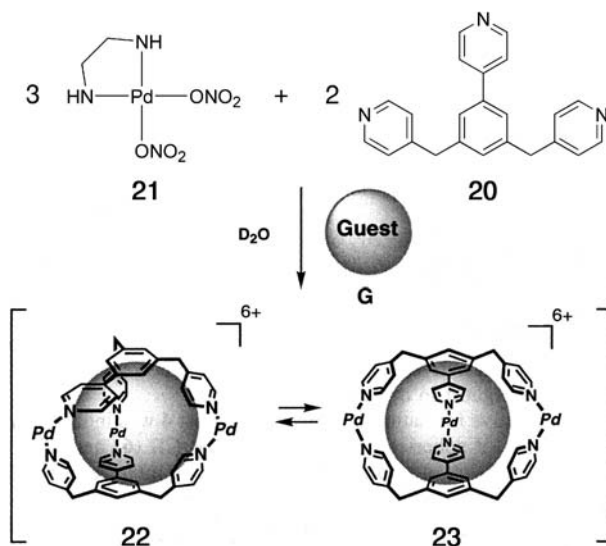


Fig. 15 Formation of trigonal prismatic coordination complexes from tripyrindine ligand **20** and angular connector **21**. Upon guest encapsulation, a dynamic equilibrium between chiral cage **22** and achiral **23** is observed. Reprinted with permission from [75]. Copyright 1999 American Chemical Society

encapsulation (Fig. 15) [75]. A dynamic equilibrium between chiral cage **22** and achiral compound **23** was observed depending on the shape of the guest molecule. Whereas the addition of “flat” 1,3,5-benzenetricarboxylic acid led to the formation of chiral cage **22**, the addition of more spherical guests such as CBrCl₃ or carbontetrabromide led primarily to the formation of achiral cage **23**. This shape preference is explained by molecular modelling studies that indicate a “flattened” cavity within the cage **22** as compared to the more spherical shape found in compound **23**. Despite the C_{2v} symmetrical structure of the tripyrindine ligand **20**, cage structure **22** is asymmetric because of its ligand orientation in the cage framework (Fig. 16).

The chirality of **22** was observed by diastereomeric encapsulation of *R*-mandelic acid. The observation of two diastereomers in the ¹H-NMR evidenced that the racemization of *P*-**22** to *M*-**22**, which requires the cleavage of at least two Pd–N bonds, did not take place on the NMR timescale. Notably, diastereomers were not observed when racemic mandelic acid was employed, indicating a rapid guest exchange of *R*- and *S*-mandelic acid on the NMR timescale. Modest chiral induction was obtained in a 3 : 2 diastereomeric ratio upon encapsulation of the chiral guest (*S*)-1-acetoxyethylbenzene.

Another example of a trigonal prismatic complex is the porphyrin prism **24**, also reported by Fujita and coworkers [139]. This complex is formed upon coordination of three face bridging zinc(II)-coordinated porphyrin ligands to six palladium(II) ions at the corners of the prism. Although

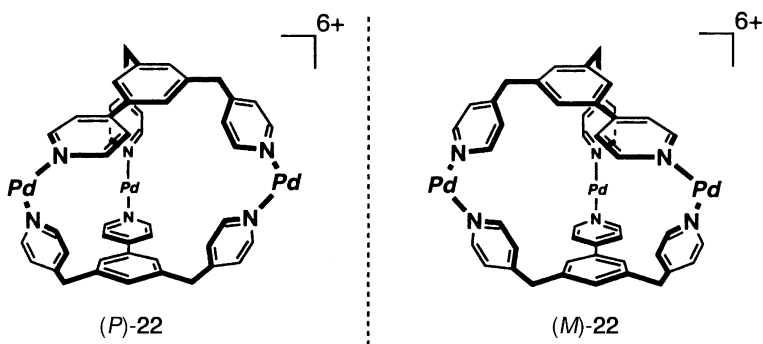


Fig. 16 Illustration of the right- (*P*) and left- (*M*) handed chirality of cage 22. Reprinted with permission from [75]. Copyright 1999 American Chemical Society

the structure originally exhibits D_{3h} (conformation A) symmetry with the palladium(II) centers at the apical positions of the prism, suitable guest molecules such as pyrene can trigger a conformational change into a chiral, C_2 symmetrical species as monitored by ^1H -NMR spectroscopy (Fig. 17). Addition of powdered pyrene to a solution of 24 and heating at 80 °C for 3 h results in desymmetrization of the prismatic structure due to pyrene encapsulation. A large upfield shift in the ^1H -NMR pyrene signals indicates guest inclusion within the cavity, which was further confirmed by integration of the ^1H -NMR signals and cold-spray ionization mass spectrometry. Based on molecular modelling analysis, the authors suggest that the guest binding triggered the apical to equatorial flipping of two Py-Pd-Py hinges at diagonal positions, thus providing C_2 -desymmetrized conformation B.

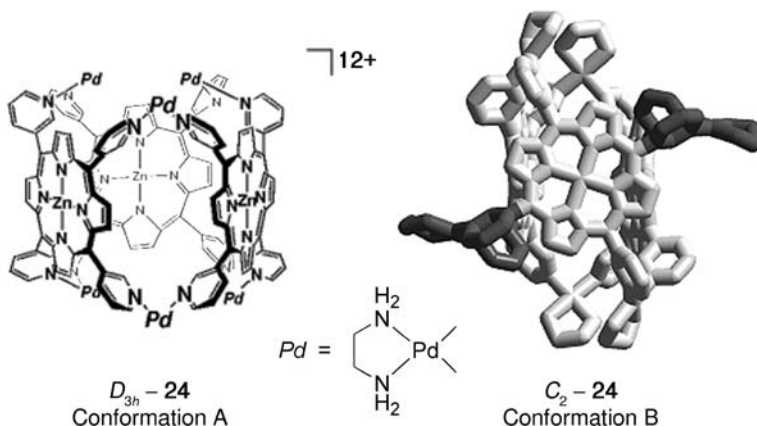


Fig. 17 Illustration of the conformational change in compound 24 from D_{3h} (conformation A) to C_2 (conformation B) symmetry upon guest (pyrene) encapsulation. Reprinted with permission from [139]. Copyright 2001 Wiley, Inc.

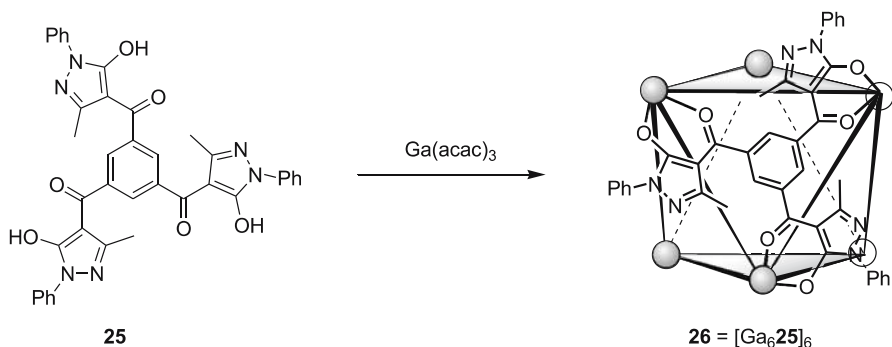


Fig. 18 Formation of the trigonal antiprism **26** upon coordination of six pyrazolone ligands **25** and six gallium(III) ions [67]

Serendipitous syntheses of trigonal antiprismatic ensembles were recently reported by Raymond and Saalfrank [67, 140]. One such assembly results from the stoichiometric reaction of a pyrazolone based ligand **25** with gallium(III) acetylacetonate, forming the $[\text{Ga}_6\text{25}_6]$ cylinder **26** with idealized D_3 symmetry (Fig. 18). The gallium(III) ions are octahedrally coordinated and define a distorted trigonal antiprism in which six ligands **25** form the equatorial faces of the cylinder, leaving gaping holes at the top and the bottom. The cylinder exists as a racemic mixture of homochiral **26** ($\Delta\Delta\Delta\Delta\Delta$ or $\Lambda\Lambda\Lambda\Lambda\Lambda$) in the solid state and in solution. **26** is remarkably enantiostable as no racemic interconversion to any of the 64 possible isomers was observed on the NMR timescale in the temperature range from -40°C to 120°C .

Two similar systems of trigonal antiprismatic geometry are represented by dimeric calixarene capsules that are also based on only five building units [141, 142]. This is illustrated for capsule **28** [141], where two ligands **27**, each with three meta-pyridyl substituents, are connected via coordination to three palladium(II) ions. Due to the meta-substitution at the coordinating pyridyl rings, the resulting capsule **28** is helically twisted (Fig. 19). The

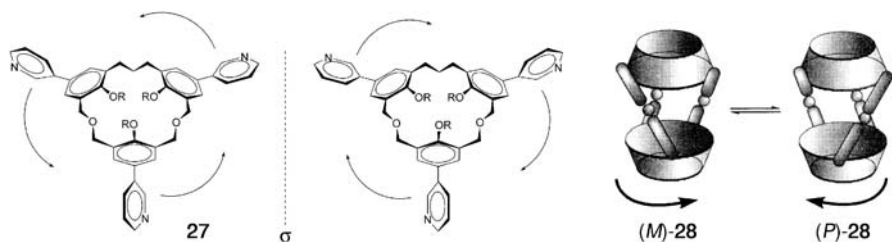


Fig. 19 Formation of the dimeric coordination capsule **28** based on the calixarene ligand **27**. The helical twist results from the orientation of the meta-substituted pyridyl units upon coordination to palladium(II) ions (represented by grey spheres). Adapted with permission from [141]. Copyright 2001 American Chemical Society

structure was elucidated in solution by NMR studies and cold-spray mass spectrometry techniques. Chiral induction was observed upon encapsulation of chiral guest molecules such as *S*-2-methylbutylammonium ions; however, the helical orientation of the diastereomeric aggregates was not established.

2.3

Tetrahedra

The most utilized chiral supramolecular architectures resemble tetrahedra. They comprise the highest symmetry observed to date for chiral molecular systems (*T* symmetry) and a variety of splendid examples are reported in the literature [15, 68, 143, 144]. Molecular tetrahedral symmetry can be represented by a number of different cage stoichiometries (Fig. 20) [143], all of which are realized in molecular systems.

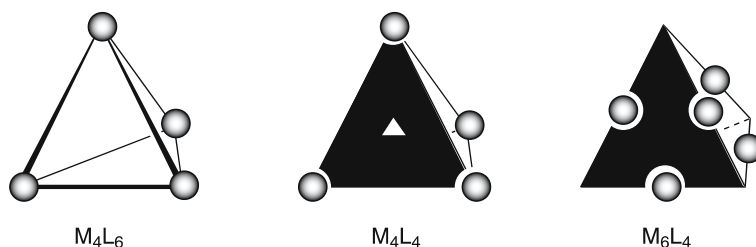


Fig. 20 Categorization of molecular tetrahedra into different cage stoichiometries M_4L_6 , M_4L_4 and M_6L_4 [143]

2.3.1

M_4L_6 Stoichiometry

The earliest example of a coordination tetrahedron was reported by Saalfrank and coworkers [144]. Their study showed the formation of the tetranuclear magnesium(II) complex **30** bridged by six tetra-carboxylate ligands **29**, representing the first reported coordination tetrahedron exhibiting M_4L_6 stoichiometry (Fig. 21). This serendipitous discovery was followed by the formation of other, pre-designed tetrahedral architectures [19, 122, 145].

In the Mg_4 **29**₆ tetrahedron **30**, the four magnesium(II) ions are coordinated by three chelating ligands **29** in an octahedral fashion. Temperature-dependent ¹H-NMR studies have shown that **30** is formed as a racemic mixture of homochiral $\Delta\Delta\Delta\Delta$ and $\Lambda\Lambda\Lambda\Lambda$ ensembles. This enantioselectivity is ensured by restricted rotation around the C – C single bond in ligand **29** imposed by the carboxylate residues. Replacement of the carboxylate residues by smaller hydrogen atoms results in ligand **31** that forms the Mg_4 **31**₆ tetrahedron **32**. Although exclusively homochiral $\Delta\Delta\Delta\Delta$ and $\Lambda\Lambda\Lambda\Lambda$ ensembles



Fig. 21 Saalfrank and co-workers reported the formation of the first molecular tetrahedron **30** [144]. Modification of the original tetra-carboxylate ligand **29** allowed the formation of tetrahedron **32** based on ligand **31** [122]

are formed and thus **30** and **32** are isostructural in the solid state, **32** shows a dynamic temperature dependence in solution that consists of four simultaneous Bailar twists at the four octahedrally coordinated magnesium(II) centers. These twists are synchronized with the sterically unhindered atropenantimerization processes around the C–C single bonds in the six ligands **31** resulting in the remarkable enantiomerization of $(\Delta\Delta\Delta\Delta)$ -**32** to $(\Lambda\Lambda\Lambda\Lambda)$ -**32** without the formation of diastereomeric intermediates (Fig. 22). The activation barrier for this racemization process was determined to be 14.3 kcal/mol from variable temperature ^1H -NMR experiments.

A series of rationally designed M_4L_6 coordination tetrahedra **6**, **35** and **36** based on the *bis*-catecholate ligands **5**, **33** and **34**, respectively, was reported by Raymond and coworkers [68, 76, 146]. The tetrahedral M_4L_6 complexes form from four metal ions such as Al(III), Ga(III), In(III), Sn(IV), Ge(IV), Fe(III) and Ti(IV) that are octahedrally coordinated by six *bis*-catecholate ligands. The 2-fold symmetric ligands **5**, **33** and **34** span the edges of the tetrahedra and coincide with the C_2 symmetry axes of the assembly, while the

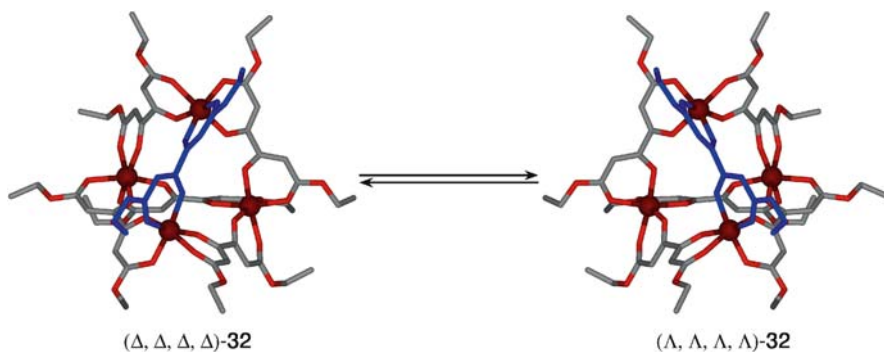


Fig. 22 Four synchronous *Bailar*-twists and six ligand atropenantimerization processes are required for the enantiomerization of $(\Delta\Delta\Delta\Delta)$ -**32** to $(\Lambda\Lambda\Lambda\Lambda)$ -**32** [122]

metal ions are positioned on the C_3 symmetry axes of the overall T symmetric ensembles. The resulting M_4L_6 tetrahedra are rendered chiral due to helical *tris*-bidentate coordination of the catecholates to the octahedral metal centers. Furthermore, the chirality established at one vertex is mechanically coupled by the rigid backbones of ligands **5**, **33** and **34** onto the three remaining metal vertices resulting exclusively in homochiral ($\Delta\Delta\Delta\Delta$ or $\Lambda\Lambda\Lambda\Lambda$) architectures (Fig. 23). Importantly, the obtained tetrahedra **6**, **35** and **36** exhibit a molecular cavity capable of guest encapsulation. In this respect, it is noteworthy that formation of **6** occurs either with or without the presence of suitable guest molecules, whereas **35** and **36** require the presence of suitable guest molecules such as tetramethyl- and tetraethylammonium ions as thermodynamic templates to ensure formation. Without the presence of a guest template, ligand **33** forms the triple-stranded helicate **37**.

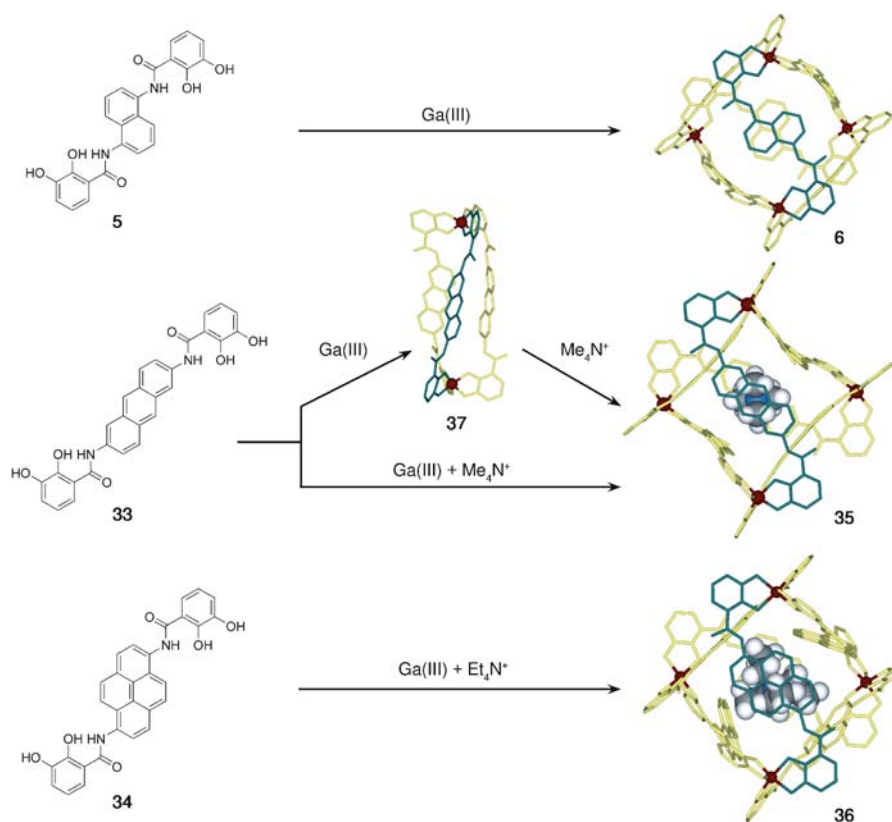


Fig. 23 Formation of a series of M_4L_6 tetrahedra **6**, **35** and **36** from the *bis*-catecholate ligands **5**, **33** and **34**. Tetrahedron **6** forms with or without the presence of suitable guest molecules [68], whereas **35** and **36** require thermodynamic guest templates [76, 146]. Without the presence of NMe_4^+ guest molecules, ligand **33** forms the dinuclear, triple helicate **37** [76]

Tetrahedron **6** represents one of the rare examples of supramolecular assemblies where complete enantiomeric resolution can be achieved. Treatment of racemic **6** with the chiral auxiliary (*S*) – *N*-methylnicotinium (s-nic, **38**) preferentially precipitates the diastereomeric ion-pair of ($\Delta\Delta\Delta\Delta$)-**638**. Once resolved, the chiral auxiliary can be replaced by achiral counter-ions such as tetramethyl- or tetraethylammonium ions, while the tetrahedra maintain their enantiopurity for at least 8 months, even upon extended heating in D₂O (Fig. 24) [119].

Tetrahedron **6** shows the remarkable ability to encapsulate a variety of monocationic species, to stabilize reactive intermediates [147], and even to catalyze chemical reactions inside the encapsulated space [25]. Chemical species that are readily encapsulated include NMe₄⁺, NEt₄⁺, PEt₄⁺, Cp₂Co⁺, Cp*₂Co⁺, Cp₂Fe⁺ and alkali-metal crown ether complexes [148] (Cp = η^5 -cyclopentadienyl; Cp* = η^5 -pentamethyl-cyclopentadienyl). The affinity of the guest molecules for the cavity depends on their size, lipophilicity, enthalpy of desolvation, and charge. The chiral environment of the cavity can be probed by employing chiral ruthenium(II) half-sandwich complexes of the general formula [CpRu-(diene)(halide)] and [Cp*Ru(diene)(halide)]. In polar media, these complexes undergo halide dissociation to form cationic solvated ruthenium(II) species, which can be encapsulated into the tetrahedral assembly [22]. Encapsulation of the chiral cation **39** reveals a striking stereochemical feature: the generation of two diastereomeric host-guest complexes. Combination of the racemic tetrahedron **6** with the racemic ruthenium(II) half-sandwich complex **39** results in four different host-guest stereoisomers (Δ /*R*, Δ /*S*, Λ /*R*, Λ /*S*), that is, two diastereomeric pairs of enantiomers (Fig. 25) [24]. At present, combination of a variety of chiral guest molecules led to observed diastereomeric ratios up to 85 : 15, which is encouraging con-

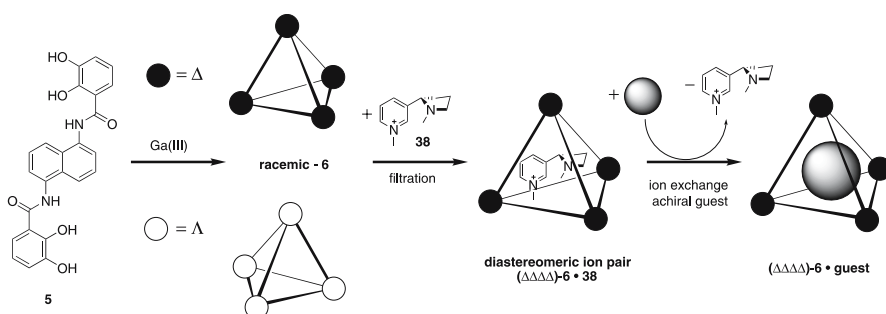


Fig. 24 Overview of the synthesis and resolution of solution stable, chiral tetrahedron **6** [119]. **a** Formation of racemic, homochiral ($\Delta\Delta\Delta\Delta$)-**6** and ($\Lambda\Lambda\Lambda\Lambda$)-**6**; **b** Chiral resolution and separation upon addition of s-nic ions (**38**) by formation of diastereomeric ion-pair ($\Delta\Delta\Delta\Delta$)-**638**; **c** Ion-exchange of chiral auxiliary **38** by achiral counterions such as NMe₄⁺ and NEt₄⁺ maintains the chirality of the resolved tetrahedra ($\Delta\Delta\Delta\Delta$)-**6**

sidering that the recognition process relies solely on weak supramolecular interactions [21, 23, 24].

In an incredible example of structural memory, tetrahedron **6** not only shows remarkable time-resolved enantioselectivity, but its chiral configuration also exhibits robustness towards substitution of edge-bridging ligands from the assembly. It was shown that as many as three (!) of the six edge bridging ligands **5** can be replaced by ligand **3** while maintaining its original chirality (Fig. 26) [149]. This is particularly remarkable since **3** originally does not form tetrahedra but rather forms M_2L_3 helicates **4**.

The previous tetrahedra exhibited anionic frameworks with the capability of cationic guest encapsulation [63, 68, 148]. Further examples of M_4L_6 tetrahedra also include cationic Co_4L_6 frameworks capable of anionic guest encapsulation as exemplified by Ward and coworkers (Fig. 27) [15, 150–152]. These cationic clusters are formed upon *tris*-bidentate coordination of the *N*-heterocyclic ligands **40**, **41** and **42** to octahedral cobalt(II) ions. The structures are trigonal pyramidal rather than tetrahedral, with the apical cobalt(II) ions exhibiting facial coordination geometries and the basal cobalt(II) ions showing meridional ligand arrangements. This overall distortion results in

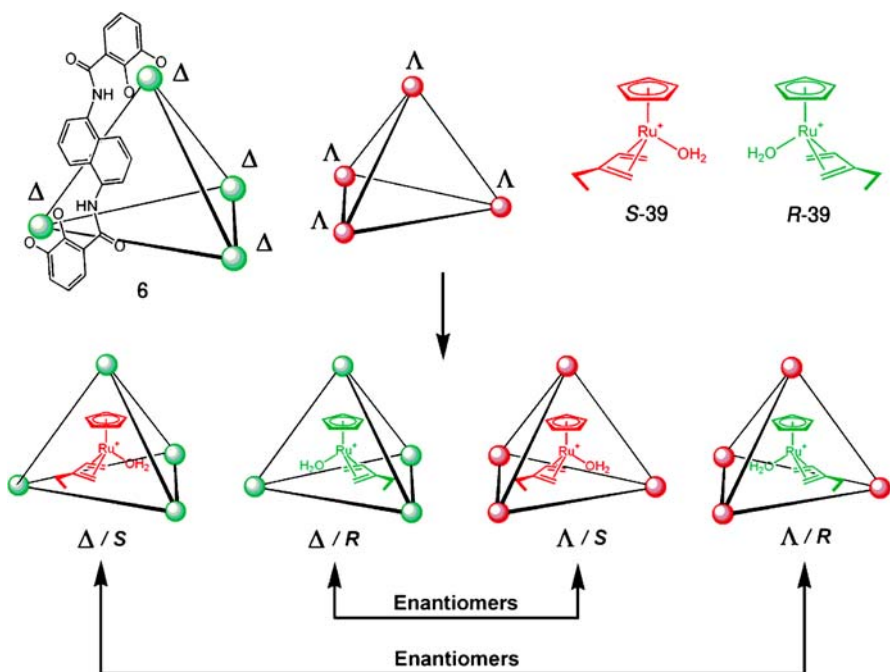


Fig. 25 Formation of two diastereomeric pairs or enantiomers by combination of racemic mixtures of tetrahedron **6** and ruthenium(II) half-sandwich complex **39**. Reprinted with permission from [24]. Copyright 2005 American Chemical Society

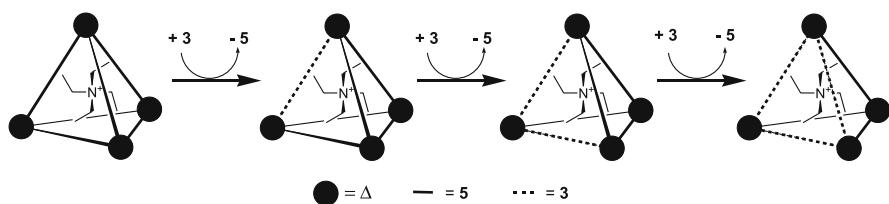


Fig. 26 Schematic representation the chiral memory effect observed in enantiomerically pure tetrahedron **6**. Ligand **3** can replace up to three bridging ligands **5** in the $(\Delta\Delta\Delta\Delta)$ -**6** tetrahedron, while still maintaining its original $\Delta\Delta\Delta\Delta$ -homochirality [149]

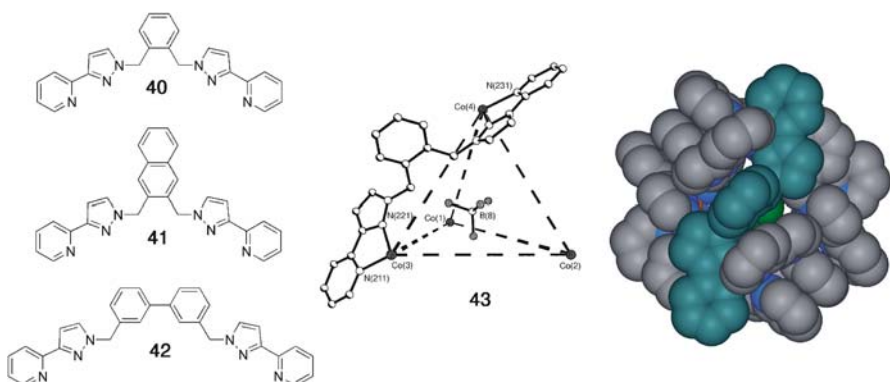


Fig. 27 Representation of the *N*-heterocyclic ligands **40**, **41** and **42** that form cationic Co_4L_6 tetrahedra. The identical coordination assemblies are illustrated by the distorted tetrahedron Co_4L_6 (**43**). Reprinted with permission from [150]. Copyright 2004 The Royal Society of Chemistry

reduced C_3 symmetry as is evidenced both in the solid state and in solution. As exemplified with tetrahedron **43** (formed from ligand **40**), the assembly encapsulates anions such as tetrafluoroborate, perchlorate, and hexafluorophosphate. Their dynamic exchange behavior in solution was monitored by NMR spectroscopy and showed no preference between encapsulated anionic species [150].

2.3.2

M_4L_4 Stoichiometry

An alternative stoichiometry in the formation of chiral tetrahedral assemblies is the utilization of *tris*-bidentate chelating, face-bridging ligands resulting in M_4L_4 tetrahedra. Three such ligands **44**, **45** and **46** of comparable size have been shown to form anionic (**47**), neutral (**48**) and cationic (**49**) M_4L_4 architectures, respectively (Fig. 28). The complexes are formed by octahedral coordination of metal ions located at the vertices of the tetrahedron, gen-

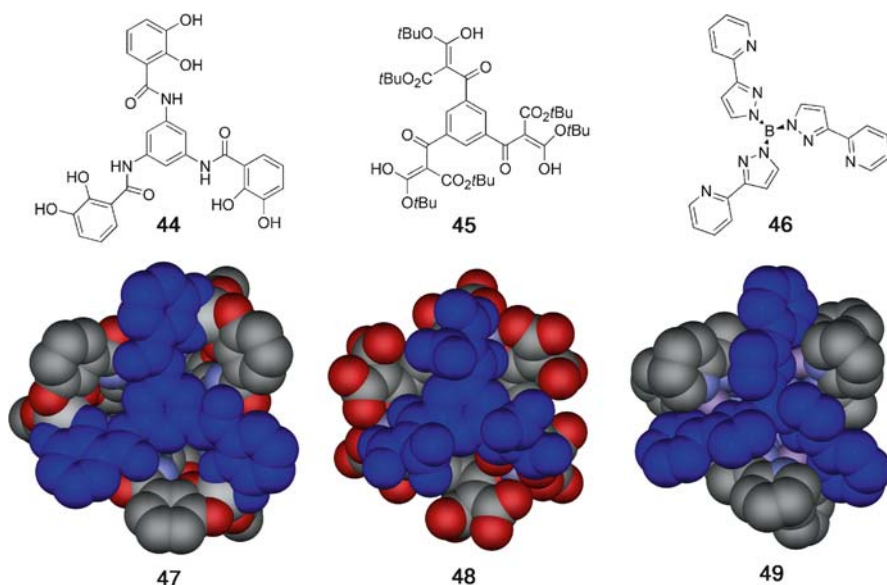


Fig. 28 Overview of the ligands **44** [105], **45** [140] and **46** [153] that form M_4L_4 tetrahedra: anionic $[M_444_4]^{8-/12-}$ (**47**); neutral $[Fe_445_4]$ (**48**) and cationic $[Mn_446_4]^{4+}$ (**49**)

erated by bidentate chelating groups from each of the three adjacent faces. The resulting tetrahedra **47**, **48** and **49** are homochiral in both solution and the solid state and exhibit cavity sizes that are too small to encapsulate guest molecules [105, 140, 153]. Anionic cluster **47** shows the greatest versatility as it is formed from a variety of metal ions such as Al(III), Ga(III), Sn(IV), Fe(III) and Ti(IV), whereas neutral **48** and cationic **49** are only reported to form from Fe(III) and Mn(II), respectively.

Subsequently, larger M_4L_4 clusters were developed that showed increased cavity sizes with potential for guest encapsulation [154, 155]. However, only tetrahedron **51**, reported by Raymond and coworkers [154], was actually shown to dynamically encapsulate guest molecules such as NMe_4^+ , NEt_4^+ and PEt_4^+ in solution. Tetrahedron **51** is based on ligand **50**, a phenyl extension of the previous described ligand **44**. The rigid phenyl extension appears necessary to ensure tetrahedron formation as it was shown that a more flexible methylene linker results in the formation of mononuclear M_1L_1 complex **52** (Fig. 29) [156].

Tetrahedra **51** were formed from a variety of metal ions such as Al(III), Ga(III), In(III) and Ti(IV) (Fig. 30). The overall charge of the anionic clusters is dependent on the metal ion employed. Trivalent metal ions result in an overall 12- charge, whereas tetravalent Ti(IV) ions reduce the charge to 8-. The compounds were unambiguously characterized in solution by NMR spectroscopy and high-resolution mass spectrometry.

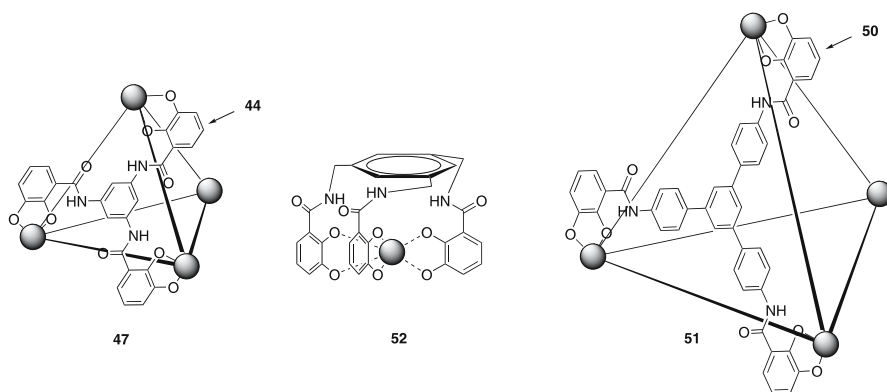


Fig. 29 Extension of the face bridging, C_3 -symmetric ligand **44** that forms M_4L_4 tetrahedron **47**. Introduction of rigid phenyl bridges in ligand **50** preserves the necessary rigidity to form tetrahedron **51** [154], whereas introduction of a flexible methylene bridge results in the formation of mononuclear M_1L_1 complex **52** [156]

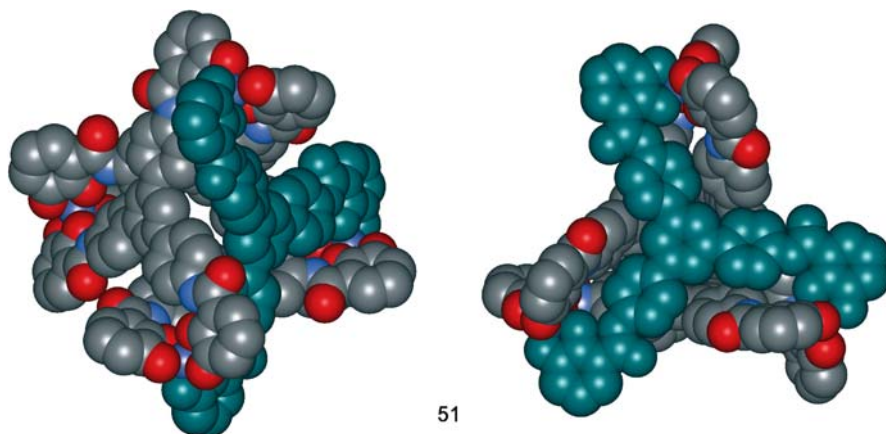


Fig. 30 Two representations of a molecular model based on M_4L_4 tetrahedra **51** that are formed from Al(III), Ga(III), In(III) and Ti(IV) ions [154]

2.3.3

M_6L_4 Stoichiometry

A third alternative in building chiral molecular tetrahedra is represented by the M_6L_4 stoichiometry, where four face bridging ligands are connected by six metal ions located on the edges of the tetrahedron. Although this exact stoichiometry has not been realized thus far, related examples are reported by Robson and Müller [143, 157]. They utilize guanidine-based ligands **53** and **54** that form tetrahedra **55** and **56**, respectively, upon reaction with cadmium(II)

chloride. Each cadmium(II) center is tetragonal pyramidal coordinated by basal coordination of two nitrogen and one phenolate oxygen atom of one ligand and a bridging phenolate oxygen atom from the adjacent tetrahedral face. This square- $[\text{Cd}_2\text{O}_2]$ bridging motif results in an overall M_{12}L_4 stoichiometry with the metal ions located close to the edges of the tetrahedron. The fifth, apical cadmium(II) coordination site is occupied by a chloro ligand. Both tetrahedra **55** and **56** resemble anionic frameworks and, upon formation, encapsulate small cationic NMe_4^+ and NEt_4^+ guest molecules. The tetrahedra are tightly closed so that no dynamic exchange of incarcer-

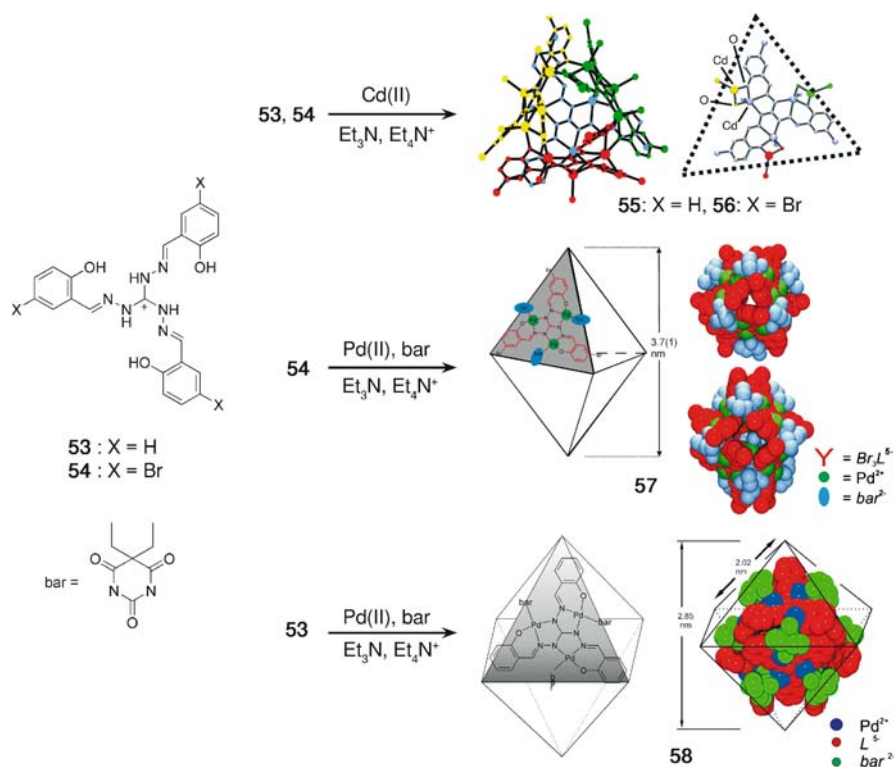


Fig. 31 Supramolecular architectures based on the face bridging and tridentate coordinating guanidine-ligands **53** ($\text{X} = \text{H}$) and **54** ($\text{X} = \text{Br}$). The screw-like orientation of the faces upon *tris*-metal coordination generates the chirality that is maintained within the final assemblies. *Tetrahedra*: both **53** and **54** form tetrahedra **55** and **56** upon cadmium(II) coordination, where the faces are linked via a square $[\text{CdO}]_2$ coordination motif; *Trigonal bipyramid* **57** is formed from ligand **54** upon palladium(II) coordination, where the face bridging occurs through palladium(II)-bar coordination; *Octahedron* **58** is formed from ligand **53** triply coordinating to palladium(II). The faces are further connected by palladium(II)-bar coordination. Adapted with permissions from [57, 143, 157, 158]. Copyrights 2004, 2005 Wiley, Inc.

ated guest molecules with charge balancing, non-encapsulated counter-ions was observed. The chirality of the assemblies originates from the screw-like orientation of each ligand upon coordinating to three cadmium(II) ions at each face of the tetrahedron, with each face exhibiting identical “screw-orientations” (Fig. 31). Furthermore, both ligands **54** and **53** can also be utilized in the formation of trigonal bipyramid **57** [158] and molecular octahedron **58**, respectively [57]. Although both of these structures are exclusively characterized in the solid state, they are discussed here as they represent an informative “modular” approach in the construction of high symmetry coordination architectures.

2.4

Trigonal Bipyramid

The sterically demanding bromo-substituted, triangular guanidine-based ligand **54** can also be utilized in the formation of the trigonal bipyramidal assembly **57** [158]. Each ligand **54** coordinates three palladium(II) centers in a tridentate manner and six of these triangular units cover the faces of a trigonal bipyramid, which are linearly connected by nine barbiturate ligands (*bar*) completing the square planar coordination sphere of the palladium(II) ions (Fig. 31). All faces exhibit identical screw-like orientations, rendering **57** chiral. The anionic framework encapsulates up to five counter-ions such as NEt_4^+ and NEt_3H^+ . Under identical reaction conditions, a partially assembled, open-sided tetrahedron was also characterized in the solid state. This structure can be seen as an intermediate in the formation of trigonal bipyramid **57** with only two triangular faces missing from completion [158].

2.5

Octahedra

Contrary to the sterically demanding bromo-substituent on ligand **54**, guanidine-based ligand **53** features a smaller hydrogen atom that allows the formation of octahedron **58** [57]. As previously observed, each ligand **53** coordinates three palladium(II) ions in a tridentate fashion resembling the trigonal faces from which octahedron **58** is formed (Fig. 31). Six of these faces are interconnected by linear coordination of 12 barbiturate (*bar*) ligands. The overall structure is chiral as all faces show identical screw-orientation of the palladium(II) coordination. Octahedron **58** resembles crystallographic *T* symmetry as the rotational twist in the faces prevents higher *O* symmetry.

Another example of a molecular octahedron is represented by assembly **60**, reported by Fujita and coworkers [56]. The ensemble is formed from six end-capped diamine palladium(II) ions that are located at the vertices of an octahedron and bridged by four C_{2v} -symmetric pyridyl ligands **59**. The self-assembly is facilitated by the presence of suitable guest molecules such as

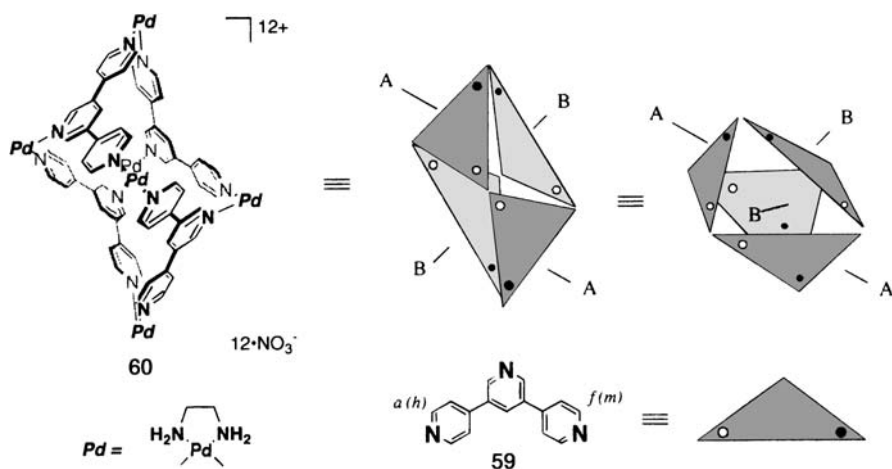


Fig. 32 Assembly of the molecular octahedron **60** from six end-capped palladium(II) corners and four C_{2v} -symmetric ligands **59**. The overall C_2 -chirality of **60** arises from the non-symmetrical arrangement of **59**. Reprinted with permission from [56]. Copyright 2002 The Chemical Society of Japan

p-dichlorobenzene and other neutral, disubstituted benzenes. The ensemble exhibits C_2 chirality where two ligands are linked together by their terminal pyridine rings, creating an S-shaped helical motif, whereas the other two ligands are linked by their center pyridine rings, resulting in a mesomeric X-shaped motif (Fig. 32). Modest chiral induction was achieved utilizing chiral ligand caps at the palladium(II) ions.

2.6

Cuboctahedra

The only example of a twisted cuboctahedron was reported by Kimura and coworkers [159]. Cuboctahedron **63** was obtained by the 4 : 4 self-assembly of *tris*(Zn^{II} -cyclen) complex **61** with trianionic trithiocyanurate (TCA^{3-} , **62**) upon guest encapsulation and was characterized both in the solid state and in solution (Fig. 33). Suitable guests are lipophilic organic molecules of matching size, such as, ([D_4]-2,2,3,3)-3-(trimethylsilyl)propionic acid (TSP), 1-adamantanecarboxylic acid, 2,4-dinitrophenol (2,4-DNP), adamantane (ADM), or the tetra-*n*-propylammonium (TPA) cation.

Each triangular TCA^{3-} unit links to three Zn^{II} -cyclen moieties through apical $Zn^{II} - S^-$ coordination, forming a triangular face of the cuboctahedron (Fig. 34, left). The rotational offset by this coordination results in either a clockwise or anti-clockwise twist of the triangular faces, rendering the overall ensemble chiral (Fig. 34, center). Furthermore, **63** contains a cavity best described as a twisted truncated tetrahedron that enables encapsulation of

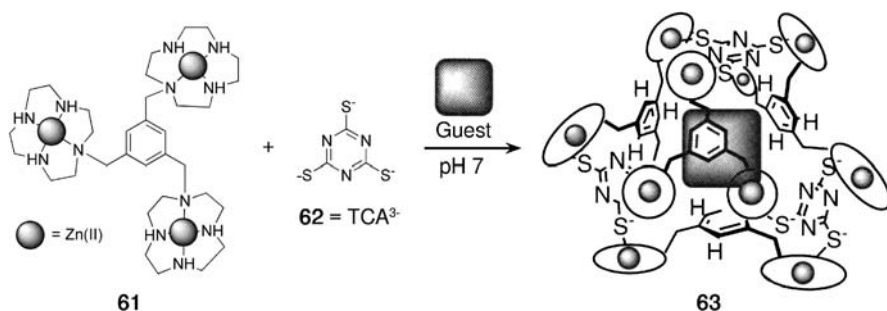


Fig. 33 Schematic representation of cuboctahedron **63** formation. Equimolar amounts of *tris*(Zn^{II}-cyclen) complex **61** react with trianionic trithiocyanurate (TCA³⁻, **62**) upon suitable guest encapsulation to form **63**. Adapted with permission from [159]. Copyright 2002 Wiley, Inc.

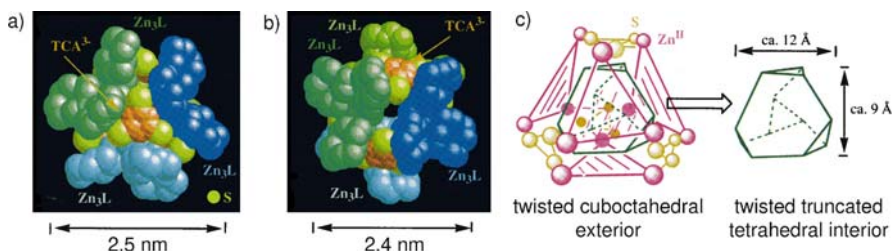


Fig. 34 Cuboctahedron **63**: **a** Space-filling representation viewed along a C_3 -symmetry axis. The four units of **61** are shown in light green, green, light blue, and blue, the 1,3,5-triazine rings of TCA³⁻ (**62**) are orange, and the sulfur ions shown in yellow; **b** Ball and stick representation of the bonding mode around TCA³⁻ in **63**; **c** The exterior framework of **63** is represented as a twisted cuboctahedron formed from four triangular faces of **61** units (purple triangles) and four triangular faces of **62** (yellow triangles). The green framework shows the inner cavity of **63**, representing a twisted, truncated tetrahedron. Adapted with permission from [159]. Copyright 2002 Wiley, Inc.

anionic and neutral guest molecules (Fig. 34, right). Chiral induction was achieved by encapsulation of chiral guest molecules such as (1*S*,2*R*,4*R*)-(-)-camphorsultam indicating that an encapsulated chiral guest can control the exterior chirality of **63**.

Although a number of impressive chiral, supramolecular architectures were not discussed in this chapter either due to their instability in solution or their inability to encapsulate guest molecules, they should not go unmentioned and are referenced to follow up for the interested reader. Some selected examples are: (i) Saalfrank and coworkers octadecametallic square box composed of 52 achiral components with molecular D_2 symmetry [160]; (ii) Ward and coworkers truncated, cationic tetrahedral cage [Co^{II}₁₂L₁₈]²⁴⁺ [161] that encapsulates four tetrafluoroborate counter-ions in the solid state; (iii) James

and coworkers “super-adamantoid” $[\text{Ag}^{\text{I}}_6(\text{trisphos})\text{X}_4]^{2+}$ ($\text{X} = \text{SO}_3\text{CF}_3^-$, ClO_4^- , NO_3^- , BF_4^-) cages, where the chirality originates from the phenyl orientation of coordinating triphos-ligands [73]; and (iv) Robson and coworkers homochiral, neutral $[\text{Cu}^{\text{II}}_8\text{L}_8]$ cube, with rotational trinuclear metal coordination around each ligand face that results in an effectively windowless shell [58, 59].

3

Conclusions and Outlook

While nature’s evolutionary development of complex hierarchical architectures resemble the blueprints for our attempts to imitate and create ensembles in a designed, architectural approach, we have only begun to understand the underlying principles that allow for the construction of highly organized assemblies. From the toolkit of supramolecular interactions, metal-ligand coordination is most promising due to the directionality and predictability of metal coordination geometries. Based on this predictability, two design approaches—the symmetry interaction and molecular library model—were developed, allowing for the construction of the diverse architectures presented. The variety of geometric polyhedra spans from simple trigonal prismatic assemblies to more complex octahedra and cuboctahedra. Although the reported molecules resemble highly symmetric constructs, the highest molecular point symmetry observed for these chiral architectures is tetrahedral *T*-symmetry. This leaves us trailing behind nature’s beautiful examples of higher octahedral *O*- and icosahedral *I*-symmetries. Further investigations will have to deepen our understanding of the basic design principles in order to enable the construction of assemblies with higher symmetry. Particular focus will thereby lie on the utilization of such ensembles in recognition processes and as chemical reaction vessels for storage, stabilization, transformations, and catalysis. Ideally, individual molecular containers will be tailor-made featuring the unique size, shape, charge, and inclusion properties required for specific chemical reactions. Tremendous progress has been made within this relatively new field of supramolecular chemistry over the last decade and many beautiful examples of coordination compounds with increasing complexity are reported, while we are continuing to explore the potential of this exciting and stimulating area of research.

Acknowledgements Our research described in this review is supported by NSF grant CHE-0317011 and by the Director, Office of Energy Research, Office of Basic Energy Sciences, Chemical Sciences Division, of the U.S. Department of Energy under contract DE-AC03-7600098.

We thank the Alexander von Humboldt Foundation for a postdoctoral scholarship to G.S. We would like further to thank Prof. Bergman and Prof. Saalfrank for their collaboration in various supramolecular projects.

References

1. Exceptions are twinned, racemic quartz crystals that are composed of both right- and left-handed helices
2. Hamilton TD, MacGillivray LR (2004) *Cryst Growth Des* 4:419
3. Sgro J-Y (2004) ICTV 8th Report: <http://virology.wisc.edu/virusworld/>
4. Rossmann MG, Arnold E, Erickson JW, Frankenberger EA, Griffith JP, Hecht HJ, Johnson JE, Kamer G, Luo M, Mosser AG, Rueckert RR, Sherry B, Vriend G (1985) *Nature* 317:145
5. Arnold E, Rossmann MG (1988) *Acta Crystallogr, Sect A* 44:270
6. Badger J, Minor I, Kremer MJ, Oliveira MA, Smith TJ, Griffith JP, Guerin DMA, Krishnaswamy S, Luo M, Rossmann MG, McKinlay MA, Diana GD, Dutko FJ, Fancher M, Rueckert RR, Heinz BA (1988) *Proc Natl Acad Sci USA* 85:3304
7. An example of an icosahedral virus is Enterobacteria phage PhiX174, PDB_ID:2BPA
8. Friedman L, Miller JG (1971) *Science* 172:1044
9. Blaschke G, Kraft HP, Fickentscher K, Kohler F (1979) *Arzneimittel-Forschung/Drug Research* 29-2:1640
10. Nakanishi T, Yamakawa N, Asahi T, Shibata N, Ohtani B, Osaka T (2004) *Chirality* 16:S36
11. Harrison PM, Arosio P (1996) *Biochim Biophys Acta* 1275:161
12. Takeda N, Umemoto K, Yamaguchi K, Fujita M (1999) *Nature* 398:794
13. Olenyuk B, Whiteford JA, Fechtenkötter A, Stang PJ (1999) *Nature* 398:796
14. Saalfrank RW, Burak R, Reihs S, Low N, Hampel F, Stachel HD, Lentmaier J, Peters K, Peters EM, von Schnering HG (1995) *Angew Chem Int Ed Engl* 34:993
15. Fleming JS, Mann KLV, Carraz CA, Psillakis E, Jeffery JC, McCleverty JA, Ward MD (1998) *Angew Chem Int Ed* 37:1279
16. Mann S, Huttner G, Zsolnai L, Heinze K (1996) *Angew Chem Int Ed Engl* 35:2808
17. Caneschi A, Cornia A, Fabretti AC, Foner S, Gatteschi D, Grandi R, Schenetti L (1996) *Chem Eur J* 2:1379
18. Hasenknopf B, Lehn J-M, Kneisel BO, Baum G, Fenske D (1996) *Angew Chem Int Ed Engl* 35:1838
19. Saalfrank RW, Burak R, Breit A, Stalke D, Herbstirmer R, Daub J, Porsch M, Bill E, Mütter M, Trautwein AX (1994) *Angew Chem Int Ed Engl* 33:1621
20. Kusakawa T, Fujita M (2002) *J Am Chem Soc* 124:13576
21. Fiedler D, Leung DH, Bergman RG, Raymond KN (2004) *J Am Chem Soc* 126:3674
22. Fiedler D, Pagliero D, Brumaghim JL, Bergman RG, Raymond KN (2004) *Inorg Chem* 43:846
23. Leung DH, Fiedler D, Bergman RG, Raymond KN (2004) *Angew Chem Int Ed* 43:963
24. Fiedler D, Leung DH, Bergman RG, Raymond KN (2005) *Acc Chem Res* 38:349
25. Fiedler D, Bergman RG, Raymond KN (2004) *Angew Chem Int Ed* 43:6748
26. Yoshizawa M, Kusakawa T, Fujita M, Yamaguchi K (2000) *J Am Chem Soc* 122:6311
27. Yoshizawa M, Takeyama Y, Okano T, Fujita M (2003) *J Am Chem Soc* 125:3243
28. Yoshizawa M, Kusakawa T, Fujita M, Sakamoto S, Yamaguchi K (2001) *J Am Chem Soc* 123:10454
29. Kusakawa T, Fujita M (1999) *J Am Chem Soc* 121:1397
30. Caulder DL, Raymond KN (1999) *J Chem Soc, Dalton Trans* 8:1185
31. Caulder DL, Raymond KN (1999) *Acc Chem Res* 32:975
32. Fujita M (1998) *Chem Soc Rev* 27:417
33. Leininger S, Olenyuk B, Stang PJ (2000) *Chem Rev* 100:853
34. Breault GA, Hunter CA, Mayers PC (1999) *Tetrahedron* 55:5265

35. Vögtle F, Dünnwald T, Schmidt T (1996) *Acc Chem Res* 29:451
36. Amabilino DB, Stoddart JF (1995) *Chem Rev* 95:2725
37. Badjic JD, Balzani V, Credi A, Silvi S, Stoddart JF (2004) *Science* 303:1845
38. Heath JR, Stoddart JF, Williams RS (2004) *Science* 303:1136
39. Collin JP, Dietrich-Buchecker C, Gavina P, Jimenez-Molero MC, Sauvage JP (2001) *Acc Chem Res* 34:477
40. Collier CP, Mattersteig G, Wong EW, Luo Y, Beverly K, Sampaio J, Raymo FM, Stoddart JF, Heath JR (2000) *Science* 289:1172
41. Collier CP, Wong EW, Belohradsky M, Raymo FM, Stoddart JF, Kuekes PJ, Williams RS, Heath JR (1999) *Science* 285:391
42. Chambron JC, Dietrich-Buchecker C, Nierengarten JF, Sauvage JP, Solladie N, Albrecht-Gary AM, Meyer M (1995) *New J Chem* 19:409
43. Chambron JC, Heitz V, Sauvage JP (1993) *J Am Chem Soc* 115:12378
44. Dietrich-Buchecker CO, Sauvage JP, Kern JM (1984) *J Am Chem Soc* 106:3043
45. Fujita M, Nagao S, Ogura K (1995) *J Am Chem Soc* 117:1649
46. Nierengarten JF, Dietrich-Buchecker CO, Sauvage JP (1996) *New J Chem* 20:685
47. Fujita M, Oguro D, Miyazawa M, Oka H, Yamaguchi K, Ogura K (1995) *Nature* 378:469
48. Livoreil A, Dietrich-Buchecker CO, Sauvage JP (1994) *J Am Chem Soc* 116:9399
49. Carina RE, Dietrich-Buchecker C, Sauvage JP (1996) *J Am Chem Soc* 118:9110
50. Dietrich-Buchecker C, Sauvage JP (1992) *New J Chem* 16:277
51. Stang PJ, Cao DH, Saito S, Arif AM (1995) *J Am Chem Soc* 117:6273
52. Stang PJ, Cao DH (1994) *J Am Chem Soc* 116:4981
53. Fujita M, Yazaki J, Ogura K (1990) *J Am Chem Soc* 112:5645
54. Beissel T, Powers RE, Raymond KN (1996) *Angew Chem Int Ed Engl* 35:1084
55. Fox OD, Drew MGB, Beer PD (2000) *Angew Chem Int Ed* 39:136
56. Kubota Y, Biradha K, Fujita M, Sakamoto S, Yamaguchi K (2002) *Bull Chem Soc Jpn* 75:559
57. Müller IM, Spillmann S, Franck H, Pietschnig R (2004) *Chem Eur J* 10:2207
58. Abrahams BF, Egan SJ, Robson R (1999) *J Am Chem Soc* 121:3535
59. Abrahams BF, Egan SJ, Robson R (1999) *J Am Chem Soc* 121:7172
60. Conn MM, Rebek J (1997) *Chem Rev* 97:1647
61. Rosokha SV, Lindeman SV, Rathore R, Kochi JK (2003) *J Org Chem* 68:3947
62. Brooker S, Ewing JD, Nelson J, Jeffrey JC (2002) *Inorg Chim Acta* 337:463
63. Parac TN, Caulder DL, Raymond KN (1998) *J Am Chem Soc* 120:8003
64. Levin MD, Stang PJ (2000) *J Am Chem Soc* 122:7428
65. Ziegler M, Miranda JJ, Andersen UN, Johnson DW, Leary JA, Raymond KN (2001) *Angew Chem Int Ed* 40:733
66. Klausmeyer KK, Rauchfuss TB, Wilson SR (1998) *Angew Chem Int Ed* 37:1694
67. Johnson DW, Xu JD, Saalfrank RW, Raymond KN (1999) *Angew Chem Int Ed* 38:2882
68. Caulder DL, Powers RE, Parac TN, Raymond KN (1998) *Angew Chem Int Ed* 37:1840
69. Cotton FA, Daniels LM, Lin C, Murillo CA (1999) *Chem Commun* 9:841
70. Heinrich JL, Berseth PA, Long JR (1998) *Chem Commun* 11:1231
71. Aoyagi M, Biradha K, Fujita M (1999) *J Am Chem Soc* 121:7457
72. Sun XK, Johnson DW, Caulder DL, Powers RE, Raymond KN, Wong EH (1999) *Angew Chem Int Ed* 38:1303
73. James SL, Mingos DMP, White AJP, Williams DJ (1998) *Chem Commun* 21:2323
74. Vilar R, Mingos DMP, White AJP, Williams DJ (1998) *Angew Chem Int Ed* 37:1258
75. Hiraoka S, Fujita M (1999) *J Am Chem Soc* 121:10239
76. Scherer M, Caulder DL, Johnson DW, Raymond KN (1999) *Angew Chem Int Ed* 38:1588

77. Fischer E (1894) *Ber Deutsch Chem Ges* 27:2985
78. Lehn J-M (1992) *Perspectives in Coordination Chemistry*. Wiley, Weinheim
79. Busch DH, Vance AL, Kolchinski AG (1996) *Templating, Self-Assembly, and Self-Organization*. Pergamon, New York
80. McMurry TJ, Raymond KN, Smith PH (1989) *Science* 244:938
81. Sauvage JP (1998) *Acc Chem Res* 31:611
82. Dietrich-Buchecker CO, Sauvage JP (1987) *Chem Rev* 87:795
83. (1989) *Webster's Unabridged Dictionary of the English Language*. Gramercy Books, New York
84. Leigh GJ (1990) *Nomenclature of Inorganic Chemistry*. Blackwell Science, Oxford
85. Cahn RS, Ingold C, Prelog V (1966) *Angew Chem Int Ed* 5:385
86. Prelog V, Helmchen G (1982) *Angew Chem Int Ed* 21:567
87. von Zelewsky A (1996) *Stereochemistry of Coordination Compounds*. Wiley, New York
88. Raymond KN, Isied SS, Brown LD, Fronczek FR, Nibert JH (1976) *J Am Chem Soc* 98:1767
89. Mills WH, Quibell THH (1935) *J Chem Soc*:839
90. Block BP, Powell WH, Fernelius WC (1990) *Nomenclature of Inorganic Chemistry-Recommendations*. Am Chem Soc, Washington, DC
91. Brown MF, Cook BR, Sloan TE (1975) *Inorg Chem* 14:1273
92. Brown MF, Cook BR, Sloan TE (1978) *Inorg Chem* 17:1563
93. The steering-wheel-convention is customized for monodentate coordination polyhedra and is similar to the Cahn-Ingold-Prelog system, whereby priorities are assigned to substituents on stereogenic centers. Instead of R/S descriptors, C (clockwise) and A (anti-clockwise) descriptors are introduced
94. Skew-lines are two non-intersecting lines that are neither orthogonal nor parallel to each other with a principal axis intersecting both skew lines orthogonally
95. The oriented skew-lines convention describes orthogonal skew lines that are not defined with the classical system. By analogy, the vector descriptors are chosen to be Δ/Δ , respectively
96. Baxter PNW, Lehn J-M, Baum G, Fenske D (1999) *Chem Eur J* 5:102
97. Baxter PNW, Lehn J-M, Kneisel BO, Baum G, Fenske D (1999) *Chem Eur J* 5:113
98. Saalfrank RW, Bernt I, Uller E, Hampel F (1997) *Angew Chem Int Ed* 36:2482
99. Cotton FA, Wilkinson G (1988) *Advanced Inorganic Chemistry*. Wiley, New York
100. Fujita M, Ogura K (1996) *Coord Chem Rev* 148:249
101. Stang PJ, Olenyuk B (1997) *Acc Chem Res* 30:502
102. Stricklen PM, Volcko EJ, Verkade JG (1983) *J Am Chem Soc* 105:2494
103. Olenyuk B, Fechtenkötter A, Stang PJ (1998) *J Chem Soc, Dalton Trans* 11:1707
104. Kusakawa T, Fujita M (1998) *Angew Chem Int Ed* 37:3142
105. Brückner C, Powers RE, Raymond KN (1998) *Angew Chem Int Ed* 37:1837
106. Caulder DL, Brückner C, Powers RE, König S, Parac TN, Leary JA, Raymond KN (2001) *J Am Chem Soc* 123:8923
107. Stang PJ, Olenyuk B, Muddiman DC, Smith RD (1997) *Organomet* 16:3094
108. Kim HJ, Moon D, Lah MS, Hong JI (2002) *Angew Chem Int Ed* 41:3174
109. Ayabe M, Yamashita K, Sada K, Shinkai S, Ikeda A, Sakamoto S, Yamaguchi K (2003) *J Org Chem* 68:1059
110. Cui Y, Ngo HL, Lin WB (2002) *Inorg Chem* 41:5940
111. Schweiger M, Seidel SR, Schmitz M, Stang PJ (2000) *Org Lett* 2:1255
112. Masood MA, Enemark EJ, Stack TDP (1998) *Angew Chem Int Ed* 37:928
113. Enemark EJ, Stack TDP (1998) *Angew Chem Int Ed* 37:932

114. Rodger A, Johnson BFG (1988) *Inorg Chem* 27:3061
115. Kepert DL (1977) *Prog Inorg Chem* 23:1
116. Pfeil A, Lehn J-M (1992) *J Chem Soc, Chem Commun* 11:838
117. Kersting B, Meyer M, Powers RE, Raymond KN (1996) *J Am Chem Soc* 118:7221
118. Meyer M, Kersting B, Powers RE, Raymond KN (1997) *Inorg Chem* 36:5179
119. Terpin AJ, Ziegler M, Johnson DW, Raymond KN (2001) *Angew Chem Int Ed* 40:157
120. Caulder DL, Raymond KN (1997) *Angew Chem Int Ed Engl* 36:1440
121. Beissel T, Powers RE, Parac TN, Raymond KN (1999) *J Am Chem Soc* 121:4200
122. Saalfrank RW, Demleitner B, Glaser H, Maid H, Bathelt D, Hampel F, Bauer W, Teichert M (2002) *Chem Eur J* 8:2679
123. Lehn J-M, Rigault A, Siegel J, Harrowfield J, Chevrier B, Moras D (1987) *Proc Natl Acad Sci USA* 84:2565
124. Carrano CJ, Raymond KN (1978) *J Am Chem Soc* 100:5371
125. Lehn J-M (1995) *Supramolecular Chemistry, Concepts and Perspectives*. Wiley, Weinheim
126. Johnson JA, Kampf JW, Pecoraro VL (2003) *Angew Chem Int Ed* 42:546
127. Cutland-Van Noord AD, Kampf JW, Pecoraro VL (2002) *Angew Chem Int Ed* 41:4667
128. Ernst RE, O'Connor MJ, Holm RH (1967) *J Am Chem Soc* 89:6104
129. Muetterties EL (1969) *J Am Chem Soc* 91:1636
130. Muetterties EL (1968) *J Am Chem Soc* 90:5097
131. Piguat C, Bernardinelli G, Hopfgartner G (1997) *Chem Rev* 97:2005
132. Albrecht M (2001) *Chem Rev* 101:3457
133. Cathey CJ, Constable EC, Hannon MJ, Tocher DA, Ward MD (1990) *J Chem Soc, Chem Commun* 8:621
134. Constable EC, Ward MD (1990) *J Am Chem Soc* 112:1256
135. Constable EC, Ward MD, Tocher DA (1991) *J Chem Soc, Dalton Trans* 7:1675
136. Krämer R, Lehn J-M, Marquis-Rigault A (1993) *Proc Natl Acad Sci USA* 90:5394
137. Baxter PNW, Lehn J-M, Baum G, Fenske D (2000) *Chem Eur J* 6:4510
138. Childs LJ, Alcock NW, Hannon MJ (2002) *Angew Chem Int Ed* 41:4244
139. Fujita N, Biradha K, Fujita M, Sakamoto S, Yamaguchi K (2001) *Angew Chem Int Ed* 40:1718
140. Saalfrank RW, Glaser H, Demleitner B, Hampel F, Chowdhry MM, Schünemann V, Trautwein AX, Vaughan GBM, Yeh R, Davis AV, Raymond KN (2002) *Chem Eur J* 8:493
141. Ikeda A, Udzu H, Zhong ZL, Shinkai S, Sakamoto S, Yamaguchi R (2001) *J Am Chem Soc* 123:3872
142. Zhong ZL, Ikeda A, Shinkai S, Sakamoto S, Yamaguchi K (2001) *Org Lett* 3:1085
143. Müller IM, Möller D, Schalley CA (2005) *Angew Chem Int Ed* 44:480
144. Saalfrank RW, Stark A, Peters K, von Schnering HG (1988) *Angew Chem Int Ed Engl* 27:851
145. Saalfrank RW, Stark A, Bremer M, Hummel HU (1990) *Angew Chem Int Ed Engl* 29:311
146. Johnson DW, Raymond KN (2001) *Inorg Chem* 40:5157
147. Ziegler M, Brumaghim JL, Raymond KN (2000) *Angew Chem Int Ed* 39:4119
148. Parac TN, Scherer M, Raymond KN (2000) *Angew Chem Int Ed* 39:1239
149. Ziegler M, Davis AV, Johnson DW, Raymond KN (2003) *Angew Chem Int Ed* 42:665
150. Paul RL, Argent SP, Jeffery JC, Harding LP, Lynam JM, Ward MD (2004) *Dalton Trans* 21:3453
151. Paul RL, Bell ZR, Jeffery JC, McCleverty JA, Ward MD (2002) *Proc Natl Acad Sci USA* 99:4883

152. Paul RL, Bell ZR, Fleming JS, Jeffery JC, McCleverty JA, Ward MD (2002) *Heteroatom Chem* 13:567
153. Amoroso AJ, Jeffery JC, Jones PL, McCleverty JA, Thornton P, Ward MD (1995) *Angew Chem Int Ed Engl* 34:1443
154. Yeh RM, Xu J, Seeber G, Raymond KN (2005) *Inorg Chem* 44:6228
155. Albrecht M, Janser I, Meyer S, Weis P, Fröhlich R (2003) *Chem Commun* 23:2854
156. Weitz FL, Raymond KN (1979) *J Am Chem Soc* 101:2728
157. Müller IM, Robson R, Separovic F (2001) *Angew Chem Int Ed* 40:4385
158. Müller IM, Möller D (2005) *Angew Chem Int Ed* 44:2969
159. Aoki S, Shiro M, Kimura E (2002) *Chem Eur J* 8:929
160. Saalfrank RW, Bernt I, Hampel F (2001) *Chem Eur J* 7:2770
161. Bell ZR, Jeffery JC, McCleverty JA, Ward MD (2002) *Angew Chem Int Ed* 41:2515

Dynamic Chirality: Molecular Shuttles and Motors

David A. Leigh (✉) · Emilio M. Pérez

School of Chemistry, University of Edinburgh, The King's Buildings, West Mains Road,
Edinburgh EH9 3JJ, UK
David.L Leigh@ed.ac.uk

1	Introduction	185
1.1	Controlled Motion at the Molecular Level; Walking in a Hurricane	186
2	Dynamic Chirality in Covalently Linked Molecular Rotors	187
3	Dynamic Chirality in Interlocked Architectures	195
3.1	Translational Isomerism in Molecular Shuttles	196
3.2	Translational Isomerism in Catenanes	198
3.3	Influencing the Expression of Chirality with Interlocked Architectures . . .	204
4	Conclusions and Outlook	206
	References	206

Abstract To appreciate the technological potential of controlled molecular-level motion one only has to consider that it lies at the heart of virtually every biological process. When we learn how to build synthetic molecular motors and machines that can interface their effects directly with other molecular-level sub-structures and the outside world it will add a new dimension to functional molecule and materials design. In this review we discuss both the influence of chirality on the design of molecular level machines and, in turn, how molecular level machines can control the expression of chirality of a physical response to an inherently achiral stimulus.

Keywords Dynamics · Chirality · Catenane · Rotaxane · Molecular shuttle · Molecular machine · Molecular motor

Abbreviations

ICD induced circular dichroism
NMR nuclear magnetic resonance
NOE nuclear Overhauser effect
TTF tetrathiafulvalene

1 Introduction

The term chirality (from the Greek *kheir* = hand) was introduced by the Scottish scientist, Lord Kelvin, a few years after Pasteur's separation of the enantiomers of tartaric acid [1]. Kelvin defined chirality as "*a property of*

any object that cannot superimpose, or overlap, completely with its own mirror image". Nature has a remarkable inclination to asymmetry at all hierarchical levels: the relative spatial location of the organs in our body, the organelles in a cellule, the configuration of key supramolecular assemblies (such as those formed by nucleic acids), the geometry of proteins, and the molecular structure of smaller building blocks (e.g. sugars and aminoacids) are all chiral [2]. In fact, due to parity violation, even atoms are weakly chiral [3, 4]. While the origin of biomolecular homochirality in evolution remains uncertain, [5], its significance throughout biology is self-evident.

However, because traditional mechanics are based on non-chiral concepts—like the Newtonian center of mass—the effects of chirality on molecular level motion have largely been overlooked [6]. This review is concerned with the relationship between mechanical motion and chirality at the molecular level; we will discuss how chirality—or its expression—can be altered through molecular motion, and how a fixed chiral configuration can help to direct motion. But first it is important to briefly describe the physics that governs motion at the molecular level since it is fundamentally different to that which governs movement in the macroscopic world and, in many respects, the differences are somewhat counterintuitive [7].

1.1

Controlled Motion at the Molecular Level; Walking in a Hurricane

Molecules and their parts move incessantly and randomly at any temperature above 0 K. This chaotic movement is termed Brownian motion after another Scottish scientist, Robert Brown, who observed it in 1827 when looking at pollen particles suspended in water through a microscope. As a consequence of this phenomenon any attempt to “push” or “pull” molecules in a particular direction by the one-off application of a force (as opposed to the continuous application of a force) will be completely swamped by the random background motion of the environment. In many ways trying to control motion at the molecular level is like trying to play pool on a table on which hundreds of balls are moving constantly and randomly. As soon as we strike the cue ball it is immediately hit by others and proceeds on a random pathway irrespective of the direction that it was initially struck.

The dominating influence of Brownian motion is not the only difference between motion at the molecular-level and in the macroscopic world. In the macroscopic world the equations of motion are governed by inertial terms (dependent on mass). This means objects do not move unless we give them specific energy to do so but once we have given them that initial impetus they keep on moving in the same direction until all that energy is dissipated. Viscous forces (dependent on surface areas) dampen motion by converting kinetic energy into heat. As objects become smaller, inertial terms decrease in importance and viscous terms begin to dominate. At the mo-

molecular level the effect of inertia is negligible so an object's behavior will be determined by the forces applied to it at that very moment, and by nothing in the past.

From a practical point of view, this change in the dominant physical terms has several implications. Firstly, when trying to produce controlled movement at the molecular level, we will need to "tame" Brownian motion rather than provoke movement by applying a force [8, 9]. This is an intimidating task. Even the motor proteins of Nature hardly begin to punch against the power of Brownian motion. A typical motor protein consumes adenosine triphosphate (ATP) at a rate of 100–1000 molecules every second, which corresponds to a maximum possible power output in the region 10^{-16} to 10^{-17} W per molecule. When compared with the random environmental buffeting of $\sim 10^{-8}$ W experienced by molecules in solution at room temperature, it is surprising that they manage any controlled motion at all [10]! But Nature has found a way around this problem. To start with, motor proteins follow a "track". Tracks reduce the degrees of freedom of the protein, so that motion does not need to be controlled in all three dimensions, only in one. Also, in order to comply with the Second Law of Thermodynamics, an external input of energy is required to do work through controlled directional motion. Motor proteins typically utilize ATP hydrolysis as an energy source, although other energy supplies can also be used. Secondly, it is reasonable to say that the same techniques and tools that have proven useful to make macroscopic machines (even very small ones) are not a good choice when trying to make molecular-sized machines. Working on the definition given above, if what we intend to do is to assemble molecular components, it seems sensible to opt for chemistry as the basic tool for the synthesis and operation of very small machines.

2

Dynamic Chirality in Covalently Linked Molecular Rotors

Control of chirality is present in many natural materials and is an intrinsic feature of living organisms [11]. Inspired by this, the search for new chemical entities in which chirality can be controlled at the molecular [12], macro-molecular [13] and supramolecular [14, 15] levels has gained great impetus in recent years.

Molecular machines can be defined as "*a subset of molecular devices (functional molecular systems) in which some stimulus triggers the controlled, large amplitude mechanical motion of one component relative to another (or of a substrate relative to the machine) which results in a net task being performed*" [9]. Since chirality is a direct consequence of the relative position of the different parts of a molecule, the intimate relationship between mechanical motion in molecular machines and chirality is self-evident.

The rotational triple energy minima about C–C single bonds follows directly from the tetrahedral geometry of saturated carbon centers [16], yet was not proven experimentally until 1936 [17]. In practice, the energy barrier to rotation around a C–C single bond is so low (ca. 3 kcal mol⁻¹) that this is an effectively barrierless process at room temperature. To achieve some kind of control over rotation about a chemical bond it is necessary to raise that energy barrier. This has typically been achieved by increasing the steric demand in the proximity of the bond around which we want to control rotation.

The restricted rotation of molecular components around a central carbon atom was first observed by Kwart and Alekman in 1968 when studying the ¹H NMR of mesityl carbonium ions, **1**, and their tetravalent precursors **2** (Fig. 1) [18].

In **1** and **2** the rotation of each mesityl ring about the bond linking it to the central carbon is relatively unrestricted. Calculations of internuclear distances between non-bonded atoms of a single pair of methyl groups, one from each ring, showed no overlap of van der Waals radii of the hydrogen atoms provided the rings could be assumed to rotate in coordination and with the same angular velocity. In other words, although both aromatic rings can rotate independently, their concerted rotation is energetically favored, so the rotation of one ring clockwise, say, leads to rotation of the other ring counter-clockwise and vice versa.

This first example inspired the design of many other similar systems, most famously those investigated in the 1970s and 1980s by Mislow and Iwamura [19]. Later, the structurally complex but conceptually similar “molecular turnstiles” **3–5** (Fig. 2) were introduced by Moore [20]. Variable temperature ¹H NMR studies on the methylene protons, *H*_a and *H*_b, showed that the central aromatic ring of **4** spins rapidly on the NMR timescale at room temperature, while spindle rotation does not occur in turnstile **5** even at 85 °C due to steric constraints.

All of these devices show a certain degree of restriction in the movement of their molecular components, but rotation occurs randomly with no control over directionality. In an attempt to achieve directional motion Kelly investigated the dynamic behavior of a so-called “molecular ratchet”, **6** [21, 22].

The structural features of **6** are identical to those of a macroscopic ratchet. The helical chirality of the helicene “pawl” generates an energy profile for

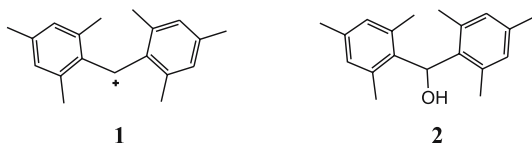


Fig. 1 Mesityl carbonium ion **1** and its tetravalent precursor **2** studied by Kwart and Alekman [18]

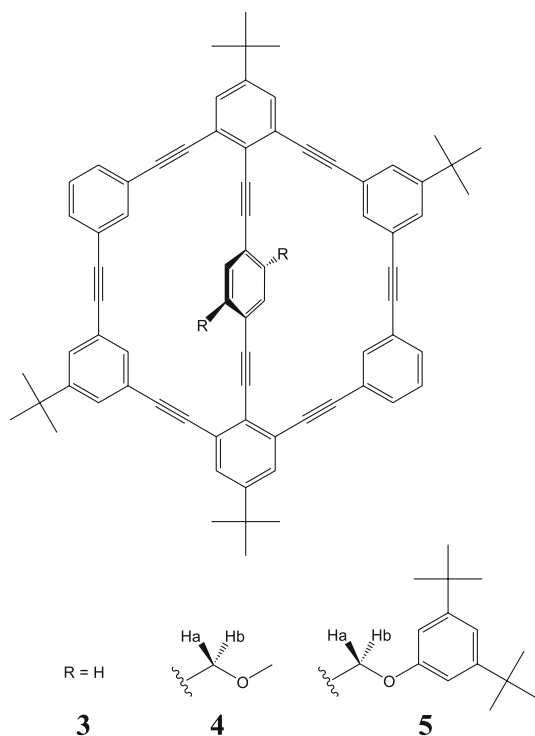


Fig. 2 “Molecular turnstiles” reported by Bedard and Moore [20]. The variable temperature ^1H NMR of protons H_a and H_b provides evidence of spindle rotation in **4** and a locked spindle in **5**

rotation of the triptycyl “wheel” that imitates the teeth on the macroscopic wheel (Fig. 3) and might be expected to make rotation in one direction an energetically favored process. However, ^1H NMR experiments showed that ro-

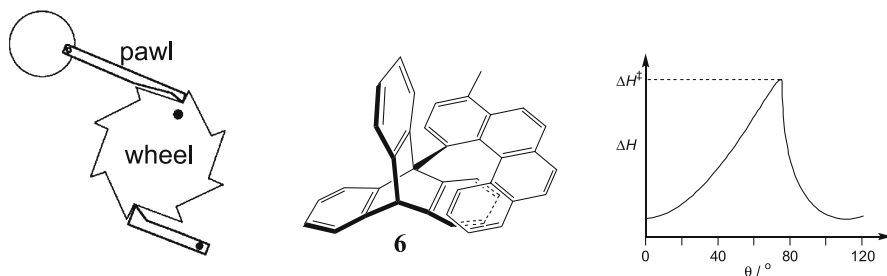
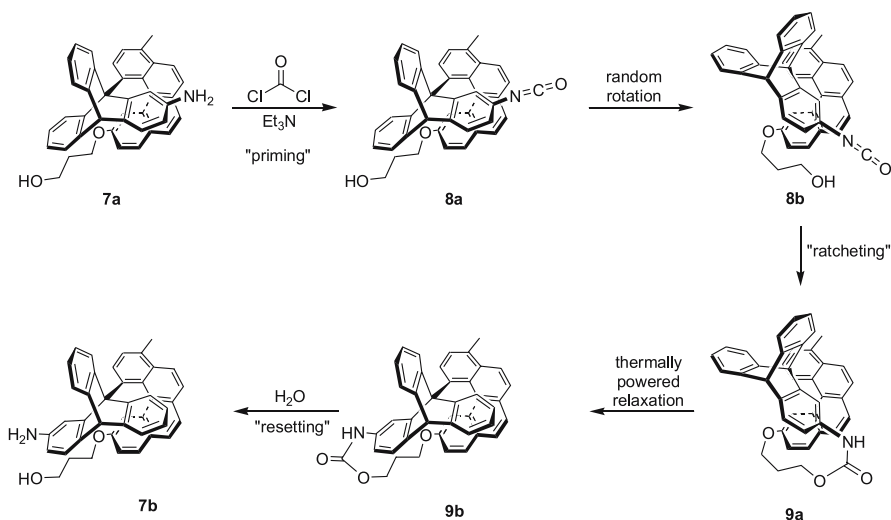


Fig. 3 Schematic representation of a macroscopic ratchet, structure of the “molecular ratchet” **6** and calculated enthalpy changes for rotation of the triptycene “wheel” around the helicene “pawl” [21, 22]

tation in **6** occurred at identical rates in both directions. In fact, such a result had been predicted by Feynman more than 30 years earlier in his celebrated discussions on a miniature ratchet-and-pawl [23]. Although unsuccessful, molecular ratchet **6** was probably the first experimental attempt at probing the relationship between chirality and molecular-level motion. Although the helicity of the pawl might superficially be expected to favor thermally-activated rotation in one direction, it does not! This outcome serves as a reminder of the differences between the macroscopic and the molecular-level worlds. In the authors' words: *"In contrast to mountain climbing, [in the molecular-level world] it is only the height of the summit, not the steepness of the terrain that matters"* [21]. If we look at the problem from the point of view of thermodynamics, the number of molecules populating a certain energetic level depends on its state functions only, not on the pathway they followed to get there. Kelly's molecular ratchet provides an illustration that the Second Law of Thermodynamics holds in the molecular world too: work cannot be exerted continuously using the thermal bath as the only energy source, no matter how clever the structural design [8].

Kelly therefore proposed **7a** (Scheme 1) [24], a modified version of the ratchet structure in which a chemical reaction is used as a source of energy to control the motion, thus preventing conflict with the Second Law.



Scheme 1 A chemically powered unidirectional rotary motor in action [24]. Priming of the motor in its initial state with phosgene (**7a** \rightarrow **8a**) allows a chemical reaction to take place when the helicene rotates far enough up the potential energy well towards the blocking triptycene arm (**8b**). This gives a tethered state, **9a**, for which rotation over the barrier to **9b** is an exoergic process that occurs under thermal activation. Finally, the urethane linker can be cleaved to give the original rotor rotated by 120° (**7b**)

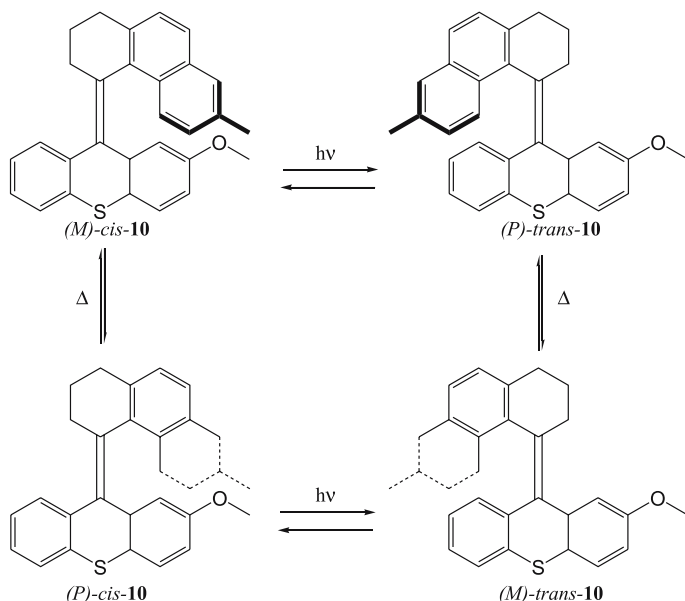
Ignoring the amino group, all three possible positions for the helicene with respect to the triptycene “spokes” are identical—the energy profile for 360° rotation would appear as three equal energy minima, separated by similar barriers, large enough to prevent rapid rotation at room temperature ($\sim 25 \text{ kcal mol}^{-1}$). Treatment of **7a** with phosgene yields isocyanate **8a**. Once the isocyanate has been formed, as the helicene oscillates randomly in the thermodynamic trough, sometimes the alcohol will come close enough to the isocyanate (**8b**) for a chemical reaction to occur to form urethane **9a**, resulting in “ratcheting” of the motion some way up the energy barrier. Rotation in the same direction over the energy barrier to give **9b** is now an exothermic process, while rotation in the opposite direction is virtually impossible without breaking the urethane bond. Finally, hydrolysis of urethane **9b** affords **7b** in which the chemical structure has been restored but a unidirectional 120° rotation has taken place. It is worth noting that all the rotation steps are powered thermally while the chemical reaction serves to bias Brownian motion in one direction. Again, chirality plays a central role in the functioning of this molecular rotor. Indeed, the unidirectional rotation is ultimately derived from the asymmetry of the helicene and the use of a pro-chiral triptycene.

Carbon–carbon double bonds (olefins) present significantly higher rotational barriers—typically $25\text{--}65 \text{ kcal mol}^{-1}$ —than single bonds, providing kinetic stability of both *cis* and *trans* isomers. This stability, together with the possibility of their interconversion by photoisomerization, have been exploited in the construction of a wide variety of rotors—and even directional molecular rotary motors—in which the “rotor” and “base” are connected via an olefin.

First reported in 1977 [25], Feringa’s overcrowded alkene systems account for the most abundant and significant contribution to this area [26]. Chiroptical switch **10** (Scheme 2) [27] was the first example of this kind of molecular rotor.

The system shown in Scheme 2 is based on the fact that irradiation at 250 and 300 nm yielded photostationary states of slightly different composition. Irradiation of enantiomerically pure (*M*)-*cis*-**10** or (*P*)-*trans*-**10** at 250 nm resulted in a photostationary state consisting of 68% (*M*)-*cis*-**10** and 32% (*P*)-*trans*-**10**, whereas irradiation at 300 nm yielded 64% (*M*)-*cis*-**10** and 36% (*P*)-*trans*-**10**. Thanks to the thermal stability of these pseudoenantiomers—no (*P*)-*cis* or (*M*)-*trans*-**10** were detected after irradiation—the small difference in composition of the photostationary states could be detected by circular dichroism (CD) spectroscopy. In this case, the photoinduced 180° rotation around the olefin results in a change in the helicity of the tetrahydrophenanthrene unit. Similar behavior was observed for the structurally related benzoannulated bithioxanthylidene [28].

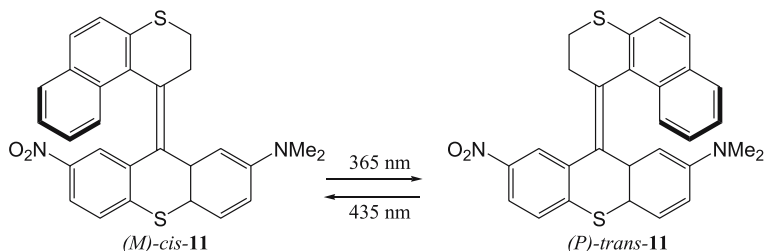
Later, a rotor that showed a much more significant difference in composition between the photostationary states was reported by the same group [29]. Molecular switch **11** features an unsymmetrically substituted donor-acceptor



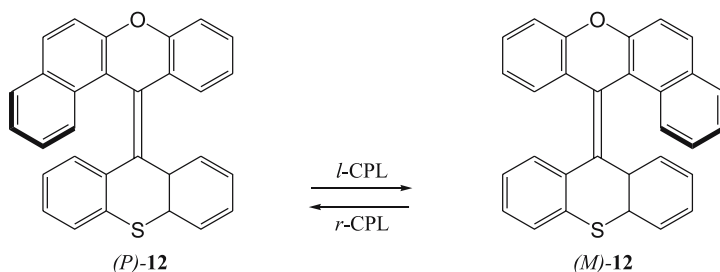
Scheme 2 Feringa's chiroptical switch based on a molecular rotor [27]. The switch functioning mechanism is based on photoinduced *cis/trans* isomerizations

rotor "base". This substitution pattern results in (*M*)-*cis*-11 and (*P*)-*trans*-11 having sufficiently different electronic absorption spectra to obtain a 30 : 70 and 90 : 10 (*M*)-*cis*-11:(*P*)-*trans*-11 ratio by irradiation at 365 nm and 435 nm respectively.

The change in chirality obtained by irradiation of 11 was sufficient to provoke the light-induced conversion of cholesteric to nematic phases in liquid crystals of 4'-(pentyloxy)-4-biphenylcarbonitrile doped with 1% w/w (*P*)-*trans*-11 [33].



Scheme 3 A highly stereoselective optical switching process [29]. Molecular switch 11 gives a 30 : 70 and 90 : 10 (*M*)-*cis*-(*P*)-*trans* ratio by irradiation at 365 nm and 435 nm, respectively



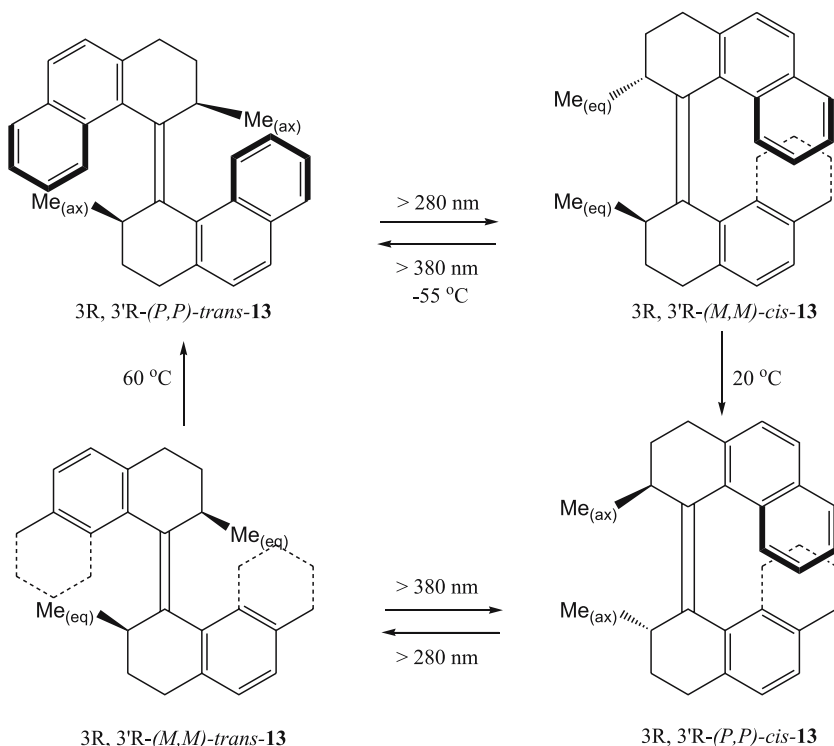
Scheme 4 Photochemical interconversion of *P* (right handed) and *M* (left handed) helicity in **12** by irradiation with *l*- or *r*-CPL [31]

In molecular switch **12** [31] the relationship between chirality and molecular motion becomes even more apparent. Indeed, irradiation of a dilute (9×10^{-5} M) hexane solution of a racemic mixture of **12** with left or right circular polarized light (CPL) at 313 nm resulted in enantioenriched solutions of (*P*)-**12** and (*M*)-**12**, although with only moderate enantiomeric excesses of 0.07 and -0.07% , respectively.

Irradiation of a stable nematic phase consisting of 20% w/w (*P/M*)-**12** and 4'-(pentyloxy)-4-biphenylcarbonitrile with *l*-CPL under similar conditions to those used in solution resulted in the formation of a cholesteric phase, showing that an optical enrichment in (*M*)-**12** was also achieved in the liquid crystalline phase.

The chiral helicity of molecules such as **12** causes the photo-induced *trans-cis* isomerization to occur unidirectionally according to the handedness of the helix. Therefore, these systems already possess many of the necessary requirements for a unidirectional molecular rotor and, indeed, the incorporation of two further stereogenic centers allowed realization of the first synthetic molecular rotor capable of achieving a full and repetitive 360° unidirectional rotation (Scheme 5) [32]. Irradiation of (*3R,3'R*)-(*P,P*)-*trans*-**13** at $\lambda > 280$ nm, causes chiral helicity-directed unidirectional rotation of the upper half relative to the lower portion (as drawn), at the same time switching configuration of the double bond and inverting the helicity to give (*3R,3'R*)-(*M,M*)-*cis*-**13**. Unlike previously investigated systems, this form is not thermally stable at temperatures above -55°C as the methyl substituents are placed in unfavorable equatorial positions. At ambient temperatures the system relaxes via a thermally activated helix inversion thus continuing to rotate in the same direction to yield (*3R,3'R*)-(*P,P*)-*cis*-**13**. Irradiation of this new species ($\lambda > 280$ nm) results in photoisomerization and helix inversion to give (*3R,3'R*)-(*M,M*)-*trans*-**13**. Once more, the methyl groups are in unfavorable equatorial positions and thermal relaxation (this time temperatures $> 60^\circ\text{C}$ are required) completes the 360° rotation.

As each different step in the cycle involves a change in helicity, the unidirectional process can be observed by the change in the circular dichroism

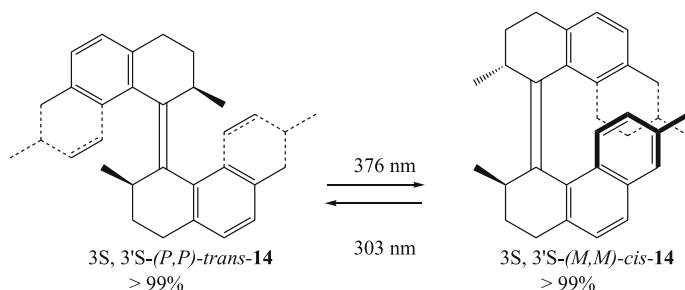


Scheme 5 Feringa's unidirectional rotor [32]. The 360° unidirectional rotation is achieved in a four-step process involving alternative photo-isomerization of the double bond and thermal interconversion of helicity

spectrum at each stage. The four different states can be populated depending on the precise choice of wavelength and temperatures, while irradiation at temperature above 60 °C results in random rotation.

Later, the same group reported second [33] and third [34] generation molecular rotors, based on the same basic design, in which structural variations allowed for faster 360° rotation. An even more significant improvement is molecular rotor **14** in which apparently perfect diastereomeric selection can be achieved by alternative irradiation at 303 and 376 nm [35].

Although, as we have already stressed, analogies between the macroscopic and the molecular world often lead to misunderstandings and must be used carefully, it is tempting to compare the relationship between chirality and motion in Feringa's systems with that seen in a macroscopic example: the windmill. When the wind blows at the vanes of a windmill, its rotor immediately “knows” which direction to rotate in. When blown at by the same wind, two “enantiomeric” windmills will rotate in opposite directions, and if the vanes were symmetric with respect to the axis of rotation, the windmill just



Scheme 6 A molecular rotor with apparently perfect stereocontrol, recently reported by Feringa and co-workers [35]

wouldn't rotate. Similarly, it is the pre-determined chirality of these molecular systems that decides their direction of rotation.

3

Dynamic Chirality in Interlocked Architectures

Because of their extraordinary dynamic properties, interlocked architectures [36–38] are particularly well suited for the development of molecular machinery [9]. Catenanes (from the Latin *catena* = chain) are molecules in which two or more macrocycles are interlocked. Rotaxanes (from the Latin *rota* = wheel and *axis* = axle) are molecular species in which one or more macrocycles are threaded onto a linear component and de-threading is prevented by bulky “stoppers” (Fig. 4).

Because the components of these species are not covalently but mechanically connected, they can move relative to each other in well-defined ways. One component can serve as a “track” that restricts the degrees of freedom along which the other component can move, greatly facilitating the possibility of

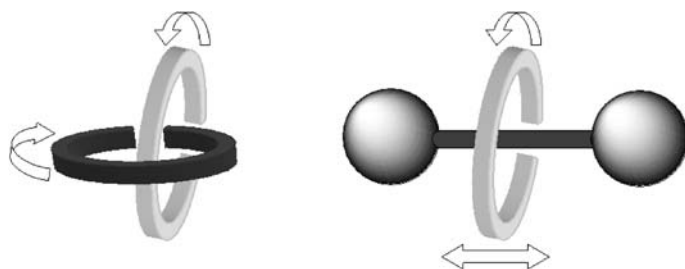


Fig. 4 Cartoons representing a [2]catenane and a [2]rotaxane. The arrows show the main possible large-amplitude movements of one component with respect to the other: “pirouetting” (curved arrows) and “shuttling” (double-headed arrow)

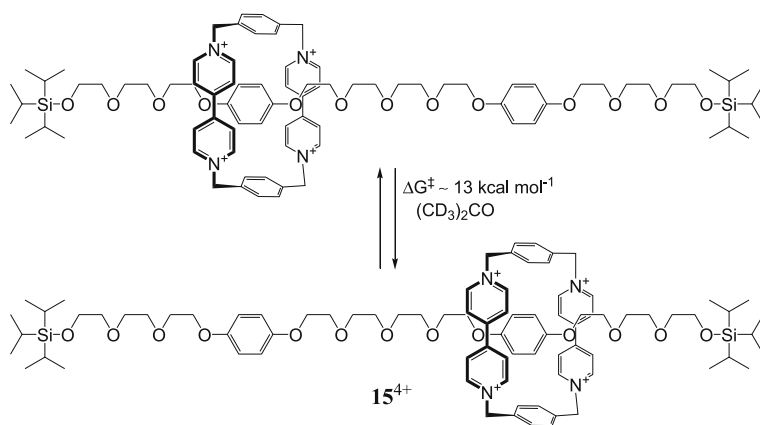
achieving controlled molecular motion. There are two main kinds of possible large-amplitude motion in catenanes and rotaxanes: “pirouetting”, in which one ring rotates around the other—in the case of catenanes—or around the thread—in the case of rotaxanes; and “shuttling”, in which the macrocycle moves along the thread.

3.1

Translational Isomerism in Molecular Shuttles

The spatial arrangement of the components of interlocked molecules requires definition of a new stereochemical term: co-conformation. This refers to the relative positions of the non-covalently linked components with respect to each other [39]. By analogy to conformational changes within classical molecules, the relative movements of the submolecular constituents of interlocked species are termed co-conformational changes. If the thread in a rotaxane is decorated with more than one possible binding sites (“stations”) for the macrocycle, the two or more possible states in which the macrocycle binds to different stations are termed *translational isomers*. In the absence of kinetic barriers, these isomers are in thermodynamic equilibrium, and the macrocycle will distribute its time between the alternative stations depending on their binding affinity according to a Boltzmann distribution. If the binding sites have accessible free activation energy barriers between them and are located far enough apart so that the shuttling movement can be distinguished from any other internal motions, shuttling of the macrocycle along the thread can be observed spectroscopically.

A [2]rotaxane containing two degenerate and well-separated stations on its thread can be considered the simplest example to study the shuttling phenomenon [40]. In such a system the macrocycle shuttles back and forth



Scheme 7 The first molecular shuttle, 15^{4+} [40]

between the two energetically identical stations, spending exactly half of its time over each of them. The first two-station [2]rotaxane of this kind, **15**⁴⁺, was reported by Stoddart and co-workers in 1991 [40].

Molecular shuttle **15**⁴⁺ consists of a tetracationic cyclophane macrocycle, a linear thread containing two hydroquinol stations and a polyether spacer. The macrocycle binds the stations via $\pi - \pi$ and charge-transfer interactions between the electron-poor cyclophane and the electron-rich hydroquinols. As explained above, because both stations are energetically degenerate (they are chemically identical) the macrocyclic unit has no preference for either of them and randomly shuttles between them, in this case at a rate of $k = 2360 \text{ s}^{-1}$ in $(\text{CD}_3)_2\text{CO}$ at 34°C , measured by ^1H NMR spectroscopy. It was already noted in Stoddart's seminal 1991 paper that including two stations of different binding affinity in the thread could allow a stimuli-induced change of position of the macrocycle in a molecular shuttle.

The minimum requirements to achieve stimuli-responsive molecular shuttles of this type are (Fig. 5): Firstly, one of the stations must be able to be switched between a state in which it shows high affinity (green) and another one in which it shows low affinity (pink) for the macrocycle. Secondly, we require a non-switchable station (orange) which exhibits a binding affinity somewhere between the high and low affinity states of the switchable one. The macrocycle populates the stations following a Boltzmann distribution according to the difference in binding affinities. Therefore, when the switchable

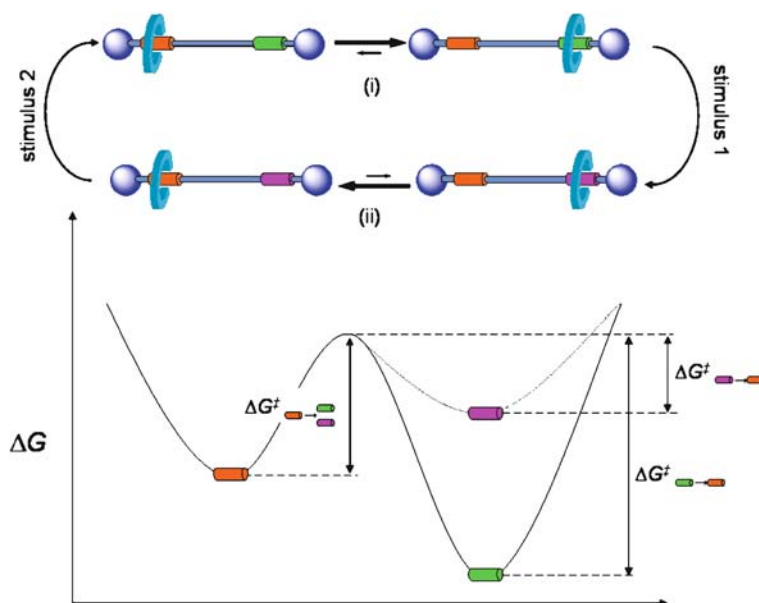


Fig. 5 Idealized free energy profiles for a switchable molecular shuttle

station is in its high affinity state, (i), the macrocycle spends most of its time over the green station because its binding affinity is higher than that of the intermediate non-switchable station. When the switchable station is addressed with stimulus 1 it is transformed into its low affinity state. In this new state, (ii), the macrocycle will reside preferentially over the non-reactive station which is now the one with the highest affinity. The system should ideally be reversible by application of another stimulus, 2 (Fig. 5).

Figure 5 also indicates how the net flow of macrocycles from one station to the other is achieved. The external stimulus does not directly induce directional motion of the macrocycle. Instead, by destabilizing the initially preferred binding site (stimulus 1) and/or increasing the binding strength of the less populated station (stimulus 2), the system is put out of co-conformational equilibrium. Relaxation towards the new global energy minimum subsequently occurs via biased Brownian motion. In state (i) the activation energy for shuttling from the green to the orange station is greater than that for the reverse process. Consequently, macrocycles shuttle “faster” from the orange to the green station than in the opposite direction. This results in a net flux of macrocycles to the green station until the new equilibrium concentration at each station is reached. When stimulus 1 is applied the difference in activation energies is reversed. It is now energetically easier to shuttle from the pink to the orange station than in the opposite direction, so the system relaxes to an equilibrium in which the macrocycle spends most of its time over the orange station.

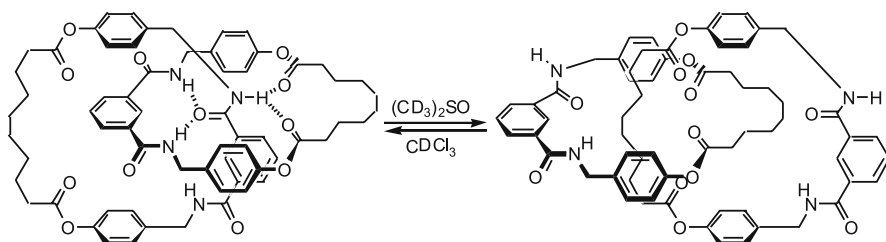
In these systems, chirality and sub-molecular motion stem directly from each other, thus showing an even more intimate relationship. Many different kinds of stimuli have been used to provoke such changes in co-conformation including pH-change [41–47], redox processes [41, 47–49], the nature of the environment [50], photochemistry [51, 52], temperature (entropy-driven shuttling) [53] and reversible covalent chemistry [54].

3.2

Translational Isomerism in Catenanes

The fundamental principles of controlling shuttling in rotaxanes and rotation in catenanes are the same. For example, homocircuit [2]catenane **16** [55] acts somewhat like a two station degenerate shuttle such as **15**. In halogenated solvents such as CDCl_3 , the two macrocycles in **16** interact through hydrogen bonding between their aromatic-1,3-diamide groups (Scheme 8). In a hydrogen bond-disrupting solvent such as $(\text{CD}_3)_2\text{SO}$, however, the preferred co-conformation has the amides exposed on the surface, where they can interact with the polar environment, while the hydrophobic alkyl chains are buried in the middle of the molecule.

In heterocircuit [2]catenane **17**⁴⁺, the tetracationic cyclophane initially encircles the more electron-rich tetrathiafulvalene station (TTF) as evidenced

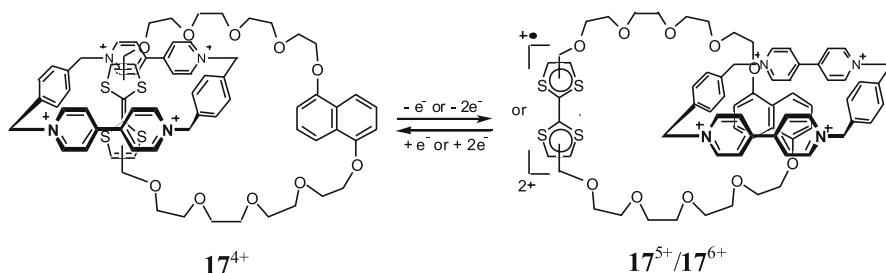


Scheme 8 Translational isomerism in an amphibilic benzylic amide [2]catenane **16** [55]

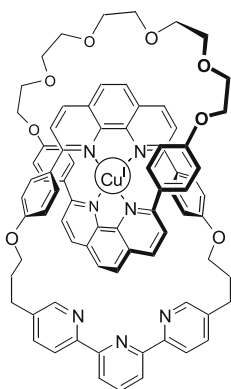
by ^1H NMR, UV-Vis spectroscopy and cyclic voltammetry [56]. Oxidation of the TTF to either its radical cation or dication can be achieved chemically or electrochemically. This oxidation results in complete movement of the cyclophane away from the cationic residue to the hydroxynaphthalene unit. The process can be reversed by reduction of the TTF unit back to its neutral state. There is, however, no control over which direction the motion occurs; the cyclophane has a choice of two identical routes between the stations and half the molecules will rotate one way, the other half the other (Scheme 9).

Sauvage has demonstrated both electrochemical and photochemical control over ring motions in a catenane, **18** [57, 58]. The observed behavior of the catenane is essentially similar to the analogous rotaxane, the only difference being that the 4-coordinate to 5-coordinate (dpp \rightarrow terpy) shuttling process is slower in the catenane and the reverse step is faster. Again, the issue of directionality is not addressed in this system.

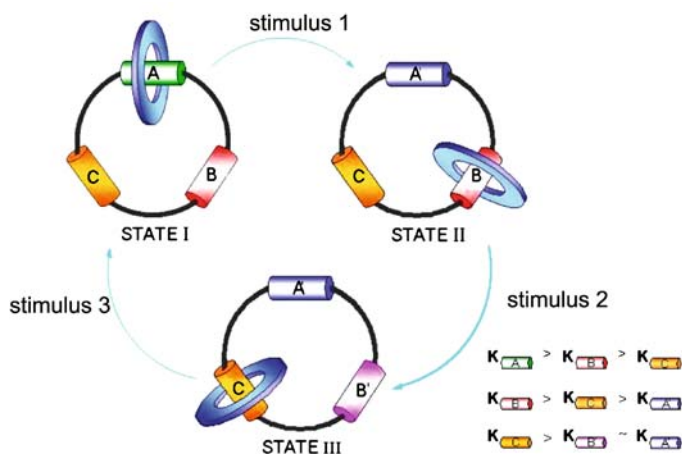
In 2003, Leigh and co-workers reported the first example of unidirectional rotation in a catenane system [59]. A [2]catenane in which one of the macrocycles is larger and displays three binding stations of different affinity for the smaller one was designed. Two of those stations can be addressed by different stimuli in an orthogonal fashion, altering the order of relative binding affinities and provoking the smaller macrocycle to move sequentially from A to B to C to achieve net full rotation around the bigger one (Fig. 7).



Scheme 9 Chemically and electrochemically driven translational isomer switching of [2]catenane **17** [56]



18

Fig. 6 Heterocircuit switchable catenate 18**Fig. 7** Stimuli-induced sequential movement of a macrocycle in a [2]catenane [59]

The chemical structures of [2]catenane 19 and the related [3]catenane 20 (Fig. 8) were conceived as an extension of their work on molecular shuttles. The larger macrocycle in 19 comprises two fumaramide stations with differing macrocycle binding affinities. In station B (red) the methyl groups on the fumaramide motif cause it to have lower affinity than the standard fumaramide station. The non-methylated fumaramide station (station A, green) is located next to a benzophenone unit. This allows selective, photosensitized isomerization of station A by irradiation at 350 nm. Station B (red) can be photoisomerized by direct irradiation at 254 nm. The third station, a succinic amide ester (station C, orange), is not photoactive and is intermediate in macrocycle binding affinity between the two fu-

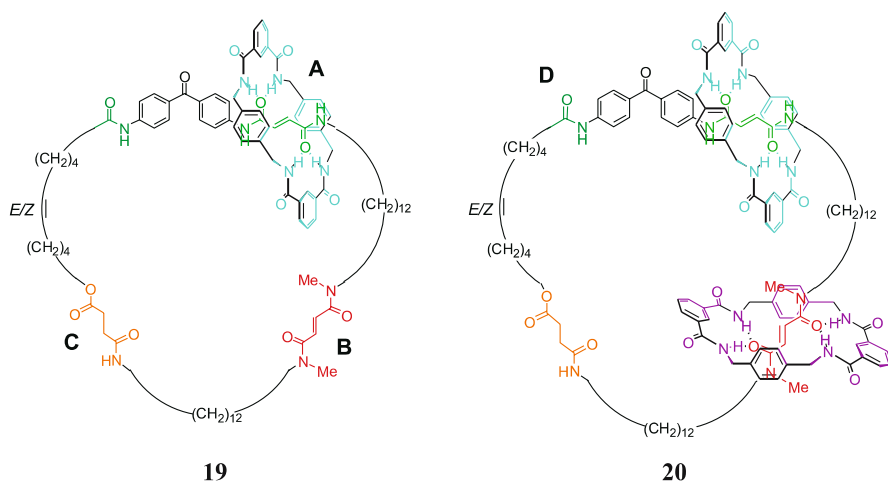


Fig. 8 [2]Catenane **19** and [3]catenane **20**, shown as their *E,E*-isomers [59]

maramide stations and their maleamide counterparts. A fourth station, an isolated amide group (shown as D in **20**) which can make fewer intercomponent hydrogen bond contacts with the smaller macrocycle than A, B or C, is also present but only plays a significant role in the behavior of the [3]catenane, **20**.

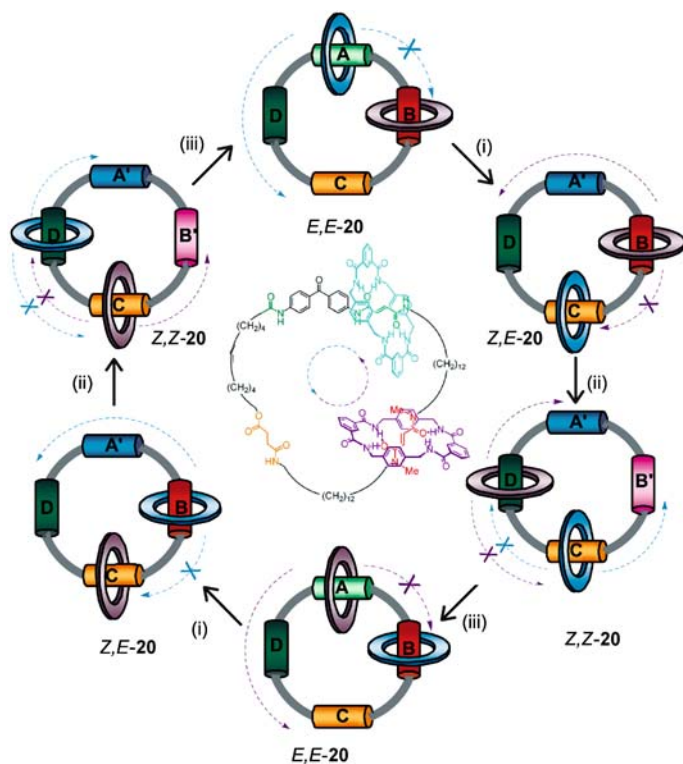
Let us first consider the behavior of [2]catenane **19**. In the initial state (state I in Fig. 7), the small macrocycle resides on the green, non-methylated fumaramide station. Isomerization of this station by sensitized irradiation at 350 nm (green \rightarrow blue) destabilizes the system and the macrocycle finds its new energy minimum on the red station (state II). Subsequent photoisomerization of this station by direct irradiation at 254 nm (red \rightarrow pink) forces the macrocycle to move onto the succinic amide ester unit (orange, state III). Finally, heating the catenane (or treating it with photo-generated bromine radicals or piperidine) results in isomerization of both the *Z*-olefins back to their *E*-forms (pink \rightarrow red and blue \rightarrow green) so that the original order of binding affinities is restored and the macrocycle returns to its original position on the green station (state I).

The ^1H NMR spectra for each diastereomer show excellent positional integrity of the small macrocycle at all stages of the process. However, rotation of the small macrocycle does not occur unidirectionally.

To bias the direction the macrocycle takes at each of the transformations, temporary barriers would be required in order to restrict Brownian motion in one particular direction. Such temporary barriers are intrinsically present in [3]catenane **20** (Fig. 8 and Scheme 10). Irradiation at 350 nm of *E,E*-**20** causes counter-clockwise rotation of the light-blue macrocycle to the succinic amide ester (orange) station to give *Z,E*-**20**. The light-blue macrocycle cannot rotate clockwise because the purple macrocycle effectively blocks that route.

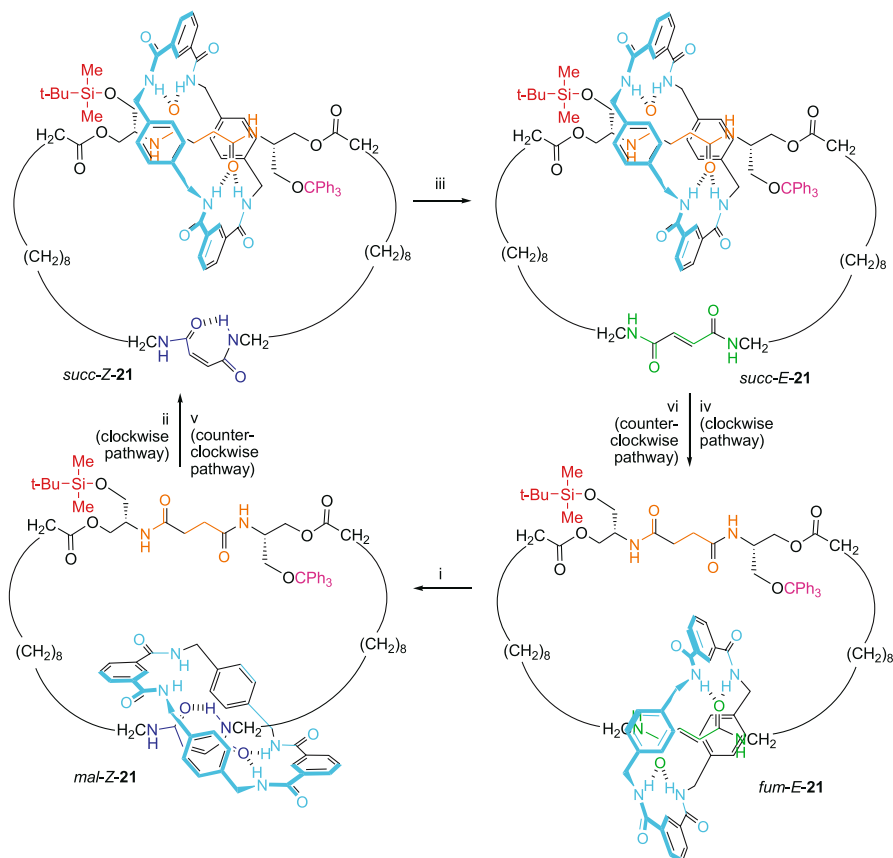
Photoisomerization of the remaining fumaramide group is achieved by direct irradiation at 254 nm and causes the purple macrocycle to relocate to the single amide (dark green) station (*Z,Z*-**20**). Again, this occurs in a counter-clockwise fashion because the clockwise route is blocked by the light-blue macrocycle. This process, each macrocycle first moving and then blocking a direction of passage for the other macrocycle, is repeated throughout the sequence of transformations shown in Scheme 10. After three diastereomer interconversions, *E,E*-**20** is again formed but 360° rotation of each of the small rings has not yet occurred, they have only swapped places. Complete unidirectional rotation of both small rings occurs only after the synthetic sequence (i)–(iii) has been completed twice.

Recently, Hernández et al. reported the first catenane system in which unidirectional rotation can be achieved in either direction [60]. Catenane **21** works by biasing Brownian motion with the aid of chemically labile kinetic barriers. The system is a simple [2]catenane in which the route that the smaller macrocycle can take between two stations on the larger can be se-



Scheme 10 Unidirectional rotation in a four station [3]catenane, **20**. (i) 350 nm, CH₂Cl₂, 5 min, 67%; (ii) 254 nm, CH₂Cl₂, 30 min, 50%; (iii) Δ, 100 °C, C₂H₂Cl₄, 24 h, 95% [59]

lected by the manipulation of steric barriers. The small ring is made to move around the larger one by applying a series of chemical reactions. Remarkably, the sense of rotation (clockwise or counter-clockwise) is governed solely by the order in which these reactions are carried out (see Scheme 11 legend).



Scheme 11 Operation of a reversible synthetic molecular motor, 21 [60]. The motor consists of two mechanically interlocked rings; the larger ring can be considered a track for the smaller ring to move around. The smaller ring starts on the fumaramide station (*fum-E-21*). Photoisomerization of the fumaramide to maleamide with ultra-violet light (254 nm) places the system out of equilibrium; the preferred position for the macrocycle would now be the succinamide station but the bulky protecting groups (trityl ether and TBDMS) act as kinetic barriers, blocking both routes to it (*mal-Z-21*). Selectively removing and replacing either blocking group allows the macrocycle to move to the succinamide station by biased Brownian motion (*succ-Z-21*). Re-isomerization of the maleamide to fumaramide using piperidine generates *succ-E-21*. Now removal/re-attachment of the second blocking group allows the ring to return to its original position, completing the full rotation. The choice of blocking group to be removed/reinstalled in the first and second place determines the direction of rotation

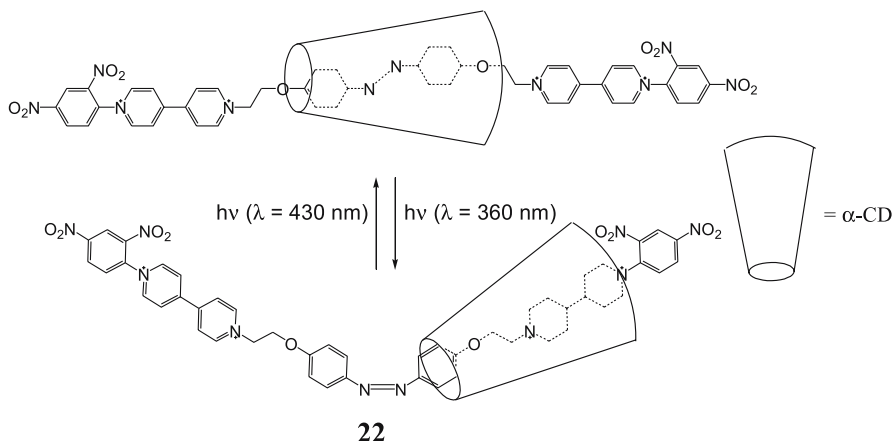
Catenane **21** is, in fact, a minimalistic molecular motor, since every fragment it contains is strictly necessary to perform repetitive, unidirectional motion. In the absence of kinetic barriers—blocking groups—the small ring would rotate between the stations without control over the directionality. On the other hand, the fumaramide-maleamide isomerizations act as balance-breaking reactions, allowing the small macrocycle to utilize Brownian motion to move energetically downhill—from maleamide to succinamide to fumaramide.

3.3

Influencing the Expression of Chirality with Interlocked Architectures

The relationship between chirality and motion in interlocked architectures is not limited to translational (or rotational) isomerism. In some cases, the characteristics of the mechanical bond can also help express or suppress the expression of chirality.

The first example of a photoresponsive [2]rotaxane, published in 1997 by Nakashima and co-workers, is one of those cases [61]. Molecular shuttle *E/Z*-**22**⁴⁺ consists of an α -cyclodextrin macrocycle, and a tetracationic thread containing an azobiphenoxy moiety, very closely related to azobenzene, and two bipyridinium stations. The well-known *E* – *Z* isomerizations of azobenzenes and the ability of cyclodextrins to bind lipophylic compounds in water are exploited in this system to achieve shuttling. When the azobiphenoxy station is in its *trans* form, *E*-**22**⁴⁺, the cyclodextrin encapsulates it preferentially over the more hydrophilic bipyridinium station (Scheme 12).



Scheme 12 Photochemically driven shuttling movement of an α -cyclodextrin in an azobenzene-containing thread through reversible *E/Z* photoisomerization [61]

The shuttling process was confirmed by ^1H NMR and NOE experiments, and significantly also resulted in changes in the circular dichroism spectrum, suggesting that the change in position also affected the influence of the chirality of the cyclodextrin upon the aromatic regions of the thread.

In a study of chiral dipeptide [2]rotaxanes it was found that the presence of an intrinsically achiral benzylic amide macrocycle near to the chiral center could induce an asymmetric response in the aromatic ring absorption bands [62]. This induced circular dichroism (ICD) effect was stronger in apolar solvents (Fig. 9), where intercomponent interactions are maximized, showing a direct relationship to the “tightness” with which the macrocycle binds the chiral thread. Computer simulations showed that chirality is transmitted from the amino acid asymmetric center on the thread via the achiral macrocycle to the aromatic rings of the achiral C-terminal stopper.

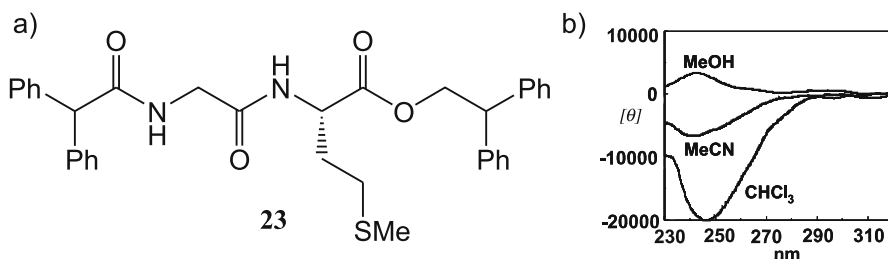
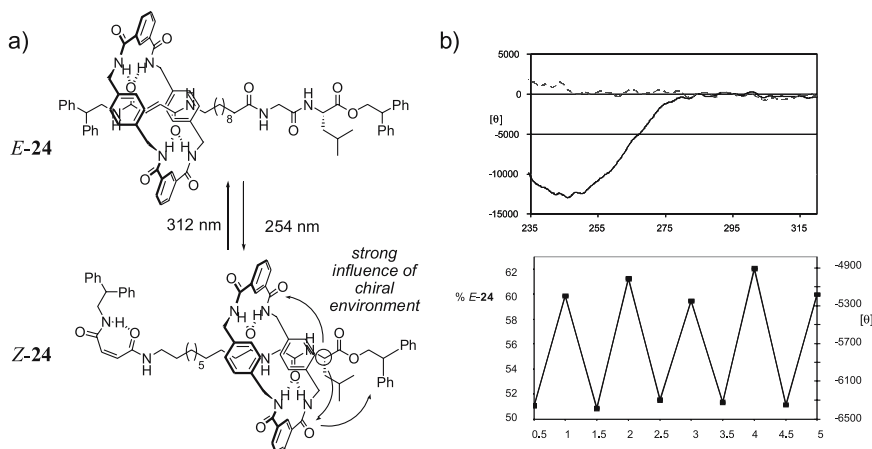


Fig. 9 **a** Molecular structure of the Gly-Met dipeptide rotaxane **23** and **b** CD spectrum of solutions of **23** in MeOH, MeCN and CHCl_3 [62]

These observations led to the design of chiroptical switch *E/Z*-**24** which utilizes the same fumaramide–maleamide isomerization seen in the previous catenanes (Scheme 13) [63]. In this case, however, the presence of a chiral dipeptide unit as a second, non-reactive station confers the shuttle its unique properties. In the *E*-**24** form, the macrocycle is held over the fumaramide template, far from the chiral center in the peptidic station. Consequently, the CD response in the aromatic region is flat, as observed for the free thread. In the *Z*-**24** isomer, where the macrocycle resides on the peptide station, close to the *L*-Leu residue, a strong and negative (ca. $-13 \text{ k deg cm}^2 \text{ dmol}^{-1}$ at 246 nm) CD response is observed. Remarkably, thanks to a small difference in the UV-Vis spectra of the *E* and *Z* forms, it was possible to achieve two photostationary states of different composition by irradiation at 254 nm (photostationary state 56 : 44 *Z* : *E*) and 312 nm (photostationary state 49 : 51 *Z* : *E*). This modest difference was enough to produce a large net change ($> 1500 \text{ deg cm}^2 \text{ dmol}^{-1}$) in the elliptical polarization response that is reproducible over several cycles of irradiation. Unlike chiroptical switches in which the presence of or the handedness of chirality is intrinsically altered, *E/Z*-



Scheme 13 **a** Chemical structure and switching mechanism of molecular shuttle *E*/Z-24. **b** Above: CD spectra of *E*-24 (dashed) and Z-24 (solid line). Below: Percentage of *E*-24 in the photostationary state (from ^1H NMR data, 400 MHz, CD_3CN , 298 K) after alternating irradiation at 254 nm (half integers) and 312 nm (integers) for five complete cycles. The second *Y* axis shows the CD absorption at 246 nm

24 remains chiral and non-racemic, with the same handedness, throughout the changes in translational isomerism; it is the *expression* of chirality that is altered.

4

Conclusions and Outlook

The relationship between chirality and molecular-level motion is a complex one. Chirality is not an inherent requirement for generating directional motion and yet in some cases it is precisely what causes molecular level motion to proceed in one direction only. New generations of molecular machines will undoubtedly shed more light on this matter; for instance in establishing the processes for which chirality is an absolute requirement in their design. Conversely, some molecular machines have the ability to dramatically influence the expression of chirality through controlled submolecular motion. This feature has potential application in data storage, displays and switchable catalysis.

References

1. Pasteur L (1848) Ann Chim 24:458
2. Lough WJ, Wainer IW (2002) Chirality in Natural and Applied Science. Blackwell, Oxford

3. Hegstrom RA, Chamberlain JP, Seto K, Watson RG (1988) *Am J Phys* 56:1086
4. Bouchiat M-A, Bouchiat C (1997) *Rep Prog Phys* 60:1351
5. Quack M (2002) *Angew Chem Int Ed* 41:4618
6. Gilat G (1999) arXiv:physics: 9904026 v1
7. Purcell EM (1977) *Am J Phys* 45:3
8. Astumian RD (1997) *Science* 276:917
9. Kay ER, Leigh DA (2005) Synthetic Molecular Machines. In: Schrader AD, Hamilton AD (eds) *Functional Artificial Receptors*. Wiley-VCH, Weinheim
10. Astumian RD, Hänggi P (2002) *Phys Today* 55:33
11. Gardner M (1964) *The Ambidextrous Universe*. Basic Books, New York
12. Feringa BL, van Delden RA, Koumura N, Geertsema EM (2000) *Chem Rev* 100:1789
13. Cornelissen JJLM, Rowan AE, Nolte RJM, Sommerdijk NAJM (2001) *Chem Rev* 101:4039
14. Orr GW, Barbour LJ, Atwood JL (1999) *Science* 285:1049
15. Lehn J-M (2002) *Science* 295:2400
16. Eliel EL, Wilen SH (1994) *Stereochemistry of Organic Compounds*. Wiley, New York
17. Kemp JD, Pitzer KS (1936) *J Chem Phys* 4:749
18. Kwart H, Alekman S (1968) *J Am Chem Soc* 90:4482
19. Iwamura H, Mislow K (1988) *Acc Chem Res* 21:175
20. Bedard TC, Moore JS (1995) *J Am Chem Soc* 117:10662
21. Kelly TR, Tellitu I, Sestelo JP (1997) *Angew Chem Int Ed Engl* 36:1866
22. Kelly TR, Sestelo JP, Tellitu I (1998) *J Org Chem* 63:3655
23. Feynman RP, Leighton RB, Sands M (1963) *The Feynman Lectures on Physics*, vol 1 (chap. 46). Addison-Wesley, Reading, MA
24. Kelly TR, De Silva H, Silva RA (1999) *Nature* 401:150
25. Feringa BL, Wynberg H (1977) *J Am Chem Soc* 99:602
26. Feringa BL (2001) *Acc Chem Res* 34:504
27. Feringa BL, Jager WF, De Lange B, Meijer EW (1991) *J Am Chem Soc* 113:5468
28. Feringa BL, Jager WF, De Lange B (1993) *Chem Commun*: 288
29. Jager WF, de Jong JC, De Lange B, Huck NPM, Meetsma A, Feringa BL (1995) *Angew Chem Int Ed Engl* 34:348
30. Feringa BL, Huck NPM, van Doren HA (1995) *J Am Chem Soc* 117:9929
31. Huck NPM, Jager WF, de Lang B, Feringa BL (1996) *Science* 273:1686
32. Koumura N, Zijlstra RWJ, van Delden RA, Harada N, Feringa BL (1999) *Nature* 401:152
33. Koumura N, Geertsema EM, van Gelder MB, Meetsma A, Feringa BL (2002) *J Am Chem Soc* 124:5037
34. ter Wiel MKJ, van Delden RA, Meetsma A, Feringa BL (2003) *J Am Chem Soc* 125:15076
35. van Delden RA, ter Wiel MKJ, Feringa BL (2004) *Chem Commun*: 200
36. Amabilino DB, Stoddart JF (1995) *Chem Rev* 95:2725
37. Sauvage J-P, Dietrich-Buchecker C (eds) (1999) *Molecular Catenanes, Rotaxanes and Knots: A Journey Through the World of Molecular Topology*. Wiley-VCH, Weinheim
38. Balzani V, Credi A, Raymo FM, Stoddart JF (2000) *Angew Chem Int Ed* 39:3348
39. Fyfe MCT, Glink PT, Menzer S, Stoddart JF, White AJP, Williams DJ (1997) *Angew Chem Int Ed Engl* 36:2068
40. Anelli PL, Spencer N, Stoddart JF (1991) *J Am Chem Soc* 113:5131
41. Bissell RA, Cordova E, Kaifer AE, Stoddart JF (1994) *Nature* 369:133
42. Martinez-Diaz MV, Spencer N, Stoddart JF (1997) *Angew Chem Int Ed Engl* 36:1904

43. Ashton PR, Ballardini R, Balzani V, Gomez-Lopez M, Lawrence SE, Martinez-Diaz MV, Montalti M, Piersanti A, Prodi L, Stoddart JF, Williams DJ (1997) *J Am Chem Soc* 119:10641
44. Keaveney CM, Leigh DA (2004) *Angew Chem Int Ed* 43:1222
45. Gatti FG, Leigh DA, Nepogodiev SA, Slawin AMZ, Teat SJ, Wong JKY (2001) *J Am Chem Soc* 123:5983
46. Marcus Y (1993) *Chem Soc Rev* 22:409
47. Armaroli N, Balzani V, Collin J-P, Gavina P, Sauvage J-P, Ventura B (1999) *J Am Chem Soc* 121:4397
48. Brouwer AM, Frochot C, Gatti FG, Leigh DA, Mottier L, Paolucci F, Roffia S, Wurpel GWH (2001) *Science* 291:2124
49. Altieri A, Gatti FG, Kay ER, Leigh DA, Martel D, Paolucci F, Slawin AMZ, Wong JKY (2003) *J Am Chem Soc* 125:8644
50. Lane AS, Leigh DA, Murphy A (1997) *J Am Chem Soc* 119:11092
51. Altieri A, Bottari G, Dehez F, Leigh DA, Wong JKY, Zerbetto F (2003) *Angew Chem Int Ed* 42:2296
52. Gatti FG, Leon S, Wong JKY, Bottari G, Altieri A, Morales MAF, Teat SJ, Frochot C, Leigh DA, Brouwer AM, Zerbetto F (2003) *Proc Nat Acad Sci* 100:10
53. Bottari G, Dehez F, Leigh DA, Nash PJ, Perez EM, Wong JKY, Zerbetto F (2003) *Angew Chem Int Ed* 42:5886
54. Leigh DA, Perez EM (2004) *Chem Commun*: 2262
55. Leigh DA, Moody K, Smart JP, Watson KJ, Slawin AMZ (1996) *Angew Chem Int Ed Engl* 35:306
56. Asakawa M, Ashton PR, Balzani V, Credi A, Hamers C, Mattersteig G, Montalti M, Shipway AN, Spencer N, Stoddart JF, Tolley MS, Venturi M, White AJP, Williams DJ (1998) *Angew Chem Int Ed Engl* 37:333
57. Livoreil A, Dietrich-Buchecker CO, Sauvage J-P (1994) *J Am Chem Soc* 116:9399
58. Livoreil A, Sauvage J-P, Armaroli N, Balzani V, Flamigni L, Ventura B (1997) *J Am Chem Soc* 119:12114
59. Leigh DA, Wong JKY, Dehez F, Zerbetto F (2003) *Nature* 424:174
60. Hernandez JV, Kay ER, Leigh DA (2004) *Science* 306:1532
61. Murakami H, Kawabuchi A, Kotoo K, Kunitake M, Nakashima N (1997) *J Am Chem Soc* 119:7605
62. Asakawa M, Brancato G, Fanti M, Leigh DA, Shimizu T, Slawin AMZ, Wong JKY, Zerbetto F, Zhang S (2002) *J Am Chem Soc* 124:2939
63. Bottari G, Leigh DA, Perez EM (2003) *J Am Chem Soc* 125:13360

Supramolecular Surface Chirality

Karl-Heinz Ernst

Empa, Swiss Federal Laboratories for Materials Testing and Research,
 Überlandstrasse 129, 8600 Dübendorf, Switzerland
karl-heinz.ernst@empa.ch

1	Introduction	211
1.1	Chirality at Surfaces	211
1.2	Structures of Clean Surfaces	213
1.3	Experimental Aspects	215
1.3.1	Molecular Deposition	216
1.3.2	STM	216
1.3.3	LEED	218
2	Achiral Molecules at Surfaces	219
2.1	Surface-Induced Chirality	219
2.2	Molecular Rearrangement	221
2.3	Reaction-Induced Chirality	222
2.4	Assembly-Enforced Chirality	223
2.5	Substrate Lattice-Induced Chirality	224
3	Chiral Recognition in Two Dimensions	226
3.1	Enantiomorphism at Surfaces	226
3.1.1	Chiral Patterns in Close-Packed Monolayers	227
3.1.2	Chiral Clusters, Chains and Rings	231
3.1.3	Losing the Expression: Achiral Lattices from Chiral Molecules	234
3.2	Spontaneous Resolution	236
3.3	Enantiospecific Surface Chemistry	243
3.4	Diastereoisomeric Recognition	244
4	Amplification of Chirality in Two Dimensions	245
4.1	Homochirality from Prochiral Precursors	245
4.2	Homochiral Pseudo-Racemic Systems	246
4.3	Magnetic Field-Induced Enantiomeric Excess	248
5	Outlook	249
	References	249

Abstract Two-dimensional supramolecular chemistry on surfaces is strongly governed by directional forces, and expression of chirality in two dimensions is quite pronounced due to confinement to the plane. In particular the absence of certain symmetry elements has a strong influence on pattern formation. With the appearance of scanning tunneling microscopy, two-dimensional supramolecular chirality has become a popular issue in the field of surface self-assembly during the last decade. By using recent examples from literature, a conceptual overview on different aspects of surface chirality will be given.

The main topics are adsorption-induced chirality, chiral recognition, transfer of chirality from single molecules into supramolecular structures, and cooperatively driven chiral amplification phenomena.

Keywords 2D self-assembly · Chiral surfaces · Crystallization · Enantiomorphism · Molecular monolayers

Abbreviations

1D	one-dimensional
2D	two-dimensional
3D	three-dimensional
[7]H	heptahelicene
8CB	4-cyano-4'-octibiphenyl
AA	arachidic anhydride
AES	Auger electron spectroscopy
AFM	atomic force microscopy
bcc	body centered cubic
CCW	counterclockwise
CW	clockwise
$\Delta\Phi$	workfunction change
ee	enantiomeric excess
fcc	face-centered cubic
hcp	hexagonal close-packed
hopg	highly ordered pyrolytic graphite
HREELS	high-resolution electron energy loss spectroscopy
ISA	5-[10-(2-methylbutoxy)decyloxy] isophthalic acid
LC	liquid crystal
LEED	low-energy electron diffraction
MAA	methylacetoacetate
ML	monolayer
MMC	molecular modeling calculations
NN	1-nitronaphthalene
NP	naphtho[2,3-a] pyrene
PVBA	4-trans-2-(pyridyl-4-yl-vinyl) benzoic acid
RAIRS	reflection-absorption infrared spectroscopy
RT	room temperature
SDA	4,4'-stilbene dicarboxylic acid
SIMS	secondary ion mass spectrometry
STM	scanning tunneling microscopy
SU	succinic acid
SubPC	chloro[subphthalocyaninato] boron(II)
TA	tartaric acid
TPD	temperature programmed desorption
UHV	ultra-high vacuum
XPS, XPD	X-ray photoelectron spectroscopy, -diffraction

1

Introduction

1.1

Chirality at Surfaces

Since the 1990s, surface chirality has received increasing attention. The original motivation for studying chirality at surfaces came from a classic field of surface science, namely, heterogeneous catalysis. Enantioselective catalysis on a solid support is a promising approach with a high potential for sustainable pharmaceutical synthesis. By coadsorbing a chiral modifier on the catalytically active metal surface, a bias towards enantioselectivity is introduced. In addition, new thin film devices for optical and electronic applications substantially increased the interest in self-assembly phenomena of large organic molecules on solid substrates¹.

A more fundamental concern in investigating chiral molecules at surfaces comes from the aspect of chiral recognition. Ever since Pasteur's separation of enantiomorphous TA-salt crystals and his realization that there is a connection between crystal enantiomorphism and the handedness of the molecular building blocks, there has been a growing interest in understanding the mechanisms of chiral resolution during crystallization at the molecular level. Moreover, the transfer of chirality into mesoscopic structures—a very important issue in liquid crystal science—is difficult to predict in three dimensions, but 2D model systems help to get insight. In particular, the possibility to study these processes with sub-molecular resolution on surfaces by exploitation of STM has substantially increased the number of molecular surface science publications during the last ten years.

Supramolecular chemistry on crystalline surfaces is governed to a large extent by lateral interactions. Nevertheless, the substrate plays an important role in mediating these interactions. Intermolecular recognition on a surface, for example, can take place only if the adsorbate–substrate interaction allows the molecules to meet each other. Therefore, the choice of the substrate plays a decisive role. Too strong interactions immobilize molecules and do not leave room for 2D supramolecular chemistry or may even induce decomposition; too weak adsorbate–substrate interactions cause high mobility and 2D crystallization phenomena will not occur.

The interplay between lateral forces and interaction with the substrate is illustrated in Fig. 1. The adsorption energy ΔE_{ad} of a single atom or molecule is modulated laterally due to the atomic corrugation of the crystalline surface. At low temperatures, the molecule will be in its ground state and immobile. In order to migrate on the surface, the molecule must overcome the acti-

¹ In contrast to the meaning in synthetic chemistry, throughout this review “substrate” stands for the solid support of adsorbed molecules.

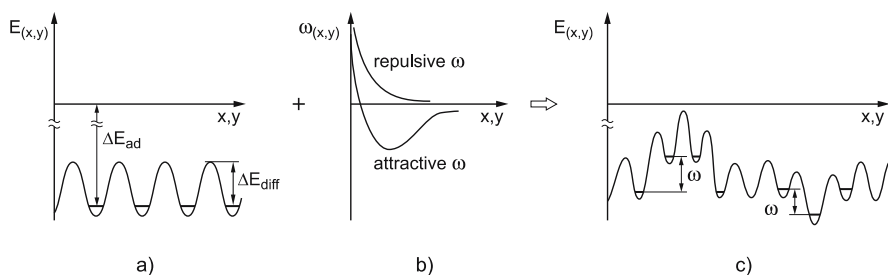


Fig. 1 Modulation of adsorption energy due to lateral interactions between molecules on surfaces: **a**) potential diagram of a single molecule on a crystalline surface. **b**) potential curves for repulsive and attractive lateral interaction ω . **c**) lateral repulsion lowers the adsorption energy (left), attraction leads to an increase in adsorption energy (right). The adlayer periodicity is the result of the balance of lateral molecular interaction, i.e., extent of repulsion allowed in a close-packed molecular layer, and the energy gain with increased adsorption. Reproduced with permission of the author [1]

vation barrier ΔE_{diff} . At higher coverage, lateral forces between molecules become more prominent and have an influence on the interaction with the substrate. Attractive forces between molecules cause an increase of the adsorption energy, while repulsion between adsorbates lowers the adsorption energy. The latter is often observed in close-packed monolayers. When finally the amount of repulsion energy within one layer becomes as strong as the adsorption energy of a single molecule, the saturation coverage at that particular temperature is reached. Under these conditions, theory predicts the strongest chiral discrimination forces [2]. That is, any steric influence becomes substantially large and molecular shape and symmetry determine the outcome [3]. For the same reason, an energetically favored adsorption site for the single molecule at low coverage may switch to a different binding site at high packing density. This subtle balance between lateral intermolecular interaction and molecule-substrate interaction determines the long-range 2D molecular crystal structure and is the most important aspect of this review.

This contribution is restricted to supramolecular chiral phenomena on solid surfaces. Neither interaction of molecules with chiral inorganic surfaces [4], nor chiral amphiphilic molecules at the air–water interface are considered [5–8]. It is the intent of this review to present principle aspects of surface chirality. That is, examples are used to highlight typical chiral assembly mechanisms and structures. Most of these examples, however, belong to more than one aspect presented within this review. Hopefully, this set-up will be accessible to the reader who is not working with surfaces as well as informative to those who are familiar with the subject.

In order to give the non-specialist a basis, the remainder of this section gives a short introduction into the methodologies of surface science and to

important experimental techniques for studying self-assembly phenomena on solid surfaces. Section 2 deals with chirality induction due to confinement of molecules at surfaces. Chiral recognition in two dimensions and 2D supramolecular chiral structures will be presented in Sect. 3. Section 4 treats chiral amplification and homochirality based on cooperative molecular phenomena followed by a short summary.

1.2

Structures of Clean Surfaces

The arrangement of atoms on solid surfaces strongly affects the supramolecular structure of adsorbates. Cleaving a crystal parallel to crystal planes reveals defined surface structures. These crystal planes are denoted by the Miller indices (hkl), which are the integer ratios of the reciprocal unit vectors where the particular plane intercepts the crystal coordinates x , y and z . If a plane is parallel to one or two axes, it intercepts at infinity; consequently, the Miller index is zero. Three different cuts through the fcc lattice and the corresponding surface structures are shown in Fig. 2. These are the low-index planes (100), (110) and (111) (Fig. 2a–c, respectively). The obtained surface lattice symmetries for the top-most atomic layer are quadratic, rectangular and hexagonal (Fig. 2d–f). Depending on the cut, similar surface geometries can be obtained for bcc and hcp crystals [9]. Ni, Cu, Ag, Au, Pt, Pd and Rh are examples of fcc metals, but few of their clean surface structures deviate from the bulk geometries and undergo a so-called reconstruction. The topmost layer may show a different periodicity or an up-down buckling of the surface atoms. Examples of surfaces undergoing reconstruction are Pt(110), Au(110) and Au(111).

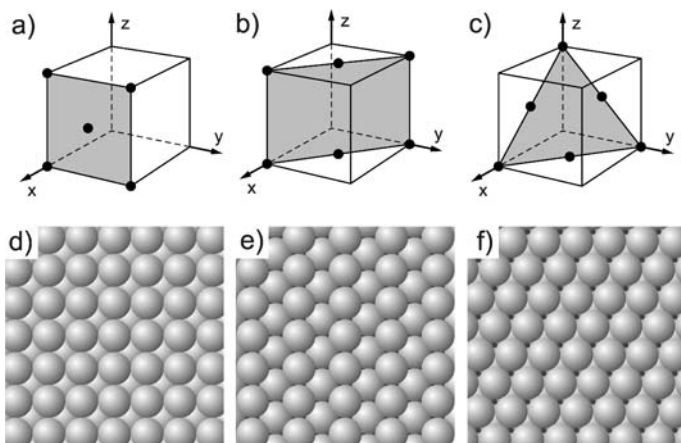


Fig. 2 The low-index planes (100), (110) and (111) of the fcc-crystal (a–c), and the corresponding surface lattice structures. Reproduced in part with permission of the author [1]

Surface reconstruction after adsorption of gases or organic molecules is a also common phenomenon [1, 9].

A popular substrate for solid–liquid interface studies is hopg. Cleaving the crystal perpendicular to the c -axis leads to the well-defined honeycomb-structured basal plane (Fig. 3).

In order to describe the 2D crystal lattice periodicities of the adsorbate unit cell, two notations are used in the literature: the Wood notation [10] and the matrix notation [11]. For the latter, the transformation matrix $(\mathbf{m}_{11}\mathbf{m}_{12}, \mathbf{m}_{21}\mathbf{m}_{22})$ links the adsorbate lattice vectors $(\mathbf{b}_1, \mathbf{b}_2)$ to the substrate vectors $(\mathbf{a}_1, \mathbf{a}_2)$ via:

$$\begin{pmatrix} \mathbf{b}_1 \\ \mathbf{b}_2 \end{pmatrix} = \begin{pmatrix} \mathbf{m}_{11} & \mathbf{m}_{12} \\ \mathbf{m}_{21} & \mathbf{m}_{22} \end{pmatrix} \begin{pmatrix} \mathbf{a}_1 \\ \mathbf{a}_2 \end{pmatrix}, \quad \text{i.e.,} \quad \mathbf{b}_1 = \mathbf{m}_{11}\mathbf{a}_1 + \mathbf{m}_{12}\mathbf{a}_2 \quad \text{and} \quad \mathbf{b}_2 = \mathbf{m}_{21}\mathbf{a}_1 + \mathbf{m}_{22}\mathbf{a}_2$$

The Wood notation describes the adsorbate structure periodicity by the ratios of the unit vectors of the adlattice and the substrate unit vectors. In addition, if a rotation is required to bring substrate and adlattice to coincide, the value of the rotation angle is given. Primitive or centered unit cells can be distinguished by p or c in front of the parentheses. The three examples shown in Fig. 4 are denoted as $p(2 \times 2)$, $(\sqrt{2} \times \sqrt{2})R45^\circ$ or $c(2 \times 2)$, and $(\sqrt{3} \times \sqrt{3})R30^\circ$ in Wood notation, or as $(2 \ 0, 0 \ 2)$, $(2 \ 0, 1 \ 1)$ and $(2 \ 0, -1 \ 1)$ in matrix notation (from left to right, respectively). In order to further specify or to distinguish from other possibilities, sometimes crystallographic symmetry symbols are added to the Wood notation. For example, $(2 \times 1)p2mg$ stands for a primitive (2×1) cell with two mirror planes and a glide plane, which is substantially different to $p(2 \times 1)$ or $c(2 \times 1)$ structures. In order to have consistent labeling, the choice of the proper unit cell is also important. Different assignment procedures give rise to much confusion, although rules for the appropriate choice of vectors and angles have been established [12].

If an adlattice is oriented in an oblique angle with respect to the substrate, e.g., $0^\circ < \varphi < 30^\circ$ for a surface lattice with hexagonal symmetry, two mirror-

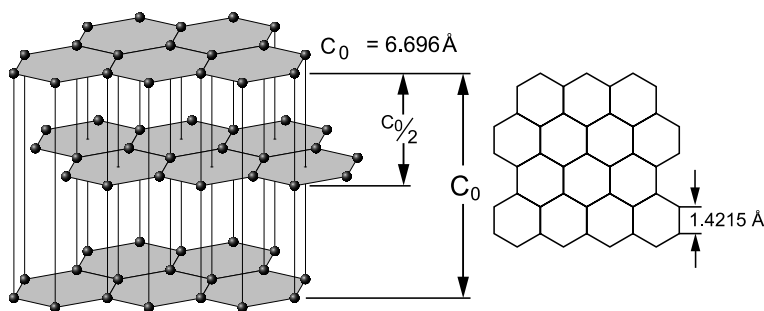


Fig. 3 Lattice of hopg. The basal plane of the hexagonal lattice structure is commonly used for adsorption studies from solution

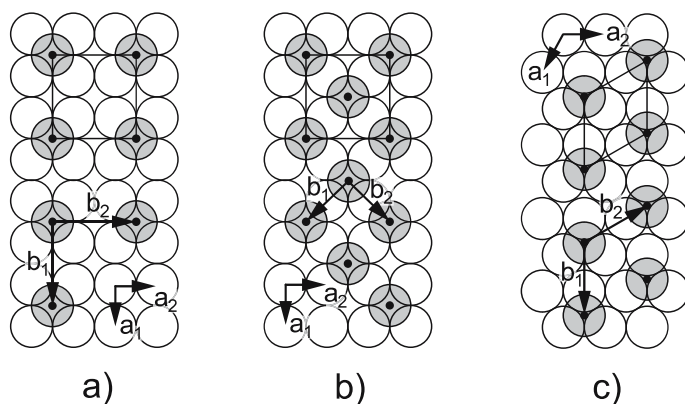


Fig. 4 Examples for adsorbate lattice structures on (100) and (111) fcc-surfaces. The choices of unit vectors for adlattice and substrate lattice are indicated. Adatoms are shown in grey. Instead of the four-fold and three-fold coordination sites for the adsorbates, the same adlayer periodicities can result for sites with different coordination; e.g., on *top* or *bridge sites*

like alignments must be expected. In this case, rotation and translation are not sufficient to bring both domains to coincide. An example of this “lattice-chirality” is discussed in Sect. 2.5.

If a rotation operation must be included in order to bring two domains on a surface to coincide, we speak of “rotational domains”. If, by no means, a regular adlattice can be brought into a periodic relation with the underlying substrate lattice, the superstructure is incommensurate. In this case, the lateral interactions are so strong that the substrate registry cannot govern the lateral order.

1.3

Experimental Aspects

Investigating 2D self-assembly at the molecular level provides new insight into complex intermolecular interactions. These model studies are usually performed under well-defined conditions in order to have more control on complicated surface processes [13]. This includes single-crystal substrates which allow the application of diffraction techniques.

There has been substantial progress in experimental and theoretical surface analytical methods over the last years. Methods based on X-rays and UV light for diffraction, absorption, or photoelectron spectroscopies benefit from new generation synchrotron light sources. To name a few, surface experimental methods include XPS, AES and SIMS for investigating the surface chemistry; $\Delta\Phi$ and TPD for adsorption energetics and kinetics; as well as XPD, RAIRS, HREELS, LEED and STM for molecular and surface structure

determination. Being able to deliver information on the long-range structure of molecular films, the latter two are by far the most important methods for studying supramolecular chemistry on surfaces and will be introduced briefly in this section.

1.3.1

Molecular Deposition

Self-assembly phenomena on solid substrates are usually studied in ultra-high vacuum (UHV) or at the liquid–solid interface. Surface analytical methods involving electrons require vacuum. But UHV has also the advantage that reactive metal and metal oxide surfaces can be used as substrate since the very low background pressure also guarantees long investigation times on a non-altered sample.

Adsorbate layers in UHV are obtained by evaporation of molecules. Liquid organic substances usually have a sufficient vapor pressure to be directly admitted to the vacuum chamber via leak valves. Larger molecules must be heated so their vapor pressure becomes substantial. Here, organic molecular beam deposition is the method of choice under UHV conditions. The solid substance is sublimed and collimated by a Knudsen cell. Because the sticking coefficient of larger molecules on surfaces at RT is usually at unity, this method does not affect the background pressure. However, not all species can be adapted to UHV, such as those with relatively low thermal stability and/or high molecular weight (i.e., macromolecules), not allowing sublimation.

Adsorption from the liquid phase is experimentally much easier (cheaper), but requires, even for highest-purity solvents, chemical inert substrates, e.g., hogg, or selective adsorbate systems, like thiols on gold.

As mentioned above, the choice of substrate is crucial for tuning the lateral mobility. This problem might also be addressed in part by temperature control. Cooling can lower mobility so that the 2D gas aggregates into 2D crystals. If mobility on a particular substrate is not sufficient, it can be increased by heating. However, this could raise the probability of decomposition or desorption. Low temperatures, on the contrary, put constrain on experimental control that comes with cooling with liquid nitrogen or helium.

1.3.2

STM

This method is undisputedly the most important innovation in this field since the advent of the “surface science founding methods” AES and XPS in the 1960s [14]. It has revolutionized surface structure determination and is an extremely powerful method for investigating 2D molecular pattern formation. Applications also include biology, electrochemistry, solid state physics, as well as atomic and molecular manipulation. Although most of the studies

are performed under UHV, ambient conditions and the liquid–solid interface allow high-resolution STM imaging as well [15]. STM analysis also benefits to a great extent from the regularity of crystalline substrates.

The principle set-up of an STM experiment is illustrated in Fig. 5. A tungsten tip as one electrode and the electrically conductive sample as the other leave a finite probability of electrons to tunnel through the gap in between. The tunneling current depends exponentially on the tip–sample distance and is used for exact distance control. The relative positioning of tip and sample is achieved via piezoelectric actuated x – y – z manipulation. The x – y map of the tunneling current at constant bias voltage, for example, delivers electronic and topographic features of the surface. However, this spatial variation of tunneling current actually reflects the local density of states [16]. Nevertheless, STM provides good insight into molecular ordering in 2D molecular monolayers. Depending on the sign of polarity between tip and sample, tunneling occurs either from the tip to the surface into unoccupied states or from the sample's occupied states into the tip. Via bias-current (I – V) curves, this method is sensitive to the electronic structure of the substrate–adsorbate system. This makes STM a spatially resolved spectroscopy for electronic states of adsorbate systems. It allows further manipulation of single molecules and atoms at the surface [17], or even breaking and formation of chem-

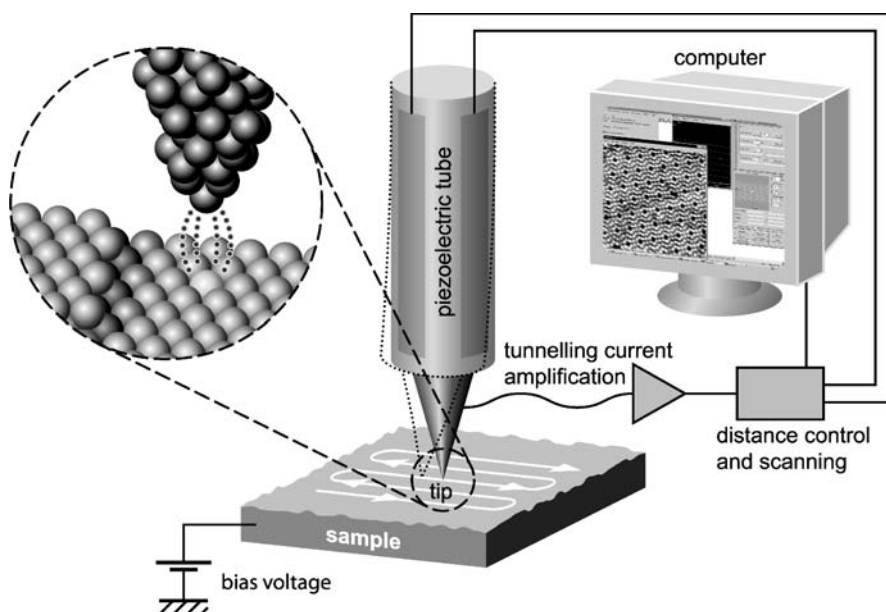


Fig. 5 Schematic presentation of the STM experiment. The tunneling current is utilized for distance control of an electrode above the sample surface and maps spatially resolved the geometric and electronic properties of surfaces

ical bonds [18]. Although cumbersome, supramolecular structures could be built in this way via human intervention and then compared to natural self-assembly.

For molecular systems at surfaces, one must take into account that STM may interfere with natural assembly. That is, the tip-molecule interaction may induce disorder during scanning operation. In other words, defined molecular 2D crystals can be distorted by this method, not allowing true geometric analysis. Again, low temperatures in UHV or saturated monolayer systems, in general, help to circumvent this problem.

Shortly after the invention of STM, another scanning probe microscopy has been developed, which is based on the force between a bendable probe and the surface. The atomic or scanning force microscope (AFM or SFM) is now the most popular tool in nanoscience. Constant progress allows today lateral resolution which is comparable to STM.

1.3.3

LEED

Determination of lateral periodicities in the self-assembled layer is an important goal in surface analysis. 2D surface crystal structures are best studied with low energy electrons, since their escape depth, contrary to X-rays, is basically limited to the top-most atomic layers. Consequently, LEED has become the most important method in surface monolayer crystallography. However, single-crystalline substrates are required. Via this technique, 2D supramolecular chiral lattice structures on single crystal surfaces had already been observed in 1978 [19].

The typical experimental set-up is shown in Fig. 6. Mono-energetic collimated electrons, with energies usually between 20 to 500 eV, are backscattered from the crystal surface onto a fluorescent screen, whereby only the elastically scattered electrons are allowed to pass the grids of an electron optic in front of the screen. Because of their wave-like behavior, the electrons are diffracted at the crystal lattice and the interference maxima become visible at the fluorescent screen.

A LEED pattern is the projection of the reciprocal lattice. The unit cells of molecular adlattices are usually larger than the atomic substrate lattice, which results in smaller reciprocal vectors and smaller distances between the superstructure spots of the reciprocal adlattice.

LEED does not only reveal the relative periodicities of the adsorbate mesh with respect to the substrate lattice. Applying dynamical scattering theory, i.e., modeling the scattering intensity of diffracted beams versus electron energy (so-called I-V curves), allows determination of absolute positions of atoms on the surface [20]. Unfortunately, the complexity of the method limits the number of atoms per unit cell and makes it applicable only to atomic or small-molecule lattices.

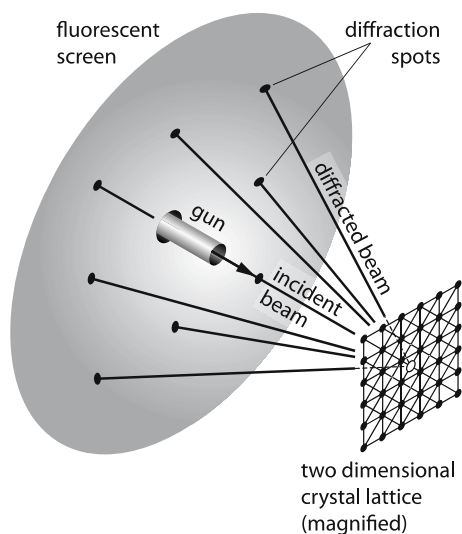


Fig. 6 Backscattering of low energy electrons from a single crystal surface. Reproduced with permission of the author [1]

2

Achiral Molecules at Surfaces

If chiral molecules are adsorbed on a surface, the supramolecular system will be always chiral. There are, however, ways of creating single motifs or layers devoid of reflection symmetry due to interaction of achiral molecules, belonging to the C_{nh} , C_s , or C_i point groups, with the achiral surface [21]. All adsorption-induced chirality processes have in common that both enantiomers will be created as long as no further bias for single handedness is present. At a global level, the surface remains achiral, but at a local level, spontaneous symmetry breaking is a common phenomenon.

This section deals with principle ways of inducing chirality at surfaces. Some of the following examples could be listed under more than one category and most of them are strongly influenced by the crystalline substrate.

2.1

Surface-Induced Chirality

If only the presence of the surface itself destroys the mirror symmetry of the free species, i.e., even without any distortion of the molecular backbone, the two resulting enantiomers cannot be superimposed by translation and rotation within the plane. The resulting absolute configuration depends on which enantiotopic face of the molecule is turned towards the substrate. Interconversion is only possible by reflection with the mirror plane perpen-

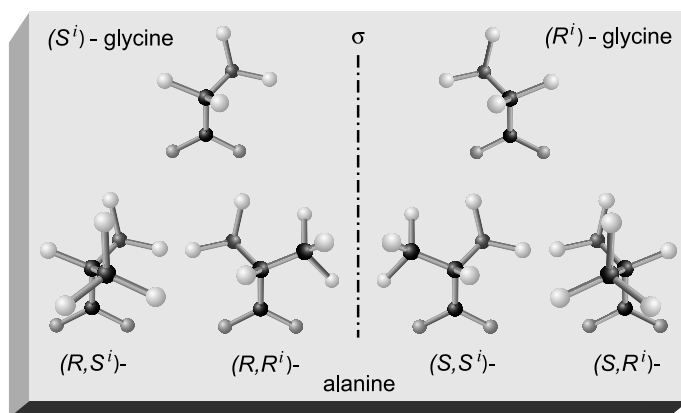


Fig. 9 Top-view on enantiomers and diastereoisomers of adsorbed glycine and alanine. The amino nitrogen and the two oxygen atoms form bonds to the surface and create a chiral footprint configuration. The surface-induced absolute configuration, as indexed with a superscripted *i*, is specified using CIP-rules and by giving an atom or group closer to the surface a higher priority

A molecule may also lose mirror symmetry if the presence of the surface induces non-equivalence of otherwise identical groups. This is shown for the theoretical example of methane in tilted adsorption geometry (Fig. 8). Another example is the amino acid glycine. In tilted geometry, it will become chiral on the surface [22]. This surface-induced handedness, in turn, gives rise to four diastereomeric configurations for alanine on a surface (Fig. 9).

2.2

Molecular Rearrangement

The interaction with the surface or the influence of adjacent molecules in a close-packed supramolecular film may force the single molecule into a chiral conformation. On hpg, the molecular arrangement of long-alkyl chain molecules is largely based on $C-H \cdots \pi$ interactions of methylene groups with the top graphite layer, stretching out the alkyl chains parallel to the surface [23]. AA, for example, can be aligned either in an achiral or chiral geometry (Fig. 10). The specific interaction to the substrate mesh, in combination with a dense-as-possible packing arrangement, as observed via STM, led to a chiral conformation (Fig. 10b) [24].

For the inherently chiral (*R, R*)- and (*S, S*)-TA, a zigzag distortion has been confirmed experimentally via XPD [25]. DFT calculations, however, predicted also for achiral (*R, S*)-TA and SU on Cu(110) a chiral zigzag conformation after deprotonation of both carboxyl groups (Fig. 11) [26]. Indeed, observations of long-range chiral patterns suggest this geometry [27–29].

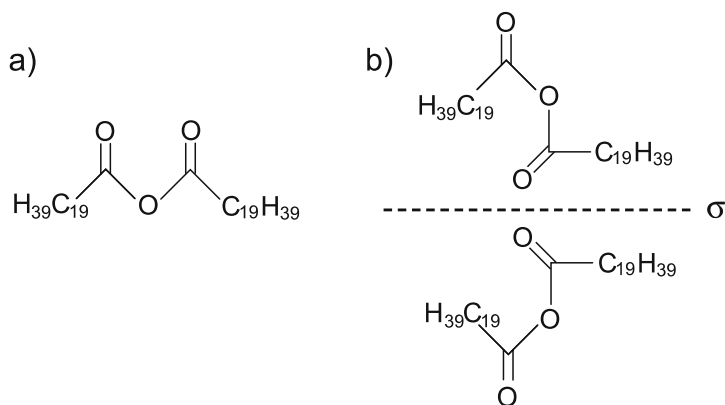


Fig. 10 Chirality due to molecular arrangement. *Top-view* on achiral and chiral configurations of AA on hopg. The nonadecyl groups stretch out into zigzag configurations on hopg (not shown)

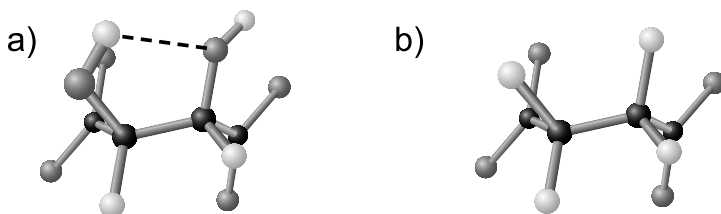


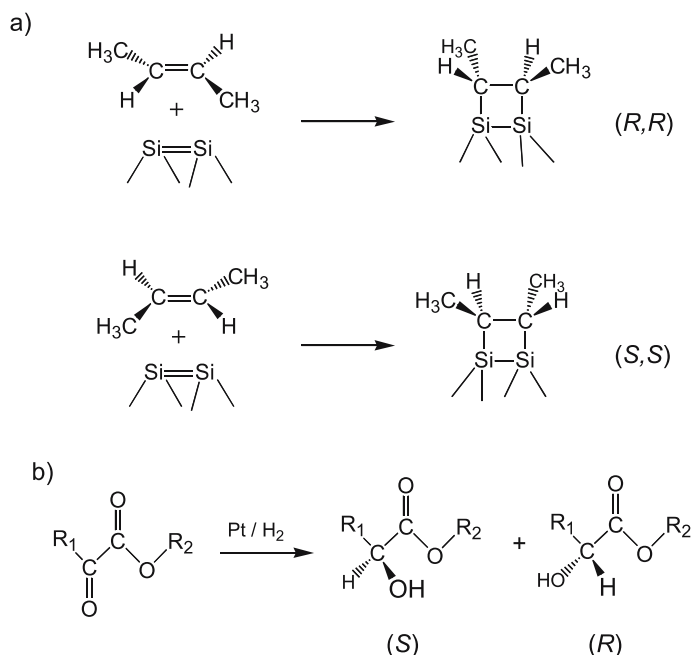
Fig. 11 *Top-view* of ball and stick models of (*R,S*) tartaric acid (**a**) and succinic acid (**b**) in chiral zigzag arrangements on Cu(110). The interaction with the surface atoms causes deprotonation of the carboxyl groups in first place and forces both species into chiral conformations. For (*R,S*)-TA, a stabilizing intramolecular hydrogen bond is indicated as a *dashed line*

2.3

Reaction-Induced Chirality

A pro-chiral molecule may turn chiral after undergoing a symmetry breaking chemical reaction on a surface. An example where covalent bonds to surface atoms are formed is the reaction of *trans*-2-butene with Si(100) [30]. As with purely adsorption-induced chirality, the relative alignment of the prochiral reactant with respect to the surface plane determines the handedness of the adsorbate complex (Scheme 1a).

As mentioned in the introduction heterogeneously catalyzed hydrogenation of prochiral species is industrially important. The relative alignment of the prochiral species to the surface determines the direction of hydrogen attack, and, thus, the handedness of the product. Enantioselectivity can be introduced by co-adsorbed chiral modifiers. These influence the align-



Scheme 1 **a** The [2 + 2] cycloaddition product of prochiral *trans* 2-butene with Si dimers of the Si(100) surface leads to chiral adsorbate complexes. **b** Hydrogenation of prochiral α -keto esters over platinum is a heterogeneously catalyzed reaction leading to chiral alcohols. Using cinchonidin as chiral modifier makes this surface reaction enantioselective. In a similar fashion, TA-modified nickel is a highly enantioselective catalyst for β -keto ester hydrogenation

ment of the reactant so that identical enantiotopic faces are turned towards the surface. Most prominent are hydrogenation of functionalized ketones on *cinchona*-modified platinum group metal catalysts (Scheme 1b) [31] and hydrogenation of β -keto carboxylic acid esters and ketones on tartaric acid-modified nickel catalysts [32].

2.4

Assembly-Enforced Chirality

Chiral supramolecular architectures are sometimes formed by molecules that stay achiral as a single entity. Hence, chirality arises just because of close-packed self-assembly on the surface. The single pentane molecule in its linear configuration remains achiral. For the close-packed monolayer, a rectangular unit cell has been identified by neutron diffraction. In addition, a tilt of the molecular axis with respect to the adlattice vectors would make the whole layer chiral [33]. For a particular mirror domain, the tilt angle ψ can be either turned clockwise or counterclockwise (Fig. 12).

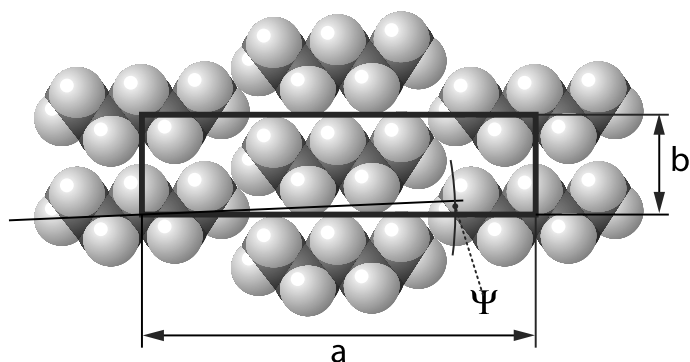


Fig. 12 Pentane on hopg forms at 11 K a rectangular unit cell. A small tilt angle Ψ of the molecular axis with respect to the adsorbate lattice vectors a and b would break the mirror symmetry of the layer. Reproduced with permission of the authors [33]

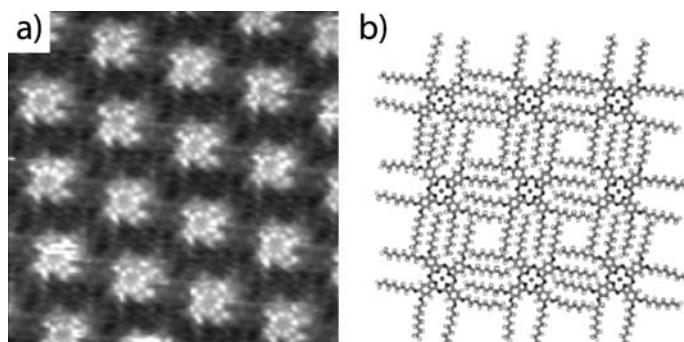


Fig. 13 **a** The STM image (12.8 nm \times 12.8 nm) of CuPcOC8 on hopg reveals rotated structures due to interdigitation of the alkyl chains, as shown in the structure model **(b)**. Reprinted in part with permission from [35]. Copyright (2000) American Chemical Society

For discotic molecules with long alkyl side chains, 2D assembly also often leads to mirror-symmetry-broken structures. In addition to steric hindrance and superlattice formation, the mechanism involves conformational mobility of the side chain [34]. This has been shown for the Cu-phthalocyanine derivative CuPcOC8 on hopg using STM (Fig. 13). The C_{4v} -symmetric molecule forms dense layers with interdigitated alkyl chains. This forces the molecules into a rotated structure [35, 36].

2.5

Substrate Lattice-Induced Chirality

In order to explain the chirality induction processes in the previous examples, we simply had to take the presence of an isotropic surface into account. Nev-

ertheless, the surface crystallography has in some of these cases an influence on (chiral) pattern formation. If the substrate mesh is considered, more ways of creating chirality arise. A simple chiral motif is a linear molecule; e.g. CO or N₂, tilted in an oblique angle with respect to a highly symmetric lattice direction.

Another commonly observed case of lattice-enforced chirality is the formation of mirror domains in close-packed monolayers. The interplay of lateral and perpendicular interactions leads to a chiral supramolecular arrangement; i.e., two mirror-like surface structures are observed. Benzene adsorbed under ultra-high vacuum (UHV) conditions on Ni(111) is a classic example. At RT, the benzene ring is centered above a bridged site between two surface atoms. Higher lateral packing densities are achieved below 270 K, with the molecules forced into three-fold adsorption sites leading to a saturation coverage of one molecule per seven surface atoms [37]. Shown in Fig. 14a is a model for this $(\sqrt{7} \times \sqrt{7})R19.1^\circ$ structure. Since the domain size rarely exceeds the diameter of the probing electron beam, both domains contribute to the diffraction pattern. Therefore, the LEED pattern, as schematically shown in Fig. 14b, is the superposition of the reciprocal lattices of both mirror domains. Other examples for mirror domain structures of benzene are $(\sqrt{19} \times \sqrt{19})R23.4^\circ$ on Rh(111), $(\sqrt{13} \times \sqrt{13})R13.9^\circ$ on Ru(001), including coadsorbed CO, and $(\sqrt{21} \times \sqrt{21})R10.9^\circ$ on Os(0001) [38].

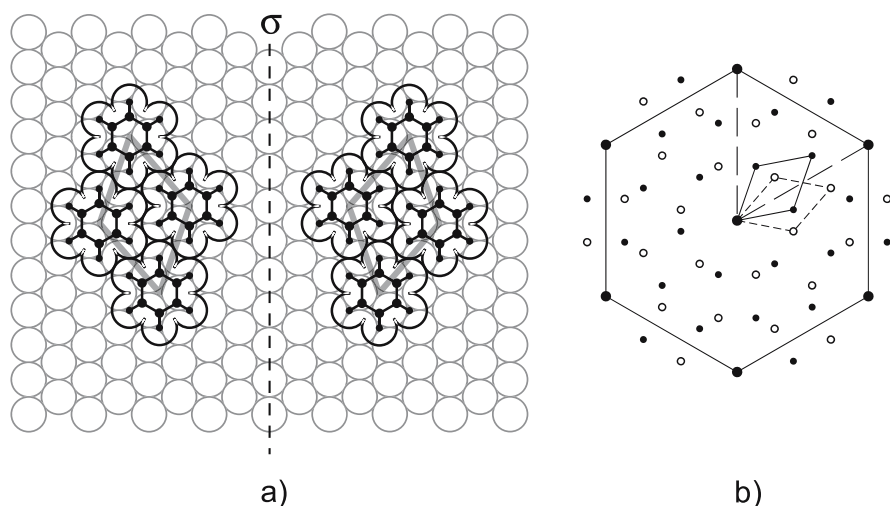


Fig. 14 **a** Benzene on Ni(111) forms mirror domains with the mirror plane parallel to the [110] surface lattice direction. The unit cell is rotated either by $+19.1^\circ$ or by -19.1° with respect to the [110] direction of the substrate. The van der Waals radii around the hydrogen atoms show that the structure is closely packed. **b** Schematic drawing of the LEED pattern. The unit cell periodicity of substrate (*large hexagon*) and adlayer for both mirror domains (*small hexagonal prisms*, *open and closed circles*) are indicated

Interestingly, there are two levels of chirality involved here. If benzene were replaced by single atoms, one would still observe mirror domains, i.e., a LEED pattern with identical diffraction spot periodicities. The loss of mirror symmetry then comes solely from the relative alignment of adsorbate and substrate lattice. For benzene molecules, however, the relative azimuthal alignment within the adsorbate unit cell already presents a chiral arrangement. Consequently, the two benzene mirror unit cells alone cannot be superimposed. Although forced into this alignment by a regular substrate, just the adsorbate unit cell plus molecular orientation—like the above-mentioned pentane example—represents a 2D supramolecular chiral system. Practically, there is no difference between the examples in Sects. 2.4 and 2.5. The distinction is based on the extent of interactions, that is, if substrate–adsorbate or the lateral interactions prevail.

3

Chiral Recognition in Two Dimensions

Chiral recognition at surfaces occurs at different levels and in different ways. Chiral expression becomes especially obvious in the formation of chiral motifs. That is, chirality is transferred from the single molecule into a supramolecular enantiomorphous structure. Moreover, enantioselective interactions between identical or different species are decisive for spontaneous resolution or play an important role in cooperative phenomena.

We will find in this section that different electrostatic intermolecular forces, e.g. dipole–dipole, quadrupole–quadrupole, van der Waals, and acceptor–donor interactions contribute to chiral recognition. Most important, however, are hydrogen bonding and steric interactions.

Beside the presented supramolecular systems on surfaces, it is worth mentioning that recognition of chiral sites on crystalline surfaces has been reported in biomineralization or at the solid–liquid interface [39–41]. Enantioselective interactions with kink sites of metal surfaces have been demonstrated for the electro-oxidation of *R*- and *S*-glucose over Pt and for desorption of chiral molecules from Cu(543) [42, 43].

3.1

Enantiomorphism at Surfaces

There are several ways for molecules to transfer chirality into supramolecular structures. The typical examples presented in this section are distinguished whether chiral expression occurs in the close-packed monolayer or in smaller molecular aggregates. The case that chiral molecules in ordered structures do not show a supramolecular chiral motif is also discussed here, since it also highlights the balance between lateral and perpendicular acting forces.

3.1.1

Chiral Patterns in Close-Packed Monolayers

Pure enantiomers at surfaces form in most cases 2D enantiomorphous structures in close-packed monolayers. That is, chirality is transferred from the single molecule into a long-range chiral motif at the surface. The created motifs are mirror images for the opposite enantiomers. This was clearly observed via STM for helically shaped aromatic [7]H on Cu(111) [44]. Close to monolayer saturation, handed pinwheel structures were observed (Fig. 15a, top), with M-[7]H-pinwheels having the opposite handedness as P-[7]H-pinwheels. In addition, at full monolayer coverage “three-molecule-cloverleaf” units show opposite tilt angles with respect to the adsorbate lattice unit cell (Fig. 15a, bottom).

Molecular modeling calculations (MMC) revealed that these structures are governed by steric constraints. The lowest-energy structure for the close-packed monolayer delivers identical adsorption sites for all molecules of the unit cell. Their azimuthal orientations, however, are different. Similar to the frustrated lattice structures observed for crystalline polymers of single helicity, e.g., isotactic poly(propylene) [45, 46], not all helices can be aligned “in phase”. The azimuthal orientations, in turn, depend strongly on the helicity of the molecules, so that opposite structures are generated for the enantiomers. Assuming that the brightest features of the STM images reflect the off-centered topmost part of the molecular helix, the MMC structures

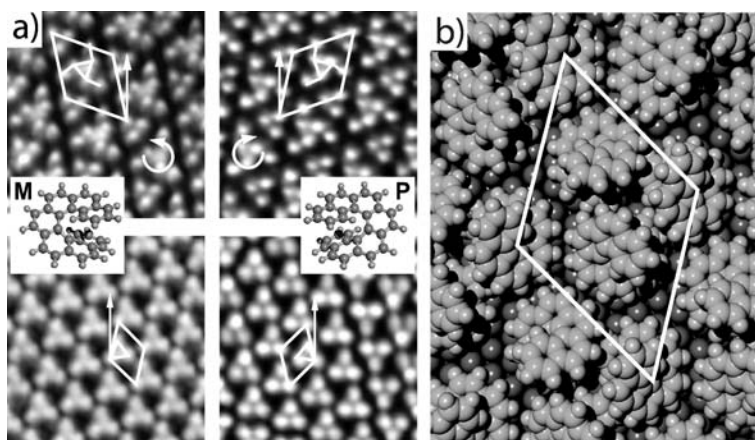


Fig. 15 **a** M-[7]H forms at 95% of the saturated monolayer CW-rotated pinwheels (*top, left*) while CCW-rotated pinwheels are observed via STM for P-[7]H (*top, right*) [44]. At full ML opposite tilt angles of cloverleaf clusters with respect to the adlattice are observed (*bottom*). Images: 10 nm × 10 nm. Reprinted with permission from Wiley. **b** Model for the M-[7]H cloverleaf structure obtained from MMC. Minimal repulsion is achieved for certain relative azimuthal orientations

agree well with the experimentally observed STM structures [44]. [7]H on Cu(111) thus stands for short-range sterically controlled supramolecular self-assembly mediated by the surface lattice.

At the solid–liquid interface, solvent molecules may also become coadsorbed into the monolayer. Dissolved in heptanol, ISA forms on hopg lamellae in which the larger lamella ΔL_1 reflects the interdigitated ISA alkyl chains (Fig. 16) and the shorter lamella is composed of 1-heptanol molecules [47]. The zigzag alignment of the ISA alkyl chains on hopg, in combination with the handedness of the stereogenic center, yields opposite tilt angles of the lamella axis with respect to the substrate lattice for the two enantiomers. The chiral expression is further transferred via intermolecular hydrogen bonding between the ISA head groups and the hydroxyl groups of the heptanol. The aligned achiral solvent molecule is rotated, with respect to the ΔL_1 lamella axis: clockwise for (*S*)-ISA and counterclockwise for (*R*)-ISA.

The opposite supramolecular chiral motif is always observed for opposite enantiomers, but which handedness will be expressed in the supramolecular assembly of a particular enantiomer is difficult to predict. An example for opposite-handed supramolecular structures built by equally handed monomers is the formation of chiral rosettes with olig(*p*-phenylene vinylene) derivatives on hopg (Fig. 17). Again, the interplay of lateral hy-

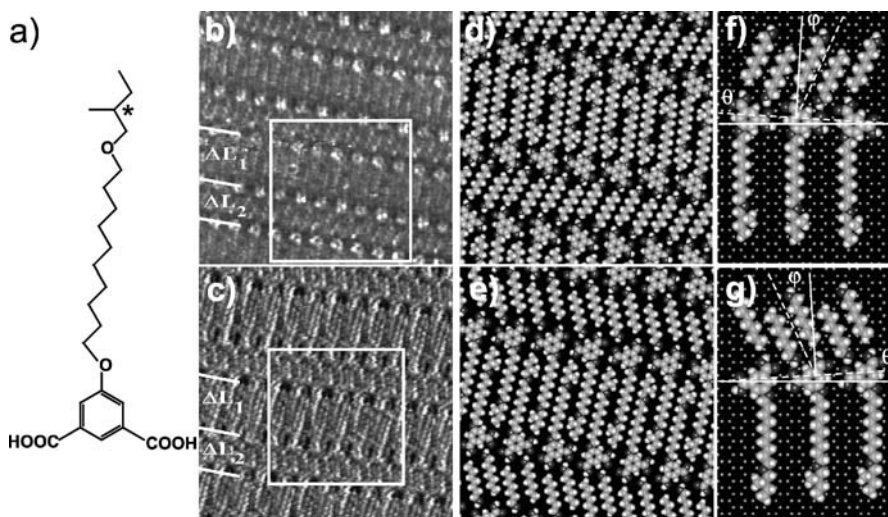


Fig. 16 STM images (**b**: $11.7 \times 11.7 \text{ nm}^2$, **c**: $11.5 \times 11.5 \text{ nm}^2$) and structure models (**d,e**) for the enantiomorphous lamella structures induced by adsorption of ISA (**a**) on hopg from a 1-heptanol solution [47]. For opposite enantiomers, opposite lamella tilt angles (θ) are observed. The large lamella ΔL_1 is built up from pure ISA enantiomers, while the smaller ΔL_2 lamella consists of coadsorbed achiral 1-heptanol molecules. The ISA chirality is transferred to the coadsorbed solvent molecules via opposite alignment angles φ (**f,g**). Reprinted with permission from Wiley

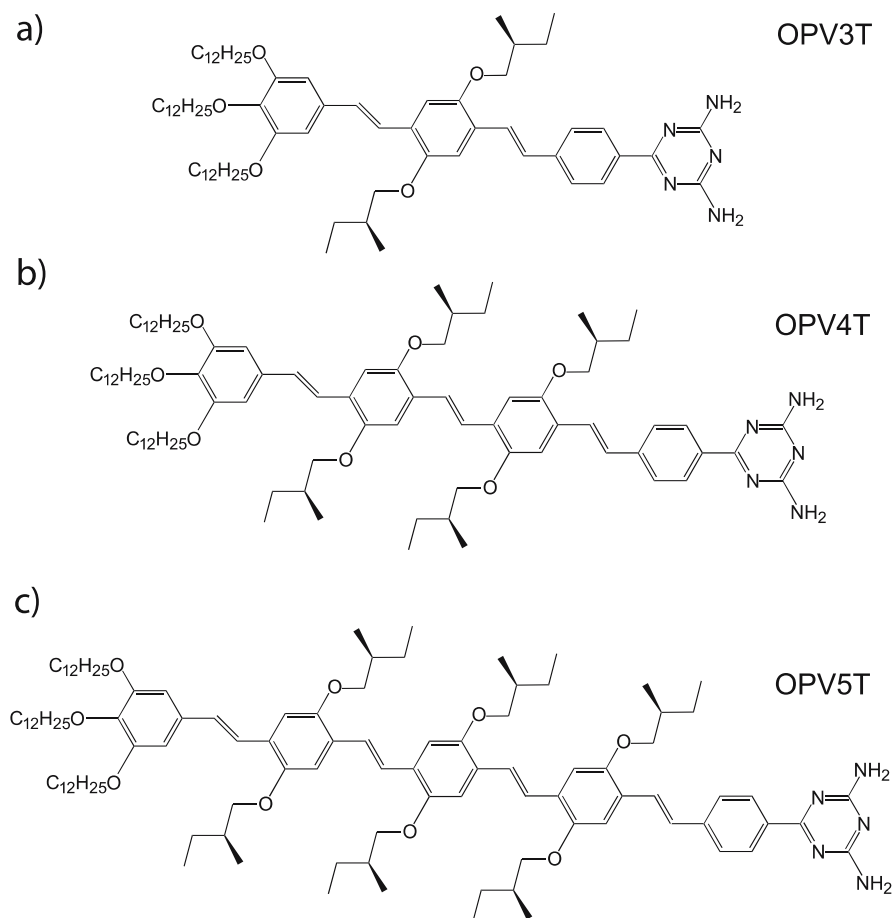


Fig. 17 Oligo(*p*-phenylene vinylene) derivatives (a) OPV3T, (b) OPV4T, and (c) OPV5T

drogen bonding and molecule-substrate interaction govern the pattern formation [48].

Although all stereogenic centers in the side chains have identical handedness, OPV3T forms a CW-rotating rosette, while OPV4T and OPV5T generate CCW-rotated rosettes (Fig. 18). These wheel structures are based on a hydrogen bonding network between six terminal diaminotriazine units. Detailed structure models suggest that for OPV4T and OPV5T denser lateral packing is achieved in a CCW-rotated alignment. For OPV3T, however, this would impose an unfavorable steric interaction between alkyl chains and the terminal phenyl rings, explaining the CW-rotated wheel formation.

The pinwheel structure is not only observed for chiral adsorbates. An early example was reported for small molecules at low temperatures on graphite in UHV (Fig. 19). Neutron and electron diffraction experiments as well as

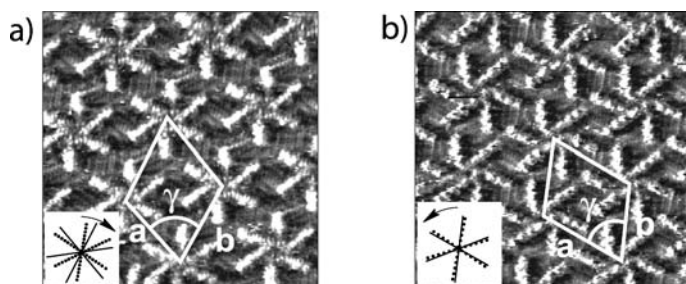


Fig. 18 STM images of OPV3T (14.4 nm × 14.4 nm) and OPV4T (18.4 nm × 18.4 nm) showing opposite rotation directions [48]. Reprinted with permission from Wiley

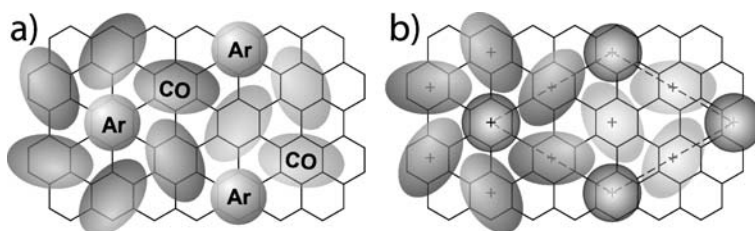


Fig. 19 Pinwheel structures formed by CO adsorbed on hopg: **a** commensurate $\text{Ar}(\text{CO})_3$ lattice, **b** pure but incommensurate $\text{CO}(\text{CO})_3$ layer. Reproduced with permission of the authors of [49, 50]

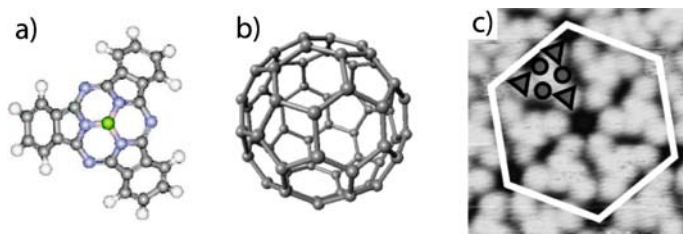


Fig. 20 SubPc **(a)** and C_{60} **(b)** form at 1 : 1 ratio on the Ag(111) surface a six-molecule pin-wheel structure [51]. The STM image **(c)**, 13.6 nm × 13.6 nm) reveals locally only clusters of equal handedness. All subPc molecules (*triangles*) of a single pinwheel are rotated into the same direction. Reprinted with permission from Wiley

mean-field calculations suggested that quadrupole–quadrupole interactions between flat-lying CO molecules favor a pinwheel structure [49]. Coadsorbed argon atoms, having no quadrupole moment, act like lattice vacancies in the center of the wheel. A similar structure, based on static LEED analysis only, has been proposed for pure CO layers in which one molecule in the unit cell, adsorbed in a different geometry (probably in upright adsorption geometry),

serves as the vacancy [50]. In the latter case, however, the structure is incommensurate along one highly symmetric substrate direction.

Electron acceptor–donor interactions should favor intermixing different species at equimolar ratios. This has been confirmed for coadsorption of C_{60} and the three-fold symmetric subPC on Ag(111) [51]. Among other structures, pinwheels are formed under local spontaneous symmetry breaking (Fig. 20). The pinwheels contain three C_{60} and three subPC molecules, which are azimuthally rotated. Because C_{60} acts as an electron acceptor and subPC as a donor, an anti-parallel dipole alignment governs the packing. However, the chiral wheel alignment must be attributed to lateral van der Waals forces in combination with steric repulsion and substrate registry. That is, the densest packing on the Ag(111) surface is achieved by rotating the three subPC molecules plus occupation of a certain surface site. Only one handedness was presented in the original paper, but we assume that both structures have been observed.

3.1.2

Chiral Clusters, Chains and Rings

If lateral attractive forces prevail and mobility of the single unit is sufficient, supramolecular assemblies can be observed at low coverages. This is often observed for intermolecular hydrogen-bonded systems on substrates not interacting too strongly with the adsorbents; e.g., noble metals (Au, Ag) and hogg. A remarkable example is the decamer formation of NN (Fig. 7b) on gold(111) observed via STM at 5 K [52]. The Au(111) substrate embodies alternating domains of hcp- and fcc-stacked surface atoms. At sufficient terrace size, the domain orientations rotate by 120° and form a herringbone structure [53]. The NN molecules nucleate first at the fcc elbows of the herringbone structure. NN decamers are comprised of eight equally handed molecules at the periphery surrounding two opposite handed molecules in the core [54]. This gives the whole cluster a chiral shape (Fig. 21). Also observed were homochiral tetramers [54]. The relatively strong intermolecular hydrogen bonds in a decamer even allowed manipulation of the clusters. Utilizing the STM, a one-by-one lateral separation of opposite-handed clusters was performed like in the classical Pasteur experiment, but this time at the nanoscale [52].

A striking example of mesoscopic pattern formation governed by intermolecular hydrogen bonding on noble metal surfaces is PVBA (Fig. 7a) on Au(111) and Ag(111) [55]. Due to head-to-tail hydrogen bonding between carboxyl and pyridine groups, linear chains are formed (Fig. 22). In addition, hydrogen bonds between aryl hydrogen and the carbonyl oxygen induce formation of twin chains. Since these hydrogen bonds are sensitive to the handedness of the adsorbed PVBA, homochiral recognition between two single strands of a twin chain is observed. The strands are several μm long. The distance between parallel running chains depends on the coverage, since the

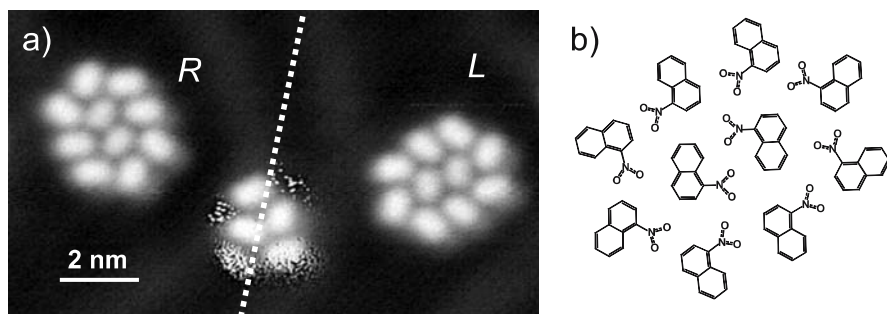


Fig. 21 **a** STM image of chiral clusters formed by ten NN molecules on Au(111) [52]. **b** Structure model for the alignment within a decamer. Reprinted with permission from Wiley

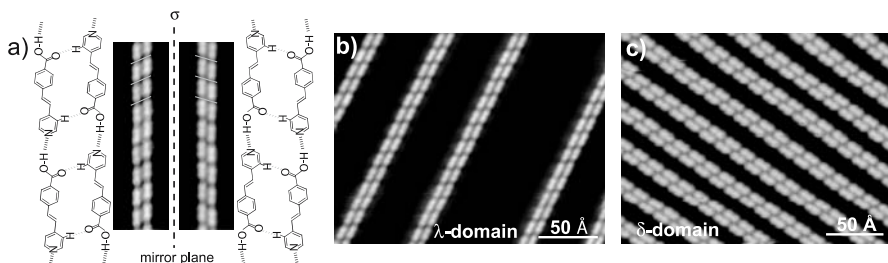


Fig. 22 **a** PVBA forms enantiomorphous twin chains of homochiral composition on Ag(111) and Au(111). **b,c** Depending on the coverage the twin chain distances vary, indicating repulsion between them. Only equally handed chains are observed within one domain. Reprinted with permission from [55]. Copyright (2001) American Physical Society

twin chains do not attract each other. Ignoring metastable deviations, no opposite handed chains have been observed within these gratings; i.e., chiral correlation is extended over large distances without apparent direct molecular contact. However, the mechanism put forward for explaining these homochiral gratings embraces twin chains as the template and metastable triple chains deviating from the template once a fourth chain is formed. The interconversion of enantiomers, e.g. by rotation of the pyridine vinylene group during a partial lift-off from the surface, as a possible alternative for building these long-range homochiral gratings, has been excluded for energetic reasons. Instead, an intramolecular transfer of the carboxyl hydrogen from one oxygen atom to the other in the metastable third chain has been proposed. If we compare this PVBA/Au(111) example with the system PVBA/Pd(111), it becomes clear that mobility of single molecules is very important for chiral pattern formation. Much stronger adsorbate–substrate interactions allow only formation of dimers and trimers on Pd(111) [56].

Homochiral hydrogen bonded linear chiral structures have also been reported for adenine on Cu(110) [57]. In a 2D network of adenine molecules, a number of different intermolecular hydrogen bonds between homo- or heterochiral pairs are possible. The calculated energies for most of these pairs do not differ much [58], but the most stable homochiral hydrogen bridged pair (Fig. 23a) agrees well with a model suggested by STM [57]. The pairs, in turn, are connected via other hydrogen bonds that come into play due to the best fit to the substrate lattice (Fig. 23b). Again, intermolecular lateral bonding and the substrate-adsorbate interactions contribute to the pattern formation. Depending on the handedness of its building blocks, the dimer chain is either aligned parallel along the (1,2) or the $(-1,2)$ direction on the surface; i.e., CW- or CCW-rotated away from the [001] surface direction.

A beautiful example for hierarchical chiral structures is the spontaneous self-assembly of 5,6,11,12-tetraphenylnaphtacene (“rubrene”) on Au(111) [59]. The backbone of the sterically overcrowded rubrene is helically twisted, and its handedness can be directly observed in highly resolved STM images. Beside homochiral chains, rubrene forms a ring structure of five equally handed units, which, in turn, self-assemble into a ring structure containing ten of the pentamers (Fig. 24). Within the pentamers, the monomers are equally rotated for close interdigitation in a gear wheel-like fashion. CCW or CW rotation is representative of the handedness of the monomers. Depending on their chirality, ten pentamers in a pentacontamer are either rotated CW or CCW (Fig. 24c). The handedness of the monomer is thus transferred step-by-step into the supramolecular ring unit of 50 monomers.

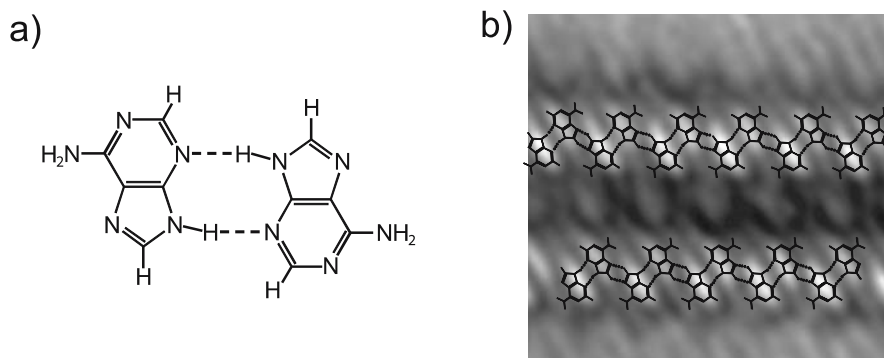


Fig. 23 The most stable hydrogen bonded 2D conformation has been calculated for homochiral pairs of adenine (**a**). The STM image (**b**, $4.2\text{ nm} \times 4.2\text{ nm}$) suggests that these homochiral pairs are connected via other hydrogen combinations into linear chains on Cu(110). Reprinted with permission from [57]. Copyright (2002) American Chemical Society

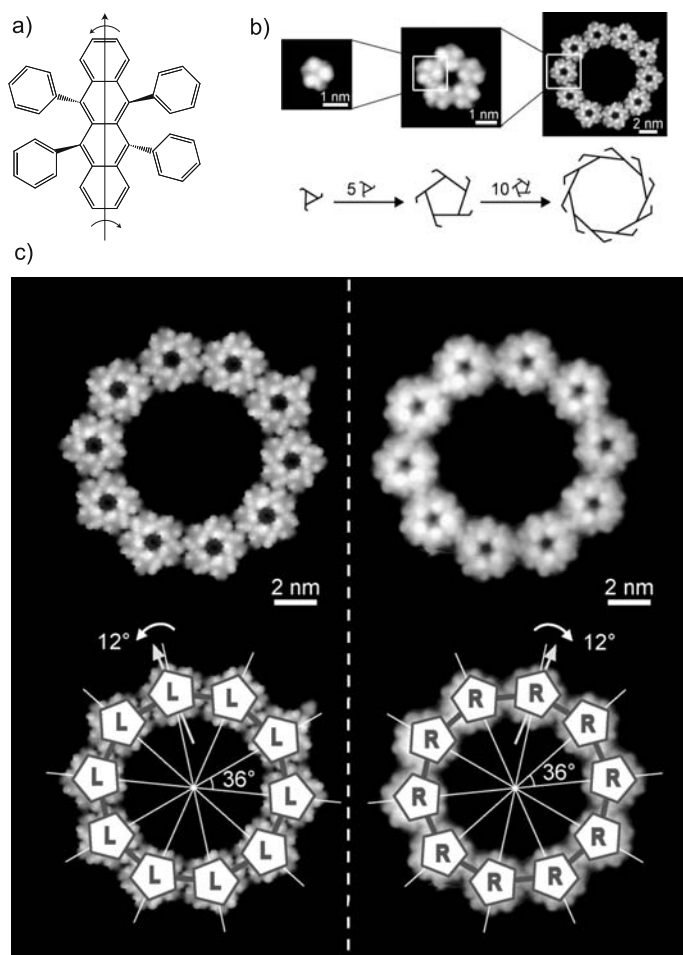


Fig. 24 Hierarchical homochiral self-assembly as observed via STM on Au(111): Chirally distorted rubrene (a) self-assembles in a first step into homochiral pentagons and these, in a second step, into homochiral rings containing 50 monomers, (b) [59]. Within these pentacontamers, all ten pentamers are rotated equally 12° with respect to the virtual spokes of the wheel (c). Reprinted with permission from Wiley

3.1.3

Losing the Expression: Achiral Lattices from Chiral Molecules

In three dimensions, chiral molecules always crystallize in chiral space groups. In order to transfer molecular chirality into supramolecular structures on a surface, the interaction forces must allow the molecular asymmetry to come into play. Very strong interactions with the substrate may force the molecules to align in a symmetry that is strictly dictated by the substrate. Typical examples

are the rectangular adlattices generated by alanine and glycine on Cu(110) and Cu(100) [19, 21, 60–69]. Both species become deprotonated at RT, and annealing to 420 K leads to a tridentate bonding configuration; i.e., carboxylate atoms and the amino group bind to copper atoms of the surface [21]. The adlattice structure formation is governed only by this footprint interaction on the (110) and (100) grid (Table 1), which is so strong that the inherent molecular chirality does not come into play. If not annealed, a chiral (2 – 2, 5 3) phase can be observed for enantiopure alanine on Cu(110) [64, 69].

Another example is the adsorption of prochiral 1,2,4-benzene tricarboxylic acid on Cu(100). As determined via X-ray absorption studies, this molecule has a tilted local geometry on the surface. The adsorbate complex is therefore chiral [70]. The long range ordered adlattice, however, has $p(3 \times 3)$ periodicity; i.e., the molecules are strictly aligned by the quadratic substrate mesh.

(*R,R*)-TA crystallizes in different enantiomorphous superstructures on Cu(110), but at a coverage of 0.25 molecules per substrate atom, the monotartrate species forms an achiral $c(4 \times 2)$ or $(4\ 0, 2\ 1)$ structure [71]. In contrast to the bitartrate in its sawhorse geometry, only a single molecular site is connected to the substrate and chirality is not transferred into the lattice structure. Under these conditions, chiral resolution cannot be expected (see below) [72].

With the chiral center located in a side chain that is bent away from the surface, an achiral lattice is formed by the chiral diacetylene isophthalic acid derivative at the 1-octanol/graphite interface [73]. Because of the relatively weak interaction between the dangling chiral side chains, the achiral part of the molecule interacting with the substrate dominated the pattern formation.

The interaction of molecules with substrate atoms at step edges is usually stronger than with those of a flat terrace. This has consequences for the long-range structure, if the number of step edges becomes considerably large. The Cu(332) surface has a high step density and its (111)-terraces have a width of only 1.2 nm. The distance perpendicular to the steps is just sufficient for one [7]H molecule, and only formation of molecular rows parallel to the steps is possible. This 1D confinement and a specific molecule-step in-

Table 1 The most stable DFT structures of glycine and alanine on Cu(110) and Cu(100) surfaces have rectangular symmetry [60]

	Cu(110)	Cu(100)
Glycine	(3×2) heterochiral	$c(4 \times 2)$ homochiral/ (4×2) heterochiral (“ (2×2) grid”)
Alanine (enantiopure)	(3×2)	$c(4 \times 2)$ homochiral/ (4×2) diastereomeric (“ (2×2) grid”)
Alanine racemic	(3×2) heterochiral	(4×2) heterochiral (“ (2×2) grid”)

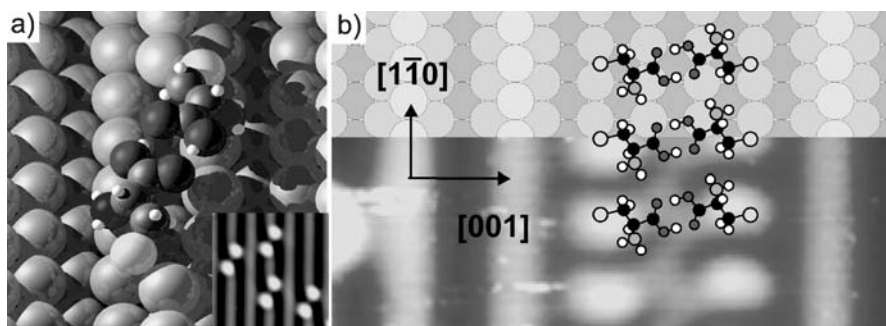


Fig. 25 **a** Homochiral pairs are observed in STM after adsorption of racemic cysteine. *L*-cysteine pairs are tilted CW away from the $[1\bar{1}0]$ substrate direction as clearly observed via STM (*inset*). Reprinted with permission of the authors. **b** Superposition of the most stable structure obtained from DFT calculations and a STM image acquired after annealing of a *D*-cysteine layer at 380 K. By removing the top-most atomic row underneath the cysteine double row structure the (1×1) Au(110) surface is restored. Reprinted with permission from [78]. Copyright (2004) American Physical Society

teraction interfere with the azimuthal transfer mechanism observed on the Cu(111) surface [44]. For the M-enantiomer all molecules were found to occupy an identical azimuthal orientation, not allowing the transfer of helicity into the molecular layer [74].

In the last example here, the interaction of the amino acid cysteine with the Au(110) surface is so strong that a rearrangement of the substrate occurs. The clean Au(110) surface is (1×2) “missing row” reconstructed; i.e., along the $[001]$ direction every second atomic row of this fcc(110) surface (see Fig. 2e) is missing. Upon adsorption of cysteine, however, this reconstruction is lifted locally. At low coverage, homochiral pairs are observed in STM that show, depending on their handedness, opposite tilt angles with respect to the substrate lattice (Fig. 25a) [75]. In combination with specific surface sites occupied by the sulfur atom and amino group, this homochiral recognition is well-explained via the classical three-point contact model [76, 77]. DFT calculations suggested that under every cysteine pair the surface atoms of the densely packed row are etched away. After prolonged annealing at 380 K, unidirectional growth of cysteine double rows is observed (Fig. 25b) [78]. This process goes hand-in-hand with the deconstruction of the Au surface under the cysteine double rows and forces them into an alignment parallel to the $[1\bar{1}0]$ direction.

3.2

Spontaneous Resolution

The most discussed issue in chiral surface science is whether enantiomeric lateral separation occurs after adsorption of racemates. Compared to the

230 space groups of 3D crystals there are only 17 lattices, of which five are chiral. In three dimensions, racemic crystals outnumber chiral conglomerates, but for 2D systems a higher probability of enantiomeric separation has been proposed [79]. Beside lower entropic contributions in 2D, common 3D symmetry elements do not exist on a surface. That is, the inversion center and glide planes or screw axes parallel to the surface are not possible [80]. On the other hand, metastable racemic structures can be the result on a surface with limited mobility. In contrast to crystallization from solution, UHV experiments with coverages up to one monolayer allow only 2D mass transport. Crystallization at full monolayer coverage due to cooling is a disorder–order transition and may lead to metastable racemic structures if lateral long-range mass transport is hindered. But if the barrier for chiral interconversion is small, the low-energy homochiral structure could form without lateral mass transport.

Initially, almost all studied systems seemed to confirm the hypothesis of 2D lateral enantiomeric separation [81]. However, recent reports shine a different light on 2D conglomerate formation [82–88]. Early studies were biased by experimental approach, that is, molecules containing polar groups favor formation of intermolecular hydrogen bonds, and strong lateral interactions lead to more stable networks for STM at RT. Strong and directional interactions, in turn, support chiral recognition in two dimensions. Low temperature STM studies, on the contrary, allow investigation of order phenomena of a wider range of molecules.

One of the early examples for enantiomeric separation was phenylglycine on Cu(110) [89]. The racemic mixture shows in LEED a superposition of two mirror domains, while for the pure enantiomers only the respective single enantiomorphous domain is observed. Like for the above-mentioned benzene/Ni(111) structure, the primary electron beam probes both enantiomorphous domains in case of the racemate. However, to conclude lateral resolution based only on co-existence of mirror domains, is a doubtful procedure, since a non-separated racemate may form—just like achiral molecules—mirror domains as well. For phenylglycine/Cu(110), nevertheless, mixtures with excess of one enantiomer showed the corresponding LEED spots with higher intensity than the opposite mirror domain diffraction spots, strongly supporting the separation scenario. That is, the LEED intensity, which is proportional to the total area of the corresponding mirror domains, scaled linearly with ee. The STM image of two opposite homochiral mirror domains of phenylglycine on Cu(110) are shown in Fig. 26. The fact that the local structure within the domains is identical with the structure observed after adsorption of enantiopure phenylglycine finally confirms the spontaneous resolution for the racemate.

A remarkable example of spontaneous resolution is the adsorption of achiral NP (Fig. 7c) on the reconstructed Au(111) surface [90]. Within one domain only one handedness has been observed by highly-resolved STM. Since

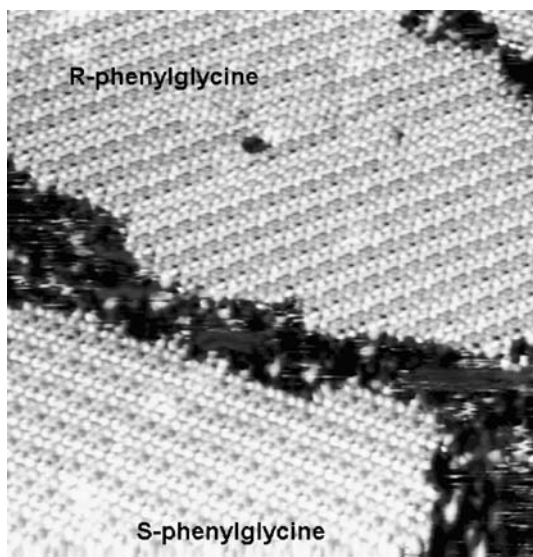


Fig. 26 STM image ($27\text{ nm} \times 27\text{ nm}$) showing two enantiomorphous domains of R- and S-phenylglycine on Cu(110) after adsorption of the racemate. Courtesy of N.V. Richardson

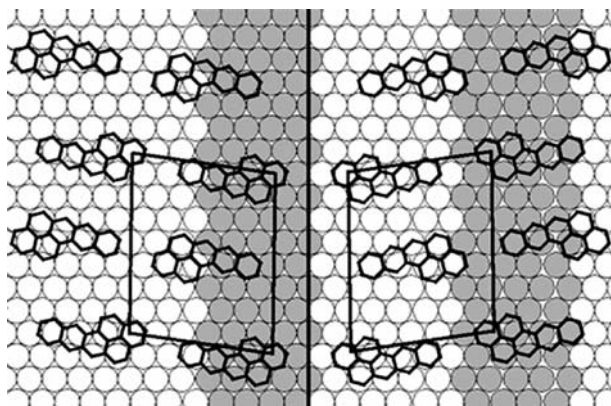


Fig. 27 NP on Au(111) forms enantiomorphous homochiral domains. Grey areas represent up-lifted atoms of the reconstructed clean surface. Reprinted in part with permission from [90]. Copyright (2003) American Chemical Society

the NP layer is not densely packed to such an extent that this packing results from steric reasons, we assume that the equal handedness is substrate mediated. The homochiral alignment must stem from occupation of favored substrate binding sites. The model in Fig. 27 shows the terminal C6 rings atop sites of substrate atoms, and the white and grey areas represent the hcp and fcc stacked domains of the reconstructed Au surface. Reflection of a single

molecule does not lead to identical (energetically favored) adsorption sites. A racemic lattice for adjacent molecules is thus avoided. This exemplifies the role of the substrate in 2D supramolecular chemistry. For this system, a second homochiral structure built up by “69” pairs has been identified [91].

Among the systems showing lateral resolution is the above-mentioned long-alkyl-chain-ISA/heptanol/hopg system [47]. Prochiral 1,5-bis(3'-thia-alkyl) anthracenes, on the other hand, have been demonstrated to show either lateral resolution or 2D racemate formation [85]. Highest packing density is achieved when the terminal bonds of the alkyl chain are oriented parallel to the aryl-C1 bonds (Fig. 28). Consequently, interdigitation of alkyl chains with an even number of bonds aligns anthracenes of adjacent rows with opposite enantiotopic faces toward the surface (Fig. 28a). Adding one methylene group to the alkyl chain, in turn, switches the assembly from the 2D racemate to a 2D conglomerate (Fig. 28b).

Chiral 9,10-iodine-substituted octadecanol is another example of a system that does not undergo spontaneous resolution on hopg [84]. Adjacent rows are packed head-to-head interacting via hydrogen bonding between the OH-groups. A parallel orientation of alkyl chains is best achieved for the same enantiomers. STM further reveals that the optical isomers have different apparent heights and are separated into different rows. That is, closest packing is achieved by pointing the iodine atoms away from the surface for one enantiomer and being buried underneath the alkyl chain for the other enantiomer.

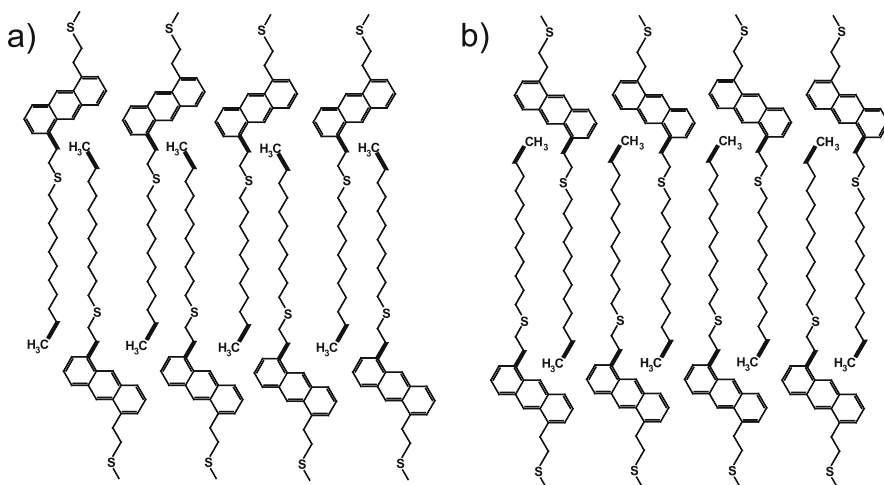


Fig. 28 Model structure for bis-thiaalkylanthracene derivatives on hopg. Depending on alkyl chain length, either crystallization as 2D racemate (**a**) or spontaneous resolution (**b**) occurs. Terminal bonds of the alkyl chains and the aryl-C1 alkyl chain (*bold sticks*) are forced into a parallel arrangement by steric means. Reproduced with permission of the authors [85]

It is worth mentioning that in this orientation on the surface, the two enantiomers of a single pair are not superimposable by a glide plane operation with the plane perpendicular to the surface. Consequently, a heterochiral pair forms a chiral entity and the lattice is “pseudo-racemic”.

Although devoid of alkyl chains, [7]H on Cu(111) forms, similar to 9,10-iodo-octadecanol and the anthracene derivative shown in Fig. 28a, a racemic lattice structure. Conglomerate formation was initially concluded from LEED, because the mirror domain pattern observed for the racemate was identical to the superimposed patterns of the pure enantiomers [92]. STM images, however, delivered different lattice structures for the mirror domains of the racemate and the pure enantiomers [93]. High-resolution STM and MMC finally showed that the enantiomorphous domains are racemic [88]. We will return to this system in more detail in Sect. 4.

Depending on the local molecular adsorption geometry, lateral interactions can vary substantially. Therefore, 2D-resolution may switch for a single compound. The already mentioned TA/Cu(110) system undergoes, depending on temperature and/or coverage, different types of phase transitions. Upon thermal activation, bitartrate species are formed from the initially generated monotartrate species at RT [71]. With increasing coverage, however, the newly adsorbed TA molecule hydrogenates the doubly deprotonated C_2 -symmetric bitartrate species to monotartrate again [71, 94]. Besides this new local adsorption geometry, the enantiomorphous (9 0, 1 2) lattice disappears and an achiral (4 0, 1 2) lattice is formed [71]. For racemic TA, a lateral resolution occurs only for the bitartrate species where homochiral (9 0, 1 2) and (9 0, -1 2) domains are present [72]. The non-enantiomorphous (4 0, 1 2) monotartrate lattice, however, is heterochiral; but as we will see in the next section, the “achiral” enantiopure and racemic (4 0, 1 2) lattices still show subtle differences.

The “2D chiral” systems of NN and PVBA do not need a change in local adsorbate geometry in order to show a chiral phase transition [83, 86]. Homochiral structures have been observed for PVBA (Fig. 7a) and SDA on Cu(100) [95]. A CW-rotated structure contains exclusively λ -PVBA, while the CCW-rotated structure contains only δ -PVBA (Fig. 29) [86]. Increasing the PVBA coverage above 0.05 molecules per copper atom induces a phase transition into a single achiral structure that possesses two mirror planes (Fig. 29c). Highly resolved STM shows that this structure is now comprised of a δ -/ λ -PVBA racemate and that the unit cell contains equal numbers of CCW- and CW-rotated units.

A coverage dependence of 2D conglomerate or racemate formation was first observed for NN on Au(111). In that case, the transition from homochiral chain structures to heterochiral 2D domains is strongly influenced by the hcp-fcc substrate reconstruction sites of the substrate [83].

The fate of resolution is actually determined by the free energy of the system; i.e., the energy difference between homo- and heterochiral structure.

If this energy difference is very small, coexistence of both can be the result. For glycine on Cu(100), several structures have been proposed [61]. DFT calculation clearly favored a (4×2) homochiral and a $(4 \times 2)pg$ heterochiral/“pseudo (2×2) ” structure (Fig. 30) over other possible structures [67]. Because of a very small energy difference between these two structures, they are expected to coexist on the surface (see Table 1).

Finally, we mention a remarkable example of lateral resolution reported for supramolecular nanostructures on hopg [96]. Held together by 72 hydrogen bonds, the molecular nanostructure is formed from three melamine-substituted calix[4]arene units and twelve 5,5-diethylbarbiturate molecules (Fig. 31a). The nanostructure, basically a stack of four rosettes, has chiral symmetry. With its components all being achiral, both enantiomers are formed upon self-assembly in solution. Deposition of the tetra-rosettes on hopg leaves this nanostructure intact and allows surface self-assembly. AFM studies revealed close-packed 2D lattices formed by the tetra-rosettes on hopg

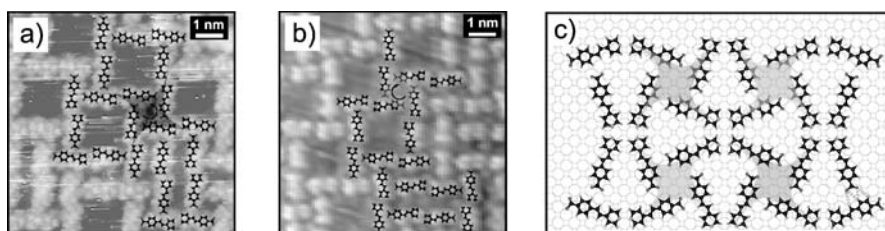


Fig. 29 **a,b** Clockwise and counterclockwise rotated domains contain exclusively λ - or δ -PVBA molecules, respectively. **c** At coverages exceeding the critical value of one molecule per 20 Cu-atoms, a butterfly structure comprising both enantiomers is formed. Reprinted in part with permission from [86]. Copyright (2005) American Chemical Society

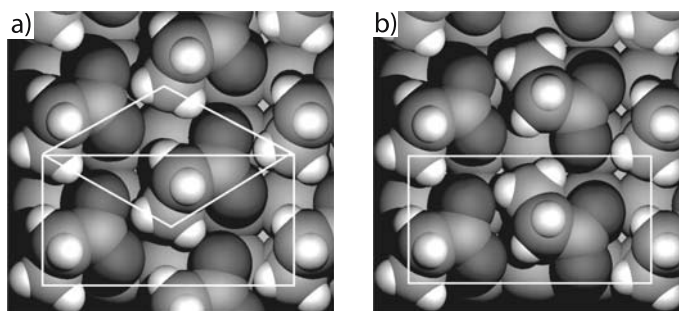


Fig. 30 Lowest energy configurations for glycine on Cu(100). **a** Homochiral $c(4 \times 2)$ glycine layer, as indicated by the rectangular cell. Also shown is the $(\sqrt{2} \times \sqrt{2})45^\circ$ unit cell. **b** Heterochiral $(4 \times 2)pg$ structures of glycine on Cu(100). Ignoring the handedness, the molecules form a (2×2) grid on the surface. Reprinted in part with permission from [67]. Copyright (2005) American Chemical Society

(Fig. 31b). In addition to rotational symmetry reflecting the symmetry of the substrate, mirror-like structures have been observed. Taking into account the extent of lateral interactions due to the large size of the nanostructures, this observation strongly suggests that the P and M enantiomers of

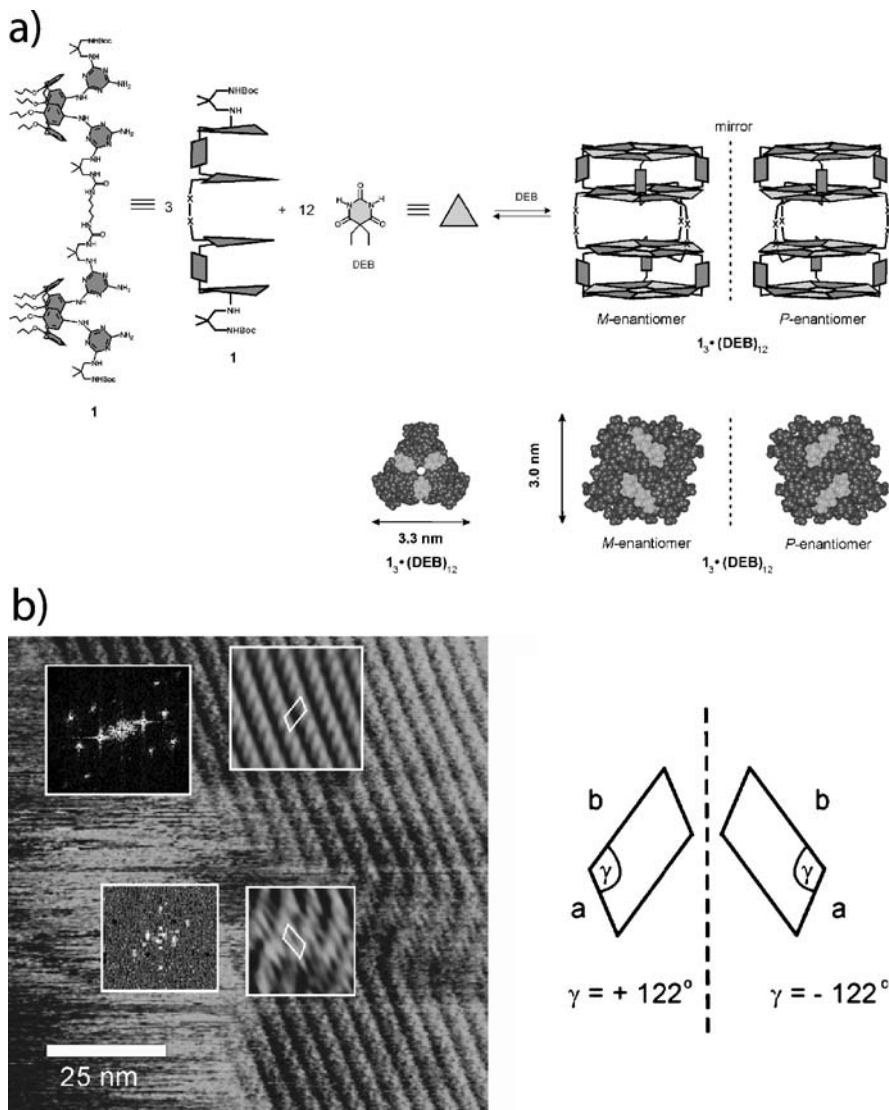


Fig. 31 Self-assembly of chiral nanostructures on hopg. Melamine-calix[4]arene units self-assemble with diethylbarbiturate (DEB) into chiral tetra-rotosettes (a) [95]. The nanostructures form different 2D domains with unit cells being mirror images of each other (b). Reprinted with permission from Wiley

the tetra-roses undergo spatial resolution and crystallize in 2D homochiral domains.

3.3

Enantiospecific Surface Chemistry

Since pre-adsorbed chiral modifiers like cinchonidin or TA are assumed to influence the adsorption geometry of prochiral keto-esters, we deal here with intermolecular chiral recognition on a surface. However, whether supramolecular features or single reactant-modifier interactions play a role in these processes is not clear. Chiral voids between long-range ordered enantiomorphous domains have been proposed as enantioselective reaction sites [97] and the homochiral alignment of MAA due to coadsorbed long-range ordered (*R,R*)-TA on Ni(100) has been shown directly in STM [98]. Long-range ordered structures, on the other hand, were suspected to suppress the single molecule-modifier interaction and were blamed for low enantioselectivity [99].



Scheme 2 Decomposition reaction of monotartrate on Cu(110)

The influence of chirality in a 2D supramolecular array on a chemical reaction has clearly been demonstrated recently [100]. The thermally induced decomposition reaction of mono-TA on Cu(110) in vacuum (Scheme 2) is catalyzed by free surface sites. Since the decomposition, in turn, creates active sites, the reaction is under autocatalytic control. In addition, the stability of monotartrate is enhanced due to the close-packed monolayer structure not allowing interaction of upper parts of the molecule with the surface in the first place. This leads upon heating to complete decomposition in a small temperature interval (i.e. 1.6 K) once the reaction has started. Because the gaseous decomposition products desorb instantaneously at decomposition temperature, a sharp pressure rise is observed. Therefore, this type of autocatalytic decomposition was coined “surface explosion” [101]. The initial step requires a rearrangement of the upper part of the molecule in order to get in contact with the surface in a densely packed environment, and that is where the supramolecular chirality, i.e., the handedness of adjacent molecules, plays a role. As already mentioned, racemic monotartrate is not enantioseparated on Cu(110), but forms at 405 K the same $c(4 \times 2)$ lattice structure as enantiopure TA; i.e., with identical periodicity and coverage. A direct comparison of decomposition temperature and decomposition kinetics of both structures reveals remarkable differences which were assigned to a supramolecular ensemble effect (Table 2). The decomposition temperature for the enantiopure structure exceeds the one for the racemic structure by 8 K. The higher stability of the enantiopure structure can be explained by the more extended

Table 2 Comparison of decomposition data of enantiopure and racemic monotartrate monolayers on the copper surface

	ΔE kJ mol^{-1}	A s^{-1}	T_{dec} K
<i>R, R</i>	162	10^{15}	517
rac.	142	10^{14}	509

H-bonding network, whereby the initial “unhinging” process from the lateral mesh of next neighbors has a higher activation barrier than for the racemic structure.

3.4

Diastereoisomeric Recognition

In addition to the chiral interactions of enantiomers, interactions of dissimilar chiral species are fundamentally important. As described above, adenine becomes chiral upon adsorption and forms homochiral dimer chains on Cu(110). These chains are tilted $\pm 19.5^\circ$ with respect to the [001] surface direction. This tilt makes the sites right next to an enantiomorphous supramolecular chain chiral! Consequently, the interactions of inherently chiral molecules with both chain types are energetically nonequivalent. This

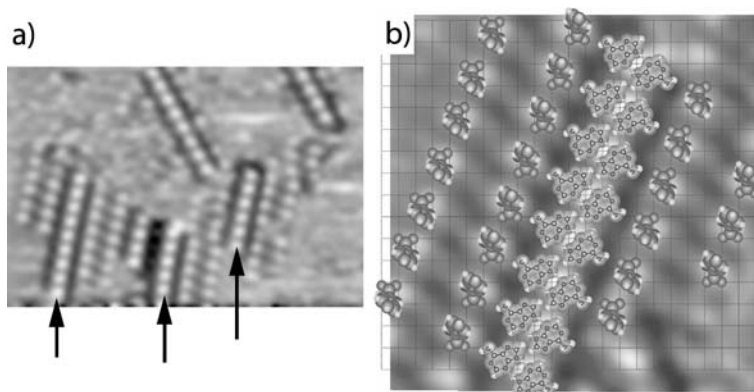


Fig. 32 Enantiospecific recognition between the nucleic acid base adenine and the amino acid phenylglycine on Cu(110) [102]. **a** STM image ($15 \text{ nm} \times 10 \text{ nm}$) of coadsorbed *S*-phenylglycine and alanine. Only the CW-rotated adenine double rows, marked by *arrows*, are decorated with *S*-phenylglycine double rows. **b** Structure model superimposed on the STM image of adenine/*S*-phenylglycine. The carboxylate oxygens and the N atom have been placed atop Cu atoms. Reprinted with permission of the authors

has been beautifully demonstrated for phenylglycine coadsorbed with adenine. *S*-phenylglycine was found to bind only to adenine double chains that were CW rotated with respect to the [001] surface direction (Fig. 32) [102]. Interestingly, the adenine double rows were decorated with double rows of phenylglycine on both sides. Hydrogen bonding and dipole–dipole interactions in combination with preferred substrate sites have been put forward as dominating lateral interaction forces. With the carboxyl and amino group of phenylglycine bound to specific Cu-atoms and hydrogen bonding to the adenine amino group, the three-point contact model explains the chiral recognition of the first phenylglycine row. The relatively large inter-row spacing of the phenylglycine double rows, however, suggests a stronger role of the surface. Local strain or charge density waves, for example, have been discussed in order to explain voids or large distances between molecular structures [103, 104].

4

Amplification of Chirality in Two Dimensions

One of the most recent observations in supramolecular surface chirality is the induction of homochirality on surfaces via cooperatively amplified interactions in molecular monolayers. As discussed in Sect. 2, adsorption-induced chirality leads to both mirror motifs. However, in the presence of additional chiral bias, “lattice homochirality” can be installed in the entire molecular layer. Such bias comes from a chiral dopant, small ee or physical fields in combination with symmetry breaking of the surface.

Chiral amplification phenomena have been observed for helical polyisocyanate copolymers and were coined as the “sergeants-and-soldiers” principle and “majority rule” [105, 106]. Small amounts of chiral groups in the side chain or small ee gave enough bias for single helicity in the entire polymer chain. Because helix reversals are energetically unfavorable, a small symmetry breaking influence suffices to induce single helicity [107]. Both effects were explained by a one-dimensional random field Ising model based on cooperative interactions of the polymer backbone units [108, 109].

4.1

Homochirality from Prochiral Precursors

The coadsorption of chiral molecules into racemic layers is an efficient way to induce further asymmetrization towards single handedness. While in heterogeneous chiral catalysis the stationary ratio of modifier and reactant at the surface is assumed to be one, a small amount of chiral dopant can be sufficient for induction of homochirality on the entire surface! SU on Cu(110), for example, forms two enantiomorphous domains in its bisuccinate phase [27].

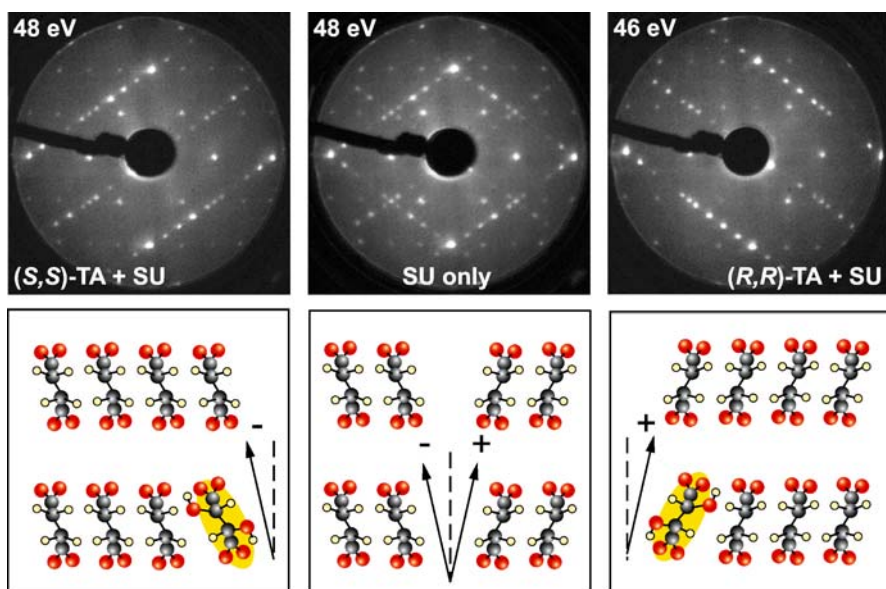


Fig. 33 Homochirality induced by chiral doping in enantiomorphous succinic acid (SU) monolayers observed by LEED. Doping with 2 mol% (S,S)-TA (*left*) or 2 mol% (R,R)-TA (*right*) allows only formation of one enantiomorphous mirror domain, while the undoped SU layer shows both domains (*middle*). Reprinted with permission from [28]. Copyright (2004) American Chemical Society

It is reasonable to assume that the molecules in these domains have opposite handedness. Doping the SU layer with one TA enantiomer suppresses completely the formation of one mirror domain and installs global homochirality [28]. The opposite TA enantiomer suppresses the opposite SU enantiomorph (Fig. 33). Since hydrogen bonds between the bisuccinate molecules cannot be expected to play a role, one must consider a substrate-mediated mechanism. That is, a chiral footprint onto the surface acts as a chiral bias and suppresses opposite handedness in the adjacent adsorbate complex. A chiral footprint reconstruction has also been proposed for the TA/Ni(110) system [110]. The same type of homochirality inductions have been shown for (S,S)- or (R,R)-TA-doped (R,S)-TA monolayers on Cu(110) [29].

4.2

Homochiral Pseudo-Racemic Systems

The equivalent to the majority rule, but in two dimensions, has been reported recently for [7]H on Cu(111). In that case, a small ee induces homochiral long-range order [88]. As mentioned above, the two [7]H enantiomers crystallize in a 2D racemic lattice, which forms two enantiomorphous do-

main [93]. The difference of both mirror domains is based on the relative alignment of two enantiomers in a heterochiral pair on the surface (Fig. 34). A glide plane operation connects the two enantiomers but is not a symmetry operation for this 2D lattice. Because of steric constraints, any ee is expelled from these racemic enantiomorphous domains during crystallization. From the domain boundaries, however, the excess molecules have an influence on the relative alignment of the heterochiral pairs at the domain edge. M-[7]H excess favors formation of λ -domain pairs and P-[7]H excess ρ -domain pairs. This chiral bias is amplified by the cooperative interaction among heterochiral pairs, strongly favoring an equal alignment. Like helix reversals in a polymer chain, opposite alignment would create energetically unfavorable mirror domain boundaries. Even for the racemate, these boundaries are rarely observed on a single terrace, and locally spontaneous symmetry breaking occurs. Nevertheless, the number of λ - and ρ -domain decorated terraces is equal. From ee = ± 0.08 on, the entire surface—although still close to racemic content—is driven into a homochiral arrangement during 2D crystallization and only λ - or ρ -domains are observed. In contrast to the SU-TA-doped system, where the molecular frame of the molecule is switched to its mirror configuration, interconversion between both structures here requires only a change in relative position of both enantiomers of a heterochiral pair. Chiral resolution is not required. Similar studies performed with chiral long alkyl chain formamide on hopg under 1-heptanol did not reveal any amplification mechanism; the domain orientation scaled directly with ee [111].

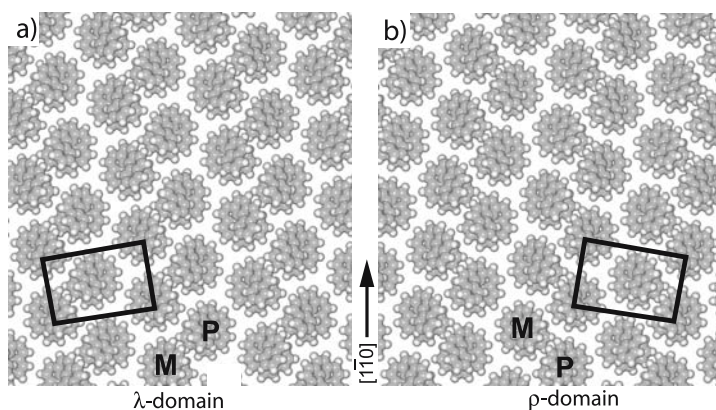


Fig. 34 Racemic but enantiomorphous structures of [7]H on Cu(111) [88]. Opposite tilt angles with respect to a highly symmetric substrate direction of heterochiral M–P double rows create left-tilted λ domains (a) and right-tilted ρ domains (b). The sign of the tilt angle is determined by the relative position of the M–P enantiomers in a heterochiral pair

4.3

Magnetic Field-Induced Enantiomeric Excess

Surface-induced ordering in LCs has been known for a long time, but the reverse process, i.e., ordering of the adsorbate layer due to oriented molecules in the fluid above the surface, is quite a new phenomenon [112]. Although the alignment of a single molecule is still governed by the substrate lattice, formation of certain rotational or mirror domains can become unfavorable if the molecules in the liquid phase are pre-aligned. For a nematic fluid, this can be achieved by a magnetic field. Because of the collective interactions in the LC, the weak magnetic forces are magnified and induce polar order. If for prochiral LC-molecules a pre-alignment is maintained in an oblique angle with respect to a highly symmetric substrate lattice dur-

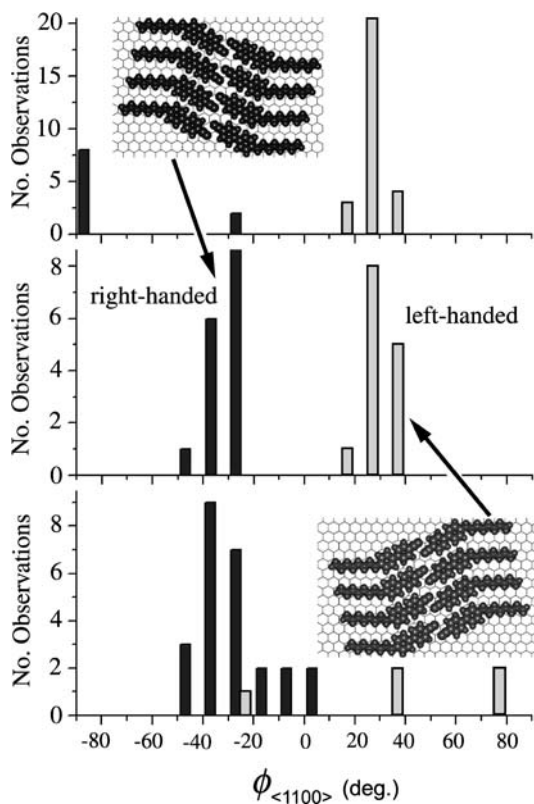


Fig. 35 Magnetic field aligned LC molecules show a preferred formation for single enantiomorphism on hopg [112]. With the field vector pointing either $+19^\circ$ or -19° away from the $\langle 1100 \rangle$ directions, either left- or right-handed domains prevail (*top* and *bottom*), the vector aligned parallel to the $\langle 1100 \rangle$ directions has no effect. Reprinted with permission of Wiley

ing adsorption, chiral symmetry breaking can occur. Such an effect has been reported for 8CB when cooled down from 100 °C to RT in a field of 1.2 Tesla [113]. This LC molecule itself forms enantiomorphous lamella structures on hopg [114].

With the field directed in an angle of -19° or $+19^\circ$ with respect to the $\langle 1100 \rangle$ directions of hopg, the vast majority of domains shows identical enantiomorphism (Fig. 35). As already realized by Faraday and Lord Kelvin more than 100 years ago, a magnetic field alone has no chirality. Furthermore, it is not strong enough to realign adsorbed molecules. The chiral symmetry breaking is actually induced by the surface during adsorption of the polar ordered 8CB. While the cyano head group tends to be aligned parallel to the magnetic field and the alkyl chain prefers alignment parallel to the $\langle 1100 \rangle$ surface directions, any oblique angle of the bulk director with respect to the substrate breaks the left-right symmetry during adsorption. Once locked in, however, the alignment is amplified by the supramolecular monolayer structure forcing additional molecules into homochiral alignment.

5

Outlook

Chiral surface science is still in its infancy. Most of the information has been gathered during the last few years only. With the further development of experimental and theoretical tools, in particular DFT methods, much new insight on 2D intermolecular interactions will be achieved in the near future. Chirality is a wonderful approach in order to better understand complex molecular interactions. Many cooperative phenomena ruling supramolecular processes are still waiting to be understood and to be described on a molecular level. From the riddle of the transfer of molecular structure into the shape of (enantiomorphous) crystals to the influence of small impurities deciding the outcome of macroscopic shape, a 2D model systems will help to understand these complex mechanisms. Beyond that, well-characterized 2D systems are an excellent starting point in studying the structural transfer mechanisms into the 3D world.

Acknowledgement I thank André Niederer for his help drawing the figures.

References

1. Christmann K (1991) Introduction to Surface Physical Chemistry. Springer, Berlin Heidelberg New York (Steinkopf, Darmstadt)
2. Schipper PE, Harrowell PR (1983) J Am Chem Soc 105:723
3. Ward M (2003) Nature 426:615

4. Hazen RM, Sholl DS (2003) *Nat Mater* 2:367
5. Nandi N, Vollhardt D (2003) *Chem Rev* 103:4033
6. Kuzmenko I, Rapaport H, Kjaer K, Als-Nielsen J, Weissbuch I, Lahav M, Leiserowitz L (2001) *Chem Rev* 101:1659
7. Weissbuch I, Kuzmenko I, Berfeld M, Leiserowitz L, Lahav M (2000) *J Phys Org Chem* 13:426
8. Stine KJ (2002) *Encyclopedia of Surface and Colloid Science*. Marcel Dekker, New York, p 1017
9. Masel RI (1996) *Principles of Adsorption and Reaction on Solid Surfaces*. Wiley, New York
10. Wood EA (1964) *J Appl Phys* 35:1306
11. Park RL, Madden HH Jr (1968) *Surf Sci* 11:188
12. Unertl WN (1996) Physical structure. In: Holloway S, Richardson NV (eds) *Surface crystallography, handbook of surface science* 1. Elsevier, Amsterdam, chap. 1
13. Ertl G, Küppers J (1985) *Low Energy Electrons and Surface Chemistry*, 2nd ed. Wiley-VCH, Weinheim
14. Paparazzo E (2003) *Nat Mater* 2:351
15. De Feyter S, De Schryver FC (2005) *J Chem Phys B* 109:4290
16. Tersoff J, Hamann DR (1985) *Phys Rev B* 31:805
17. Jung TA, Schlittler RR, Gimzewski JK, Tang H, Joachim C (1996) *Science* 271:181
18. Hla SW, Bartels L, Meyer G, Rieder KH (2000) *Phys Rev Lett* 85:2777
19. Atanasoska LL, Buchholz JC, Somorjai GA (1978) *Surf Sci* 72:189
20. Pendry JB (1994) *Surf Sci* 299/300:375
21. Barlow S, Raval R (2003) *Surf Sci Rep* 50:201
22. Chen Q, Frankel DJ, Richardson NV (2002) *Surf Sci* 497:37
23. DeFeyter S, De Schryver (2003) *Chem Soc Rev* 32:139
24. Cai Y, Bernasek SL (2005) *J Phys Chem B* 109:6233
25. Fasel R, Wider J, Quitmann C, Ernst KH, Greber T (2004) *Angew Chem Int Ed* 43:2853
26. Barbosa LAMM, Sautet P (2001) *J Am Chem Soc* 123:6639
27. Humblot V, Ortega Lorenzo M, Baddeley CJ, Haq S, Raval R (2004) *J Am Chem Soc* 126:6460
28. Parschau M, Romer S, Ernst KH (2004) *J Am Chem Soc* 126:15398
29. Parschau M, Kampen T, Ernst KH (2005) *Chem Phys Lett* 407:433
30. Lopinski G, Moffat DJ, Wayner DDM, Wolkow RA (1998) *Nature* 392:909
31. Baiker A (2000) *J Mol Catal A: Chemical* 163:205
32. Izumi Y (1983) *Adv Catal* 32:215
33. Kruchten F, Knorr K, Volkmann UG, Taub H, Hansen FY, Matthies B, Herwig KW (2005) *Langmuir* 21:7507
34. Charra F, Cousty J (1998) *Phys Rev Lett* 80:1682
35. Qiu X, Wang C, Zeng Q, Xu B, Yin S, Wang H, Xu S, Bai C (2000) *J Am Chem Soc* 122:5550
36. Qiu X, Wang C, Yin S, Zeng Q, Xu B, Bai C (2000) *J Phys Chem B* 104:3570
37. Steinrück HP, Huber W, Pache T, Menzel D (1989) *Surf Sci* 218:293
38. Neuber M, Schneider F, Zubrägel C, Neumann M (1995) *J Phys Chem* 99:9160 and refs therein
39. Weissbuch I, Addadi L, Lahav M, Leiserovitz L (1991) *Science* 253:637
40. Bouropoulos N, Weiner S, Addadi L (2001) *Chem Eur J* 7:1881
41. Orme CA, Noy A, Wierzbicki A, McBride MT, Grantham M, Teng HH, Dove PM, DeYoreo JJ (2001) *Nature* 411:775

42. Ahmadi A, Attard GA, Feliu J, Rodes A (1999) *Langmuir* 15:2420
43. Horvath JD, Gellman A (2002) *J Am Chem Soc* 124:2384
44. Fasel R, Parschau M, Ernst KH (2003) *Angew Chem Int Ed* 42:5178
45. Stocker W, Schumacher M, Graff S, Thierry A, Wittmann JC, Lotz B (1998) *Macromolecules* 31:807
46. De Rosa C (2003) *Top Stereochem* 24:71
47. De Feyter S, Grim PCM, Rücker M, Vanoppen P, Meiners C, Sieffert M, Valiyaveetil S, Müllen K, De Schryver FC (1998) *Angew Chem Int Ed Engl* 37:1223
48. Miura A, Jonkheijm P, De Feyter S, Schenning APHJ, Meijer EW, Schryver FC (2005) *Small* 1:131
49. Yoo H, Fain SC Jr, Satija S, Passell L (1986) *Phys Rev Lett* 56:244
50. Yoo H, Fain SC Jr (1985) *Surf Sci* 151:361
51. de Wild M, Berner S, Suzuki H, Yanagi H, Schlettwein D, Ivan S, Barattoff A, Güntherodt H-J, Jung TA (2002) *ChemPhysChem* 3:881
52. Böhrringer M, Morgenstern K, Schneider WD, Berndt R (1999) *Angew Chem Int Ed* 38:821
53. Barth JV, Brune H, Ertl G, Behm RJ (1990) *Phys Rev B* 42:9307
54. Böhrringer M, Morgenstern K, Schneider WD, Berndt R, Mauri F, De Vita A, Car R (1999) *Phys Rev Lett* 83:324
55. Weckesser J, De Vita A, Barth JV, Cai C, Kern K (2001) *Phys Rev Lett* 87:096101
56. Kim BI, Cai C, Deng X, Perry SS (2003) *Surf Sci* 538:45
57. Chen Q, Frankel DJ, Richardson NV (2002) *Langmuir* 18:3219
58. Kelly REA, Kantorovich LN (2005) *Surf Sci* 589:139
59. Blüm M-C, Čavar E, Pivetta M, Patthey F, Schneider WD (2005) *Angew Chem Int Ed* 44:5334
60. Toomes RL, Kang JH, Woodruff DP, Polcik M, Kittel M, Hoefl JT (2003) *Surf Sci Lett* 522:L9
61. Efsthathiou V, Woodruff DP (2003) *Surf Sci* 531:304
62. Egawa C, Iwai H, Kabutoya M, Oki S (2003) *Surf Sci* 532:233
63. Iwai H, Tobisawa M, Emori A, Egawa C (2005) *Surf Sci* 574:214
64. Barlow SM, Louafi S, Le Roux D, Williams J, Muryn C, Haq S, Raval R (2004) *Langmuir* 20:7171
65. Rankin RB, Sholl DS (2004) *Surf Sci* 548:301
66. Rankin RB, Sholl DS (2005) *Surf Sci Lett* 574:L1
67. Rankin RB, Sholl DS (2005) *J Phys Chem B* 109:16764 and refs therein
68. Sayago DI, Polcik M, Nisbet G, Lamont CLA, Woodruff DP (2005) *Surf Sci* 590:76
69. Barlow SM, Louafi S, Le Roux D, Williams J, Muryn C, Haq S, Raval R (2005) *Surf Sci* 590:243
70. Dmitriev A, Spillmann H, Lin N, Barth JV, Kern K (2003) *Angew Chem Int Ed* 42:2670
71. Ortega Lorenzo M, Haq S, Bertrams T, Murray P, Raval R, Baddeley CJ (1999) *J Phys Chem B* 103:10661
72. Romer S, Behzadi B, Fasel R, Ernst KH (2005) *Chem Eur J* 11:4149
73. Zhang J, Gesquière A, Sieffert M, Klapper M, Müllen K, De Schryver FC, De Feyter S (2005) *Nano Lett* 5:1395
74. Fasel R, Cossy A, Ernst KH, Baumberger F, Greber T, Osterwalder J (2001) *J Chem Phys* 115:1020
75. Kühnle A, Linderroth TR, Hammer B, Besenbacher F (2002) *Nature* 415:891
76. Easson LH, Stedman E (1933) *Biochem J* 27:1257
77. Booth TD, Wahnnon D, Wainer IW (1997) *Chirality* 9:96

78. Kühnle A, Molina LM, Linderroth TR, Hammer B, Besenbacher F (2004) *Phys Rev Lett* 93:086101
79. Arnett EM, Chao J, Kinzig B, Stewart MV, Thompson O, Verbiar RJ (1982) *J Am Chem Soc* 104:389
80. Lahav M, Leiserowitz L (1999) *Angew Chem Int Ed* 38:2533
81. Pérez-García L, Amabilino DB (2002) *Chem Soc Rev* 31:342
82. De Feyter S, Gesquière A, Wurst K, Amabilino DB, Veciana J, De Schryver FC (2001) *Angew Chem Int Ed* 40:3217
83. Böhringer M, Schneider WD, Berndt R (2000) *Angew Chem Int Ed* 39:795
84. Cai Y, Bernasek SL (2003) *J Am Chem Soc* 125:1655
85. Wie Y, Kannappan K, Flynn GW, Zimmt MB (2004) *J Am Chem Soc* 126:5318
86. Vidal F, Delvigne E, Stepanow S, Lin N, Barth JV, Kern K (2005) *J Am Chem Soc* 127:10101
87. Cai Y, Bernasek SL (2005) *J Phys Chem B* 109:4514
88. Fasel R, Parschau M, Ernst KH (2006) *Nature* 439:449
89. Chen Q, Lee CW, Frankel DJ, Richardson NV (1999) *Phys Chem Comm* 9
90. France CB, Parkinson BA (2003) *J Am Chem Soc* 125:12712
91. France CB, Parkinson BA (2004) *Langmuir* 20:2713
92. Ernst KH, Kuster Y, Fasel R, Müller M, Ellerbeck U (2001) *Chirality* 13:675
93. Ernst KH, Parschau M, Fasel R (2004) *J Surf Sci Nanotech* 2:136
94. Ortega Lorenzo M, Humblot V, Murray P, Baddeley CJ, Haq S, Raval R (2002) *J Catal* 205:123
95. Stepanov S, Lin N, Vidal F, Landa A, Ruben M, Barth JV, Kern K (2005) *Nano Lett* 5:901
96. Schönherr H, Crego-Calama M, Vansco JG, Reinhoudt DN (2004) *Adv Mater* 16:1416
97. Ortega Lorenzo M, Baddeley CJ, Muryn C, Raval R (2000) *Nature* 404:376
98. Jones TE, Baddeley CJ (2002) *Surf Sci* 519:237
99. Bonello JM, Williams FJ, Lambert RM (2003) *J Am Chem Soc* 125:2723
100. Behzadi B, Romer S, Fasel R, Ernst KH (2004) *J Am Chem Soc* 126:9176
101. Falconer JL, Madix RJ (1974) *Surf Sci* 46:473
102. Chen Q, Richardson NV (2003) *Nat Mater* 2:324
103. Hermse CGM, van Bavel AP, Jansen APJ, Barbosa LAMM, Sautet P, van Santen RA (2004) *J Phys Chem B* 108:11035
104. Lukas S, Witte G, Wöll C (2002) *Phys Rev Lett* 88:28301
105. Green MM, Reidy MP, Johnson RJ, Darling G, O'Leary DJ, Wilson G (1989) *J Am Chem Soc* 111:6452
106. Green MM, Garetz BA, Munoz B, Chang H, Hoke S, Cooks RG (1995) *J Am Chem Soc* 117:4181
107. Green MM, Park JW, Sato T, Teramoto A, Lifson S, Selinger RLB, Selinger JV (1999) *Angew Chem Int Ed* 38:3138
108. Selinger JV, Selinger RLB (1997) *Phys Rev E* 55:1728
109. Selinger JV, Selinger RLB (1996) *Phys Rev Lett* 76:58
110. Humblot V, Haq S, Muryn C, Hofer WA, Raval R (2002) *J Am Chem Soc* 124:503
111. Mamdouh W, Uji-i H, Gesquière A, De Feyter S, Amabilino DB, Abdel-Mottaleb MMS, Veciana J, De Schryver FC (2004) *Langmuir* 20:9628
112. Mougous JD, Brackley AJ, Foland K, Baker RT, Patrick DL (2000) *Phys Rev Lett* 84:2742
113. Berg AM, Patrick DL (2005) *Angew Chem Int Ed* 44:1821
114. Smith DPE (1991) *J Vac Sci Technol B* 9:1119

Supramolecular Chiral Functional Materials

David B. Amabilino (✉) · Jaume Veciana

Institut de Ciència de Materials de Barcelona (CSIC), Campus Universitari de Bellaterra,
08193 Cerdanyola del Vallès, Spain
amabilino@icmab.es

1	Introduction	254
1.1	Why Chiral Functional Materials?	254
1.2	Preparing Supramolecular Chiral Materials	254
2	Supramolecular Chirality in Systems of Interest in Molecular Electronics	255
2.1	Conductivity in Materials	255
2.2	Chiral Conductors Incorporating Small Molecules	256
2.3	Chiral Polymeric Conductors	259
3	Stereochemistry of Supramolecular Liquid Crystals	263
3.1	Intrinsically Chiral Supramolecular Liquid Crystals	264
3.2	Induced Chirality in Achiral Liquid Crystals	269
3.3	Spontaneous Resolution in Achiral and Racemic Liquid Crystals	274
4	Gels	277
5	Chiral Magnets	281
6	Materials with Interesting Optical Properties	288
6.1	Colourants	288
6.2	Nonlinear Optical Materials	292
6.3	Luminescent Materials	293
7	Conclusion and Outlook	294
	References	294

Abstract The preparation of chiral functional materials with new, improved, and interesting properties is aided tremendously by control of the spatial arrangement of the functional units within them. The use of non-covalent interactions is absolutely critical in this regard, and the molecular–supramolecular balance has to be strictly controlled. The conducting, magnetic and optical properties of chiral materials whose function is profoundly influenced by supramolecular chemistry will be reviewed. Special emphasis is placed on the control of helical arrangements in liquid crystalline systems, in which both chiral induction and spontaneous resolution are important phenomena which can be controlled.

Keywords Conductors · Chiral induction · Gels · Liquid crystals · Magnetism

Abbreviations

hfac Hexafluoroacetylacetone
AFM atomic force microscopy
CD circular dichroism

CPL	circularly polarised light
CSA	camphorsulphonic acid
IR	infrared
LB	Langmuir–Blodgett
LC	liquid crystal
OPV	oligophenylenevinylene
PANI	poly(aniline)
PEDOT	poly(ethylenedioxythiophene)
Pc	phthalocyanine
PT	poly(thiophene)
SEM	scanning electron microscopy
TEM	transmission electron microscopy
TTF	tetrathiafulvalene

1

Introduction

1.1

Why Chiral Functional Materials?

Chirality is inherent to most biological materials. It is essential to the functioning and the growth of many living things, where it is manifested in the twisted shapes of shells or the entwined vines of climbing plants, for example. It determines the smells and flavours that we sense, and the action of the drugs that cure us [1]. Unlike the vast majority of materials which function in the natural world, synthetic materials have been achiral, by and large. However, chirality in materials can have very beneficial consequences [2]. Not only is optical activity presented, but the structural aspects that asymmetry endows on the products can lead to useful, surprising and unique physical effects. In general, specific interactions of chiral compounds with polymers is responsible for their separation during chromatography [3], and in liquid crystal displays chirality is a key player [4]. Bearing in mind that other contributions will treat aspects of supramolecular polymers, in this chapter we shall concentrate on molecular materials with a function—be it electronic, magnetic, optical, etc.—in which the chemistry beyond the molecule is particularly important, and where the role of chirality is evident. Chiral supramolecular materials do not only show structural chirality and optical activity, they present the chance to investigate the combination of different phenomena and explore their synergies.

1.2

Preparing Supramolecular Chiral Materials

The balance between molecular structure and supramolecular organisation is essential in the preparation of materials if their properties are to be of any

interest. While studies of the basic rules of self-assembly [5], crystal engineering [6] and the like abound, the use of non-covalent interactions in materials in general is complicated by the fact that the very units that are included to control the arrangement of the functional units can dilute or nullify any effect [7]. For chiral materials this statement is even more true.

The two general ways of preparing chiral materials—spontaneous resolution and chiral induction—are both valid and have been exploited. In the first, non-chiral building blocks come together in a chiral sense thanks to non-covalent interactions to form, at random, either left-handed or right-handed superstructures [8, 9]. The problem with this approach from a practical viewpoint is that the enantiomers must be separated from each other. In a more controllable fashion, chirality can be induced into a material by incorporating stereogenic centres into the components [10–16] or—to a lesser extent—by forming the materials under a physical chiral “field” [17]. These approaches have afforded supramolecular materials that will be detailed in the following sections, subdivided into the type of property that they display.

2

Supramolecular Chirality in Systems of Interest in Molecular Electronics

2.1

Conductivity in Materials

The transport of electrons through materials—electrical conductivity—is an important phenomenon for a number of reasons. The motion of electrons in low dimensional molecular materials (with a mixed valence nature and that have a band structure) has provided great insight into the mechanisms of transport, and many materials based on organic building blocks have been prepared which meet the requirements for these properties [18–20]. Usually, conducting salts are of two types: charge transfer complexes and charge transfer salts. Both types contain stacks of molecules in close contact through which the electrons may flow. In general, electrons preferentially flow through networks formed by one of the components of these ionic compounds giving rise to metallic conductivities. The dimensionality of the solid state structure determines directly the space available to the mobile electron, thus non-covalent interactions play a critical role. The use of conducting polymers in a number of technologically important applications is well documented [21–24]. Here, the conductivity takes place along and between the chains, principally through a hopping mechanism resulting in semiconducting properties. Therefore, the organisation of the polymers can have very dramatic consequences on their conductivity in the bulk.

Conductivity in chiral materials is a topic of great interest presently because of the possibilities of observing chiral electron movement in mate-

rials [25, 26], although this notion is not new [27, 28]. Also, the synergy between chirality and conductivity in polymeric systems raises a number of interesting opportunities in sensing materials or systems with optical properties. All of these applications are particularly relevant given the growing interest in molecular electronics in general [29, 30].

2.2

Chiral Conductors Incorporating Small Molecules

The two types of molecular conductors, charge transfer salts and charge transfer complexes, are formed by the combination of electron donor and acceptor which crystallise in segregated stacks with partial transfer of charge, and by oxidation or reduction of the active component in a solution which contains an electrolyte whose ions are incorporated into the salt, respectively. In principle, one could imagine two ways to introduce chirality in these systems: to prepare the charge transfer salts and complexes with intrinsically chiral donor or acceptor molecules, or to prepare the salts with chiral counter-ions. Both of these approaches have yielded chiral salts with conducting properties. The molecules most widely employed to generate conducting regions in these salts are those derived from tetrathiafulvalene, TTF (Fig. 1).

A great number of chiral TTFs have been prepared [31, 32], and some of their charge transfer salts have been crystallised. The π -donor **1** can be electrocrystallised to give a salt $\text{I}_2 \cdot \text{PF}_6$, which has a conductivity of $\approx 5 \Omega^{-1} \text{ cm}^{-1}$ at room temperature and metallic behaviour when cooled down [33]. While the structure of the crystals is chiral, the structure of this salt and other related ones [34] has an essentially achiral stack of donor molecules, which are pseudo-centrosymmetric [35]. The methyl groups at the periphery of the molecule are apparently not sufficient to cause a truly chiral stack of donors, which prefer to stack in parallel arrangements with partial overlap of the π -systems in the solid state, a situation which is true for the majority of the efforts to prepare salts of this type (even if the salts are metallic).

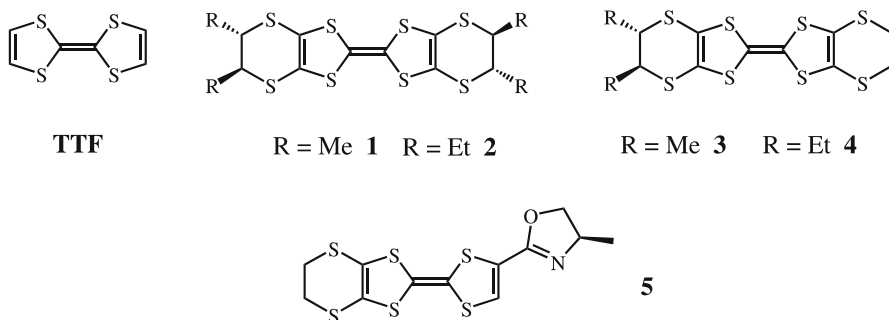


Fig. 1 TTF and some of the chiral donor molecules derived from it

A very nice example in which racemic and both enantiopure conducting salts were prepared involves the donor **5**, where an oxazoline ring is used as the source of chirality [36]. Again, the molecules stack parallel to each other (the β form), with the neighbours in the stack located head-to-tail (Fig. 2). The real advantage of chirality in this system turned out to be that in the enantiopure 2 : 1 salts with hexafluoroarsenate (which crystallise in the $P1$ space group) the order in the crystal is much greater than that in the corresponding racemic compound (which crystallises in the $P1$ space group). In the latter, the oxazoline ring is disordered such that the *s-cis* and *s-trans* conformers of the *R* and *S* enantiomers, respectively, occupy the same crystallographic position (Fig. 2), while in the enantiopure salts there is slight disorder in the ethylenedithio group (as there is in the racemic compound) but not in the chiral part. The mixed valence nature of the salts and the efficient packing means that the samples are metallic at room temperature—the racemic compound has a conductivity of approximately 10 S cm^{-1} , while that of the enantiomers is 100 S cm^{-1} —and show broad minima in resistivity at around 230 K. The reason for the difference in conductivity by an order of magnitude is the disorder in the structures, which favours localisation of the charge carriers.

The donor (*S,S*)-**3** forms two different polymorphs when it forms a salt with perchlorate anions, one of which shows a crystalline packing somewhat different to those described above, in which the donors form orthogonally oriented dimers in a sheet (κ type packing) [37]. Pseudo-symmetry again prevails here, at the centre of the dimer, despite a slight homochiral twist at the central $\text{C}=\text{C}$ bond. The salt is weakly metallic. Meanwhile, the compound **2**

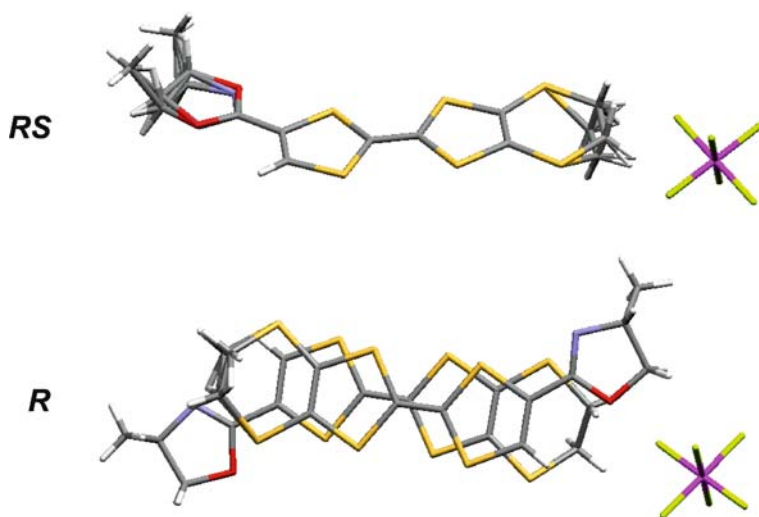


Fig. 2 Views of the crystal structures of salt $5_2 \cdot \text{AsF}_6$ as the racemic compound (*top*) and *R* enantiomer (*bottom*) [36]

in its racemic undoped state is interesting in the sense that it resolves spontaneously, crystallising in the space group $P4_32_12$ (with the racemic crystals pertaining to $P4_32_12$ inferred but not proven) [38]. However, the salts obtained from the racemic compound are neither chiral nor conducting.

One approach to chiral conductors using the counterions as the source of asymmetry is that employed in the preparation of a conductor based on bis(ethylenedithio)-tetrathiafulvalene (BEDT, Fig. 3) [39]. When this organic donor is electrocrystallised in the presence of the L-tartrate salt $K_2[Sb_2(L-tart)_2]$ the compound that is formed is $BEDT_3Sb_2(L-tart)_2 \cdot MeCN$. Thus, the BEDT is in a mixed valence state, with two third charge per molecule on average. The salt, which pertains to the $P2_12_12_1$ space group, has layers of donor molecules and ions derived from BEDT which alternate with layers of the chiral counter-ions.

The stack of BEDT is of the so-called α -phase. The sulphur–sulphur contacts between the stacks ($S \cdots S$ distances $\approx 3.47 \text{ \AA}$, shorter than the sum of the van der Waals radii of 3.6 \AA) and within the stack ($S \cdots S$ distances $\approx 4.1\text{--}4.2 \text{ \AA}$) give the layers a decidedly two-dimensional character. The BEDT donors are related by a two-fold screw axis, and therefore have no real chiral nature (the molecules have pseudo-centre symmetry). There are several hydrogen bonds between the hydrogen atoms of the ethylene groups of BEDT and the carboxylate groups of the counter-ion. The material is a semiconductor, where the conductivity falls as the temperature is lowered, from about 1 S cm^{-1} at room temperature.

The great challenge in this area of research, then, is to be able to form a chiral stack of the planar organic donors and their ions in a crystalline form, and much of the problem arises from the inability of chemists to prepare compounds which will stack in a helical form in the crystal. In Sect. 5 of this

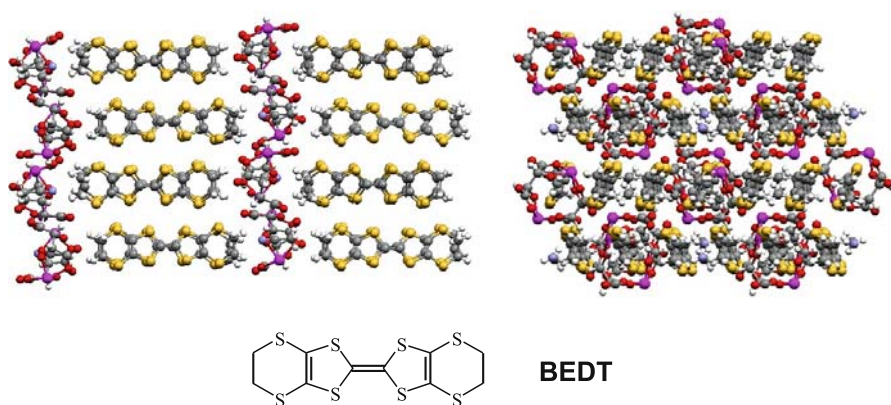


Fig. 3 Views of the crystal structure of the enantiopure salt $BEDT_3Sb_2(L-tart)_2 \cdot MeCN$ in which the stacks of BEDT molecules can be appreciated [39]

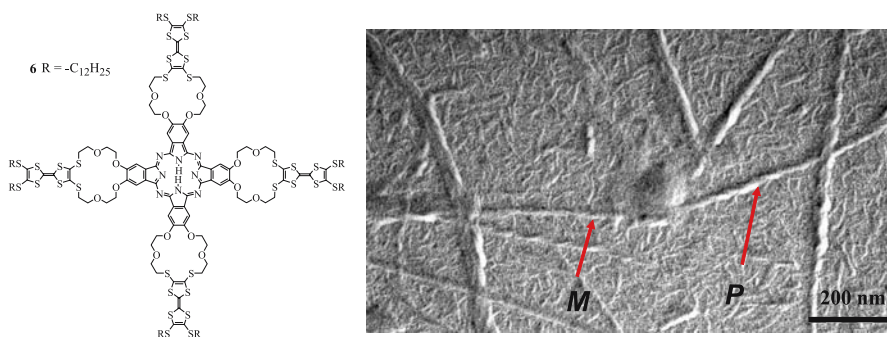


Fig. 4 The TTF-bearing Pc **6** and a TEM image of the helical fibres it forms [45]

chapter we describe interesting recent results that may go some way to meeting this challenge. We should also point out that the preparation of chiral conductors using helicene-type molecules is potentially very interesting [40]. Although useful helicenes have been synthesised [41–43], their conducting properties have not been reported.

A strategy that may find a more practical possible remedy to the difficulty in preparing helices in crystals is to prepare self-assembling molecules that form conducting fibres. There are a number of examples of phthalocyanines (Pcs) which form supramolecular chiral fibres [44]. One such molecule is the TTF-bearing Pc **6**, which although achiral forms helical fibres from dioxane–chloroform mixtures, according to TEM microscopy (Fig. 4) [45]. The forces that hold these aggregates together are probably between the TTF moieties and the phthalocyanine aromatic surface. The doping and study of conductivity is pending.

2.3

Chiral Polymeric Conductors

Intrinsically chiral conducting organic polymers—in which the stereogenic centre is contained in a pendant sidechain—can show significant optical activity thanks to their aggregation. Perhaps the prime example is that of polythiophene (PT) derivatives, which show very weak optical activity in solvents in which the material is readily soluble, but when they are dissolved in solvents where dissolution is less favourable the macromolecules aggregate and very significant optical activity is recorded [46]. The aggregates also reveal odd-even effects [47]. That is, when the position of the stereogenic centre is positioned at each consecutive carbon atom in the chain the Cotton effects resulting from the polymer alternate sign. The origin of this optical activity, which is expressed in a very strong Cotton effect of the $\pi-\pi^*$ transition of the polymer chain, is believed to be a result of the self-assembly of molecules that are mainly planar (Fig. 5) [48]. The chirality of the aggregates

is not only manifested in absorption, but also in the luminescence properties of the aggregates, where circularly polarised luminescence is observed [48]. More examples of this kind of phenomenon will be given in the section on optical properties (see Sect. 6).

The supramolecular chirality in PTs can also be promoted by metal ion binding when suitable groups are used as side chains. When chiral oxazoline was used as a pendant moiety, addition of copper(II) triflate to a chloroform solution of the polymer caused a dramatic increase in the optical activity [49]. Most notably, the Cotton effects observed in the CD spectrum grow from practically zero to quite significant values in the region of the polymer backbone transitions. The polymer is very sensitive to regioregularity, since the random polymer is not as optically active when treated with metal ions as the regioregular form. Proof for aggregation was also provided by AFM measurements, which revealed round aggregates.

In a similar vein, aggregates of other conjugated polymers have been discovered, with the focus of this research being directed at the optical properties of the materials (see Sect. 6). Another interesting aspect of these materials is the possibility of changing the optical activity by oxidising the polymers. A representative example is that of films of poly[(*R*) or (*S*)-1,4-bis(2-(3',4'-ethylenedioxy)thienyl)-2-benzoic acid 1-methyl heptyl ester] prepared by electropolymerisation [50], which shows strong Cotton effects in the region of the π - π^* transition of the polymer chain, indicative of the kind of aggregate mentioned above. In common with other PTs, in the oxidised state virtually no optical activity is observed in the visible region, but cycling back to the neutral state restored the activity. This kind of chiral PT can also be used to sense chiral anions by cycling the voltage [51]. All of these examples concerned intrinsically chiral polymers, where the stereogenic centre is incorporated during the synthesis.

The preparation of chiral conductors is perhaps most easily achieved by supramolecular induction in preformed achiral conducting polymers. Al-

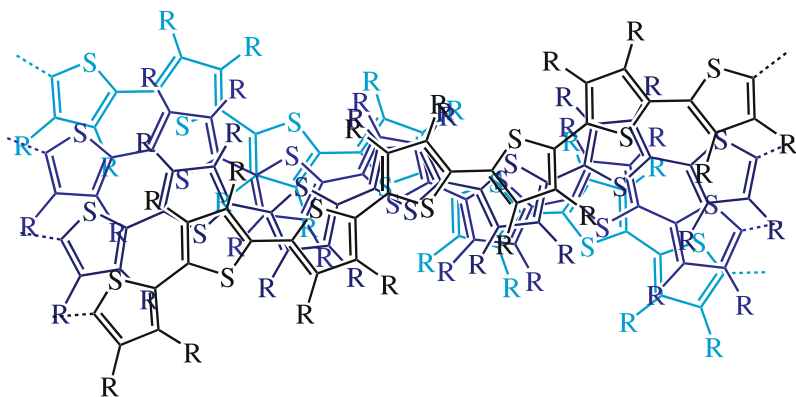
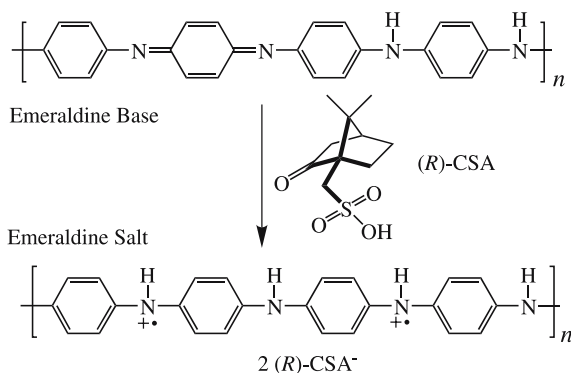


Fig. 5 Possible aggregated form of chiral polythiophene derivatives [48]

though the structures are not as well defined as those in the previous section, the availability of poly(aniline) (PANI), PT and the like makes them a logical choice for many potential applications. A classic example is that of PANI, which in its half oxidised emeraldine base guise can be easily doped to the emeraldine salt form—which is conducting—by treatment with strong acids (Scheme 1). 10-Camphorsulphonic acid (CSA) is a chiral dopant that is readily available in both its enantiomeric forms, and can be used to treat emeraldine base and generate optically active PANI.

Films have been prepared from cresol which showed a large Cotton effect in the region of the absorption bands of the doped PANI [52]. The maxima in the Cotton effects could not be seen in the conducting samples which have absorption maxima in the near IR (the range of CD spectrometers is limited), but partial de-doping allowed observation of an exciton splitting. In this initial report, it was stated that no Cotton effect could be observed for the solution of the salt in *meta*-cresol solution. The absence of any CD absorption bands in films prepared using other chiral acids as dopants prompted the authors to imply a specific binding of the CSA to the PANI through both sulphonate and ketone groups. The substrate used for casting the films was shown to have a significant effect on the optical activity. This sensitivity to surroundings was accentuated when a study of the water content of the salt was performed [53]. Doping of the emeraldine base dissolved in *N*-methylpyrrolidinone with (*S*)-CSA produced a positive Cotton effect at 450 nm when the system was relatively dry (3–5% water content), but when the water content was greater than 50% a negative effect was observed. Casting of the solutions onto quartz gave the same Cotton effects as observed in solution. This observation could explain some discrepancies between the signs of the Cotton effects reported in this system [54–57].

In addition to the optical activity of the samples, CSA also has beneficial effects on the conductivity of the polymer when compared with other dopants [58, 59], and can be exploited for systems used for chiral recogni-



Scheme 1 Doping of PANI in its emeraldine base form with CSA

tion. When the PANI-CSA thin film system is dedoped (with ammonium hydroxide) the chirality remains in the polymer backbone, as seen by CD spectroscopy, but disappears when the dedoped polymer is redissolved showing the supramolecular origin of the chirality [60]. The chiral films obtained after de-doping could be used to bind amino acids stereoselectively in aqueous solution. The authors hypothesise that hydrogen bonding within the polymer maintains a chiral pocket. The selectivity is particularly good for phenylalanine [61], an effect which can be observed electrochemically [62].

It is also possible to prepare chiral PANI by in situ polymerisation with CSA, and in this case the reaction can afford chiral nanotubes [63]. The optically active materials contain nanotubes with 80 to 200 nm outer diameter and an internal diameter of between 20 and 40 nm, as revealed through microscopy images. A self-assembly process was proposed in which anilinium cations and CSA anions form micelles which act as templates for the growing polymer chains. Nanotubes are also formed when (*R*)- or (*S*)-2-pyrrolidone-

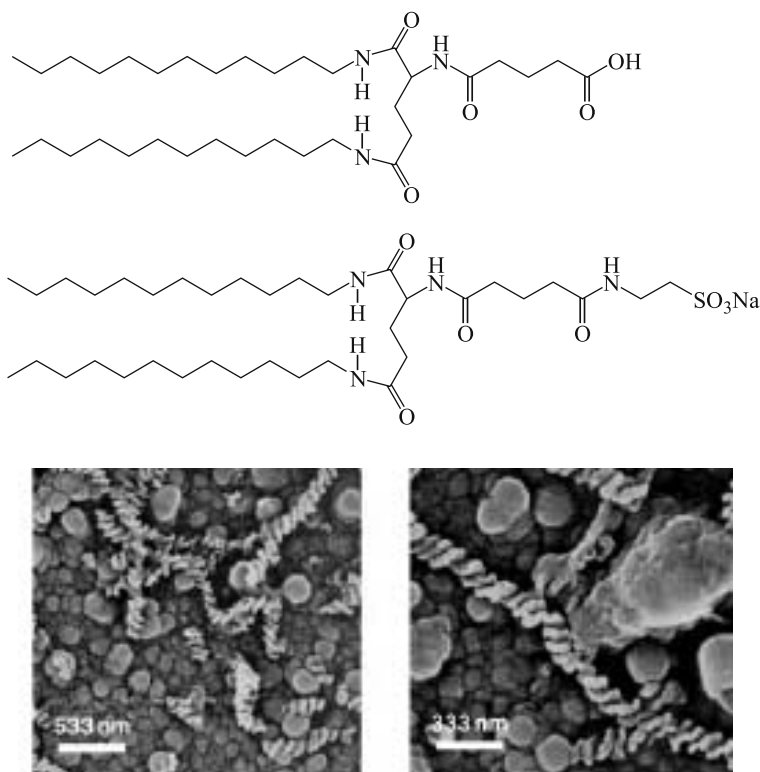


Fig. 6 Lipid molecules used to template the formation of helical fibres of conducting polymers. The SEM images correspond to PEDOT formed using the sulphonate lipid as a template. TEM image reprinted with the permission of Wiley [66, 67]

5-carboxylic acid was used as dopant in the in situ polymerisation. The bulk material is optically active and weakly conducting [64].

In these examples it was not possible to visualise any chiral structure with a microscope, but when PANI was prepared using poly(acrylic acid) as an in situ template, helical microwires were visualised [65]. In an even more general sense, helical fibres of PANI, poly(ethylenedioxythiophene) (PEDOT), and poly(pyrrole) were prepared using synthetic lipids as templates [66, 67]. The synthetic lipid molecules used are shown in Fig. 6 along with some of the helical fibres of PEDOT that are formed when the sulphonate salt is used to shape the fibres during the polymerisation. The procedure involves growing the fibres by electrochemical polymerisation onto an ITO electrode with the lipid molecules in the electrolyte.

3

Stereochemistry of Supramolecular Liquid Crystals

The role of supramolecular chemistry in materials is perhaps expressed most impressively in liquid crystals, in which slight variations of chiral content can lead to dramatic influences in the properties of the mesophases. The helical sense of these mesophases is determined not only by intrinsically chiral mesogens but also by the use of dopants which more often than not interact with achiral host LCs to generate chiral phases (Fig. 7). These phenomena are important both scientifically and technologically, most notably for the chiral smectic and cholesteric liquid crystal phases [68–71]. These materials—as small molecules and as polymers [72, 73]—are useful because their order

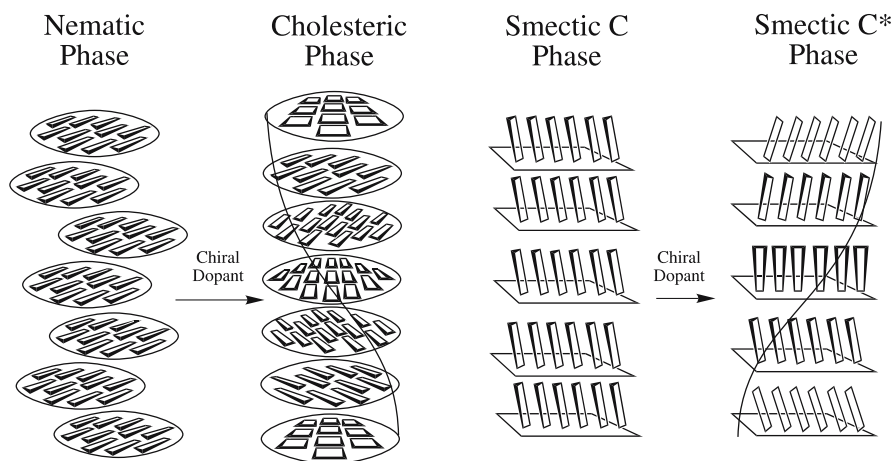


Fig. 7 Induction of chiral mesophases in achiral LCs by addition of chiral dopants

can be switched by application of an electric field thanks to their ferroelectricity [74–76], and they are useful components for systems with optical applications, because they can selectively reflect polarised light (see Sect. 6). Non-covalent interactions play an important role in the ordering of these liquid crystals.

The consequences of supramolecular chemistry in this area is so wide that it is impossible to give a comprehensive account of the subject in this short general review. We will instead focus on examples which are more contemporary and appealing from the authors' perspective, and encourage the interested reader to read the general reviews that we have cited.

3.1

Intrinsically Chiral Supramolecular Liquid Crystals

A vast array of covalent molecules have been synthesised over the years in the search for LCs that show the useful cholesteric and ferroelectric smectic C* phases, often on a trial and error basis ignoring the interactions between the molecules. The idea that one could think of the interactions between the molecules as a kind of molecular recognition came from the careful analysis of the conformations of molecules in the layers [77, 78]. The arguments are based on the symmetry limitations of the angle formed by the alkyl chain and the phenyl benzoate moiety in the molecules that were the subject of this study. A molecular recognition site within the phase was used as the basis for these “speculations”, which have actually proved rather successful. The actual interactions between molecules are usually weak, but the formation of layers of aromatic and aliphatic units in these mesophases gives rise to their unique properties.

On the other hand, the preparation of liquid crystals in general using intermolecular hydrogen bonds as a structuring element to form a rigid core of calamitic and other mesogens is reasonably well established [79, 80]. While the simple dimerisation of benzoic acids was the first in this area [81], perhaps the most investigated supramolecular synthon is the dimer formed by benzoic acids with pyridine derivatives [82], which has been used for a very wide variety of achiral and chiral LC systems. For example, ferroelectric LCs can be prepared from achiral polysiloxanes with 4-alkoxybenzoic acid side chains in combination with optically active *trans*-stilbazole. The ferroelectric properties are determined through the proportion of stilbazole to polymer units, as well as the length of the alkyl spacers in the structures [83]. The same principle can be used with simple benzoic acid derivatives [84]. The nature of the mesophases (the smectic A phase is observed as well as the smectic C*) and the temperature intervals they display depend on the number of carbon atoms as well as the proportions of the components. A study of one of the mixtures showed that the 1 : 1 complex does not actually give the widest temperature range of the chiral phase. Rather, when 25% of the chiral stilbazole

was added the temperature range of the smectic C* phase was between 72 and 124 °C, after which a chiral nematic (cholesteric) phase was observed up to the clearing point at 138 °C.

The valency of the hydrogen bond donors and acceptors can be varied to produce chiral mesophases [85]. Mixtures of the divalent 4,4'-bipyridine with 4-[(*S*)-2-methylbutoxy]benzoic acid in ratios between 1 : 9 and 4 : 6 show LC behaviour, but the chiral mesophases are exhibited for only a small range of compositions [86]. Here, the cholesteric and a blue LC phase were observed. The association of the acid to the bipyridine was confirmed by a crystal structure of the 1 : 2 complex.

Cholesteric liquid crystals based on branched systems have been prepared by the self-assembly of non-mesomorphic molecular components thanks to the same carboxylic acid pyridine hydrogen bond [87]. The mixture of the two components shown in Fig. 8 gives rise to a material that exhibits an enantiotropic mesophase which shows a focal-conic fan texture under a polarising microscope, a feature that is characteristic of a cholesteric phase with relatively short helical pitch. It is interesting that this phase is generated, because the rod-like structure which normally gives the cholesteric phase is clearly not preferential in the branched supramolecular topology that is generated.

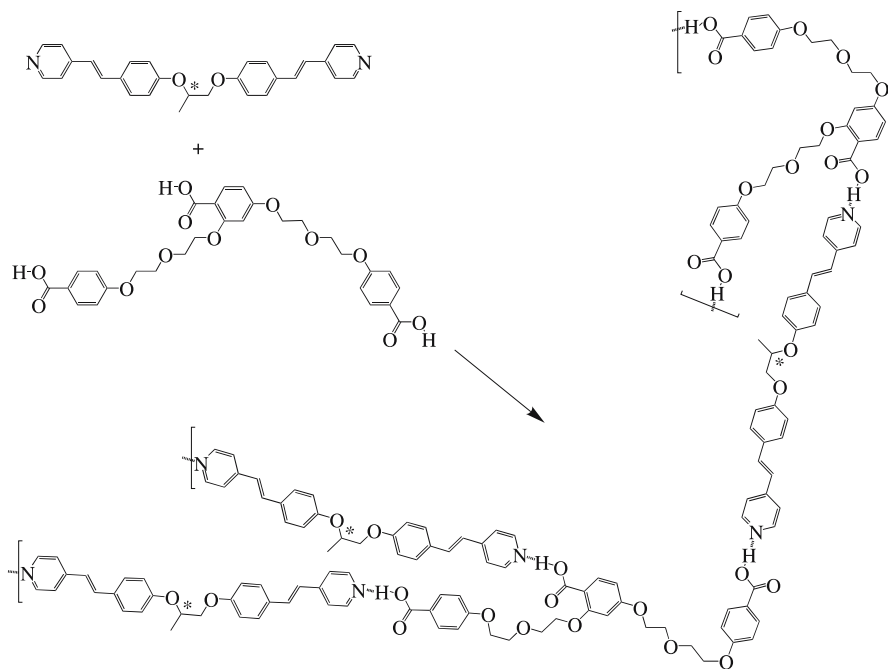


Fig. 8 The self-assembly of chiral networks presenting cholesteric LC phases [87]

This topology has the potential for a high degree of supramolecular cross-linking.

One of the most classic examples of chiral expression in thermotropic liquid crystals is that of the stereospecific formation of helical fibres by diastereomers of tartaric acid derivatised either with uracil or 2,6-diacetylamino pyridine (Fig. 9) [88]. Upon mixing the complementary components, which are not liquid crystals in their pure state, mesophases form which exist over very broad temperature ranges, whose magnitude depend on whether the tartaric acid core is either *D*, *L* or *meso* [89]. Electron microscopy studies of samples deposited from chloroform solutions showed that aggregates formed by combination of the meso compounds gave no discernable texture, while those formed by combinations of the *D* or *L* components produced fibres of a determined handedness [90]. The observation of these fibres and their dimensions makes it possible that the structural hypothesis drawn schematically in Fig. 9 is valid. This example shows elegantly the transfer of chirality from the molecular to the supramolecular level in the nanometer to micrometer regime.

Lyotropic (in solvent) cholesteric mesophases have been observed for self-assembled guanosine derivatives. In water, the compounds shown in Fig. 10 generate left-handed columnar aggregates [91]. When the concentration is sufficiently high, cholesteric phases are formed which also have a left-handed twist, as determined by CD spectroscopy. The same tetrameric motif is present in the lyomesophases formed by more lipophilic guanosine deriva-

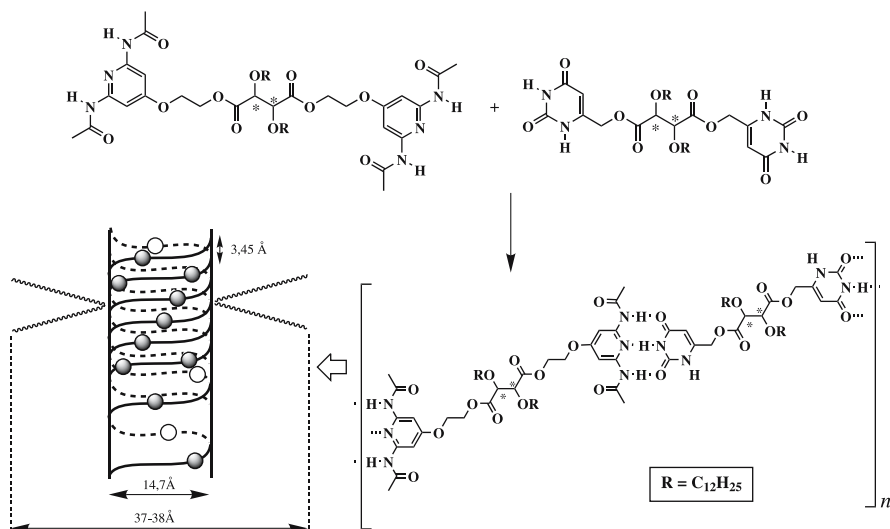


Fig. 9 The self-assembly of complementary chiral tartaric acid derivatives which self-assemble giving liquid crystalline materials [88]

tives when they complex potassium ions [92]. In this case the metal ions are located in between the disc-like tetramers and aid in the formation of the LC. The optical activity of these derivatives increases very dramatically upon introduction of the alkali cation as observed by CD spectroscopy in tetrachloroethane. In hexane the optical activity of the cholesteric phase is increased even further.

The preparation of a cubic phase with supramolecular chirality was achieved using a branched folic acid derivative incorporating glutamic acid residues (Fig. 11) as the source of chirality [93]. The pterin rings of folic acid residues are able to form a cyclic tetramer as a result of two hydrogen bonds between the components. Depending on the number of carbon atoms in the alkyl substituents, the compounds form columnar phases over a wide temperature range, and for **8** and **9** form cubic phases at temperatures above 130 °C. Addition of sodium triflate stabilises the cubic phase for **7**, and the salt is incorporated into the other mesophases. It was implied that the cation resides between stacked tetramers. Supramolecular chirality is expressed for both the columnar and the cubic phases, as revealed by vari-

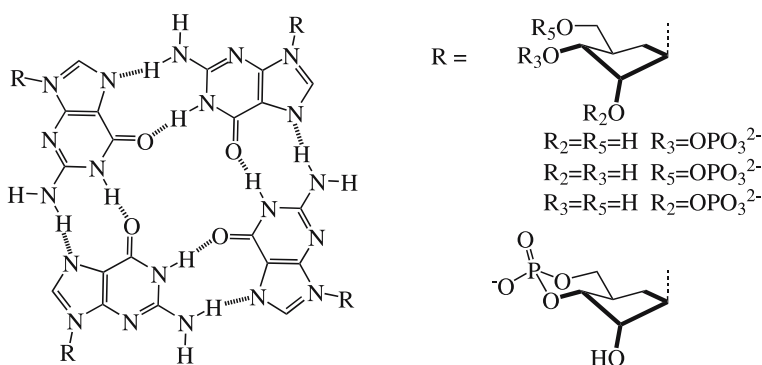


Fig. 10 Guanosine derivative tetramers that form lyotropic cholesteric phases [91]

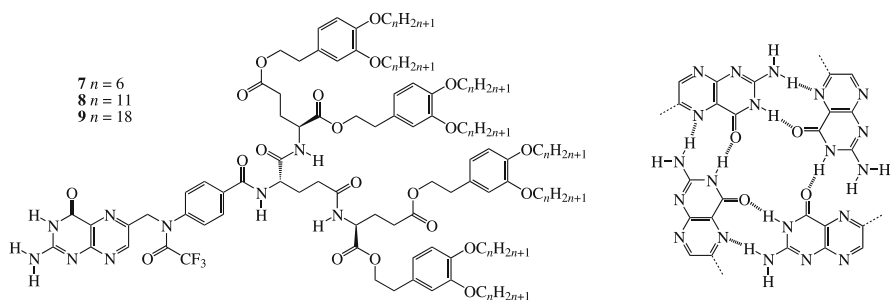


Fig. 11 The chiral folic acid derivatives **7**, **8** and **9**, which display mesophases thanks to the formation of a supramolecular cyclic tetramer by the pterin rings (right) [93]

able temperature CD studies. The induced chirality in the cubic phase for compound **8** is dependent on the presence of the sodium ion. It is an interesting example of an achiral ion that influences the expression of chirality in a material.

The chirality of the glutamate residues has been sequentially modified, and it has been shown that the mesophases are maintained, but their optical activity can be changed by these modifications [94]. The formation of chiral structures in chloroform solutions of these compounds is assisted by the addition of sodium cations, while in dodecane the ions are not necessary for the chiral expression.

Metallomesogens have been shown to form helical supramolecular organisations in their mesophases [95]. Chiral oxazoline complexes with various metal ions and six alkyl chains did not show LC behaviour, but when mixed with trinitrofluorenone form achiral smectic A phases [96]. Furthermore, when a branch was included in the structure of the ligands (Fig. 12) the corresponding complexes with copper(II) and palladium(II) form columnar mesophases which have a helical organisation [97]. The presence of the stereogenic centre near the central metal ion in these complexes (Fig. 12) is enough to cause the parallel molecules to stack in a tilted manner with

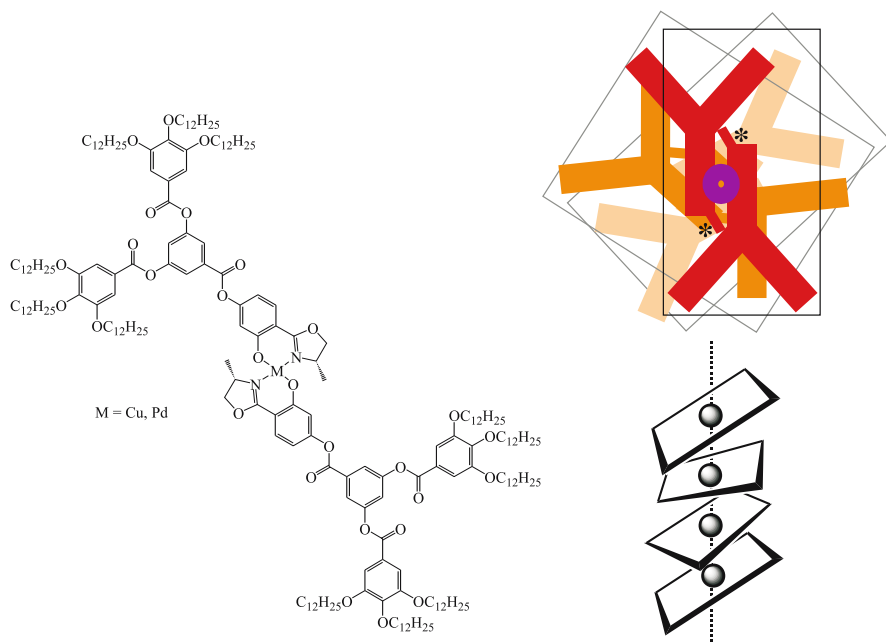


Fig. 12 Chiral metallomesogen based on a chiral oxazoline core and representations of its helical organisation from above (*top right*) and side-on (*bottom right*) to the helix axis [97]

each molecule twisted by 60° with respect to the next, as shown by the X-ray diffraction pattern in oriented mesophases. The CD spectra of the mesophases confirm this analysis. An exciton coupled signal is observed, whereas in solution the compounds show a single Cotton effect in their spectra, a clear sign that the organisation of the molecules has influenced the chiroptical properties. Interestingly, the racemic mixture and the mixture of diastereomers show a similar type of organisation, suggesting that spontaneous resolution occurs in the mesophase.

The position of the stereogenic centres has an important influence on the helix that is observed in this kind of metallomesogen, it can give rise to discotic phases that exhibit ferroelectric switching [98]. Oxovanadium(IV), copper(II) and palladium(II) β -diketonates bearing ten chiral chains derived from lactic acid showed room temperature discotic phases, seen most clearly by optical microscopy in which Maltese cross patterns were observed [99]. X-ray diffraction proved a rectangular columnar arrangement in which the planes of the molecules are tilted with respect to the column axis and with respect to each other. This organisation allows switching of the molecular orientation when introduced in electro-optic cells. A ferroelectric response was seen from the clearing temperature at around 150°C down to around 80°C (at which temperature the samples become too viscous to reorient at an appropriate speed). An electro-optic effect was observed for all the complexes when an alternating electric field was applied.

3.2

Induced Chirality in Achiral Liquid Crystals

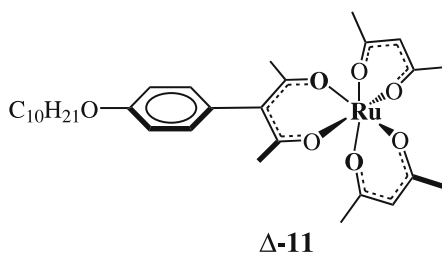
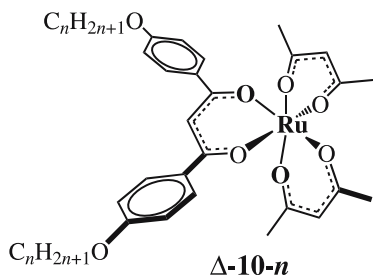
The induction of chirality in liquid crystals (LCs) has a long history [100–104]. The supramolecular induction can be used to assign absolute configurations [105–108], conformations of molecules [109, 110] and the interplay between inter- and intra-molecular interactions [111], and models can be developed to justify the sense of the inductions that are observed. Twisting powers of dopants—the twist per mole—can be pushed to extraordinary values [112]. Given the history and vast body of work, we will focus here on the more contemporary aspects of work in this area.

In general, the chirality of the cholesteric phases are indicated by the sign and magnitude of the cholesteric pitch, which in turn depends on the helical twisting power and the concentration. At a fixed concentration for a given compound the pitch depends on the enantiopurity of the compound. An ingenious method for easily evaluating enantiomeric purity was described recently [113]. This method involves the functionalisation of biphenyl derivatives with chiral groups and the use of these adducts to induce a cholesteric phase. The colour of the induced cholesteric reveals the enantopurity of the sample, once a set of standard measurements have been done. It is a visual chiral indicator, which can be used with micrograms of chiral material.

Recently, the importance of the structure of chiral metal complexes on the handedness of the mesophases induced in a nematic LC was exemplified [114]. The chiral metal complexes **10** and **11**—in which the alkyl substituents are aligned almost perpendicularly to the C_2 axis in the former and parallel in the latter—show very different induction phenomena. Not only are the induced helicities in the nematic LC of opposite sense for the two compounds, but the helical twisting power of **10** is much higher than that of **11**. The reason for these differences is the way in which the molecules are incorporated into the host nematic phase and exert their force upon it to create the twist between the layers.

While the vast majority of studies on chiral induction were mainly concerned with the induction of the chiral (twisted) nematic or cholesteric phase, more recently induction of the smectic C^* phase in the smectic C has come to the fore, with a special emphasis on the way chirality is transferred between molecules [115]. It should also be noted that comparison of the chiral induction phenomena in the two types of LC phase and in other media can provide useful information concerning mechanisms of transfer and amplification of stereochemical “information” [116].

The calamitic (rod-like) molecules in the smectic C phase are organised in layers with the long axes of the molecules at an angle to the normal to the layer plane. Judicious choice of a chiral dopant forces this angle into a helical arrangement whose vector lies perpendicular to the layer plane, with a pitch of a few microns. It is believed that the induction mechanism involves a host–guest type interaction, in such a way that an orientational bias is inferred on the host. These chiral superstructures may be induced by molecules with stereogenic centres in the alkyl chains attached to rigid cores. The relatively high flexibility of the stereogenic centre in general induces chirality in host phases with a wide variety of structural features. Meanwhile, when rigid atropoisomeric cores are present in the dopant molecules, more specific interactions take place between host and guest and a more pronounced dependence on the structure of the two is observed [115]. The substituted biphenyl derivative **12** (Fig. 13) acts as a dopant by interacting with smectic C liquid crystals of the type which contain a phenyl pyrimidine core (**13**) in such a way that a preferred axially chiral conformation of the host is in-



duced by the dopant guest, and this conformation is propagated through the layers [117–119].

Chirality can be induced in discotic polymeric liquid crystals based on triphenylene residues by the addition of chiral π -electron deficient dopants [120]. The achiral polymers were constructed by linking the triphenylene groups through their sides with a methylene spacer ($x = 10$, Fig. 14) such that a stack of the aromatic residues can form, and the alkyl substituents ensure the liquid crystalline mobility. With achiral alkyl chains no chiral phase was observed. When the electron-deficient fluorene derivative **14** (in either of its enantiomeric forms) was added a charge transfer complex is formed and a very strong Cotton effect was observed in the CD spectra of thin films of these mesophases, which were stabilised by addition of the dopant. The Cotton effect arises from the triphenylene chromophores, as witnessed by the fact that chiral polymers of the same type show similar signals. This method constitutes an appealing way to generate chiral discotic liquid crystals.

Just as chiral induction can be realised in discotic liquid crystals, it can also be realised in assemblies of disc-like molecules or disc-like aggregates. As far as molecules are concerned, C₃-symmetrical trisamides (Fig. 15), which actually exhibit discotic liquid crystalline phases, also form chiral columnar stacks through π - π interactions when dissolved in apolar solvents, which are depicted schematically in Fig. 15 [121]. An achiral compound of this type (**15**) exhibits no optical activity in dodecane, but when the compound is dissolved in the chiral (*R*)-(-)-2,6-dimethyloctane significant Cotton effects (only slightly less intense than those observed in a chiral derivative) are detected. The chiral disc-like trisamide **16** can also be used as a dopant at concentrations as low as 2.5% to induce supramolecular chirality in the stacks of achiral compound. In this case, the presence of the additional hydrogen

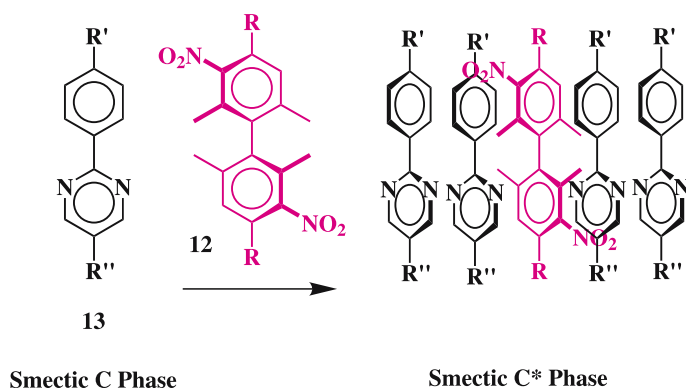


Fig. 13 The doping of a smectic C mesogenic phase with an atropoisomeric biphenyl dopant [117]

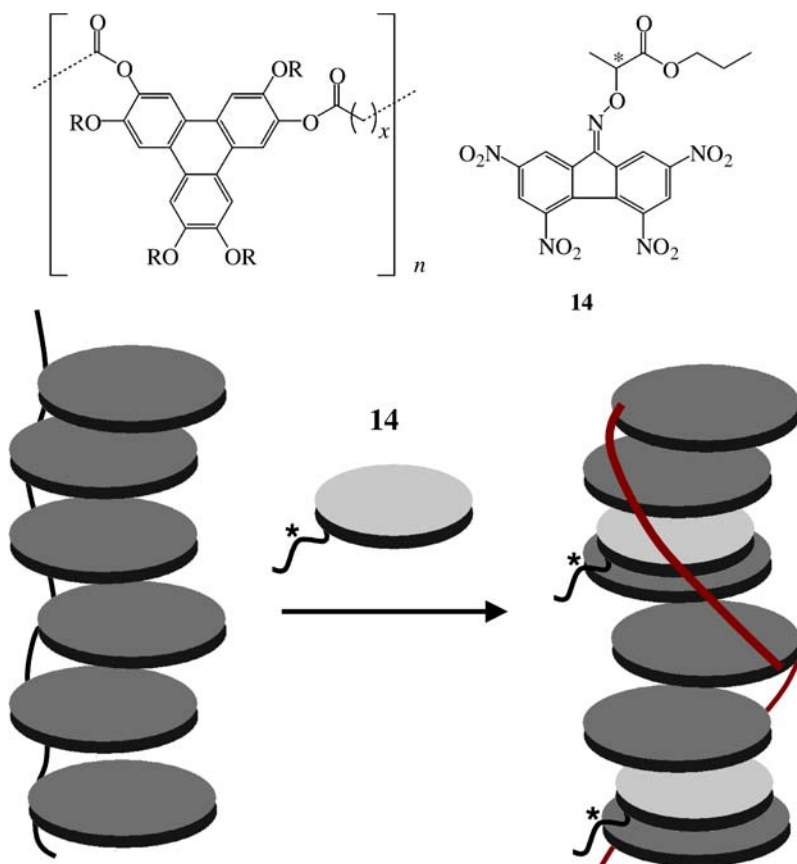


Fig. 14 An achiral discotic polymer and the chiral dopant used to induce chiral columnar packing, as represented schematically in the lower part [120]

bonds in the form of the self-complementary urea unit is detrimental to chiral induction.

The induction effect can also be used to prepare materials which can be reversibly switched with light when a suitable chromophore is used as the dopant [122]. For example, switching of fulgide derivatives incorporating a binaphthyl group caused reversible changes in helical pitch in a cholesteric [123]. Also, when the planar chiral compound **17** (Fig. 16) is introduced as an equimolar mixture of the *M-cis* and *P-trans* isomers into a nematic liquid crystal (4'-pentyloxy-4-biphenylcarbonitrile) no cholesteric LC phase is formed, but when the system is irradiated with light at 435 nm, an excess of the *M-cis* atropoisomer is formed in the solution, and a cholesteric LC phase is induced (Fig. 16) [124]. In a sample with 1% (weight) of the chiral compound the pitch was found to be 12.3 μm . Subsequent irradiation with 365 nm light generated *P-trans*-**17**, which induces a cholesteric pitch of

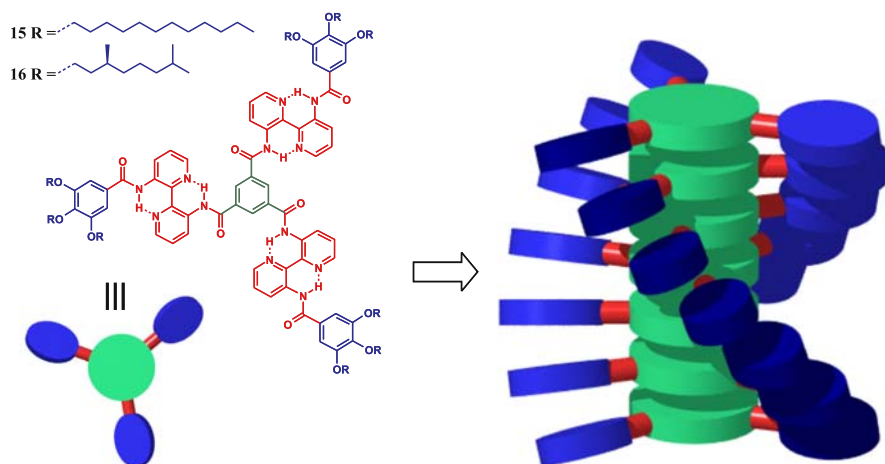


Fig. 15 Self-assembly of an intramolecularly hydrogen bonded disc-like molecule [121]

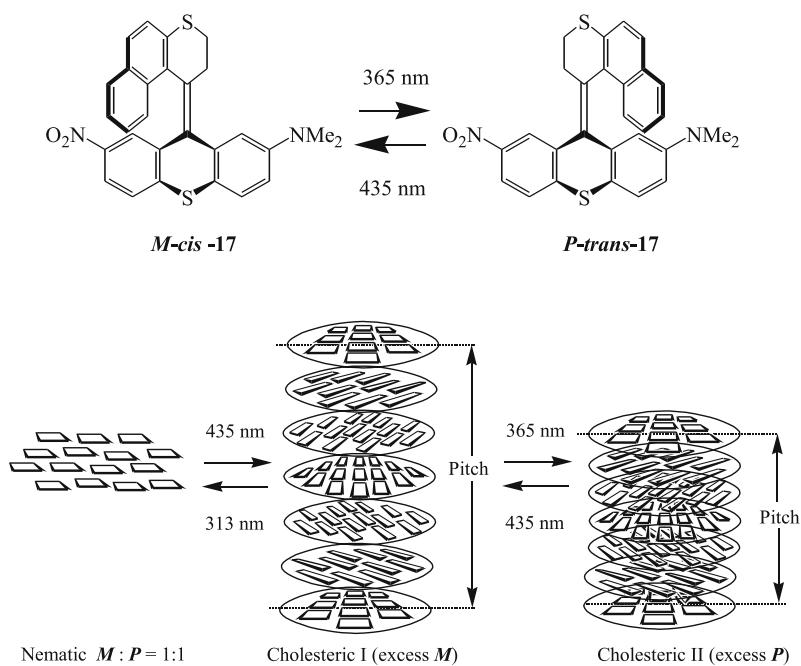


Fig. 16 Reversible photochemical cholesteric LC induction promoted in a nematic liquid crystal (4'-pentyloxy-4-biphenylcarbonitrile)

only 5.3 μm . In addition, the helical sense of the cholesteric phase is inverted. Thus, the switching of axial chirality in the molecule results in a switching of the cholesteric state. The same switching is seen when a mixture of the corresponding *M-trans* and *P-cis* atropisomers is introduced. In addition, the nematic phase can be regenerated by irradiating at 313 nm, which produces equal proportions of *M* and *P* isomers at the photostationary state.

Using similar effects, the colour of the liquid crystalline material can be tuned [125]. In addition, a similar molecule has been used for dynamic control of chirality using circularly polarised light (CPL). When a nematic mixture of 4'-pentyloxy-4-biphenylcarbonitrile containing a racemic crowded alkene related to **17** was illuminated with left-handed CPL, an excess of the *M* atropisomer was generated and a left-handed cholesteric phase formed [126]. The nematic phase could be regenerated by illuminating with linearly polarised light, or the opposite-handed cholesteric LC could be formed by illuminating with right-handed CPL, albeit that long irradiation times (90 min) were necessary.

Photoswitching can also be achieved in the ferroelectric smectic C^* phase by using achiral azobenzene dopants in chiral phases [127] or using chiral thioindigo dopants in achiral hosts [128, 129]. In the latter case, the dopant molecule was specifically designed to invert the sign of the spontaneous polarisation in the smectic C^* phase upon irradiation. The polarisation is changed by varying the transverse dipole moment of the molecule upon isomerisation, as it is this factor which determines the helical sense in these LCs. Aggregation of the dyes is a possible reason for the lower efficiency of the dopant as its concentration is increased in the host smectic. In any case, the bulk chiral properties of the LC material are modified by minute changes in stereochemistry at the molecular level.

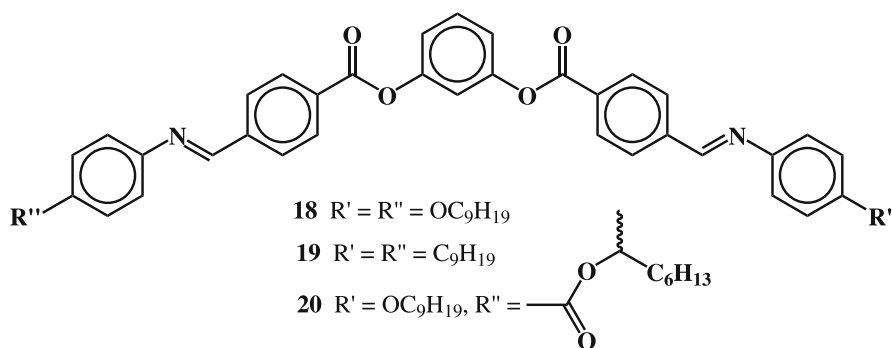
3.3

Spontaneous Resolution in Achiral and Racemic Liquid Crystals

Spontaneous formation of chiral LC phases from achiral mesogens—an equivalent to spontaneous resolution of achiral compounds in crystals but in a fluid phase—is a relatively recent phenomenon [9, 130–132]. The first compounds discovered with this extraordinary property were the “bent-core” or “banana-shaped” mesogens [133, 134].

A detailed analysis of the high temperature mesophase formed by the achiral compounds **18** and **19** revealed spontaneous resolution and an extraordinary stereochemical complexity of the systems at the supramolecular level [132].

The molecules form tilted layers that pack to give either racemic or enantiopure stacks which are defined by three supramolecular factors (Fig. 17) [133] (i) the chirality (tilt angle) of each layer, *P* or *M* with respect to the normal to the layer plane; (ii) the relative interlayer clinicity *in the tilt*



plane, either synclinic or anticlinic, and; (iii) The relative directions of the polar axes (P, defined by the C – H bond direction at the central 1,3-phenylene ring) of the layers, either ferroelectric (parallel axes) or antiferroelectric (antiparallel axes). Thus, there are the four possible phases depicted in Fig. 17.

Freely suspended thin films of **18** and **19** have chiral layers of molecules, as evidenced by depolarised reflected light microscopy in conjunction with small applied electric fields. The layers stack on top of each other with alternating chirality giving a racemic compound [134]. When the materials were located in electro-optic cells, two different polymorphs were observed in the transmission polarised light micrographs: [134] a more abundant racemic compound ($\text{SmC}_\text{S}\text{P}_\text{A}$), and a minority conglomerate $\text{SmC}_\text{A}\text{P}_\text{A}$. Proof of the enantiomeric domains came by switching an applied electric field in opposite directions, and noting opposite optical twisting of the extinction brushes

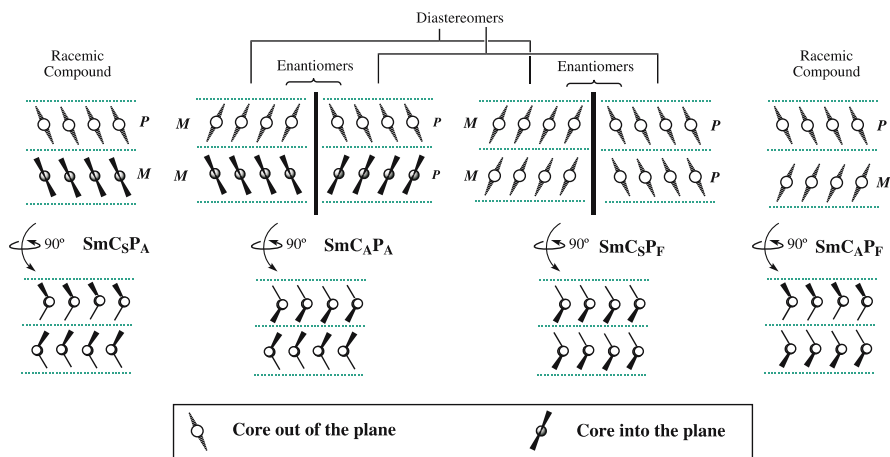


Fig. 17 The stereochemical possibilities for packing in bent-core molecule phases

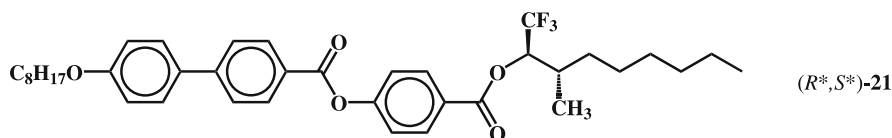
depending on the field direction and the domain. The metastable minority domains are formed predominantly by warming the lower temperature phase. The origin of this remarkable discovery probably resides in the conformational chirality of the core of the molecule, arising from twisting of the aromatic rings joined by ester or imine units which can be of *P* or *M* chirality, and this twisting is then transferred hierarchically through supramolecular interactions.

A shrewd design strategy based on the observations outlined above and precedents in other LCs led to the preparation of a molecule (**20**) which favours anticlinic unions between the smectic layers: it is a ferroelectric liquid crystalline conglomerate. [135] In the *polar plane* the ferroelectric SmC_5P_F is anticlinic and the 1-methylheptyloxycarbonyl group promotes anticlinic interfaces in other mesogens. The racemate **20** forms the so-called B7 LC phase (SmC_5P_F in Fig. 17), as confirmed by the characteristic behaviour of the phase in electric fields. Another very interesting observation in this type of material [136–138] is that when the isotropic phase is cooled to the B7 phase left- and right-handed helical ribbons and tubes are observed with a polarised light microscope, another example of spontaneous resolution.

Supramolecular chemistry can be used to create the bent cores that give rise to the symmetry breaking in this family of liquid crystals [139]. The formation of a complex between a calamitic benzoic acid derivative and a bent core terminated with a pyridyl group—neither of which display mesomorphic behaviour—gave rise to a material which displayed SmCP mesophases. The achiral bent cores can also give rise to symmetry breaking when they are attached to flexible polymeric chains, such as poly(siloxane) [140].

More classical calamitic (rod-shaped) mesogens can also form conglomerates. The *unlike* racemic mixture (with two stereogenic centres with opposite configurations with respect to each other, which exist as *RS* or *SR*) of compound **21** with two stereogenic centres in its tail forms a smectic phase in an electro-optic cell [141]. The diastereomers show electro-optic switching of the mesophase akin to chiral compounds (racemates and achiral compounds normally show no switching because there is no net dipole). Evidence for conglomerate formation was also revealed in the textures of the smectic phase in a polarising microscope. This spontaneous resolution, which was not observed in the corresponding homologues with just one substituent in the chain, was attributed to a bent orientation of the alkyl chain with respect to the rigid core of the molecule, and its greater rigidity when two substituents are present in the chain [142].

Achiral nematic-type LCs formed by certain *trans*-4-alkylcyclohexane carboxylic acids [143] and 4-*n*-alkyloxybenzoic acids [144] also show signs of spontaneous resolution. These molecules form a dimer at low temperatures arising from hydrogen bonding between acid groups in a complementary manner, which can interconvert with a dimer united by a single hydrogen bond, and eventually dissociate at higher temperatures. The chirality



was inferred from textures observed in the polarised transmission micrographs during cooling from the isotropic phase, which were characteristic of cholesteric rather than nematic phases. The latter were observed on further cooling, although near the surface chiral grains were still observed. The author's hypothesis implied surface anchoring of the acids, followed by oligomerisation of the open singly hydrogen-bonded aggregate to generate a chiral superstructure [144]. The surface attachment is reversible, since the chiral domains appear randomly throughout the cell on heating cycles. While the explanation is still rather vague, this is a nice example of how a surface might initiate supramolecular chirality spontaneously.

The bent core molecules do not only exhibit spontaneous resolution in smectic phases. One achiral derivative resolves in a nematic phase in this fluid state [145], while a substituted oxadiazole which forms a biaxial nematic phase also segregates [146]. The bent core clearly has a special stereochemical influence as a result of the effects it induces beyond the molecule, at least for liquid crystals.

4

Gels

The term gels refers to a range of materials which are grouped under the general definition: A dilute mixture of two or more components which form a separate uninterrupted phase throughout the system [147, 148]. This classification includes chemical gels—where covalent bonds create the continuous network—and physical gels which are maintained by non-covalent interactions, which concern us here.

In general, low molecular weight molecules that gel fluids do so by forming an infinite entangled network of supramolecular fibres in the solvent [149, 150]. Hydrogen bonds and van der Waals interactions are both important in the formation of a good gel, but crystallisation has to be avoided. Thus, a delicate balance of the intervening intermolecular interactions must be achieved in order to hinder the crystallisation of compounds favouring the gel formation.

Amide derivatives of *trans*-1,2-diaminocyclohexane have proven to be particularly reliable gelators (Fig. 18). A simple alkylamide derived from this compound can gelate a wide range of organic liquids—from hexane to acetonitrile, ethyl acetate to silicone oil—in concentrations below ten grams per litre of liquid. In the case of hexane, one molecule of gelator interacts with

around 600 of the solvent [151]. Chemical constitution is also a crucial issue: The *cis* isomer forms no gels at all. IR studies of the gels formed by the *trans* isomer shows stretching vibrations typical of amide groups involved in the formation of hydrogen bonds. CD spectra of loose gels show very significant exciton coupled Cotton effects, the most intense of which appears at 212 nm (positive for the *S,S* enantiomer and negative for *R,R*) which disappear when the gel is heated and the solution becomes isotropic. Direct evidence for the formation of helical fibres in the gel was obtained by TEM imaging on a stained loose gel. Intertwined aggregates formed from these fibres, with widths of 40–70 nm and pitches of around 150 nm, were observed. The helices were always right-handed for the *R,R* sample, and the opposite for the enantiomer. The proposed structure for the molecular aggregate involves antiparallel chains of hydrogen-bonded amides (Fig. 18). These aggregates must come together to form the helical tapes seen in the TEM images, which in turn interact by van der Waals forces with the solvent.

Thermoreversible liquid crystalline gels can be prepared using the same gelling agent [152, 153]. Figure 19 shows the phase transition behaviour of the mixture of **22** and the nematic LC 4-pentyl-4'-(cyano)biphenyl as a function of mol.-% of **22**. These mixtures exhibit two transitions, gel–gel and gel–sol. It is worth noticing that two thermally reversible gel states with order and disorder are achieved. The sol–gel transition temperature from isotropic liquid to gel increases as the molar ratio of **22** increases while the other transition temperature remains unchanged, being almost identical to the isotropic–nematic

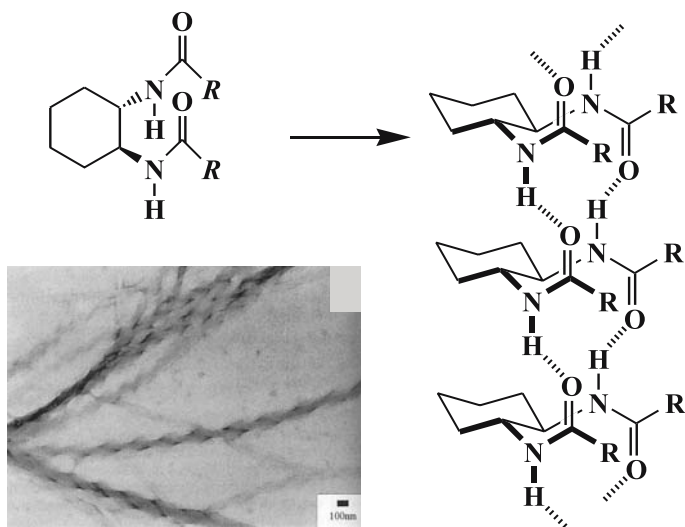


Fig. 18 Proposed structure for the molecular aggregate formed by the *trans*-(1*R*,2*R*)-bis(alkylamino)cyclohexane and a TEM image showing the helical fibres in one of the gels. TEM image reprinted with the permission of Wiley [151]

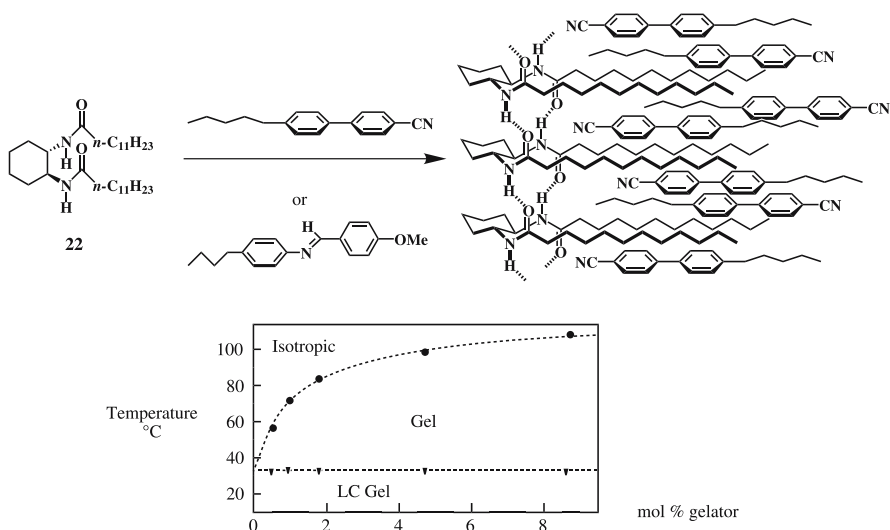


Fig. 19 Phase transition behaviour of the mixture of **22** and the LC 4-pentyl-4'-(cyano)biphenyl (nematic: 24–35 °C) as a function of their molar ratios and proposed structure for the molecular aggregates

transition temperature of the pure nematic compound. Another interesting result is that the sol–gel transition is not dependent on the structure of the mesogenic compound, as revealed by the thermal behaviour of the gels formed by the LC 4-(methoxy)-benzylidene-4'-(butyl)aniline (nematic: 22–47 °C) and **22**. In this particular case the sol–gel transition temperature is identical to the previous case while the sol–gel transition occurs at 45 °C.

Incorporation of urea functions onto the diaminocyclohexane scaffold also produces very good gels of organic solvents and oils [154–156]. The co-operative nature of aggregation in these gel systems was studied elegantly by employing enantiomeric bis-urea cyclohexanes incorporating azobenzene units as photoisomerisable guest chromophores to probe the chiral microenvironment [157]. Spectroscopic methods showed differences in the rates of isomerisation of the azobenzene group when it was incorporated into gels containing majority gelators of opposite handedness, and therefore implied that chiral recognition plays an important role in determining the structure of the gels.

Ionic compounds can also gelate solvents, perhaps one of the nicest examples being that of dicationic gemini surfactants in which tartrate is used as the counterion and source of chirality [158], because it shows the very important role of chirality on the property of the salt. When either D- or L-tartrate dianions and dimers of cetyltrimethylammonium cations are combined, stable gels are formed in chlorinated solvents, but neither the mixture of enantiomers nor the *meso* tartrate form a gel. The structure of the gelator

aggregates in these organic solvents is presumably a kind of inverse micelle. The authors invoked both hydrogen bonding and electrostatic interactions between the bridged pairs of ions, and subsequently developed a model for the interaction in membranes derived from the same materials [159]. The compounds also gel water, but this time the racemic mixture does form a gel. The textures formed by the enantiomers in the gels in both chloroform and water are very long helical fibres about 20 nm in width and with a pitch of about 130 nm in chloroform and 250 nm in water. The D- and L-enantiomers give fibres of opposite handedness, and the mixture of the two enantiomers in water shows plates. The authors proposed that the gels are multilayers with either tails or head exposed to the solvent depending on its polarity.

Amido alcohols are often good candidates for the formation of organogels. Chiral bis(amino alcohol)oxalamides are capable of gelating a variety of organic compounds. The structural basis for the fibres observed in the gels was obtained by X-ray crystallography [160]. The structures are comprised of layers of molecules in which chains form through amide hydrogen bonds. These chains unite through weaker hydrogen bonds involving the hydroxyl groups (Fig. 20). The capacity of the compounds to gel solvents is very sensitive to the chiral modification. TEM images show fibres without any chiral morphology. A variety of functionalised gluconamides [161, 162] and their metal complexes also form gels in a range of solvents. The helical nature of the aggregates can be visualised in some cases by TEM [163]. In particular, it is interesting that the compounds can be used to gel acrylates, and that polymerisation starting from the gelled state leads to imprinted structures. Although the helical nature of the fibres was not obvious in the morphological features in the polymer, this may lead to a number of interesting opportunities [164]. The sensitivity of the morphology of gels to chiral composition has

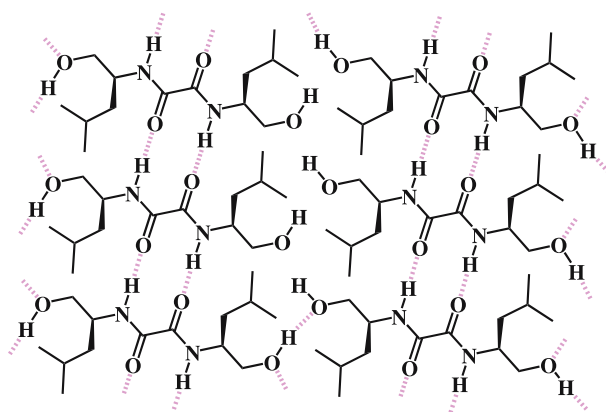
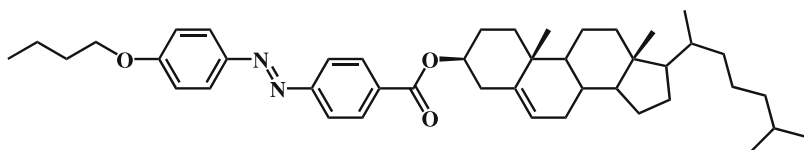


Fig. 20 Layers formed in the crystals of a chiral bis(amino alcohol)oxalamide

also been shown for two-component gels incorporating dendritic peptides as one of the components and an aliphatic diamine as the other [165].

The incorporation of azobenzene moieties into gel-forming molecules can afford materials which switch from solution to gel and the reverse upon irradiation, as shown elegantly for cholesterol derivatives such as **23** [166]. CD spectroscopy is a very useful tool for the observation of the helical aggregates that are formed in the gel state, because they have a significant optical activity, while the solution state is virtually devoid of it. Interestingly, some of the derivatives showed a sensitivity of their chirality on the cooling rate from the isotropic solutions. The opposite handedness of aggregates was not only seen by CD spectroscopy but also by SEM. A light-driven transition was caused by irradiating at 330–380 nm from the gel state, with the azobenzene in the *trans* conformation, to the solution state, where the azobenzene is in the *cis* conformation (which does not pack efficiently). The reverse process was achieved by irradiating at wavelengths longer than 460 nm.

The use of the gel state to transfer supramolecular into molecular chirality has been elegantly demonstrated for the dithienylethene derivative **24**, which can be converted to the closed form **25** with UV radiation [167]. Compound **24** can exist as two diastereomers with opposite helicity (Fig. 21). When **24** is irradiated in solution a 1 : 1 mixture of the diastereomers of **25** was obtained, so there was no transfer of chirality during the reaction. When the same reaction is carried out in the gelled state—which shows fibres with a clear helical structure—by irradiating at 313 nm, a 98 : 2 ratio of diastereomers in a yield of 40% at the photostationary state was obtained. The result shows clearly that there is a preference for one of the conformational diastereomers in the gelled state thanks to induction from the stereocentres near the hydrogen bonding sites which presumably drive the fibre formation. Curiously, the new state of the gel is metastable, as a heating and cooling cycle of the diastereomeric **25** gave fibres with an inverted helicity, as revealed by CD spectroscopy. Thus, performing the ring-opening reaction with visible light can lead to a metastable form of the gel formed by **24**, which was otherwise inaccessible. It is a beautiful example of the interplay between molecular and supramolecular chirality leading to a sophisticated molecular material.



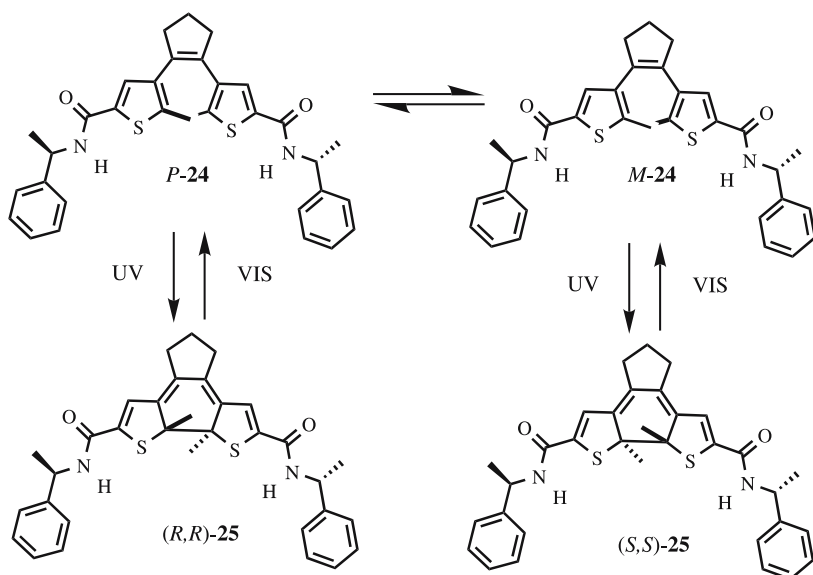


Fig. 21 The different open (24) and closed (25) states of a chiroptical switch in a gel

5

Chiral Magnets

There has been a surge of interest in the preparation of chiral molecular magnets as a result of the seminal work which showed the presence of magnetochiral dichroism in luminescence from a paramagnetic complex in solution [168]. The use of non-covalent interactions in the preparation of chiral molecular magnets of organic and metallo-organic nature will be reviewed, with special reference to the pathways of chiral induction, and the relation between supramolecular structure and optical activity in the systems.

A number of purely organic chiral radicals have been prepared which exhibit optical activity and paramagnetic nature at room temperature [169–174], while at low temperatures the interactions between the unpaired electrons are antiferromagnetic. Perhaps the most thoroughly investigated system to date is that of the phenyl nitronyl nitroxides [175]. This system can have four diastereomeric conformations in the molecular sense, where the twist in the imidazolyl unit and the angle between this ring and the phenyl substituent can be positive or negative (Fig. 22) [176]. Which diastereomer is adopted in the crystals of the compounds depends largely on the interactions in the solid.

A series of radicals bearing side chains derived from the same enantiomer of lactic acid show all four of the possible diastereomers depending on the position and nature of the lactate residue (ester or acid) and the other substituents [177]. The compounds bearing acid groups invariably form

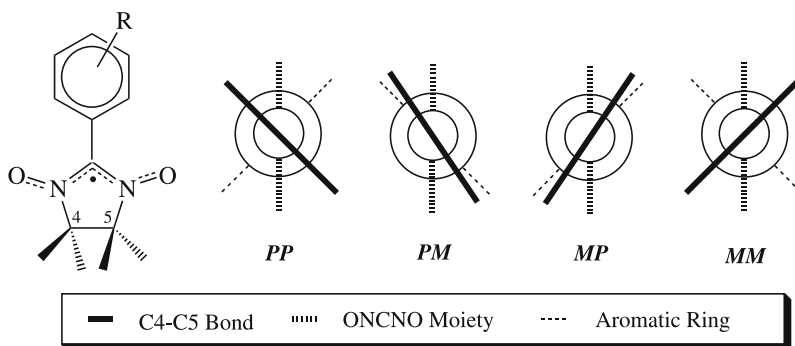


Fig. 22 The chiral conformations exhibited by phenyl nitronyl nitroxides

hydrogen-bonded chains in the crystals by interaction with the nitroxide groups [178]. CD spectroscopy in the solid state is particularly useful for determining the optical activity of the compounds as a function of the molecular and supramolecular structures [179].

A purely organic chiral nitroxide which shows liquid crystalline behaviour as well as intriguing magnetic properties and a dependence on the enantiomeric nature has been reported [180]. The reason for studying the compounds was to increase the sensitivity of mesophases to magnetic and electric fields. The racemic modification of the radical, which displays a nematic phase, proved to be more sensitive to alignment than the cholesteric phase with the enantiomers present. It was proposed that the compounds may also be used to study the dynamic nature of mesophases by electron paramagnetic resonance spectroscopy.

The low optical activity and the absence of ferromagnetic order in the purely organic compounds makes them inadequate for the observation of magnetochiral effects [181], and therefore coordination compounds incorporating the radicals are more interesting. The combination of the nitronyl nitroxides with metal hexafluoroacetylacetonate (hfac) can produce molecular magnets [182]. When manganese(II) is used as the metal ion and the complex with the nitroxide ligands provides a coordination polymer, the antiferromagnetic interaction between the metal and the radical gives rise to ferrimagnetic chains which order at low temperatures. A chiral complex of a phenyl nitronyl nitroxide with manganese hfac is actually known [183]. A phenyl nitronyl nitroxide with a methoxy group in the *para* position to the radical forms a 3_1 helical coordination polymer in the solid state (Fig. 23). There are no significant non-covalent interactions between the chains. The complex orders magnetically at about 4.8 K. The isomorphous cobalt complex can also be prepared, but the formation of a chiral structure is extremely sensitive to the substitution pattern on the nitroxide [184], added to which the

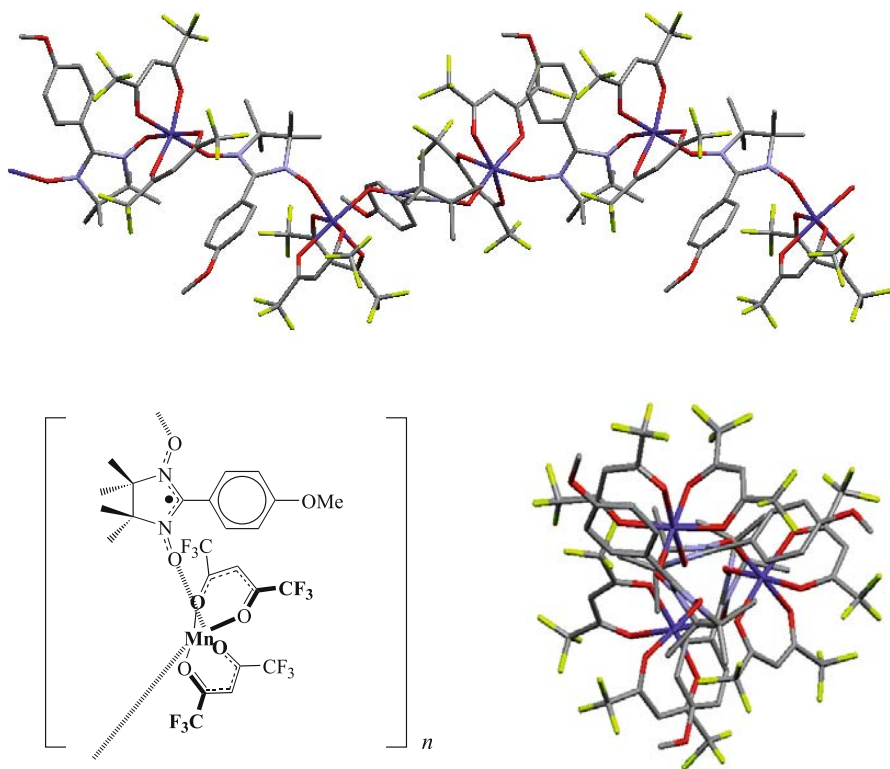


Fig. 23 A spontaneously resolved chiral complex between $\text{Mn}(\text{hfac})_2$ and a phenyl nitronyl nitroxide which is a magnet

collection of crystals is racemic. Therefore, chiral induction is a better way to prepare optically active magnets.

Chiral induction from anions or organic ligands to metal ion centres is well documented, if not entirely predictable because of high coordination numbers and multitude of metal ions [10]. When the chiral nitroxide (*R*)-3MLNN is crystallised with manganese(II) hfac a coordination polymer is formed in which the chirality in the ligand induces a chiral Λ configuration in the manganese coordination sphere [185], as shown in Fig. 24. Interestingly, the chiral conformation adopted by the ligand—regarding the helicity between the phenyl ring and the imidazolyl ring and the imidazolyl ring itself—is of the same type as that seen in the isolated ligand's crystal structure. The optical activity of radical ligand in the free state and in the complex is quite different, because of the charge transfer taking place between the two, as revealed in the solid state CD spectra (Fig. 24). The Cotton effect at approximately 460 nm in the complex is at a wavelength of low absorption, which is good for observing magnetochiral dichroism. In addition to being optically

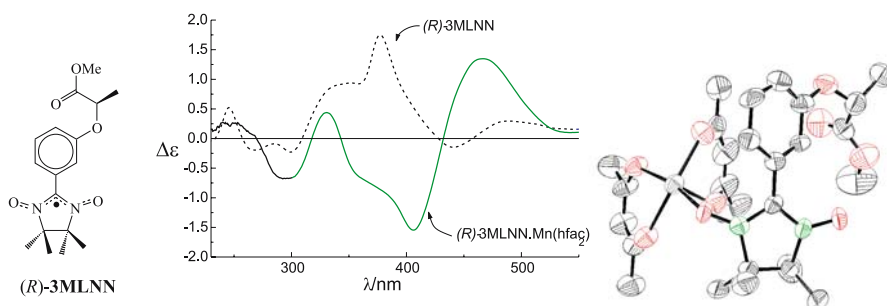


Fig. 24 The radical (R)-3MLNN, the monomeric unit in the crystal structure of the complex with $\text{Mn}(\text{hfac})_2$, and the solid state CD spectra of the two in KBr

active, this metal-radical-based material is interesting since it is a magnet at low temperatures.

In addition to these nitronyl nitroxides, bisnitroxides which have a triplet ground state can be used to link metal centres to generate molecular magnets [186]. Making use of a chiral derivative of just such a bisnitroxide, an optically active metamagnet was prepared using $\text{Mn}(\text{II})(\text{hfac})_2$ as the source of metal ion [187, 188]. The complex consists of alternating organic ligands and metal ions in a 2_1 chain. Here, the complex could even be identified in solution by CD spectroscopy, unlike the previous cases. Attempts to extend this approach to chiral triradicals have also led to partial success [189], although no structural data are available to our knowledge.

A quite remarkable case of spontaneous resolution in a magnetic system was found when tetrathiafulvalene (TTF) was electrocrystallised in the presence of mellitate anions [190, 191]. Electrochemical oxidation of TTF was carried out in the presence of metillic acid and pyridine, leading to the formation of hexagonal plates of the salt $[\text{TTF}^+]_2[\text{C}_6(\text{COO})_6\text{H}_4^{2-}]$, which has the crystal structure shown in Fig. 25. The salt, which belongs to the space groups $P6_222$ or $P6_422$ depending on the enantiomer, contains a helical stack of TTF radical cations which coincides with the 6_2 screw axis, while the metillate anions form a double helical hydrogen-bonded chain around this stack. This kind of regular stacking in flat π -functional materials is virtually without precedent [192]. In fact, in the present case, one of the two crystallographically independent TTF units is partially disordered [as shown in Fig. 25 (iii)]. Unfortunately, magnetic susceptibility measurements show that the chain of radicals has a singlet ground state, with the TTF units thought to be dimerised. The disorder in the crystal gives rise to a higher than expected paramagnetic contribution to the susceptibility, but even so it corresponds to only 1.7% of the radicals. Nonetheless, it is an intriguing material which may provide inspiration for new magnets or conductors. Indeed, the preparation of the corresponding tetramethyl-TTF [193] and ethylenedithio-TTF [191]

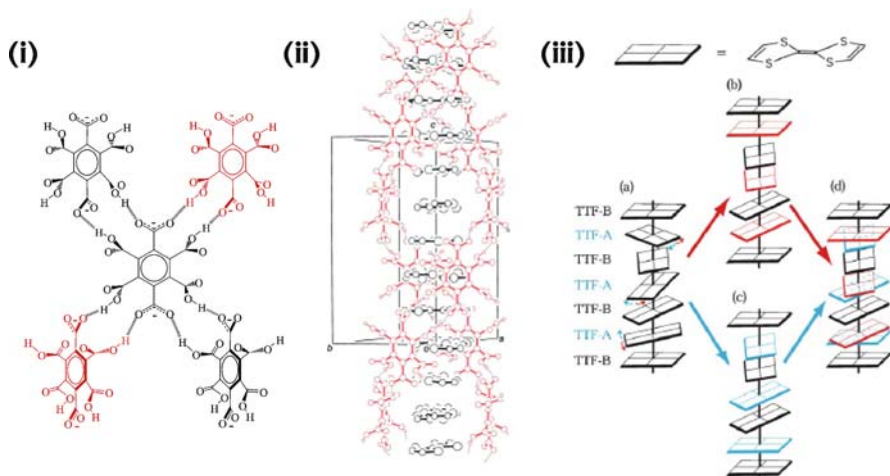


Fig. 25 Representations of parts of the solid state structure of the salt $[\text{TTF}^+]_2[\text{C}_6(\text{COO})_6\text{H}_4]^{2-}$. (i) The hydrogen bonds between the mellitate ions. (ii) The helically arranged TTF cation radicals in the double helix of mellitate anions. (iii) Disorder in the stacks, (a) shows the regular helix, (b) and (c) two dimer faults and (d) the average column with disorder in the A site. Adapted and reprinted with the permission of the Royal Society of Chemistry [191]

salts has already been achieved, although here the packing is achiral in either sheets or channels with different topology and topography to the chiral salt.

Spontaneous resolution can afford chiral coordination polymers [194]. A particularly nice example of this phenomenon is the formation of azide-linked manganese complexes in which twisted diazine ligands complete the coordination sphere [195, 196]. It is an interesting case in that partial spontaneous resolution takes place, because the racemic compound is also formed along with the chiral one, which contains a 2_1 chain of manganese ions linked by the diazine unit. Both compounds are weak ferromagnets. The spontaneous resolution process is sensitive to the ligand that is employed, slight changes result in the formation of racemic compounds or conglomerate [196].

The coordination chemistry of oxalate (ox , $\text{C}_2\text{O}_4^{2-}$) compounds provides a series of very interesting compounds from the stereochemical and magnetic points of view [197]. Most frequently the compounds form honeycomb layers in the presence of transition metal ions, in which the stereochemistry of the metal ion coordination sphere alternates between Δ and Λ . However, a three-dimensional homochiral structure is also possible. On the other hand, the negative charge of the oxalates necessitates the incorporation of cations between them, which provides the opportunity to introduce chirality and additional functionality in materials. The compound formed between homochiral manganese II oxalate and iron II tris-2,2'-bipyridine (bpy) with formula $[\text{Mn}_2^{\text{II}}(\text{ox})_3]_n^{2n-} [\text{Fe}^{\text{II}}(\text{bpy})_3]_n^{2+}$ crystallises in the space group $P4_132$.

The formal oxalate subunits act as three-directional connecting points and form a well-defined 3D 3-connected 10-gon net (10,3). Three cations occupy the spaces. This is a helical supramolecule that orders antiferromagnetically on cooling below 13 K [198, 199]. Changing the nature of the metal ions coordinated by the oxalate and bipyridine units gives rise to magnets [200, 201], or to compounds which show energy or electron transfer [202, 203], and even to complexes which exhibit spin transitions [204]. In particular, the use of resolved Cr(ox)_3^{2-} as a building block for these three-dimensional chiral materials has proven particularly fruitful, giving complexes which show marked optical activity—as shown by CD spectroscopy—and magnetic ordering [205–207].

Ferrimagnets based purely on the magnetic interaction between more strongly coupled transition metal ions have the potential to provide materials with much higher transition temperatures than the examples cited so far. The complex formed when manganese(II) perchlorate and potassium hexacyanochromate are mixed with (S)-1,2-diaminopropane ($\text{C}_3\text{H}_{10}\text{N}_2$) dihydrochloride affords a compound with empirical formula $\text{K}_{0.4}[\text{Cr(CN)}_6][\text{Mn(S)} - \text{C}_3\text{H}_{10}\text{N}_2](\text{S}) - \text{C}_3\text{H}_{10}\text{N}_2\text{H}_{0.6}$ in which four cyanide groups are coordinated to the Mn(II) ions giving helical dimetallic loops, whose chirality is determined by the coordinated diamine [208]. The crystals belong to the space group $P6_1$. Magnetic measurements reveal that the compound is a three-dimensional ferrimagnet with an ordering temperature of 53 K, relatively high for a molecular material. Varying the experimental conditions for the crystallisation gives a two-dimensional network in which there are four coordinating cyanide groups to the manganese ion again, but there is no additional amine in the structure, which pertains to the $P2_12_12_1$ space group [209]. The compound orders ferrimagnetically at 38 K, as witnessed both by magnetisation experiments and magnetic circular dichroism spectroscopy, which shows very intense Faraday effects below the transition temperature and 400 nm. Replacing the amine in the previous examples by D- or L-amino alanine produces a three-dimensional chiral ferrimagnet with a triple helical stranded structure in the $P6_3$ space group [210]. In contrast to the previous structures, the manganese ion is surrounded by the chiral ligands which links these cations to give helical chains which in turn come together. There are three manganese ions per chromate, and all the cyanide groups coordinate to them. The ferrimagnet orders at 35 K. This compound is unique, in that it may possess a helical spin structure. Hexacyanoferrate has also been used as a building block for the construction of chiral magnets in which the optical activity originates from enantiomers of *trans*-cyclohexane-1,2-diamine coordinated to nickel or copper(II) ions [211, 212].

The preparation of chiral magnetic materials is not limited to those that show paramagnetism and magnetic ordering. Another important phenomenon is that of spin crossover, as it can lead to bistable systems, that in addition can be switched by light [213, 214]. A homochiral spin crossover

compound incorporating iron(II) and iron(III) centres was achieved by spontaneous resolution during the crystallisation of iron(III) nitrate with the tripodal ligand tris{[2-((imidazole-4-yl)methylidene)amino]-ethyl}amine in the presence of base [215]. Two-dimensional sheets are present in the crystals where the di- and tri-valent iron cations (both surrounded by the tripodal ligand) are linked to each other by imidazole to imidazolate hydrogen bonds. The proof of the conglomerate was shown in the CD spectra of the enantiomeric crystals. The material was shown to undergo a spin state transition both thermally and under light irradiation from the low spin state which exists at low temperatures to the high spin state (which predominates above 150 K). The chiral material provides an advantage over others, in that the spin state can be read out using optical rotation at long wavelengths, which does not disturb the spin state of the material, and therefore makes the compound interesting as a model for data storage using these methods.

6

Materials with Interesting Optical Properties

6.1

Colourants

Colourants are perhaps the oldest recognised synthetic molecular materials, and they present a wide range of properties, both optical and other, and a varied supramolecular chemistry [216, 217]. Several chiral dyes are known and their aggregates have been studied [218, 219]. Here we shall concentrate on the more recent advances in the area.

Achiral dyes have been shown to aggregate into structures which spontaneously resolve *and* generate an enantiomeric excess of one of the chiral supramolecular assemblies. A series of benzimidocyanine dyes (**26**) shows spontaneous generation of chirality in dilute basic aqueous solutions [220]. The chirality is observed when measuring the CD spectra of the dyes *J*-aggregates (named after one of their discoverers, Jelley), which present optical activity in the two absorption bands (a Davydov-split band) shifted to long wavelength with respect to the longest wavelength band of the isolated molecule. Addition of dilute aqueous NaOH to ethanolic solutions of the dyes containing isolated molecules produces optimum induction of chirality. Proof that the CD spectra observed were not artefacts (linear dichroism) was achieved by embedding the aggregates in a polymeric matrix and observing the spectrum at defined angles [221].

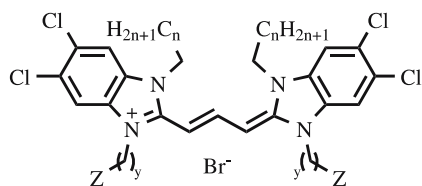
A statistical plus-minus distribution of the sign of chirality is observed. The formation of the chiral aggregates is reversible by cooling or heating the sample, a procedure which causes the formation of a different achiral aggregate. This effect bears witness to the equilibrium state of the system, and

might point to a type of spontaneous resolution either as a result of multiple nucleation centres or under racemising conditions, where small chiral aggregate fragments break off a growing chiral supermolecule and initiates the growth of another larger supermolecule.

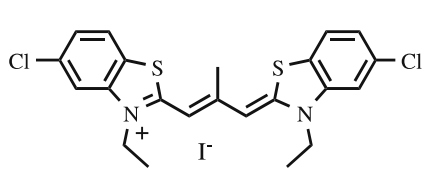
Chiral systems of biological origin or inspiration can behave as templates for the formation of chiral dye aggregates. DNA can be used as a template for dye aggregates to generate chiral superstructures in which dye molecules form end-to-end dimers [222]. Very recently, a role reversal has been achieved, in that a chiral dye has induced a chiral conformation on a peptide nucleic acid duplex [223]. The addition of adenosine 5'-triphosphate (ATP) to aqueous solutions of the dichloro-substituted thia-carbocyanine dye **27** produced an immediate colour change and the appearance of Cotton effects in the areas of the visible spectrum corresponding to H-aggregated dyes [224]. The aggregates grow and separate from the dispersions as fibrous microstructures. TEM images showed that nanowires can be formed, with a width of about 10 nm and several micrometers long. No fibres were observed for either components, and other phosphates do not lead to fibres either; the phenomenon is specific to ATP. The assembly-disassembly is thermally reversible, and heating-cooling cycles give rise to more homogeneous wires. Unlike the aggregation of dyes with macromolecular biological systems, this example gives rise to continuous dye aggregates with excitation-delocalisation, and energy migration within them is expected.

Supramolecular chiral induction into dye chromophores can also be achieved in totally synthetic systems. Interpenetrated ion pairs of cyanine dyes and chiral borate anions show that the twisting of the dye is important for the observation of the induced optical activity by CD spectroscopy [225]. The incorporation of merocyanine dyes into synthetic self-assembled systems provides important information about their stability and chirality [226].

Dyes can also be incorporated into hydrogen-bonded superstructures using the complementarity of the hydrogen bond donors and acceptors. The addition of a perylene bisimide dye to chiral dialkyl melamine derivatives leads to aggregates (Fig. 26) which show induced circular dichroism in the dye part of the assembly in methylcyclohexane as well as the formation of mesoscopic fibres when the solvent is evaporated [227]. The melamine compounds



26 ($Z = \text{COOH}, \text{SO}_3\text{Na}, n \geq 6, y = 2, 3$)



27

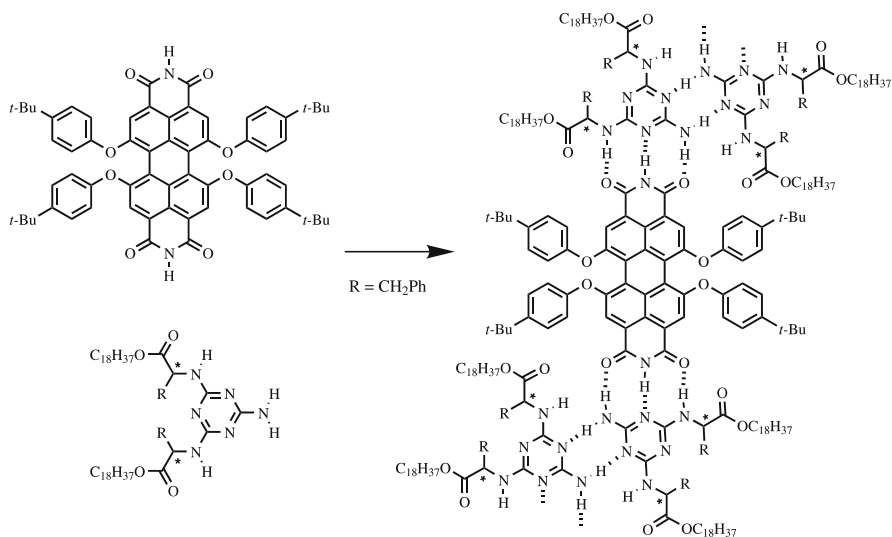


Fig. 26 The assembly of a perylene imide dye with a chiral melamine derivative to give chiral supramolecular chains

themselves are capable of forming aggregates, but because of the strength of bonding between the imide and amine groups, the dye's incorporation is favoured. In addition, within these aggregates the perylene moieties stack with each other, even at very low proportions of the dye with respect to the melamine. The assembly process is sensitive to the type of substituent at the stereogenic centres in the melamine derivative. The exciton coupling seen in the CD spectra allowed assignment of the handedness of the assemblies.

In a very different way, various N-substituted chiral perylenes have been prepared and their assembly in the presence of p-type materials was studied [228]. When the perylenes were mixed with oligo(para-phenylene vinylene) compounds in methylcyclohexane, "orthogonal self-assembly" took place, in which aggregates of the perylenes and oligomers formed separately. Indeed, in this solvent, the perylenes form aggregates, a phenomenon which was proven by variable temperature CD experiments in which intense signals were observed at low temperature, which vanished when the temperature was raised sufficiently. Spin casting of solutions onto mica resulted in fibres of these assemblies containing the two supramolecular networks, which were observed by AFM. When toluene was used as the solvent, neither orthogonal self-assembly nor fibre formation took place. In films prepared from both solvents, electron transfer takes place.

Porphyrins are very interesting chromophores for optically active compounds [229], especially in the realm of chiral supramolecular materials. More frequently than not they are used as chiral reporters of host stereochemistry by interaction of guests with the centre of the ring [230–234], and

the chirality induced in the porphyrin can even be “memorised” [235, 236]. These compounds also provide a particularly interesting example of chiral expression in an achiral chromophoric system that is displayed upon aggregate formation by the multiply charged porphyrins. The family of 4-sulfonatophenyl porphyrins shown in Fig. 27 form *J*-aggregates in their diprotonated form (in which all the pyrrole rings bear protons) in water as a result of the electrostatic interaction between the anionic and cationic parts of the molecule [237]. The aggregation was detected by absorption spectroscopy as well as by CD spectroscopy. This result shows that when aggregation occurs in the absence of a vortex, spontaneous symmetry breaking takes place giving dextro or levo-rotary aggregates in a random way [238]. However, when the aggregates are formed while the solutions are stirred in one direction, the vortex leads to assemblies of one handedness [239]. It is believed that the molecules form ribbon-like aggregates which kink during their formation in one sense or the other, as shown schematically in Fig. 27, and this gives rise to the chirality. The authors believe that this vortex-induced chiral effect may be useful in soft materials, catalysis, and even that it might explain the genesis of chirality in prebiotic times. Subsequently, self-replication of chiral memory has been demonstrated in related porphyrin systems [240], and the hierarchical assembly process has been influenced using the sergeants and soldiers effect [241]. Self-assembly can also be effected in organic solvents for systems related to chlorophyll [242].

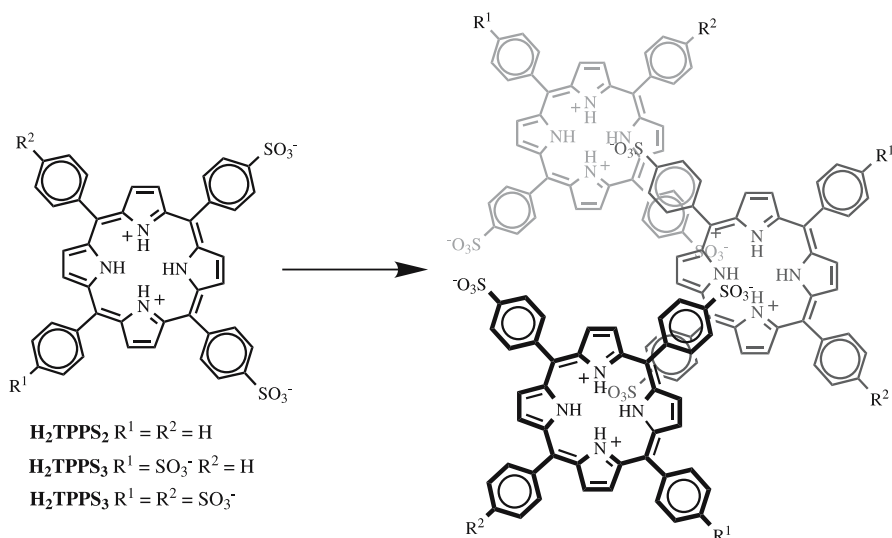


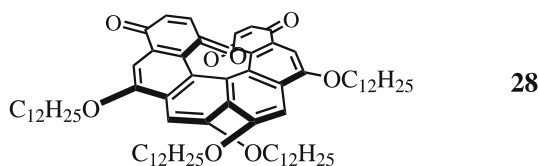
Fig. 27 Charged porphyrins which self-assemble in water to give chiral aggregates

6.2

Nonlinear Optical Materials

The preparation of materials which display non-linear optical properties—the frequency multiplication of light—can benefit enormously from simultaneous control of supramolecular structure and chirality. For the observation of second-order non-linear optical (NLO) effects, the existence of a non-centrosymmetric structure is a prerequisite [243]. So the use of chiral materials increases the chances of having an effect [244], although the magnitude can be almost nullified by the adoption of pseudo-centre symmetry. Polar order is required, and therefore control of the supramolecular structure in these chiral systems is also essential. Crystal engineering can be used for the organisation of chiral molecules, as nicely shown for a chiral quinoid compound which organises via hydrogen bonds between the molecules [245], or in coordination chemistry for the preparation of chiral networks [246]. However, other organisational techniques are preferred.

A beautiful example of supramolecular control over the scale of the second-order non-linear optical response is that of the helicenebisquinone **28**. In its non-racemic form, this compound self-assembles into fibres in which the molecules are organised in hexagonally packed columnar stacks [247], which have huge optical activity [248]. The racemic form does not generate fibres at all. Films of the molecules were prepared by the Langmuir–Blodgett (LB) technique, up to 60 layers, and the non-linear optical properties were measured [249]. The intensity of the second harmonic for the non-racemic sample is approximately 1000 times that of the racemic film, which corresponds to an increase in susceptibility of approximately 30-fold. An interpretation of the data collected implied that not only was polar order important, but the intrinsic chiral form of the molecular and supramolecular organisation was vital to explain the magnitude of the effect. In the films prepared by the LB method, AFM measurements of the non-racemic sample show much longer nanometre scale fibres than does the racemic sample, and the order of these fibres is more homogeneous. This observation suggests that packing of the different enantiomers in single fibres is not favoured, while those of single enantiomers is. The dominance of chiral tensor components and the high NLO activity—despite the non donor-acceptor character in the molecule—constituted a conceptually important step in this area.



Liquid crystals are interesting supramolecular systems which can show second harmonic generation when they are aligned appropriately. Ferroelectric LCs [250] as well as bent-core molecules have been used to this purpose, and show reasonable second harmonic generation [251]. These materials combine non-linear optical effects with simple processing procedures on account of their liquid crystalline flow characteristics and the possibility of organising them with electric and magnetic fields.

6.3

Luminescent Materials

The organisation of luminescent materials is interesting for a number of reasons. Chiral supramolecular systems that have been extensively investigated because of their potential applications in light-emitting diodes or photodiodes are the substituted oligophenylenevinylenes (OPVs). In particular, the use of the ureido-s-triazine as a hydrogen-bonding unit has been particularly productive in the organisation of the OPV units [252, 253]. The dimerisation of these groups (Fig. 28) affords nanoscopic dimeric aggregates in solution, which are able to assemble further to generate columnar stacks resulting from the stacking of the π -functional unit. The stacks are made chiral by the incorporation of the 2-methylbutyl group, a fact that is witnessed in apolar solvents by intense CD activity. AFM measurements have confirmed the formation of the fibres on surfaces [253]. Fast migration of charges is seen in the stacks [254], a phenomenon that has been successfully modelled in a way that implies excitation delocalisation over the acceptor molecules [255]. The chiral side groups are key in the organisation and functions of these supramolecular systems.

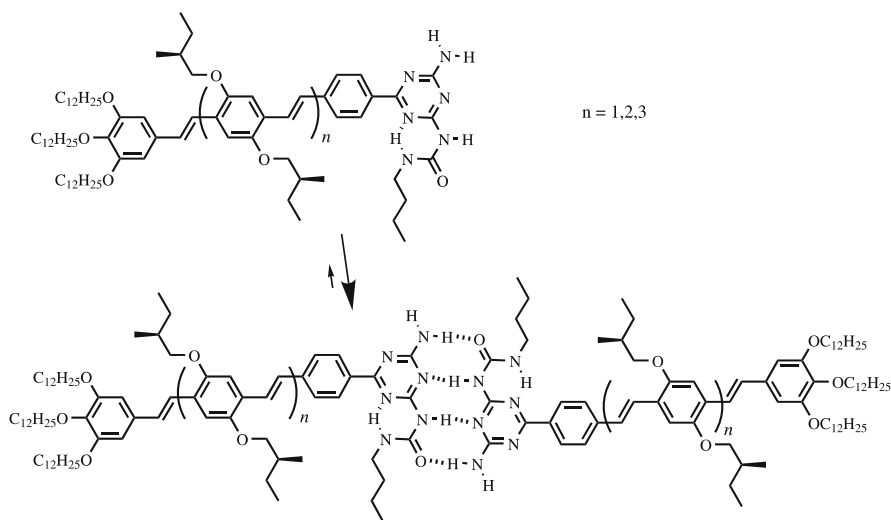


Fig. 28 Self-assembling oligophenylenevinylenes

When an appropriate asymmetric influence is exerted on a luminescent material, it is possible that circularly polarised light is generated. This can be achieved by embedding a light-emitting compound in a chiral liquid crystal, and such is the case for an oligofluorene in a chiral nematic phase [256]. In this case, in optimised processing and compositional factors, nearly pure right-handed luminescence was achieved, and practical applications were implied. This phenomenon arises because the helical structure of the cholesteric phase suppresses the luminescence of one handedness when the wavelength coincides with the selective reflection band of the LC, letting the other circularly polarised light through. A very broad spectral range for circularly polarised luminescence was achieved by combining a calamitic hole-transporting chiral nematic glass as host and indirectly exciting a dye embedded in the material [257].

7

Conclusion and Outlook

A wide variety of chiral functional materials exist, and the development of the liquid crystalline variety has seen remarkable development, from their use as display components to their potential as second harmonic generation materials. Chiral conductors are still a real challenge for the materials scientist today, and much needs to be learned in order to arrange the generally planar molecules used in a reliable way. The preparation of truly chiral spin arrangements in magnetic systems is proving a similarly formidable task, although great strides are being made in this area. The use of chiral induction for the preparation of chiral materials is still in its infancy, with relatively few examples and applications, in clear contrast to biological materials. There are opportunities for the use of supramolecular chiral induction [258] to produce functional systems with new and interesting properties.

Acknowledgements We warmly thank all the researchers that have contributed to the research in this area that has been performed in our laboratories, and to the organisations that finance our research at the present time: The European Commission for the Marie Curie RTN CHEXTAN (MRTN-CT-2004-512161), the Network of Excellence MAGMANet (515767-2) and the Integrated Project NAIMO (NMP4-CT-2004-500355), and the DGI, Spain (Projects No. BQU 2003-00760 and MAT 2003-04699). We also thank Dr. “Bert” Meijer (Eindhoven University of Technology, Holland) for supplying the graphics for Fig. 15.

References

1. Collins AN, Sheldrake GN, Crosby J (1992 and 1997) Chirality in Industry vols. I and II. Wiley, Chichester
2. Green MM, Nolte RJM, Meijer EW (2003) Topics in Stereochemistry 24. Chiral Materials. Wiley, Chichester

3. Beesley TE, Scott RPW (1998) *Chiral Chromatography*. Wiley, Chichester
4. Gray GW, Kelly SM (1999) *J Mater Chem* 9:2037
5. Lindoy LF, Cook J (2000) *Self-Assembly in Supramolecular Systems*. RSC, Cambridge
6. Braga D, Grepioni F (2004) In: Atwood J, Steed J (eds) *Encyclopedia of Supramolecular Chemistry*. Marcel Dekker Inc, New York, p 357–363
7. Veciana J, Rovira C, Amabilino DB (1999) *Supramolecular Engineering of Synthetic Metallic Materials*. NATO ASI Series C, 518. Kluwer Academic, Dordrecht
8. Jacques J, Collet A, Wilen SH (1994) *Enantiomers, Racemates, and Resolutions*. Krieger Publishing Company, Malabar, Florida
9. Pérez-García L, Amabilino DB (2002) *Chem Soc Rev* 31:342
10. Knof U, von Zelewsky A (1999) *Angew Chem Int Ed* 38:302
11. Green MM, Cheon KS, Yang SY, Park JW, Swansburg S, Liu W (2001) *Acc Chem Res* 34:672
12. Cornelissen JJLM, Rowan AE, Nolte RJM, Sommerdijk NAJM (2001) *Chem Rev* 101:4039
13. Mateos-Timoneda MA, Crego-Calama M, Reinhoudt DN (2004) *Chem Soc Rev* 33:363
14. Yashima E, Maeda K, Nishimura T (2004) *Chem Eur J* 10:42
15. Amabilino DB, Veciana J (2004) In: Atwood J, Steed J (eds) *Encyclopedia of Supramolecular Chemistry*. Marcel Dekker Inc., New York, p 245–252
16. Keizer HM, Sijbesma RP (2005) *Chem Soc Rev* 34:226
17. Avalos M, Babiano R, Cintas P, Jiménez JL, Palacios JC, Barron LD (1998) *Chem Rev* 98:2391
18. Ferraro JR, Williams JM (1987) *Introduction to Synthetic Electrical Conductors*. Academic Press, London
19. Farges J-F (1994) *Organic Conductors: Fundamentals and Applications*. Marcel Dekker, Inc., New York
20. Nalwa HS (2001) *Handbook of Advanced Electronic and Photonic Materials and Devices*, vol 3. High- T_c Superconductors and Organic Conductors. Academic Press, London
21. Shirakawa H (2001) *Angew Chem Int Ed* 40:2574
22. MacDiarmid AG (2001) *Angew Chem Int Ed* 40:2581
23. Heeger AJ (2001) *Angew Chem Int Ed* 40:2591
24. Nalwa HS (2001) *Handbook of Advanced Electronic and Photonic Materials and Devices*, vol 8. Conducting Polymers. Academic Press, London
25. Krstic V, Rikken GLJA (2002) *Chem Phys Lett* 364:51
26. Coronado E, Galan-Mascaros JR (2005) *J Mater Chem* 15:66
27. Booth S, Wallace NK, Singhal K, Bartlett PN, Kilburn J (1998) *J Chem Soc, Perkin Trans* 1:1467
28. Akagi K, Piao G, Kaneko S, Higuchi I, Shirakawa H, Kyotani M (1999) *Synth Met* 102:1406
29. Carroll RL, Gorman CB (2002) *Angew Chem Int Ed* 41:4378
30. Maruccio G, Cingolani R, Rinaldi R (2004) *J Mater Chem* 14:542
31. Wallis JD, Griffiths J-P (2005) *J Mater Chem* 15:347
32. Griffiths J-P, Nie H, Brown RJ, Day P, Wallis JD (2005) *Org Biomol Chem* 3:2155
33. Wallis JD, Karrer A, Dunitz JD (1986) *Helv Chim Acta* 69:69
34. Zambounis JS, Pfeiffer J, Papavassiliou GC, Lagourvados DJ, Terzis A, Raptopoulou CP, Delhaes P, Ducasse L, Fortune NA, Murata K (1995) *Solid State Commun* 95:211
35. Wallis JD, Dunitz JD (1988) *Acta Cryst C* 44:1037
36. Réthoré C, Avarvari N, Canadell E, Auban-Senzier P, Fourmigué M (2005) *J Am Chem Soc* 127:5748

37. Zambounis JS, Mayer CW, Hauenstein K, Hilti B, Hofherr W, Pfeiffer J, Bürkle M, Rihs G (1992) *Adv Mater* 4:33
38. Kini AM, Parakka JP, Geiser U, Wang H-H, Rivas F, DiNino E, Thomas S, Dudek JD, Williams JM (1999) *J Mater Chem* 9:883
39. Coronado E, Galán-Mascarós JR, Gómez-García CJ, Murcia-Martínez A, Canadell E (2004) *Inorg Chem* 43:8072
40. Treboux G, Lapstun P, Wu Z, Silverbrook K (1999) *Chem Phys Lett*
41. Okubo H, Nakuno D, Anzai S, Yamaguchi M (2001) *J Org Chem* 66:557
42. Sooksimuang T, Mandal BK (2002) *J Org Chem* 68:652
43. Rajca A, Miyasaka M, Pink M, Wang H, Rajca S (2004) *J Am Chem Soc* 126:15211
44. Engelkamp H, Middelbeek S, Nolte RJM (1999) *Science* 284:785
45. Sly J, Kasák P, Gomar-Nadal E, Rovira C, Górriz L, Thordarson P, Amabilino DB, Rowan AE, Nolte RJM (2005) *Chem Commun* 1255
46. Langeveld-Voss BMW, Peeters E, Janssen RAJ, Meijer EW (1997) *Synth Met* 84:611
47. Ramos-Lermo E, Langeveld-Voss BMW, Janssen RAJ, Meijer EW (1999) *Chem Commun* 791
48. Langeveld-Voss BMW, Janssen RAJ, Meijer EW (2000) *J Mol Struct* 521:285
49. Goto H, Okamoto Y, Yashima E (2002) *Chem Eur J* 8:4027
50. Goto H, Soo Y, Akagi K (2005) *Macromol Rapid Commun* 26:164
51. Lemaire M, Delabouglise D, Garreau R, Guy A, Roncali J (1988) *J Chem Soc Chem Commun* 658
52. Havinga HH, Bouman MM, Meijer EW, Pomp A, Simenon MMJ (1994) *Synth Met* 66:93
53. Egan V, Bernstein R, Hohmann L, Tran T, Kaner RB (2001) *Chem Commun* 801
54. Majidi MR, Kane-Maguire LAP, Wallace GG (1994) *Polymer* 35:3113
55. Majidi MR, Kane-Maguire LAP, Wallace GG (1995) *Polymer* 36:3597
56. Barisici JN, Innis PC, Kane-Maguire LAP, Norris ID, Wallace GG (1997) *Synth Met* 84:181
57. Aboutanos V, Kane-Maguire LAP, Wallace GG (2000) *Synth Met* 114:313
58. Cao Y, Andreatta A, Heeger AJ, Smith P (1989) *Polymer* 30:2305
59. Cao Y, Smith P, Heeger AJ (1992) *Synth Met* 48:91
60. Guo H, Knobler CM, Kaner RB (1999) *Synth Met* 101:44
61. Huang J, Egan VM, Guo H, Yoon J-Y, Briseno AL, Rauda IE, Garrell RL, Knobler CM, Zhou F, Kaner RB (2003) *Adv Mater* 15:1158
62. Sheridan EM, Breslin CB (2005) *Electroanalysis* 17:532
63. Zhang L, Wan M (2005) *Thin Solid Films* 477:24
64. Yang Y, Wan M (2002) *J Mater Chem* 12:897
65. Lu X, Yu Y, Chen L, Mao H, Wang L, Zhang W, Wei Y (2005) *Polymer* 46:5329
66. Hatano T, Bae A-H, Takeuchi M, Fujita N, Kaneko K, Ihara H, Takafuji M, Shinkai S (2004) *Angew Chem Int Ed* 43:465
67. Hatano T, Bae A-H, Takeuchi M, Fujita N, Kaneko K, Ihara H, Takafuji M, Shinkai S (2004) *Chem Eur J* 10:5067
68. Solladié G, Zimmermann RG (1984) *Angew Chem Int Ed Engl* 23:348
69. Goodby JW (1991) *J Mater Chem* 1:307
70. Fukuda A, Takanishi Y, Isozaki T, Ishikawa K, Takezoe H (1994) *J Mater Chem* 4:997
71. Demus D, Goodby JW, Gray GW, Spiess H-W (1998) *Handbook of Liquid Crystals*. Wiley, Weinheim
72. Chiellini E, Galli G (1987) In: Fontanille M, Guyot A (eds) *Recent Advances in Mechanistic and Synthetic Aspects of Polymerisation*. D Reidel Publishing, Dordrecht, p 425–450
73. Zentel R (1989) *Adv Mater* 2:321

74. Meyer RB, Liebert L, Strzelecki L, Keller P (1975) *J Phys Lett (Paris)* 36:L69
75. Clark NA, Handschy MA, Lagerwall ST (1983) *Mol Cryst Liq Cryst* 94:213
76. Walba DM (1995) *Science* 270:250
77. Walba DM, Slater SC, Thurmes WN, Clark NA, Handschy MA, Supon F (1986) *J Am Chem Soc* 108:5210
78. Walba DM, Razavi HA, Horiuchi A, Eidman KF, Otterholm B, Haltiwanger RC, Clark NA, Shao R, Parmar DS, Wand MD, Vohra RT (1991) *Ferroelectrics* 113:21
79. Paleos CM, Tsiourvas D (1995) *Angew Chem Int Ed Engl* 34:1696
80. Kato T, Fréchet MJM (1995) *Macromol Symp* 98:311
81. Bennett GM, Jones B (1939) *J Chem Soc* 420
82. Kato T, Fréchet MJM (1989) *Macromolecules* 22:3818
83. Kumar U, Fréchet MJM, Kato T, Ujiie S, Timura K (1992) *Angew Chem Int Ed Engl* 31:1531
84. Kihara H, Kato T, Uryu T, Ujiie S, Kumar U, Fréchet MJM, Bruce DW, Price DJ (1996) *Liquid Crystals* 21:25
85. Kato T, Fréchet MJM, Wilson PG, Saito T, Uryu T, Fujishima A, Jin C, Kaneuchi F (1993) *Chem Mater* 5:1094
86. Grunert M, Howie RA, Kaeding A, Imrie CT (1997) *J Mater Chem* 7:211
87. Kihara H, Kato T, Uryu T, Fréchet MJM (1998) *Liquid Crystals* 24:413
88. Lehn JM (1993) *Makromol Chem, Macromol Symp* 69:1
89. Fouquey C, Lehn JM, Levelut AM (1990) *Adv Mater* 2:254
90. Gulik-Krzywicki T, Fouquey T, Lehn JM (1993) *Proc Natl Acad Sci USA* 90:163
91. Gottarelli G, Proni G, Spada GP (1997) *Liquid Crystals* 22:563
92. Pieraccini S, Gottarelli G, Mariani P, Masiero S, Saturni L, Spada GP (2001) *Chirality* 13:7
93. Kato T, Matsuoka T, Nishii M, Kamikawa Y, Kanie K, Nishimura T, Yashima E, Ujiie S (2004) *Angew Chem Int Ed* 43:1969
94. Kamikawa Y, Nishii M, Kato T (2004) *Chem Eur J* 10:5942
95. Serrano JL, Sierra T (2003) *Coord Chem Rev* 242:73
96. Lehmann M, Sierra T, Barberá J, Serrano JL, Parker R (2002) *J Mater Chem* 12:1342
97. Barberá J, Cavero E, Lehmann M, Serrano JL, Sierra T, Vázquez T (2003) *J Am Chem Soc* 125:4527
98. Serrano JL, Sierra T (2000) *Chem Eur J* 6:759
99. Barberá J, Iglesias R, Serrano JL, de la Fuente MR, Palacios B, Pérez-Jubindo MA, Vázquez JT (1998) *J Am Chem Soc* 120:2908
100. Friedel G (1922) *Ann Phys, Paris* 18:273
101. Buckingham AD, Ceasar GP, Dunn MB (1969) *Chem Phys Lett* 3:540
102. Gottarelli G, Spada GP, Solladié G (1986) *New J Chem* 10:691
103. Saeva FD, Wysocki JJ (1971) *J Am Chem Soc* 93:5928
104. Saeva FD (1979) In: Saeva FD (ed) *Liquid Crystals: The Fourth State of Matter*. Dekker, New York, p 249–273
105. Pirkle WH, Rinaldi PL (1980) *J Org Chem* 45:1379
106. Gottarelli G, Mariani P, Spada GP, Samorí B, Forni A, Solladié G, Hibert M (1983) *Tetrahedron* 39:1337
107. Gottarelli G, Hibert M, Samorí B, Solladié G, Spada GP, Zimmermann R (1983) *J Am Chem Soc* 105:7318
108. Pieraccini S, Donnoli MI, Ferrarini A, Gottarelli G, Licini G, Rosini C, Superchi S, Spada GP (2003) *J Org Chem* 68:519
109. Arnone C, Gottarelli G, Spada GP, Spinelli D, Exner O (1986) *J Mol Struct* 147:307
110. Rosini C, Rosati I, Spada GP (1995) *Chirality* 7:353
111. Kuball H-G, Brüning (1997) *Chirality* 9:407

112. Kuball H-G, Weiss B, Beck AK, Seebach D (1997) *Helv Chim Acta* 80:2507
113. van Delden RA, Feringa BL (2001) *Angew Chem Int Ed* 40:3198
114. Yoshida J, Sato H, Yamagishi A, Hoshino N (2005) *J Am Chem Soc* 127:8453
115. Lemieux RP (2001) *Acc Chem Res* 34:845
116. Amabilino DB, Ramos E, Serrano J-L, Sierra T, Veciana J (1998) *J Am Chem Soc* 120:9126
117. Lazar C, Radke JP, Hartley CS, Glaser MA, Lemieux (2001) *Chem Mater* 13:1692
118. Hartley CS, Lazar C, Wand MD, Lemieux RP (2002) *J Am Chem Soc* 124:13513
119. Lazar C, Yang K, Glaser MA, Wand MD, Lemieux RP (2002) *J Mater Chem* 12:586
120. Green MM, Ringsdorf H, Wagner J, Wüstefeld R (1990) *Angew Chem Int Ed Engl* 29:1478
121. van Gorp JJ, Vekemans JAJM, Meijer EW (2002) *J Am Chem Soc* 124:14759
122. Feringa BL, van Delden RA, Koumura N, Geertsema EM (2000) *Chem Rev* 100:1789
123. Yokoyama Y, Sagisaka T (1997) *Chem Lett* 687
124. Feringa BL, Huck NPM, van Doren HA (1995) *J Am Chem Soc* 117:9929
125. van Delden RA, Koumura N, Harada N, Feringa BL (2002) *PNAS* 99:4945
126. Huck NPM, Jager WF, de Lange B, Feringa BL (1996) *Science* 273:1686
127. Komitov L, Tsutsumi O, Ruslim C, Ikeda T, Ichimura K, Yoshino K (2001) *J Appl Phys* 89:7745
128. Dinescu L, Lemieux RP (1999) *Adv Mater* 11:42
129. Vlahakis JZ, Wand MD, Lemieux RP (2004) *Adv Funct Mater* 14:637
130. Niori T, Sekine T, Watanabe J, Furukawa T, Takezoe H (1996) *J Mater Chem* 6:1231
131. Sekine T, Niori T, Watanabe J, Furukawa T, Choi SW, Takezoe H (1997) *J Mater Chem* 7:1307
132. Link DR, Natale G, Shao R, MacLennan JE, Clark NA, Körblová E, Walba DM (1997) *Science* 278:1924
133. Walba DM, Körblová E, Shao R, MacLennan JE, Link DR, Glaser MA, Clark NA (2000) *J Phys Org Chem* 13:830
134. Pelzl G, Diele S, Weissflog W (1999) *Adv Mater* 11:707
135. Walba DM, Körblová E, Shao R, MacLennan JE, Link DR, Glaser MA, Clark NA (2000) *Science* 288:2181
136. Pelzl G, Diele S, Jákli A, Lischka Ch, Wirth I, Weissflog W (1999) *Liq Cryst* 26:135
137. Lee CK, Chien LC (2000) *Ferroelectrics* 243:231
138. Dierking I, Sawade H, Heppke G (2001) *Liq Cryst* 28:1767
139. Gimeno N, Ros MB, Serrano JL, de la Fuente MR (2004) *Angew Chem Int Ed* 43:5235
140. Keith C, Reddy RA, Tschierske C (2005) *Chem Commun* 871
141. Takanishi Y, Takezoe H, Suzuki Y, Kobayashi I, Yajima T, Terada M, Mikami K (1999) *Angew Chem Int Ed* 38:2354
142. Mikami K, Yajima T, Kojima J, Terada M, Kawauchi S, Shirasaki H, Okuyama K, Suzuki Y, Kobayashi I, Takanishi Y, Takezoe H (2000) *Mol Cryst Liq Cryst* 346:41
143. Torgova SI, Komitov L, Strigazzi A (1998) *Liq Cryst* 24:131
144. Torgova SI, Petrov MP, Strigazzi A (2001) *Liq Cryst* 28:1439
145. Pelzl G, Eremin A, Diele S, Kresse H, Weissflog W (2002) *J Mater Chem* 12:2591
146. Görtz V, Goodby JW (2005) *Chem Commun* 3262
147. Flory JP (1974) *Faraday Discuss Chem Soc* 57:7
148. van Esch JH, Feringa BL (2004) *Encyclopedia of Supramolecular Chemistry*. Marcel Dekker, New York, p 586–596
149. Terech P, Weiss RG (1997) *Chem Rev* 97:3133
150. van Esch J, Schoonbeek F, De Loos M, Veen EM, Kellogg RM, Feringa BL (1999) In: Ungaro R, Dalcanele E (eds) *Supramolecular Science, Where it is and Where it is Going*. NATO ASI Series C 527. Kluwer Academic. Dordrecht, p 233–259

151. Hanabusa K, Yamada M, Kimura M, Shirai H (1996) *Angew Chem Int Ed Engl* 35:1949
152. Kato T, Katsuna T, Hanabusa K, Ukon M (1998) *Adv Mater* 10:606
153. Kato T, Kondo G, Hanabusa K (1998) *Chem Lett* 193
154. Hanabusa K, Shimura K, Hirose K, Kimura M, Shirai H (1996) *Chem Lett* 885
155. van Esch J, De Feyter S, Kellogg RM, De Schryver FC, Feringa BL (1997) *Chem Eur J* 3:1238
156. van Esch J, Schoonbeek F, de Loos M, Kooijman H, Spek AL, Kellogg RM, Feringa BL (1999) *Chem Eur J* 5:937
157. de Loos M, van Esch J, Kellogg RM, Feringa BL (2001) *Angew Chem Int Ed* 40:613
158. Oda R, Huc I, Candau SJ (1998) *Angew Chem Int Ed* 37:2689
159. Berthier D, Buffeteau T, Léger JM, Oda R, Huc I (2002) *J Am Chem Soc* 124:13486
160. Makarević J, Jokić M, Raza Z, Štefanić Z, Kojić-Prodić B, Žinić M (2003) *Chem Eur J* 9:5567
161. Fuhrhop JH, Schneider P, Boekema E, Helfrich W (1988) *J Am Chem Soc* 110:2861
162. Köning J, Boettcher C, Winkler H, Zeitler E, Talmon Y, Fuhrhop JH (1993) *J Am Chem Soc* 115:693
163. Hafcamp RJH, Kokke BPA, Danke IM, Geurts HPM, Rowan AE, Feiters MC, Nolte RJM (1997) *Chem Commun* 545
164. Gu W, Lu L, Chapman GB, Weiss RG (1997) *Chem Commun* 543
165. Hirst AR, Smith DK, Feiters MC, Geurts HPM (2004) *Chem Eur J* 10:5901
166. Murata K, Aoki M, Suzuki T, Harada T, Kawabata H, Komori T, Ohseto F, Ueda K, Shinkai S (1994) *J Am Chem Soc* 116:6664
167. de Jong JJD, Lucas LN, Kellogg RM, van Esch JH, Feringa BL (2004) *Science* 304:278
168. Rikken GLJA, Raupach E (1997) *Nature* 390:493
169. Scheffler K, Höfler U, Schuler P, Stegmann HB (1988) *Mol Phys* 65:439
170. Mäurer M, Scheffler K, Stegmann HB, Mannschreck A (1991) *Angew Chem Int Ed Engl* 30:602
171. Joerss E, Schuler P, Maichle-Moessmer C, Abram S, Stegmann HB (1997) *Enantiomer* 2:5
172. Schuler P, Schaber FM, Stegmann HB, Janzen E (1999) *Magn Reson Chem* 37:805
173. Tamura R, Susuki S, Azuma N, Matsumoto A, Toda F, Kamimura A, Hori K (1994) *Angew Chem Int Ed Engl* 33:878
174. Sedó J, Ventosa N, Ruiz-Molina D, Mas M, Molins E, Rovira C, Veciana J (1998) *Angew Chem Int Ed* 37:330-333
175. Amabilino DB, Veciana J (2001) In: Miller JS, Drillon M (eds) *Magnetism-Molecules to Materials*, vol II: Molecule Based Materials. Wiley, Weinheim
176. Minguet M, Amabilino DB, Cirujeda J, Wurst K, Mata I, Molins E, Novoa JJ, Veciana J (2000) *Chem Eur J* 6:2350
177. Minguet M, Amabilino DB, Wurst K, Veciana J (2001) *J Solid State Chem* 159:440
178. Minguet M, Amabilino DB, Vidal-Gancedo J, Wurst K, Veciana J (2002) *J Mater Chem* 12:570
179. Minguet M, Amabilino DB, Wurst K, Veciana J (2001) *J Chem Soc, Perkin Trans 2* 670
180. Ikima N, Tamura R, Shimono S, Kawame N, Tamada O, Sakai N, Yamauchi J, Yamamoto Y (2004) *Angew Chem Int Ed* 43:3677
181. Minguet M, Luneau D, Paulsen C, Lhotel E, Gorski A, Waluk J, Amabilino DB, Veciana J (2003) *Polyhedron* 22:2349
182. Caneschi A, Gatteschi D, Sessoli R, Rey P (1989) *Acc Chem Res* 22:392
183. Caneschi A, Gatteschi D, Rey P, Sessoli R (1991) *Inorg Chem* 30:3936

184. Caneschi A, Gatteschi D, Lalioti N, Sangregorio C, Sesoli R (2000) *J Chem Soc, Dalton Trans* 3907
185. Minguet M, Luneau D, L'hotel E, Villar V, Paulsen C, Amabilino DB, Veciana J (2002) *Angew Chem Int Ed* 41:586
186. Iwamura H, Inoue K, Koga N (1998) *New J Chem* 201
187. Kumagai H, Inoue K (1999) *Angew Chem Int Ed* 38:1601
188. Inoue K, Kumagai H, Markosyan AS (2001) *Synth Met* 121:1772
189. Ghalsasi PS, Inoue K, Samant SD, Yakhmi JV (2001) *Polyhedron* 20:1495
190. Kobayashi N, Naito T, Inabe T (2004) *Adv Mater* 16:1803
191. Inabe T (2005) *J Mater Chem* 15:1317
192. Wang Z, Enkelmann V, Negri F, Müllen K (2004) *Angew Chem Int Ed* 43:1972
193. Inabe T, Kobayashi N, Naito T (2004) *J Phys IV France* 114:449
194. Nakayama K, Ishida T, Takayama R, Hashizume D, Yasui M, Iwasaki F, Nogami T (1998) *Chem Lett* 497
195. Gao EQ, Bai SQ, Wang ZM, Yan CH (2003) *J Am Chem Soc* 125:4984
196. Gao EQ, Yue YF, Bai SQ, He Z, Yan CH (2004) *J Am Chem Soc* 126:1419
197. Decurtins S (1999) *Phil Trans R Soc Lond A* 357:3025
198. Decurtins S, Schmalle HW, Schneuwly P, Ensling J, Güthlich P (1994) *J Am Chem Soc* 116:9521
199. Decurtins S, Scmalle HW, Pellaux R, Huber R, Fischer P, Ouladdiaf B (1996) *Adv Mater* 8:647
200. Coronado E, Galán-Mascarós, Gómez-García CJ, Martínez-Agudo JM (2001) *Inorg Chem* 40:113
201. Pointillart F, Train C, Gruselle M, Villain F, Schmalle HW, Talbot D, Gredin P, Decurtins S, Verdaguer M (2004) *Chem Mater* 16:832
202. Decurtins S, Scmalle HW, Pellaux R, Schneuwly P, Hauser A (1996) *Inorg Chem* 35:1451
203. Hauser A, Riesen H, Pellaux R, Decurtins S (1996) *Chem Phys Lett* 261:313
204. Sieber R, Decurtins S, Stoeckli-Evans H, Wilson C, Yufit D, Howard JAK, Capelli SC, Hauser A (2000) *Chem Eur J* 6:361
205. Malézieux B, Andrés R, Brissard M, Gruselle M, Train C, Herson P, Troitskaya LL, Sokolov VI, Ovseenko ST, Demeschik TV, Ovanesyan NS, Mamed'yarova IA (2001) *J Organomet Chem* 637-639:182
206. Andrés R, Brissard M, Gruselle M, Train C, Vaissermann J, Malézieux B, Jamet JP, Verdaguer M (2001) *Inorg Chem* 40:4633
207. Ovanesyan NS, Makhaev VD, Aldoshin SM, Gredin P, Boubekeur K, Train C, Gruselle M (2005) *J Chem Soc, Dalton Trans* 3101
208. Inoue K, Imai H, Ghalsasi PS, Kikuchi K, Ohba M, Okawa H, Yakhmi JV (2001) *Angew Chem Int Ed* 40:4242
209. Inoue K, Kikuchi K, Ohba M, Okawa H (2003) *Angew Chem Int Ed* 42:4810
210. Imai H, Inoue K, Kikuchi K, Yoshida Y, Ito M, Sunahara T, Onaka S (2004) *Angew Chem Int Ed* 43:5618
211. Coronado E, Gómez-García CJ, Nuez A, Romero FM, Rusanov E, Stoeckli-Evans H (2002) *Inorg Chem* 41:4615
212. Coronado E, Giménez-Saiz C, Martínez-Agudo JM, Nuez A, Romero FM, Stoeckli-Evans H (2003) *Polyhedron* 22:2440
213. Güthlich P, Hauser A, Spiering H (1994) *Angew Chem Int Ed Engl* 33:2024
214. Sato O (2003) *Acc Chem Res* 36:692
215. Sunatsuki Y, Ikuta Y, Matsumoto N, Ohta H, Kojima M, Iijima S, Hayami S, Maeda Y, Kaizaki S, Dahan F, Tuchagues JP (2003) *Angew Chem Int Ed* 42:1614
216. Lincke G (2003) *Dyes and Pigments* 59:1

217. Hao Z, Iqbal A (1997) *Chem Soc Rev* 26:203
218. Reichardt C (1995) *J Phys Org Chem* 78:61
219. Eggers L, Kolster K, Buss V (1997) *Chirality* 9:243
220. Kirstein S, von Berlepsch H, Böttcher C, Burger C, Ouart A, Reck G, Dähne S (2000) *Chem Phys Chem* 146
221. Spitz C, Dähne S, Ouart A, Abraham HW (2000) *J Phys Chem B* 104:8664
222. Seifert JL, Connor RE, Kushon SA, Wang M, Armitage BA (1999) *J Am Chem Soc* 121:2987
223. Renikuntla BR, Armitage BA (2005) *Langmuir* 21:5362
224. Morikawa M-a, Yoshihara M, Endo T, Kimizuka N (2005) *J Am Chem Soc* 127:1358
225. Owen DJ, VanDerveer D, Schuster GB (1998) *J Am Chem Soc* 120:1705
226. Prins LJ, Thalacker C, Würthner F, Timmerman P, Reinhoudt DN (2001) *Proc Natl Acad Sci USA* 98:10042
227. Thalacker C, Würthner F (2002) *Adv Funct Mater* 12:209
228. van Herrikhuyzen J, Syamakumari A, Schenning APHJ, Meijer EW (2004) *J Am Chem Soc* 126:10021
229. Huang X, Nakanishi K, Berova N (2000) 12:237
230. Mizuno Y, Aida T (2003) *Chem Commun* 20
231. Kubo Y, Ishii Y, Yoshizawa T, Tokita S (2004) *Chem Commun* 1394
232. Guo YM, Oike H, Aida T (2003) *J Am Chem Soc* 126:716
233. Borovkov VV, Hembury GA, Inoue Y (2004) *Acc Chem Res* 37:449
234. Monti D, Cantonetti V, Venanzi M, Ceccacci F, Bombelli C, Mancini G (2004) *Chem Commun* 972
235. Mizuno Y, Aida T, Yamaguchi K (2000) 122:5278
236. Lauceri R, Purrello R (2005) *Supramolecular Chemistry* 17:61
237. Rubires R, Crusats J, El-Hachemi Z, Jaramillo T, López M, Valls E, Farrera JA, Ribó JM (1999) *New J Chem* 189
238. Ribó JM, Crusats J, Sagués F, Claret J, Rubires R (2001) *Science* 292:2063
239. Rubires R, Farrera J-A, Ribó JM (2001) *Chem Eur J* 7:436
240. Laureci R, Raudino A, Gurrieri S, Monsù-Scolaro L, Micali N, Purrello R (2002) *J Am Chem Soc* 124:894
241. De Napoli M, Nardis S, Paolesse R, Vicente MGH, Lauceri R, Purrello R (2004) *J Am Chem Soc* 126:5934
242. Balaban TS, Bhise AD, Fischer M, Linke-Schaetzel M, Roussel C, Vanthuyne (2003) *Angew Chem Int Ed* 42:2140
243. Prasad PN, Williams DJ (1991) *Introduction to Non-linear Optical Effects in Molecules and Polymers*. Wiley, New York
244. Barron LD (1982) *Molecular Light Scattering and Optical Activity*. Cambridge University Press, Cambridge
245. Ravi M, Gangopadhyay P, Rao DN, Cohen S, Agranat I, Radhakrishnan TP (1998) *Chem Mater* 10:2371
246. Evans OR, Lin W (2002) *Acc Chem Res* 35:511
247. Lovinger AJ, Nuckolls C, Katz TJ (1998) *J Am Chem Soc* 120:264
248. Nuckolls C, Katz TJ, Katz G, Collings PJ, Castellanos L (1999) *J Am Chem Soc* 121:79
249. Verbiest T, Van Elshocht S, Kauranen M, Hellemans L, Snauwaert J, Nuckolls C, Katz TJ, Persoons A (1998) *Science* 282:913
250. Liu JY, Robinson MG, Johnson KM, Walba DM, Ros MB, Clark NA, Shao R, Doroski D (1991) *J Appl Phys* 70:3426
251. Ortega J, Gallastegui JA, Folcia CL, Etxebarria J, Gimeno N, Ros MB (2004) *Liq Cryst* 31:579

252. Schenning APHJ, Jonkheijm P, Peeters E, Meijer EW (2001) *J Am Chem Soc* 123:409
253. Jonkheijm P, Hoebein FJM, Kleppinger R, von Herrikhuyzen J, Schenning APHJ, Meijer EW (2003) *J Am Chem Soc* 125:15941
254. Hoebein FJM, Herz LM, Daniel C, Jonkheijm P, Schenning APHJ, Silva C, Meskers SCJ, Beljonne D, Phillips RT, Friend RH, Meijer EW (2004) *Angew Chem Int Ed* 43:1976
255. Beljonne D, Hennebicq E, Daniel C, Herz LM, Silva C, Scholes GD, Hoebein FJM, Jonkheijm P, Schenning APHJ, Meskers SCJ, Phillips RT, Friend RH, Meijer EW (2005) *J Phys Chem B* 109:10594
256. Chen SH, Katsis D, Schmid AW, Mastrangelo JC, Tsutsui T, Blanton TN (1999) *Nature* 397:506
257. Woon KL, O'Neill M, Richards GJ, Aldred MP, Kelly SM, Fox AM (2003) *Adv Mater* 15:1555
258. Mateos-Timoneda MA, Crego-Calama M, Reinhoudt DN (2004) *Chem Soc Rev* 33:363

Author Index Volumes 251–265

Author Index Vols. 26–50 see Vol. 50
Author Index Vols. 51–100 see Vol. 100
Author Index Vols. 101–150 see Vol. 150
Author Index Vols. 151–200 see Vol. 200
Author Index Vols. 201–250 see Vol. 250

The volume numbers are printed in italics

- Ajayaghosh A, George SJ, Schenning APHJ (2005) Hydrogen-Bonded Assemblies of Dyes and Extended π -Conjugated Systems. 258: 83–118
- Albert M, Fensterbank L, Lacôte E, Malacria M (2006) Tandem Radical Reactions. 264: 1–62
- Alberto R (2005) New Organometallic Technetium Complexes for Radiopharmaceutical Imaging. 252: 1–44
- Alegret S, see Pividori MI (2005) 260: 1–36
- Amabilino DB, Veciana J (2006) Supramolecular Chiral Functional Materials. 265: 253–302
- Anderson CJ, see Li WP (2005) 252: 179–192
- Anslyn EV, see Houk RJT (2005) 255: 199–229
- Araki K, Yoshikawa I (2005) Nucleobase-Containing Gelators. 256: 133–165
- Armitage BA (2005) Cyanine Dye–DNA Interactions: Intercalation, Groove Binding and Aggregation. 253: 55–76
- Arya DP (2005) Aminoglycoside–Nucleic Acid Interactions: The Case for Neomycin. 253: 149–178
- Bailly C, see Dias N (2005) 253: 89–108
- Balaban TS, Tamiaki H, Holzwarth AR (2005) Chlorins Programmed for Self-Assembly. 258: 1–38
- Balzani V, Credi A, Ferrer B, Silvi S, Venturi M (2005) Artificial Molecular Motors and Machines: Design Principles and Prototype Systems. 262: 1–27
- Barbieri CM, see Pilch DS (2005) 253: 179–204
- Barchuk A, see Daasbjerg K (2006) 263: 39–70
- Bayly SR, see Beer PD (2005) 255: 125–162
- Beer PD, Bayly SR (2005) Anion Sensing by Metal-Based Receptors. 255: 125–162
- Bier FE, see Heise C (2005) 261: 1–25
- Blum LJ, see Marquette CA (2005) 261: 113–129
- Boiteau L, see Pascal R (2005) 259: 69–122
- Borovkov VV, Inoue Y (2006) Supramolecular Chirogenesis in Host–Guest Systems Containing Porphyrinoids. 265: 89–146
- Boschi A, Duatti A, Uccelli L (2005) Development of Technetium-99m and Rhenium-188 Radiopharmaceuticals Containing a Terminal Metal–Nitrido Multiple Bond for Diagnosis and Therapy. 252: 85–115
- Braga D, D’Addario D, Giaffreda SL, Maini L, Polito M, Grepioni F (2005) Intra-Solid and Inter-Solid Reactions of Molecular Crystals: a Green Route to Crystal Engineering. 254: 71–94
- Brebion F, see Crich D (2006) 263: 1–38

- Brizard A, Oda R, Huc I (2005) Chirality Effects in Self-assembled Fibrillar Networks. 256: 167–218
- Bruce IJ, see del Campo A (2005) 260: 77–111
- del Campo A, Bruce IJ (2005) Substrate Patterning and Activation Strategies for DNA Chip Fabrication. 260: 77–111
- Chaires JB (2005) Structural Selectivity of Drug-Nucleic Acid Interactions Probed by Competition Dialysis. 253: 33–53
- Chiorboli C, Indelli MT, Scandola F (2005) Photoinduced Electron/Energy Transfer Across Molecular Bridges in Binuclear Metal Complexes. 257: 63–102
- Collin J-P, Heitz V, Sauvage J-P (2005) Transition-Metal-Complexed Catenanes and Rotaxanes in Motion: Towards Molecular Machines. 262: 29–62
- Collyer SD, see Davis F (2005) 255: 97–124
- Commeyras A, see Pascal R (2005) 259: 69–122
- Correia JDG, see Santos I (2005) 252: 45–84
- Costanzo G, see Saladino R (2005) 259: 29–68
- Credi A, see Balzani V (2005) 262: 1–27
- Crestini C, see Saladino R (2005) 259: 29–68
- Crich D, Brebion F, Suk D-H (2006) Generation of Alkene Radical Cations by Heterolysis of β -Substituted Radicals: Mechanism, Stereochemistry, and Applications in Synthesis. 263: 1–38
- Cuerva JM, Justicia J, Oller-López JL, Oltra JE (2006) Cp_2TiCl in Natural Product Synthesis. 264: 63–92
- Daasbjerg K, Svith H, Grimme S, Gerenkamp M, Mück-Lichtenfeld C, Gansäuer A, Barchuk A (2006) The Mechanism of Epoxide Opening through Electron Transfer: Experiment and Theory in Concert. 263: 39–70
- D'Addario D, see Braga D (2005) 254: 71–94
- Darmency V, Renaud P (2006) Tin-Free Radical Reactions Mediated by Organoboron Compounds. 263: 71–106
- Davis F, Collyer SD, Higson SPJ (2005) The Construction and Operation of Anion Sensors: Current Status and Future Perspectives. 255: 97–124
- Deamer DW, Dworkin JP (2005) Chemistry and Physics of Primitive Membranes. 259: 1–27
- Deng J-Y, see Zhang X-E (2005) 261: 169–190
- Dervan PB, Poulin-Kerstien AT, Fechter EJ, Edelson BS (2005) Regulation of Gene Expression by Synthetic DNA-Binding Ligands. 253: 1–31
- Dias N, Vezin H, Lansiaux A, Bailly C (2005) Topoisomerase Inhibitors of Marine Origin and Their Potential Use as Anticancer Agents. 253: 89–108
- DiMauro E, see Saladino R (2005) 259: 29–68
- Dobrawa R, see You C-C (2005) 258: 39–82
- Du Q, Larsson O, Swerdlow H, Liang Z (2005) DNA Immobilization: Silanized Nucleic Acids and Nanoprinting. 261: 45–61
- Duatti A, see Boschi A (2005) 252: 85–115
- Dworkin JP, see Deamer DW (2005) 259: 1–27
- Edelson BS, see Dervan PB (2005) 253: 1–31
- Edwards DS, see Liu S (2005) 252: 193–216
- Ernst K-H (2006) Supramolecular Surface Chirality. 265: 209–252
- Escudé C, Sun J-S (2005) DNA Major Groove Binders: Triple Helix-Forming Oligonucleotides, Triple Helix-Specific DNA Ligands and Cleaving Agents. 253: 109–148

- Fages F, Vögtle F, Žinić M (2005) Systematic Design of Amide- and Urea-Type Gelators with Tailored Properties. 256: 77–131
- Fages F, see Žinić M (2005) 256: 39–76
- Fechter EJ, see Dervan PB (2005) 253: 1–31
- Fensterbank L, see Albert M (2006) 264: 1–62
- Fernández JM, see Moonen NNP (2005) 262: 99–132
- Fernando C, see Szathmáry E (2005) 259: 167–211
- Ferrer B, see Balzani V (2005) 262: 1–27
- De Feyter S, De Schryver F (2005) Two-Dimensional Dye Assemblies on Surfaces Studied by Scanning Tunneling Microscopy. 258: 205–255
- Flood AH, see Moonen NNP (2005) 262: 99–132
- Fujiwara S-i, Kambe N (2005) Thio-, Seleno-, and Telluro-Carboxylic Acid Esters. 251: 87–140
- Gansäuer A, see Daasbjerg K (2006) 263: 39–70
- Garcia-Garibay MA, see Karlen SD (2005) 262: 179–227
- Gelinck GH, see Grozema FC (2005) 257: 135–164
- George SJ, see Ajayaghosh A (2005) 258: 83–118
- Gerenkamp M, see Daasbjerg K (2006) 263: 39–70
- Giaffreda SL, see Braga D (2005) 254: 71–94
- Grepioni F, see Braga D (2005) 254: 71–94
- Grimme S, see Daasbjerg K (2006) 263: 39–70
- Grozema FC, Siebbeles LDA, Gelinck GH, Warman JM (2005) The Opto-Electronic Properties of Isolated Phenylenevinylene Molecular Wires. 257: 135–164
- Guiseppi-Elie A, Lingerfelt L (2005) Impedimetric Detection of DNA Hybridization: Towards Near-Patient DNA Diagnostics. 260: 161–186
- Di Giusto DA, King GC (2005) Special-Purpose Modifications and Immobilized Functional Nucleic Acids for Biomolecular Interactions. 261: 131–168
- Hansen SG, Skrydstrup T (2006) Modification of Amino Acids, Peptides, and Carbohydrates through Radical Chemistry. 264: 135–162
- Heise C, Bier FF (2005) Immobilization of DNA on Microarrays. 261: 1–25
- Heitz V, see Collin J-P (2005) 262: 29–62
- Higson SPJ, see Davis F (2005) 255: 97–124
- Hirst AR, Smith DK (2005) Dendritic Gelators. 256: 237–273
- Holzwarth AR, see Balaban TS (2005) 258: 1–38
- Houk RJT, Tobey SL, Anslyn EV (2005) Abiotic Guanidinium Receptors for Anion Molecular Recognition and Sensing. 255: 199–229
- Huc I, see Brizard A (2005) 256: 167–218
- Ihmels H, Otto D (2005) Intercalation of Organic Dye Molecules into Double-Stranded DNA – General Principles and Recent Developments. 258: 161–204
- Indelli MT, see Chiorboli C (2005) 257: 63–102
- Inoue Y, see Borovkov VV (2006) 265: 89–146
- Ishii A, Nakayama J (2005) Carbodithioic Acid Esters. 251: 181–225
- Ishii A, Nakayama J (2005) Carboselenothioic and Carbodiselenoic Acid Derivatives and Related Compounds. 251: 227–246
- Ishi-i T, Shinkai S (2005) Dye-Based Organogels: Stimuli-Responsive Soft Materials Based on One-Dimensional Self-Assembling Aromatic Dyes. 258: 119–160

- James DK, Tour JM (2005) *Molecular Wires*. 257: 33–62
- Jones W, see Trask AV (2005) 254: 41–70
- Justicia J, see Cuerva JM (2006) 264: 63–92
- Kambe N, see Fujiwara S-i (2005) 251: 87–140
- Kano N, Kawashima T (2005) *Dithiocarboxylic Acid Salts of Group 1–17 Elements (Except for Carbon)*. 251: 141–180
- Karlen SD, Garcia-Garibay MA (2005) *Amphidynamic Crystals: Structural Blueprints for Molecular Machines*. 262: 179–227
- Kato S, Niyomura O (2005) *Group 1–17 Element (Except Carbon) Derivatives of Thio-, Seleno- and Telluro-Carboxylic Acids*. 251: 19–85
- Kato S, see Niyomura O (2005) 251: 1–12
- Kato T, Mizoshita N, Moriyama M, Kitamura T (2005) *Gelation of Liquid Crystals with Self-Assembled Fibers*. 256: 219–236
- Kaul M, see Pilch DS (2005) 253: 179–204
- Kaupp G (2005) *Organic Solid-State Reactions with 100% Yield*. 254: 95–183
- Kawasaki T, see Okahata Y (2005) 260: 57–75
- Kawashima T, see Kano N (2005) 251: 141–180
- Kay ER, Leigh DA (2005) *Hydrogen Bond-Assembled Synthetic Molecular Motors and Machines*. 262: 133–177
- King GC, see Di Giusto DA (2005) 261: 131–168
- Kitamura T, see Kato T (2005) 256: 219–236
- Komatsu K (2005) *The Mechanochemical Solid-State Reaction of Fullerenes*. 254: 185–206
- Kriegisch V, Lambert C (2005) *Self-Assembled Monolayers of Chromophores on Gold Surfaces*. 258: 257–313
- Lacôte E, see Albert M (2006) 264: 1–62
- Lahav M, see Weissbuch I (2005) 259: 123–165
- Lambert C, see Kriegisch V (2005) 258: 257–313
- Lansiaux A, see Dias N (2005) 253: 89–108
- Larsson O, see Du Q (2005) 261: 45–61
- Leigh DA, Pérez EM (2006) *Dynamic Chirality: Molecular Shuttles and Motors*. 265: 185–208
- Leigh DA, see Kay ER (2005) 262: 133–177
- Leiserowitz L, see Weissbuch I (2005) 259: 123–165
- Lhoták P (2005) *Anion Receptors Based on Calixarenes*. 255: 65–95
- Li WP, Meyer LA, Anderson CJ (2005) *Radiopharmaceuticals for Positron Emission Tomography Imaging of Somatostatin Receptor Positive Tumors*. 252: 179–192
- Liang Z, see Du Q (2005) 261: 45–61
- Lingerfelt L, see Guiseppi-Elie A (2005) 260: 161–186
- Liu S (2005) *6-Hydrazinonicotinamide Derivatives as Bifunctional Coupling Agents for ^{99m}Tc-Labeling of Small Biomolecules*. 252: 117–153
- Liu S, Robinson SP, Edwards DS (2005) *Radiolabeled Integrin $\alpha_v\beta_3$ Antagonists as Radiopharmaceuticals for Tumor Radiotherapy*. 252: 193–216
- Liu XY (2005) *Gelation with Small Molecules: from Formation Mechanism to Nanostructure Architecture*. 256: 1–37
- Luderer F, Walschus U (2005) *Immobilization of Oligonucleotides for Biochemical Sensing by Self-Assembled Monolayers: Thiol-Organic Bonding on Gold and Silanization on Silica Surfaces*. 260: 37–56

- Maeda K, Yashima E (2006) Dynamic Helical Structures: Detection and Amplification of Chirality. 265: 47–88
- Magnera TF, Michl J (2005) Altitudinal Surface-Mounted Molecular Rotors. 262: 63–97
- Maini L, see Braga D (2005) 254: 71–94
- Malacria M, see Albert M (2006) 264: 1–62
- Marquette CA, Blum LJ (2005) Beads Arraying and Beads Used in DNA Chips. 261: 113–129
- Mascini M, see Palchetti I (2005) 261: 27–43
- Matsumoto A (2005) Reactions of 1,3-Diene Compounds in the Crystalline State. 254: 263–305
- McGhee AM, Procter DJ (2006) Radical Chemistry on Solid Support. 264: 93–134
- Meyer LA, see Li WP (2005) 252: 179–192
- Michl J, see Magnera TF (2005) 262: 63–97
- Milea JS, see Smith CL (2005) 261: 63–90
- Mizoshita N, see Kato T (2005) 256: 219–236
- Moonen NNP, Flood AH, Fernández JM, Stoddart JF (2005) Towards a Rational Design of Molecular Switches and Sensors from their Basic Building Blocks. 262: 99–132
- Moriyama M, see Kato T (2005) 256: 219–236
- Murai T (2005) Thio-, Seleno-, Telluro-Amides. 251: 247–272
- Nakayama J, see Ishii A (2005) 251: 181–225
- Nakayama J, see Ishii A (2005) 251: 227–246
- Nguyen GH, see Smith CL (2005) 261: 63–90
- Nicolau DV, Sawant PD (2005) Scanning Probe Microscopy Studies of Surface-Immobilised DNA/Oligonucleotide Molecules. 260: 113–160
- Niyomura O, Kato S (2005) Chalcogenocarboxylic Acids. 251: 1–12
- Niyomura O, see Kato S (2005) 251: 19–85
- Oda R, see Brizard A (2005) 256: 167–218
- Okahata Y, Kawasaki T (2005) Preparation and Electron Conductivity of DNA-Aligned Cast and LB Films from DNA-Lipid Complexes. 260: 57–75
- Oller-López JL, see Cuerva JM (2006) 264: 63–92
- Oltra JE, see Cuerva JM (2006) 264: 63–92
- Otto D, see Ihmels H (2005) 258: 161–204
- Palchetti I, Mascini M (2005) Electrochemical Adsorption Technique for Immobilization of Single-Stranded Oligonucleotides onto Carbon Screen-Printed Electrodes. 261: 27–43
- Pascal R, Boiteau L, Commeyras A (2005) From the Prebiotic Synthesis of α -Amino Acids Towards a Primitive Translation Apparatus for the Synthesis of Peptides. 259: 69–122
- Paulo A, see Santos I (2005) 252: 45–84
- Pérez EM, see Leigh DA (2006) 265: 185–208
- Pilch DS, Kaul M, Barbieri CM (2005) Ribosomal RNA Recognition by Aminoglycoside Antibiotics. 253: 179–204
- Pividori MI, Alegret S (2005) DNA Adsorption on Carbonaceous Materials. 260: 1–36
- Piwnica-Worms D, see Sharma V (2005) 252: 155–178
- Polito M, see Braga D (2005) 254: 71–94
- Poulin-Kerstien AT, see Dervan PB (2005) 253: 1–31
- Procter DJ, see McGhee AM (2006) 264: 93–134
- Quiclet-Sire B, Zard SZ (2006) The Degenerative Radical Transfer of Xanthates and Related Derivatives: An Unusually Powerful Tool for the Creation of Carbon–Carbon Bonds. 264: 201–236

- Ratner MA, see Weiss EA (2005) 257: 103–133
Raymond KN, see Seeber G (2006) 265: 147–184
Rebek Jr J, see Scarso A (2006) 265: 1–46
Renaud P, see Darmency V (2006) 263: 71–106
Robinson SP, see Liu S (2005) 252: 193–216
- Saha-Möller CR, see You C-C (2005) 258: 39–82
Sakamoto M (2005) Photochemical Aspects of Thiocarbonyl Compounds in the Solid-State. 254: 207–232
Saladino R, Crestini C, Costanzo G, DiMauro E (2005) On the Prebiotic Synthesis of Nucleobases, Nucleotides, Oligonucleotides, Pre-RNA and Pre-DNA Molecules. 259: 29–68
Santos I, Paulo A, Correia JDG (2005) Rhenium and Technetium Complexes Anchored by Phosphines and Scorpionates for Radiopharmaceutical Applications. 252: 45–84
Santos M, see Szathmáry E (2005) 259: 167–211
Sauvage J-P, see Collin J-P (2005) 262: 29–62
Sawant PD, see Nicolau DV (2005) 260: 113–160
Scandola F, see Chiorboli C (2005) 257: 63–102
Scarso A, Rebek Jr J (2006) Chiral Spaces in Supramolecular Assemblies. 265: 1–46
Scheffer JR, Xia W (2005) Asymmetric Induction in Organic Photochemistry via the Solid-State Ionic Chiral Auxiliary Approach. 254: 233–262
Schenning APHJ, see Ajayaghosh A (2005) 258: 83–118
Schmidtchen FP (2005) Artificial Host Molecules for the Sensing of Anions. 255: 1–29 Author Index Volumes 251–255
De Schryver F, see De Feyter S (2005) 258: 205–255
Seeber G, Tiedemann BEF, Raymond KN (2006) Supramolecular Chirality in Coordination Chemistry. 265: 147–184
Sharma V, Piwnica-Worms D (2005) Monitoring Multidrug Resistance P-Glycoprotein Drug Transport Activity with Single-Photon-Emission Computed Tomography and Positron Emission Tomography Radiopharmaceuticals. 252: 155–178
Shinkai S, see Ishi-i T (2005) 258: 119–160
Sibi MP, see Zimmerman J (2006) 263: 107–162
Siebbeles LDA, see Grozema FC (2005) 257: 135–164
Silvi S, see Balzani V (2005) 262: 1–27
Skrydstrup T, see Hansen SG (2006) 264: 135–162
Smith CL, Milea JS, Nguyen GH (2005) Immobilization of Nucleic Acids Using Biotin-Strept(avidin) Systems. 261: 63–90
Smith DK, see Hirst AR (2005) 256: 237–273
Stibor I, Zlatušková P (2005) Chiral Recognition of Anions. 255: 31–63
Stoddart JF, see Moonen NNP (2005) 262: 99–132
Suk D-H, see Crich D (2006) 263: 1–38
Suksai C, Tuntulani T (2005) Chromogenetic Anion Sensors. 255: 163–198
Sun J-S, see Escudé C (2005) 253: 109–148
Svith H, see Daasbjerg K (2006) 263: 39–70
Swordlow H, see Du Q (2005) 261: 45–61
Szathmáry E, Santos M, Fernando C (2005) Evolutionary Potential and Requirements for Minimal Protocells. 259: 167–211
- Taira S, see Yokoyama K (2005) 261: 91–112
Tamiaki H, see Balaban TS (2005) 258: 1–38
Tiedemann BEF, see Seeber G (2006) 265: 147–184

- Tobey SL, see Houk RJT (2005) 255: 199–229
Toda F (2005) Thermal and Photochemical Reactions in the Solid-State. 254: 1–40
Tour JM, see James DK (2005) 257: 33–62
Trask AV, Jones W (2005) Crystal Engineering of Organic Cocrystals by the Solid-State Grinding Approach. 254: 41–70
Tuntulani T, see Suksai C (2005) 255: 163–198

Uccelli L, see Boschi A (2005) 252: 85–115

Veciana J, see Amabilino DB (2006) 265: 253–302
Venturi M, see Balzani V (2005) 262: 1–27
Vezin H, see Dias N (2005) 253: 89–108
Vögtle F, see Fages F (2005) 256: 77–131
Vögtle M, see Žinić M (2005) 256: 39–76

Walschus U, see Luderer F (2005) 260: 37–56
Walton JC (2006) Unusual Radical Cyclisations. 264: 163–200
Warman JM, see Grozema FC (2005) 257: 135–164
Wasielewski MR, see Weiss EA (2005) 257: 103–133
Weiss EA, Wasielewski MR, Ratner MA (2005) Molecules as Wires: Molecule-Assisted Movement of Charge and Energy. 257: 103–133
Weissbuch I, Leiserowitz L, Lahav M (2005) Stochastic “Mirror Symmetry Breaking” via Self-Assembly, Reactivity and Amplification of Chirality: Relevance to Abiotic Conditions. 259: 123–165
Williams LD (2005) Between Objectivity and Whim: Nucleic Acid Structural Biology. 253: 77–88
Wong KM-C, see Yam VW-W (2005) 257: 1–32
Würthner F, see You C-C (2005) 258: 39–82

Xia W, see Scheffer JR (2005) 254: 233–262

Yam VW-W, Wong KM-C (2005) Luminescent Molecular Rods – Transition-Metal Alkynyl Complexes. 257: 1–32
Yashima E, see Maeda K (2006) 265: 47–88
Yokoyama K, Taira S (2005) Self-Assembly DNA-Conjugated Polymer for DNA Immobilization on Chip. 261: 91–112
Yoshikawa I, see Araki K (2005) 256: 133–165
You C-C, Dobrawa R, Saha-Möller CR, Würthner F (2005) Metallosupramolecular Dye Assemblies. 258: 39–82

Zard SZ, see Quiclet-Sire B (2006) 264: 201–236
Zhang X-E, Deng J-Y (2005) Detection of Mutations in Rifampin-Resistant *Mycobacterium Tuberculosis* by Short Oligonucleotide Ligation Assay on DNA Chips (SOLAC). 261: 169–190
Zimmerman J, Sibi MP (2006) Enantioselective Radical Reactions. 263: 107–162
Žinić M, see Fages F (2005) 256: 77–131
Žinić M, Vögtle F, Fages F (2005) Cholesterol-Based Gelators. 256: 39–76
Zipse H (2006) Radical Stability—A Theoretical Perspective. 263: 163–190
Zlatušková P, see Stibor I (2005) 255: 31–63

Subject Index

- Amplification 47
Antiprism 162
- Bailer twist 156
Barbituric acid 11
Benzylic amide [2]catenane 199
Bipyramid, trigonal 175
Bis(ethylenedithio)-tetrathiafulvalene 258
- Calix[4]arene capsules 16, 19, 29
10-Camphorsulphonic acid 261
Capsules 16
–, cylindrical dimeric 23
–, dimeric, ion pairing 20
–, racemic 29
–, tetrameric 21
Catenanes 185
–, translational isomerism 198
Chains 231
Chirality, assembly-enforced 223
–, reaction-induced 222
–, stirring-induced 126
–, surface-induced 219
Chirality sensing 47
Chirogenesis, supramolecular 93
Clean surfaces 213
Clusters 231
Coencapsulation 40
Conductors 253
–, polymeric 259
Coordination assemblies, racemization 147, 155
Crystallization 210
Cuboctahedra 176
 α -Cyclodextrin 204
- Deposition, molecular 216
2,6-Diacylamino pyridine 266
- Dimelamines-barbituric acid assemblies 11
Dimelamines-cyanurate assemblies 14
Dynamics 185
- Enantiomeric excess, magnetic field-induced 248
Enantiomorphism 210, 226
Enantioselective synthesis, chiral memory effect 35
Encapsulation 39
- Feringa's chiroptical switch 192
– unidirectional rotor 194
Fumaramide stations 200
- Gels 253, 277
–, chirality sensing 78
G-quadruplex assemblies 25
Guest inclusion 147
- Helical aggregates 47, 49
– –, chiral amplification 55
– –, chirality sensing 60
Helical chirality, memory and storage 74
Helical macromolecules 47, 61
Helical polymers, supramolecular assembly 80
Helicates 49, 159
–, circular 162
Helix 47
– inversion, chirality sensing 71
Hexa-*peri*-hexabenzocoronene 50
Homochirality, prochiral precursors 245
Host, cylindrical 38
Host-guest interactions 90, 147
Hydrogen bond 1
- Induction 253

- Interlocked architectures 204
– –, dynamic chirality 195
- Lattices, achiral 234
LEED 218
Liquid crystal 79, 253, 269
- M4L4 stoichiometry 171
M4L6 stoichiometry 166
M6L4 stoichiometry 173
Magnetic field-induced enantiomeric excess 248
Magnets/magnetism 253, 281
Mechanical coupling 157
Melamine, chiral cyanurate assembly 10
Metallomesogen 268
Molecular deposition 216
Molecular machine 185
Molecular monolayers 210
Molecular motor 185
Molecular ratchet 189
Molecular rotors 187
Molecular shuttle 185
– –, translational isomerism 196
Molecular switch 192
Molecular turnstiles 189
Monolayers, close-packed 227
– –, molecular 210
- Non-covalent synthesis 1
Nonlinear optical (NLO) materials 292
- Octahedra 175
- PANI-CSA 261
Peptido calix[4]arene capsules 19
Phthalocyanines 259
Pirouetting 195
Poly(ethylenedioxythiophene) (PEDOT) 263
- Poly(phenylacetylene)s 62
Polythiophene (PT) 259
Porphyrinoids 97
– –, achiral/racemic 93, 105
– –, chirality 90, 117
– –, dimeric/oligomeric 139
– –, monomeric 126, 131
– –, racemic 126
– –, supramolecular 105
Pseudo-racemic systems, homo-chiral 246
- Ray-Dutt twist 156
Rings 231
Rosettes, double 11
– –, enantiopure 35
Rotaxane 185
- Self-assembly, 2D 210
Shuttling 195
Softball, capsule 31
– –, chiral enantio-enriched 37
STM 216
Stoichiometry, M4L4 171
Substrate lattice-induced chirality 224
Supramolecular chemistry/architectures 93, 126, 147, 159
Surfaces 210
– –, achiral molecules 219
– –, chirality 210
– –, enantiomorphism 226
Switch, molecular 192
- Tennis ball capsule 30
Tetrahedra 166
Translational isomers 196
Tris-melamine, chiral cyanurate assembly 10
- Weak interactions 1